AD 744595

AGARD-LS-53

AGARD

ADVISORY GROUP FOR AEROSPACE RESEARCH & DEVELOPMENT

7 RUE ANCELLE 92 NEUILLY SUR SEINE FRANCE

DDC
RECEIVED
JUL 11 1972
C

AGARD LECTURE SERIES No. 53

on

Airframe/Engine Integration

NORTH ATLANTIC TREATY ORGANIZATION

Reproduced by
NATIONAL TECHNICAL
INFORMATION SERVICE
U S Department of Commerce
Springfield VA 22151

DISTRIBUTION AND AVAILABILITY
ON BACK COVER

NORTH ATLANTIC TREATY ORGANIZATION

ADVISORY GROUP FOR AEROSPACE RESEARCH AND DEVELOPMENT

(O' ANISATION DU TRAITE DE L'ATLANTIQUE NORD)

AGARD Lecture Series No.53

AIRFRAME/ENGINE INTEGRATION

A.Ferri

Lecture Series Director

Details of illustrations in
this document may be better
studied on microfiche

The material in this book has been assembled to support a Lecture Series under the sponsorship of the Propulsion and Energetics Panel and the Consultant and Exchange Program of AGARD.

THE MISSION OF AGARD

The mission of AGARD is to bring together the leading personalities of the NATO nations in the fields of science and technology relating to aerospace for the following purposes:

- Exchanging of scientific and technical information;
- Continuously stimulating advances in the aerospace sciences relevant to strengthening the common defence posture;
- Improving the co-operation among member nations in aerospace research and development;
- Providing scientific and technical advice and assistance to the North Atlantic Military Committee in the field of aerospace research and development;
- Rendering scientific and technical assistance, as requested, to other NATO bodies and to member nations in connection with research and development problems in the aerospace field.
- Providing assistance to member nations for the purpose of increasing their scientific and technical potential;
- Recommending effective ways for the member nations to use their research and development capabilities for the common benefit of the NATO community.

The highest authority within AGARD is the National Delegates Board consisting of officially appointed senior representatives from each Member Nation. The mission of AGARD is carried out through the Panels which are composed for experts appointed by the National Delegates, the Consultant and Exchange Program and the Aerospace Applications Studies Program. The results of AGARD work are reported to the Member Nations and the NATO Authorities through the AGARD series of publications of which this is one.

Participation in AGARD activities is by invitation only and is normally limited to citizens of the NATO nations.

The material in this publication has been reproduced directly from copy supplied by AGARD or the author.

Published May 1972

629.7.058.4
621.438:629.7.022

Printed by Technical Editing and Reproduction Ltd
Harford House, 7–9 Charlotte St, London, W1P 1HD

PREFACE

This Lecture Series is sponsored by the Propulsion and Energetics Panel and the Consultant and Exchange Program, and is a review of some of the work of the Ad Hoc Committee for Airplane Engine Interference.

The basic concepts related to optimizing airplane installations are described, and some of the analytical and experimental methods used for the investigation of such interference are reviewed in detail. Subsonic, transonic, and supersonic ranges are considered.

The interference problems are discussed in two groups: (1) inlet-airplane interference; and (2) nozzle and exhaust jet, and airplane interference. A detailed discussion of different experimental techniques presently used by different laboratories is given. A critical review of the shortcomings of some of the new techniques used is presented. The problem related to dynamics of the engine inlet-engine nozzle integration is reviewed, and a consistent set of definitions of airplane and engine characteristics is given.

A round table discussion with the participation of all the speakers concludes the Lecture Series presented in four different NATO nations (USA, France, Germany and England), from 22 June to 4 July 1972.

A.Ferri
Lecture Series Director

LIST OF SPEAKERS

Lecture Series Director Professor A.Ferri
Director
Aerospace Laboratory
New York University
177th St. and Harlem River
Bronx, New York 10453
USA

Mr P. Antonatos
Chief
Flight Mechanics Division
Air Force Flight Dynamics Laboratory AFFDL/FX
Wright-Patterson AFB
Ohio 45433
USA

Dipl. Ing.F.Aulehla
Messerschmitt-Bölkow-Blohm GmbH
Unternehmensbereich Flugzeuge
D 8 München 80
Postfach 80 11 60
Germany

Mr E.C.Carter
Deputy Chief Aerodynamicist
Aircraft Research Association Ltd
Manton Lane
Bedford, Beds.
England

Dr A.Fuhs
Department of Aeronautics
Naval Postgraduate School
Monterey, California 93940
USA

Mr F.Jaarsma
National Aerospace Laboratory
Sloterweg 145
Amsterdam 17
The Netherlands

Dr Demetrius Zonars
Chief Scientist
Department of the Air Force
Air Force Flight Dynamics Laboratory (AFSC)
Wright-Patterson AFB,
Ohio 45433
USA

CONTENTS

	Page
PREFACE	iii
LIST OF SPEAKERS	iv
	Reference
INTRODUCTORY LECTURE – ENGINE AIRPLANE INTERFERENCE – DEFINITION OF THE PROBLEM AND RELATED BASIC FLUID DYNAMIC PHENOMENA by A.Ferri	1
INLET/AIRPLANE INTERFERENCE AND INTEGRATION by P.P.Antonatos	2
EXPERIMENTAL DETERMINATION OF INLET CHARACTERISTICS AND INLET AND AIRFRAME INTERFERENCE by E.C.Carter	3
NOZZLE/AIRFRAME INTERFERENCE AND INTEGRATION by F.Aulehla and K.Lotter	4
EXPERIMENTAL DETERMINATION OF NOZZLE CHARACTERISTICS AND NOZZLE AIRFRAME INTERFERENCE by F.Jaarsma	5
DYNAMIC CHARACTERISTICS OF ENGINE INLETS by D.Zonars	6
ENGINE INTEGRATION AND THRUST/DRAG DEFINITION by A.E.Fuhs	7

ENGINE AIRPLANE INTERFERENCE

DEFINITION OF THE PROBLEM AND RELATED BASIC FLUID DYNAMIC PHENOMENA

by

Antonio Ferri
Director, Aerospace Laboratory
Astor Professor of Aerospace Sciences
New York University
Bronx, New York 10453

1. INTRODUCTION

In the past, the development of aerodynamic technology has been based on the use and application of scaling criteria which have permitted the investigation of many aerodynamic configurations by means of wind tunnel tests where carefully instrumented small scale models are investigated experimentally. The extensive use of similarity laws, in order to investigate alternate solutions for a given problem, is somewhat unique for the aeronautical industry, and is probably one of the reasons for the rapid progress of this industry.

The basic similarity laws for aerodynamics requires simulation of nondimensional parameters such as Reynolds and Mach numbers, and for high Mach numbers, the Nusselt and Prandtl numbers. In view of the difficulties encountered in simulating all of the parameters in wind tunnel tests, we have learned to extrapolate data from one condition to another; however, in some ranges of speed we have found difficulties in performing these extrapolations. Besides the effects due to testing at different similarity numbers, other effects are present that sometimes make it difficult to extrapolate small scale test results to full scale. Such effects are due to imperfect simulation of the physical and geometrical parameters involved in the experiments. The presence of tunnel walls creates substantial changes in the flow fields at subsonic and especially at transonic speeds. The presence of the support of the model produces interference with the model flow, especially at subsonic and transonic speeds. Aeroelastic effects interfere with accurate simulation. In addition, the lack of simulation of the engine flow introduces in some instances substantial differences between the aerodynamics of the actual airplane and of the model tested. The purpose of this series of lectures is to discuss the last problem in some detail, to review some of the most recent advances and some of the unresolved problems in this field, and to suggest possible improvements of better techniques and fields of research directed toward a better understanding of the problem. In order to outline the problems involved with the lack of correct representation of the engine flow, I will review as an introduction some of the characteristics related to interference between the airplane and the engine , and their effects on the calculated performances of the airplane. The problems are somewhat different at subsonic and transonic speeds and at supersonic speed; therefore, I will discuss the two velocity regimes separately, First, I will review the effects of the engine on the airplane.

2. INTERACTION OF THE ENGINE FLOW ON THE AIRPLANE

2.1 Subsonic and transonic speeds

The engine thrust is defined by the variation of total momentum of the flow entering the engine between free stream conditions existing far ahead of the engine and the conditions occurring at the exit of the engine. The engine, by increasing the total momentum of this flow, produces internal thrust; but at the same time generates external forces that affect the drag and lift of the airplane. The drag production is due to either viscous losses or shock losses. Therefore, in order to analyze the effect of the engine, we must analyze the effect of the shocks and viscous phenomena produced by the engine on the flow outside. The engine induces large pressure variations in the region in front of the engine and behind the engine that can influence the aerodynamic properties of the airplane including lift and pitching moments. In order to understand qualitatively such effects, consider first an isolated axially symmetric engine nacelle. At very low flight speed a turbojet engine acts as a hollow body having a distribution of sinks and sources at the axis. In the front we have sinks that accelerate the flow. Because the flow velocity at the inlet entrance is much larger than the flight velocity, in the front, the streamtube entering the inlet is a rapidly converging streamtube, Fig. 1. The flow is accelerated and heated by the engine, and at low speed the streamtube leaving the engine is much smaller than the free streamtube and the streamtube at the inlet; therefore, the sink strength is larger than the strength of the sources. The air leaving the engine mixes with the outside air. Such mixing occurs with a variation of streamtube area; thus, the interference between engine flow and external flow extends downstream of the engine. The mixing produces a variation of cross-sectional area that is equivalent to a displacement thickness corresponding to the mixing process. Such variation of area of the streamtube produces a variation of static pressure equivalent to the pressure produced by a body of cross-sectional area equal to the variation due to mixing. Therefore, if the nacelle is placed in the vicinity of an airframe, the nacelle induces a flow field that affects lift moments and skin friction drag of the airplane.

In the absence of the flow field induced by the airplane, the shape of the streamtube of the flow entering and leaving the engine can be determined analytically. In the subsonic region, before localized supersonic regions appear in the flow, linear theory permits determining the streamtube shape in front and behind provided that a mixing analysis is combined with the linearized theory in order to determine the shape of the mixing. Such types of analyses are available, and a computer program can be easily generated provided that the turbulent transport properties are assumed from experimental information.

A more complex analysis can be performed for the transonic region by means of the linearized transonic analysis or by more complex transonic analyses based on relaxation in time dependent methods. However,

all of these analyses should include the mixing regions behind the engine in order to use the correct boundary conditions for the problem. Such a region incorrectly is not considered as a part of the problem in some of the work presently under way. Presently, such analyses are not performed systematically for any new engine, and are not required as a part of an engine's characteristics in spite of the fact that the results could be useful in order to evaluate engine performance when installed in the airplane. The shape of the mixing displacement thickness depends strongly on the cycle of the engine In general, if we consider the mixing of two streams having the same γ, the variation of the cross-sectional area due to mixing at constant pressure after complete mixing is given by:

$$\Delta A \sim (H_1/u_1 - H_2/u_2)\ (u_1 - u_2)$$

where the ΔA is the increase of the streamtube area at constant pressue, H_1 and H_2 the total enthalpy of the two streams and u_1, u_2 the velocities of the streams. For an engine, the jet velocity u_1 is always larger than the external velocity $u_1 > u_2$. At low flight velocities u_2 is small and H_2/u_2 is larger than H_1/u_1; therefore, the mixing between the external flow and the engine flow tends to produce a converging streamtube. In a bypass engine, we must consider three streams. The engine flow can have a value of H_1/u_1 larger or smaller than the value of H_2/u_2 of the fan flow, depending on the compression ratio of the fan and flight velocity. At low flight speed, the value of H_2/u_2 increases rapidly when the fan compression ratio decreases. Then at low speed for an engine having low pressure ratio fans, the converging of the streamtube downstream of the jet due to the mixing of the engine flow and fan flow is very large.

Figure 1 indicates schematically the variation of streamtube area of a bypass engine having bypass ratio 6 and 40,000 lbs takeoff thrust, at flight Mach numbers of 0.15 sea level. The streamtube converges from an area of 120 ft^2 corresponding to free stream conditions to an area of 50 ft^2 at the exit. The displacement of the mixing is negative; therefore,the streamtube continues to converge. Consider now an airplane having engines placed in nacelles under the wings. When we perform a model test in order to determine airplane performances, we should represent this flow field correctly; therefore, if we do not use engine simulators, we should insert under the wing bodies having roughly the shape of the streamtube of the engine. However, the interaction among the airplane flow fields and the jet flow fields changes the local pressure, which therefore changes the equivalent body shape; then, the equivalent body shape is nonsymmetrical and is not known "a priori" from a calculation for a uniform flow field. These interaction effects, however , can be determined by means of an iteration procedure. Often, experiments are made where the nacelles are either not represented, or are represented by ducts having the same external shape as the engines and passing some flow through. The second approach is less satisfactory than the first because in the absence of an engine simulator placed inside the nacelle, the mass flow entering the inlet of the nacelle is much less than the engine mass flow (unless the exhaust area is increased) because a pressure drop occurs inside the nacelle. Then the streamtube shape entering the nacelle is quite different than in flight, and the flow field in front of the engine and behind it is quite different from the corresponding flow field in the airplane. These effects are large at all speeds, and are important especially at transonic speeds.

Figure 2 gives an indication of the difference of streamtube cross section required at the exit for different engine cyles, and for the case of a cowling without an engine simulator when the inlet mass flow is matched. The data are for $M_\infty = 0.90$. The figure also gives the streamtube of an engine simulator which simulates accurately entrance conditions, exit Mach number, exit area, and exit pressure; but not exit temperature for a typical turbojet and turbofan. In the data presented, it is assumed that the engine simulator has a compressor that compresses the air entering the inlet which is simulated, while the turbine that drives the compressor is driven by compressed air carried in from the outside through a channel. Then the exit mass flow is larger than the entrance mass flow and includes inlet air and turbine air. Such additional air balances the lack of heat addition; then the area Mach number and pressure are matched at the inlet. For the turbojet engine, a case where transition from laminar to turbulent mixing occurs at some distance from the nozzle is also shown. The differences of streamtubes are large, and in some cases can be important.

Figure 3 gives an indication of the differences between the streamtube area for engine simulators used in this type of testing for a bypass engine and an actual engine. In this simulation at $M_\infty \sim 0.85$, the entrance mass flow through the inlet is less than in the actual mass flow engine (14% less); the pressure ratio through the fan is the same, the exit area of the main engine is smaller, and the flow from the engine simulator is cold; therefore, the same discrepancy as shown in Fig. 2 exists for the mixing region. The difference in streamtube area for four engines in full scale corresponds to 17 ft^2 initially, and becomes 32 ft^2 at some distance. The importance of these effects should be evaluated, and if important, corrections to the experimental data should be introduced.

Two alternate solutions are suggested:

(1) test without nacelles and make analytical corrections,

(2) use engine simulators.

The first approach is already used during the preliminary design phase; however, corrections are seldom performed in spite of the fact that they are possible for podded engines. The second solution requires more complex and expensive apparatus, and even with the additional complications, cannot give a completely satisfactory simulation; therefore, even in this case analytical methods that permit estimating such lack of complete simulation should be used.

The experimental results in wind tunnels are usually corrected for wall effects; however, numerical methods are not yet available to evaluate corrections for engine interference on the airplane. Such methods could be generated within the ability of present analytical methods for podded engines as used in transport airplanes. The problem for engines imbedded in the fuselage is more complex, and requires further investigations; however, some correction is possible even for this case. The methods to be used

are fairly simple because superposition of solutions is possible (e.g., Ref. 1). Numerical programs based on superposition of solutions can define the equivalent body shape that represents the engine flow as a function of the flow field produced by the airplane for subsonic flow. Then by using, as an input, experimental data that defines the flow field of the airplane without the engine, the flow field induced by the engine on the airplane can be determined. If required, interaction procedures could be used in order to obtain a second order correction on the streamtube shape. The basic concept suggested here is to use a combination of computers. The wind tunnel is used as an analog computer for the data simulation of the airplane flow field because of its ability of determining viscous flow effects and three-dimensional flow. Then a digital computer is used to determine the equivalent body that represents the engine, flow in the presence of the airplane flow, and the influence of such a body on the airplane. The use of engine simulators simplifies somewhat the experimental problem; however, even in this case the simulation is not perfect and therefore the influence of the differences should be evaluated. The problem becomes more difficult when transonic flow is present because in this velocity range, the numerical analyses are much more complex, and at the same time the effects of variation of cross-sectional area of the engine flow are more important. Presently, research is in progress for the analysis of the flow field around nacelles as shown in Fig. 3. Unfortunately, in the analysis it is assumed that the streamtube leaving the engines does not mix with the external flow; therefore, the boundary conditions downstream of the fan and the engines are not representative. The effect of the mixing of the fan flow can be introduced as a correction of the boundary conditions, and can be determined in advance from the determination of the displacement thickness obtained from a calculation of the mixing; however, the introduction of the mixing of the flow field downstream is more difficult because it affects the pressure distribution.

2.2 Supersonic speed

The interaction of the engine on the airplane at supersonic speed is limited to the region downstream of the inlet. Such interaction is very important and can be utilized to produce lift or reduce drag of the airplane. In many installations we can define an L/D of the engine defined as the increase in lift due to engine interference, divided by the additional external drag produced by the engine. The fact that the inlet and inlet spillage produces not only drag, but also lift is important, and is a factor in the selection of the inlet configuration and engine position.

The basic conceptional principles for the utilization and analysis of favorable engine airplane interference has been given in Ref. 2. Consider Fig. 4 (taken from Ref. 2), the equivalent body that represents the variation of streamtube entering the engine can be represented as a distribution of singularities. The singularities are sources and sinks for axially symmetric configurations, and multipoles for nonsymmetrical configurations. Both the airplane and the equivalent body induce a flow field that can be calculated. The front part of the body produces a pressure rise in the rear part of the wing, decreasing pressure drag and increasing lift, while the front part of the wing produces a pressure rise in the rear part of the body decreasing the pressure drag of the body. The effect of such flow fields can be evaluated by simple integral relations if the interaction is felt by flat surfaces, or it requires numerical integration if the surfaces are not flat. In any case, the pressure field induced by the equivalent body can be evaluated and the variations due to interference can be obtained provided that linear theory can be applied.

Figure 5 indicates inviscid polar diagrams for an isolated wing, and a wing and additional body conveniently shaped,placed under the wing. The body increases the shock drag and also the lift; therefore, the L/D is increased by the presence of the new body. The possibility of increasing lift is important because it tends to decrease the penalties due to external compression for the inlet. As mentioned previously, the analysis of the interference effects can be performed easily when linear theory is utilized. Improvements on this type of analysis can be obtained by using the Whitham type of analysis which is used extensively for the analysis of sonic boom. In this case, the intensity of the perturbation is still given by the linear theory; however, the propagation of the perturbation is given along a Mach line or shock that takes into account the change of speed of sound, and the effect of velocity disturbances; therefore, the Mach line is not inclined at μ_∞ (Mach angle of the undisturbed velocity) with the flight velocity but at $(\mu+\theta)_{local}$ where μ is the local Mach angle and θ the inclination of the velocity. Either linear theory, or experimental data that gives the flow field produced by the inlet, or more accurate theory can be used to determine the disturbances produced at the surface of the body that represents the engine streamtube. The propagation of such disturbances is determined by the second order theory of Whitham as described in Refs. 3 and 4. The interaction and reflection of such waves with the airplane surface is determined by linear theory. Then the effect of interaction on local pressure is obtained by two components. The first is proportional to the local velocity perturbation produced by the equivalent body, the propagation of which is analyzed in second order; the second contribution is obtained by assuming that a source sink distribution is present, defined by the local component of the velocity perturbation normal to the airplane surface generated by the equivalent body representing the engine. The intensity and distribution of sources and sinks is proportional to this normal component. Then the velocity and pressure at any point generated by this distribution can be obtained from linear theory, and the second component of the interaction determined.

At high Mach numbers, this type of analysis is unsatisfactory because all analyses depend on the validity of linear theory. Then either experimental investigations, or more complex analyses, are required in order to obtain the perturbation flow field at small distances from the inlet. Time dependent types of analyses are attractive for such investigations. The extrapolation to larger distances can be obtained with the method described above, or with improvements of the method as described in Refs. 5 and 6. The distance where extrapolation is possible is defined by the necessity of existence of a solution given by linear theory at the distance considered; therefore, it is a function of the Mach number and local intensity of the disturbance.

3. INTERACTION OF THE AIRPLANE FLOW FIELD ON THE ENGINE PERFORMANCES

The effect of the flow field produced by the airplane on the engine performance is strong for engines imbedded in the fuselage and is smaller for podded engines. Usually, for podded engines, simple corrections

can be introduced on the isolated engine performances in order to take care of such effects. However, in some cases, at low flight speed and for high bypass engines, even for podded engines the interaction of the airplane flow field can be important when the airplane changes substantially the pressure field at the exit of the fan. This local change of pressure affects the split between engine and fan mass flow, and therefore the bypass ratio. In addition, this pressure field induced by the airplane is not uniform; it can produce nonsteady fluctuation in the flow of the fan by producing peripheral variations of the pressure at the exit of the fan. These effects can be present only at low speed because at high subsonic speed the flow leaving the fan becomes sonic or supersonic even for low fan pressure ratio engines.

While the flow induced by the airplane does not affect substantially the engine performances, when podded engines are sidered, the flow can affect the external drag of the nacelle. Because of the presence of the airplane, large cross flows can exist at the exit of the jet. Such cross flows at transonic speed and supersonic speed can affect substantially the nacelle drag of the engine. Some mismatch of static pressure of flow direction is presented at the exit of the fan flow, or engine flow. Then some local separation takes place near the nozzle exit. This separation usually is beneficial because it tends to decrease over-expansion and therefore drag, Fig. 6.

The local separation and the amount of drag depends on the momentum and temperature thickness of the boundary layer. Such quantities are strongly affected by the presence of cross pressure gradients and cross flows because they distribute the boundary layer nonuniformity around the nozzle. Therefore, the airplane pressure field can modify the nozzle performances and the nacelle drag. (This effect will be discussed in more detail later on.)

The problem of interference is of primary importance when the engine inlets and nozzles are either part of the fuselage or are located on the lower surface of the wing. In these cases, the flow induced by the wing or by the fuselage interacts with the inlet and the nozzle of the engine and affects engine performances directly. This problem is especially important for airplanes that must have supersonic capabilities and good performances at transonic speeds, and must operate efficiently and at high angles of attack during maneuvers. For these configurations, the airplane and engine flow are closely interdependent; therefore, the effects of the airplane flow on the engine performances, and of the engine flow on the airplane performances, are of primary importance. The compromise of the inlet and nozzle design for a given engine, selection of the best engine cycle, and engine location, must take into account from the beginning interference effects. The flow field produced by the fuselage in locations convenient for inlets either at subsonic, transonic, or supersonic velocities, is highly nonuniform especially at large angles of attack. The cross flow generated by lack of axial symmetry, or angle of attack, produces vortices and regions of local separation that start in the front region of the fuselage which can enter the engine inlet. The non-uniformities entering the inlet generate large distortions in the inlet flow that either can be unacceptable for the compressors or the fans, or can produce penalties in performance. A large amount of experimental information has become available recently in this field (e.g., Ref.7). Such results indicate the importance of the problems and some possible solutions; some of the most important results will be discussed later on. Here, I will limit my attention to discussing possible analytical contributions to the understanding of the problem. The inviscid flow field can be analyzed accurately at subsonic and supersonic speed. Recently, analytical methods have been developed also for transonic speed; however, such available analytical methods are not fully utilized in airplane design practice. The reason is that the boundary layer effects cannot be predicted by analysis as accurately as the inviscid effects, and they produce important modifications on the flow field. The boundary layer properties and the production of separated regions are a function only of local pressure gradients. The recent availability of a large amount of experimental information in this field gives indications of such dependence; therefore, it will probably be possible in the future to generate analytical prediction methods of the flow field taking into account the presence of boundary layers, provided that the available experimental data are utilized to define the properties of the boundary layer. When the available information is used, a generalized numerical program could probably be generated that defines approximately the flow field and permits extrapolating experimental data performed at low Reynolds number to higher Reynolds numbers. The availability of such a type of analysis would help the designer. Such analysis could indicate promising directions of configuration changes required to eliminate an existing problem, and could help during preliminary design to select the more promising locations of air intakes and engines, and fuselage shapes in a given airplane configuration. The integration of analytical and experimental information in a numerical method for fuselage flow analysis, should be the next step of the research program in this field. Such a type of analysis should cover the subsonic, transonic, and supersonic ranges.

In connection with the interference between airplane and inlet flow at subsonic and transonic speed, careful attention should be given to the interpretation of experimental data. Often the airplane interference on an inlet is determined experimentally in wind tunnels by determining the forces on the region of the airplane configuration extended in front of the inlet in the vicinity of the inlet, and on the inlet, without correct representation of the rear part of the airplane. Such measurements can be highly misleading at subsonic and transonic speeds.

Assume, for example, that we investigate the effect of a ramp AB placed in front of an inlet, as shown in Fig. 7, and we want to compare the drag of a given airplane inlet combination at subsonic or transonic speed for the case where the inlet has ramp AB (configuration a), and for the case of an inlet without the ramp (configuration b). If we measure the force only in the front part of the airplane, in front of section S-S for the same inlet mass flow, then we find that the ramp produces an additional "apparent" drag because the streamline entering the inlet is inviscid and has a bump where the pressure is above atmospheric. However, such a drag is balanced by a thrust in the rear part of the airplane. Therefore, at subsonic speed, this "ramp drag" is mainly due to the testing technique and is not an actual increase in drag of the airplane unless the recovery in the rear part of the airplane is reduced by viscous phenomena. This can be seen immediately if we analyze the pressure distribution in a subsonic "bump" as shown in Fig. 8. The pressure along a corrugated surface at subsonic speed is symmetrical and the pressure in the front part balances the pressure in the rear. Therefore, if the total displacement is zero, the inviscid drag is also zero. The two possible sources of drag are viscous effects and localized shocks. The viscous losses and formation of localized shocks occur in the region of the airplane that is not

represented in the test, and therefore cannot be measured. Any measurement of losses at subsonic and transonic speeds without a careful investigation of the downstream conditions can lead to incorrect conclusions The only valid investigation for this type of test is an investigation that attempts to determine the presence and defines the intensity of additional viscous and shock losses independently of the pressure field.

A similar type of comment applies to the experimental investigation of the boundary layer scoops either at subsonic or supersonic speeds. In all inlets attached to the fuselage or wing, the boundary layer produced on the surfaces in front of the inlet is directed outside of the inlet by boundary layer diverters or scoops that connect the low velocity flow inside or in front of the inlet to a region of lower pressure. The drag of such scoops depends on the pressure variation of the boundary layer flow. A large part of the flow in the scoops is either transonic or subsonic; therefore, the flow has subsonic characteristics and the pressure variation inside the scoop depends substantially on the downstream conditions. Such conditions depend on many parameters; e.g., the geometry of the rear part of the airplane, the Reynolds number of the tests, and on the angle of attack of the airplane. Therefore, experiments on boundary layer scoops should, as a first step, prove that the downstream conditions are correctly represented. This could be done by measuring the pressure on the airplane in the region of the boundary layer scoops and by checking that the pressure in this region is reproduced in the inlet tests. Often this type of proof is missing in the report describing such experiments.

4. INTERACTION BETWEEN ENGINE FLOW AND EXTERNAL FLOW NEAR THE NOZZLE

One of the most important interactions between the airplane induced flow and the engine flow occurs in the region of the engine nozzle. Here, especially at transonic speeds, a large percentage of the airplane drag is generated. Such a drag is controlled by the interaction between the internal and external flows; therefore, the most complex compromise between external and internal performances is required in the selection of nozzle design. The difficulty is increased by the fact that the effect on the external drag is not included in the definition of engine performances, and by the fact that in practice two independent engineering design groups are responsible for the designs of the configuration of the nozzle that controls the internal flow and for the configuration of the external shape of the fuselage.

The presence of large external drag in the region of the nozzle exit is somewhat related to the characteristics of the engine design. The flow leaving the turbine has low exit Mach number, and is discharged through annulus; therefore, the turbine diameter is much larger than the diameter of the minimum area of the nozzle where the flow is sonic. In order to minimize heat and viscous losses, the transition from the turbine to the nozzle is short; therefore, the rear part of the engine has a very rapid converging section at the end. Only for supersonic flight a diverging section follows the converging nozzle reducing the difference between turbine and exit nozzle diameter. Therefore, this effect is maximum at transonic speed. For example, for a typical bypass engine for a subsonic transport, the ratio between the diameter of the engine in the turbine region to the nozzle of the main flow is of the order of 1:4 - 1:6. This rapid convergency of the engine tends to produce large local overexpansion that tends to produce pressure drag. When the engine is placed on a pod, the local external area change can be balanced by an area increase produced by a different component of the airplane, such as the wing or the fuselage; therefore, the effect on overall drag at transonic speed can be minimized. However, when the engines are placed in the fuselage, usually the nozzles are located at the end of the fuselage, then this compensation is impossible. Therefore, at transonic speed substantial drag is generated by this region for airplanes having engines in the fuselage. The main reason for the selection of the positioning of the engine in the rear part of airplanes of this type,is due to the fact that the exhaust gases of the jet are at high temperature; therefore, the solution where the engines are placed in front, and the gases are discharged underneath the fuselage would produce severe aerodynamic heating for the skin of the fuselage in contact with the jet. Many parameters affect the drag near the jet exhaust, some of which are related to the airplane design, others are defined by the details of the engine design. A correct representation of all the parameters involved in a small scale experiment is extremely difficult, and the importance of some of the parameters cannot be defined "a priori;" however, presently the possible importance of some of these parameters is not clearly recognized. A detailed discussion, therefore, of such interaction could be useful. Consider first an axial symmetric installation similar to the case of a single jet airplane. Usually, the inside flow generated by the engine has several streams mixing inside the nozzle, each having different stagnation properties. Figures 9 and 10 indicate two different possible configurations. The first has a converging nozzle, the second used for supersonic airplanes has a converging, diverging section.

Figure 9 schematizes either a jet engine or a bypass engine where the bypass flow is discharged ahead of the engine nozzle.The flow at point c includes the bypass and the engine flows, and only some cooling air is discharged between the airplane shell and the nozzle engine. In the converging region of the fuselage, some separation occurs in the outside that tends to decrease the drag of the airplane. The separation region is controlled by several flow parameters. The flow in front of point B is locally supersonic at transonic and supersonic flight speeds; therefore, the flow outside is qualitatively similar to the flow over a supersonic or transonic wing in the region of separation. The separation point B is a function of the boundary layer profile in front of B. In this case, because of the difference of the separation in the wing, both velocity and temperature profiles must be considered as parameters since some heat transfer takes place between the structure of the engine and the boundary layer due to the fact that the inside flow has higher temperature than free stream. At transonic speed, the separation of the boundary layer produces an envelope shock and the Mach number downstream at point D is of the order of one. Then the pressure rises from D to C, and at C the pressure is higher than at D. The position of B depends on the ability of the flow along the streamline BDC to overcome the pressure rise between B and C. At B, the velocity along the streamline is zero, at D it is higher than zero and at C is again zero. The velocity profiles are qualitatively indicated in Fig. 9. The pressure rise requires a balance between shear forces and pressure gradients and is accomplished by the work due to the shear produced by the velocity gradients normal to the streamline. This shear depends on the characteristics of the flow inside; the flow at A expands because the flow at the jet is slightly underexpanded. Due to this underexpansion, the pressure

at C depends on the characteristics of the inside flow that affects the pressure distribution along AC. In addition, the shear along AC contributes substantially to accelerating the flow in the separated region, DC; therefore, the shear along AC, and the pressure along AC, depend on the inside properties of the flow and on the outside properties of the flow. Then additional parameters that are important for the definition of point B and of the pressure along BA, are velocity and temperature profiles of the boundary layer flow at A, expansion process of the internal flow related to the flow distribution at the nozzle exit, velocity and temperature profiles of the boundary layer of the external flow at B, in addition to the main properties such as total enthalpy, Mach number, and pressure of all flows. The mixing along EF between cooling flow and main flow affects directly the pressure along AC, because it defines the profile of the velocity at A; therefore, such mixing must also be considered in experiments.

In addition to these flow quantities, other parameters are of primary importance. The pressure rise along BC and AC is related to shear due to turbulent mixing. The mixing is affected by swirl of the flow, by leakage of the flow across the sections of the variable nozzle. Therefore, a representative test requires the control of many other parameters above the ratio of the jet Mach number and pressure at A. For this reason, it is improbable that the use of engine simulators in the form of small rocket engines, or turbojet engines, that simulate only a few overall properties of the flow can give significant qualitative results without substantial additional tests of analyses that investigate the importance of the parameters not simulated. For example, the presence of coolant flow in the outside of the engine, or leakage of engine flow through the nozzle, is usually not considered in nozzle tests. Such flows can have significant effects because they define the velocity and temperature profiles at A. The scale of the turbulent fluctuations of the engine flows in the presence of swirl are also important parameters of the problem because the turbulent mixing along AC depends on such quantities. Such quantities could and should be measured in the tests of the actual engine, and scaled correctly in the simulation. The scaling laws, however, have not yet been clearly determined.

The mass flow of the secondary flow 1 depends on the pressure distribution at E, which is controlled by the shape of the nozzle and by the mixing occurring before A, and by the pressure at A. The possibility exists that the mixing between secondary and primary flow is slow, and that a reverse flow takes place in the outside and inside of the nozzle, Fig. 9b.

When the nozzle has a divergent section following the throat, then the separation at transonic speed, or at low subsonic speed occurs in the inside, Fig. 10a; while at higher Mach numbers and at design speed occurs outside, Fig. 10b. Again, the separation region is controlled by the mixing of the inside flows, and by their interaction with the outside flow, which is controlled by the details of the inside flow such as temperature and velocity profiles, turbulence level, and scale, in addition to stagnation properties and geometry of the nozzle.

In some instances part of the external flow is used to fill the engine nozzle, which is designed for supersonic performances, Fig. 11. Then mixing takes place between the cooling flow and the external flow, and between these flows and the main jet. The external flow first expands and then is compressed through a shock wave. The expansion and the shock produce external drag that must be considered as part of the engine performance. The problem is similar to the problem described before; however, here the mixing process inside is more complex. Here the details of the external boundary layer are extremely important because they define the amount of expansion occurring outside and the amount of mass flow entering the engine.

In actual applications, the flow outside the nozzle is three-dimensional. Then the pressure at A of Fig. 9 is also three-dimensional. As a consequence, the secondary flow 1 of Fig. 9 and the secondary flow 3 coming from the outside in Fig. 11 are not axially symmetric. The mass flow of these streams changes around the periphery of the nozzle, concentrating in the region of low local pressure. This effect makes the problem extremely complex and more difficult to investigate. It is clear that such complex phenomenon cannot be investigated by tests of wind tunnel models of airplane configurations alone even if complex engine simulators are used. Experimental programs, with a combination of isolated nozzle engines, where external flows and three-dimensional effects are simulated and engine simulators installed on the airplane are used, are the more promising.

Presently, the research in this field is unsatisfactory because it has been directed mainly toward the determination of selecting satisfactory nozzle designs, rather than toward a better understanding of the influence of the different parameters and development of good testing criteria. Many of the parameters such as properties of secondary flow, turbulence level, or effects of nozzle leakage, and three-dimensional flow, are usually not considered in present tests; therefore, substantial additional basic work is required before a satisfactory, analytical, and experimental technique is developed, that permits evaluating nozzle airplane interference.

5. CONCLUDING REMARKS

This brief introduction indicates that substantial additional research work is required in the field of engine airplane interference. We will follow up with a detailed discussion of some of the most important problems. Here, only one conclusion will be made.

In the problem of engine interference, like in many other important problems, the tendency in the past has been to rely mainly on experimental data; this should be changed. New approaches are required where analog and digital simulation is integrated, where the wind tunnel or test stand furnishes analog data. Then, corrections generated by numerical methods are introduced to these data in order to improve the results obtained. Such approaches should be used extensively in preliminary design, and in the determination of engine and airplane performances.

6. REFERENCES

1. Ward, G.N., "Linearized Theory of Steady High-Speed Flow." Cambridge University Press, 1955.

2. Ferri, A., Clarke, J.H., and Ting, L., "Favorable Interference in Lifting Systems in Supersonic Flow." Journal Aeronautical Sciences, Vol. 24, No. 11, November 1957, pp. 798-804.

3. Whitham, G.B., "The Flow Pattern of a Supersonic Projectile." Comm. Pure Appl. Math., 5:301-48, 1952.

4. Walkden, F., "The Shock Pattern of a Wing-body Combination Far From the Flight Path." Aero. Quart., 9:164-94, 1958.

5. Landahl, M., Ryhming, I., and Lofgren, P., "Nonlinear Effects on Sonic Boom Intensity." NASA Third Conference on Sonic Boom Research, NASA SP-255, October 1970, pp. 3-15.

6. Landahl, M. Ryhming, I., Sorensen, H., and Drougge, G., "A New Method for Determining Sonic Boom Strength from Near-Field Measurements." NASA Third Conference on Sonic Boom Research, NASA SP-255, October 1970, pp. 285-95.

7. Ferri, A., "Engine Airplane Interference and Wall Corrections in Transonic Wind Tunnel Tests." AGARD AR 36-71.

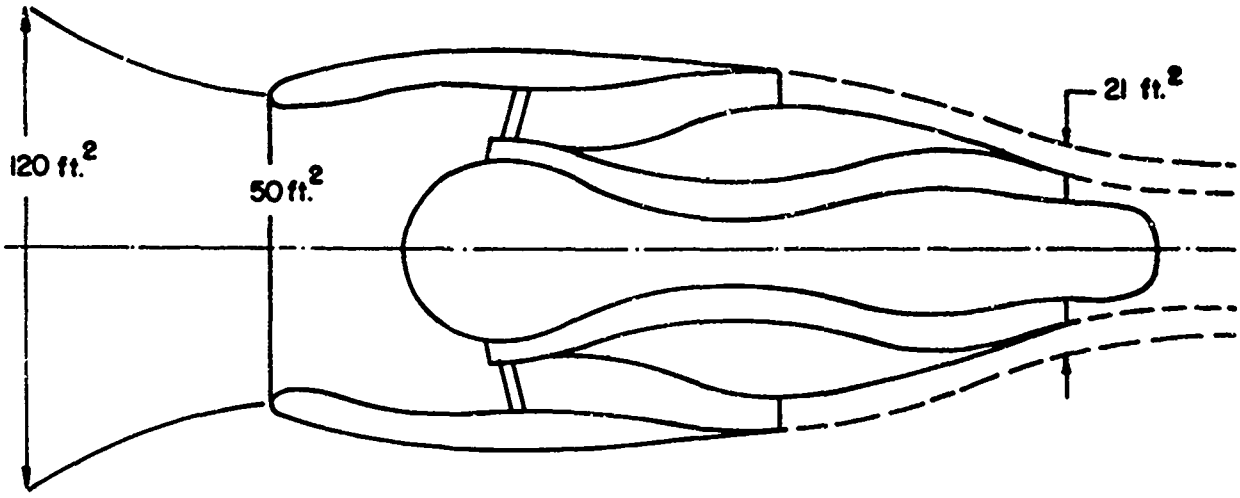

Fig. 1 Streamtube variation for typical bypass engine at M = 0.15

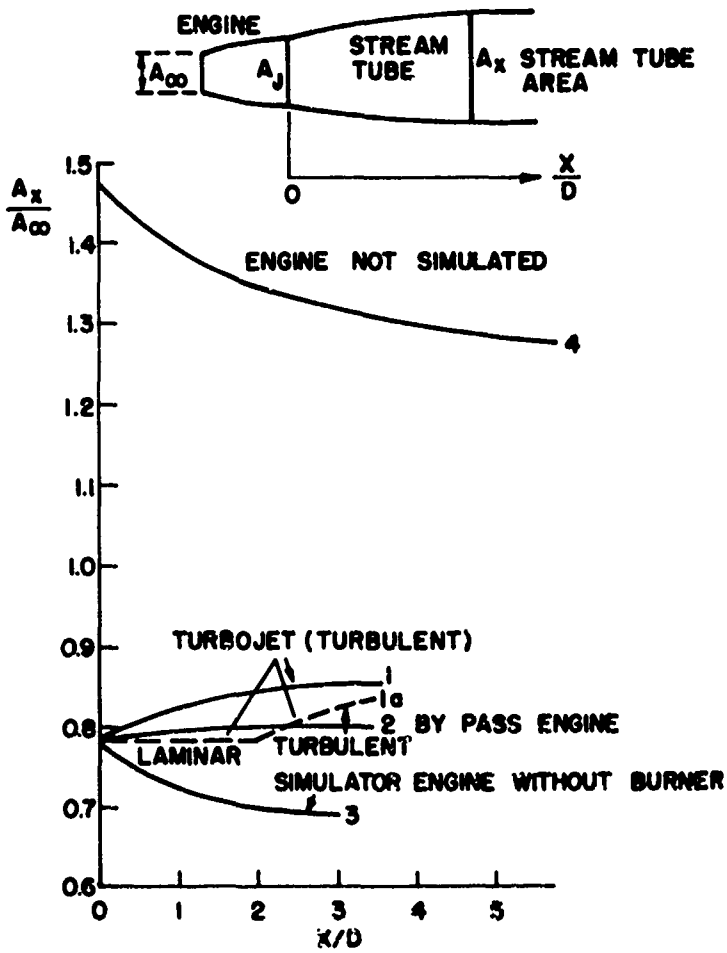

Fig. 2 Variation of streamtube area at M = 0.90, across and downstream of the engine

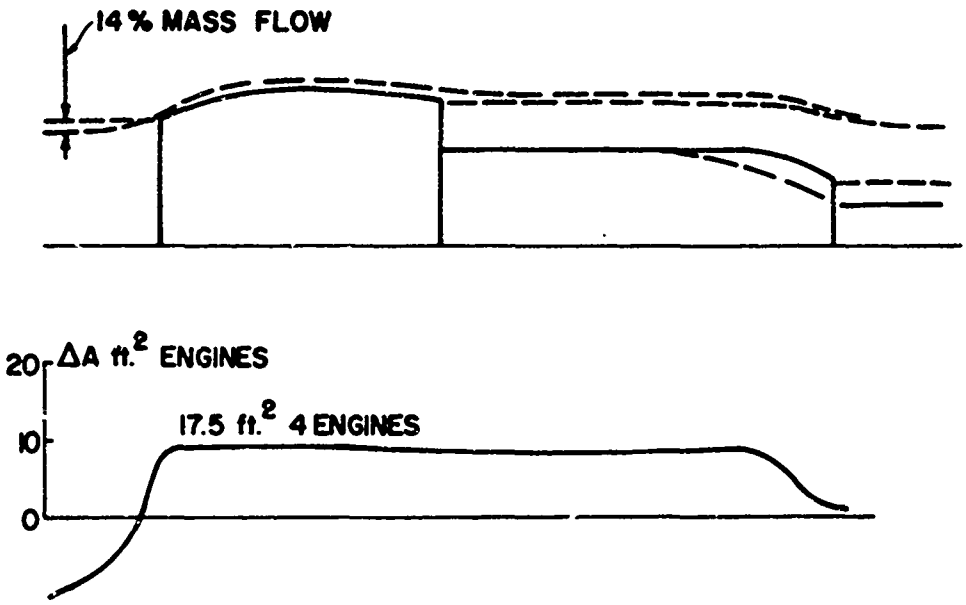

Fig. 3 Difference in streamtube area between engine and engine simulator

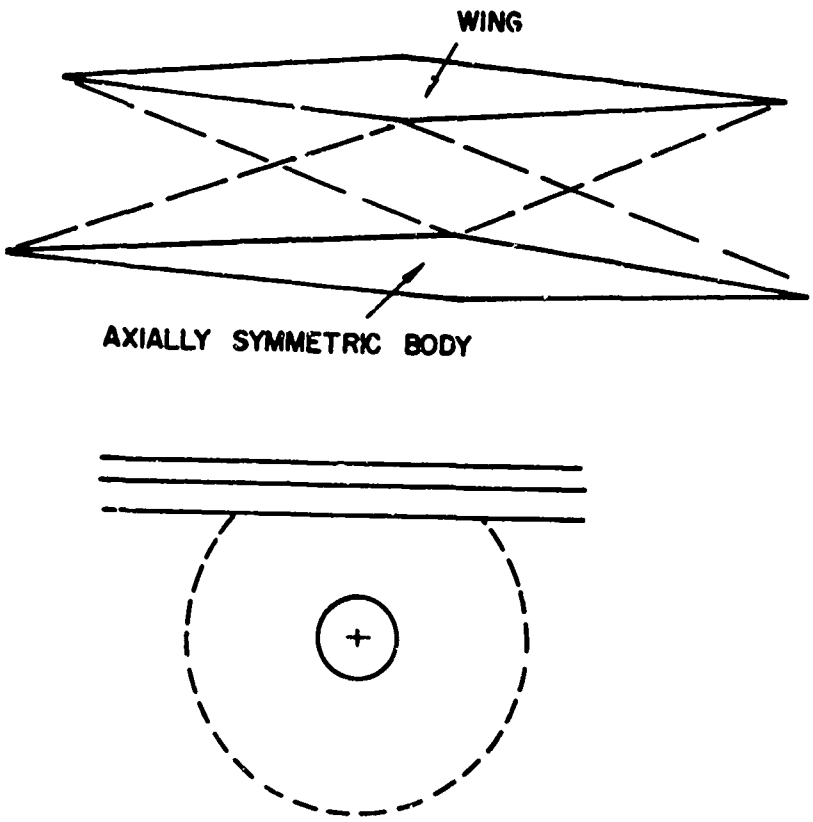

Fig. 4 Schematic indication of beneficial interference

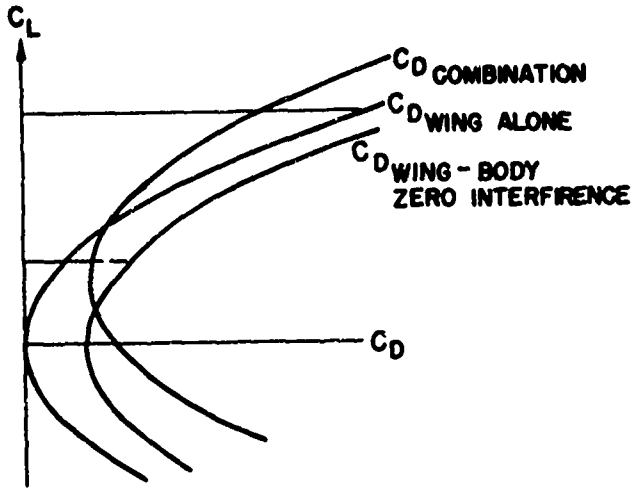

Fig. 5 Variation of polar diagram due to interference

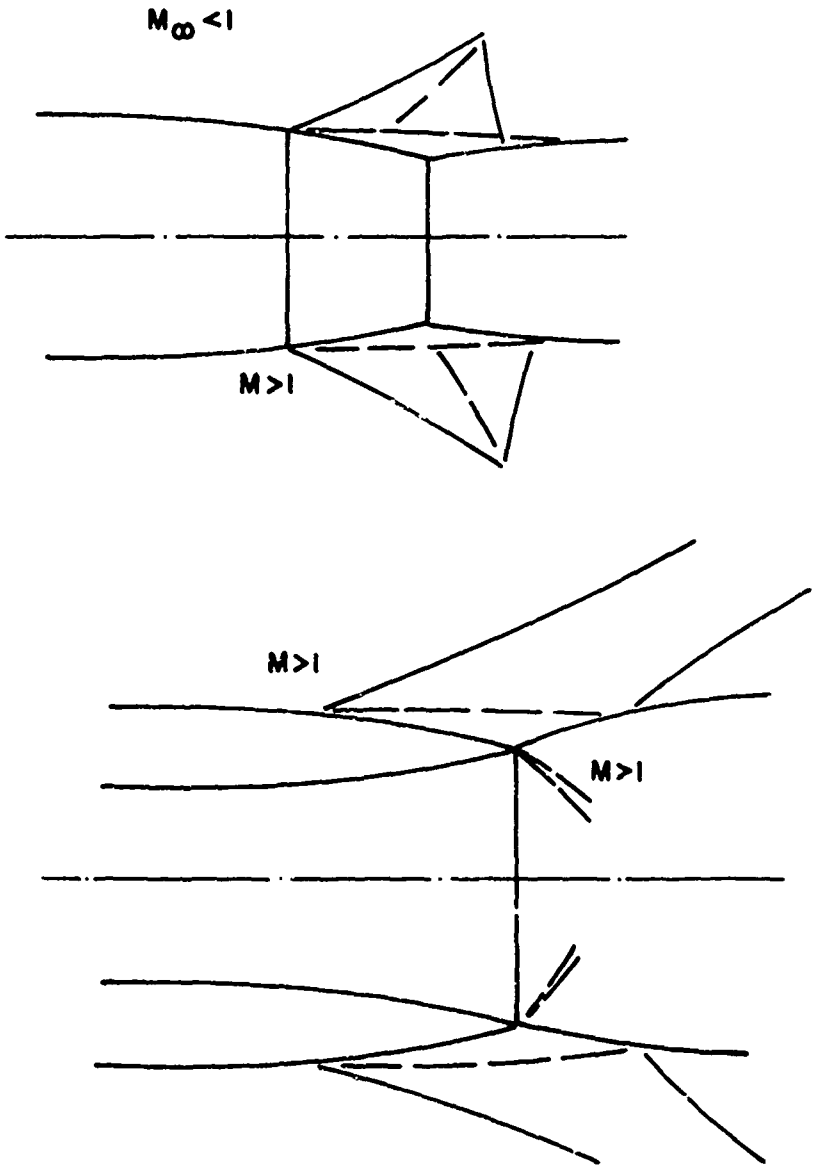

Fig. 6 Decrease of pressure drag due to local separation

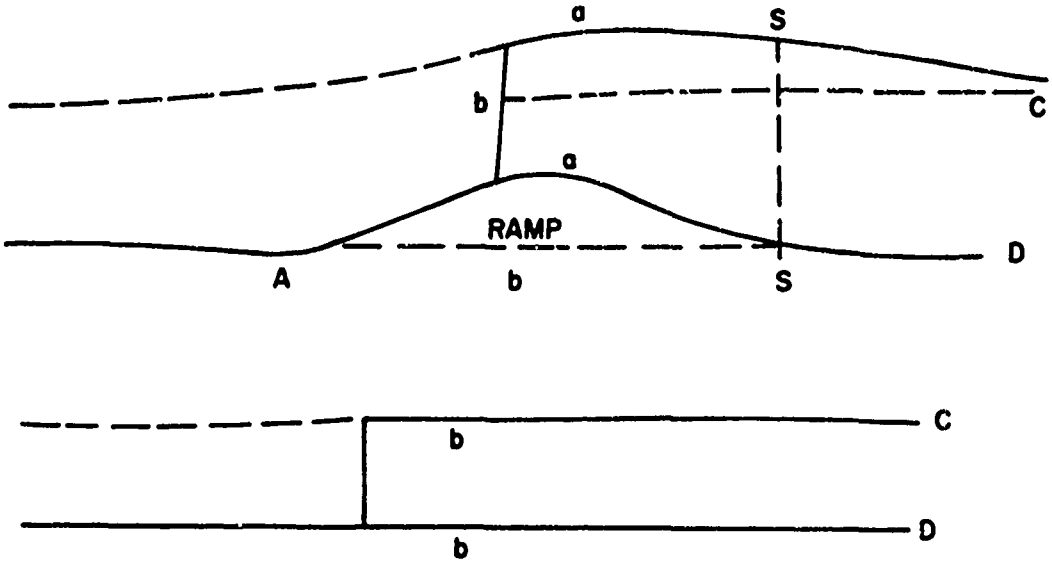

Fig. 7 Apparent pressure drag produced by inlet ramp

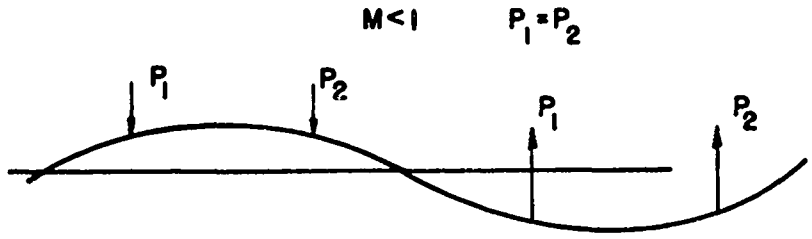

Fig. 8 Pressure on a subsonic "bump"

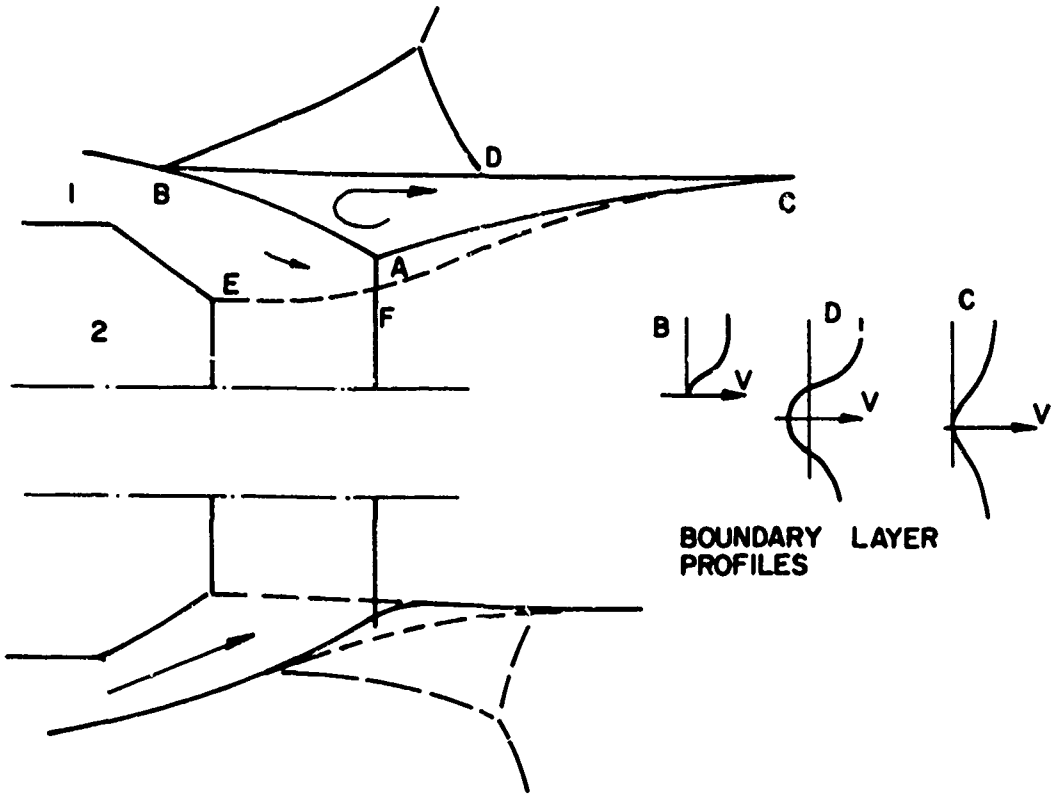

Fig. 9 Interaction between jet exhaust and external flow in a converging nozzle

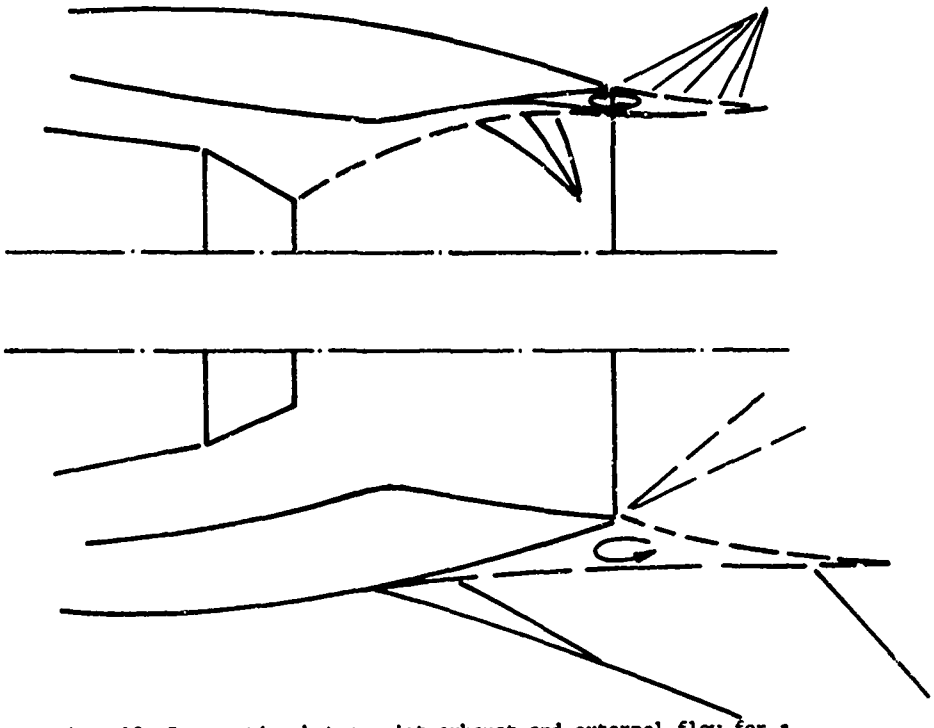

Fig. 10 Interaction between jet exhaust and external flow for a converging diverging nozzle

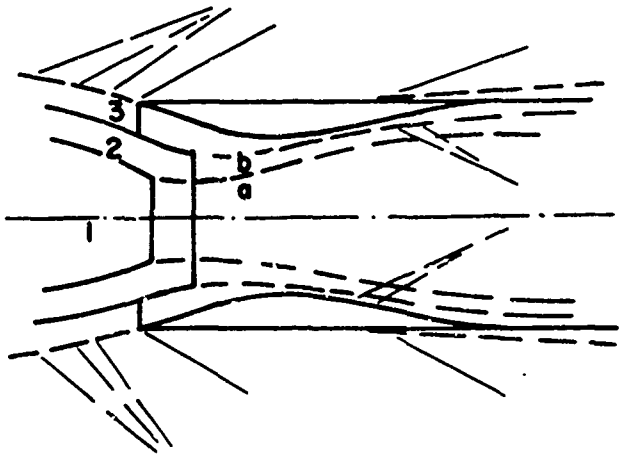

Fig. 11 Nozzle with outside additional flow.

INLET/AIRPLANE INTERFERENCE AND INTEGRATION

by

Philip P. Antonatos
Director, Flight Mechanics Division

Lewis E. Surber
Technical Manager, Internal Aerodynamics Group

Donald J. Stava
Aerospace Engineer

Air Force Flight Dynamics Laboratory
Wright-Patterson Air Force Base, Ohio
USA

SUMMARY

Discussions will be presented on the basic technological problems and potential solutions relating to the development of inlet and airframe design criteria. Results of the analytical and experimental work conducted will be presented emphasizing details of closely coupled inlet airframe concepts. Inlet flow fields generated by basic forebody and forebody/wing combinations will be reviewed together with an analysis of the effects of variations in fuselage shape, forebody camber, wing geometry and inlet position. Problems associated with boundary layer development and vortex ingestion will be discussed in terms of their effect on inlet design. Attitude effects such as angle of attack and angle of yaw will be reviewed. The losses due to spillage, bleed and bypass flows will be analyzed as they affect vehicle performance. Criteria will be reviewed to minimize such loss for the development of optimal inlet/airframe performance. Specific problems relating to the subsonic-transonic flight regime and the supersonic regime will be presented.

LIST OF SYMBOLS

A	Area
AXI	Axisymmetric
A_o/A_c	Capture Area Ratio or Mass Flow Ratio
B.L.	Boundary layer
C_D	Drag coefficient $D/q_o A_c$
C_L	Lift coefficient $L/q_o A_c$
C_R	Thrust Correction Factor
D	Drag, diameter
D_x	Distortion parameter
ECS	Environmental Control System
F	Thrust
h	Wing/cowl spacing
h_t	Throat height
IN	Inches
INBD	Inboard
K_{ADD}	Actual Spillage Drag/Theoretical Additive Drag
L	Lift
M	Mach Number
m	Mass flow
P,p	Pressure
q	Dynamic pressure
SFC	Specific Fuel Consumption
V.G.	Vortex Generators
W	Weight flow
x	Axial distance
y	Lateral distance
α	Angle-of-Attack, incidence
β	Angle-of-Sideslip
Δ	Quantity change
δ	Boundary Layer height
δ_2, θ_R	Variable ramp deflection angles
θ_L	Cowl lip angle
$\angle$	Angle

Subscripts:

o, ∞	Free Stream
2	Compressor face
ADD	Additive
BL,bl	Bleed
BP,BYP	Bypass
c	Capture
D	Drag
DD	Drag Divergence
INT	Interference
i	ideal
L	Local conditions, Lift
Max	Maximum
Min	Minimum
N,n	Net Value
p	Pitot condition
RMS	Root Mean Square
T,t	Total conditions
TH	Throat
u	Unstart condition

1.0 Inlet Influence on Aircraft Performance

The inlet/airplane integration problem, basically, is the requirement for efficient, uniform delivery of air to the aircraft engine at all operating conditions. In the case of turbine engine aircraft operating in the subsonic/supersonic Mach Number range, inlet performance is measured in terms of its effect on both the thermodynamic performance of the engine and the aerodynamic performance of the airframe. Several parameters are involved in the determination of inlet performance, including total pressure recovery, flow distortion and turbulence at the engine compressor face, additive drag, cowl lip suction, boundary layer bleed drag, bypass drag, and boundary layer diverter drag. There is also an effect of variations in inlet mass flow ratio on aircraft lift and drag which must be taken into account. Most of the inlet related losses stem from the fact that turbojet and turbofan engines, in order to power aircraft efficiently throughout a large flight envelope, demand a wide range of mass flow ratios. If the inlet is sized to meet a supersonic high altitude flight engine demand efficiently, there is a great deal of excess airflow at transonic Mach Numbers (Figure 1-1). Some of the inlet airflow may be required for boundary layer control (inlet bleed), environmental control systems, or propulsion system cooling, (Figure 1-2) but all of this excess flow must experience some loss in momentum as it is diverted or processed. It is the job of the inlet designer to reduce these losses and momentum losses of the actual engine airflow to a minimum while maintaining low weight and system complexity.

1.1 Total Pressure Recovery

The engine face average total pressure recovery is of prime interest due to its direct effect on engine thrust. One method for correcting engine thrust for the effect of total pressure recovery specifies:

$$\frac{\Delta F_N}{F_N} = \left[1.0 - {}^{P_{T_2}}/_{P_{T_o}} \right] C_R$$

where: F_N = net thrust

P_{T_2}/P_{T_o} = Total Pressure Recovery

C_R = Correction factor

Typical values of the correction factor, C_R, for turbojet and turbofan engines fall between 1.1 and 1.6 over the Mach Number 0.8 to 2.2 range as shown in Figure 1-3.

1.2 Inlet Flow Distortion

As seen by the compressor face airfoils, inlet flow distortion is actually a velocity distortion, but has typically been expressed in terms of total pressure variations for the sake of simplicity. The most apparent effect of flow distortion on the turbine engine is a downward shift of the engine surge line (see Figure 1-4). This shift is primarily due to the fact that many of the compressor blades are operating closer to stall in the distorted flow. If the distortion is sufficient to alter the blade lift-curve slopes, operating line efficiency will be changed so that the distortion results in a shift along the engine operation line to a lower operating pressure ratio. If surge margin loss due to flow distortion is greater than anticipated, the engine may have to be derated in order to allow sufficient margin for engine transients and other effects shown in Figure 1-5. The primary effect of inlet turbulence, as shown, is to drop the surge line even closer to the operating line, but it can also be expressed as an expansion of the operating line into a band.

1.3 Inlet Drag

Propulsion installation penalties not affecting the actual engine airstream are normally expressed in terms of drag - either as separate increments or as variations to the airframe drag polar. Additive Drag is the momentum loss of the airstream defined by the capture area, A_c, as excess flow is diverted around the inlet (Figure 1-6). Some of this lost momentum may be recovered in Lip Suction as the diverted flow accelerates over the cowl, creating a low pressure region which acts in the thrust direction. Boundary Layer Bleed Drag and Bypass Drag are defined as the combination of (1) momentum lost by these flows from the time they are taken into the inlet till they exit the aircraft and (2) exit door pressure drags. Diverter Drag (occasionally included in inlet drag) is simply the momentum lost in airflow that is turned by the boundary layer diverter measured by the integration of pressures on its surface.

1.4 Installed Performance

These effects all find their way into the equation defining the total forces acting on an airplane in straight and level flight.

$$F_{total} = F_N + \Delta F_{N_{inlet}} + \Delta F_{N_{exhaust}} + D_{aero}$$

where: F_N = Installed engine thrust including effects of inlet recovery and distortion, internal nozzle performance, engine thrust and power extraction.

$\Delta F_{N_{inlet}}$ = All drag increments between the D_{aero} configuration and a model which reproduces the range of inlet mass flow ratios and all other inlet-related flows (bleed and bypass).

$\Delta F_{N_{exhaust}}$ = All drag increments between the D_{aero} configuration and a model which reproduces the real afterbody/nozzle geometry, flow fields, and critical operating parameters.

D_{aero} = Airplane exterior friction and pressure drag plus additive drag of the air entering the inlet.

As mentioned previously, the propulsion system performance effects must be considered together with weight penalties in order to assure the best mission performance. An example of such a trade study is shown in Figure 1-7 where several inlet types were considered for a mixed mission aircraft. Note that the relative importance of the two missions may have a rather large impact on the final choice of inlet design. Also, advantages in supersonic performance gained through a sophisticated inlet design may be negated by the associated increase in aircraft weight. The quest for high component performance cannot be achieved at the expense of total aircraft performance and reliability. Keeping this admonition in mind, it must be realized that consideration of the topics in this lecture is most certainly necessary, but not sufficient to assure optimum mission performance. This discussion will include only the items involved in inlet performance and the assurance of inlet-engine compatibility.

2.0 Forebody Flow Fields

Continuing development of turbine engines for transonic/supersonic flight applications has, among other things, led to tighter control of the surge margin with fewer unknowns allowed in the inlet performance and flow distortion levels. In determining inlet performance, therefore, it is necessary to define (1) how the airframe distorts flow entering the inlet and (2) how the inlet reacts to upstream flow variations. The importance of the first item can be seen from the comparison of performance of a simple fixed geometry two-dimensional inlet design integrated with several different tactical fighter forebody shapes (Figure 2-1). The second requirement (definition of inlet reaction) stems from the fact that different inlet types may react to external flow field distortion in a variety of ways. One method of defining and controlling flow distortion is shown in Figure 2-2. Use of this artificial flow field has been made in a comparison of two-dimensional and axisymmetric external compression inlet data in both uniform flow and identical distorted flow fields (Figure 2-3). This flow field distortion has a greater effect on the axisymmetric inlet and the effect differential increases with Mach Number. Inlet sensitivity to upstream flow distortion is extremely important in the establishment of forebody or forebody/wing flow field uniformity requirements.

A number of programs have been conducted to give some definition of forebody flow fields, but much of the data available is for rather crude designs and has obtained only pitot or total pressure profiles of the flow. Other investigations have been accomplished for specific aircraft designs, but have not been published formally or lack sufficient variety to be of use to a designer. The most recent programs to generate reasonably accurate measurements of important flow field parameters, have been accomplished for highly maneuverable supersonic tactical fighter aircraft. The ensuing discussion of forebody flow fields, therefore, will be concentrated in this area.

2.1 Side-Mounted Inlet Flow Fields

There are a great many variables involved in the study of side mounted inlet flow fields. Amoung these variables are nose shape, fuselage underbody shape, canopy shape, nose droop, fuselage camber, fuselage aspect ratio and inlet position with respect to the canopy. Two test programs in particular are of interest for the purpose of studying the influence of these variables. The first investigation, referred to hereafter as Program "F"*, has been performed in small (1/12) scale using a basic forebody shape consistent with typical fighter designs (Figure 2-4). Provisions have been made in this model for variations in nose shape, fuselage underbody shape and canopy shape. Measurements of the flow field have been accomplished with a rake of three cone probes remotely controlled to map the flow field at a given fuselage axial position (Figure 2-5). The most thorough comparisons in this program have been accomplished for the various fuselage shapes. An example of variations in fuselage effect is shown in Figure 2-6 for a supersonic maneuvering flight condition ($M_o = 2.2$, $\alpha_o = 20^o$). The local angle-of-attack (α_L) contours are quite similar, where $\alpha_L = 22^o$, but closer to the fuselage lower corner the influence of geometry variations show up in the $\alpha_L = 26^o$ contours. As a general rule it appears that more flat-bottomed, square cornered fuselage shapes tend to influence flow further from the fuselage and generate greater flow distortion in the lower

*Program F - "An Investigation of Airframe-Inlet Interaction" conducted by Fairchild Hiller Corporation for the USAF.

inboard corner of the inlet. In the case of local sideslip (β_L) flow, Figure 2-7 indicates little in the way of a consistent trend, but again suggests that the influence of flow shed by the flat-bottomed fuselages at high angle of attack tends to penetrate the inviscid flow away from the body more deeply.

Another program, referred to as "G"**, was performed in larger scale (approximately 1/4 scale) on several forebodies which represented a somewhat different concept in fighter design, having greater body camber, a more prominent canopy and further aft positioning of the inlets (Figure 2-8). A comparison of somewhat similar fuselage shapes between the two programs (F and G) in Figure 2-9 indicates very great differences in the two flow fields. The differences were so great, in fact, that one of the models from program "F" was modified to represent model A-1 from program "G" and re-tested. The result of this follow-on test was gratifying to the extent that the flow field of the modified model was much more like the A-1 model from program "G" (Figure 2-10). On the other hand, these results point out another problem in that there are a great many variables in vehicle forebody design which have a major effect on the composition of inlet flow fields. In program "F" it has been found that the effect of nose shape on inlet flow fields is conditioned by the aircraft canopy shape. The canopy itself has a significant effect on inlet flow fields, but the nature of this effect is dependent upon the relative axial location of the inlet on the fuselage.

A more accurate and detailed comparison of some of the fuselage shape effects can be determined from program "G" on models A-1, A-1-1 (a modification of A-1), and A-2, representing increasing fuselage lower shoulder radii. As an example, Figure 2-11 shows local angle-of-attack (α_L) and angle-of-sideslip (β_L) contours for model A-1-1 at Mo = 2.2 and $\alpha_o = 20^o$. Values of α_L in the lower part of the field are less than α_o due to flow deflection by the forebody nose. As the flow moves upward around the fuselage and the influence of flow expansion over the top of the fuselage is felt, α_L values increase rapidly. Sideslip effects are most prominent in the lower inboard region of the flow field due to the shedding of flow from the high pressure region under the fuselage. The influence of the fuselage shape is shown in Figures 2-12 and 2-13 where selected local flow angularity contours are compared for the three different fuselage shapes. Little effect of the shape changes on α_L is seen in the lower part of the flow field (Figure 2-12), but in the middle inboard region the sharper-cornered model A-1-1 generates significantly higher flow angularity. Shifting attention to the effect of fuselage shape on local sideslip (Figure 2-13), an altogether different sensitivity pattern is observed. In this case, $\beta_L = 0^o$ contours in the upper part of the flow field are least affected whereas major variations are seen in the $\beta_L = 6^o$ contours in the lower part. Here it is noted that the sharp-cornered fuselage at high angle of attack sheds flow laterally, influencing sideslip angularity at rather large distances from the fuselage in the lower portion of the flow field. The more rounded A-1 fuselage does not influence the flow at such large distances, but creates large β_L higher in the flow field. A significant improvement, however, is observed with the A-1 forebody shape. In this case, underbody flow is shed more nearly in an upward direction, creating much less sideslip at the lower inboard corner of the inlet. Additional insight into the flow field effects is provided by Figure 2-14, a comparison of boundary layer development for the three fuselage shapes at this flight condition. The more rounded fuselage shape results in higher energy airflow adjacent to the fuselage. Mach 2.2 flight at $\alpha_o = 20^o$ has been used for the purpose of convenient data comparison and near-maximum flow field effects, but the same general observations can be made for Mach 1.6 flight at $\alpha_o = 20^o$ (Figures 2-15, 2-16) or $\alpha_o = 15^o$ (Figures 2-17, 2-18).

At this point it is worth while to explore the utility of theoretical analysis in the determination of these flow fields. There are, of course, many different types of analysis which could be applied - from very simple hand calculations to highly complex computer programs requiring large amounts of computer running time to obtain a single solution. A relatively simple analysis has been chosen for program "G" which uses the method of characteristics and linear theory to define flow field angularity. Subsonic (Mo = 0.90) and supersonic (Mo = 1.50, 2.50) solutions are compared with applicable data in Figures 2-19, 2-20, 2-21. At the subsonic Mach Number (Figure 2-19), small perturbations to linear theory works reasonably well in both α_L and β_L prediction up to an aircraft angle-of-attack (α_o) of 10°. Application of the small perturbations to a method of characteristics solution at Mo = 1.50, however, does not approximate experimental α_L data well at the same α_o (Figure 2-20) and gives only fair approximation of the β_L contours. For Mach 2.50, neither α_L nor β_L values are estimated well by this technique (Figure 2-21). Other methods of analysis such as a three-dimensional method-of-characteristics solution are being explored to generate more accurate supersonic flow field predictions which are still reasonably simple and economical to apply.

2.2 Shielded Inlet Flow Fields

Inlet shielding may be used to reduce local angles-of-attack at the inlet face during maneuvering flight, but this technique of airframe-inlet integration must still be accomplished very carefully in order to assure inlet-engine compatibility. As an example, Figure 2-22 shows the inlet flow fields for two different fuselage shapes from program "F", both "shielded" by a top-mounted wing. During maneuvering flight, low energy flow moves upward from the high pressure fuselage underbody region, but when it intercepts the adverse pressure gradient imposed by the wing, this

**Program G - "Project Tailor-Mate, An Investigation of Supersonic Inlet Design and Airframe-Inlet Integration" conducted by General Dynamics/Convair for the USAF.

flow separates and has a tendency to travel outward with the wing outwash - directly into the path of the inlet. It can be observed from the data in Figure 2-22 that the more nearly square fuselage cross section results in the most uniform inlet flow field (unlike the case of side-mounted inlets). Apparently, the sharper cornered fuselage, tends to delay the shedding of underbody low energy flow and "channels" the wing-body flow somewhat, reducing the formation of large vortex flow in the inlet region.

The integration problem can be relieved substantially by means of a low-wing installation such as the configurations (models B-3 and B-4) shown in Figure 2-23 from program "G". The basic compatibility advantages of this type of configuration over side-mounted inlet installations is shown in Figure 2-24, where reduced flow field angularity and reduced Mach Number ahead of the inlet can both contribute to improved inlet performance. On the other hand, this type of shielded inlet demands careful design of a very short subsonic diffuser and may also result in increased vehicle structural weight.

Investigation of the wing-shielded inlet position indicates that the ideal design for inlet-engine compatibility would be a completely flat underbody surface. An example of this indication taken from boundary layer rake data on model B-4 is shown in Figure 2-25. The original B-4 model with the rounded lower fuselage profile tends to promote boundary layer separation in the fuselage/wing outwash flow. Refairing of the lower surface to the flatter B-4-1 model profile proved to be a highly satisfactory solution to the separation problem.

Inlet flow fields may also be affected by missile installation. Figure 2-26 illustrates the effect of a semi-submerged missile installation on the B-4 model at Mo = 1.4. In addition to the α_L, β_L gradients shown, there is a reduction in flow field total pressure associated with the missile installation.

As with the side-mounted models, experiment is compared with theory in Figures 2-27, 2-28, and 2-29. The same basic type of analysis has been employed in all cases. At Mo = 0.9 and 1.50, β_L is predicted reasonably well whereas α_L is somewhat inaccurate. The flow field inaccuracies at Mo = 2.50 are considered to be of somewhat more concern due to their magnitude and the increased inlet sensitivity to flow variations at the higher Mach Numbers. The analysis also predicted that the average inlet flow field total pressure recovery at Mo = 2.50 would be approximately 4% lower than the measured value of $\frac{P_{T_L}}{P_{T_o}} = 0.99$.

2.3 Forebody/Wing Design Philosophy

In spite of the many variables associated with forebody/wing design which affect inlet flow fields, some basic design principals can be derived from the information which has been generated. There has been a sufficient amount of data generated to establish approximate flow field conditions for a wide range of basic configurations. Relatively simple flow field analysis techniques may be used with confidence up to Mach Numbers of approximately 1.5 and aircraft angles-of-attack up to 10°. Improved analysis techniques are required for higher supersonic Mach Numbers. There are major integration problems to be solved for any type of airframe/inlet installation, but several variables can be manipulated for any configuration type to improve the inlet flow field.

Side-mounted inlets for supersonic maneuvering aircraft must incorporate effective fuselage boundary layer diverters and be capable of acceptable operation in the free stream at angles-of-attack at least as high as the aircraft experiences and with α_L gradients of 50% to 75% of $\alpha_{o_{MAX}}$. They must also be able to tolerate relatively high β_L conditions associated with maneuvering flight. Inlets designed for shielded positions may be much less tolerant to angles-of-attack, but, depending on the type of installation, may have to provide for considerable boundary layer diversion (top-mounted wing) or accept moderate levels of local sideslip (bottom-mounted wing). The sensitivity and performance of inlets integrated with aircraft designs will be considered in subsequent sections.

3.0 Inlet Performance and Flow Distortion

The general subject of inlet integration with airframes embraces a huge matrix of design possibilities. There have been many inlet and airframe/inlet designs developed and tested over the past several years with only a few ever having actually found their way into prototype or production flight hardware. The designs for which performance data exist include axisymmetric, two-dimensional, and three-dimensional designs employing both external and mixed compression. They include podded and fuselage-integrated installations; side-mounted, wing-shielded, fuselage-shielded, top-mounted and nose installations. They incorporate wide variations in cowl shape, ramp geometry, boundary layer bleed, throat design, diffuser shape (and length), bypass design, side plate shape and fuselage boundary layer diverter design. It would not, of course, be practical to attempt a comprehensive review of all the technical problems and the results of the investigations associated with all of these design variations. As an alternative, selected programs and their results will be used which highlight some of the more difficult problems associated with inlet performance and flow distortion.

3.1 Subsonic/Transonic Inlets

Speaking strictly in terms of total pressure recovery and compressor face flow distortion, the problems associated with subsonic/transonic design aircraft are not felt to warrent much attention in this discussion. Generally speaking, the inlets for these applications are sized for cruise altitude and Mach Number and require no variable geometry, bypass, boundary layer bleed or control complexities in order to provide satisfactory operation. They are usually characterized by generously rounded cowl lips and are either podded or fuselage integrated in such a way that no appreciable amount of low energy air or vortex flows are likely to be ingested. Some designs have incorporated blow-in doors for low-speed, low-altitude flight, but when safety of flight is a prime consideration, the inlet cowl is usually sized sufficiently large to avoid the added complexity of variable geometry, e.g., fixed geometry cowl retrofit on the Boeing 747. If inlets for this class of aircraft were to be placed in the wing or fuselage shadow, careful tests would have to be conducted to assure non-ingestion of vortices or other separated flows during any realistic flight condition. The problems associated with such inlet testing are covered in a separate discussion on experimental investigation techniques.

3.2 Supersonic Inlets - External Compression

External compression inlet performance, in general, is less sensitive to external flow field variations than mixed compression inlet performance. Consequently, supersonic aircraft required to perform acceptably over wide ranges of altitude, maneuver condition and Mach Number typically employ external compression designs in which terminal shock movement can act as a flow control device without endangering stability of the basic inlet flow field. The examination of performance aspects of inlet/airplane interference and integration, then, can best be illustrated using this type of an inlet.

3.2.1 Side-Mounted Inlets

As observed previously (Figure 2-3), the performance of both axisymmetric and two-dimensional inlets is affected to varying degrees by the type and level of external flow field distortion. An idea of the relative suitability of these two design types for side-mounted installations can be observed (for the same two inlets) in a comparison of the isolated supersonic angle-of-attack performance of both in Figure 3-1. The fundamental structure of the two-dimensional inlet flow field remains stable to higher angles-of-attack, resulting in less turbulence and total pressure distortion at the compressor face. This same type of comparison can be made using two installed inlets from the previously mentioned program "G". Performance variations with Mach Number (Figure 3-2) and angle-of-attack (Figure 3-3) again point out the inlet-engine compatibility advantages of the two-dimensional design (A-1) over the axisymmetric design (A-2).

Some of the differences in performance can be traced back to the slightly different forebody flow fields noted in section 2. This forebody effect was checked by testing the two-dimensional A-1 inlet on both the A-1 and A-2 forebodies. Figure 3-4 gives comparisons of the basic inlet performance and Figure 3-5 gives an overall compatibility assessment of each installation. The cross-hatched envelopes in Figure 3-5 encompass all time-averaged distortion index data point values versus the corresponding levels of inlet turbulence of the inlets as indicated. These envelopes are, in turn, compared to the region of assured stability defined in the figure for a typical high performance turbofan engine. It is obvious that the more rounded A-2 fuselage underbody shape would be preferable for the side-mounted inlet installation.

The influence of forebody shape is not sufficient, however, to account for the differences in the inlet-engine compatibility of the two-dimensional and axisymmetric inlets as indicated in Figure 3-6. These α_0, β_0 compatibility envelopes were prepared by checking the distortion and turbulence levels of each α_0, β_0 test point with the screening curve of Figure 3-5. In order to study the performance differences of the two inlet types in greater detail, total pressure surveys measured by rakes positioned in the inlet ducts are presented in Figures 3-7 and 3-8. Mach 2.2 data from the A-1 inlet shows that energy levels in the flow fall off slightly with increasing angle-of-attack, α_0, but the basic flow field maintains its structure. In inlet A-2, however, pressures drop off rapidly with α_0 in the upper part of the inlet where flow separation is experienced. This flow separation is fairly well localized at $\alpha_0 = 5^\circ$. At $\alpha_0 = 15^\circ$ though, the separation spreads rapidly and affects the entire flow at the compressor face. The performance problem for side-mounted axisymmetric inlets in supersonic maneuvering flight is seen as a very fundamental flow interaction. It might be possible to reduce this problem somewhat by employing variable spike geometry biased with airplane angle-of-attack in which high α_0 operation calls for the second cone angle to be increased on the lee (upper) side of the spike and possibly reduced slightly on the lower side.

3.2.2 Wing-Shielded Inlets

Expanding the comparison of inlet types for given installations, Figure 3-9 adds to a previous illustration, showing now the performance of axi-symmetric and two dimensional inlets in wing-shielded flow fields (B-3 and B-4 respectively) as well as side-mounted flow fields. Judging from this figure alone, both wing-shielded inlets would appear to have substantial advantages in performance and

compatibility over the side-mounted inlets for highly maneuverable supersonic aircraft. This view, however, is modified considerably when the effects of sideslip are examined in Figure 3-10 and taken into account. The performance of the wing-shielded 2-D inlet (B-4) drops off sharply with any leeward (negative) angle-of-sideslip. Reference to diagnostic instrumentation in the duct (Figure 3-8 is used as an example), reveals the reason for the β_0 sensitivity. From these pressure measurements in the duct, it is observed that the adverse sideslip flow creates a massive flow separation at the inboard sideplate leading edge which spreads as the flow progresses through the duct, resulting in low average total pressure recovery and high distortion at the compressor face station. On the other hand, negative sideslip flow impinging on the inboard side of the wing-shielded half axisymmetric inlet cowl is deflected by the spike so that the flow is effectively turned and remains attached. Using the distortion versus turbulence limit curve presented earlier, flight maneuver inlet-engine compatibility envelopes have been prepared for each of the inlets discussed (Figure 3-12). From these envelopes and the preceding discussion it would appear that the two-dimensional inlet for side-mounted installations have fundamental advantages to offer the designer of supersonic fighter aircraft.

3.2.3 Influence of Component Design Variations

Although the foregoing considerations suggest what is possibly the easiest line of approach, there are a number of techniques that can be employed to improve the performance of any given inlet design. Several of these will be identified and discussed briefly in succeeding paragraphs.

One important technique for improving the inlet performance of maneuvering aircraft is proper scheduling of flow bypass. In the case of the side-mounted two-dimensional inlet, increases in α_0 force the inlet to spill large amounts of excess flow. The basic mechanism for this increased spillage is forward movement of the normal shock, but this may allow a slipstream from the oblique/normal shock interaction to enter the inlet or precipitate other interaction phenomena unfavorable to efficient inlet operation. Getting rid of some of this excess air by means of throat slot bypass is seen from Figure 3-13 to offer definite advantages in terms of fundamental inlet performance. The bypass schedule used for this research inlet (Program "G") started at very low values at $\alpha_0 = 0^\circ$ for all Mach numbers, but at $\alpha_0 = 20^\circ$, it ranged from 0% of engine mass flow at Mo = 0.9 to 35% at Mo = 1.6 to nearly 70% at Mo = 2.50. A rigorous trade study should take bypass drag into account, but it must be remembered that the condition spoken of here is transient and the bypass is being employed primarily for the sake of inlet-engine compatibility.

Boundary layer bleed may also be employed in the inlet to control shock-wave boundary layer interaction and prevent massive flow separation. Isolated results for such a study of the program "G" side-mounted axisymmetric inlet are shown in Figure 3-14 for perforated bleed ahead of a throat bypass slot. Peak performance was obtained at approximately 2.5% bleed flow over the Mach Number range studied (Mo = 2.0-2.5). The amount of bleed required to obtain such a peak may vary widely depending on bleed location, boundary layer conditions, and terminal shock strength.

Inlet-engine compatibility can be affected quite significantly by subsonic diffuser design. The portion of the inlet downstream of the throat may act as either a flow distortion reducer or amplifier. Assuming that the design is accomplished with reasonable care, the critical compatibility design parameter is usually duct length. Flow separation and turbulence at the inlet throat can be corrected by low diffusion rates and flow mixing downstream of the inlet throat. Using the A-1 inlet from program "G" as an example again, Figure 3-15 illustrates the dramatic improvement in inlet-engine compatibility criteria achieved by a straight-pipe diffuser extension of approximately 40%. Other investigations have shown similar if not as dramatic results. Using duct length to achieve compatibility is expensive in terms of system weight though, and should be employed only when high levels of inlet throat flow distortion can not be avoided.

In the case of shielded inlets where the subsonic diffuser must be quite short, rapid diffusion in the subsonic duct is unavoidable. In such a case vortex generators may be used to energize the boundary layer aft of the terminal shock in an attempt to maintain attached flow in the region of high adverse pressure gradient. An example of the effectiveness of their use is illustrated in Figure 3-16 showing only the effect of adding vortex generators on the wing-shielded half-axisymmetric inlet spike (model B-3) to those already in place on the cowl. The only observable effect in this case is a reduction in inlet turbulence during maneuvering flight, but other applications could conceivably show more significant results.

Cowl lip shape has been used as a variable in a number of inlet designs in order to improve external compression inlet performance in the transonic and low supersonic Mach Number range. An alternate, blunted cowl lip has been employed on the program "G" wing-shielded two-dimensional inlet test (model B-4) in an attempt to make its performance more acceptable in maneuvering flight. As can be seen in Figure 3-17, improvements are measured, but the inboard flow separation still increases rapidly with negative sideslip. The use of increased cowl lip bluntness to achieve improved inlet-engine compatibility has also found its way into operational aircraft, the F-111 being a notable example.

Another inlet design variable which has been used successfully in some cases to improve inlet-engine compatibility is sideplate design of two-dimensional inlets. Variations of this parameter were tested on both the side-mounted and wing-shielded inlets of program "G" without notable impact on any of the performance parameters. It should be noted that sideplate geometry is a rather difficult design feature to optimize during wind tunnel tests due to its dependence on fuselage boundary layer development and flow interaction phenomena which are to some degree affected by the test Reynold's Number.

The discussion of the influence of component design has not been intended to be completely comprehensive either in terms of the number of useful design parameters or their effect on inlet performance. It is considered, however, to give some valid trends and useful design criteria for the effective integration of airframe and propulsion systems on supersonic fighter aircraft.

3.3 Supersonic Inlets - Mixed Compression

When aircraft missions require extended flight at Mach Numbers in the 2.0 to 3.0 + range, external compression inlet applications become much less desirable in spite of their inherent stability and simplicity. At Mo = 3.0, for instance, a typical two-dimensional external compression inlet might have a final compression ramp angle of about 40° with a cowl lip angle of approximately 25° to 30°. The cowl drag which results from this high lip angle can more than offset the pressure recovery potential of the design. On the other hand, a mixed compression inlet can, by means of a series of reflected shocks, accomplish the same efficient flow diffusion while maintaining low cowl drag (see Figure 3-18). A few of the Inlet-Airplane Interference and Integration problems associated particularly with these mixed compression inlets will be discussed in this section.

Both two-dimensional and axisymmetric designs are used for mixed compression inlets. The two-dimensional inlet tends to be somewhat heavy (as with the external compression designs), but is less sensitive to angle-of-attack than an axisymmetric inlet and sometimes easier to integrate with an airframe design. Axisymmetric inlet advantages lie in light weight and relative shortness for a given application, but even with translating and collapsing centerbodies it is extremely difficult for this inlet type to provide the broad range of mass flows demanded by high pressure ratio turbofan engines.

Some of the different mixed compression inlet design types are illustrated in Figure 3-19. The configuration possibilities vary widely, but all share a few fundamental problems when integrated with aircraft designs. In the case of wing-mounted inlets (YF-12, SR-71) the integration problem may be limited to effects of airplane angle-of-attack. For side-mounted inlets (Foxbat), the additional variable of fuselage boundary layer development must be considered. Most applications, however, are wing-shielded (B-70, TU-144, Boeing/NASA SST designs, and B-1 design) and must be properly integrated with the wing flow field to overcome potential problems of inlet-inlet interference, wing boundary layer-inlet shock interaction, flow field distortions, and/or transient flow disturbances.

In order to produce high thermodynamic performance, a mixed compression inlet must approximate critical operation (terminal shock just aft of the throat) requiring precise, rapid response control of throat flow conditions. The research and development effort to this end has investigated several aspects of airframe-inlet design. An example of an inlet (axisymmetric Mach 2.5 design) used in this manner is shown in Figure 3-20.

NASA investigations have explored the sensitivity of this axisymmetric inlet to angle of attack variations and upstream flow distortion. As angle of attack is increased, an over compression develops on the inlet leeward side and a localized region of subsonic flow develops just prior to inlet unstart. Substantial improvements have been achieved simply by redistribution of spike and cowl bleed further upstream in the inlet (Figure 3-21). Small upstream flow distortions (on the order of $\Delta M_L = 0.10$) do not affect performance or flow distortion significantly. Study of the use of vortex generators in this inlet type indicate that their use ahead of an unbled shock-boundary layer interaction could provide flow improvements, but not as much as a good bleed system.

Another investigation of this inlet has coupled it with a turbojet engine mounted under a simulated wing to study interaction phenomena. Unstarts from engine stalls create transient disturbances up to 2.4 to 2.8 inlet face diameters ahead of the inlet with the lateral extent of this disturbance requiring adjacent inlet spacing of more than 4 diameters to avoid mutual interference. Wing over-pressures in the vicinity of the cowl lip have reached transient values of 10 times the wing flow field static pressure. The extent of interaction can be reduced either by increasing diverter height or decreasing boundary layer height (Figure 3-22). When the inlet is started (terminal shock swallowed) performance is not affected by proximity of the inlet to the wing unless cowl lip actually intercepts the wing boundary layer.

Other NASA programs have been conducted to explore two-dimensional inlet design. Figure 3-23 shows a typical design of a Mach 3.0 design inlet which employs variable compression ramps, a translating cowl, ramp and sideplate bleed, and throat vortex generator variations. Contrary to the axisymmetric inlet tests, it has been found in testing this inlet over $1.55 \leqslant Mo \leqslant 3.2$ that the vortex generators are effective in reducing distortion. Optimum boundary layer interaction control and inlet performance is achieved by means of a combination of distributed bleed, vortex generators, and diffuser shape (Figure 3-24). The performance of this inlet is more sensitive to angle-of-attack than angle-of-sideslip, but flow distortion is not affected by small values of either parameter (Figure 3-

4.0 Inlet Drag

As shown earlier, (Figure 1-7) inlet drag is critical in the determination of aircraft performance. However, its relative importance will be dependent on the mission requirements. Certainly achieving minimum drag in a long range, single point design aircraft (SST, 747, etc) is much more important than in a short range highly maneuverable fighter. In the latter system, engine stability and compatibility may be critical allowing some penalties in inlet drag to achieve this end. Designs which achieve minimum inlet drag do not necessarily achieve minimum aircraft drag or maximum installed engine thrust. Similarly, some designs that tend to reduce drag may impose cost, weight, complexity, reliability, or maintainability problems which, when considered over the operational lifetime of the aircraft system, may negate the benefit of a slight drag reduction. Also, advances in inlet and engine technology, such as variable capture inlets and the variable area turbine, will offer the potential for still further trade considerations. Commercial and military applications may also dictate still other drag and/or performance considerations.

4.1 Inlet Drag Bookkeeping

Although the problems associated with measurement of inlet drag and the assessment of thrust-drag bookkeeping is the subject of subsequent lectures it is useful at this time to include a few statements on these subjects to set the stage for the following discussion of inlet drag.

It has become the practice of many contractor and government agencies, to assess as inlet drag, all drag associated with the captured streamtube and its variations with engine demand and/or aircraft operating conditions. Several bookkeeping procedures are currently being used to account for these inlet drag terms, the engine thrust, and the aircraft drag to arrive at the installed aircraft performance. While the variety of procedures can cause some difficulties in the evaluation or comparison of contractor's performance estimates, the division of thrust and drag forces is immaterial in the final performance calculation (provided that all forces are accounted for once and only once).

Analytically, this buildup is somewhat easier to accomplish satisfactorily. Most problems arise when experimental determination and validation of performance is sought. Typically, two models are employed, one aerodynamic model being used to obtain the aircraft aerodynamic and stability characteristics and one propulsion model used to obtain the inlet performance and drag characteristics. Additional models are employed to obtain the exhaust nozzle drag characteristics. Generally the aerodynamic model is run with a flow-through inlet at some reference mass flow, and the inlet drag at this condition is included in the aircraft drag polar. The inlet drag variations with inlet mass flow ratio are then obtained from a propulsion drag model and applied as incremental drags to obtain performance at points other than the reference mass flow conditions.

In experimental measurements, various reference mass flow conditions have been used, but it would appear that a mass flow near critical or choked conditions should be employed such that it can be tested on both the aerodynamic and propulsion models. A reference mass flow ratio of 1.0 generally requires an additional model variation and data extrapolation that gives rise to possible errors.

Further problems arise when experimental verification of inlet drag predictions are sought. Seldom is a model built in such a way that the individual inlet component drags can be identified as readily as can be done analytically. For instance, inclusion of a sidewall bleed system may require the external geometry to be modified to provide a bleed passage. Thus, the drag measurement may be in error because the proper flow conditions have not been duplicated. If the proper cowl contours are used, however, it may not be possible to include the inlet bleed, and again the measured drag will not be correct. Conversely, in the analytical build-up, not only are the proper internal and external geometries duplicated at all times, but also the internal and external flow fields. Analytical techniques also lend themselves to easy identification and isolation of the various drag components.

4.2 Inlet Drag - Definition

Earlier, Sections 1.3 and 1.4 alluded to some of the principle inlet drag components considered during inlet design and installed propulsion system performance determination. Employing the thrust-drag accounting system mentioned previously (in which the inlet drag at the reference mass flow condition is included in the aircraft polar) the inlet drag, D_I, may be expressed as the incremental change due to mass flow variations. Thus:

$$D_I = \Delta D_{ADD} + \Delta D_{COWL} + D_{BL} + D_{BYP} + \Delta D_{INT}$$

where ΔD_{ADD} = incremental change in additive drag (pre-entry drag)
ΔD_{COWL} = incremental change in cowl pressure drag (lip suction)
D_{BL} = bleed system drag
D_{BYP} = bypass system drag
ΔD_{INT} = interference drag = incremental change in aircraft drag due to inlet operation and change in inlet drag to aircraft installation effects

Using this scheme, inlet diverter drag as well as inlet friction and pressure drags at the reference flow conditions are charged against the aircraft polar. Also chargeable to the basic aircraft drag would be the drag associated with any inlet flows required for ECS, engine bay cooling or purge air, leakage, or other similar required flows which are invarient with engine throttle demand.

4.3 External Compression Inlets

4.3.1 Spillage Drag

Generally, the additive drag and lip suction components are combined into a common spillage drag term. The importance of D_{ADD} has been discussed many times. In an aircraft requiring transonic flight at sea level, the theoretical additive drag could cause a 40% degradation in aircraft range. For an aircraft designed for a $M_o = 3$ cruise, the additive drag could amount to 20% of the airplane drag at a subsonic cruise condition. Fortunately in practice this entire penalty is seldom experienced. Proper contouring of the external cowl shape can result in appreciable lip suction effects due to increased velocities and decreasing pressures on the forward portions of the cowl lip. The magnitude of the lip suction effects may result in the cancellation at subsonic and transonic speeds of up to 80% of this drag for subsonic inlets and up to 50% for supersonic inlets. This is indicated in Figure 4-1 using the K_{ADD} factor, which is the ratio of actual spillage drag to theoretical additive drag. Of course in the selection of any inlet the absolute drag level must be determined for use in performance estimates.

Many test results have shown that appreciable flow spillage can be accomodated with little drag penalty when the inlet throat Mach Number is kept high. This can be accomplished by means of increasing the compression surface angles to reduce throat area. Presented in Figure 4-2 is some typical data obtained from a two dimensional variable ramp inlet. As can be seen, increasing the ramp angle can result in an appreciable reduction in inlet drag at a constant engine demand. However, the reduction in throat area results in increases in both steady state and time varient diffuser exit flow distortion as well as a decrease in total pressure recovery due to the higher throat Mach numbers. Assuming that the distortion generated is within engine tolerances, inlet operation at the highest ramp angle and lowest drag would be desired. However, for the data presented here, operation at the high ramp angle incurs a 3% loss in recovery and a 50% reduction in inlet drag. Employing the sensitivity factors shown in the Figure for a typical flight condition, it is readily apparent that the loss in recovery results in a much larger increase in SFC than the benefits reduced drag level can offset. At a typical high altitude cruise condition operation at a second ramp angle of $\delta_2 = 15^o$ would result in a 4% loss in SFC, while at sea level this would be decreased to approximately 1% SFC loss. Operation at some intermediate condition however, such as $\delta_2 = 5^o$ would be of benefit because there is a substantial drag reduction with essentially no loss in recovery.

4.3.2 Bypass Drag

When one considers the drag of the bypass system, a drag tradeoff occurs between the spillage and bypass drag such that the minimum inlet drag may occur at an airflow condition less than that for minimum spillage drag. A typical trade study is shown in Figure 4-3 where the increments of spillage and bypass drags are shown along with the airflow associated with minimum drag for constant engine demand. Again, this is an ideal situation and does not consider the interference of the bypass air on aircraft drag and stability characteristics. In operational use, the bypass air must be dumped and this usually occurs in an unfavorable location such as above the wing. Data shown in Figure 4-4 indicate some of the impact of the bypass system operation on the yawing and rolling characteristics of the B-70.

Depending upon the amount of excess inlet air, it may be possible to either bypass the air around the engine and use it in the exhaust nozzle or base region to improve nozzle performance or it may be dumped overboard through various doors, slots or nozzles. Figure 4-5 shows typical drag increments experienced during an acceleration depending upon the air being dumped overboard or used to augment the exhaust nozzle flow. For this case the benefits of the ejector nozzle are quite evident. Figure 4-6 shows some typical drag characteristics for various means of discharging the bypass flow. It is clear that proper design of the bypass exits can significantly reduce this drag penalty. Of course, proper accounting of added weight penalties and aircraft drag increments due to the bypass system must be included in the total system analysis.

4.3.3 Effect of Inlet Shape

The inlet geometry essentially governs the inlet drag characteristics and, as shown in Figure 4-1, the cowl lip can significantly influence the inlet drag characteristics. Figure 4-7 indicates the level of aircraft drag sensitivity to slight modifications of the external cowl lip geometry. However, the external cowl lip geometry (as well as the internal cowl lip geometry) that results in the minimum drag is dependent on the local flow angularity approaching the lip. This flow angularity is, of course, highly dependent upon both the compression surface geometry and flight condition. Figure 4-8 presents some of the drag characteristics of a two dimensional variable

ramp inlet and it is evident that the ramp geometry effects are significant. Increasing the ramp angle, however, may require an increase in the turning angle required by the cowl lip to satisfy aircraft design requirements. Illustrated in Figure 4-9 are typical inlet drag characteristics for varying internal lip angularity. Thus, the drag reduction possible with increased ramp angle can be offset by the increased cowl drag resulting from flow turning requirements.

Several investigations have shown that axisymmetric conical inlets have less drag than two-dimensional ramp inlets with equal throat/capture area ratios and equivalent ramp or cone angles. Typical data are shown in Figure 4-10. This characteristic can be explained by the relief provided by the three dimensional spillage of the cone resulting in lower flow spillage angles, i. e. the flow deflection is less than the two dimensional configurations, resulting in lower drag.

Inlet sideplate geometry also can have a significant effect on the inlet drag characteristics. Studies of various sideplate configurations have been conducted and certain characteristics have been obtained. K_{ADD} factors for various sideplate configurations in Figure 4-11 showed very significant benefits of cut back sideplates in the transonic regime. The mechanism for drag reduction here is a combination of sideplate suction effects and the three dimensionality of the side spillage which reduces the spillage flow angularity and, hence, drag.

4.3.4 Effects of Inlet Installation

The effect of inlet spillage and bypass on total aircraft drag and even on exhaust nozzle performance should not be overlooked because they can impose an appreciable drag increment. These effects generally are not accounted for since sophisticated models and analyses are required to accurately assess their contribution and impact on aircraft performance.

As mentioned earlier, the effects of the aircraft forebody on inlet drag should be considered. Inlet drag characteristics have been investigated experimentally for isolated inlets, forebody integrated inlets, and for inlets in simulated forebody flow fields. It can be seen in Figure 4-12, that while the absolute level of drag varies with the degree of forebody flow simulation, the slope of the drag curves remains constant. Therefore it appears possible that an evaluation of inlet drag characteristics may be made with isolated models.

Typical data presented in Figure 4-13 shows that there is a slight effect on the forebody lift and drag characteristics which varies with inlet mass flow ratio. This effect, however, would be highly configuration oriented and depend on inlet type and location.

The importance of inlet bleed in improving the recovery characteristics of supersonic inlets was discussed earlier. The bleed flow also imparts a drag penalty which must be accounted for to determine the optimum thrust minus drag. Bleed flow may be removed by either porous surfaces, flush slots, or ram scoops. Not only do these bleed systems affect the inlet recovery, and results in a drag increment, but they can affect the range of stable subcritical operation of the inlet. The increase in recovery achieved through the use of bleed may more than offset the drag penalty associated with the bleed flow. Data shown in Figure 4-14 shows some test results from an F-104 type inlet configuration. For this configuration the flush slot bleed resulted in the best overall performance over the supersonic range. As with bypass, the bleed air could also be ducted to the nozzle to increase thrust or dumped in a base region to reduce base drag if the base pressures are low enough.

In Section 3, the effects of the local flow field on inlet performance and distortion was discussed and showed some significant areas of impact. The local flow field similarly can influence the inlet drag characteristics. This is illustrated in Figure 4-15 where the drag characteristics of a two dimensional inlet in a horizontal and vertical orientation are presented. At nominal cruise angles of attack, there are slight differences in drag due to the local flow differences.

The effects of inlet design and orientation are further illustrated in Figure 4-16 for the four airplane designs of program "G". Using these inlet drag characteristics in vehicle performance estimates, the A-2 aircraft configuration showed the greatest range capability; 37% greater than B-4, 24% greater than B-3 and 15% greater than A-1. However, overall consideration of range and maneuverability (Figure 3-9) for the various missions considered led to the selection of A-1 as the "best compromise" airplane design.

4.4 Subsonic Inlets

For those aircraft installations featuring subsonic pod type nacelles, the problems of inlet drag are not any less serious. As cruise speeds have approached closer to sonic conditions, the problems of inlet drag and inlet-airplane interference drags have gained in significance. However, due to the emphasis on cruise conditions, the entire nacelle/cowl can be made optimum for a given flight condition and engine airflow requirement. The subsonic nacelle experiences mainly skin

friction drag and small amounts of inlet spillage and boattail drag. There are also drag contributions due to interference of the nacelle, wing, and/or fuselage. Nacelle designs featuring a long duct shrouding both fan and core flow and exiting through a common nozzle will give results that are different from a short duct featuring separate nozzle for both fan and core flow. For these systems trades of drag and weight must be performed to select the proper cowl design.

The isolation of the interference effects due to inlet spillage and nacelle shape are difficult to isolate due to the effects of the engine exhaust on the nacelle/wing flow field, which becomes more predominant as engine bypass ratios are increased. Several earlier studies presented some analytical results of the effects of nacelle placement on aircraft lift and drag. The predominance of this data is for the lower transonic speed regime. As the cruise flight conditions approach Mach 1.0, the drag divergence Mach number (M_{DD}) of the cowl becomes important as does its sensitivity to inlet mass flow ratio. Some recent studies have shown that the cowl can be designed so that the M_{DD} is insensitive to inlet airflow requirements. This is shown in the data of Figure 4-17 for two typical long duct cowls, one designed for operation at near $M_0 = 1$, the other a typical $M_0 = 0.8$ design.

4.5 Mixed Compression Inlets

As with subsonic inlets, the mixed compression inlet is usually designed for a given cruise condition. An optimum balance of inlet drag and performance can be achieved for this design point. Inlet drag, however, can rise drastically when the aircraft is required to operate at some other flight condition. At the supersonic design point, inlet spillage drag can be kept to a minimum and inlet bypass drag can also be minimized by proper inlet/engine matching. During transient conditions, e.g. aircraft maneuver or engine mismatch, some bypass drag may be encountered, but the short duration of such adverse conditions usually makes their impact on aircraft range negligible. Inlet bleed drag on the other hand, may become significant, since mixed compression inlets susally require appreciable design point bleed flow rates to maintain high efficiency levels and internal flow stability. Thus, it becomes very important for this class of inlets to obtain a design with a minimum of inlet bleed flow requirements and then maximize the bleed exhaust system performance to recover as much of the bleed flow momentum as possible. Figure 4-18 shows some of the drag characteristisc of various types of bleed exit systems.

The mixed compression inlet is generally selected for operation at cruise speeds above Mach 2.5; but if the mission requires an extensive transonic flight condition, extensive drag penalties can occur. The possible extent of this penalty is illustrated in Figure 4-1. Referring back to Figure 1-7 and comparing configurations 1 and 4, it can be seen that for a typical subsonic mission, the mixed compression inlet incurs approximately a 30% decrease in range, 21% of which is just due to the increased spillage drag of the inlet with the remainder due to the weight. The increased spillage drag of the mixed compression inlet results from a sharp cowl lip and reduced lip suction effects. On the supersonic mission however, the external compression inlet suffers only a net 7% decrease in range. For this case the range loss due to the increased drag and lower recovery of the external compression inlet is cut in half as a result of the weight savings of the external inlet system. This again points out that drag should not be considered as an independent variable.

5.0 Conclusions

Forebody/wing design plays an important role in inlet performance and inlet-engine compatibility. Side mounted designs are quite sensitive to forebody camber and fuselage underbody shape. Shielded designs are most sensitive to wing placement. A low-wing, flat-bottomed vehicle design appears to provide the fewest shielded-inlet design complications.

Current theoretical analysis techniques for estimating forebody and forebody/wing flow fields are severely limited for application to supersonic flight maneuvers. Future design development could benefit considerably by screening potential designs with an economical but relatively accurate analysis procedure.

Supersonic external compression inlet design for highly maneuverable aircraft is heavily dependent upon vehicle design. Inlet-engine compatibility considerations clearly favor two-dimensional inlets for side-mounted installations, but axisymmetric inlets have proved best for the wing-shielded design. Increased subsonic diffuser length appears to be the simplest technique for improving compatibility characteristics, but careful system development should explore flow bypass scheduling, boundary layer bleed, duct vortex generators, cowl lip shape, and/or inlet sideplate design as potential solutions with less weight penalty.

Supersonic mixed compression inlet designs are normally incorporated on higher design point Mach Number aircraft with little requirement for high speed maneuverability. High total pressure recovery requirements demand near-critical operation. Many of the previously mentioned inlet design variations may be employed to improve performance, but careful design and tuning of the boundary layer bleed system appears to be one of the most important. Shielded designs must include consideration of transient flow conditions which could cause intolerable inlet/inlet interference or inlet/wing interference.

The assessment of inlet drag characteristics is critical to the determination of aircraft performance. However, the evaluation of the propulsion system drag must not be evaluated independently of the aircraft drag characteristics or the weight and other influencing factors. The critical factor that remains is the assessment of total aircraft thrust minus drag and care must be taken both analytically and experimentally to assure that all appropriate components are accounted for.

References

1. Inlets and Nozzles for Aerospace Engines, AGARD Propulsion and Energetics Panel 38th Meeting, Sandefjord, Norway, 13-17 Sep 1971; AGARD-CP-91-71.

2. Aerodynamics of Power Plant Installation, AGARD Fluid Dynamics Panel, Tennessee, U.S.A., AGARDograph 103, Parts 1 and 2, October 1965.

3. Choby, D. A.; "Tolerance of Mach 2.50 Axisymmetric Mixed-Compression Inlets to Upstream Flow Variations", Lewis Research Center, NASA TM X-2433, January 1972.

4. Mitchell, G. A., and Johnson, D. F.; "Experimental Investigation of the Interaction of a Nacelle-Mounted Supersonic Propulsion System with a Wing Boundary Layer", Lewis Research Center; NASA TM X-2184, March 1971.

5. Mitchell, Glenn A.; "Experimental Investigation of the Performance of Vortex Generators Mounted in the Supersonic Portion of a Mixed-Compression Inlet", Lewis Research Center; NASA TM X-2405, November 1971.

6. Wong, D. and Anderson, W. E.; "Experimental Investigation of a Large-Scale, Two-Dimensional, Mixed Compression Inlet System - Performance at Supersonic Conditions, M_0 = 1.55 to 3.2", Ames Research Center; NASA TND-6392, June 1971.

7. Jane's All the World's Aircraft, 1971

8. Internal Aerodynamics Lecture Course, Presentation at Wright-Patterson AFB, Ohio by North American Rockwell Corp., 1968.

9. "Investigation of Airframe-Inlet Interaction" - Data Report, Fairchild Hiller/Republic Aviation Division, 1970-71.

10. "Project Tailor-Mate" - Data Reports, General Dynamics/Convair Aerospace Division, 1970-71.

11. "Supersonic Inlet Investigation" - Data Report, Northrop Corporation, 1971.

12. Mount, Joseph; Journal of Aircraft, Vol. 2, No. 5, "Effect of Inlet Additive Drag on Aircraft Performance", Sep-Oct 1965.

13. Muller, George, and Gasko, William; Journal of Aircraft, Vol. 4, No. 3, "Subsonic-Transonic Drag of Supersonic Inlets", May-June 1967.

14. Dobson, M. D., and Goldsmith, E.; "The External Drag at Subsonic and Supersonic Speeds of Fuselage-Side Air Intakes for Strike-Fighter Aircraft", RAE TM Aero 1259.

15. Richey, G. K., Stava, D. J., Brimelow, B., Bush, H. I.; "Airframe-Propulsion Integration for Future Aircraft Systems", SAE Paper 680288, April 1968.

16. Rall, F. T.; "Aircraft and Propulsion Operational Considerations Related to Inlet Design", AGARD CP 27, Sep 1967.

17. McVey, F. D., Phillips, E. J., and Rejeske, J. V.; Proceeding of the Air Force Airframe-Propulsion Compatibility Symposium, "Experimental Investigation of Transonic Inlet Drag", AFAPL TR 69-107, June 1969.

18. McVey, F. D., Rejeske, J. V., and Phillips, E. J.; "Experimental Evaluation of Inlet Drag Characteristics in the Transonic Mach Number Regime", AFAPL TR 68-119, Nov 1968.

19. "Propulsion System Integration and Test Program", NA 68-939, Part IV

20. Stitt, T. E., McKevett, F. X., and Smith, A. B.; "Effect of Throat Bleed on the Supersonic Performance of a Half-Conical Side-Inlet System", NACARM E55J07, Jan 1956.

Acknowledgement

Source material for this paper has included data from several programs which have not yet resulted in final documents suitable for referencing. Consequently, the authors gratefully acknowledge the work of personnel from General Dynamics, Fairchild Hiller, and Northrop whose efforts on USAF contracts have contributed heavily to this paper.

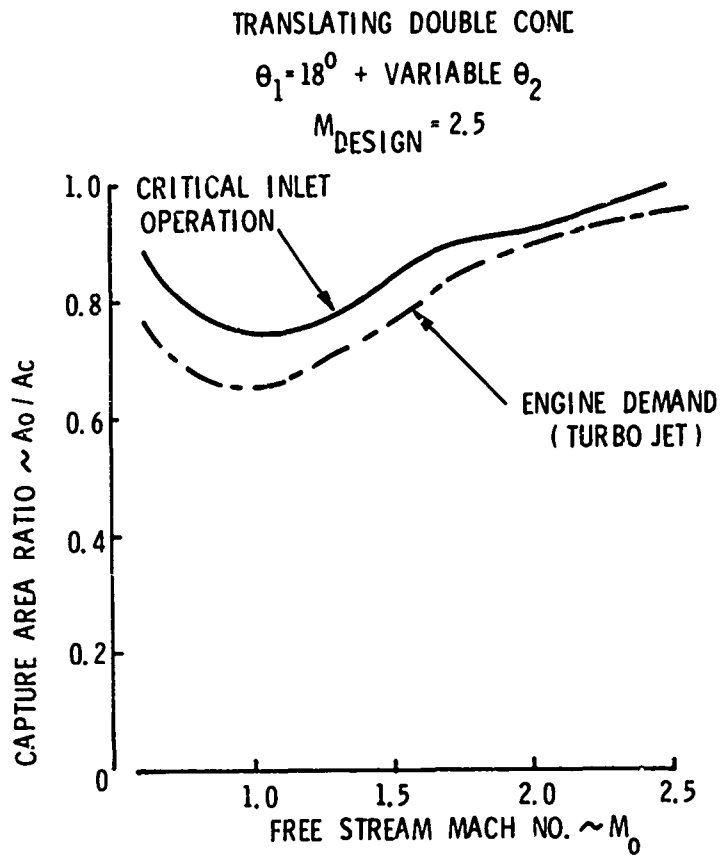

INLET-ENGINE MATCH

Figure 1–1

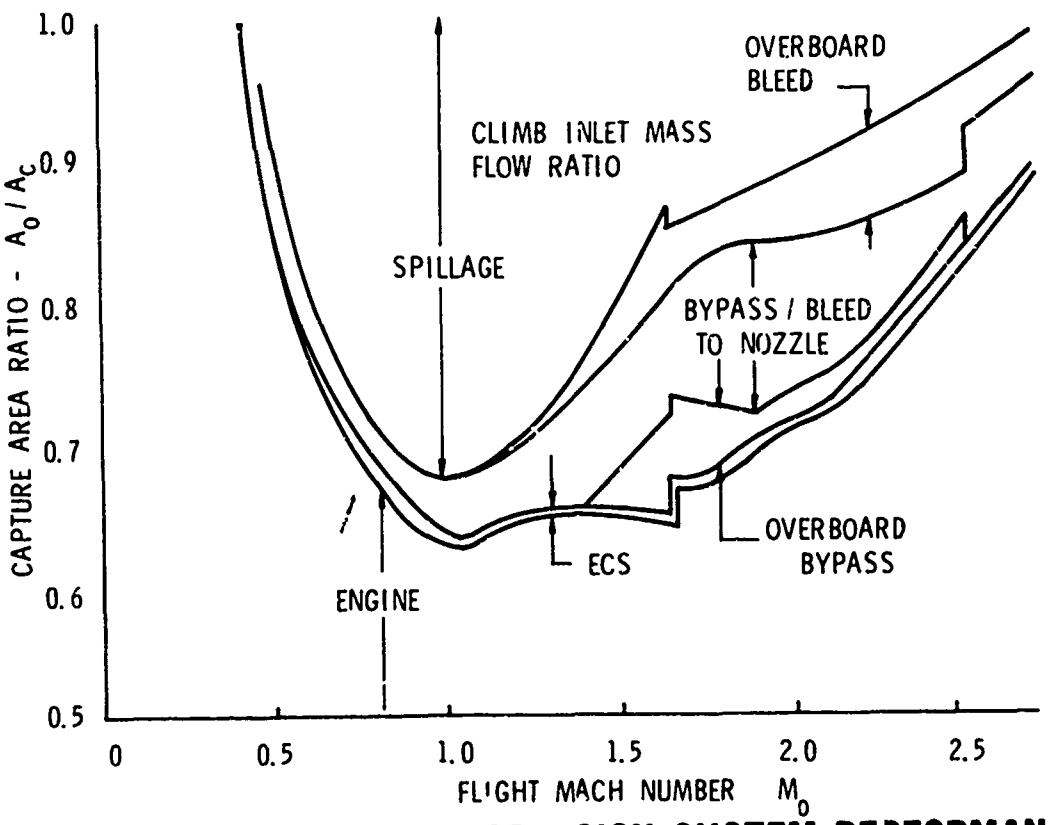

TYPICAL INSTALLED PROPULSION SYSTEM PERFORMANCE

Figure 1–2

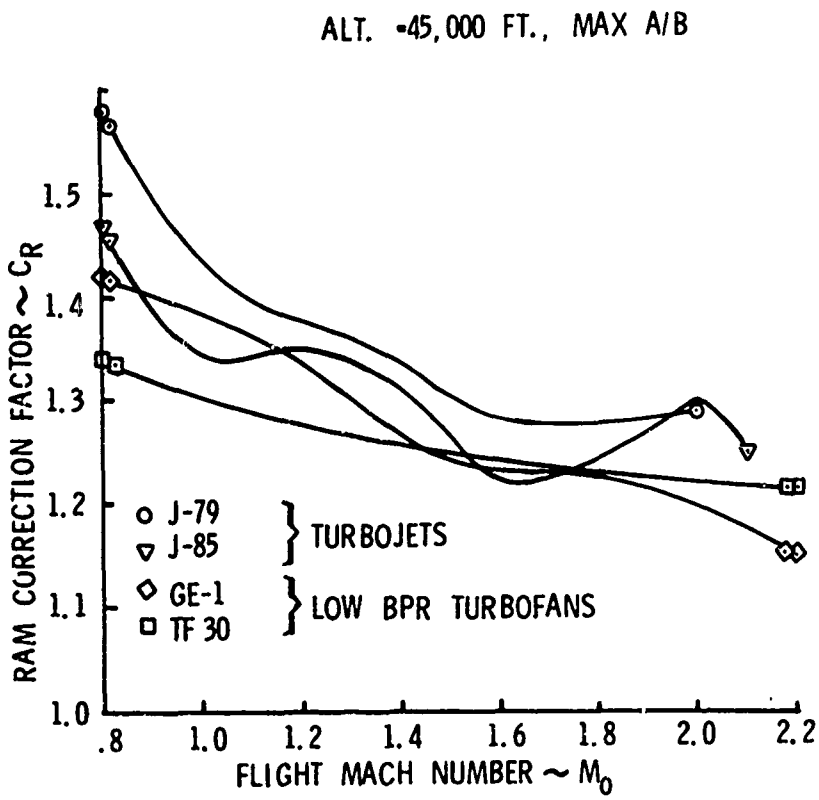

RAM CORRECTION FACTOR FOR NET THRUST

Figure 1–3

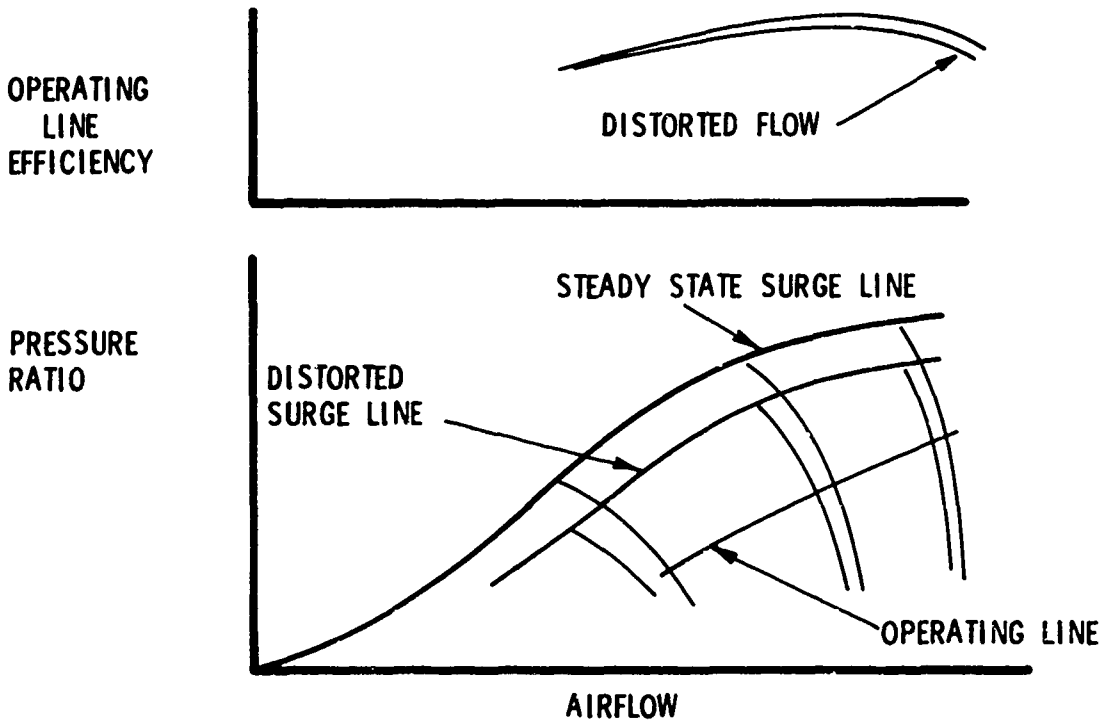

COMPRESSOR SURGE LINE CHANGE DUE TO INLET FLOW DISTORTION

Figure 1–4

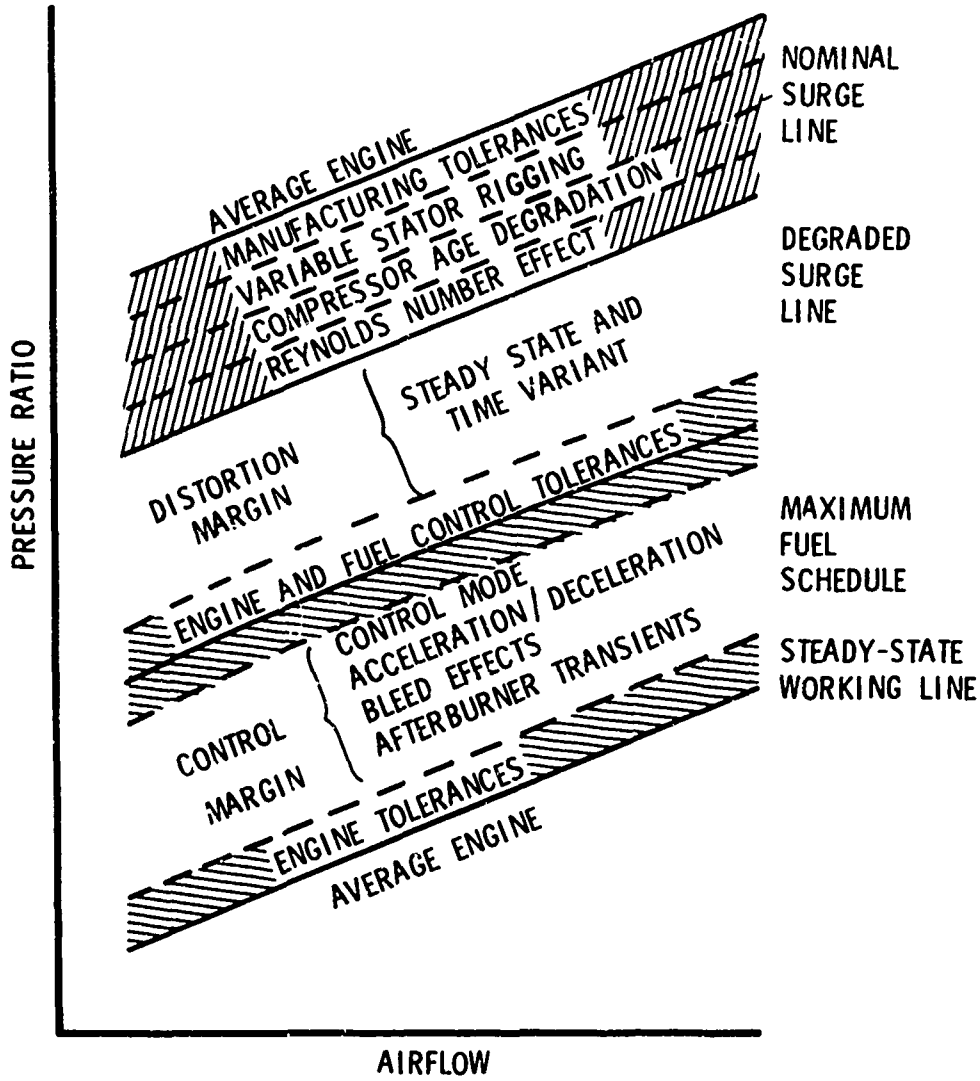

ENGINE PERFORMANCE DEGRADATION

CUMULATIVE REPRESENTATION OF FACTORS

Figure 1–5

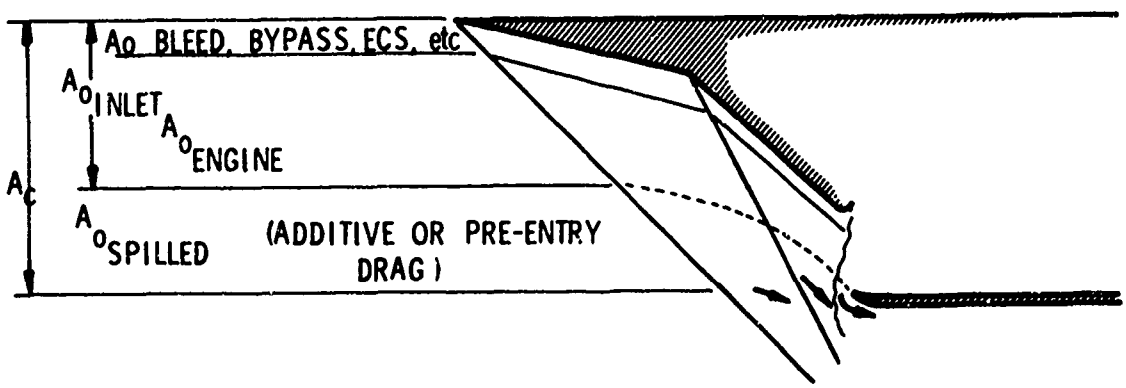

INLET SPILLAGE FLOW SCHEMATIC

Figure 1–6

CONFIG. NO	INLET TYPE	COM-PRESSION	CHARAC-TERISTICS	MACH DESIGN	
1	TWO DIM-ENSIONAL	EXTER.	SUBSON. CONTOUR COWL	2.2	
2	MODIFIED 2-D	EXTER.	SUBSON. CONTOUR COWL	2.2	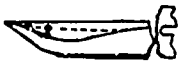
3	2-D	MIXED	SUBSON. CONTOUR COWL	2.2	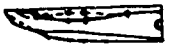
4	2-D	MIXED	SUPERSON. LOW < COWL	2.2	

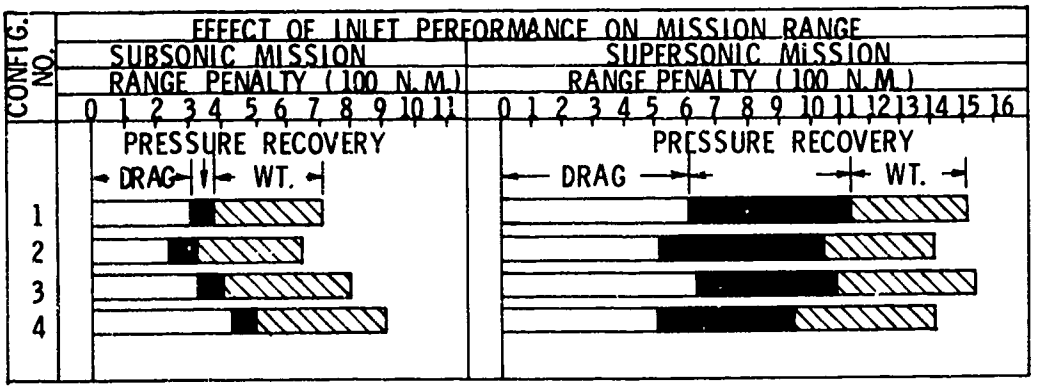

INLET TRADE STUDY RESULTS

Figure 1–7

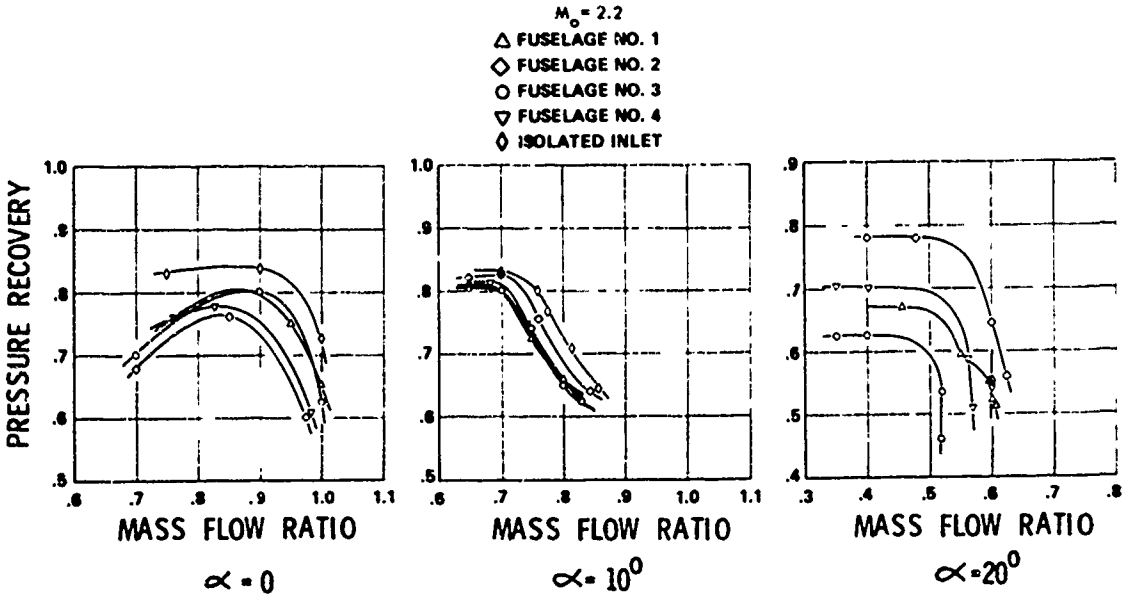

EFFECT OF FUSELAGE FLOW FIELD ON INLET PERFORMANCE

Figure 2–1

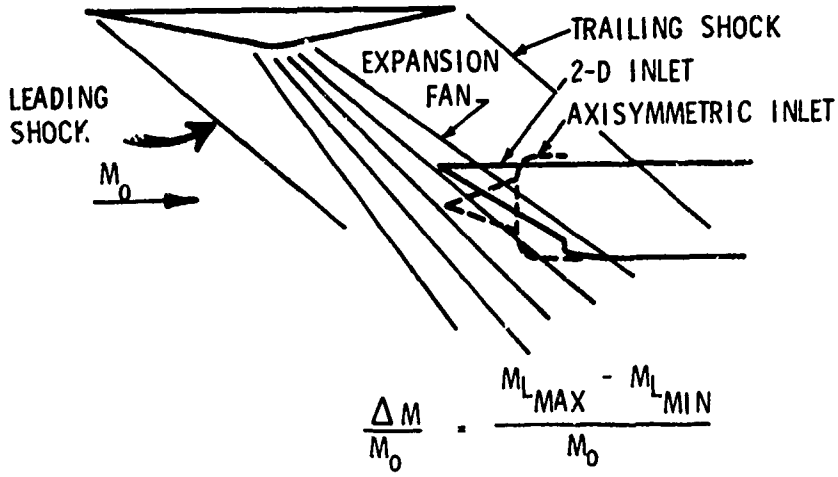

SCHEMATIC REPRESENTATION OF FLOW FIELD DISTORTION GENERATOR

Figure 2–2

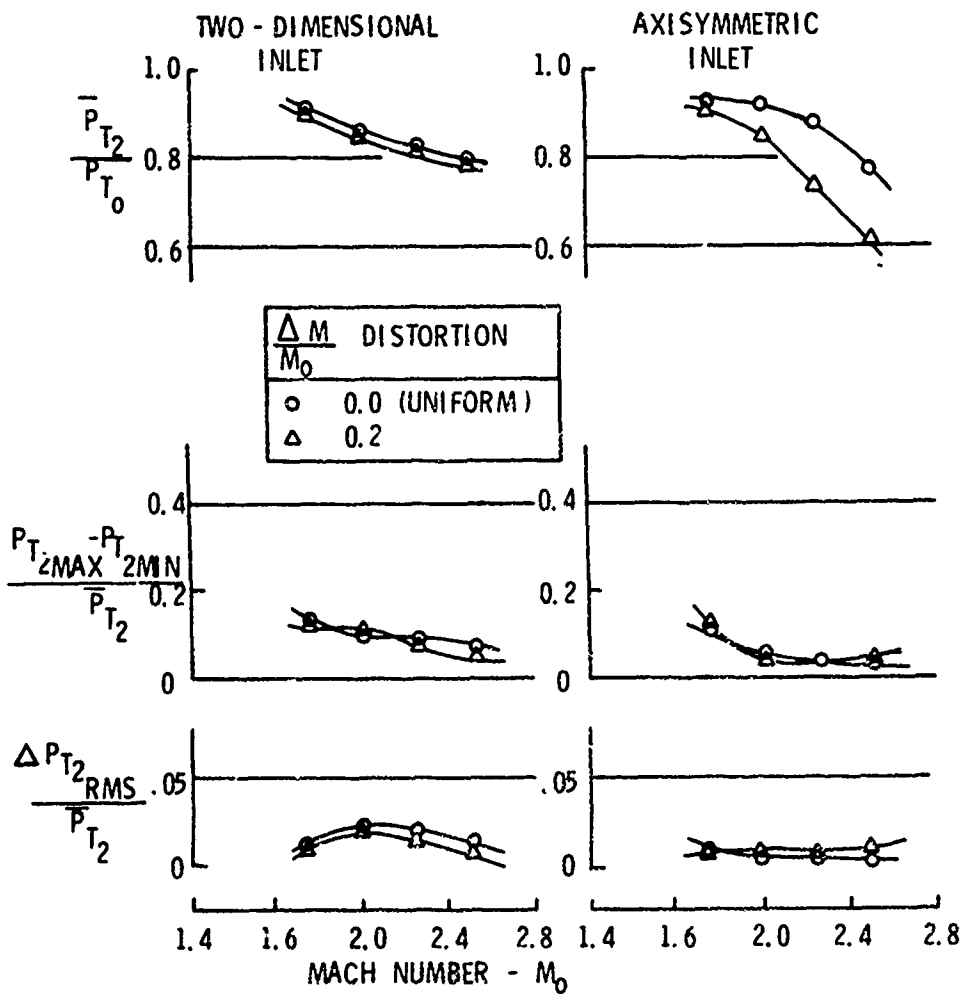

EFFECT OF UPSTREAM FLOW DISTORTION ON INLET PERFORMANCE

Figure 2–3

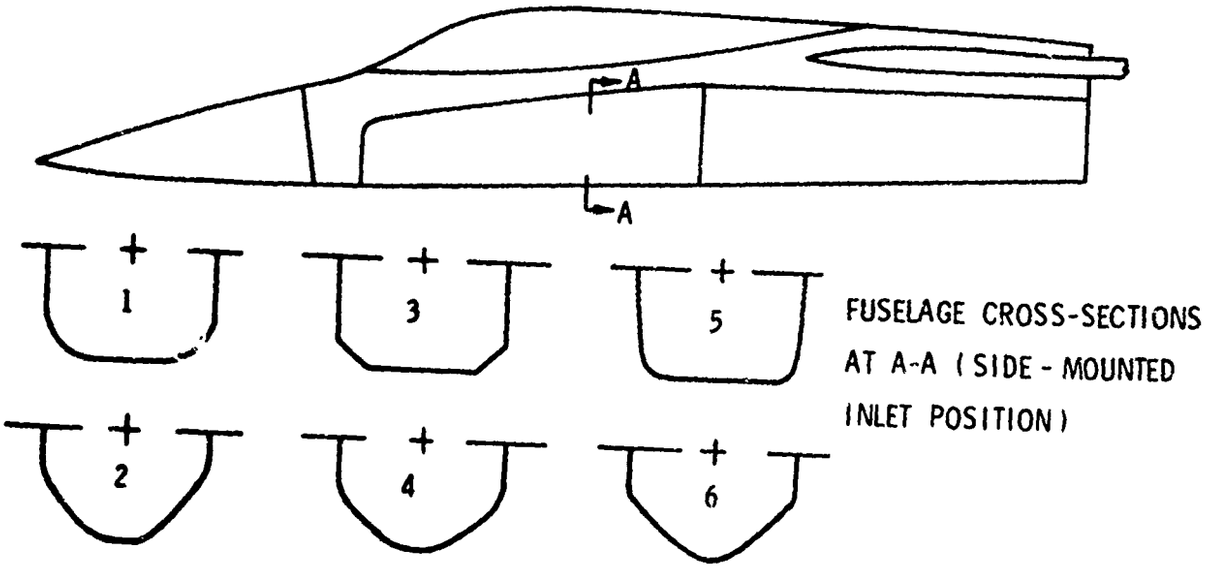

PROGRAM 'F' MODEL OUTLINE

Figure 2–4

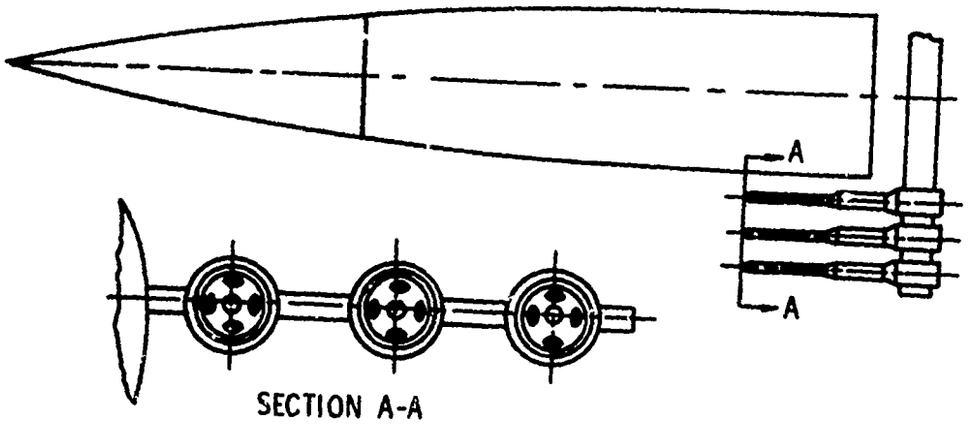

FLOW FIELD SURVEY RAKE

Figure 2–5

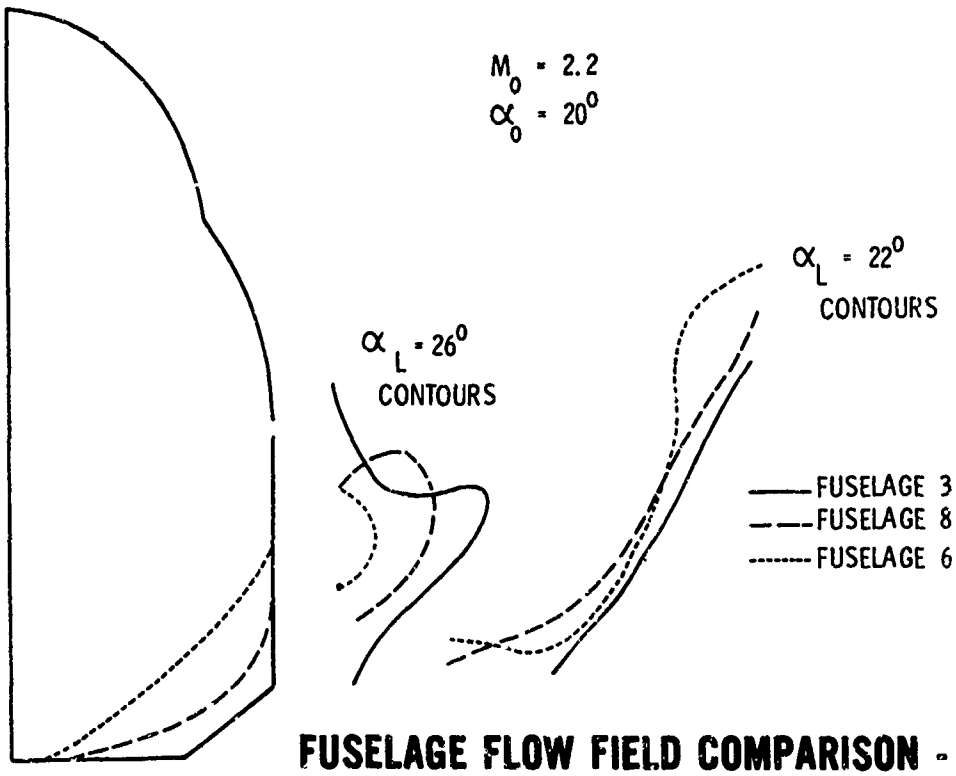

FUSELAGE FLOW FIELD COMPARISON - LOCAL ANGLE-OF-ATTACK CONTOURS

Figure 2–6

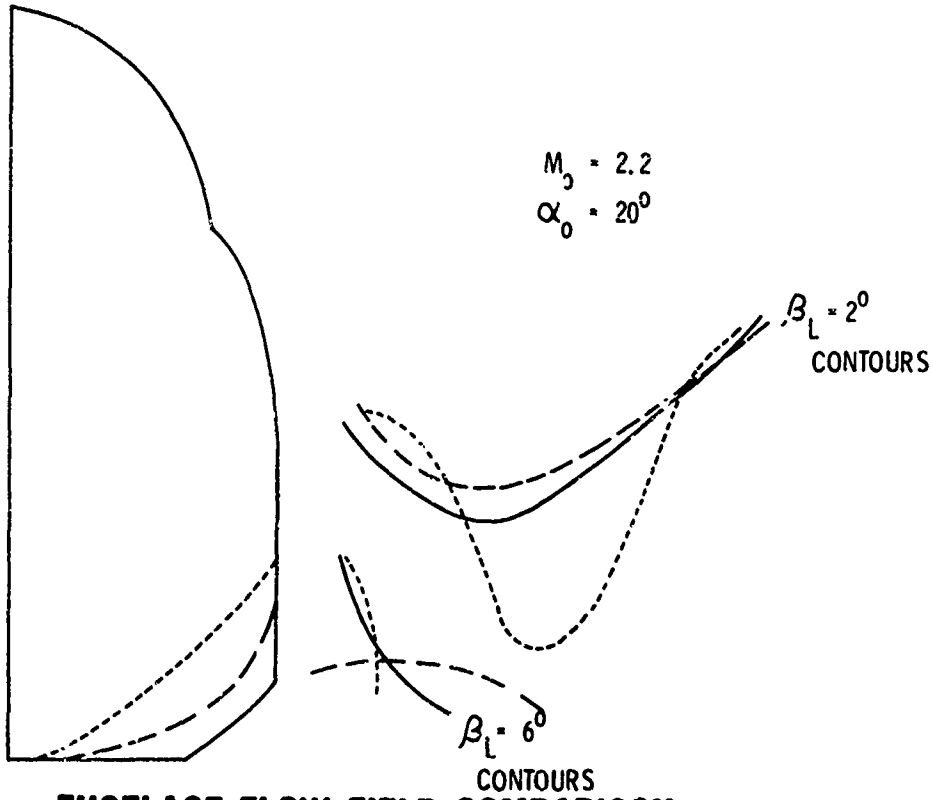

FUSELAGE FLOW FIELD COMPARISON - LOCAL ANGLE-OF- SIDESLIP CONTOURS

Figure 2–7

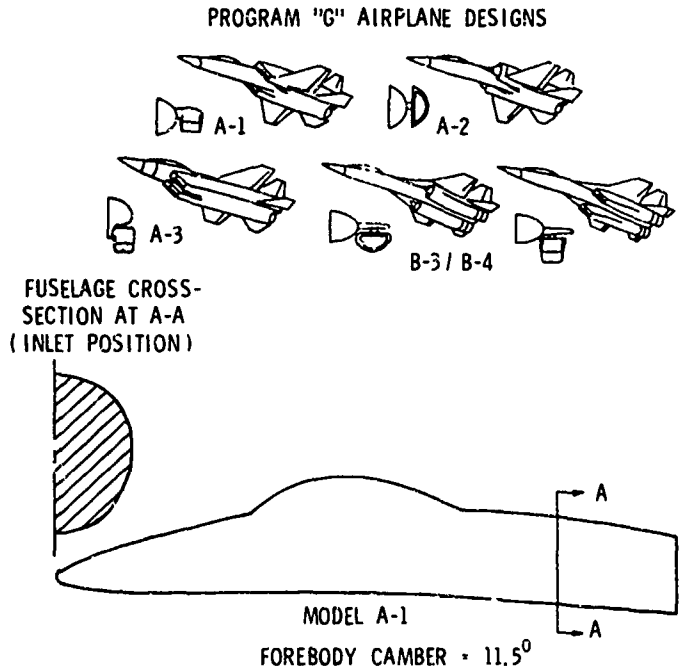

FOREBODY CONFIGURATION-PROGRAM 'G'

Figure 2–8

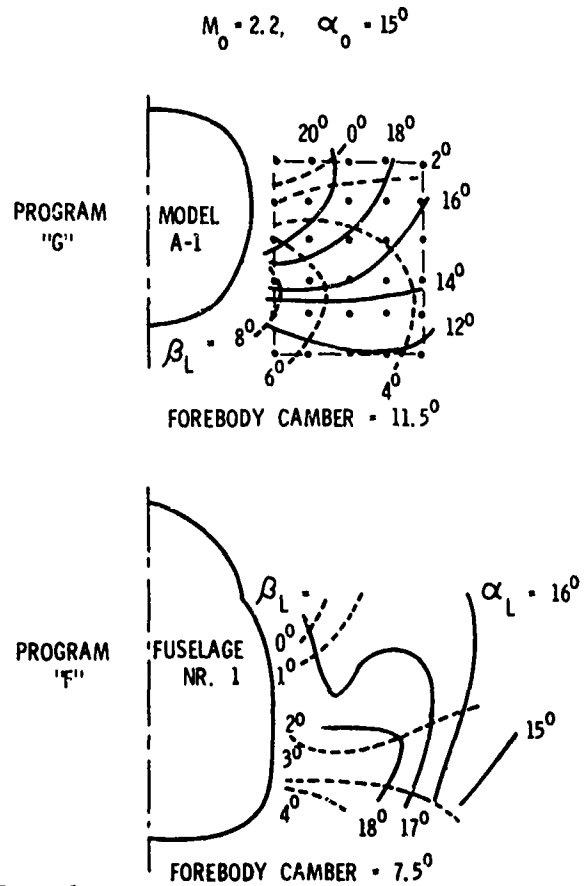

SIDE-MOUNTED INLET FLOW-FIELD DIFFERENCES IN SUPERSONIC MANEUVERING FLIGHT:

PROGRAM "G" VERSUS PROGRAM "F"

Figure 2–9

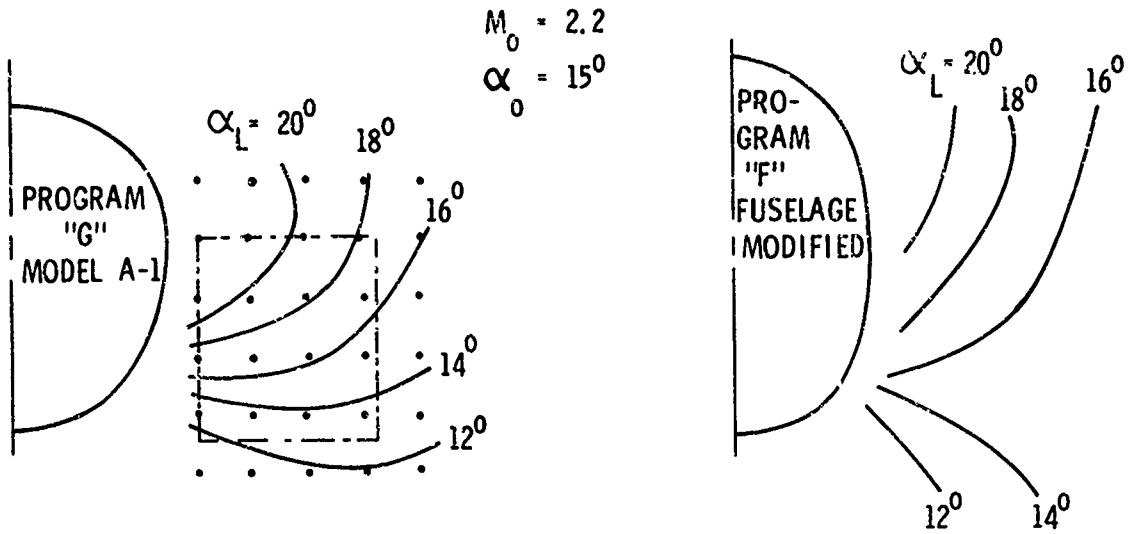

SIDE-MOUNTED INLET FLOW FIELDS:

COMPARISON OF PROGRAM "G" AND "F" MODELS WITH FUSELAGE CAMBER OF 11.5°

Figure 2–10

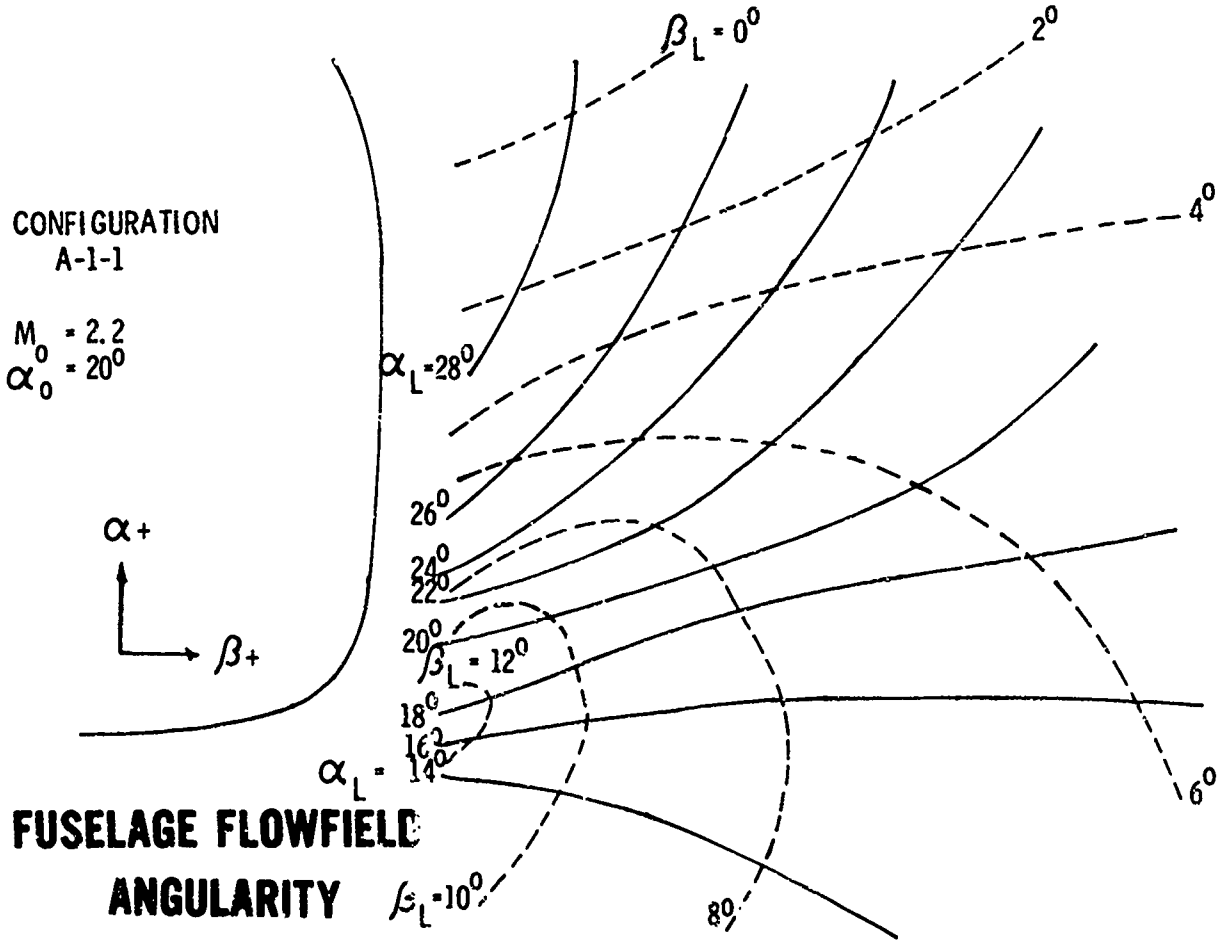

Figure 2–11

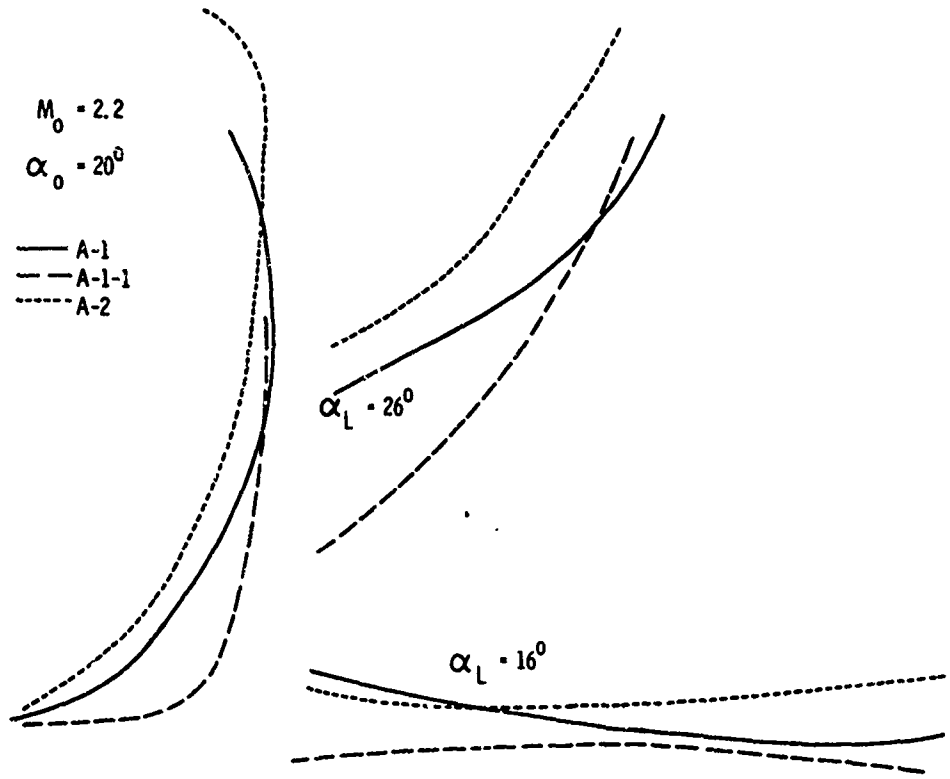

FUSELAGE FLOW FIELD COMPARISONS, LOCAL ANGLE-OF-ATTACK CONTOUR

Figure 2–12

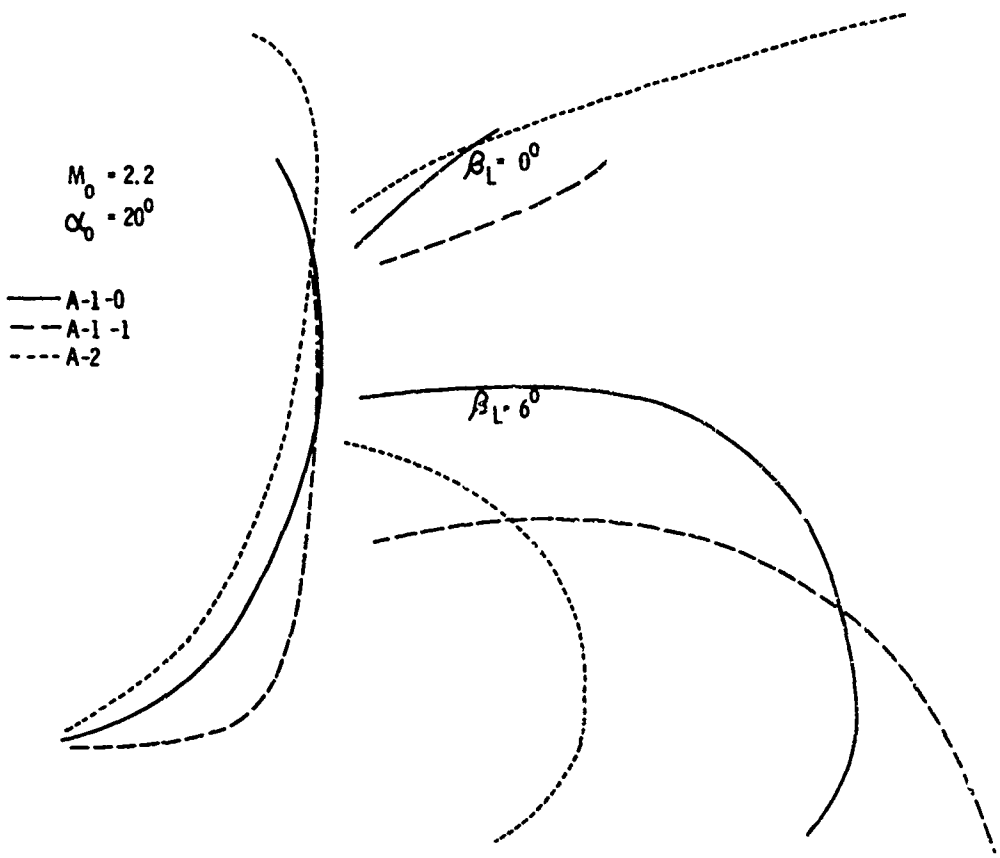

FUSELAGE FLOW FIELD COMPARISONS, LOCAL ANGLE-OF-SIDESLIP CONTOURS

Figure 2–13

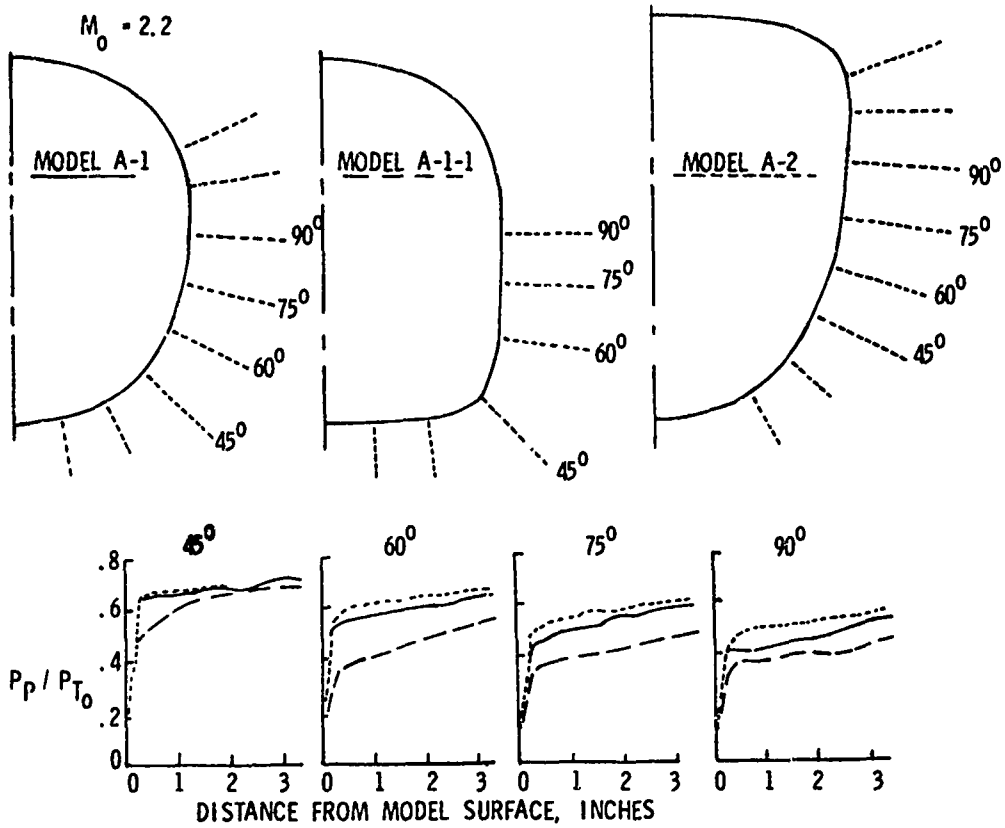

EFFECT OF FUSELAGE SHAPE ON BOUNDARY LAYER DEVELOPMENT

Figure 2–14

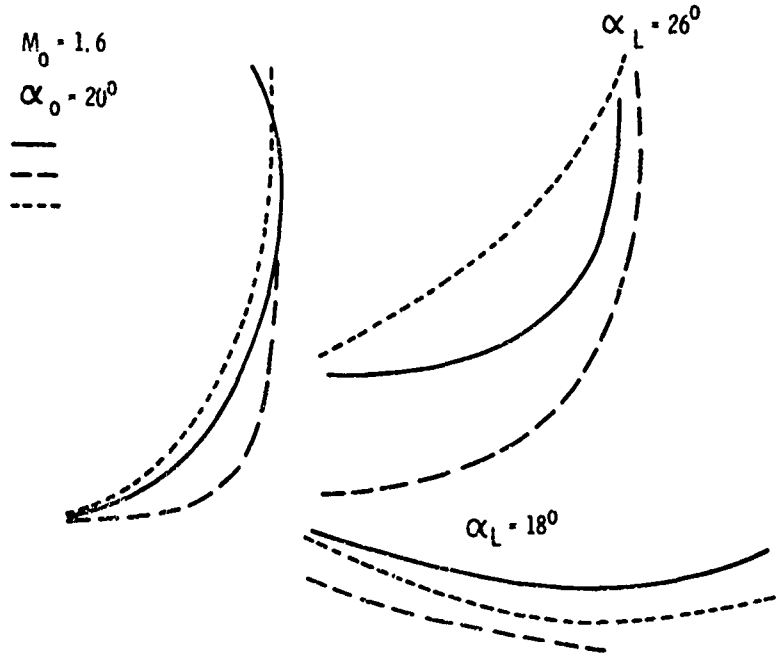

FUSELAGE FLOW FIELD COMPARISONS, ANGLE-OF- ATTACK CONTOUR

Figure 2–15

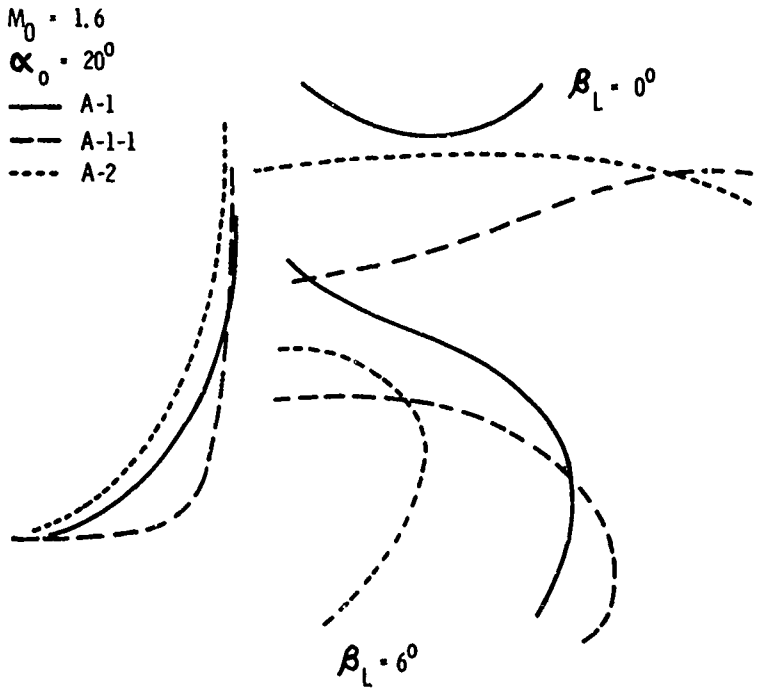

FUSELAGE FLOW FIELD COMPARISONS, ANGLE-OF-SIDESLIP CONTOURS

Figure 2–16

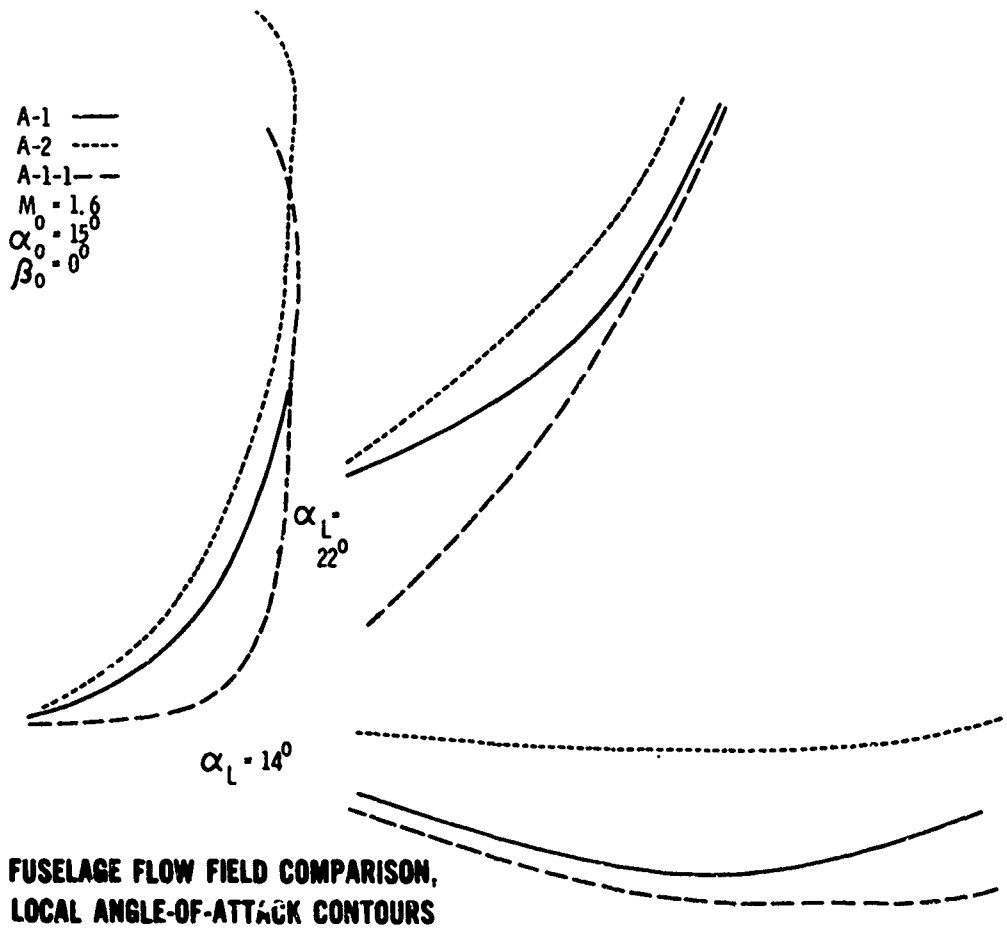

FUSELAGE FLOW FIELD COMPARISON, LOCAL ANGLE-OF-ATTACK CONTOURS

Figure 2–17

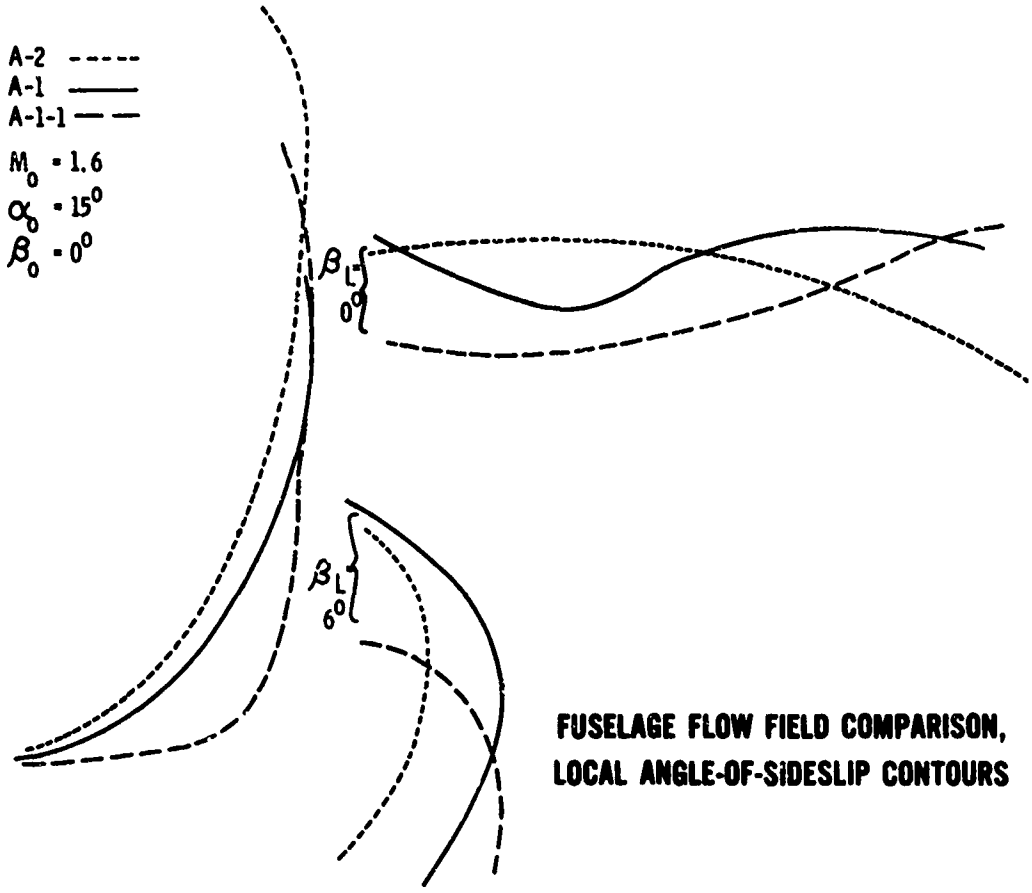

FUSELAGE FLOW FIELD COMPARISON, LOCAL ANGLE-OF-SIDESLIP CONTOURS

Figure 2–18

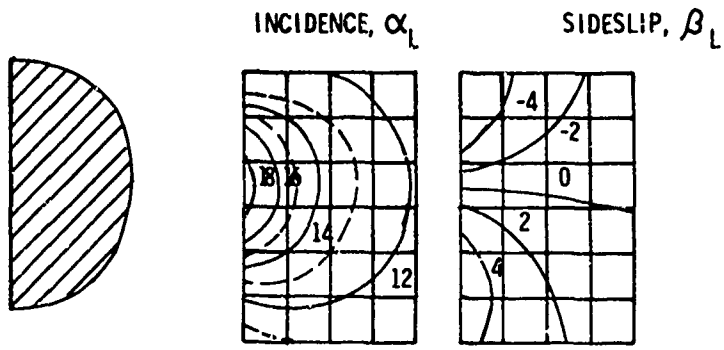

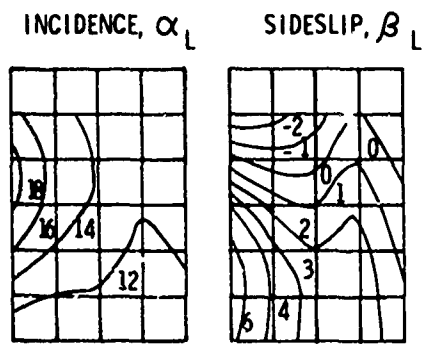

COMPARISON OF PREDICTED AND MEASURED FLOW FIELD:

CONFIGURATION A-1 AT $M_0 = 0.90$, $\alpha_0 = 10$, AND $\beta_0 = 0$

Figure 2–19

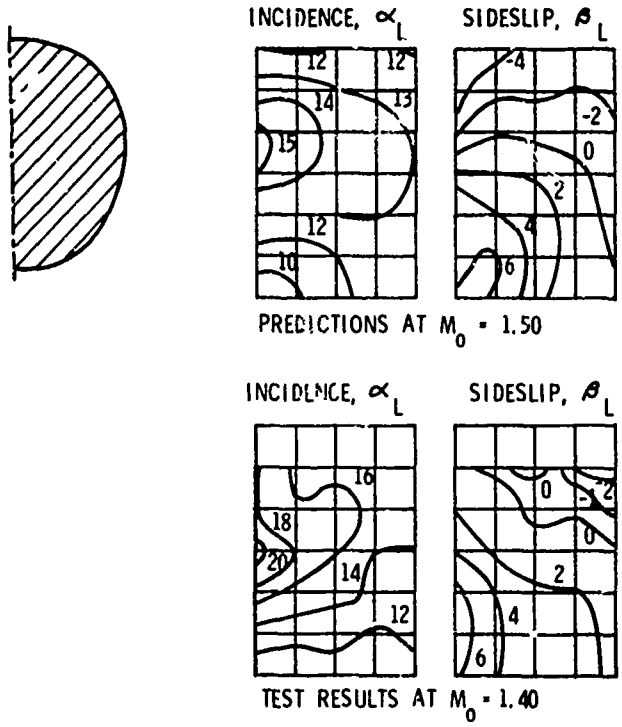

COMPARISON OF PREDICTED AND MEASURED FLOW FIELD:

CONFIGURATION A-1 AT M_0 = 1.50 VERSUS 1.40, α_0 = 10, AND β_0 = 0

Figure 2–20

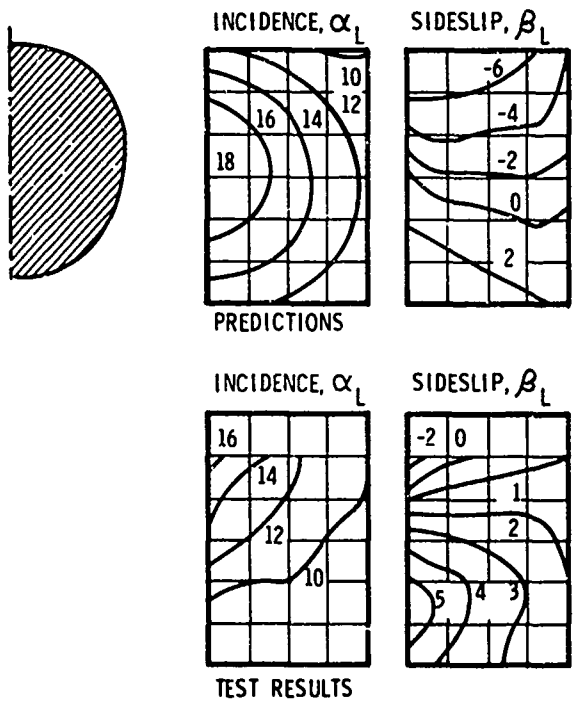

CONFIGURATION A-1 AT M_0 = 2.50, α_0 = 10, AND β_0 = 0

COMPARISON OF

PREDICTED AND MEASURED FLOW FIELD:

Figure 2–21

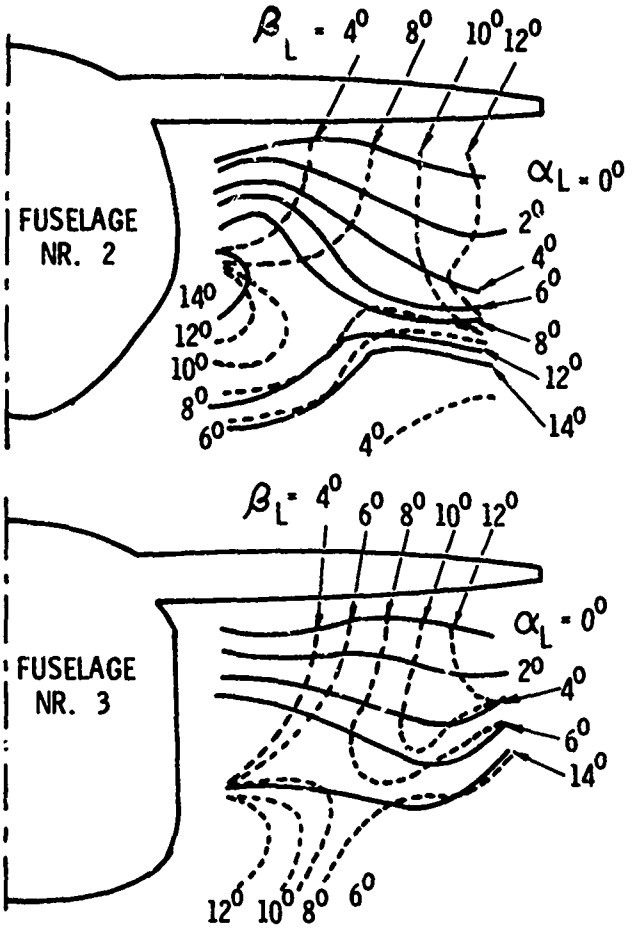

α_L = LOCAL ANGLE-OF-ATTACK β_L = LOCAL ANGLE-OF-SIDESLIP

AIRFRAME-INLET INTERACTION:

EFFECT OF FUSELAGE SHAPE ON FLOW FIELD ANGULARITY AT $M_0 = 2.2$, $\alpha_0 = 15^0$ FOR WING-SHIELDED SIDE-MOUNTED INLETS

Figure 2–22

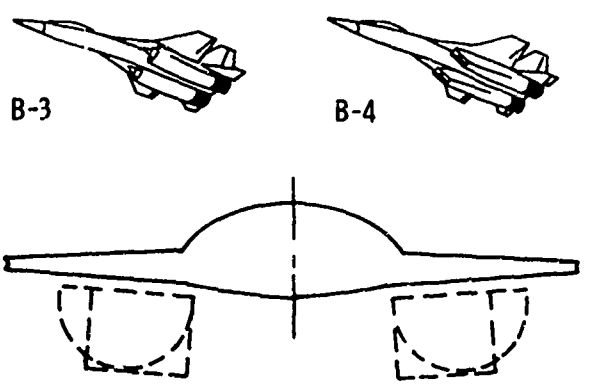

WING-SHIELDED AIRFRAME-INLET CONFIGURATIONS, MODELS B-3 AND B-4

Figure 2–23

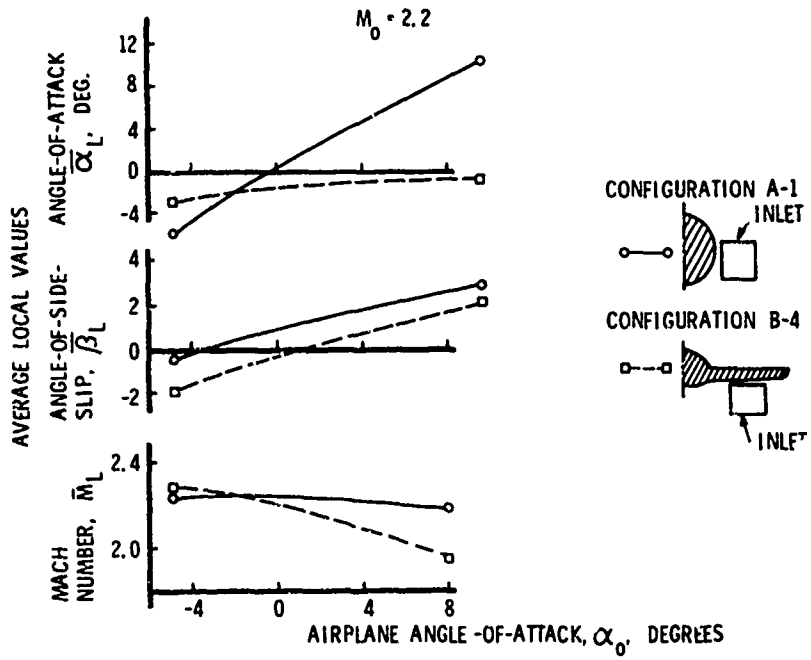

COMPARISON OF AVERAGE FLOW FIELD PROPERTIES

Figure 2–24

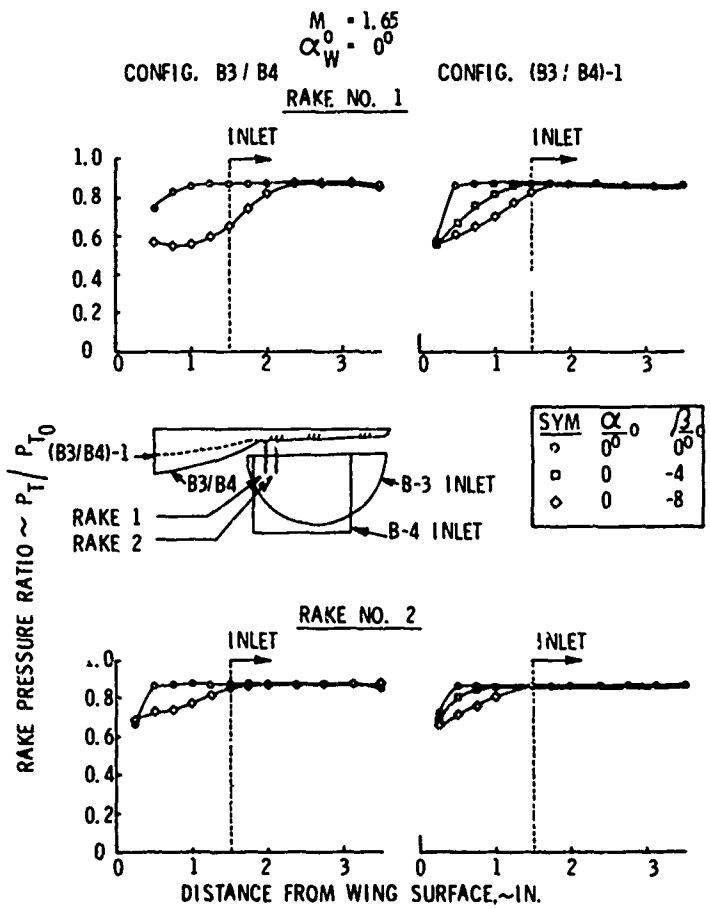

COMPARISON OF MEASURED BOUNDARY LAYER CHARACTERISTICS ON THE B-3/B-4 & (B-3/B-4)-1 FOREBODIES

Figure 2–25

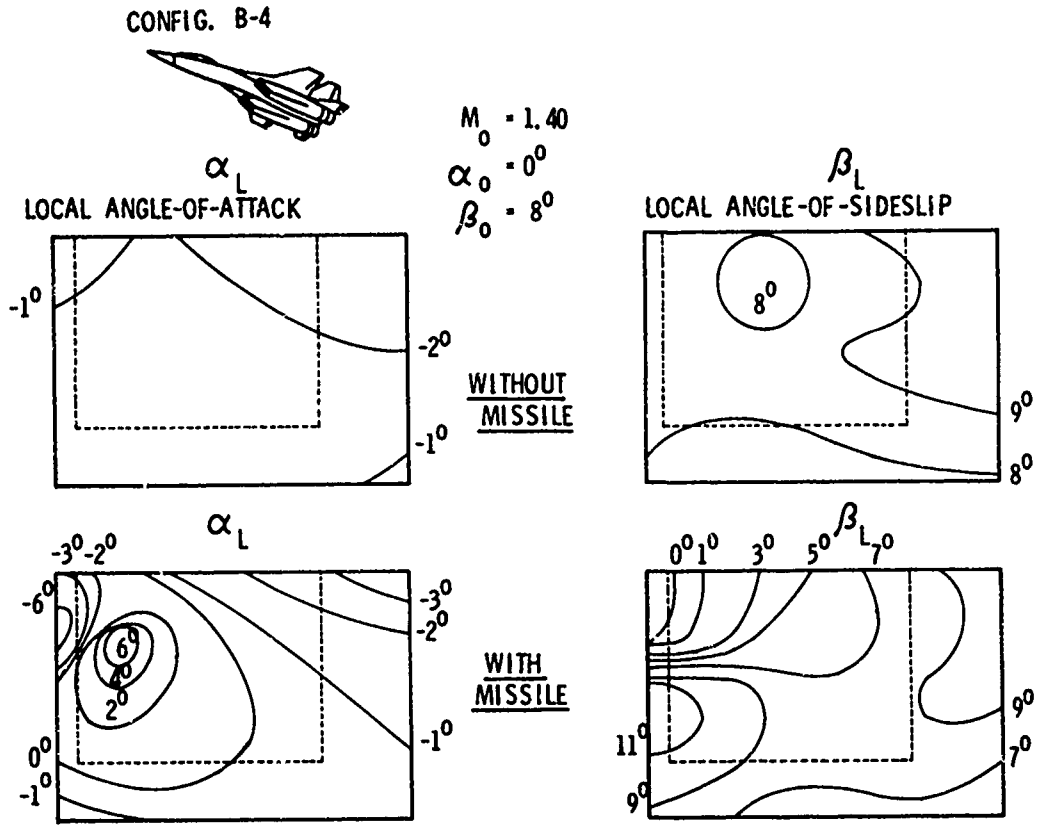

EFFECT OF MISSILE INSTALLATION ON INLET FLOW FIELD

Figure 2–26

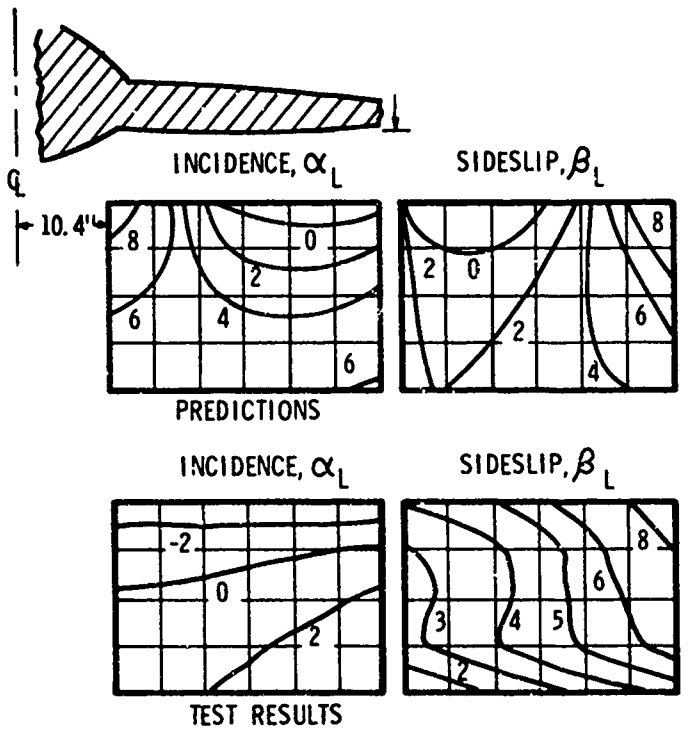

COMPARISON OF PREDICTED AND MEASURED FLOW FIELD:

CONFIGURATION B-3/B-4 AT $M_0 = 0.90$, $\alpha_0 = 10$, AND $\beta_0 = 0$

Figure 2–27

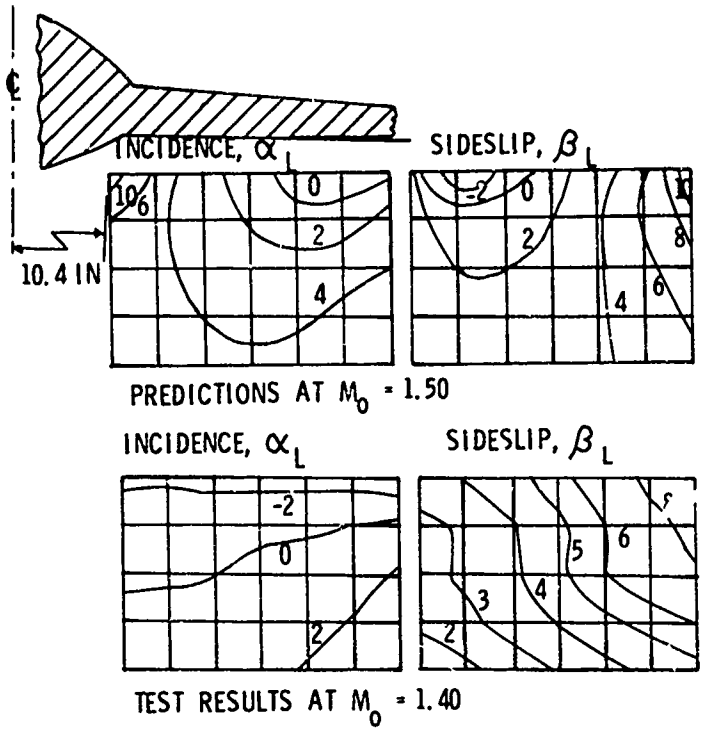

COMPARISON OF PREDICTED AND MEASURED FLOW FIELD:
CONFIGURATION B-3 / B-4 AT M_0 = 1.50 VERSUS 1.40, α_0 = 10, AND β_0 = 0

Figure 2–28

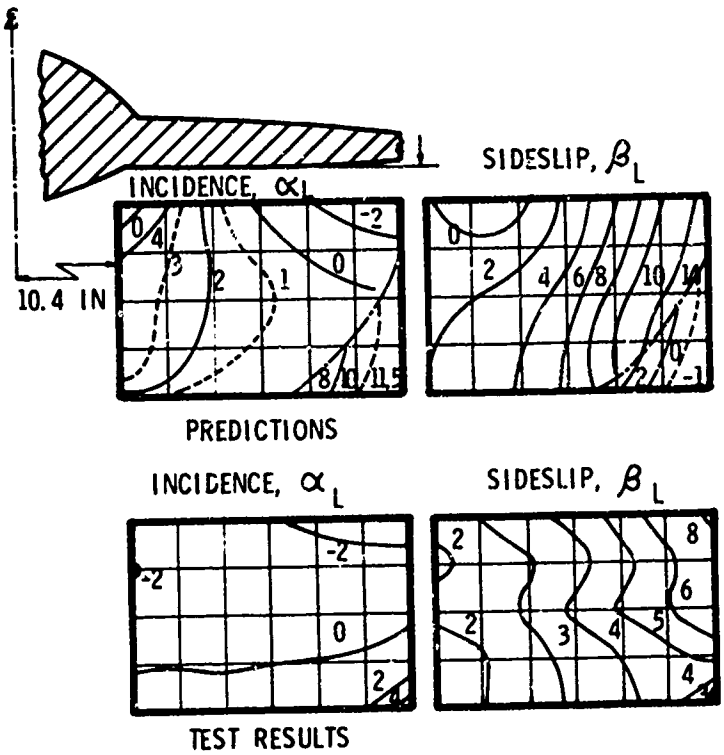

COMPARISON OF PREDICTED AND MEASURED FLOW FIELD:
CONFIGURATION B-3 / B-4 AT M_0 = 2.50, α_0 = 10, AND β_0 = 0

Figure 2–29

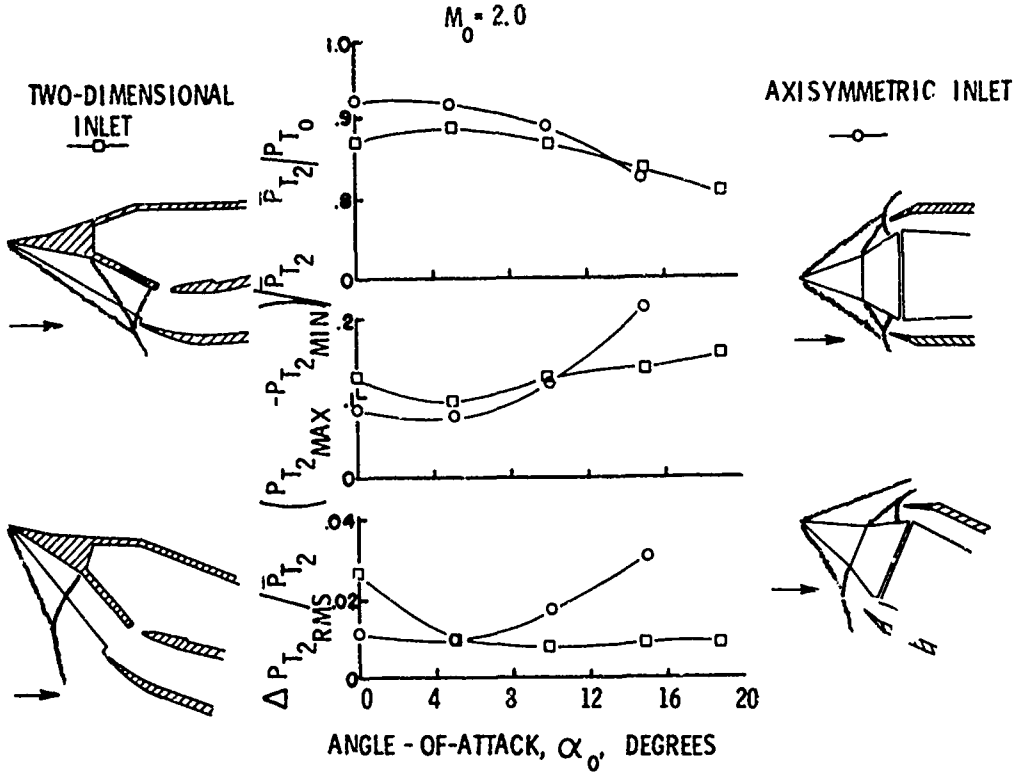

ISOLATED TWO-DIMENSIONAL VERSUS AXISYMMETRIC INLET PERFORMANCE IN MANEUVERING FLIGHT, Mo=2.2

Figure 3–1

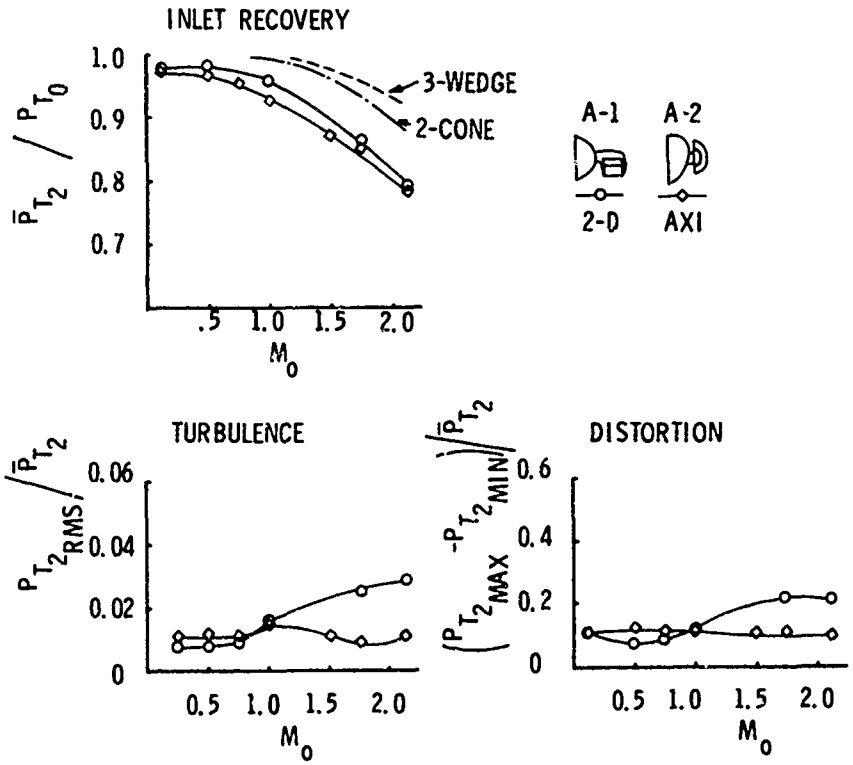

TWO-DIMENSIONAL AND AXISYMMETRIC INLET INSTALLED PERFORMANCE VARIATION WITH MACH NUMBER

Figure 3–2

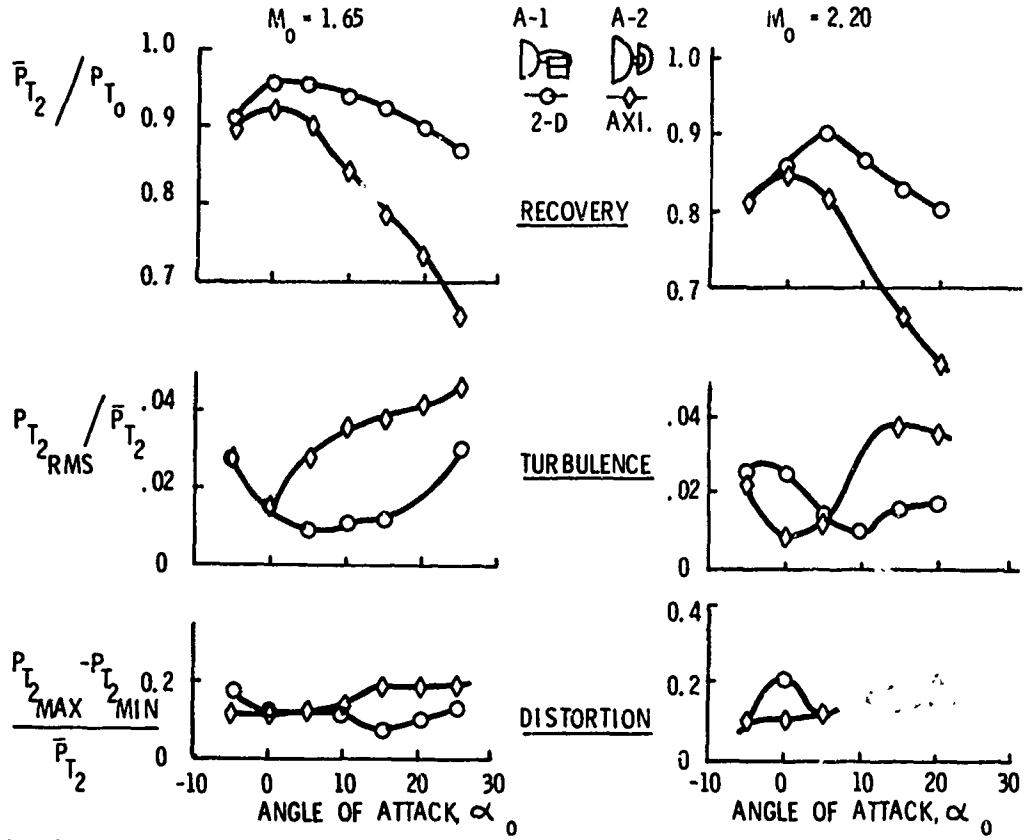

TWO-DIMENSIONAL VERSUS AXISYMMETRIC INSTALLED INLET PERFORMANCE IN MANEUVERING FLIGHT

Figure 3–3

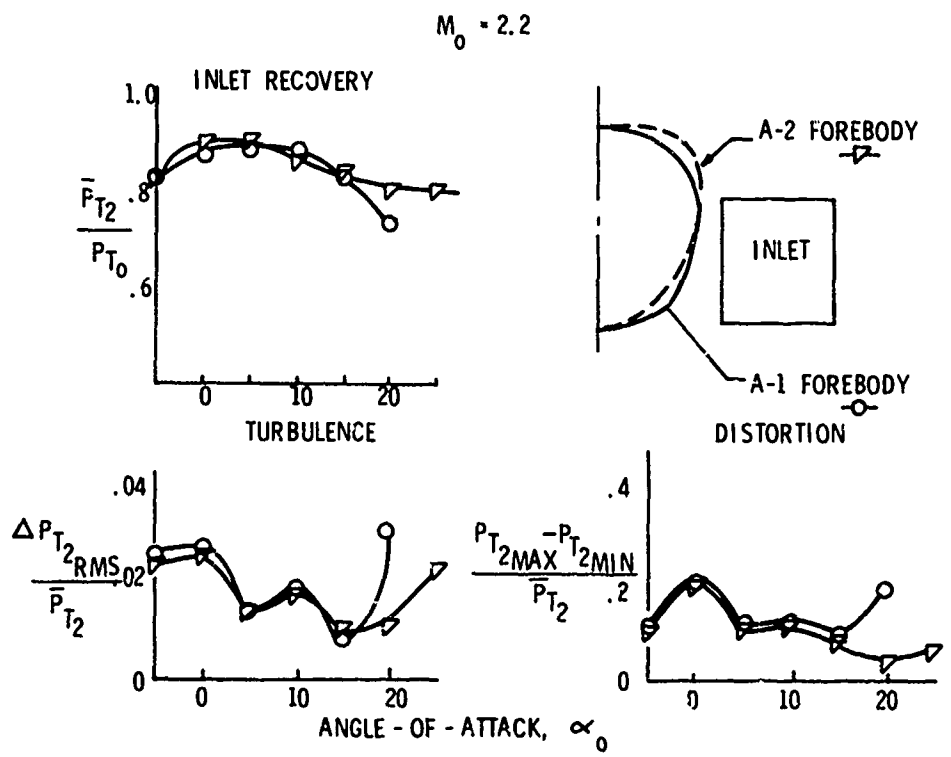

EFFECT OF FOREBODY SHAPE ON INLET PERFORMANCE PARAMETERS

Figure 3–4

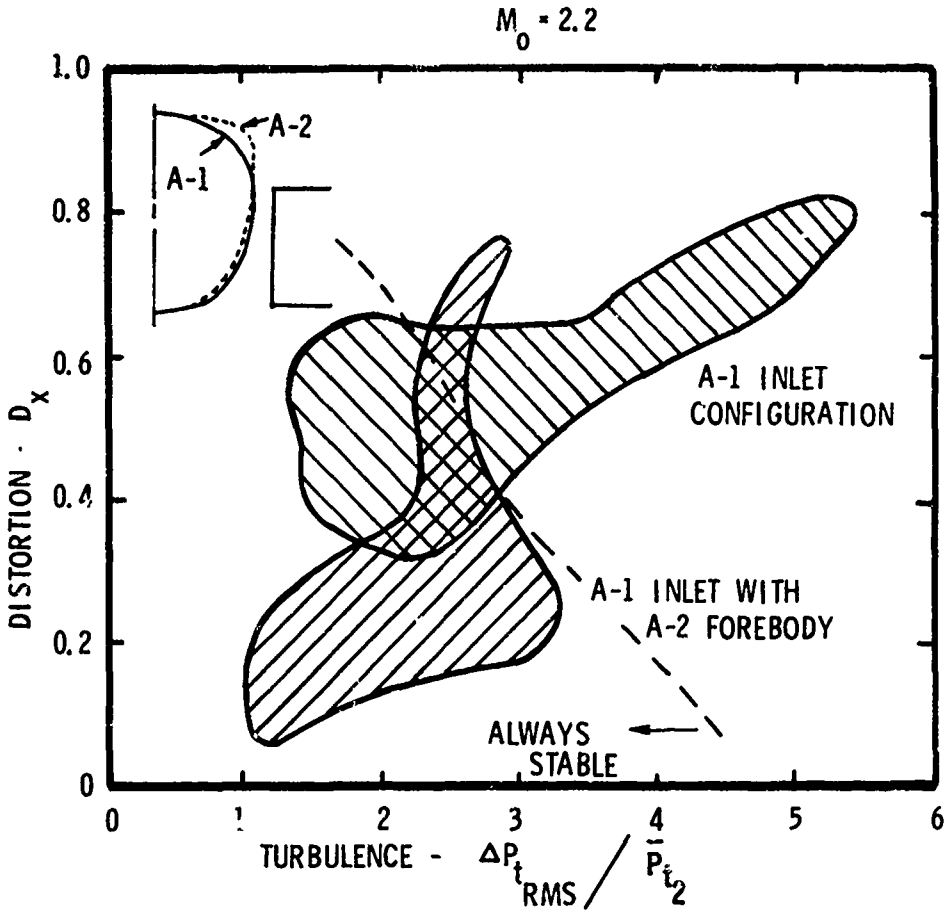

EFFECT OF FOREBODY CONTOUR ON INLET-ENGINE COMPATIBILITY

Figure 3–5

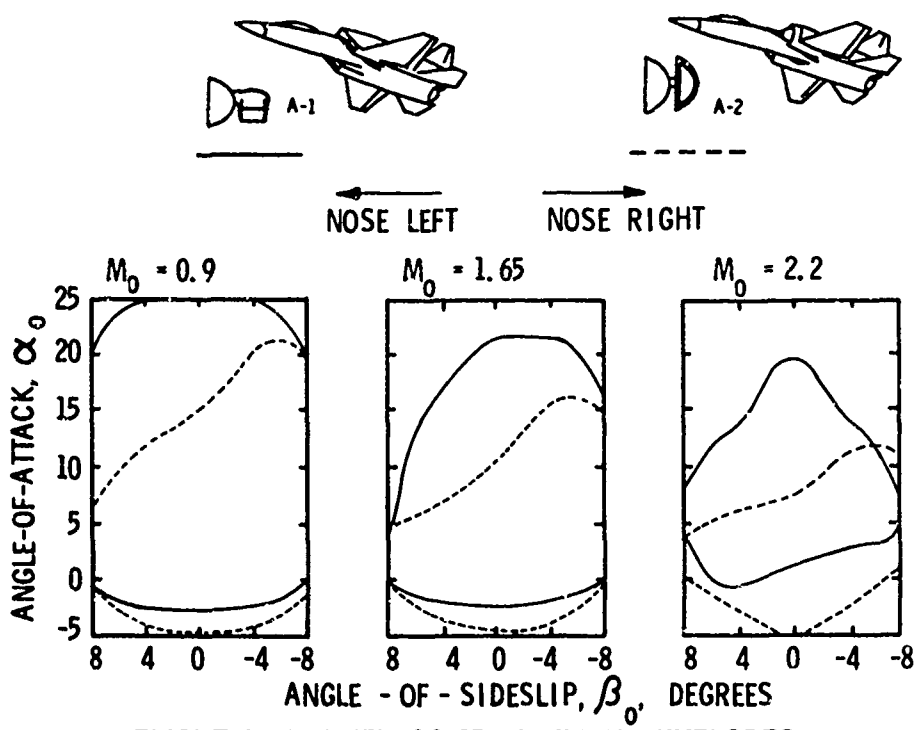

FLIGHT MANEUVER COMPATIBILITY ENVELOPES

Figure 3–6

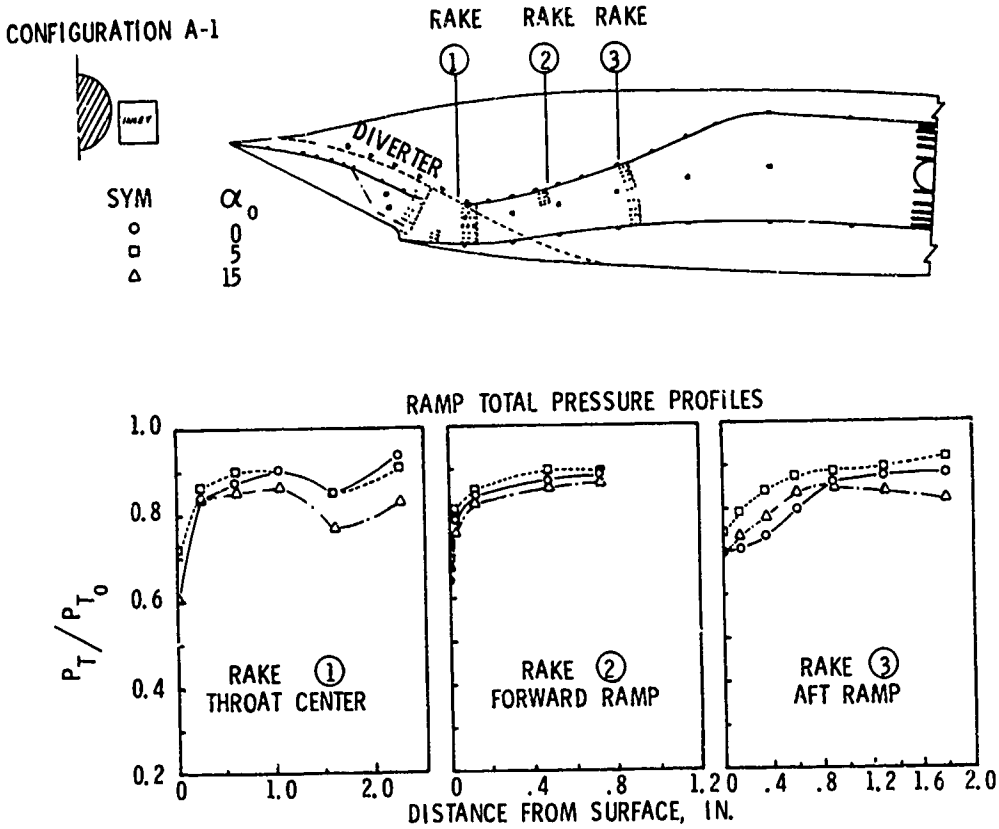

RAMP AND SUBSONIC DUCT PRESSURE PROFILES IN THE A-1 INLET, M_0=2.20

Figure 3–7

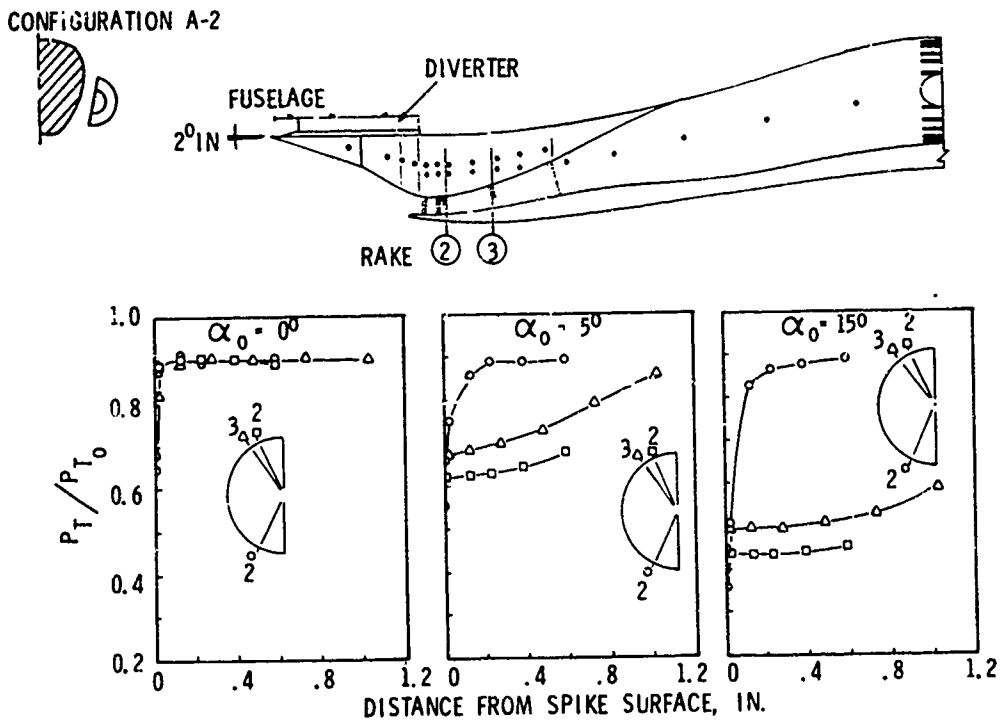

SPIKE AND SUBSONIC DUCT PRESSURE PROFILES IN THE A-2 INLET, M_0=2.00

Figure 3–8

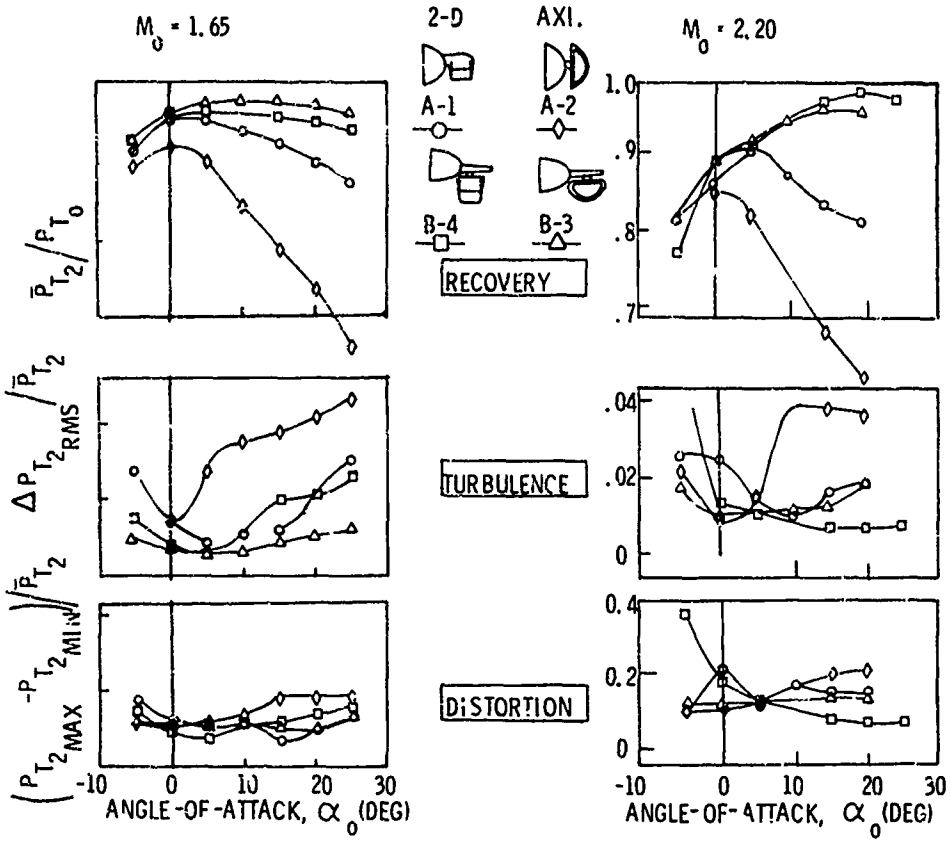

EFFECT OF ANGLE-OF-ATTACK ON INLET PERFORMANCE

Figure 3–9

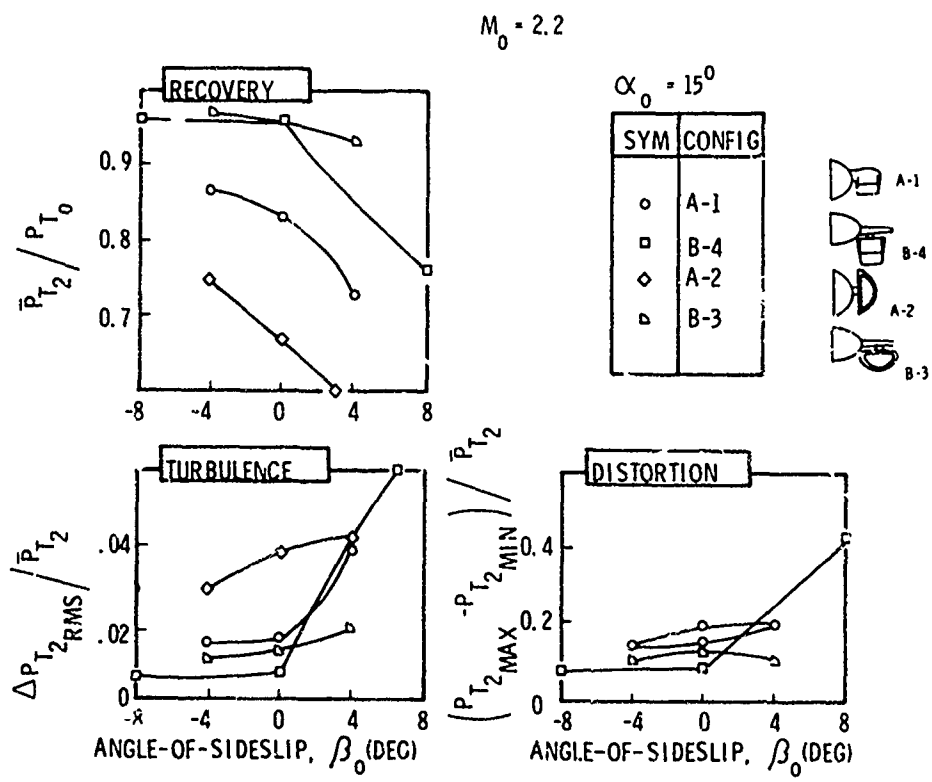

EFFECT OF ANGLE-OF-SIDESLIP ON INLET PERFORMANCE, M_0=2.2

Figure 3-10

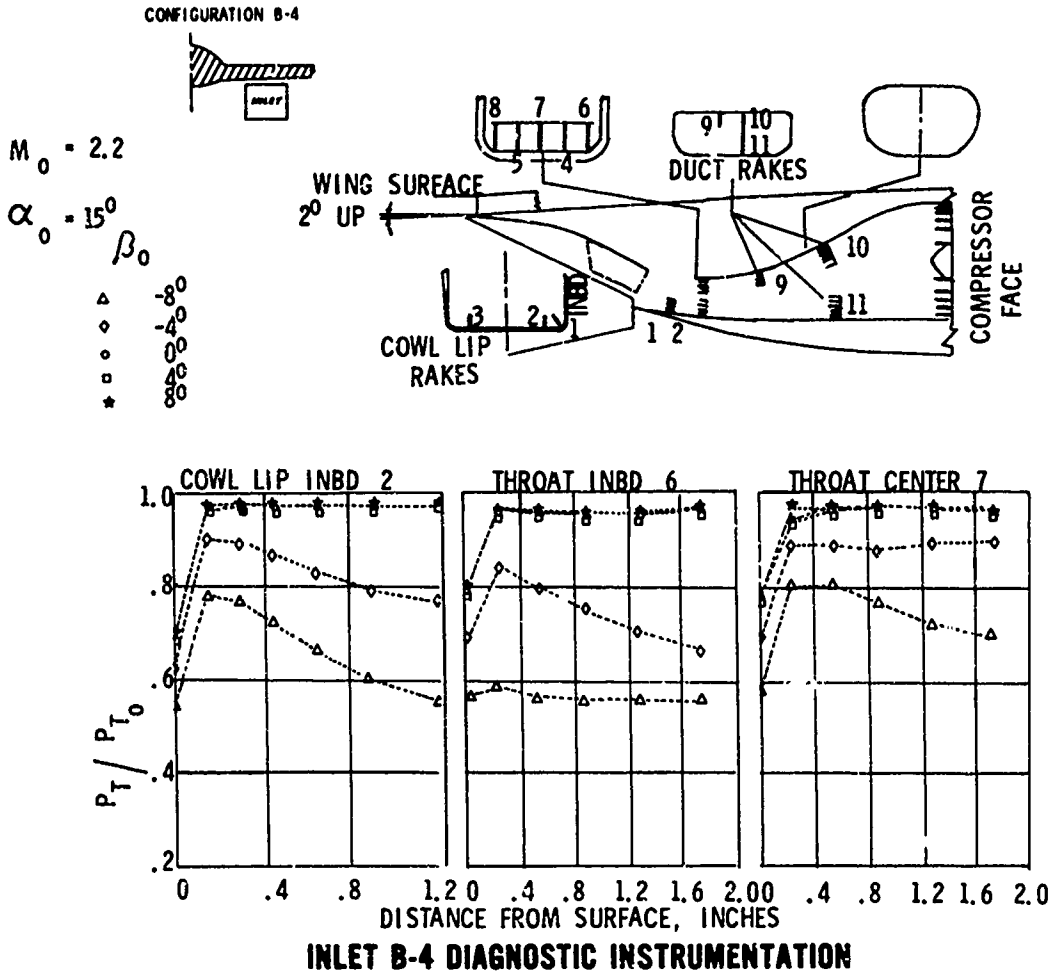

INLET B-4 DIAGNOSTIC INSTRUMENTATION

Figure 3–11

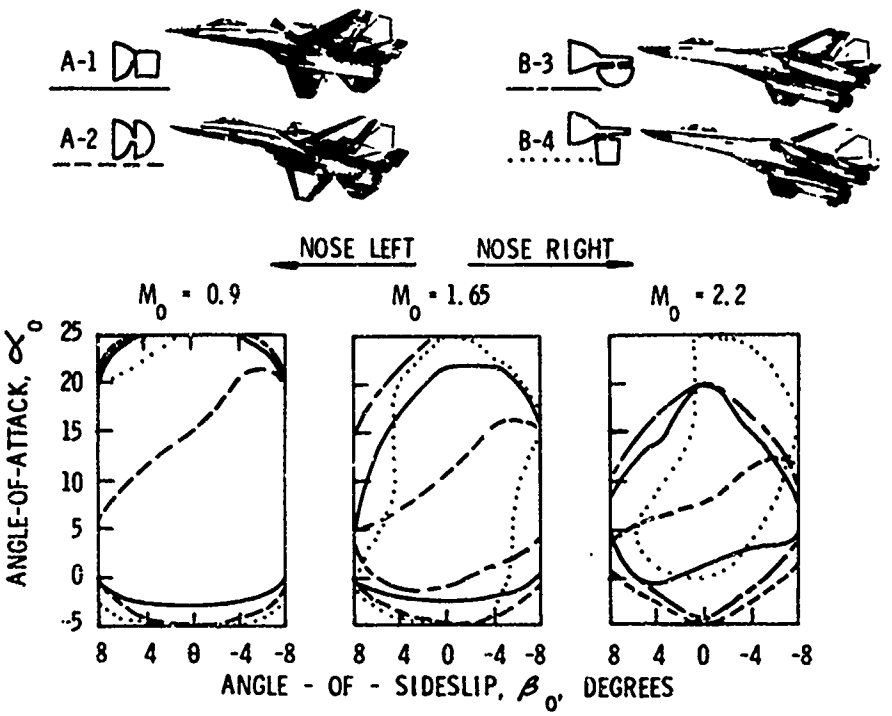

FLIGHT MANEUVER COMPATIBILITY ENVELOPES

Figure 3–12

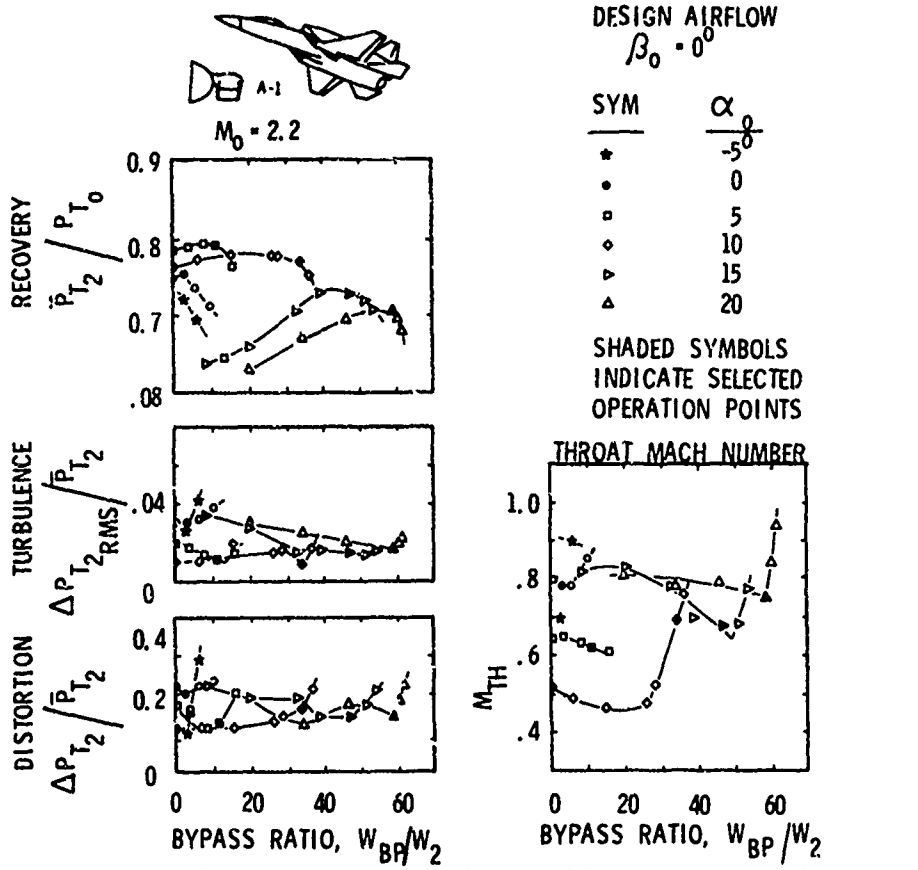

EFFECT OF BYPASS SYSTEM OPERATION ON INLET PERFORMANCE

Figure 3–13

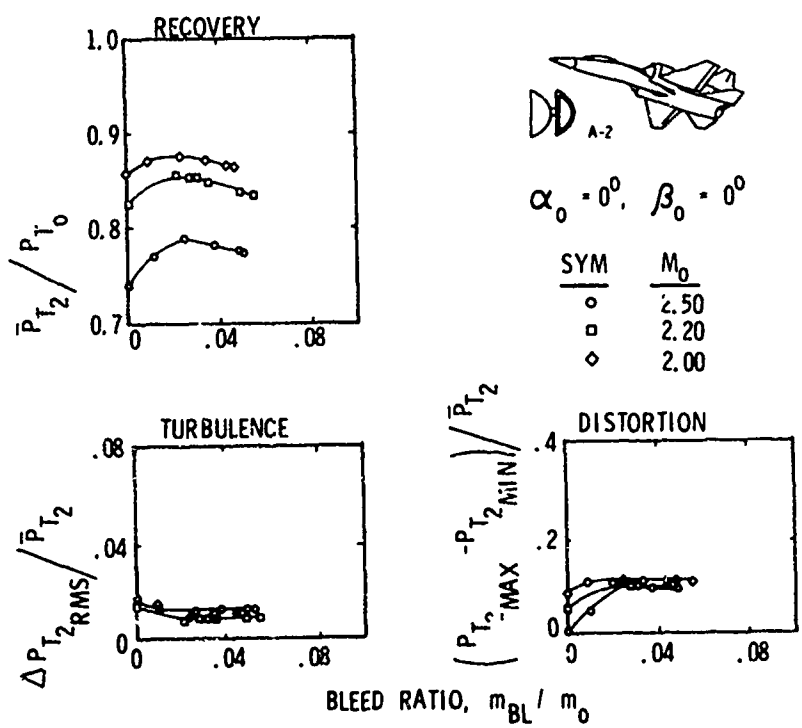

EFFECT OF BOUNDARY LAYER BLEED ON A-2 INLET PERFORMANCE

Figure 3–14

THIS
PAGE
IS
MISSING
IN
ORIGINAL
DOCUMENT

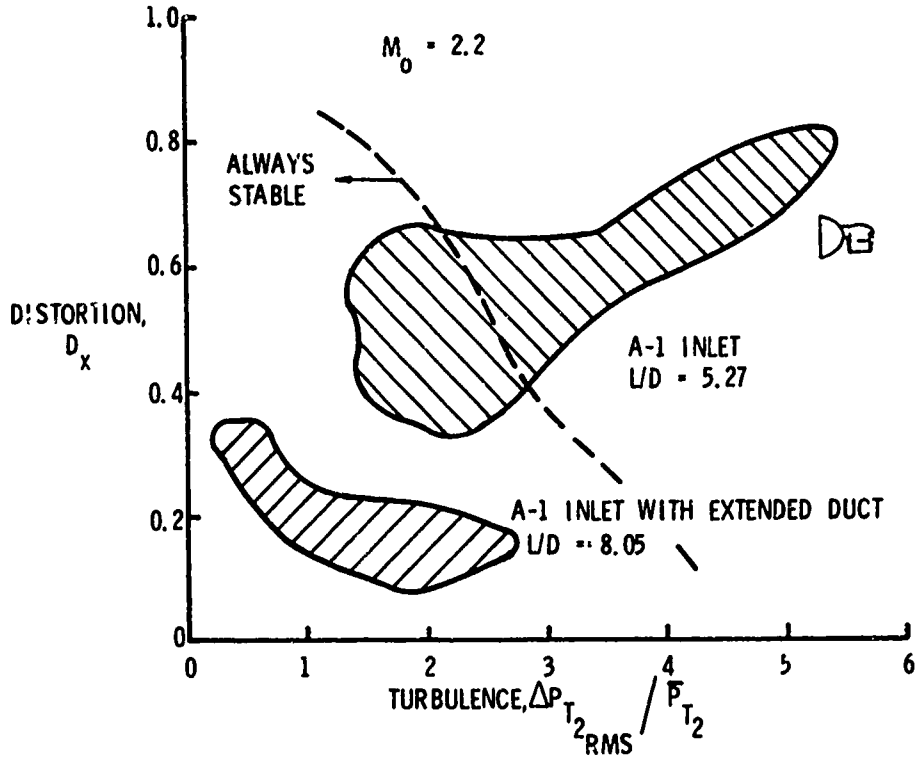

EFFECT OF DUCT LENGTH ON INLET-ENGINE COMPATIBILITY

Figure 3–15

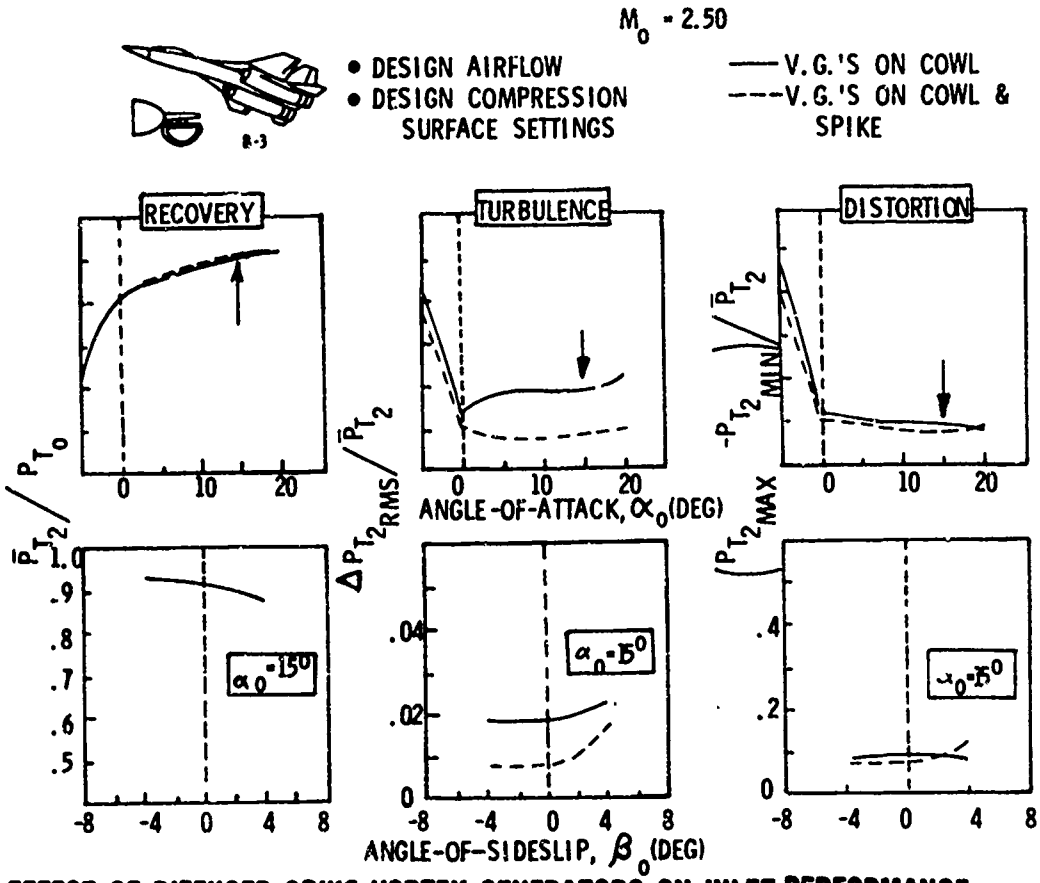

EFFECT OF DIFFUSER SPIKE VORTEX GENERATORS ON INLET PERFORMANCE

Figure 3–16

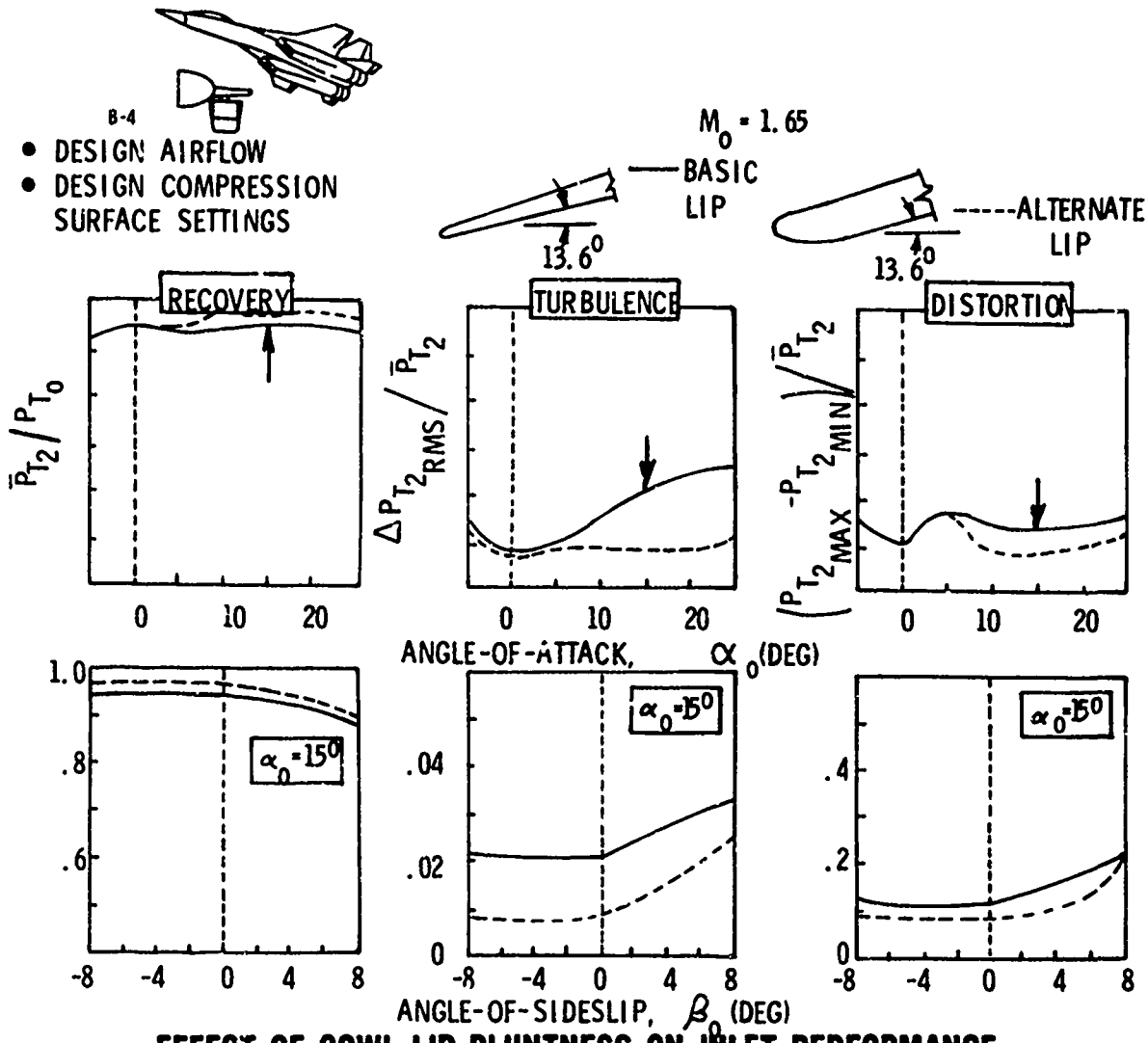

EFFECT OF COWL LIP BLUNTNESS ON INLET PERFORMANCE

Figure 3–17

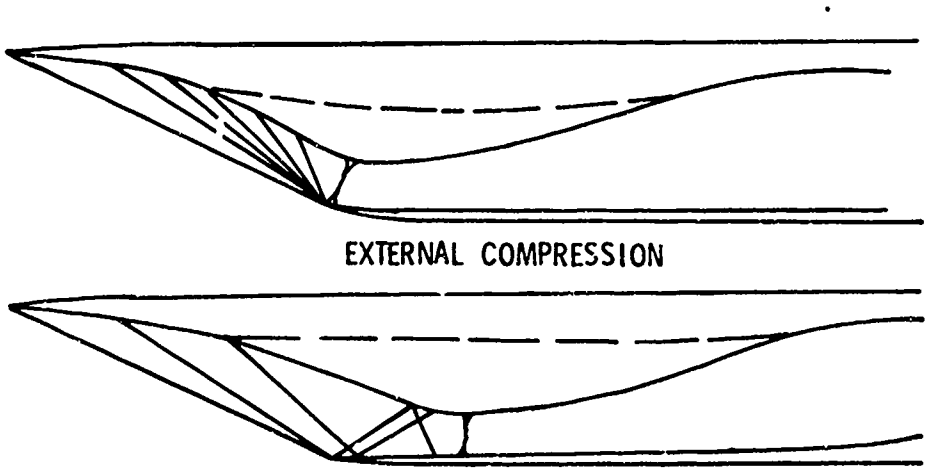

COMPARISON OF EXTERNAL AND MIXED COMPRESSION INLET TYPES

Figure 3–18

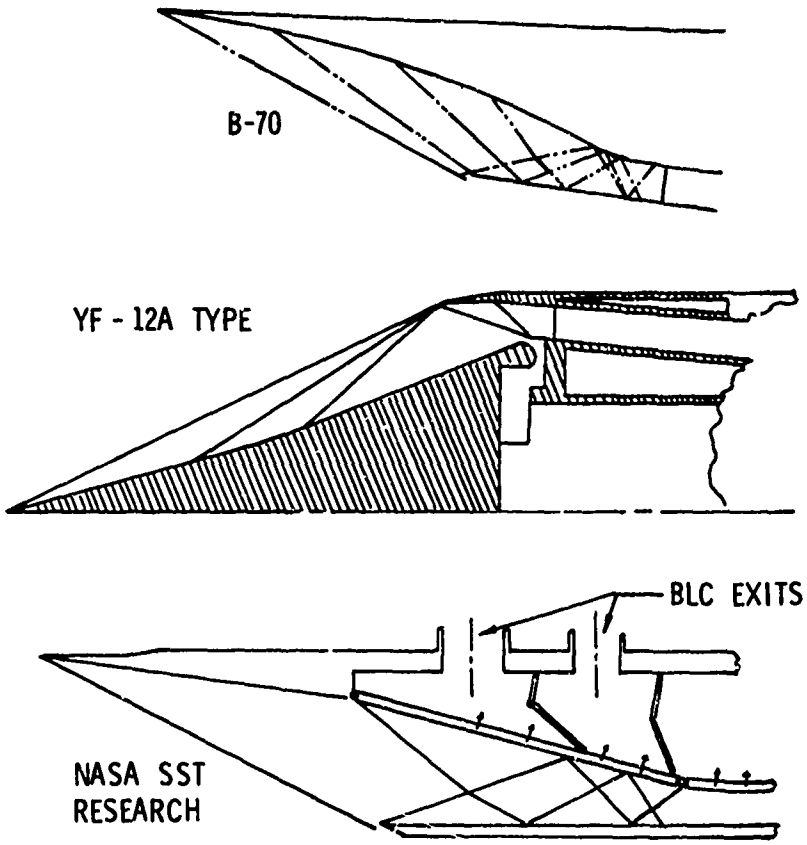

COMPARISON OF
MIXED COMPRESSION INLET DESIGN TYPES

Figure 3–19

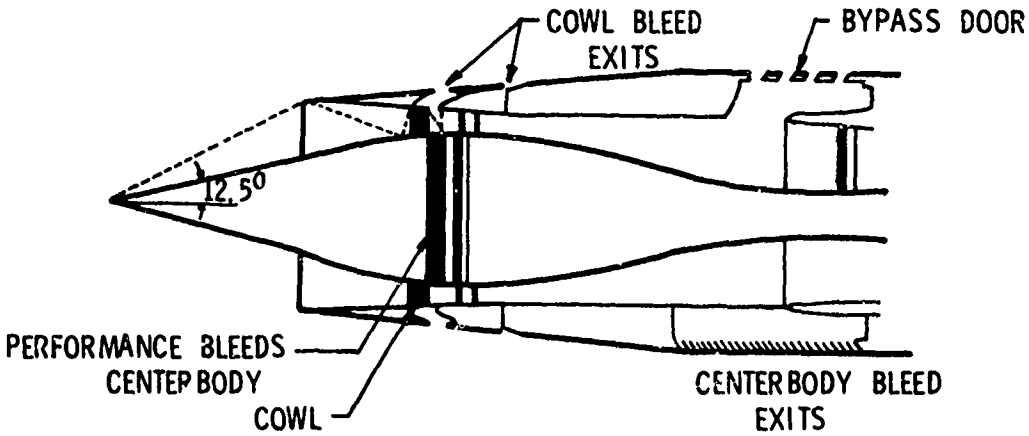

NASA RESEARCH INLET

COMPRESSION: 40% EXTERNAL, 60% INTERNAL

MACH 2.5 DESIGN AXISYMMETRIC
MIXED COMPRESSION RESEARCH INLET

Figure 3–20

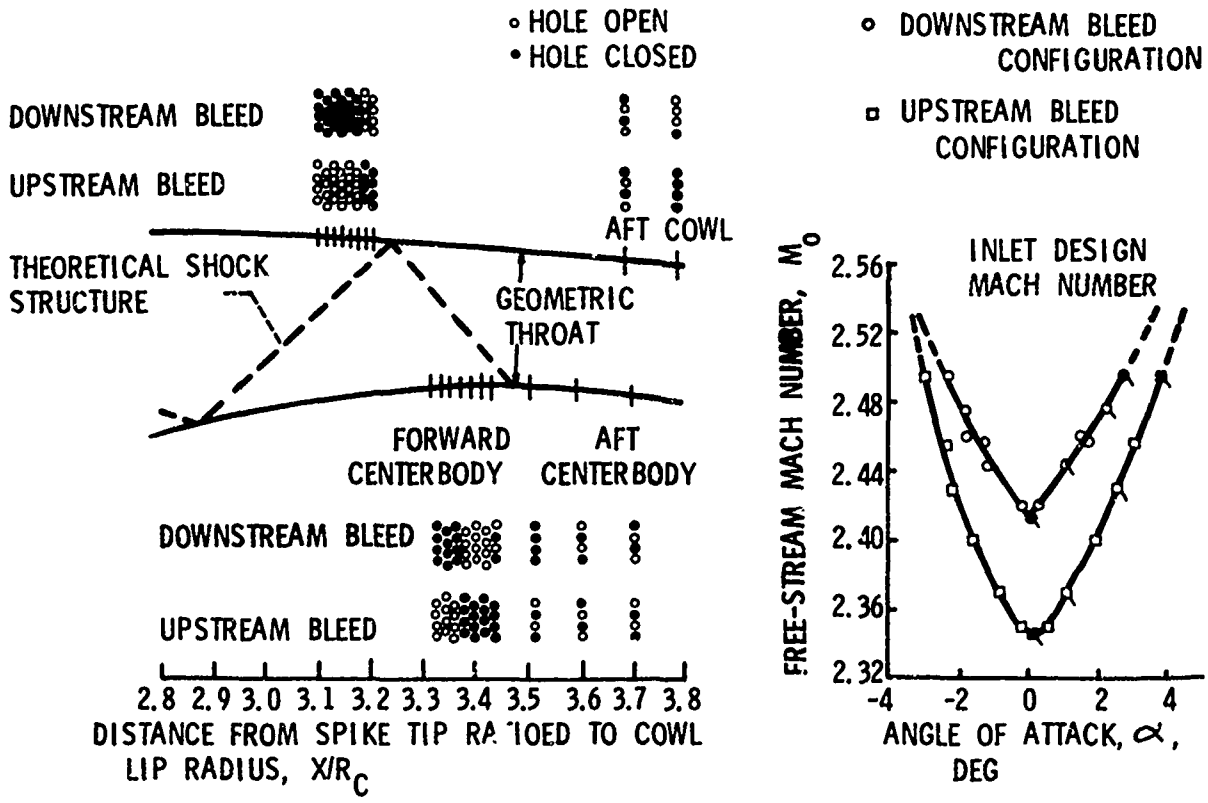

EFFECT OF BLEED DISTRIBUTION ON MIXED COMPRESSION INLET STABILITY

Figure 3–21

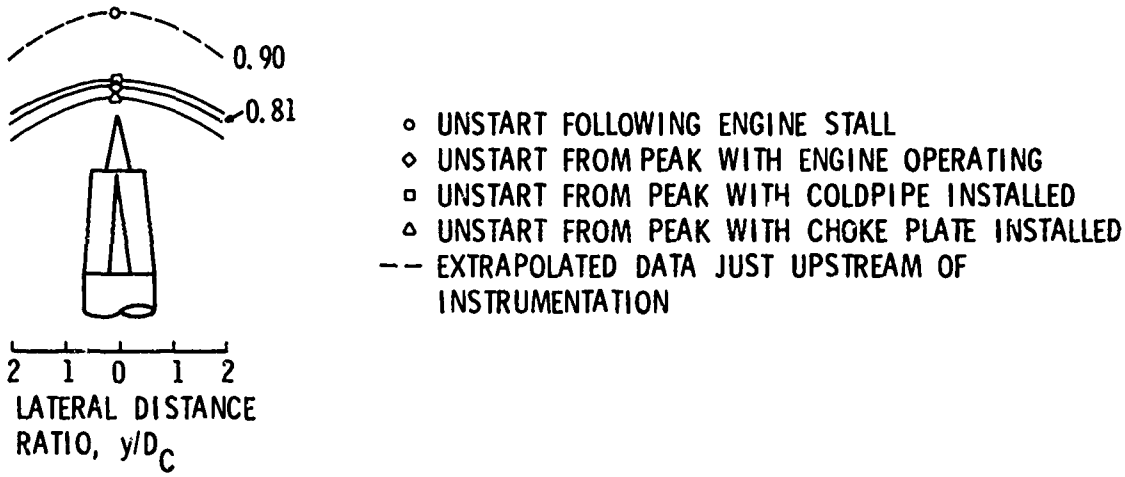

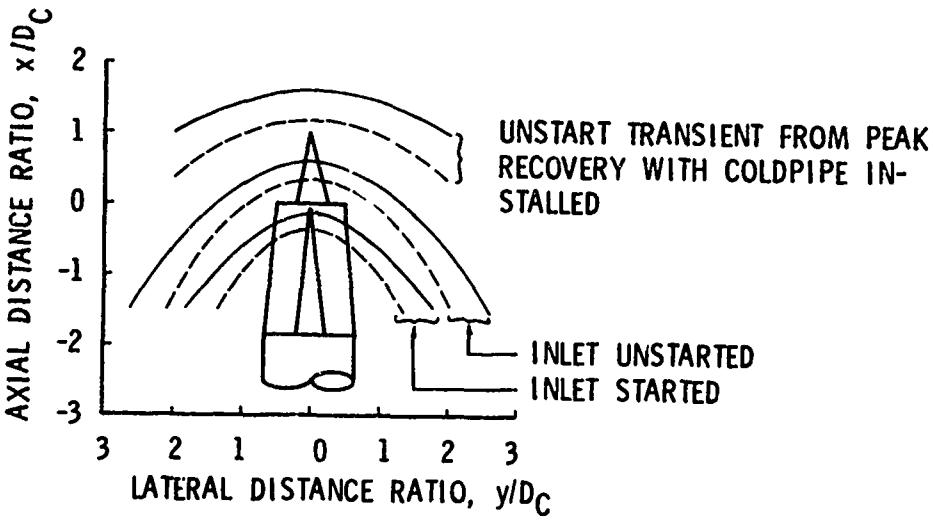

	WING BOUNDARY LAYER THICKNESS PARAMETER, δ/D_C	WING-TO-COWL LIP SPACING RATIO h/D_C	WING-TO-COWL LIP SPACING h/δ
---	0.128	0.223	1.74
——	.204	.382	1.87

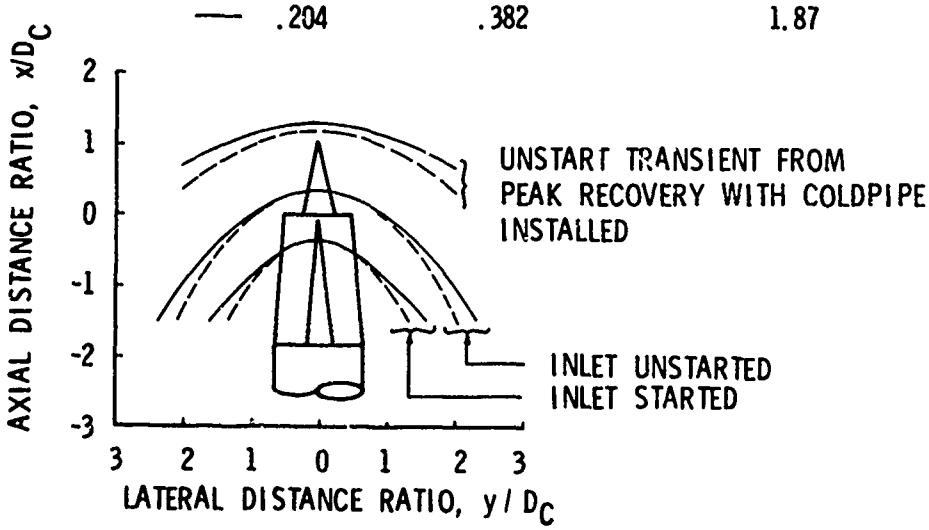

EFFECT OF BOUNDARY LAYER THICKNESS ON EXTENT OF INLET SHOCK AND WING BOUNDARY LAYER INTERACTION, M_0 =2.5

Figure 3–22

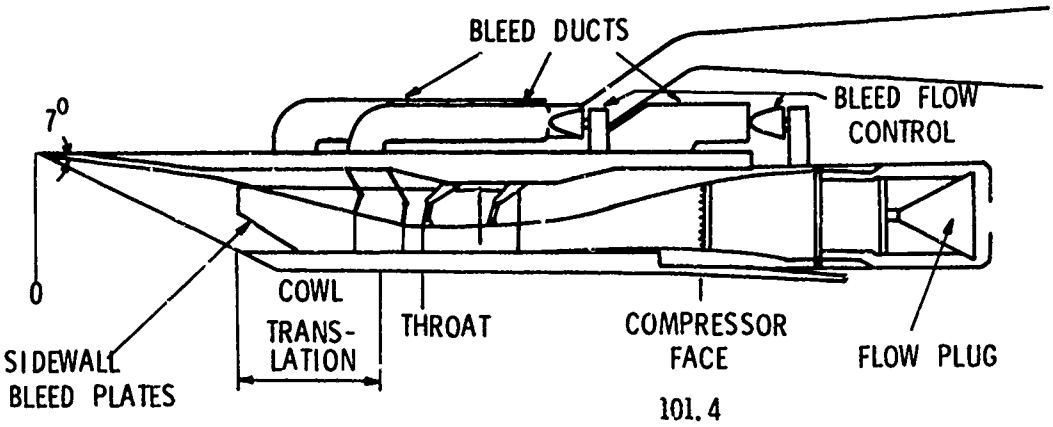

MACH 3.0 DESIGN TWO-DIMENSIONAL MIXED COMPRESSION RESEARCH INLET

Figure 3–23

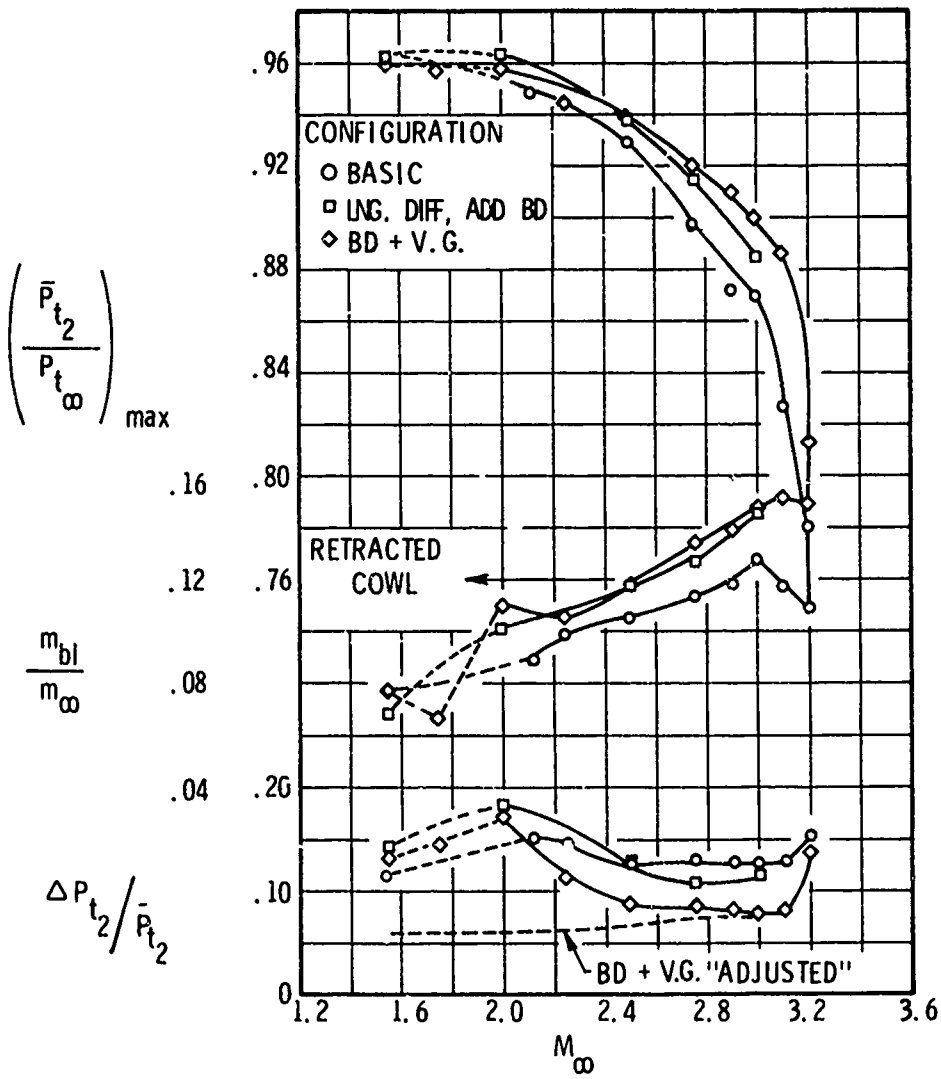

2-D INLET PERFORMANCE, EFFECT OF VORTEX GENERATORS

Figure 3–24

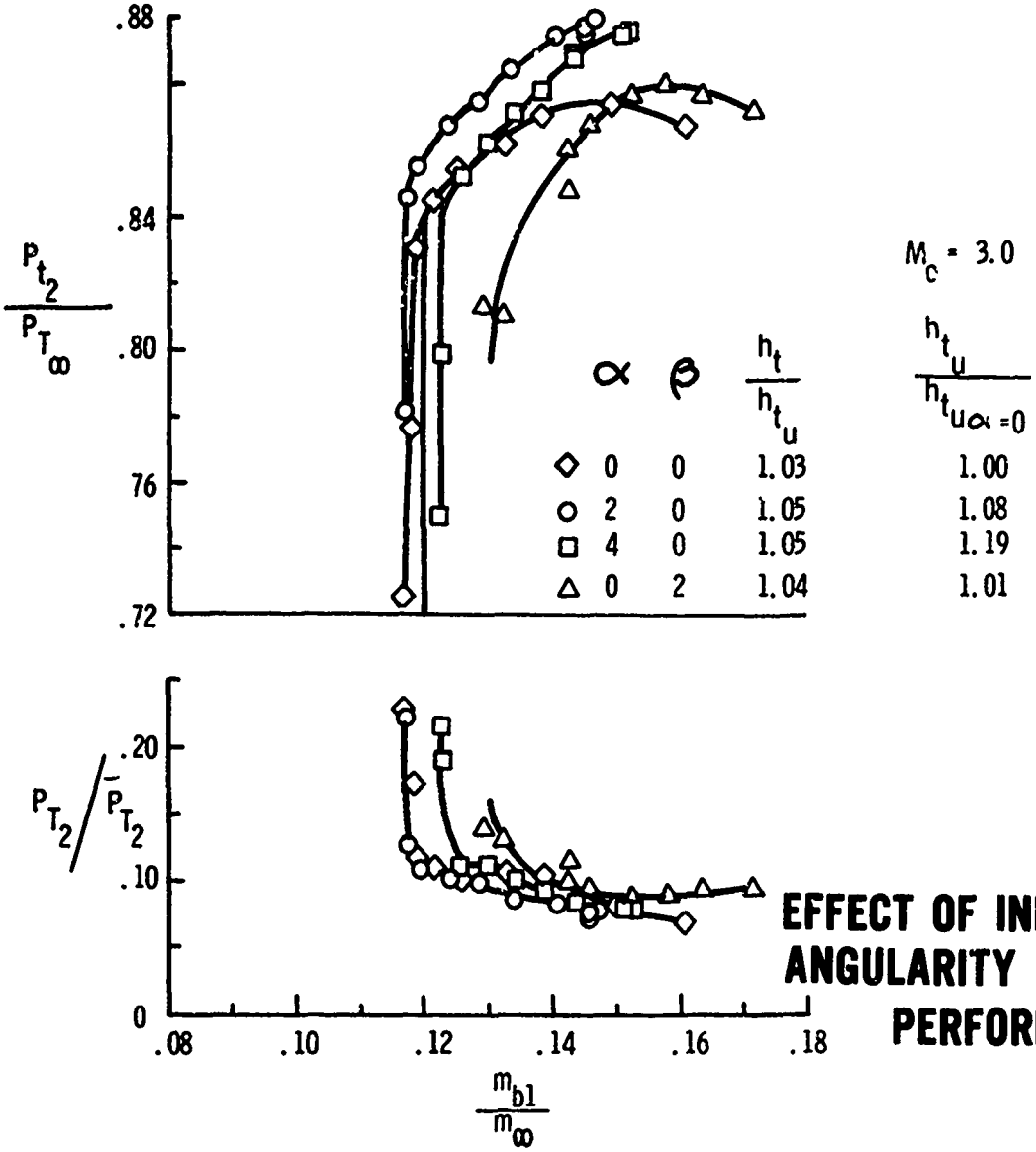

EFFECT OF INLET FLOW ANGULARITY ON INLET PERFORMANCE

Figure 3–25

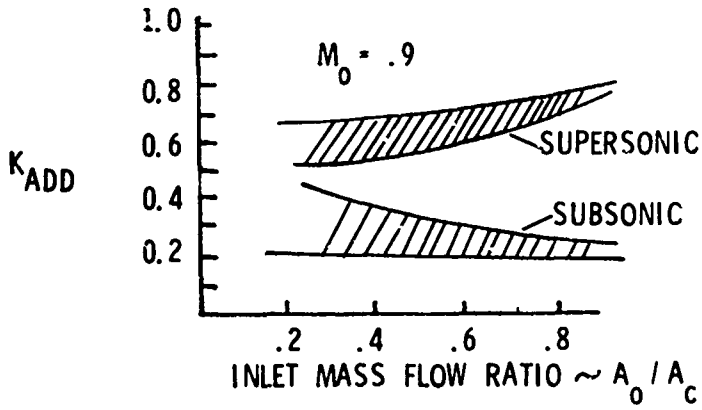

EFFECT OF INLET DESIGN ON SPILLAGE DRAG

Figure 4–1

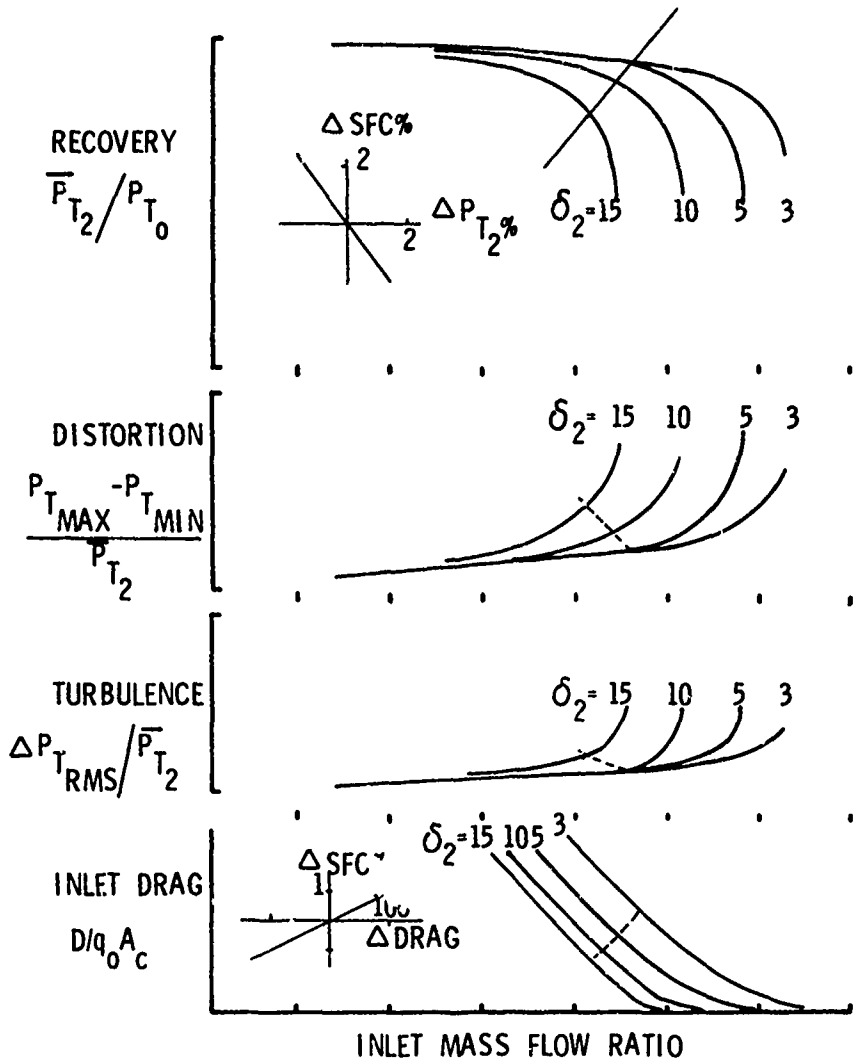

2-D VARIABLE RAMP INLET PERFORMANCE CHARACTERISTICS

Figure 4–2

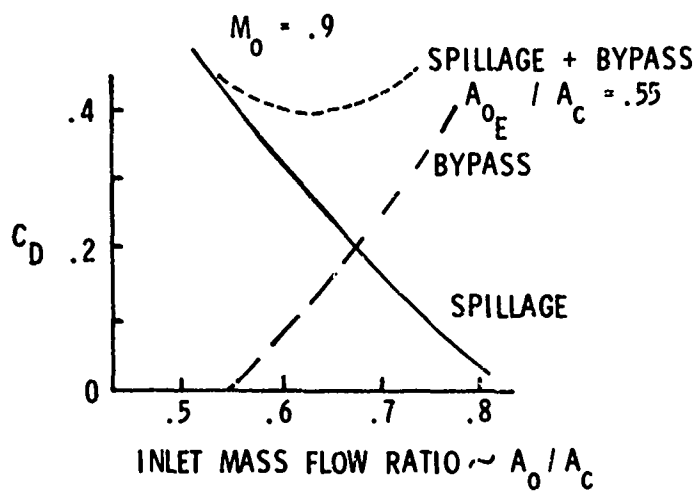

TRADEOFF OF SPILLAGE AND BYPASS DRAG

Figure 4–3

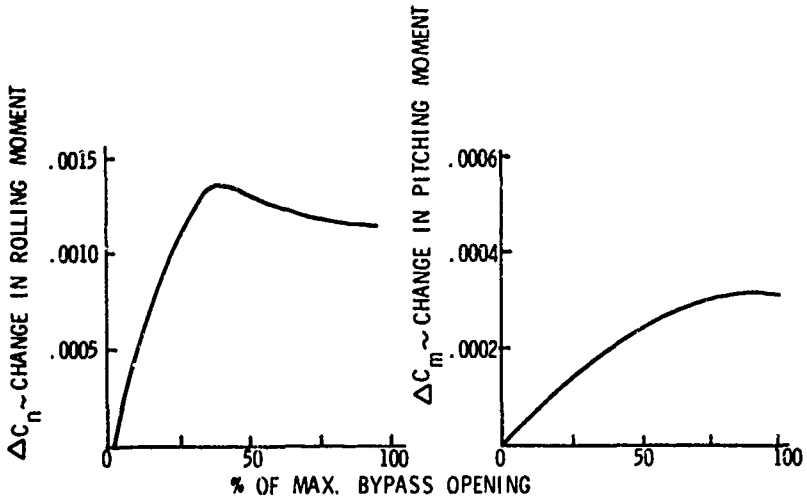

EFFECT OF BYPASS OPERATION ON AIRCRAFT STABILITY

Figure 4–4

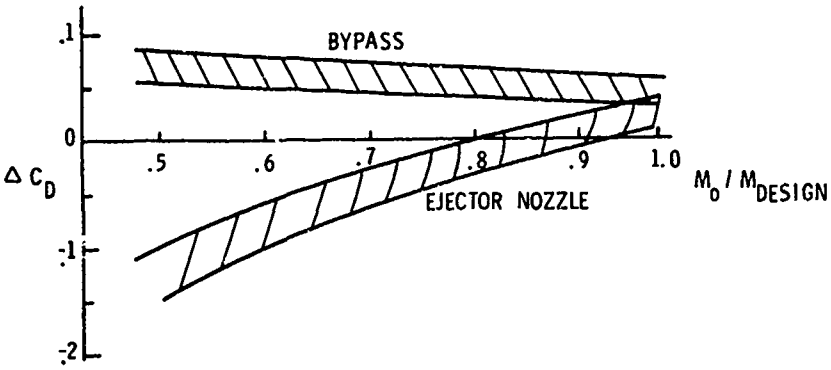

EFFECT OF SECONDARY AIR SYSTEM ON INLET DRAG

Figure 4–5

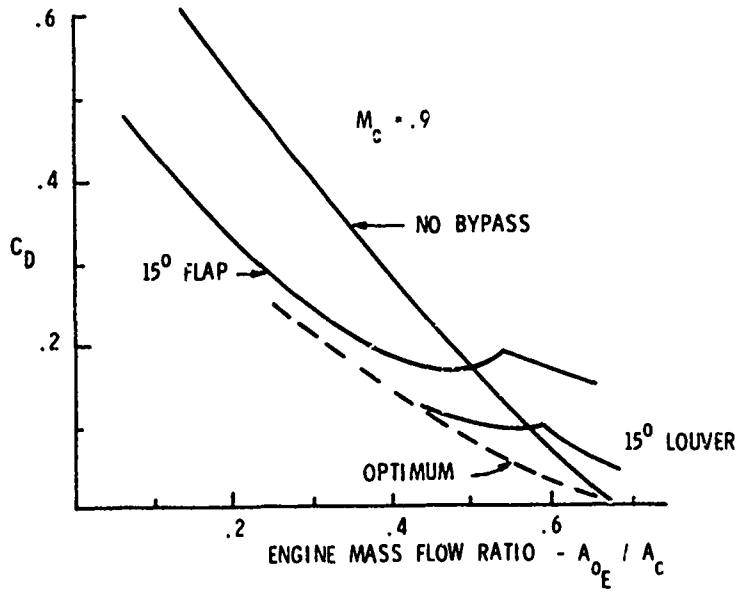

EFFECT OF BYPASS DESIGN ON INLET DRAG

Figure 4–6

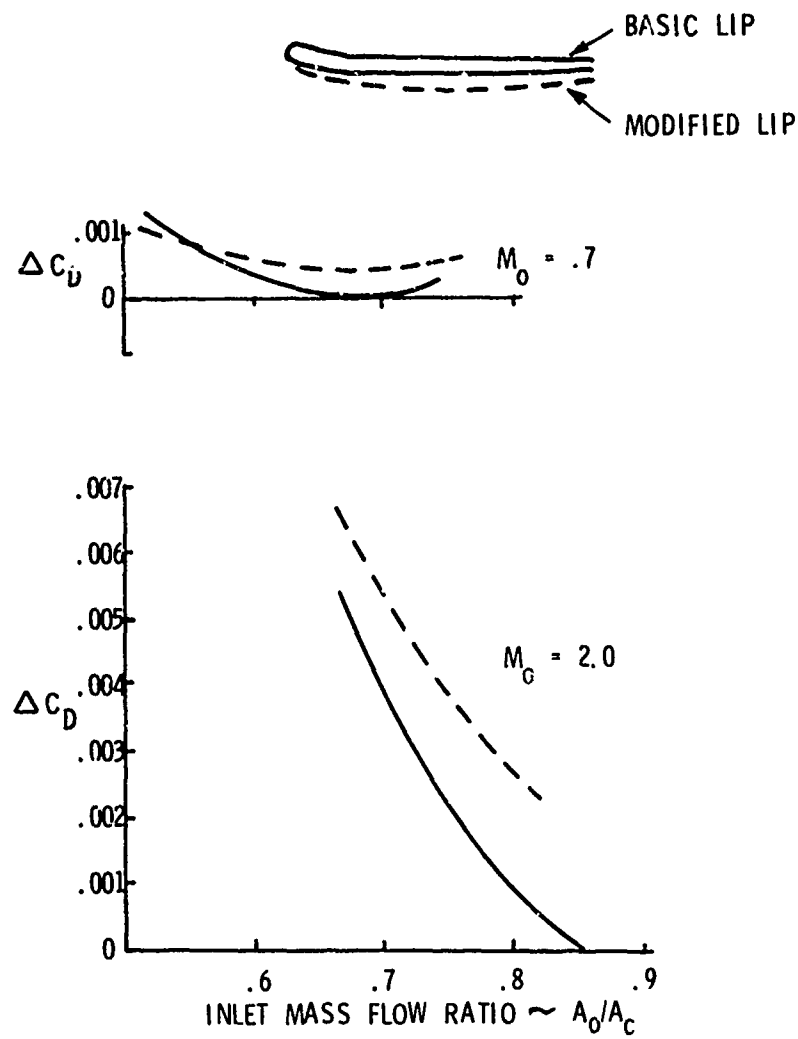

EFFECT OF LIP SHAPE ON INLET DRAG

Figure 4–7

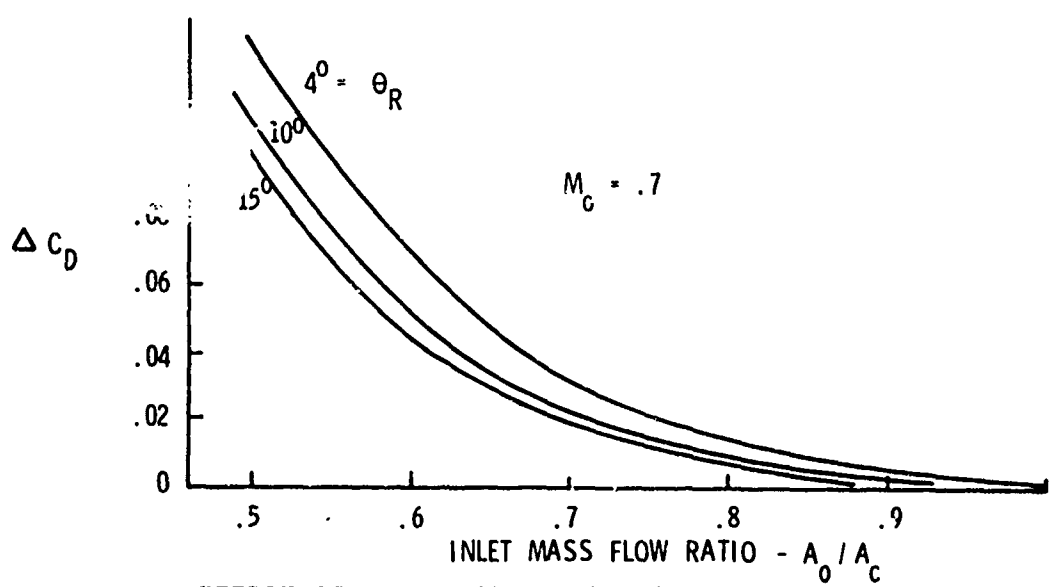

EFFECT OF INLET RAMP ANGLE ON INLET DRAG

Figure 4–8

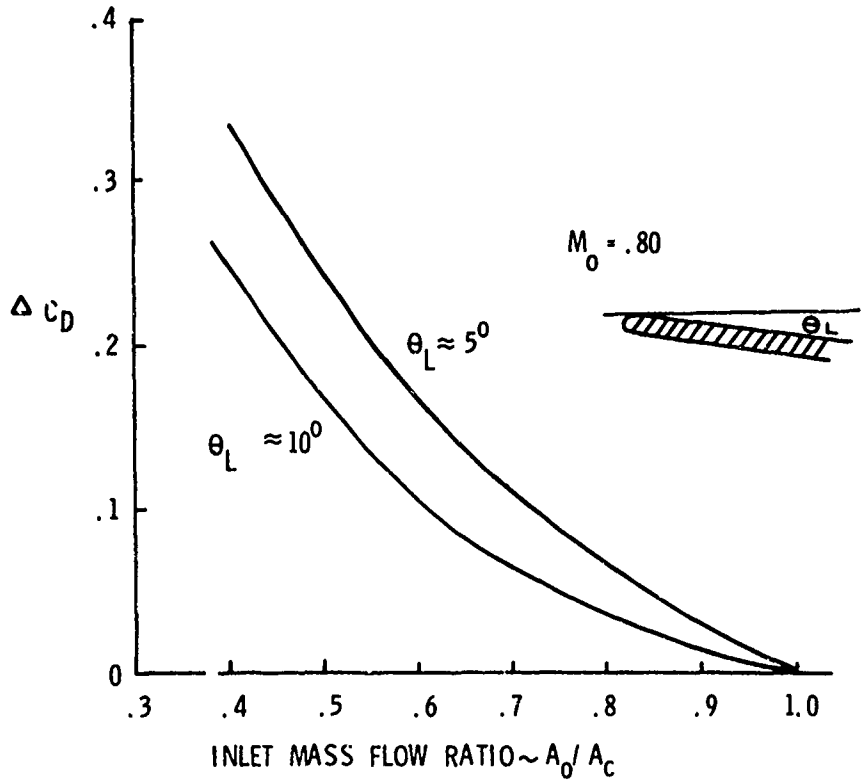

EFFECT OF INTERNAL LIP ANGLE ON INLET DRAG

Figure 4–9

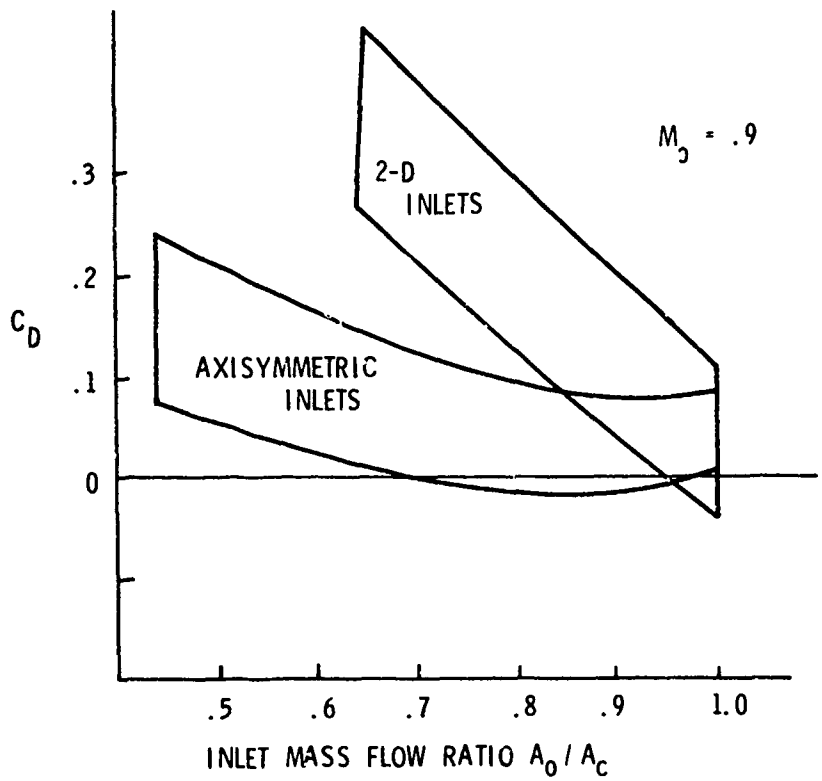

EFFECT OF INLET SHAPE ON INLET DRAG

Figure 4–10

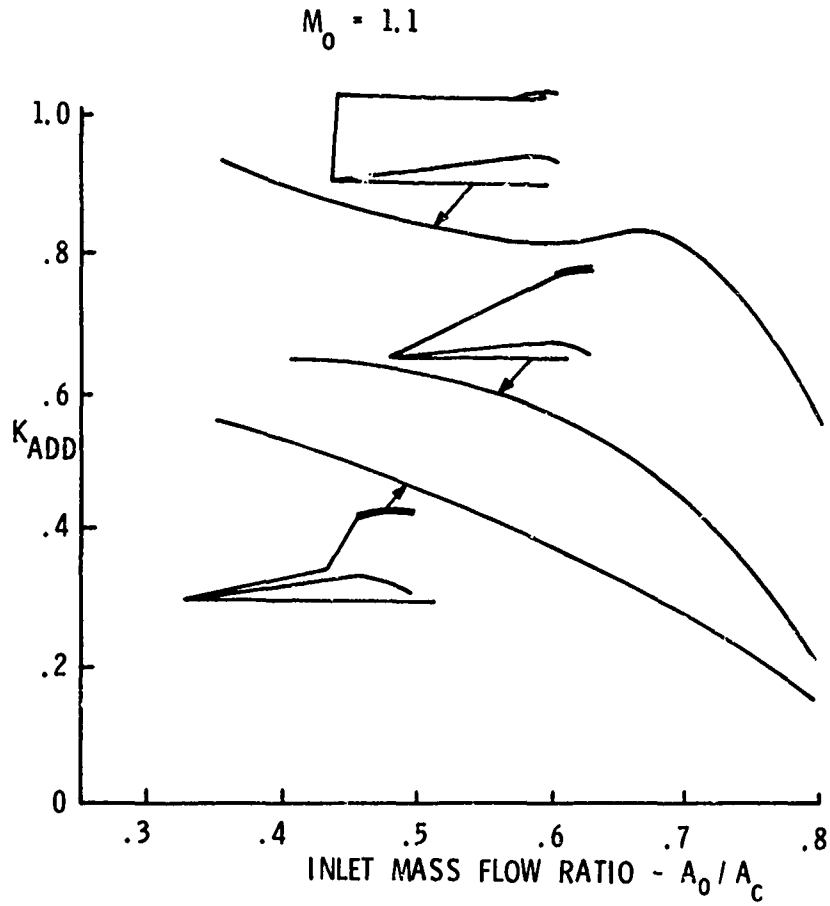

EFFECT OF SIDEPLATE SHAPE ON K_{ADD}

Figure 4–11

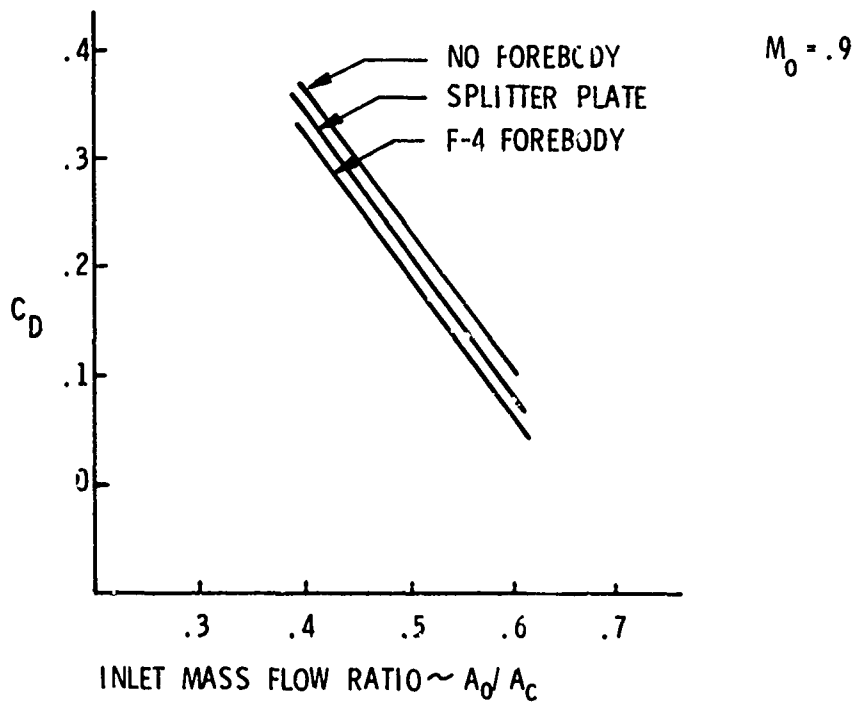

EFFECT OF FOREBODY SIMULATION ON INLET DRAG

Figure 4–12

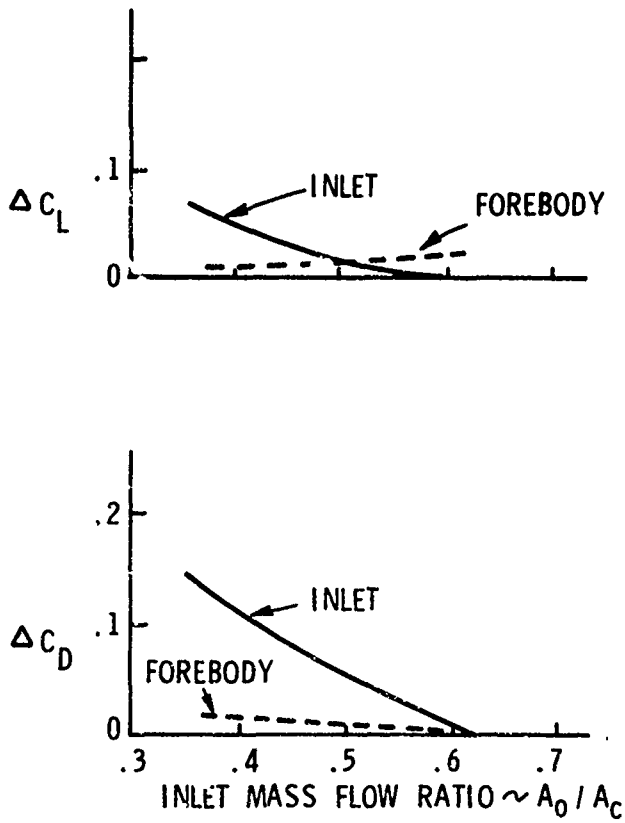

EFFECTS OF INLET MASS FLOW ON INLET AND FOREBODY LIFT AND DRAG

Figure 4-13

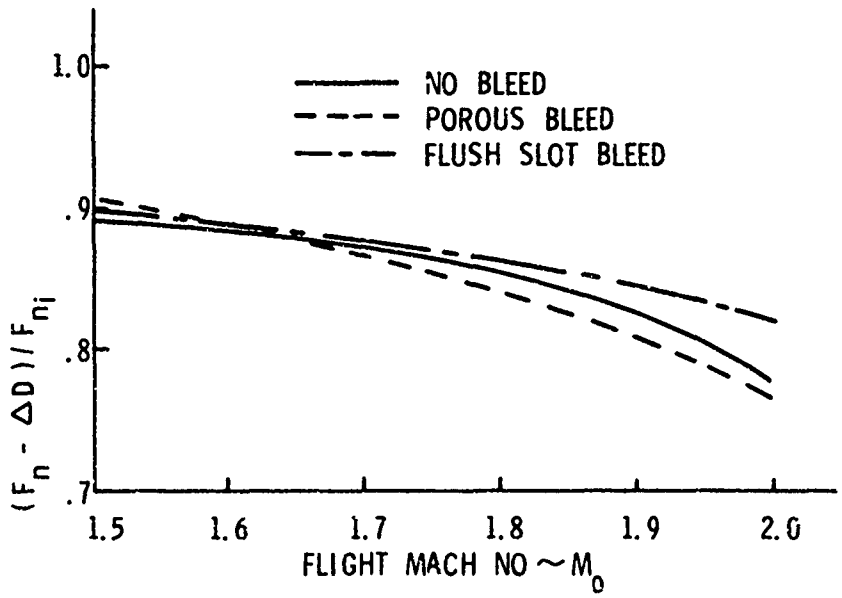

EFFECT OF BLEED SYSTEM DESIGN OF INSTALLED PERFORMANCE

Figure 4-14

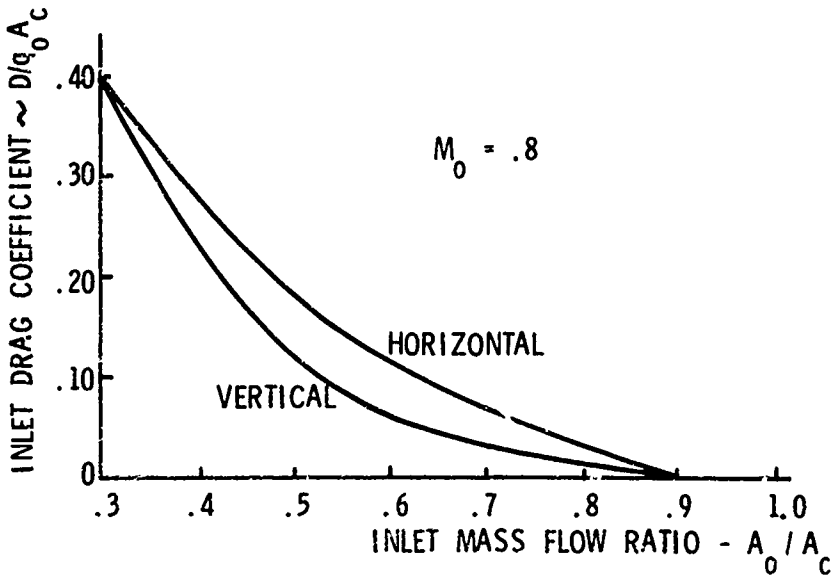

EFFECT OF ORIENTATION ON INLET DRAG

Figure 4–15

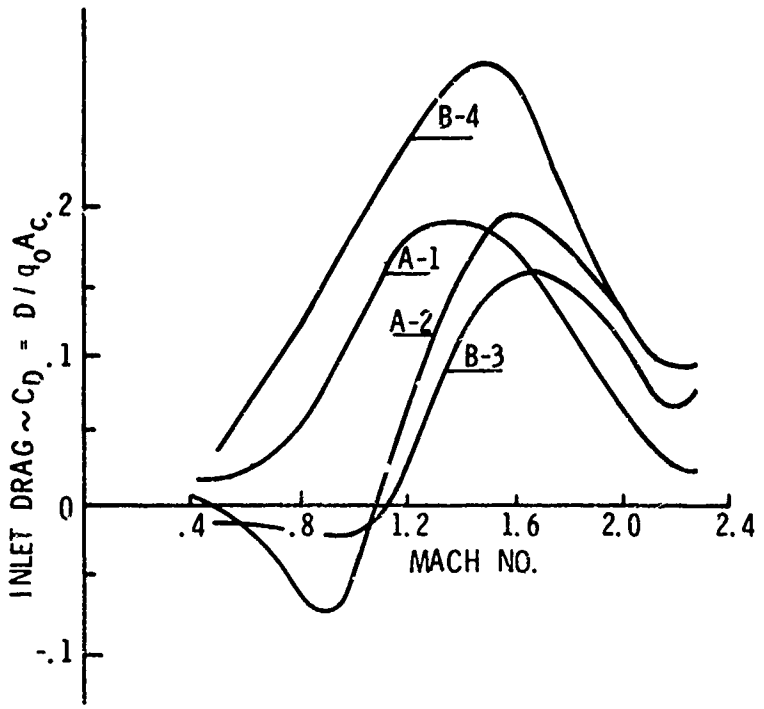

INLET DRAG CHARACTERISTICS

Figure 4–16

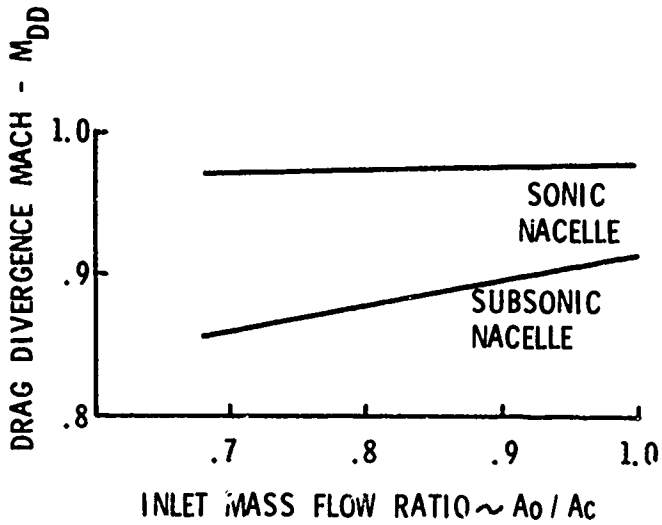

EFFECT OF NACELLE SHAPE ON DRAG DIVERGENCE MACH

Figure 4–17

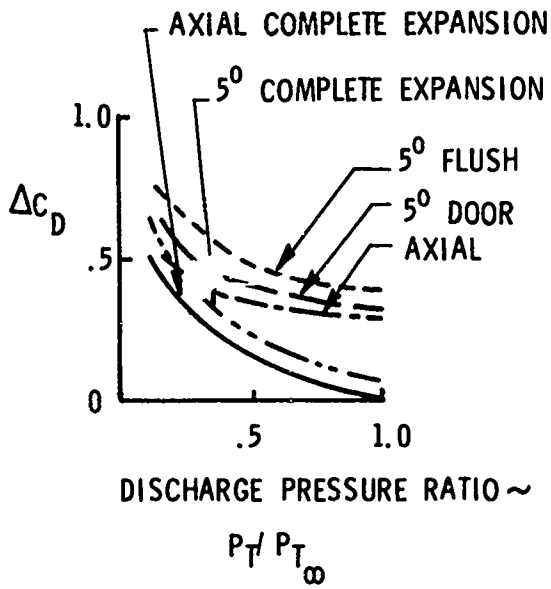

EFFECT OF BLEED SYSTEM DESIGN ON INLET DRAG

Figure 4–18

EXPERIMENTAL DETERMINATION OF INLET CHARACTERISTICS AND INLET AND AIRFRAME INTERFERENCE

by

E. C. Carter

Aircraft Research Association Ltd.
Manton Lane, Bedford, U.K.

SUMMARY

This lecture will cover basically three items; the measurement of the interference of the inlet on the airframe, the measurement of the interference of the airframe on the inlet and the measurement of the performance of the inlet/airframe combination as a whole. For some configurations and some speeds these divisions may be straightforward, for others it is only possible to consider the whole combination.

The experimental methods of determining internal and external forces are reviewed. The use of complete aerodynamic force models and partial models is discussed including the use of the full and half model tunnel techniques. Particular attention is given to drag, both basic and spillage drag, and the special techniques and accuracies required. Where necessary distinction is drawn between the use of different techniques for different inlet applications, e.g. podded installations above and below the wing and on the rear fuselage, and integrated installations on supersonic transports and fighters. Integral parts of the inlet/airframe combination such as bleeds, diverters and dump doors are considered in the experimental methods. In order to optimise inlet and airframe integration, measuring methods for flow environment and visualization are discussed.

The measurement of steady state engine face flow and distortion is discussed including the design of rakes and their interference, pressure recording methods and displays. Methods of surge simulation are described and associated unsteady measurements in the inlet. Measurement of mass flow and calibration techniques are discussed.

In the review of these methods the shortcomings of the present techniques are pointed out and where possible alternative proposals are made. These on occasion involve the use of engine simulators which are briefly described. Interference effects due to transonic tunnel flow and due to the testing methods themselves are considered, as are Reynolds number effects and methods of model scaling.

EXPERIMENTAL DETERMINATION OF INLET CHARACTERISTICS AND INLET AND AIRFRAME INTERFERENCE

by

E. C. Carter
Aircraft Research Association Ltd.
Manton Lane, Bedford, U.K.

INTRODUCTION - INLET AND AIRFRAME INTERDEPENDENCE

Transport Aircraft

For simplicity of design and test analysis a propulsion system completely independent of the airframe is most desirable. This is most nearly achieved with the large subsonic transport aircraft with underwing podded installation. The inlet is mounted well forward on the wing and tilted and toed to pick up an approach flow environment almost independent of the supporting airframe. Such an arrangement can be optimised at a design point to give intake performance equivalent to that of the isolated intake. Early designs like the B.707 and C5A had relatively long pylons which aided the independence of inlet and airframe, but currently for reasons of engine size, undercarriage height and wing position the tendency is for pylons to be greatly reduced in height with a consequent increase in inlet/wing dependence. Whilst still considering the large transport, as we move into the transonic regime the tendency is to integrate designs for low drag and area rule. Rear fuselage boundary layer ingesting intakes or integrated nacelle fuselage designs will aim at high drag-rise Mach number and a low magnitude of transonic drag rise.

For the large supersonic transport the integration philosophy has diverged into two schools - the Concorde,XB-70A,TU-144; and the Boeing supersonic transport. The former takes advantage of reduced frontal area with buried engine installations whilst accepting airframe and boundary layer interference on inlet performance; the latter takes inlet air free from viscous interference and with possible favourable interference but accepts a larger wetted area and pylon installation penalties. It is perhaps debatable where the demarkation lies between a pylon and a diverter in these configurations!

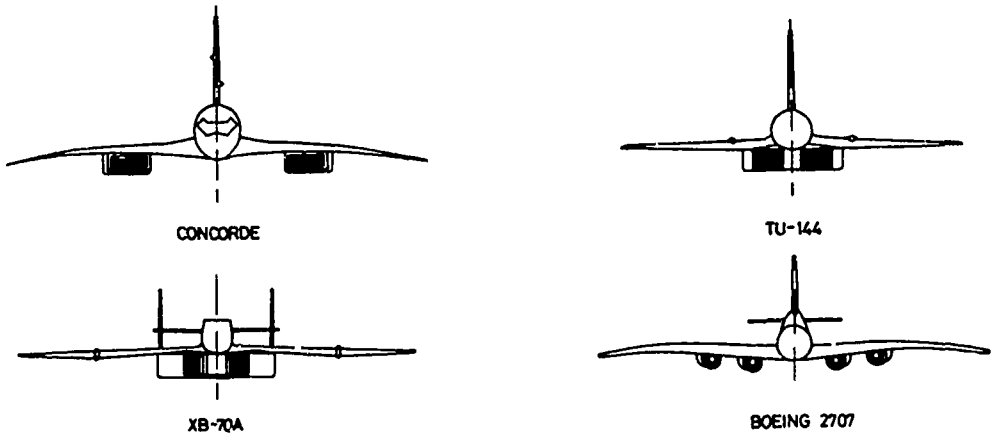

FIG.1. LARGE SUPERSONIC TRANSPORTS

Fighter Aircraft

By the very nature of the operational requirements most fighters fall into the integrated-design category irrespective of speed. For these cases, whilst design point performance is important, the off-design behaviour often dictates the final chosen configuration. Sensitivity to local Mach number changes and gradient, flow angle and body vortices strongly influence the layout although the number of different configurations, produced to meet a given specification, still remain surprisingly large. In general the fighter types cannot be so easily categorised as the transport, each case needing to be considered in its own particular application. For this reason inlet testing methods on fighters often need to be adapted to the particular configuration.

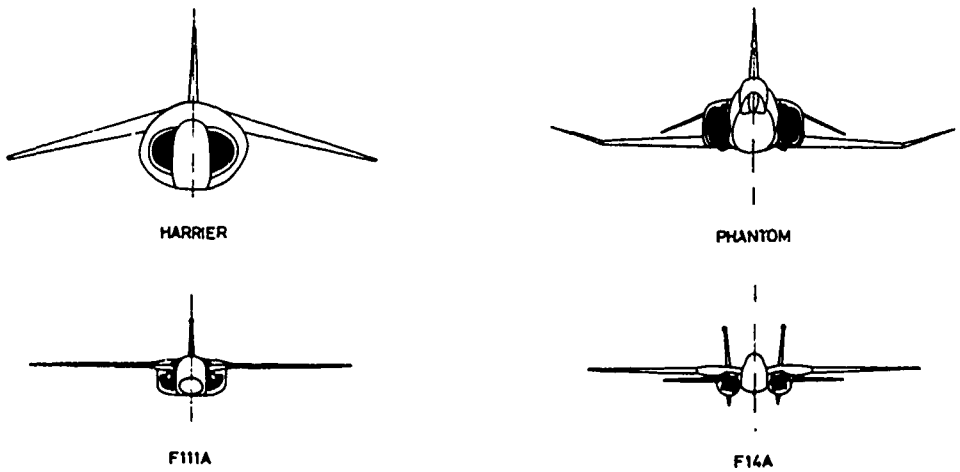

FIG.2. STRIKE FIGHTERS

Testing Requirements

Let us consider firstly what information the designer requires from his wind tunnel tests:

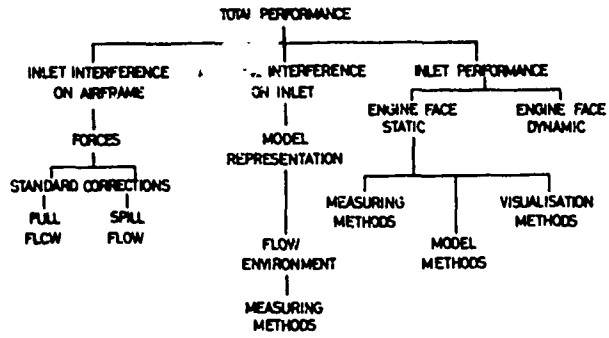

FIG.3

The methods of approach and the relative importance of the different items will be very dependent upon the particular aircraft design, its application, and speed. Careful consideration must be given to the breakdown of the tests into different models, with due allowance for the interaction of related effects, e.g. exhaust and inlet flows on the high by-pass pod.

1. INTAKE INTERFERENCE ON AIRFRAME

1.1. General corrections for internal duct flow

First in the list of all test schedules is the aerodynamic force and moment model. This is the datum model that carries the bulk of all the project testing. This is the model around which all other tests must revolve, their object being to provide correction increments to apply to the datum results. It is important that this model be very carefully planned from the start as an incorrect inlet flow representation will create a need for correction which might otherwise be avoided. It is usually axiomatic that this model will either have faired or free flow ducts, the present situation on model engines not yet being sufficiently far advanced for use in general routine testing.

Considering firstly the free flow duct, if the mass flow ratio is made correctly representative of the full scale flight conditions then the momentum of the inlet streamtube is a correctly scaled representation of the full scale momentum, hence the forces interacted between the inlet and entry streamtube will be fully representative. In these circumstances no correction needs to be made for these inlet forces and moments. The same arguments may not however be applied to the duct exit which for a free-flow model cannot in any way be representative of the full scale force and moment of an efflux. Hence in the design of this model it is preferable to make the inlet as nearly representative as possible in its mass flow capacity, by oversizing the exhaust nozzles if necessary, so that the final results will not require correction for both an unrepresentative inlet and an exhaust.

The generalised equations for the forces and moments due to internal duct flow are:

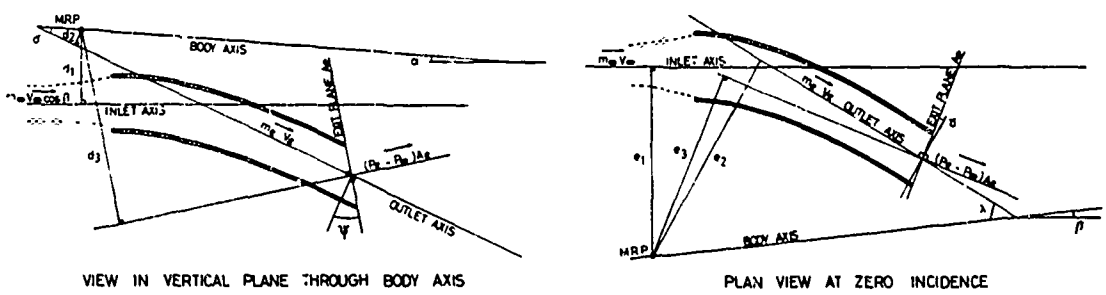

FIG.4

For stability axes:-

Drag $$D_I = \rho_\infty V_\infty^2 A_\infty \cos\beta - \left[(p_e-p_\infty)\cos(\sigma+\alpha-\psi)\cos(\lambda-\gamma)+\rho_e V_e^2 \cos\psi\cos(\sigma+\alpha)\cos\gamma\cos\lambda\right]A_e$$

Lift $$L_I = \left[(p_e-p_\infty)\sin(\sigma+\alpha-\psi)\cos(\lambda-\gamma)+\rho_e V_e^2 \cos\psi\sin(\sigma+\alpha)\cos\gamma\cos\lambda\right]A_e$$

Pitching moment $$m_I = -\rho_\infty V_\infty^2 A_\infty d_1.\cos\beta+\rho_e V_e^2 A_e d_2\cos\psi\cos\gamma + (p_e-p_\infty)A_e d_3\cos(\lambda-\gamma)$$

Sideforce $$Y_I = -\rho_\infty V_\infty^2 A_\infty \sin\beta + \rho_e V_e^2 A_e \cos\psi\cos\gamma\sin\lambda + (p_e-p_\infty)A_e\sin(\lambda-\gamma)$$

Yawing moment $$n_I = \rho_\infty V_\infty^2 A_\infty e_1 - \rho_e V_e^2 A_e e_2\cos\psi\cos\gamma - (p_e-p_\infty)A_e e_3\cos(\sigma-\psi)$$

The process of correcting model results measured with these duct forces and moments to full scale requires a knowledge of the differences in all the component items between model and full scale. In general the only terms differing significantly between model and full scale are A_e, ρ_e, p_e and V_e at the exhaust. If the captive streamtube area A_∞ is made representative then all the terms associated with the inlet momentum are fully representative of flight and so can be eliminated as correction terms in the above equations

(including ram drag of course). If however it is not possible to make the inlet flow conditions representative then it is necessary to determine a ΔA_∞ and values of e_1 and d_1. ΔA_∞ is relatively easy to measure but the position of the infinite streamtube e_1 and d_1 is much more difficult.

Drag of course, remains the exception by the nature of the definition of standard internal drag which corresponds to the standard net thrust, hence the elimination of the entry ram drag term because of its correspondence with the full scale ram drag would give values for the aircraft external drag much larger than those normally used, these values would then have to be used with gross thrust for performance calculations.

1.2. Datum Flow Representations

1.2.1. Underwing pod installations

The inlet is the least of the problems associated with the underwing pod installation. In order to minimise inlet flow distortions the designer places his inlet well ahead of the wing leading edge and adjusts the inlet centreline to align with local flow at cruise. The inlet mass flow may be correctly represented by the use of a simple free flow nacelle with appropriately sized exit, for a streamwise subsonic duct the net standard drag due to internal flow is

$$\Delta C_D = \frac{A_e}{A_{ref}} \left[\left\{ H(C_T - C_{p_e}) + \frac{2q_e}{q_\infty} \right\} \theta - C_T \right]$$

where the isentropic thrust coefficient $C_T = \frac{1}{q_\infty} \left\{ (p_e - p_\infty) + \rho_e V_e (V_e - V_\infty) \right\}$

$$C_{p_e} = \frac{p - p_\infty}{q_\infty} \; ; \; H = \frac{\delta^*}{\theta} \quad \text{at exit e ;} \quad \theta = \text{Momentum thickness at exit.}$$

For a choked duct one of the many standard internal drag equations may be used.

$$\Delta C_D = \frac{2A_\infty}{A_{ref}} - \frac{A_e}{A_{ref}} \left[C_{p_e} + \frac{2q_e}{q_\infty} \right]$$

the values of C_p and q_e/q_∞ being obtained by integration over the exit.

Interference of the intake flow on the wing flow can only be measured in a qualitative manner by using pressure plotting and even in these circumstances a true evaluation of the total interference is difficult because of the interchange of buoyancy forces between wing and nacelle which do not necessarily constitute drag. Care should be exercised in the interpretation of interference results, favourable wing interference on the pod is very easily cancelled by unfavourable wing interference.

The representation of the plume shape on the model nacelle for a high by-pass ratio is the major difficulty. For simple tests a shaped aft fan cowl is used assuming that it will have a representative interference. For more complex tests the pod may be replaced by a model fan engine, which can represent at the same time both the inlet and exit flows; the capture ratio of the inlet being reduced by (By-pass ratio)$^{-1}$ and the fan exit being representative of the total pressure and temperature.

Measurements with these simulations on configurations of the type shown in fig.5 are used to study the combined effects of inlet and exit flows on local airframe surfaces. These effects are measured as a whole and the use of this complex simulation can only be justified in its representation of the exit interference effects.

FIG.5

A limited amount of data is available on the interference of podded inlets on wing flows, it might be argued from the foregoing that this effect in isolation is of little importance if the jet flow predominates. However it can also be argued that spill flow (and all inlets do spill in relation to their highlight area) could have a more significant effect on the wing flow characteristics than the undersurface interference of the jet. If spill flow is looked upon as a local increase of wing incidence, and jet interference is looked upon as a modification of local trailing edge pressure then either of these effects could tilt the balance of a critically designed wing section. It is assumed that this has not occurred on current aircraft or that clever design has obviated its effects, but in the field of future wing designs for very high subsonic Mach numbers there will be little margin for underdesign to cope with an interference which causes premature trailing edge separation and forward movement of the upper surface shock.

It is in this realm of future testing that Reynolds number effects will predominate. Future designs will incorporate all the potential advantages of the relatively thin boundary layers of full scale flight, trailing edge flow separation will dictate the degree of permissible rear loading and premature breakdown of the wing upper surface flow due to inlet interference could be catastrophic - not only to drag and economics, but to buffet and handling in general. The spill conditions of cruise flight capture ratios may be built into the wing design but the engine failure case could be more critical than it is at present. This short digression is made to emphasise the importance of intelligent boundary layer representation at current test Reynolds numbers and to demonstrate the need for high Reynolds number facilities - at least for limited check-out purposes.

1.2.2. Over-wing installations

Whilst this may be a somewhat unusual configuration its presence cannot be ignored. In the present state of the art, as far as wing nacelle integration is concerned, it is unlikely that this type of design will be seriously contemplated for high Mach number performance. For a particular

configuration of this type two interference factors have been the subject of study.

FIG.6.

In the first experiment, fig.6, the effects of inlet spill flow were measured on rotating rakes in the plane of the fan cowl exit, using the momentum defect technique. This model was a specially enlarged version of the aircraft simulating accurately only the strictly relevant parts. These results could be compared with isolated nacelle results to determine the effects of the presence of the wing and fuselage, and in particular the wing shielding and leading edge separation effects at high incidence and Mach number. The technique was quantitatively valuable in providing the drag of the nacelle-pylon combination without the confusion of buoyancy forces. This model was also used to determine the interference effects of the wing leading edge and upper surface flow on the internal flow in the fan plane.

The second experiment[1] used a representative free flow duct to determine the interference on the aerodynamic handling. Experimental results indicated strong interference on the local wing upper surface which varied chordwise and spanwise and was dependent upon spillage, fig.7.

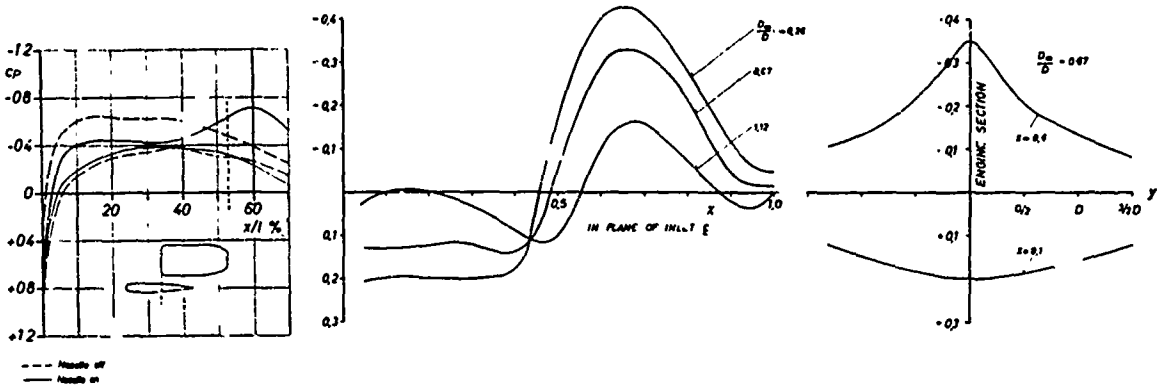

FIG.7.

The overall aerodynamic effects were measured on a conventional aerodynamic force model, fig.8, with free flow nacelle. The pitch stability was of particular concern as it was realised that the loss of wing lift associated with the interference would show mainly as a pitch change due to downwash change at the tail. The resultant effect of this was to indicate a "speed instability" in which the pitching moment for a 1g flight cruise condition showed rapid change with Mach number. Methods of correcting this problem were obtained in further wind tunnel tests on the modified model.

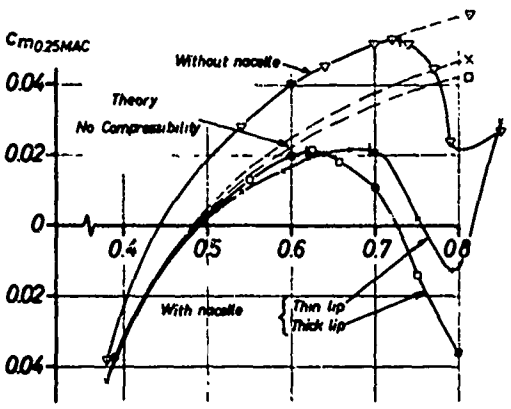

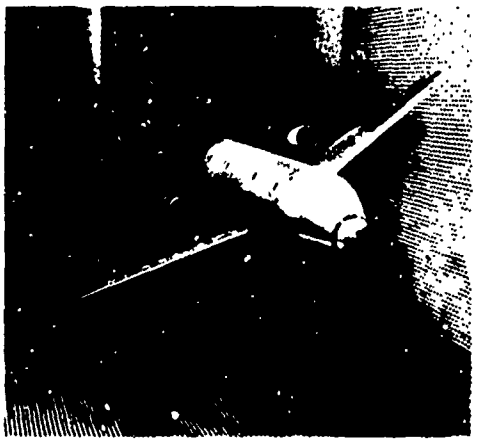

FIG.8.

1.2.3. Rear fuselage installations

Flow environment tests, described in 2.2, normally define acceptable installation areas for rear fuselage installations. The influence of the inlet and its spillage may be obtained in the same way as for the wing installation, by use of the free-flow nacelle, with the same corrections. For this configuration however, it is possible to isolate more easily the installation interference of the nacelle airframe system. This makes use of the twin sting support system, whereby the forces on the rear fuselage and nacelle are measured independent of, but in the presence of, the wing and forward fuselage.

FIG.9.

The use of this test system is best described diagrammatically:-

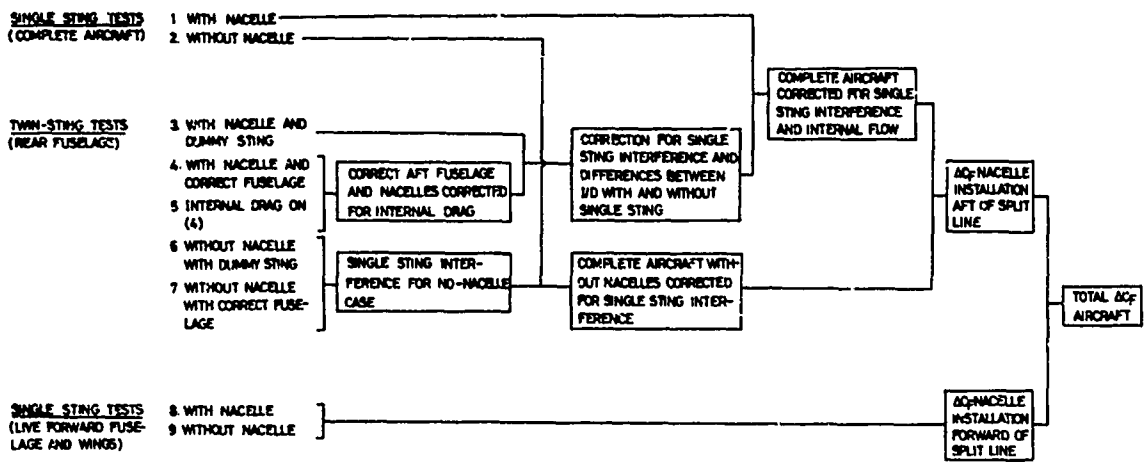

FIG.10.

The many details of this technique are beyond the scope of this lecture, some typical results[2] however are of interest.

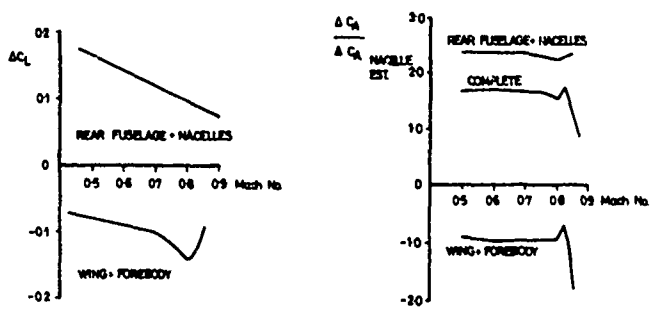

SUPER V.C10 NACELLE INTERFERENCE

FIG.11.

1.2.4. Integrated Fighter Type Configurations

This category covers a multitude of different configurations and speeds. By the very nature of the integration, the regions of interference cannot be isolated or dealt with on a piecemeal basis. It is accepted that general interference will occur and measurements are made to ensure that the effects are minimised. For this type of configuration the problems are more related to the airframe interference on the inlet which is less tolerant than the airframe.

For the aerodynamic force model the major problem is usually the choice of support system. The size of the model forces normally dictates a large sting which causes distortion near the free flow exits if their size is to be compatible with the inlet mass-flow ratio. Sting and afterbody distortion effects may be classed along with those of jet representation and can normally be simulated on special

blowing models. The inlet flow may be satisfactorily represented although varying the mass flow plug sizes can be tedious. Mutual interference of inlet and exhaust must always be considered and checked if likely to be significant. Two examples are the best way to highlight the problems, and some specific solutions.

In the first example,[3] the model was of an aircraft with twin inlets and exhaust. The exhaust was close to the rear fuselage similar to a Phantom and it was required to separate the effects of inlet flow variation and exhaust flow variation. For the inlet tests the whole aircraft was represented with free flow, hence this free-flow air exhausting from the nozzles would be at an unrepresentative pressure ratio and would give erroneous aerodynamic jet interference forces on the rear fuselage. To separate the inlet spill flow effects an extended exit duct was used which was copiously pressure plotted to determine the internal drag.

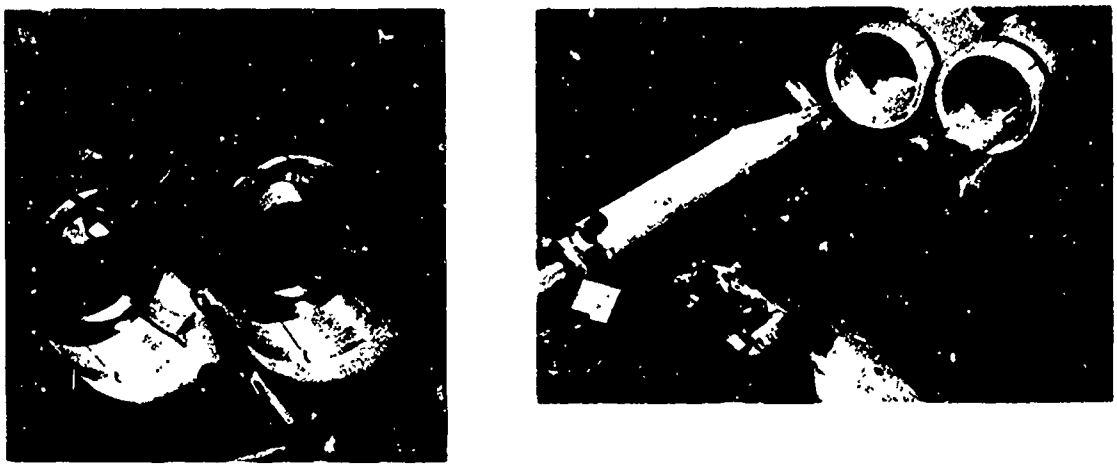

FIG.12.

To determine the basic aircraft non-spill or datum drag, the correct nozzle geometry was used, again with detailed pressure plotting. This result in conjunction with other tests enabled full separation of the various interference terms, within the limits of a cold experiment, as follows.

Test No.	Intake flow	Tailplane	Nozzle Position	Nozzle PR	Effects of :
1	Design	Yes	Correct	Recovery / W.S. Static	Datum design point
2	30% spill	Yes	Correct	"	Check datum with spill
3	Design to zero	No	Downstream	"	Spill effect
4	Faired	Yes	Correct	Approx.1 to 5	Jet effect
5	Faired	Yes	Correct	Approx.1	Datum zero jet

The second example is a model of a transonic vectored thrust aircraft which had its twin inlets feeding a single engine which in turn provided two cold forward jets and two hot rear jets. The direction of the jets was such that their influence could not be neglected in their interference on the whole aircraft flow field. The model to simulate this condition used a peripheral ejector system mounted in the model shell, this system was effectively an engine simulation in that it induced an approximately correct inlet flow and simulated reasonably well the total pressure ratios of the 4 jets - albeit cold. Conventional 6-component forces were measured on the model shell which surrounded this 'engine unit'.

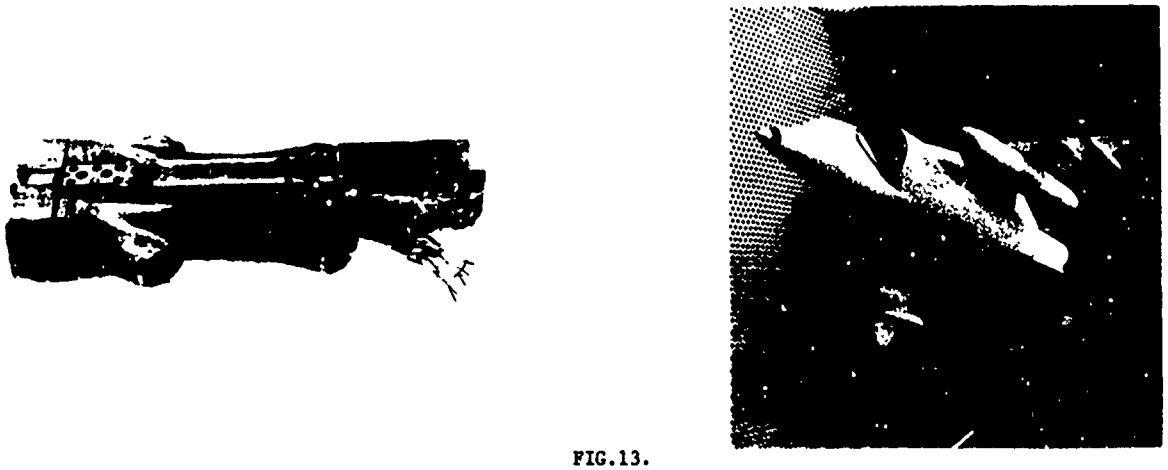

FIG.13.

This test technique was very successful, but drag was not as accurate as that measured on a conventional free flow model. In this instance the problem of external rake measurements and internal drag definition

was exchanged for the problem of satisfactory seal development with low interference and hysteresis.

1.2.5. Supersonic Transport - Slender wing configurations

Supersonic. Naturally the Concorde has dominated the European scene, demanding techniques and accuracy far in advance of those previously required. The basic supersonic aerodynamic force model was required to provide a datum drag to an accuracy better than 0.0001 in C_D. This drag figure would then be used in conjunction with the results of special tests to estimate the installed drag at a precise flight condition of fore-spill, diverter height, nozzle pressure ratio, secondary flow and many other variables.

The aerodynamic model had to be a perfect external representation with a non-spilling inlet and carefully constructed internal ducts with uniform exit flow and minimum base area. In practice, to provide a guarantee of sufficient accuracy without interference from the measuring system an auxiliary traverse gear carrying 4 pitots and a single static was used to provide a very close matrix of data from which the precise exit mass flow and momentum could be determined.

Separate calibration of the duct on a suction rig was not considered to be sufficiently accurate as the external base static pressure at the nozzle exit was variable across the exit plane due to the airframe interference and model incidence.

Two techniques of duct representation were employed:

(a) a constant area duct, with low internal drag but very non-uniform exit flow

and (b) a con-di-con duct[4] with an exit size designed to give minimum sensitivity to measuring errors in the exit plane.

In order to define the optimum duct exit, the internal drag equation is simplified from

$$D_I = m V_\infty - \int_{A_e} (p_e - p_\infty + mV)\,dA \text{ for small inlet and exit angles}$$

$$\text{to } D_I = \int_{A_e} p_e f_1(M_e)\,dA + p_\infty A_e$$

$$\text{where} \quad f_1(M_e) = \left\{ \gamma M_e^2 \left[\frac{(M.a/a^*)_\infty}{(M.a/a^*)_e} \right] - (1 + \gamma M_e^2) \right\}$$

This latter function incorporated with p_e requires the evaluation of one integration and also permits the determination of the optimum choice of M_e to minimise the magnitude of the internal drag:-

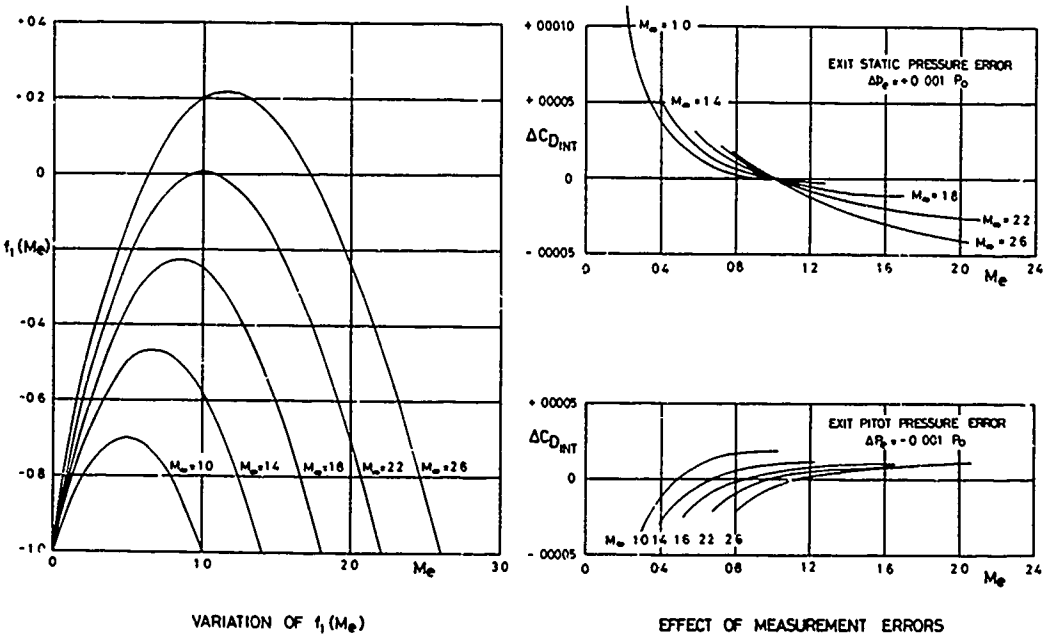

VARIATION OF $f_1(M_e)$ EFFECT OF MEASUREMENT ERRORS

FIG.14.

It will be noted from these figures that $f_1(M_e)$ is very close to zero for $M_\infty = 2.2$ and $M_e = 1.0$, in these conditions the value of $D_I \rightarrow p_\infty A_e$ both terms of which are independent of the measurements at station e. In practice of course, even for nominal sonic exit flow, local variations require elemental integration of $\left[p_e f_1(M_e)\,dA \right]$. The error curves are of interest in that they indicate a need for $M_e = 1$ to eliminate errors in p_e but varying subsonic M_e to eliminate errors in p_e. The final choice of duct design depends upon the range of M_∞ of the test and the level of absolute accuracy required. These tests provide a corrected datum result, the effects of spill are considered in 1.3.3.

Transonic. A series of tests was also required for the transonic performance including spillage. For these tests the internal shape of the duct exits was carefully faired to give a smooth contraction to a choked exit. The lower mass flow cases created a peripheral base area around the duct exits and so necessitated additional pressure plotting. Preliminary experiments showed that virtually

any external rake mounted on the base would provide interference on the absolute level of the base and duct static pressures. It was therefore essential that for transonic testing in particular, the base pressures and duct exit static pressures be measured by pressure tubes installed in the model. Total pressure profiles were obtained by multi-rake measurements which served to relate the area-weighted exit total pressure to say two reference pitot pressures in the rake. These two reference pressures could then be measured by small model-mounted pitot tubes at the same time as the base statics and duct statics and whilst the forces were being recorded. In this manner, all data was obtained in the same run, a very necessary requirement for the definition of the drag rise curve.

1.3. Effects on Inlet Spill Flow

If it is supposed that the basic force and moment results have been obtained from the standard aerodynamic model then in these tests the inlet should have been operating near its design point. In practice however because the engine demand and inlet geometry cannot be represented at all test points, it is necessary to determine the effects of this mismatch. In general, drag of primary importance in these tests, the effects on lift and pitching moment being secondary.

In principle of course it is possible to make tests on the aerodynamic model to determine the effects of spill flow. This would be done with a range of mass flow control plugs and comprehensive instrumentation in the duct exit. In practice there are various reasons why this should not be done.

(a) A special spill model can be made to a larger scale with good representation of diverters, aft spill and bleed.

(b) By reasonable aerodynamic consideration, only parts of the aircraft need be represented, hence sensitivity of particular components - drag in particular - can be enhanced.

(c) Special mass flow and momentum calibrated sections may be installed in a special model.

(d) Larger mass flow is possible in the special model by use of enlarged exits.

(e) The effect of base pressure can be measured more carefully and accurately on a special model.

(f) It is easier to install a remote moving mass flow control plug in the special model, and this permits the recording of the variation of force components directly with mass flow, in a single model test configuration.

Various different model arrangements have evolved for the determination of spill flow effects. Considering firstly the transonic pooded installation, the standard procedure is to optimise the cowl design in isolation and then by pressure plotting methods determine the interference effects of local surfaces on the installation. For wing installations these effects are generally small; for aft fuselage installations flow environment studies are a necessary preliminary to the tests on the isolated cowl.

1.3.1. Spill Drag methods for the isolated cowl (Subsonic and Transonic speeds)

Current requirements for high by-pass cowls are dictating severe design requirements. The very fact of the greatly increased mass flows which are taken through the inlet means that any spill drag increments which would be acceptable on the pure jet engine would be magnified several times for the high by-pass inlet. The size of the inlet, forces the designer into large ratios of $D_{Highlight}/D_{max}$ and the ever-increasing cruise Mach number demands high drag rise Mach number. For this reason, accurate measuring methods are needed to study the future development of inlets with high D_H/D_{max}, small L/D_{max}, and high M_{crit}. The development of the M = 1.0 transport will probably relax the small L/D requirement and perhaps reduce D_H/D_{max} somewhat but M_{crit} will obviously be predominant.

METHOD I. Cowl surface pressure plotting [5]

For the more advanced requirements with supercritical flows and shock waves, it will probably be essential to discard the determination of drag from cowl pressure plotting and boundary layer rakes. This method whilst having the advantage of copious surface pressure data for diagnostic purposes suffers from the difficulty of stagnation point definition and the calculation of additive drag,

METHOD II. Force balance [5]

These latter difficulties are avoided by the use of a force balance and internal momentum methods - as for the aerodynamic force model. This method has the advantage of measuring asymmetric cowls relatively easily.

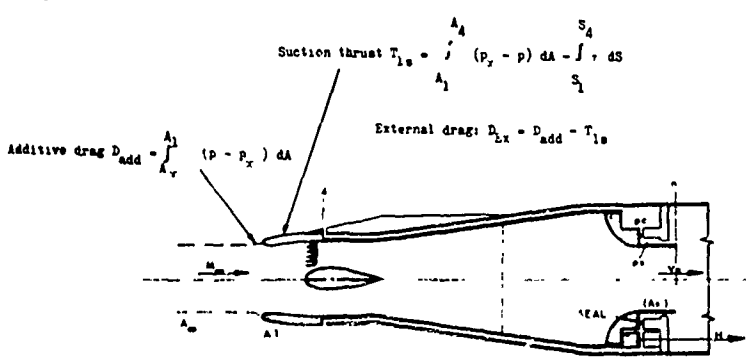

$$D_{Ex} = \dot{m}\,(V_n - V_r) + A_n(p_n - p_s) + A_d(p_c - p_x) + A_s'(p_s - p_c) - H$$

FIG.15.

METHOD III. Momentum Loss[5]

A third technique employs the momentum defect method, whereby the loss of momentum of the free stream flow which is influenced by the cowl is measured. This method requires accurate measuring techniques and does not satisfactorily provide an absolute datum drag level. However with care, accurate results of spill drag and cowl comparisons may be made.

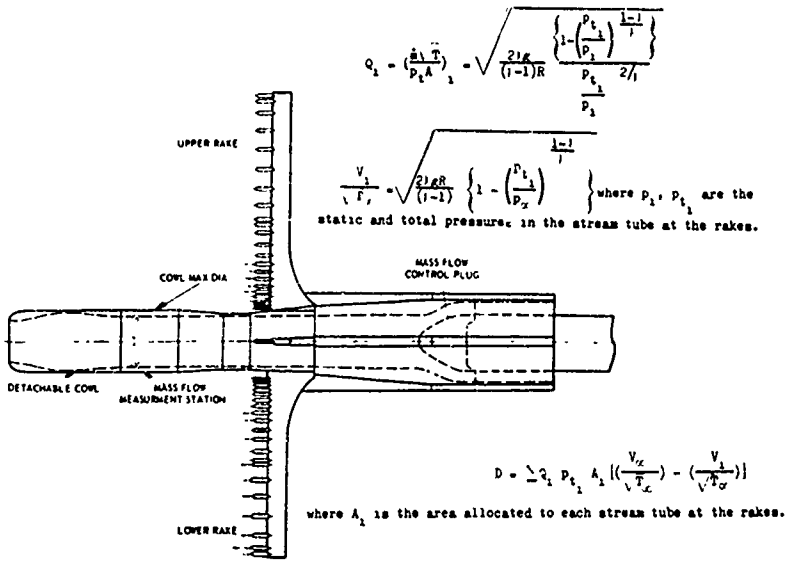

FIG.16.

Problems associated with these methods

For transonic cowls the previous assumptions of independence of forebody and afterbody are no longer valid. Rigs of the type shown in the figures must now be fully representative to the fan exit. The nacelle drag-rise condition will coincide approximately with sonic conditions at the crest and with curvatures currently applicable on short cowls for high by-pass engines the flow at the crest will be very aware of its downstream conditions. However, for free flow or sucked nacelles as used in these test rigs it is often impossible to reduce the duct diameter at the end of the cowl to be both geometrically correct and to pass the required inlet mass flow - for the model tests we do not have the fan compression to assist the reduced exit size. So it is hoped that the shape of a geometrically shortened aft cowl can be made sufficiently representative to provide correct cowl flow at the crest.

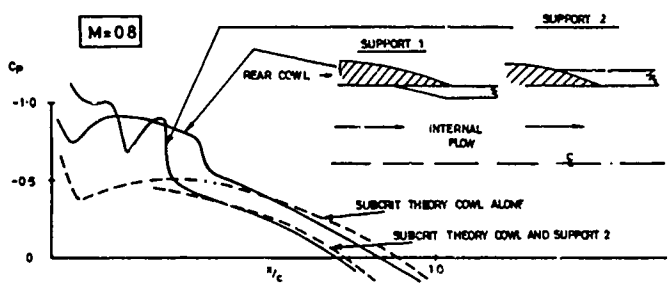

FIG.17.

It does unfortunately mean that the drag of the whole correct cowl assembly may not be measured. In addition, we have the problem of the forward pressure interference of the expanding duct or the rakes on cowl flow development. Measurements have shown these to be significant in that :

(a) The pressure field may influence the recompression on the aft cowl causing premature separation which would lead to erroneous conclusions regarding the spill drag.

(b) The pressure field will give a buoyancy force on the body which will interfere with drag measured on a balance but will not affect the wake traverse result.

Measurements of the interference effects of an expanding body, or a rake, or a support body, aft of a cowl at transonic speeds are indicated below :

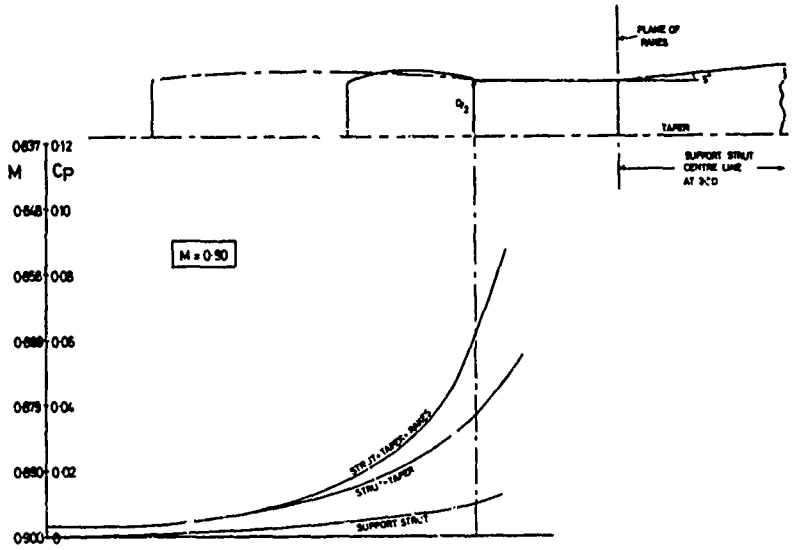

FIG.18.

(c) The very existence of these sting forward influences on the total cowl system accentuates the need for representation of the fan jet. There appears to be a strong case for the use of a fan simulator in this work. This would provide the correct representative fan pressure ratio and would permit correct geometric representation of the fan cowl. The forward influence of the expanding fan flow would then be fully representative (except for R.No.) and the total profile drag of the fore and aft cowl could be measured by the momentum-defect Method III.

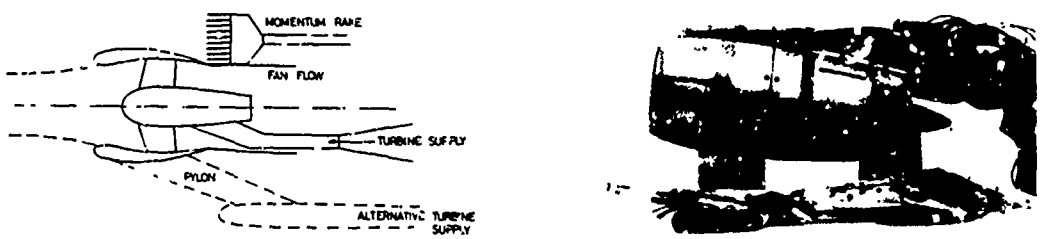

FIG.19.

It is not proposed that all experiments should be done this way but that an intelligently selected series of cowls might be tested to determine the magnitude of the problems and the interference. It is not considered that this method is easily adaptable to force balance measurements.

1.3.2. Spill drag methods for integrated installations

As previously mentioned, special models of maximum scale are used to accurately determine the effects of inlet spill flow over the full flight spectrum. The methods used follow those of the aerodynamic model and the same momentum equations apply. Models for this purpose are usually only representative in the regions where the influence of the intake and the intake spill flow might be expected to occur. For twin inlets at supersonic speeds only 1 inlet need be represented. It is usual, for example, to reduce the span of the wings, where possible, to reduce the balance loads and increase sensitivity. Such special models may be used to optimise the installation drag of the basic inlet and diverter system as well as measure spillage drag. It is common to make the fuselage section constant shortly behind the region of influence to minimise aft body effects which might mask the required measured terms.

DESIGN REQUIREMENTS

For spill interference measurements it is very desirable that mass flow should be changed during a test by remote control. This requires a motorised mass flow throttling plug which may or may not be attached to the live model.

Metric mass flow control

For the live (or metric) plug the total force on the model and plug must be accounted for in the data reduction force equations. The determination of the force associated with the plug exit flow is considerably eased if an annular mass flow plug system can be used in preference to a central plug.

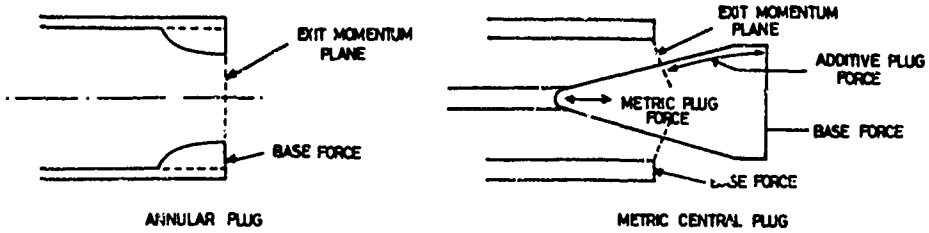

FIG.20

For this reason early tests of this type were made in a series of different test runs with interchangeable annular plugs. In this way the exit flow could be well-defined to give both accurately calibrated mass flow and momentum. This method is probably well suited to a blow-down tunnel, but is expensive and less accurate for a continuous tunnel.

The metric central plug is rarely used, this has the major disadvantage of the difficulty of defining the forces on the plug aft of the exit momentum plane which have to be accounted for in the force balance equations.

Non-metric mass flow control

This system whilst being similar to the metric plug has certain advantages in the definition of terms in the force balance equation:

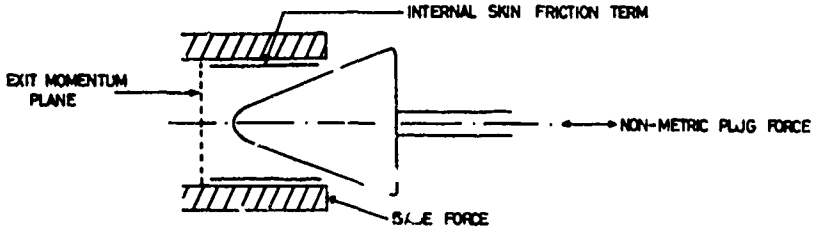

FIG.21.

In this method the momentum at the end of the live model is determined from a momentum determination at a plane upstream of the mass flow plug and an estimated or calibrated skin friction term between this station and the exit plane. The difficult and large terms on the plug behind the exit plane do not have to be accounted for in the force balance equation.

The balance of forces that exist on both the metric and non-metric plug systems is shown below:

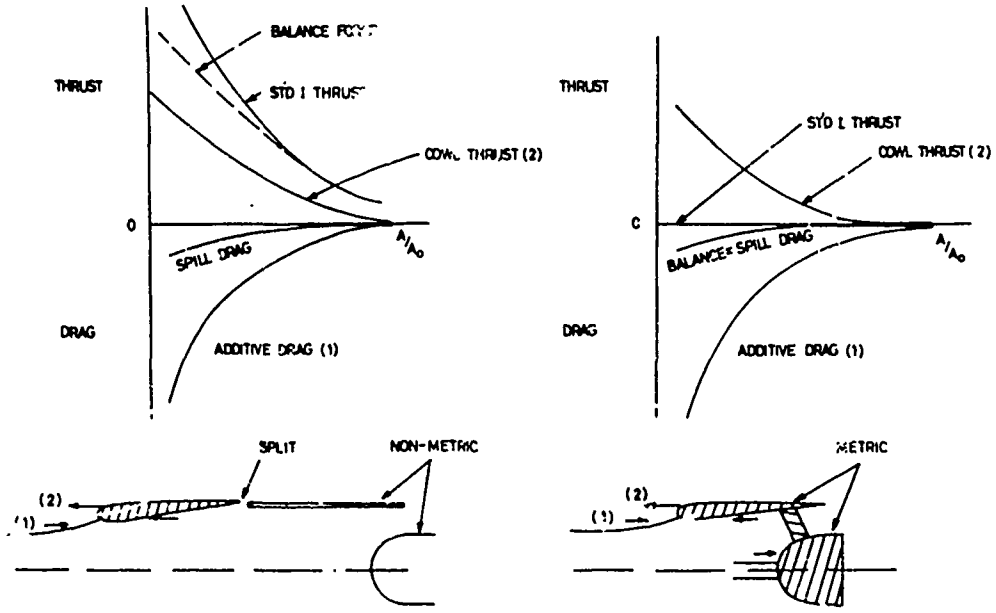

FIG.22.

Instrumentation and Calibration

It will be seen from the above terms in the force balance equation that several of the terms are of similar or greater magnitude than the resultant external drag. This imposes very stringent requirements on the instrumentation used to determine these terms, and it is for this reason that as large a model as possible should be used.

(a) Balance

The six component force and moment balance is required to provide an accuracy equal to that of the required final answer, which in turn must be equal to that of the aerodynamic force model i.e. 2 - 5 drag counts (1 drag count $\Delta C_D = 0.0001$) for a sub and supersonic fighter, 1 drag count for the subsonic transport, and better than 1 drag count for the supersonic transport.

(b) Mass flow and Momentum

It is usual to instrument the inlet drag model to measure engine mass flow, however experience has shown that with engine face distortion this instrumentation is of little value in defining true mass flow to the accuracy required in drag experiments. Current procedure is to either (1) install a calibrated venturi section or (2) use a calibrated rake, ahead of the mass flow plug.

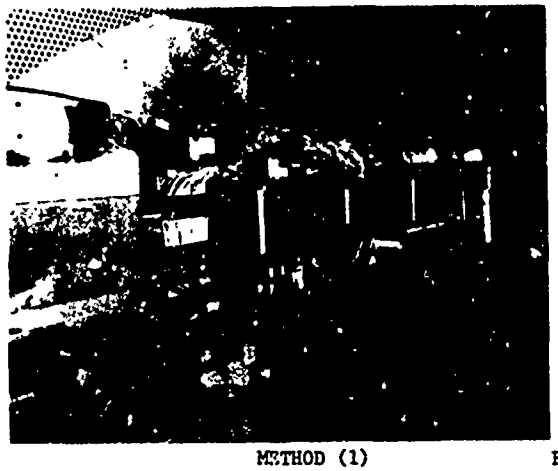

METHOD (1)

METHOD (2)

FIG.23

Reproduced from best available copy.

METHOD 1

In this method the duct is calibrated in a test cell, with an overall pressure ratio > 10:1, which contains a precision calibrated orifice plate of known discharge coefficient accurate to ½%.

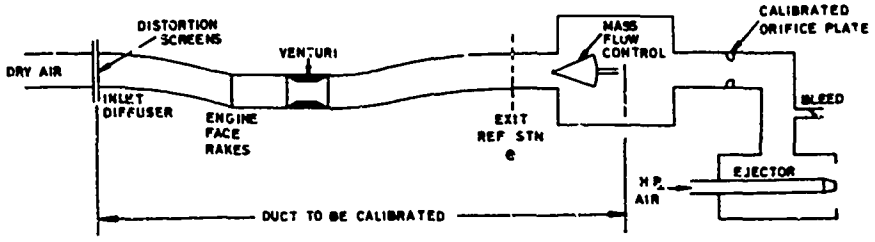

FIG.24.

Pressure measurements are made over a complete range of mass flows, these include the full engine face array, 4 wall statics + 1 pitot at the entry to the venturi, 4 wall statics in the venturi throat, and 4 wall statics in the exit. Discharge coefficients are obtained by relating the precision mass flow to that calculated using the standard venturi flow method associated with the measured upstream and throat static pressures and the venturi contraction ratio. In the particular case tested, the venturi discharge coefficient varied from 0.82 to 0.92 for venturi upstream Mach numbers from 0.1 to 0.5. The reason for the low value and large variation was probably the limitation of venturi length in this case. Tests with typical inlet distortions showed only ½% variation of the venturi discharge coefficient.

Calculation of the momentum at the internal exit station of the model uses the venturi mass flow, and wall statics at the station, the form of the equation used for net standard internal drag is

$$D_I = \frac{2 A_\infty}{A_{ref}} - \frac{A_e}{q_\infty A_{ref}} \left[(p_e - p_\infty) + \gamma p_e M_e^2 \right]$$

from the relationship $\frac{m\sqrt{T}}{A\, p_e} = f(M_e)$, with known $m\sqrt{T}$ and p_e obtain M_e, hence C_{D_I}.

Check calculations assuming a range of different total pressure distributions in the duct, whilst maintaining continuity of mass flow, have shown that the error in the slope of the spill drag v mass ratio curve should not exceed 5%.

This model has also been used with two different inlet bleed systems which are fed to precision orifices in the base. The internal force of the bleed flows is calculated in a similar manner using the area of the exit orifice and the local static and bleed mass flow.

METHOD 2[3]

The rakes used in this method, shown in the above figure, were very carefully calibrated to be consistent with the calculation of standard internal drag from

$$C_{D_I} = 2\,\frac{A_\infty}{A_{ref}} - \frac{A_{rake}}{q_\infty A_{ref}}\left[(p_{rake} - p_\infty) + \gamma\, p_{rake}\, M^2_{rake}\right]$$

The sensitive terms in this equation are A_∞, p_{rake}, and M_{rake}, where A_∞ and $(\gamma pMA)_{rake}$ are related by measured mass flow. In the example shown above the internal rakes, model duct, and exit [illegible]e calibrated for accurate measurement of mass flow. Flow through a standard orifice plate was compar[illegible] th that measured by the rake using the model duct but replacing the inlet by a 4:1 contraction bellmou[illegible] The following calibration factors are evaluated from these tests.

(1) Mass flow A_∞

For tests with a fully choked exit plug flow: $A_{exit\ effective} = A_{exit\ geometric} \cdot K_{D_P}$

where mass flow $m\sqrt{T} = Q.\ A_{ex.effective} \cdot P_{rake}$ and Q = Constant

For tests with subsonic unchoked exit plug flow: $m\sqrt{T} = K_{D_R}\,(AP)_{rake}$

(2) Mach number

In the above equation the true mean value of M_{rake} is required. This is obtained in the following way for a family of velocity profiles defined by

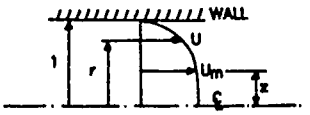

$$\frac{U}{U_m} = \left[\frac{1-r}{1-z}\right]^{\frac{1}{n}}$$

to give two constants

$$K_1 = \frac{\text{Mean Mach number from integration of velocity profile}}{\text{Mean Mach number from the discrete pitot points}}$$

$$K_2 = \frac{\text{Mean (Mach number)}^2 \text{ from integration of velocity profile}}{\text{Mean (M number)}^2 \text{ from the discrete pitot points}}$$

K_1 for a low Mach number duct flow is equal to the mass flow coefficient K_{D_R}, and theoretical calculations give a simple linear relationship between K_1 and K_2 for values of $0.2 \leq z \leq 0.8$ and $2 \leq n \leq 7$. Hence for any given inlet size a relationship is obtained between mass flow control plug position and true mass flow and M^2. These provide the necessary accurate input to the basic drag equation.

(c) Base pressures

It is essential to recess the base of the model such that a reasonably uniform pressure exists. To this end, sharp chamfered edges to the external body profile and nozzle exits should be provided. The base pressures should be measured with integral scanivalve instrumentation. The practice of using pitots mounted on a rear support with their forward facing heads very near to the base should be avoided, particularly at transonic speeds. The influence of the rake support system has been shown to have a strong influence on the base pressure.

This requirement of integral base pressure tubes also makes the measurement of pressures in annular base plugs difficult.

.3.3. Spill drag methods for slender wing installations

There is no fundamental difference between the integrated slender wing and the integrated fighter as far as measurement of internal flow effects are concerned. The full representation of the parts affected by spill flow must be provided. Methods following the proposals of 1.2.5. for a datum measurement may be used but this requires a series of different plugs each with associated internal drag measurements. However the main deterrent of this method is the need to obtain each point on a spill curve from a different test.

In one supersonic application for Concorde,[3] Method 2 of 1.3.2. was used to provide accurate measurement at the same time as continuous variation of mass flow.

It will be seen that the distortion associated with this arrangement would have precluded its use at transonic and subsonic speeds, at which conditions it would have been necessary to resort to the removable plug method. In these tests a pair of fully instrumented inlets were used measuring engine face data and providing remote variation of ramp settings and bleed. This model was capable of measuring independently the effects of throttle fore-spill, ramp spill and aft spill via dump doors. It is obvious that there are no limits to model sophistication.

FIG.25.

2. AIRFRAME INTERFERENCE ON INLET

2.1. Fore-surface representation and diverter height[3]

In the planning of any new model of an inlet-airframe system it is very desirable to arrange for the inlet to be tested in isolation and then in the presence of the airframe. This permits reasonable optimisation of some of the inlet parameters before the interference flow field is superimposed. Arrangements should also be made to vary the inlet height relative to the surface on which it is mounted to determine the importance of the interaction between the flows.

At this point we meet the almost insoluble problem in the representation of an inlet/airframe combination in scale tests. The approach boundary layer thickness at the entry plane of an inlet mounted on a model fuselage or wing surface is unrepresentatively thick. For a pitot intake without diverter or splitter plate the inlet-boundary layer interaction must inevitably be incorrect and only boundary layer suction ahead of the inlet plane can avoid unrepresentative inlet measurements, particularly when an inlet normal shock impinges on the boundary layer of the fore-surface. The usual parameter for the representation of the height of an intake on a surface is h/δ where h is the height and δ the thickness of the approach boundary layer. This parameter describes adequately the proportion of the boundary layer that is ingested by the inlet and which leads to the consequent reduction of pressure recovery at the engine face $\left(\propto \int_h^\delta \rho V^2 \, dh. \text{ for } h < \delta \right)$. It is obvious that this parameter is not adequate for small h/δ or when δ is a significant part of the height of the inlet. However for $h/\delta \approx 1.0$ this is a minor problem in comparison with the difficulty of the choice of how to represent the geometry of the inlet in the presence of an unrepresentatively thick boundary layer:

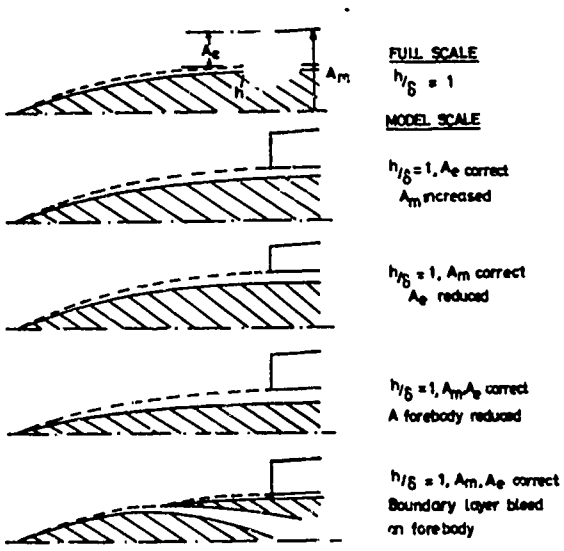

FOUR ALTERNATIVE METHODS OF REPRESENTING THE CORRECT h/δ ON A MODEL INLET AND FOREBODY

FIG.26.

The last of these alternatives appears to offer the best aerodynamic solution but the boundary layer removed by suction requires large model suction ducts and could be sensitive to incidence effects, such a scheme is also difficult if force measurements are required. A simpler and adequate alternative would seem to be (c) in which the effect of a small reduction in fineness ratio should only have minimal effect on the nose potential flow. It goes without saying that the boundary layer on the fore-surface should have transition fixed with a minimum grit or Ballotini to provide a minimum thickness turbulent boundary layer at the inlet plane. A thinner turbulent layer may be obtained with a rear band fixation on wing or fuselage if a reasonable run of laminar flow can be obtained, but this could be troublesome in the event of random natural transition ahead of the band at incidence.

The Diverter

The previous section has been concerned with the correct positioning of the inlet with respect to the local surface boundary layer. The diverter itself is of course an important interface between the inlet and airframe and it is difficult to define whether it is the problem of the inlet designer or the airframe designer: the one preferring a large h/δ, the other a zero h/δ, dependent upon who is responsible for the drag or the power plant performance. The installed drag of the diverter is obtained from tests described in section 1.2 where it is part of the datum C_{D_0} at datum or zero spill. The variation of its performance with reduced mass flow is integrated with the overall spill drag increment.

The performance of the diverter at spill and off-design conditions is only partially determined from the spill drag tests and data on the modified engine face recovery must be included in the total performance book-keeping, hence a poor diverter may provide a two-fold loss of performance. Limited pressure plotting may be done on the spill drag model or alternatively a special diverter model may be used to optimise diverter performance.

The above arrangement has been used with success supersonically to develop diverter planform shapes and divergence angles. Pressure plotting on the wing plate can be used to determine wing surface lift interference, diverter surface pressure plotting is used for drag integration.

In this test method it should be noted that the development of supersonic flow between the tunnel wall and the representative wing plate is not easy, particularly for M < 2. Some edge relief is very beneficial.

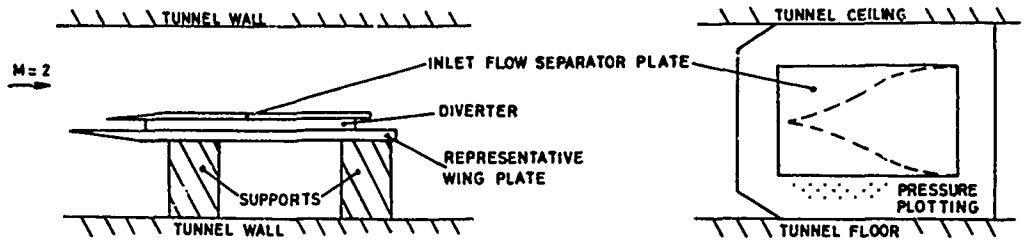

FIG.27.

2.2. Measurement of Inlet Flow Environment

Much can be done in the early stages of a design to determine the type of flow environment into which it is proposed to put the inlet. This is a desirable requirement for most configurations, excluding perhaps the underwing podded installation for subsonic and transonic flight, although measurements of cruise flow direction at the inlet usually result in a small degree of toe-in. In particular, for the inlets positioned close to surfaces or far back on a fuselage, measurements of flow direction, total pressure, and Mach number are very desirable, and of course the variation of these parameters with airframe attitude. For these measurements a 5-tube yawmeter is usually fitted either to a fixed or remotely controlled rake. This instrument, whose head angle may be chosen to match the Mach number range of the tests, can measure flow angle in two directions, total pressure and local Mach number. Calibration of the heads must be comprehensive, particularly with regard to instrument zero errors.

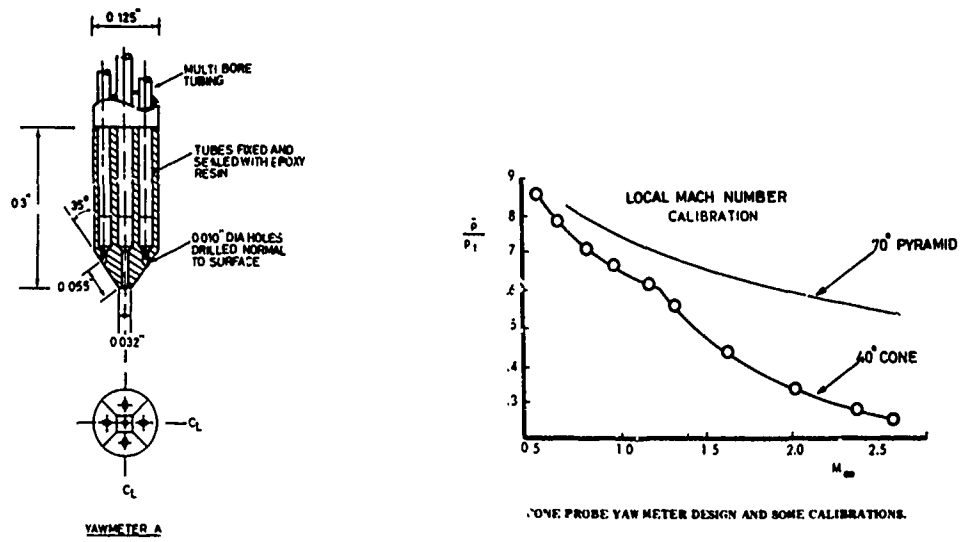

FIG.28.

The use of a 4 facet head is preferred to the conical head as this reduces the cross-flow interference. For large combined angles the accuracy is diminished but it is possible to obtain angles accurate to $\pm\frac{1}{4}^\circ$ up to 10° and ΔM of 0.02. The evaluation of total pressure comes from the pitot pressure and Mach number.

Some examples of environment survey models are shown below with illustrative results.

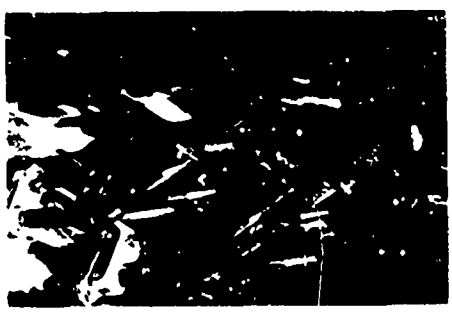

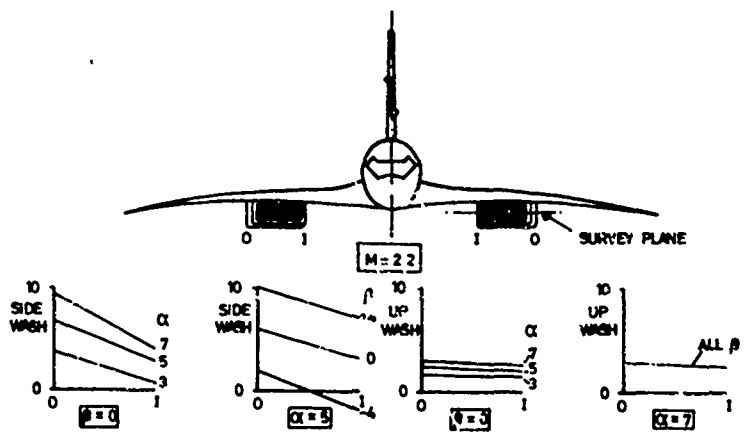

Reproduced from best available copy.

FIG.29(a).

This latter example indicates results with a simple variation of mean flow direction for an intake shielded by a wing with small pressure perturbations and with no fuselage influence.

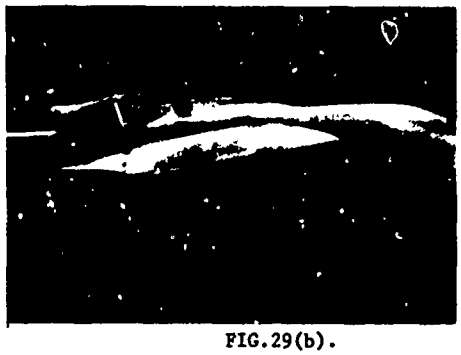

FIG.29(b).

For complex fighter-type configurations the flow environment is very involved and there is considerable scope for the use of computer analysis output data in a digestible form. The problem is similar to that of the engine face distribution and so the use of similar distortion parameters and computer contour plots are of great value.

Flow Visualisation

As a useful adjunct to the complex measuring techniques above, considerable understanding of the flow approaching the inlet may be obtained by the use of flow-visualisation techniques. For low speed performance the water tunnel is of value in demonstrating interference and model attitude effects. At all speeds, surface oil-flow methods indicate the direction of the surface flow in the vicinity of the inlet, showing clearly the existence of separations, vortices and shock waves. These methods may be used with success for internal flow studies as well.

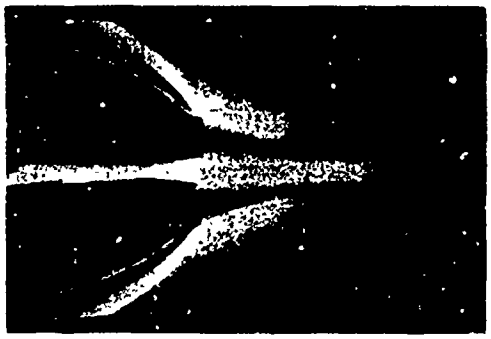

FIG.30

It is emphasized that this method essentially describes only the surface flow although experience enables reasonable speculation of the possible flow in depth.

As an addition to oil flow, the vapour screen technique has been used for qualitative data. This requires the operation of the tunnel at a controlled degree of humidity, the consequent fog density is a function of the speed of the flow environment of the model and so if a thin plane of light is shone across the model a section of the flow field is illuminated. This may be photographed from the model support and provides results of the following type.

Reproduced from best available copy.

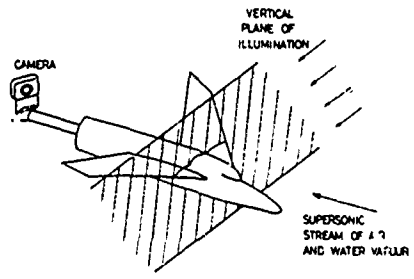

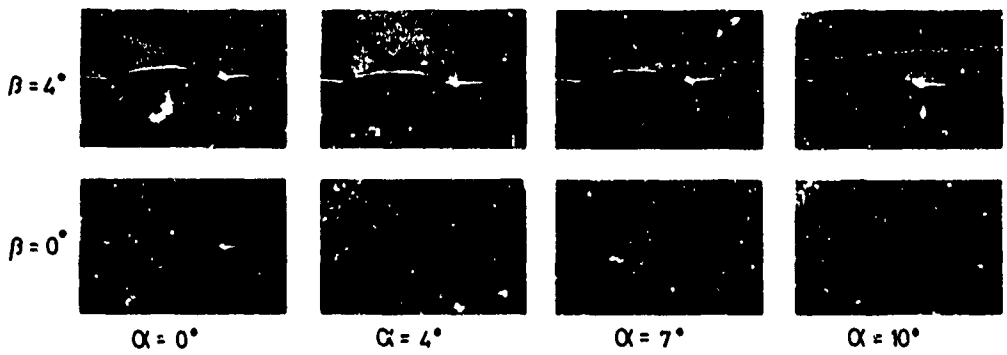

FIG.31.

3. MEASUREMENT OF THE PERFORMANCE OF INLETS

3.1. Duct and Engine Face Measurements

Rake Design

Current model methods using fixed or rotating engine face pressure rakes have been shown to give good correlating data with full scale engine measurements. Present requirements of total pressure distortion coefficients defined by engine manufacturers dictate extensive coverage of the engine face at a minimum of 12 30° sectors and if possible, 24 15° sectors. For minimum interference a two-arm rotating rake can be used with a sequence of 12 data points for every point on the inlet characteristic. This, assuming that instrumentation is no limitation, will cost approximately 12 times as much as a test using a fixed 24 arm rake. Obviously the latter is more desirable both from the economic point of view and the fact that the data is taken over a much shorter period. The question arises, what is the limiting number of fixed heads which can be used and what are the design problems of a multi-rake. Tests on two different duct arrangements have compared the results obtained with rakes carrying 2, 4, 8 and 12 arms of pitots in the first case, and 12 and 24 arms in the second case.

The first experiment used a rotating 2-arm rake to which was attached additional rakes to make up the full complement to represent 4, 8 and 12 arms. In this way comprehensive measurements could be made by rotating the rake and hence measuring pressures at close spacing in the presence of the interference rakes. These tests showed no measurable effect on total pressure distribution but the forward influence was such that the increased rake blockage increased the static pressures measured on the wall, bullet and rake. The static pressure distortion was unchanged.

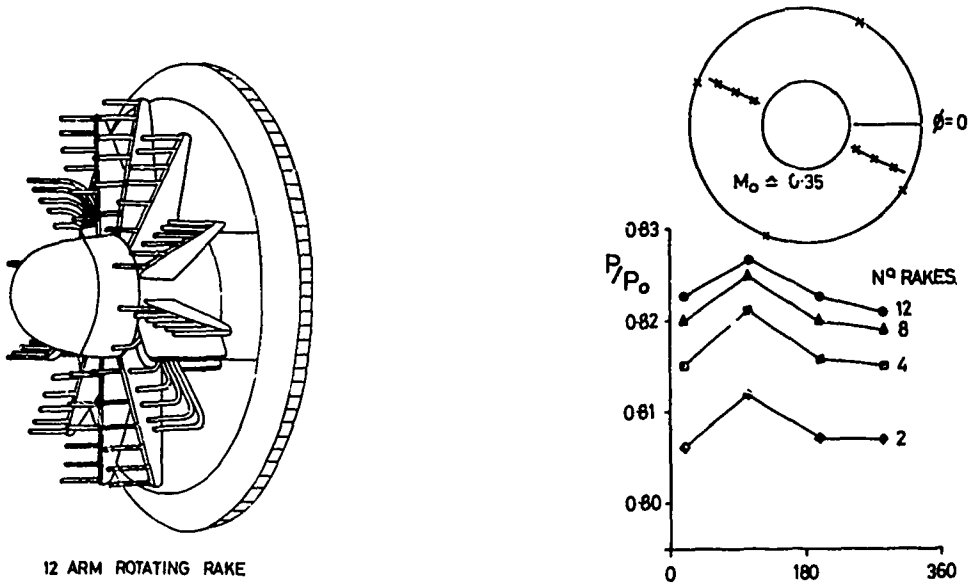

FIG.32.

The second experiment[6] compared results for a fixed 12-arm and a fixed 24-arm rake. It was found that the E.F. total pressure distortion coefficients DH, and DC 60, and the engine face pitot pressure contours, were adequately measured by the 24-arm rake but the static pressure distortion DP, was increased when the engine face Mach numbers were large enough to approach local choking in the pitot rake supports.

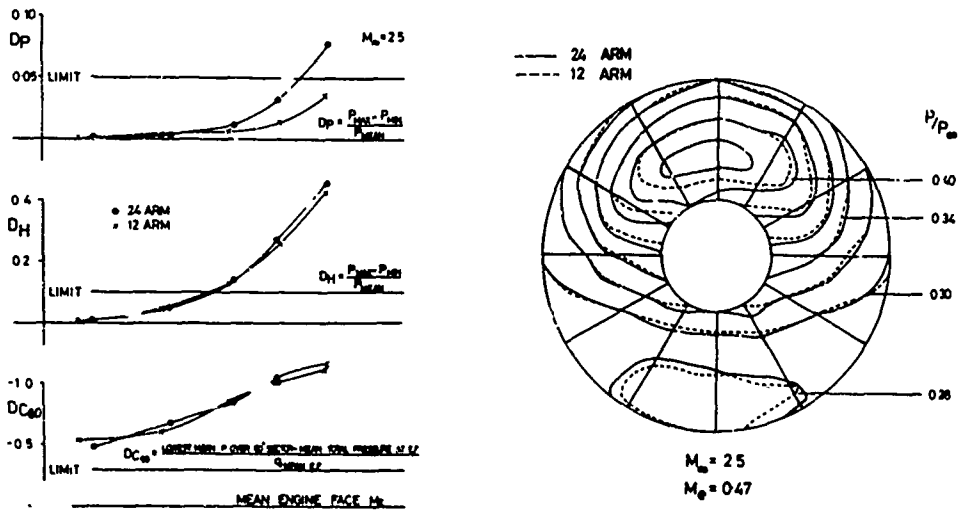

COMPARATIVE RESULTS WITH 12 ARM AND 24 ARM RAKES WITH LARGE ENGINE FACE DISTORTION

FIG.33.

In the particular installation used in the second experiment the blockage created in the uniform duct by the 24 rake arms caused choking for engine face Mach numbers near 0.5 and obviously caused static distortion for engine face Mach numbers greater than 0.35. Careful design with swept rake supports and an expanding duct in the region of the supports would permit a 24 arm rake with a frontal tube blockage of 2% to be used for engine face Mach numbers up to 0.5.

The actual measurement of static pressure on the rake may be made with heads with ogive nose leng and static holes 10d behind the shoulder, with the static hole arranged to be in the plane of or ty ahead of the pitot heads. It is not particularly common to use rake statics unless mass flow is ted from the engine face measurements - which is only done as a last resort! Even in these circumstances it is more common to place reliance on wall statics which are less dependent upon engine face flow angles. Static distortion coefficients are of relatively less importance to the engine manufacturer.

It was common practice at one stage to measure flow direction at the engine face by installing small Conrad 2-tube yawmeters, arranged to measure swirl. This was reasonably successful but the evaluation of angle requires a knowledge of local $\frac{1}{2}\rho V^2$ which in turn requires local static pressure. Use of a mean static pressure is however sufficient to ensure a calculated accuracy of 1°. Use of a standard 70° included angle head provides an instrument with a sensitivity $\frac{\Delta p}{q}$ of 0.04; calibration is generally required to determine the instrument error which can be of the order of $\pm 1^\circ$ in spite of careful manufacturing tolerances.

Number of Rakes

In the previous discussion the interference effects of multi-rakes was discussed without due reference to the specification that dictates their requirement. The usual basis for defining the closeness of pitot pressure coverage is the engine manufacturers distortion coefficients. A large number of different coefficients are in use and each may well require a different rake array. If it is assumed that each rake will have sufficient radial coverage to provide a good mean radial pressure value, then by use of error analysis with a set of typical engine face distortion patterns it is possible to define a rake rotational spacing to give a sufficiently accurate value of the required distortion coefficient.[5] Equally well this may be done experimentally using the data from a close rake spacing in which the data from some of the rakes is progressively ignored.

For example in U.K. it is common practice to use a distortion coefficient

$$DC_{60} = \frac{\text{Lowest mean total pressure over a } 60^\circ \text{ sector} - \text{Mean total pressure}_{EF}}{q_{mean_{EF}}}$$

and R = Angular position of this sector. This describes the magnitude and position of a region of low total pressure on the engine face. For different blade and engine applications, the value of 60° may be varied. For a 24-arm rake mean values of radial pressure - DC, are available at every 15°. These are combined in groups of 4 to provide a mean sector pressure over 60° - DC_{60}. There will be 24 of these values and the minimum value can be accurately determined and positioned. If data from only 12 arms is available, then only 2 arms are used to provide DC_{60} at 12 angular positions. Similarly, 6 arms each provide their own DC_{60}.

Experimental data gives the following result:

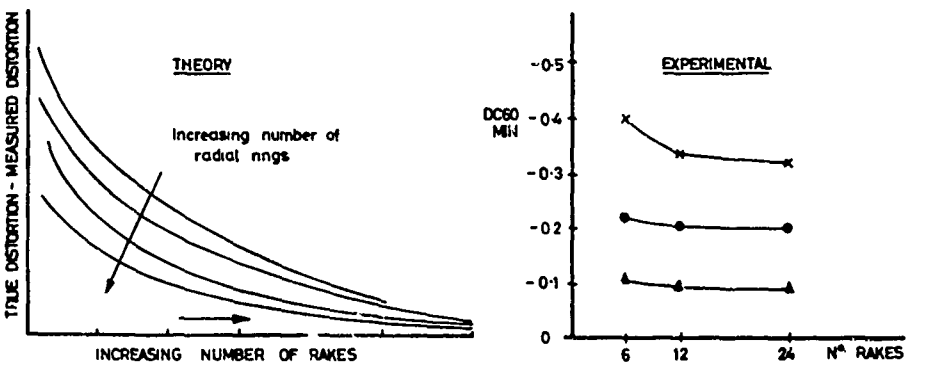

FIG.34.

3.2. Output Data

In almost all inlet tests in wind tunnels, data is recorded on a data logger via a scanning switch system. Data-taking rates vary from one facility to another depending upon the type of facility (continuous or blowdown), the total pressure level, the number of data loggers available. Rates varying from 1 port per second to 50 ports per second are used, the former being uneconomic is based on the measurement of very low pressures, the second being a blow-down tunnel requirement. This latter case requires care to ensure that carry-over pressure interference between ports does not occur. Data reduction from the data logger can be handled off-line or on-line depending upon the services at the test facility. In either case a limited amount of on-line output is desirable to ensure the best spacing of the test points, this is particularly true of subsonic and low transonic testing where the visual techniques of schlieren and shadowgraph are not always available. Equally, visual aid to detect duct instability is needed for the location of buzz points or subsonic twin-duct instability. For a simplified on-line output a limited number of the rake total pressures may be put onto individual transducers which may then be summed as analogue voltages to give a mean engine face recovery. For mass flow, $m\sqrt{T}$ may be obtained from

a transducer measurement of plug position for a sonic exit, or P and Δp for a venturi, these latter measurements being used in a simple $\sqrt{\ }$ analogue circuit. These readings may be displayed on an X - Y plotter.

Buzz and instability detection may be obtained from high-frequency-response flush-fitted pressure transducers whose output is observed on an oscilloscope or on an RMS output meter.

For a simple reversion to the old manometer techniques, a T.V. display of a scanivalve output in simulated manometer form may be produced on a T.V. screen.

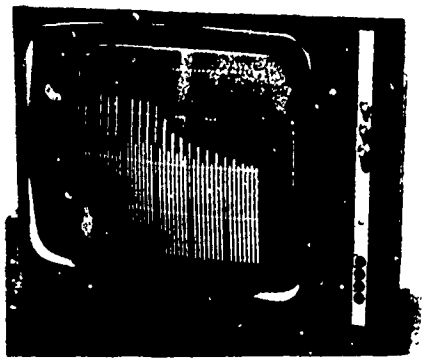

FIG.35.

A typical layout of a computer data reduction procedure may follow this scheme:

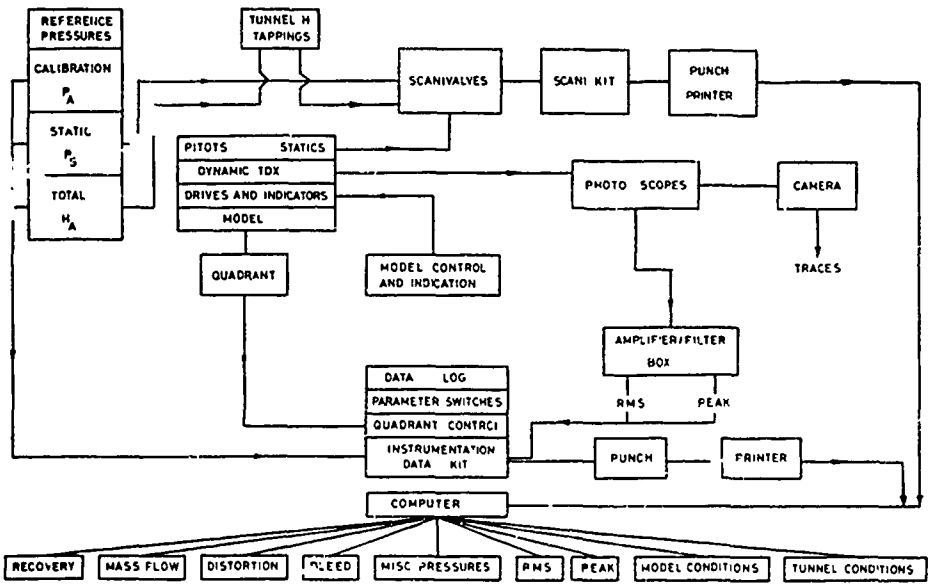

ENGINE FACE DATA REDUCTION

FIG.36.

Up to this point the production of data has been routine apart from the judicious choice of data spacing. The amount of data can however be phenomenal and the final analysis somewhat tedious. Off-line plotting of mass flow and pressure recovery with the associated distortion coefficients provides reasonable assimilation of the data and when it is necessary to improve understanding, computer contour plots of engine face distribution are produced.

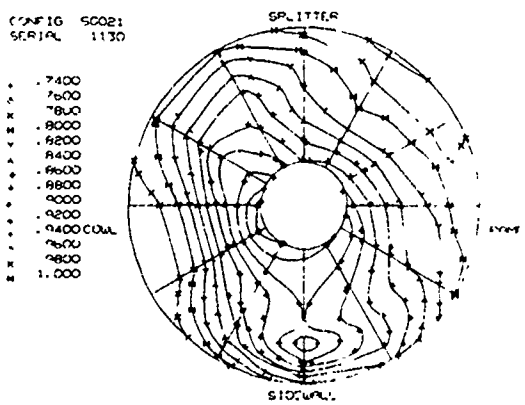

FIG.37.

3.3. Supersonic inlet flow visualisation

In all classical treatise on the subject of inlet flow visualization, the pure axi-symmetric or wedge inlet is used to demonstrate the value of schlieren and shadowgraph techniques. In practice, the integrated inlet frequently precludes these simple visualization methods. For some conditions of course, visualization methods are impossible e.g. Phantom in elevation, F14 in plan and sideslip, but it is worth noting that some configurations may use the intake wall or floor splitter plate as a device for direct shadow visualization. In the example shown, fig.38, of the tests on a single cell of a Concorde inlet the shock system was projected onto the splitter plate which was painted matt white. The photograph was obtained with an external camera on the same side as the light source. The second photograph was obtained from the shadowgraph of the external flow around the model and the internal throat flow. This was obtained as a photograph of the shadow on tracing paper on the window opposite the light source.

FIG.38.

It should be noted that the exposure time of these photographs is very long by normal standards (0.1 secs) but the resulting quality is good and for steady-state flow conditions which are normally being studied, a long exposure is more desirable.

For conditions of supercritical flow on cowls at high subsonic speeds the shadowgraph technique may be used. For tests under these conditions a porous or slotted tunnel wall is usually being used making normal visualization techniques difficult. Direct shadowgraph methods with a divergent light-source can contribute to the analysis of pressure plotting data on axi-symmetric inlets.

Reproduced from best available copy.

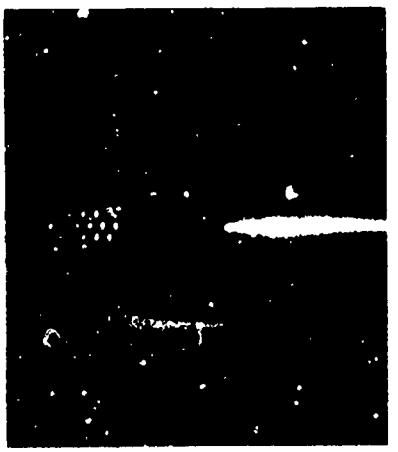

FIG.39.

3.4. Isolated and Integrated Model test Configurations

Subsonic Pod Inlets. For measurement of the internal performance of the isolated subsonic pod a model which is mounted near the tunnel centreline on a rear sting is required. Further requirements are high incidence and large inlet velocity ratios at low M. The latter requirement demands a source of external suction which is capable of choking the inlet throat at low forward speeds (M = 0.2); it i under these extreme conditions or large α and V_i/V_∞ that test results of flow distortion are of most significance. An example of such an arrangement is shown:

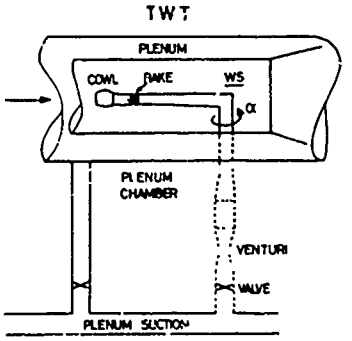

FIG.40.

Supersonic Isolated Inlet. For a clean installation that is reasonably independent of its environment and that is optimised for operation over a limited design range, much of the development can be achieved on a model of the isolated inlet at the environmental approach Mach number. For the Concorde inlet illustrated here, initial development of mutual interaction effects was studied on an isolated twin duct nacelle. On this model the effect of mismatch was studied with variable Mach number, incidence and sideslip. With this model the optimum splitter plate was obtained and boundaries of mismatch could be defined.

FIG.41.

For internal performance a single cell model has been continuously used to optimise sidewall geometry, ramp geometry, bleed configurations and many other variables. The addition of a boundary layer plate and diverter makes the inlet flow distortion more representative and permits study of these variables.

Supersonic Integrated Configurations. For the check tests of the optimised inlet a fully integrated inlet/airframe model is used. Two fully instrumented inlet cells are housed in the nacelle in the correct environment of the airframe. This represents a complex and expensive model requiring large tunnel facilities which would not be available for the many hours of development testing used on the isolated nacelles. For this type of model, care has to be taken to ensure that no forward interference from the support and mass flow control system occurs, particularly for the subsonic and transonic model versions.

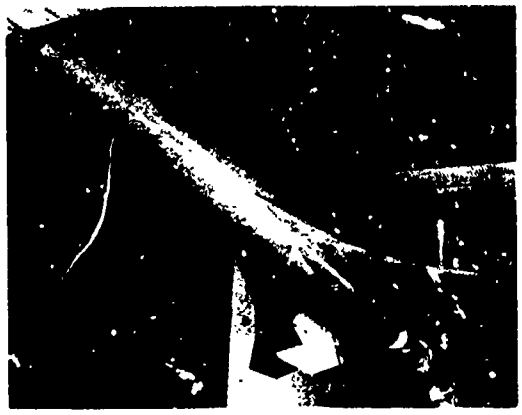

FIG.42.

Tests on this model have also been made at low forward speeds with an ejector-assisted mass flow suction to represent inlet velocity ratios greater than those available from free flow.

3.5. Mass flow measurement and control

This subject was treated in some depth in section 1.2 where it was essential to have accurate mass flow for internal drag definition. The requirements of those tests are, if anything, more stringent than those for engine performance analysis. The choice of method of measurement is large, covering:

internal (a) engine face integration (b) orifice plate (c) venturi (d) downstream rake

(e) choked or unchoked exit plug,

or external (b) and (c).

Engine-face integrations are notoriously troublesome, being very dependent upon distortion and static pressure distribution. The orifice plate normally has unacceptable losses. The venturi and downstream rake are satisfactory if far enough from the engine face distortion and if properly calibrated. The subsonic exit plug is very dependent upon exit static pressure and distribution and requires calibration, the calibrated choked exit plug is the most acceptable method if sufficient pressure ratio is available. Measurements external to the model have the advantage of controlled flow conditions at the measuring station but for transonic and subsonic tunnel conditions, external suction is required; in addition the whole length of the duct systems between inlet and measuring station must be completely

leak tight. Some examples of mass flow control plugs and measuring systems are given:

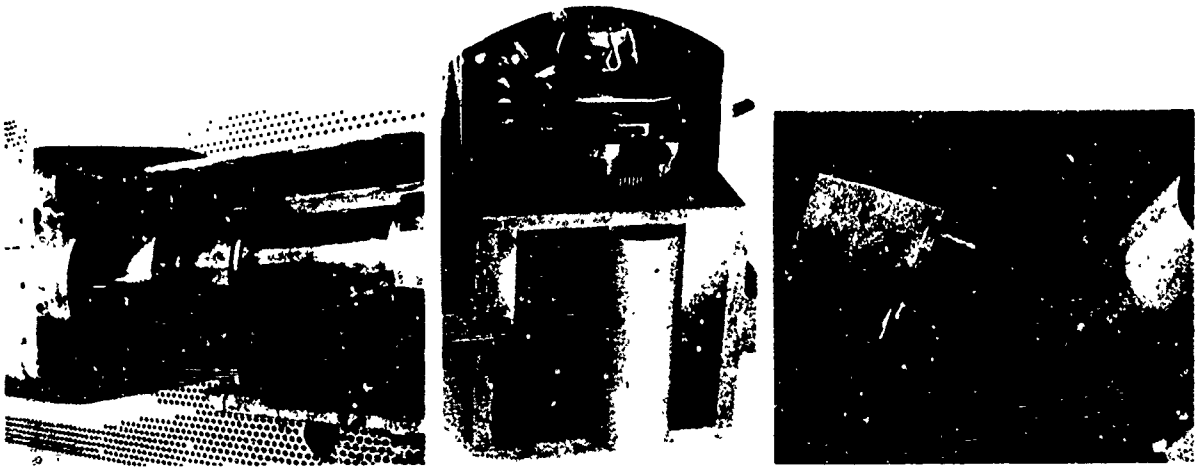

a b c

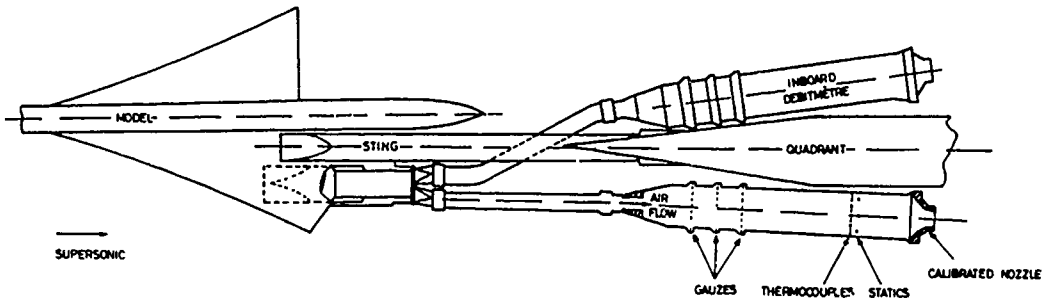

EXTERNAL MASS FLOW MEASUREMENT BY DEBITMÈTRE

FIG. 43.

d

3.6. Bleed representation and measurement

Inlet bleed ducts may in general be treated as secondary inlets in the measurement of recovery and mass flow. It is usually more difficult to instrument and provide uniform flow in bleed duct but the percentage accuracy requirements are much less and so the results are normally acceptable, i.e.½% of inlet mass flow and 2% of inlet recovery. For choked bleed exits, the problem is simplified by the use of a calibrated control plug. Venturi's may also be used with success but it should be remembered that a venturi does not know the direction of flow!

3.7. Representation of Engine Surge

Consideration will be given elsewhere to the measurements which are made to measure engine face turbulence and its use in the prediction of engine surge. In this section, the existence of surge is assumed and the experiment to determine its influence on the upstream structure and the closely associated engine, is described.

For the sake of clarity a parallel may be drawn between normal supersonic inlet buzz and surge. In the former, the instability mechanism is associated primarily with the shock system which creates a vortex or separation which causes continuous destabilisation and reform of the stable inlet flow pattern. During the unstable flow cycle the high pressure air in the inlet cavity exhausts and refills causing large variations of structural pressure load, and mutual interference on any adjacent inlet. In principle the fan or compressor stall provides a similar mechanism of inlet flow exhaust and refill, the frequency of course being different from that of buzz.

Figure 44 shows a surge valve which was fitted to the model previously shown in fig.43(c). One inlet had surge simulation whilst measurements were made on upstream transducers and in the adjacent inlet. This valve was not only capable of completely cutting off the flow but also of providing 80% flow reversal. Typical traces are shown in fig.44.

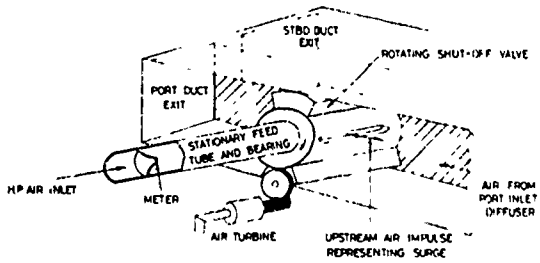

MODEL SURGE VALVE

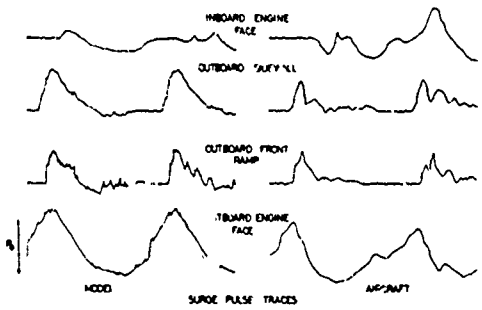

SURGE PULSE TRACES

FIG. 44.

REFERENCES

1. LOEBERT,G THOMAS,J. Engine Airframe Integration Problems peculiar to Aircraft Configurations and Nacelles mounted above the Wing. AGARD CP 27, Paper 4

2. WILLIAMS,P.R.G. STEWART, D.J. The Complex Aerodynamic Interference Pattern due to Rear Fuselage Mounted Power plants. AGARD-CP-71-71

3. GOLDSMITH, L CARTER, E.C. A Review of Methods used for the Representation of Engine Flows in High Speed Wind Tunnel Testing. A.R.A.REPORT 24, R.A.E.TECHNICAL REPORT 72012 (to be published)

4. BRITTON, J.W. Measurement of the Internal Drag of Air Breathing Installations on Slender Wing Body Combinations at Supersonic Speeds. R.A.E. TECHNICAL REPORT 65275

5. FERRI, A. JAARSMA F. Engine Airplane Interference and Wall Corrections in Transonic Wind Tunnel Tests. AGARD ADVISORY REPORT 36

6. THORNLEY,S.A.M. Tests on a 24-arm, Engine Face, Pitot Rake. A.R.A.MEMO 125.

NOZZLE/AIRFRAME INTERFERENCE AND INTEGRATION

Felix Aulehla and Kurt Lotter

Messerschmitt-Bölkow-Blohm GmbH
Unternehmensbereich Flugzeuge
D 8 München 80
Postfach 801160
Germany

SUMMARY

The lecture first discusses the main parameters involved in the interference between internal and external flow and shows also how these parameters in principle affect afterbody drag. Then the definition of rear end drag is given in the conventional way and also in a more relative manner approaching the physical optimum. Mention is made of the necessity of adapting the experimental procedure to the available theoretical methods for drag prediction during the early phase of an aircraft project.

For configurations with single and twin engines installed in the rear end of the fuselage wind tunnel test results for various nozzle concepts are presented and discussed. The geometric variations in these tests comprise boattail angle, size and location of the base, nozzle interfairings and engine spacing. The lecture describes in particular how, through the proper consideration of these geometric parameters in nozzle/airframe integration, the additional afterbody drag can be drastically reduced in the transonic flight regime.

Finally, it is shown that integrating the nozzle into the airframe requires careful optimizing of usually conflicting parameters: depending on the missions of the aircraft other factors, e.g. nozzle weight may take precedence over purely aerodynamic considerations.

LIST OF SYMBOLS

A	Area (for twin configuration: 2 nozzles)
c_D	Drag coefficient, referred to maximum fuselage cross section area, unless otherwise noticed
Δc_D	Incremental drag coefficient (over ref.)
c_f	Friction coefficient
c_F	Thrust minus drag coefficient $\frac{F-D}{F_i}$
Δc_F	Difference in c_F between ref. - model
c_N	Normal force coefficient (tail)
c_p	Pressure coefficient $\frac{P_{local} - P_o}{q_o}$
d	Diameter
D	Drag
ΔD	Incremental drag (due to jet and nozzle)
F	Measured thrust
ΔF	Thrust difference tunnel on - tunnel off
F_i	Isentropic, fully expanded thrust
l	Length from max. fuselage cross section
L	Total fuselage length
M_o	Free stream Mach number
P_o	Free stream static pressure
P_t	Total pressure
q_o	Free stream dynamic pressure
R	Radius of boattail contour
Re	Reynolds number
s	Nozzle (engine) spacing
T_o	Free stream static temperature
T_s	Structure temperature
T_t	Total temperature
W	Weight
x	Axial distance downstream of max. fuselage cross section
x'	Axial distance downstream of cylinder/boattail-juncture
$\bar{x}$	Axial distance downstream of nozzle exit
α	Nozzle divergence half angle
β	Boattail angle
δ	Boundary layer thickness
δ^*	Boundary layer displacement thickness
ε	Nozzle convergence angle
$\varkappa$	Ratio of specific heats

INDICES

AB	Afterbody	ß	Boattail (with c_D: boattail pressure drag)
BE	Back end (without nozzle)	b, ann	Annular nozzle base
FB	Forebody	e	Exit
F	Fairing	equ	Equivalent axisymmetric body
INT	Interference	f	Friction
N	Nozzle	j	Jet
RF	Reference	max	Maximum fuselage cross section
Ref	Reference	p	Pressure
T. off	Tunnel off	s	Sting
a/c	Aircraft	t	Throat
b	Base (with c_D: base pressure drag)	wet	Wetted

1. INTRODUCTION

Several years ago a trend towards aircraft purely optimized for supersonic flight became evident. More recently an increasingly wide operational spectrum is required whereby the high subsonic and transonic flight re[illegible]s, with their additional problems, are challenging the dominant position of this supersonic development. This alteration has sprung from new aerodynamic and design concepts in the field of airframe and engine research.

Today it is generally accepted that engine and airframe manufacturers cannot develop their products separately and that incompatibilities and reciprocal disturbances must be simulated and investigated for all conceivable operating conditions. But nevertheless frequent setbacks occurred because either these incompatibilities were not sufficiently taken into account or because hitherto unknown effects became of decisive importance. This lecture deals with those interference effects arising in connection with nozzle/airframe integration, with the emphasis on the high subsonic flight regime.

2. JET/AIRFRAME INTERFERENCE EFFECTS

A propulsive jet issuing from an afterbody has basically two effects on the surrounding flow field and therefore on the aircraft: firstly the jet acts like a solid body displacing the external flow secondly it normally entrains mass flow from the external stream. In subsonic flight there may be a strong upstream influence. The jet contour affects the pressure distribution on the afterbody, large changes of the afterbody shape are felt by the forebody and the jet as well (upper half of fig. 1). A typical flow pattern encountered in supersonic flight is also shown (lower half of fig. 1). In contrast to the subsonic flight condition there is limited upstream influence, since any disturbance can be propagated upstream only through the subsonic part of the boundary layer. The shock system within the jet will continue through the jet boundary and may impinge on nearby aircraft surfaces. For aircraft configurations with two or more jets the mutual interference becomes even more complex.

Computation methods available today are either not sufficiently exact or fail completely to predict the complex afterbody flow field. This is particularly true in subsonic flow incorporating boundary layer separation. Therefore, aircraft development relies heavily on wind tunnel tests with simulated jets. The aim of such tests is to obtain information on critical areas of jet/airframe interference. Depending on the location of the engine in the airplane, these interference effects may be more pronounced on wing, tails and afterbody. Normally, drag, pitching moment, pressure and temperature loads are primarily investigated as function of the various jet parameters. The correct jet simulation requires sophisticated techniques which will be covered in detail in the following lecture by Mr. Jaarsma.

The interference effects on wing, tail and rear fuselage are shown in the following three diagrams (ref. 1): Fig. 2 shows the force coefficient for the tail normal. With high tail position there is no jet effect present. The low position results in a reduced stability and a change in pitching moment for jet on/jet off. High nozzle pressure ratios cause the jet to attach resulting in strong pressure variations along the boattail associated with local fluctuations which required highly damped structure for fatigue reasons (fig. 3). Although high-temperature material was used for the boattail surface, significant secondary air flow rates had to be provided for cooling purposes. Fig. 4 shows the jet-induced pressure differences between upper and lower surface. At supersonic flight Mach numbers all pressure changes occurred on the lower wing surface while a small change was also noticed on the upper surface during subsonic flight speeds. These jet interferences introduced significant changes in pitching moment, control effectiveness, drag and wing loads.

3. INTERRELATION OF FOREBODY- AND AFTERBODY FORCES

During the last few years, intensive investigations have been devoted to the important field of jet interference on the rear end with emphasis being on thrust-minus-drag optimization. It has become common practice to separate the forces of the afterbody from those on the forebody in most test set-ups. For the better understanding of the afterbody drag problem it is useful to recall some fundamental interrelations between forebody and afterbody with respect to pressure distribution and forces for the case without jet. Fig. 5 shows, in the left half, bodies of different relative thickness in inviscid flow: though the total axial force is zero the "separating" forces, i.e. the drag on forebody and afterbody respectively, may attain large values, depending on their relative thickness. When the pressure at the maximum cross section reaches ambient pressure, which is the case with long slender bodies, the separating forces disappear. The right half of fig. 5 shows the influence of viscosity (boundary layer) on afterbody pressure distribution. Stronger boattailing reduces the amount of recompression and thus increases afterbody pressure drag.

Apart from friction the effects of boundary layer are negligible on practical forebodies. Only for long bodies are the pressure changes on the afterbody not felt on the forebody, from which it may be concluded that for slender bodies the rear end is the primary source of pressure drag. When thick fuselages with larger variations in afterbody shape are tested, measurement of afterbody forces alone yields wrong results. That is, by developing an afteroody of optimum shape one may succeed only in transferring the problem to the forward end.

4. DEFINITION OF MAIN PARAMETERS

The conventional definition of afterbody geometry and -drag is presented in fig. 6. The afterbody starts from the maximum cross section and comprises boattail and base. The total afterbody pressure drag is the sum of $c_{D,a}$ and $c_{D,b}$. These two drag components are functions of the parameters as shown in the figure. The number of parameters gradually increases, going from an axisymmetric body without jet to a twin jet configuration. Of course, there are still additional parameters defining the exact lines and local pressure- and temperature profiles,up to now considered less important.

5. AFTERBODY DRAG OF AXISYMMETRIC BODIES

In fig. 7 the effect of jet pressure ratio on base- and boattail drag is shown for axisymmetric bodies with various base sizes and given maximum cross section, jet diameter, boattail angle and with a convergent nozzle having a short cylindrical throat. Depending on base size, increasing jet pressure ratio has opposite effects on pressure drag: for small base areas, increasing jet pressure ratio produces a favorable interference in contrast to the large bases. This applies to base and boattail drag as well: at higher pressure ratios the increasing expansion of the jet causes the external and internal stream to meet at a steeper angle resulting in an increase in base- (and boattail-) pressure. For larger bases this interaction occurs only at very high jet pressure ratios beyond those shown in the diagram. As long as the external and internal stream do not impinge on each other, the aspirating effect of both flows on the body is predominant. With jet pressure ratios above 6 and the smallest base the jet interference results in a negative total pressure drag.

Fig. 8 is a cross-plot of the previous diagram at a jet pressure ratio of 3,0 and shows the effect of base size on base-,boattail- and total drag. Although there exists an optimum base size if base drag alone is considered, the total afterbody drag increases steadily with base size. As a consequence, integrating the nozzle into the rear fuselage,base areas should be avoided for moderate pressure ratios.

6. AIRPLANE DRAG ASSESSMENT

So far, single jet installations have been treated. For twin jet installations in the rear fuselage as in modern fighter airplanes, fig. 9, right half, the assessment of drag becomes more difficult. It is convenient to compare the twin jet configuration with an ideal single jet fuselage of same maximum cross section and equivalent nozzle size (ref. 2), however, of slender boattail lines in order to avoid possible flow separation. This reference afterbody has nearly zero pressure drag and is so slender that it cannot house an afterburning jet pipe (see fig. 9, left side).

The reference afterbody gains its importance by the fact that it is accessable to computation and thus allows the proper linking of experimental afterbody drag data with theoretically computed aircraft drag data. This procedure is depicted in the left half of fig. 10: Number (1) on top represents the aircraft design, the fuselage of which is transferred into an equivalent body of same cross section distribution, number (2). If, however, the aircraft afterbody is relatively short then number (2) is extended so that the computation method need not account for separation. The profile drag of this body is a function of [illegible]ds-number, Mach number, relative thickness and wetted surface and can easily be computed by st[illegible]rd methods. Particularly for twin engine installations the wetted surface may be larger than for the axisymmetric body. To obtain the correct friction drag for the aircraft, of course, this larger wetted surface has to be used. The lack of reliable afterbody drag computation methods requires special afterbody tests shown as number (3) and (4): number (3) has the same afterbody as number (2) and the forebody of the aircraft, however, reduced in length in order to better simulate the boundary layer thickness over the afterbody. Naturally, this is a compromise between correct simulation of boundary layer thickness and potential flow field. Ideally, the correct

forebody line should be duplicated with proper boundary layer control. Number (4) has the correct aircraft afterbody with proper jet simulation and with the same forebody as number (3).

The difference in afterbody plus forebody drag between (4) and (3) yields Δc_D, which is then corrected for the difference in friction drag between the same models. This corrected Δc_D consists of the incremental pressure drag with the correct jet effect and the change in thrust due to external flow affecting the jet. To obtain total airplane drag, the corrected Δc_D is added besides other drag terms to the computed profile drag of the axisymmetric body (number (2)).

While the drag assessment method described above is mostly applied during the early phase of a project when a large number of configurations usually has to be considered, a different method will be applied later in the project definition phase: that method yields airplane drag purely by testing and is shown on the right half of fig. 10: number (5) shows the complete aircraft model, normally mounted by a rear sting via an internal balance. In nearly all cases the afterbody geometry has to be modified to accomodate the sting. Intake and nozzle flow is generally unrepresentatively simulated by ram-air flowing through the ducts. The drag results obtained from the complete model must be corrected for the effects of the modified afterbody, the sting and the jet interference. These corrections may be obtained by conducting tests with afterbody models (6) and (7): model (6) duplicates the afterbody of the complete model, number (5), and has a dummy sting. Model (7) is identical to model (4), i.e by comparing it with number (6) the required corrections for jet effect, effect of external flow on thrust, effect of sting and modified afterbody geometry are obtained. Adding the other drag terms in the upper part of the figure yields total airplane drag, which ideally gives the same value as obtained by the method described in the left side of the figure (computation plus testing).

An aircraft manufacturer who is specialized in a few particular types of engine installations normally has accumulated a large number of typical afterbody drag test data which enables him to look into many configurations to find the optimum aircraft without any further testing (fig. 10, left half). Of course, there are tests to follow later for the purpose of confirmation, increase in accuracy and more detailed investigation (fig. 10, right half).

7. EXHAUST NOZZLES

An aircraft with supersonic capabilities normally has an afterburning engine. Fig. 11 shows typical jet pressure ratios for straight jet- and bypass engines versus flight Mach number, the straight jets being near the upper limit of the band. Two extreme engine operating conditions are shown: for cruise in the subsonic flight regime nozzle pressure ratio is low requiring little or no divergence. For maximum acceleration, i.e. full afterburning, the throat area is increased by a factor of about two (depending on bypass ratio). The required nozzle divergence increases gradually with increasing flight speed and reaches a value of $A_e/A_t \approx 2,6$ at nozzle pressures of 14. Besides cruise and maximum acceleration all intermediate operating conditions are possible (military, partial reheat). This equires in the ideal case a fully variable nozzle with independent variation of throat size and divergence. In many practical cases more simple systems with either purely convergent nozzles or a fixed relation in throat-to-divergence are chosen as a compromise.

On fig. 12 typical nozzle concepts are depicted.

Short convergent nozzle: This concept represents a mechanically simple lightweight nozzle. The major disadvantage from the aerodynamic point of view is the larger base in the closed position.

Iris-nozzle. With the mechanically more complex iris nozzle annular bases are avoided in all positions. As with the short convergent nozzle, large thrust losses occur at high pressure ratios since no divergence is provided.

Plug-nozzle. The necessary variation in throat area is accomplished by variation of the plug position or -geometry. As a consequence, a fixed lightweight shroud can be used. Large cooling air flows, however, are necessary for reheat operation.

The con-di iris nozzle provides some divergence in the reheat position. The variation in throat size and in divergence is coupled. Thus the con-di iris is a compromise between the simple iris and a fully variable con-di nozzle.

The simple ejector is a frequently chosen nozzle concept. Primary and secondary flaps are mechanically linked. Relatively large secondary airflows are required associated with drag penalties.

Fully variable ejector. This design yields near-optimum aerodynamic performance: throat area and divergence are independently variable. the required secondary mass flows can be kept low. Heigh weights and complex design are associated with this nozzle concept.

The isentropic ramp is difficult to adapt to varying operating conditions, which normally results in undesirable changes in pitching moment.

Blow-in-door ejector. This nozzle concept provides similar good performance as the ordinary ejector in the reheat position. In the closed position, large quantities of tertiary air are taken aboard through spring loaded flaps in order to fill the large annular base of the short primary nozzle. Large quantities of air, however, require careful handling in order to avoid losses in the sharp turnings of the secondary and tertiary flow passages. Especially this nozzle represents a highly integrated concept with respect to merging of internal and external flows. Peripheral non-uniformities (blockage) of the external flow may cause unfavorable interferences, which is particularly true with closely spaced twin jet installations.

8. AFTERBODY DRAG TEST RIGS

Inflight performance of the different nozzle concepts need to be tested in the surrounding flow field, which requires duplicating the aircraft lines at least to some extent. In the past, various afterbody drag test rigs have been developed by different groups. In fig. 13 some of these facilities are shown. The test rigs A, B, C and D measure thrust-minus-drag. Only with system A the drag of the forebody and strut is also on the balance. As may be seen from the equations on fig. 9 drag is obtained by subtracting the static gross thrust from the thrust-minus-drag term. In addition to the thrust-minus-drag measurement, system E determines the drag of the afterbody shell separately. Nozzle drag is included in the thrust-minus-drag term. System F measures forebody and afterbody drag separately in order to resolve possible changes of forebody drag caused by larger changes in afterbody geometry. So far, thrust is not measured but envisaged for a later development phase.

9. MAGNITUDE OF AFTERBODY DRAG

Fig. 14 shows the large number of models tested within a period of five years in order to develop the optimum afterbody for a twin-jet fighter aircraft. Most of these tests relate to a joint US/FRG program conducted in close cooperation between Messerschmitt-Bölkow-Blohm (MBB) and Boeing. Later some of the tested models were transferred to Pratt & Whitney and General Electric for comparative tests in the wind tunnel facilities in Hartford and San Diego respectively. Similar development work was done for different projects by others. Presented is the total airplane drag divided by the drag of the total airplane with an ideal afterbody. The ideal afterbody here again is that described in fig. 9 and 10. The worst afterbody tested in the various test series had an additional drag as high as 45 % of the total airplane drag. Nearly all of the models were twin jet installations. Large reductions of this additional drag are possible, the best coming very close to the ideal. Although soon after the early test series it became evident how a low-drag installation should basically look like, nevertheless in later test series configurations with high drag levels were tested. This was necessary in order to optimize an afterbody not only from the aerodynamic point of view but also from other considerations like weight, length, etc. These tests were conducted in different test facilities as shown in the previous figure. In some of the test facilities identical models were tested, yielding the same trends. The quintessential features of the experience obtained from the large number of investigations for optimum nozzle-airframe integration will be presented in the following diagrams.

10. AFTERBODY DRAG TEST RESULTS

10.1 Investigated Geometric Parameters

Out of the many test series those parameters which had the greatest influence on afterbody drag are listed in fig. 15.

- o Nozzle types: the various nozzle concepts are explained in fig. 12 and 16.
- o Boattail angle: the boattail angle representing the most critical parameter regarding flow separation was varied from 10° to 20°.
- o Base area: size and relative axial location of bases were investigated together with various nozzle concepts.
- o Nozzle spacing: nozzle spacing was varied from "extra narrow" to "extra wide" corresponding to values of s/d_e from zero (double-D) to 4,7.
- o Interfairing length: especially for narrow engine spacings, flow separation (effective bases) cannot be avoided except by extending fuselage portions by various amounts downstream of the nozzle exit plane.
- o Excrescences: when integrating the nozzle into the rear of the fuselage in practice many concessions from the aerodynamic side have to be made for installations like tailplane actuator, thrust reverser, levers etc. Those "excrescences" can be very detrimental in a flow field liable to separation.

Fig. 16 shows details of some nozzle- and fairing types on the models as tested in the wind tunnel. Starting from the simple short convergent nozzle, complexity gradually increases when proceeding to the complicated D-shape nozzle with its minimum engine spacing. On the right half of the figure the reduction of base areas by various types of interfairings is given.

10.2 Effect of Nozzle Type

The same nozzle concepts, in some cases even identical models, have been tested in four different test facilities (fig. 17, reheat-off). Fairly good agreement has been achieved for the short convergent nozzle. The incremental afterbody drag is about $\Delta c_D \approx 0,04$ which is explained by the large annular bases. In contrast, the blow-in-door ejector gives a larger scatter in drag. The lowest value corresponds to an idealized blow-in-door ejector with a low-drag primary nozzle and with minimum blockage in the tertiary flow passages. The following nozzle concepts have lower drag levels. Two drag levels are given for the iris nozzle, the lower value corresponding to a low boattail angle of less than 15°. The higher levels were obtained for larger boattail angles. A similar influence of boattail angle was experienced for the fully variable ejector.

It should be noted that some scatter is to be expected due to the fact that different wind tunnels with entirely different test rigs were used. Also, not always the same reference model served as a datum.

10.3 Effect of Boattail Angle

In fig. 18 the incremental drag over the drag of the single jet reference model is shown as function of boattail angle for a twin engine installation. The presence of the interfairing reduces drag by a larger amount than by reducing the boattail angle from 20° to 10°. Optimum boattail angles lie between 10° and 12°. Still lower boattail angles would result in an increase of drag due to greater friction. The interfairing was of the type FG-3 described in chapter 10.6.

10.4 Effect of Base Area

In the wind tunnel test the largest changes in drag occurred for the variation in base size (fig. 19). Geometric bases located upstream of the nozzle exit plane normally introduce flow separation, i.e. additional effective bases on adjacent surfaces, resulting in very high incremental drag levels of about 45 % of total airplane drag. The best configuration shown on the bottom of this figure has a long interfairing extending downstream of the nozzle exit plane. The additional afterbody drag is only about 4 % of the airplane total drag. Still lower values of about 2 % were achieved with a more slender boattail of 10° to 12° (see fig. 18), which represents the optimum configuration from drag point of view. This optimum shape was found after the completion of only two test series. This quick approach is largely attributed to the comparative method of the idealized single jet reference model. The certainty of being close to the physical optimum was given by the fact that the measured drag of the reference model was practically equal to the computed friction drag. Also, no configuration in any later test experienced lower drag than the reference model. The wetted surfaces of the models were comparable, i.e. equal or slightly bigger than that of the reference model

10.5 Effect of Engine Spacing

Engine spacing is one of the key parameters which define the lay-out of a new aircraft. Once a value is selected, the basic shape of the fuselage can be changed only within limits. Thorough knowledge of the associated interference effects is therefore required at an early state. In reference 3 these interference effects have been studied for various engine spacings with a newly defined interference drag (fig. 20): This interference drag is the sum of

a) change in boattail pressure drag ΔD due to presence of nozzle and jet relative to a reference end cap
b) nozzle drag D_N
c) change in engine gross thrust ΔF due to the presence of the external flow fields.

The carpet in fig. 20 shows this interference effect for various nozzle concepts and fuselage types. F-1, F-2 and F-3 have the same engine spacing but decreasing peripheral blockage (tail booms). Fuselages F-3, F-4 and F-5 had zero peripheral blockage but increasing engine spacing. The carpet plot shows that the interference drag becomes smaller with increasing engine spacing (F-3 to F-5). Considering interference drag D_{INT} by itself could lead to the wrong conclusion that the widest engine spacing (F-5) yields the optimum fuselage from performance point of view. An optimum drag configuration of course is obtained by minimizing total drag ($D_{BE} + D_{INT}$).

Taking the values from the carpet and adding the backend drag D_{BE} the next diagram (fig. 21) is obtained. In addition, similar engine spacing tests, conducted by Boeing for MBB in the Boeing test facilities, have been added in the lower part of the figure (ref. 4 and 5). In this type of diagram the minimum drag is shown for engine spacings as close as about $s/_{de} = 2.5$. For smaller engine spacings MBB tests show a steady drag rise down to an engine spacing of 1.5. For still smaller spacings the drag levels off to a value of about 0.01 at zero engine spacing. The dotted lines for these extremely narrow spacings indicate that jet pipes and the iris nozzles are squeezed together, to form the double-D concept for zero spacing.

In these Grumman tests no results are given for engine spacings lower than about 2.7. For higher engine spacings both, MBB and Grumman tests show a clear drag rise. In the Grumman tests the maximum fuselage cross section had to be increased when engine spacing was increased. Referring the drag to the actual maximum cross section yields the dotted lines. For optimization purposes, however, drag should rather be referred to the same reference area (solid lines). Here, in contrast to the MBB tests, forebody drag was not measured. Depending on relative thickness, this drag is different (see also fig. 5). Taking this effect into account the drag data for engine spacings of 4.7 should be slightly reduced.

10.6 Effect of Interfairing

As discussed already in chapter 10.4 large bases cause high drag levels. The interfairing represents a proper means to avoid such base drags. Fig. 22 shows these reductions for two different engine spacings (ref. 4 and 5). FG-1 had a base upstream of the nozzle exit of constant length l_F. With FG-2 the base was always located in the nozzle exit plane ($l_F = l_{AB}$). FG-3 and FG-4 were protruding downstream of the nozzle exit plane. With decreasing boattail angle β the length of these fairings (l_F) increases more quickly than the length of the afterbody (l_{AB}). The diagram for an engine spacing of 2.69 gives the minimum drag with a relatively long interfairing of $l_F/l_{AB} = 1.2$.

In reference 3 the effect of interfairing was investigated in a slightly different way (fig. 23): Here, base areas were kept constant for various fairing lengths. This diagram shows again that base areas should be avoided or at least not be located upstream of the nozzle exit plane.

10.7 Comparison Transonic/Supersonic

In order to compare transonic with supersonic afterbody drag in fig. 24, the results are presented as Δc_F, which is roughly the incremental drag referred to ideal gross thrust. While in the transonic regime all models of one test series had Δc_F-values within the wide band, in the supersonic range the same models had much lower drag levels with a Δc_F below 0,03. This is explained by the fact that the nozzles here were in the maximum reheat position: the ideal gross thrust is considerably higher and the projected areas of boattail and base are reduced due to the larger exit diameter of the matched convergent/divergent nozzles. The only model with a simple convergent nozzle ("conv. cusp") experienced a higher Δc_F. This is explained by the relatively high thrust losses of the convergent nozzle at high jet pressure ratios (= 10,0 at M_0 = 1,9). Subtracting those losses from the Δc_F of the "conv. cusp" yields a negative value, which will be explained as post exit thrust in the next two figures.

10.8 Post Exit Thrust

If a jet cannot fully expand inside a nozzle, it does so immediately downstream of the nozzle exit plane. Thereby the outer flow field is displaced which in turn causes the pressures on the outer surface to rise. Increasing jet pressure ratios cause the terminal shock to move forward with a separated region downstream. Thus, the boattail pressure drag is reduced. Fig. 25 illustrates this interference effect in a supersonic stream for a conical afterbody having a 5,6° cone half angle and a convergent nozzle: the higher the jet pressure ratio the higher the pressure coefficients on the boattail. This effect sometimes is referred to as "post exit thrust" indicating that some of the "lost" pressure energy is regained by the reduction in afterbody drag (ref. 6).

At supersonic flight speeds the jet pressure ratio of a turbo engine normally is high enough to require a convergent/divergent nozzle. If, however, subsonic cruise is the most important mission, the question arises whether or not the weight and complexity of a convergent/divergent nozzle is justified. Fig. 26 tries to answer this question for the aerodynamic side and in principle only ($\varkappa$=1,4), using the data from reference 6: the upper bar gives the afterbody drag of a convergent nozzle with a small base and the jet off. The second bar shows the reduction in afterbody drag due to the presence of a highly underexpanded jet ("jet effect", jet pressure ratio = 10): the boattail drag is reduced and the base drag becomes base thrust. The thrust loss due to the underexpanded jet, however, is quite large and amounts to about 7 % of the ideal gross thrust. The lowest bar gives the performance of the matched convergent/divergent nozzle with zero base: the base drag and the thrust losses, of course, are zero. Here, the boattail drag is somewhat higher than for the convergent nozzle with the underexpanded jet (middle bar). Comparing the middle and the lowest bar, gives the net difference in propulsive force divided by gross thrust, i.e. about 6,7 %. Regarding aerodynamic aspects only, the conclusions to be drawn from the above statements are that for optimum supersonic performance a (near) fully expanded nozzle is required since the gain in afterbody drag reduction cannot make up for the thrust losses of an underexpanded nozzle. In this comparison different base sizes were chosen: zero base for the con-di nozzle and a small base with a ratio d_b/d_e = 1,25 for the convergent nozzle. This is the optimum geometry for each nozzle type according to reference 6.

11. VARIABLE GEOMETRY

As shown above, a twin jet afterbody requires small boattail angles and slender interfairings between the nozzles. Depending on engine spacing these fairings may have to extend downstream of the nozzle exit plane. For the optimum engine spacings of about 2,5 these extensions are as long as about two nozzle diameters (reheat off). In fig. 27 such a fairing is shown in combination with iris nozzles in the reheat off and maximum reheat position. In the reheat condition parts of the interfairing have to be retracted or folded away to give room for the thicker jet. The diagram shows one of the many layouts investigated for such a folding mechanism. The temperature and pressure loads of course are the particular problems with such a part of airframe structure.

12. DRAG/WEIGHT TRADE-OFF

Sor far only aerodynamic drag of the afterbody optimization was considered. A complete trade-off study, however, requires taking into account a great number of additional aspects like weight, complexity, development risk, reliability, infrared suppression, acoustics etc. To a great extent the main missions of the aircraft determine how strongly these parameters are to be weighted. For short range missions and high energy manoeuvrability requirements, reduction in structural weight is more important than reduction in drag. For long range missions, however, drag usually is the most important parameter. Fig. 28 shows how changes in nozzle weight and changes in drag affect total airplane weight. A weight growth factor of 3,1 has been used for this diagram. As an example two nozzle concepts are compared: although nozzle B is about (0,5 + 0,1) % heavier than nozzle A, the overall airplane weight is about 1,5 % reduced, due to the lower drag of nozzle B. The carpet diagram is, of course, just an example and may be largely different for other missions or other aircraft.

13. CONCLUDING REMARKS

Test results presented in this lecture were obtained from facilities in which the correct simulation of jet temperature, potential flow field and external boundary layer had to be compromised. Further development of afterbody test rigs should try to eliminate these shortcomings.

It has been shown that airplane drag can be considerably reduced by providing an afterbody of optimum shape. For afterburning engines this may require the provision of variable geometry with all its associated problems of integration into the airframe.

14. REFERENCES

1	M.R. Nichols	Aerodynamics of airframe engine integration of supersonic aircraft NASA TN D-3390, August 1966
2	R.S. Armstrong S.R. Miller	Subsonic aerodynamic performance of nozzle installations in supersonic airplanes J. Aircraft Vol. 5, No. 3, page 230 - 235, May-June 1968
3	D. Migdal E.H. Miller W.C. Schnell	An experimental evaluation of exhaust nozzle/airframe interference AIAA Paper No. 69 - 430, June 1969
4	K. Lotter	Windkanalversuche an Flugzeugheckkörpern mit Zwillingstriebwerksanordnung, Ma = 0,8 bis 2,2, 1. Meßreihe Unpublished MBB-Report, EWR-Nr. 161-66, November 1966
5	H Hacker	Windkanalversuche an Flugzeugheckkörpern mit Zwillingstriebwerksanordnung, M = 0,85 - 0,95, 3. Meßreihe Unpublished MBB-Report, EWR-Nr. 37-68, February 1968
6	E.M. Cortright F.D. Kochendorfe	Jet effects on flow over afterbodies in supersonic stream NACA RM E 53H25, August 1953
7	M.P. London	VFX - The Navy's choice Space/Aeronautics, page 50 - 58, November 1968
8	W.K. Greathouse	Blending propulsion with airframe Space/Aeronautics, page 59 - 68, November 1968

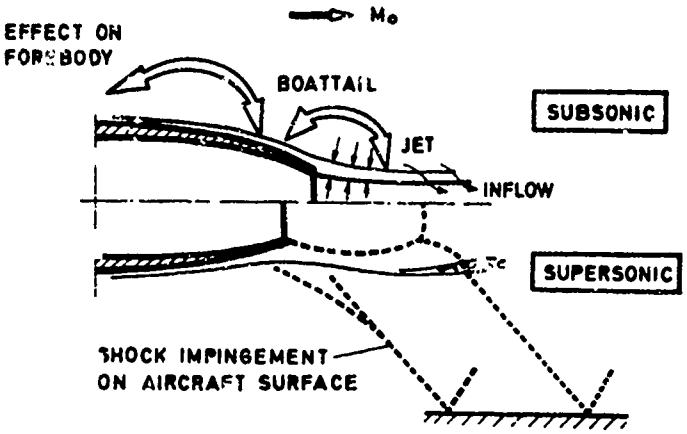

Fig. 1 Jet interference

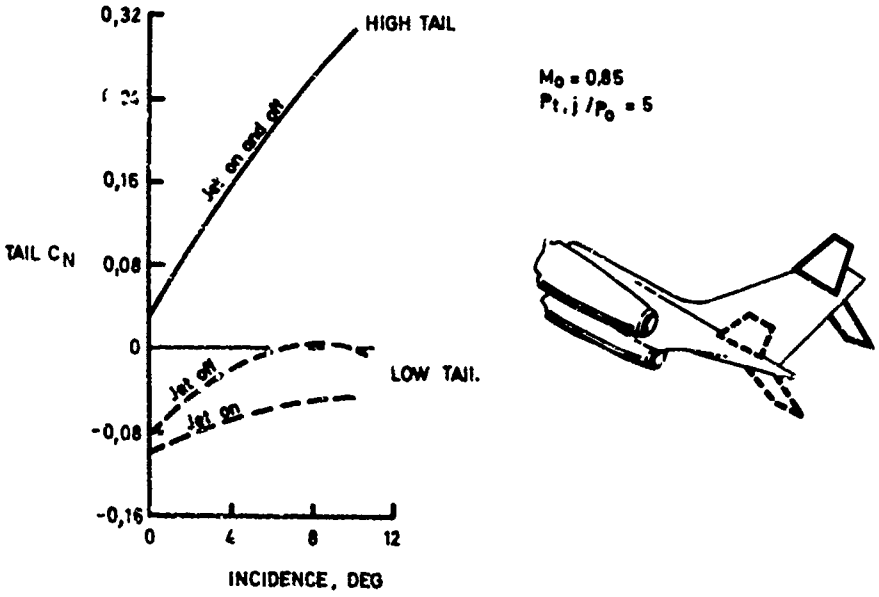

Fig. 2 Jet effect on tail normal

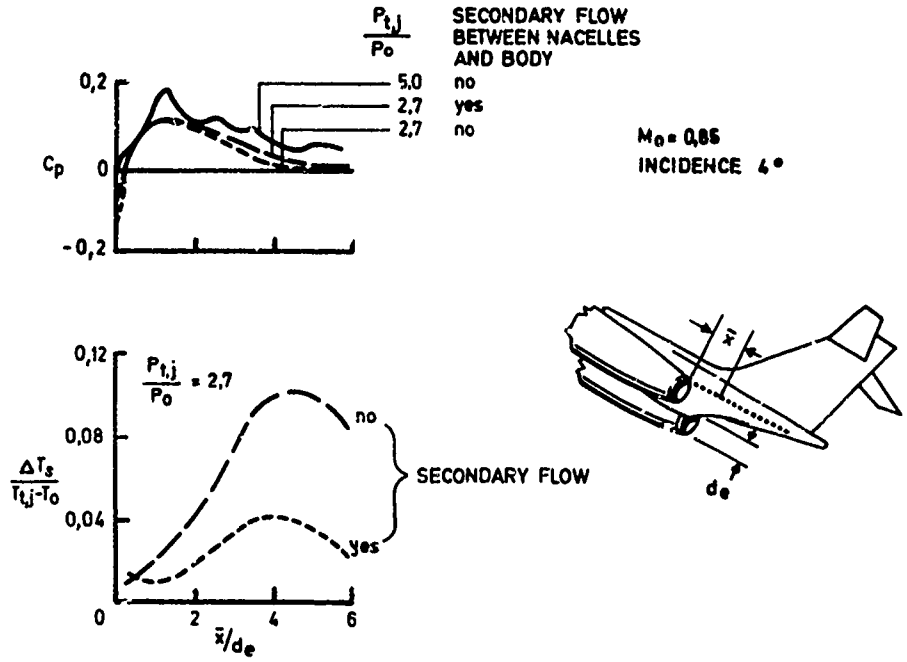

Fig. 3 Jet effects on afterbody. Pressure and temperature

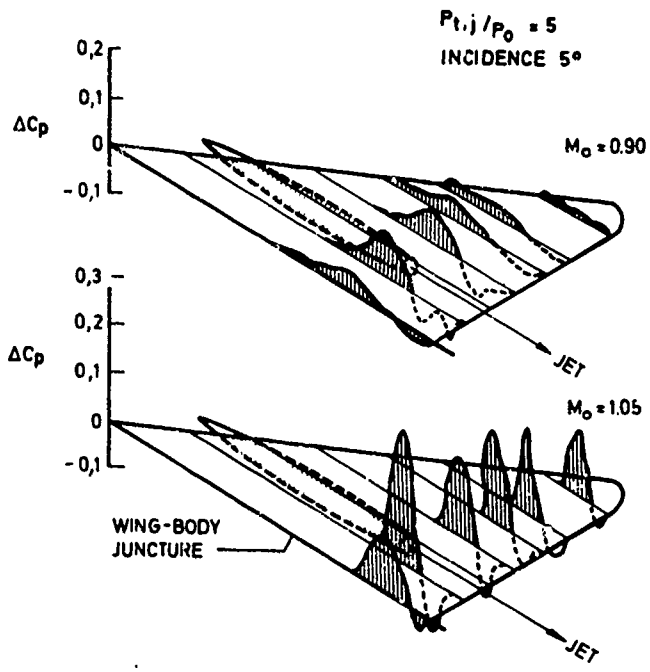

Fig. 4 Jet-induced pressure loads on wing

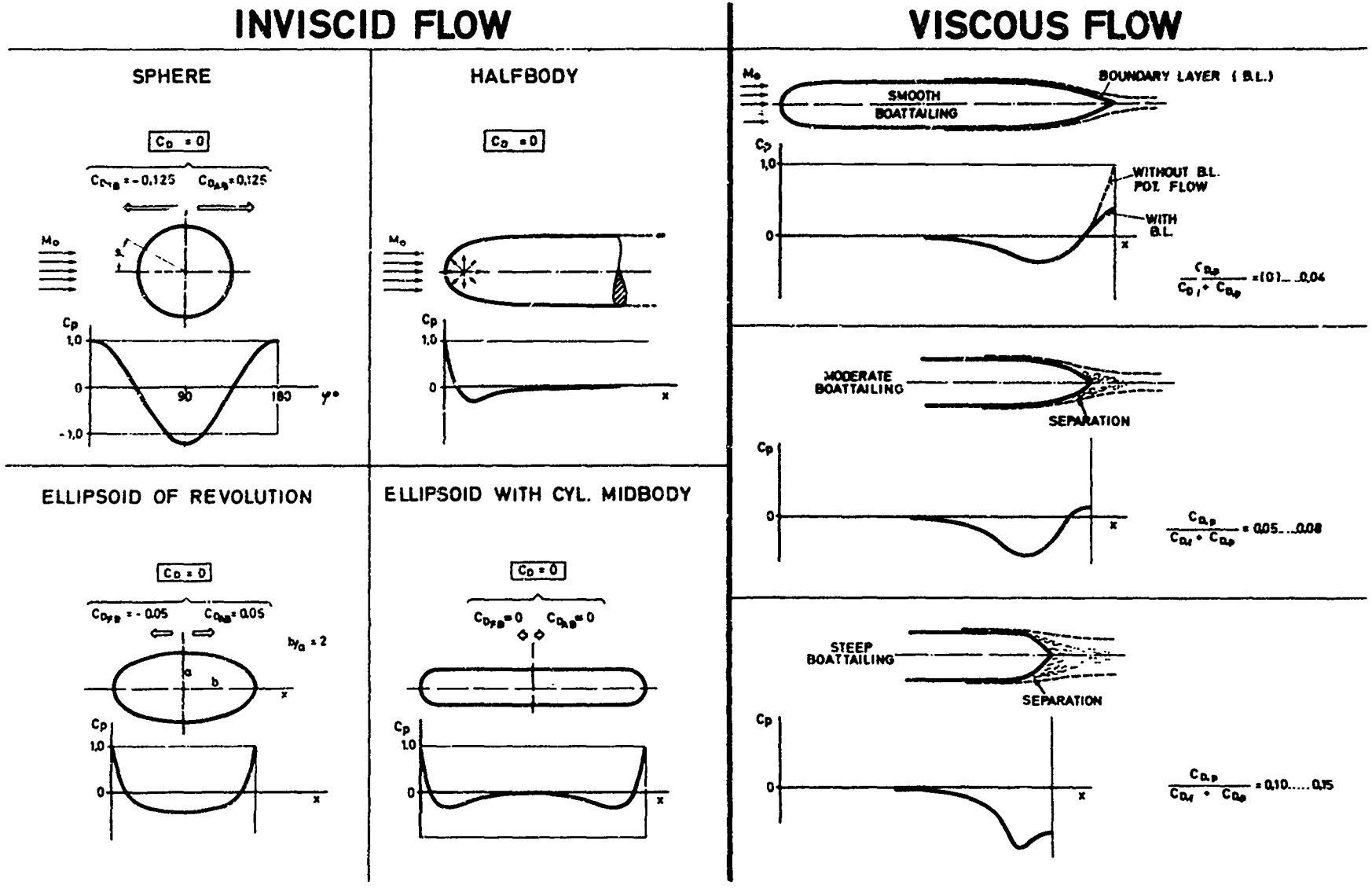

Fig. 5 Contribution of forebody and afterbody drag to total drag

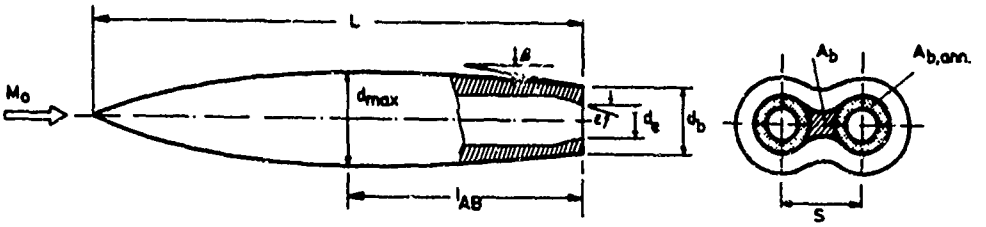

$$\underbrace{-\frac{1}{A_{max}}\int_{d_b}^{d_{max}} c_{p,\beta}\, dA}_{c_{D,\beta}} \;+\; \underbrace{-\frac{1}{A_{max}}\int_{d_e}^{d_b} c_{p,b}\, dA}_{c_{D,b}} = (c_{D,AB})_p$$

$$c_{D,\beta} \text{ and } c_{D,b} = f\Big(\underbrace{\beta, \frac{d_b}{d_{max}}, M_o, Re,}_{\text{Axisymmetric body without jet}} \underbrace{\frac{d_e}{d_{max}}, \frac{P_{t,j}}{P_o}, \frac{T_{t,j}}{T_o}, \varepsilon,}_{\text{Axisymmetric body with jet}} \underbrace{S, \frac{A_b}{A_{max}}}_{\text{Twin jet body}}\Big)$$

Fig. 6 Main parameters affecting afterbody drag

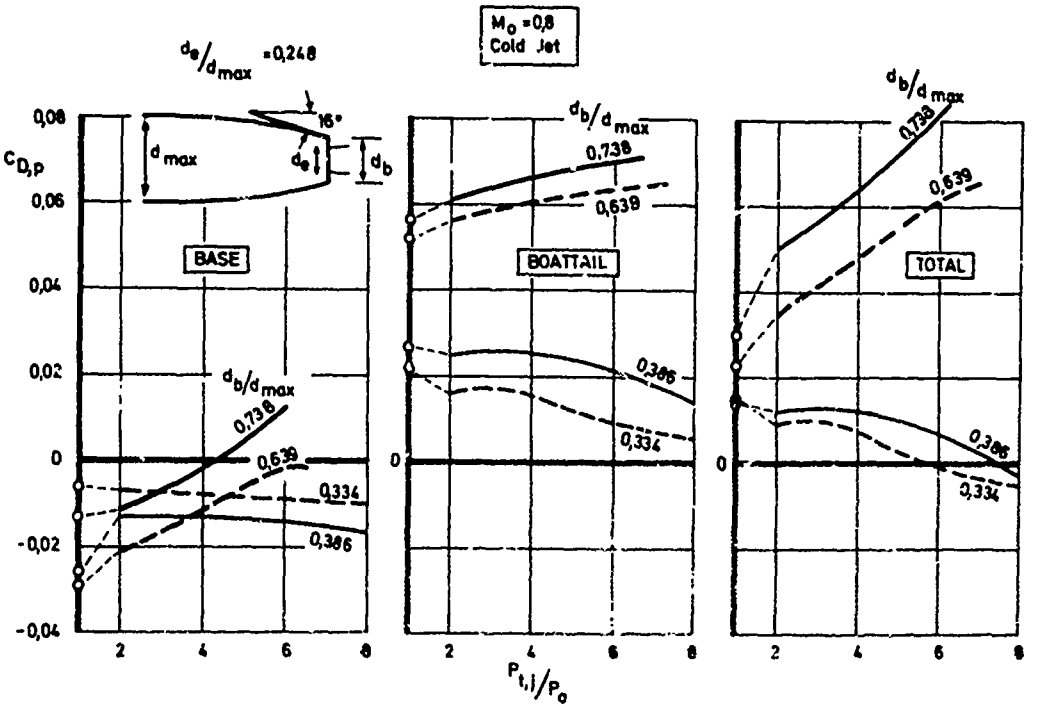

Fig. 7 Effect of jet pressure ratio on boattail-, base- and total pressure drag

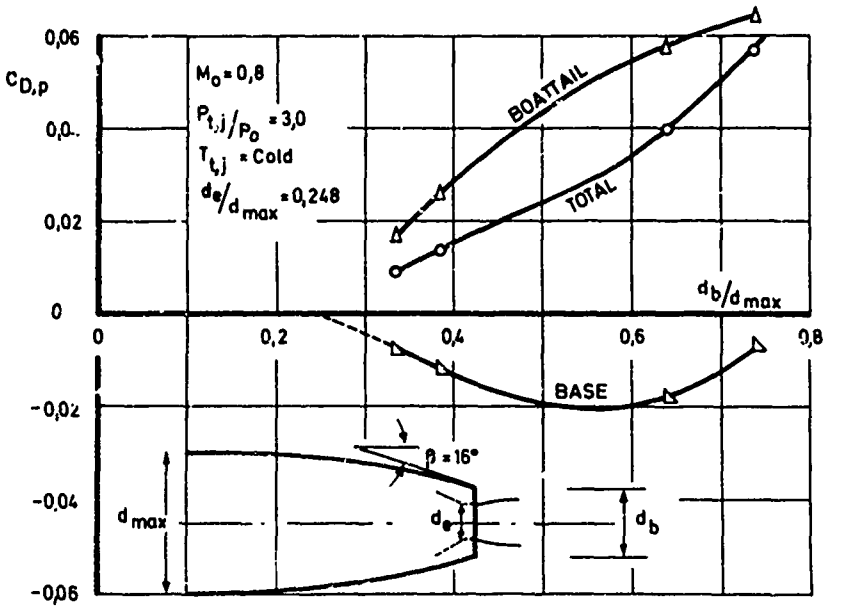

Fig. 8 Effect of base size on boattail-, base- and total pressure drag

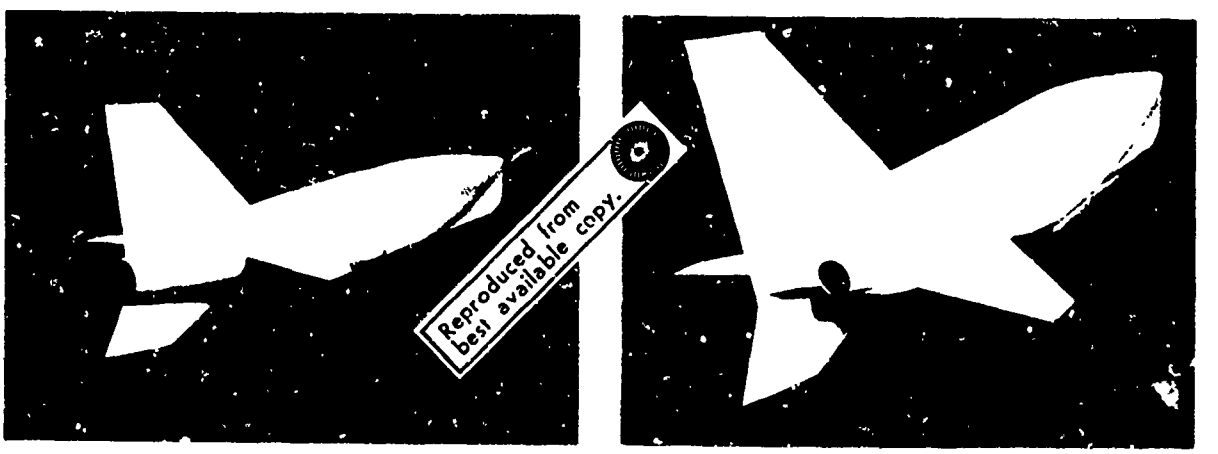

REFFERENCE AFTERBODY

TWIN - JET INSTALLATION

$$\Delta C_F = \left(\frac{F-D}{F_i}\right)_{Ref} - \left(\frac{F-D}{F_i}\right)_{Mod} \approx \frac{D_{Mod} - D_{Ref}}{F_i}$$

$$\Delta C_D = \underbrace{\left[\left(\frac{F-D}{F_i}\right)_{Ref} - \left(\frac{F-D}{F_i}\right)_{Mod}\right.}_{\text{WIND ON}} \underbrace{\left. - \left(\frac{F}{F_i}\right)_{Ref} + \left(\frac{F}{F_i}\right)_{Mod}\right]}_{\text{STATIC TEST}} \cdot \frac{F_i}{q_o \cdot A_{max}} = \frac{D_{Mod} - D_{Ref}}{q_o \cdot A_{max}}$$

Fig. 9 Comparison of typical twin jet installation with single jet reference model

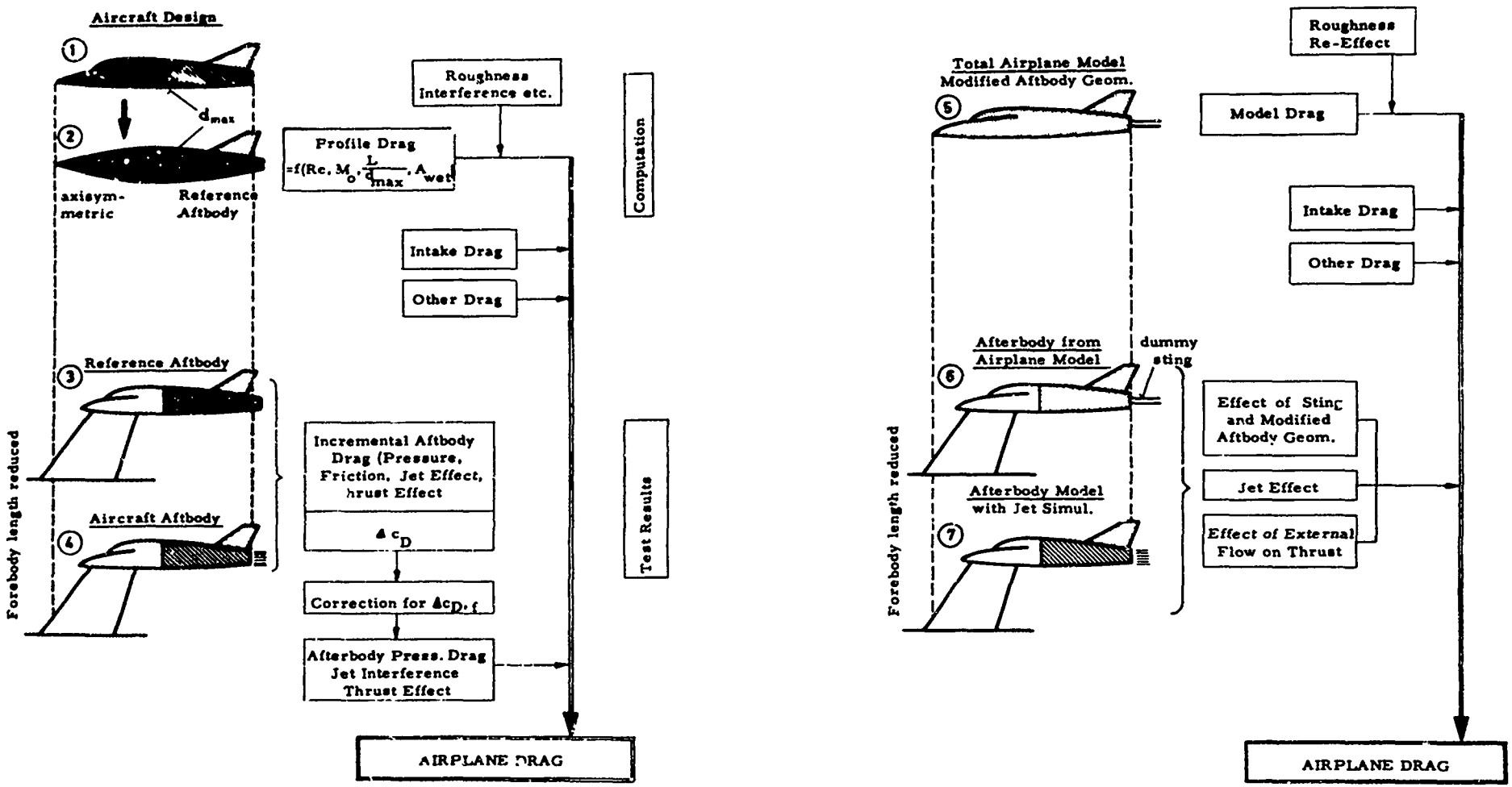

Fig. 10 Airplane drag assessment

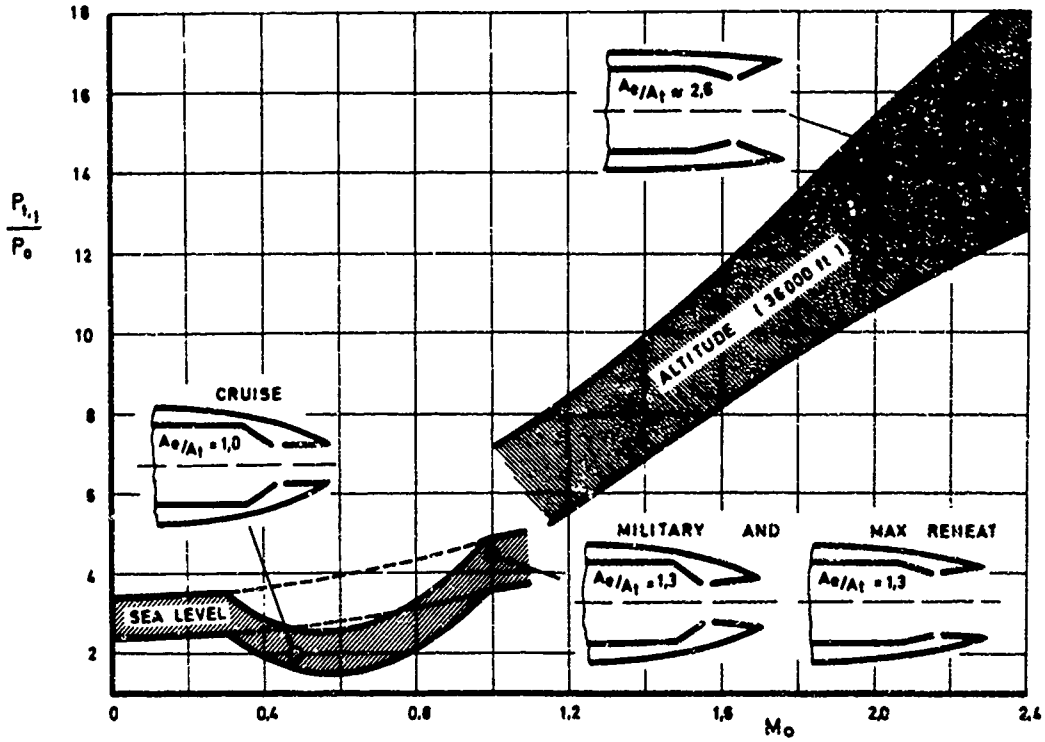

Fig. 11 Required variation of nozzle geometry

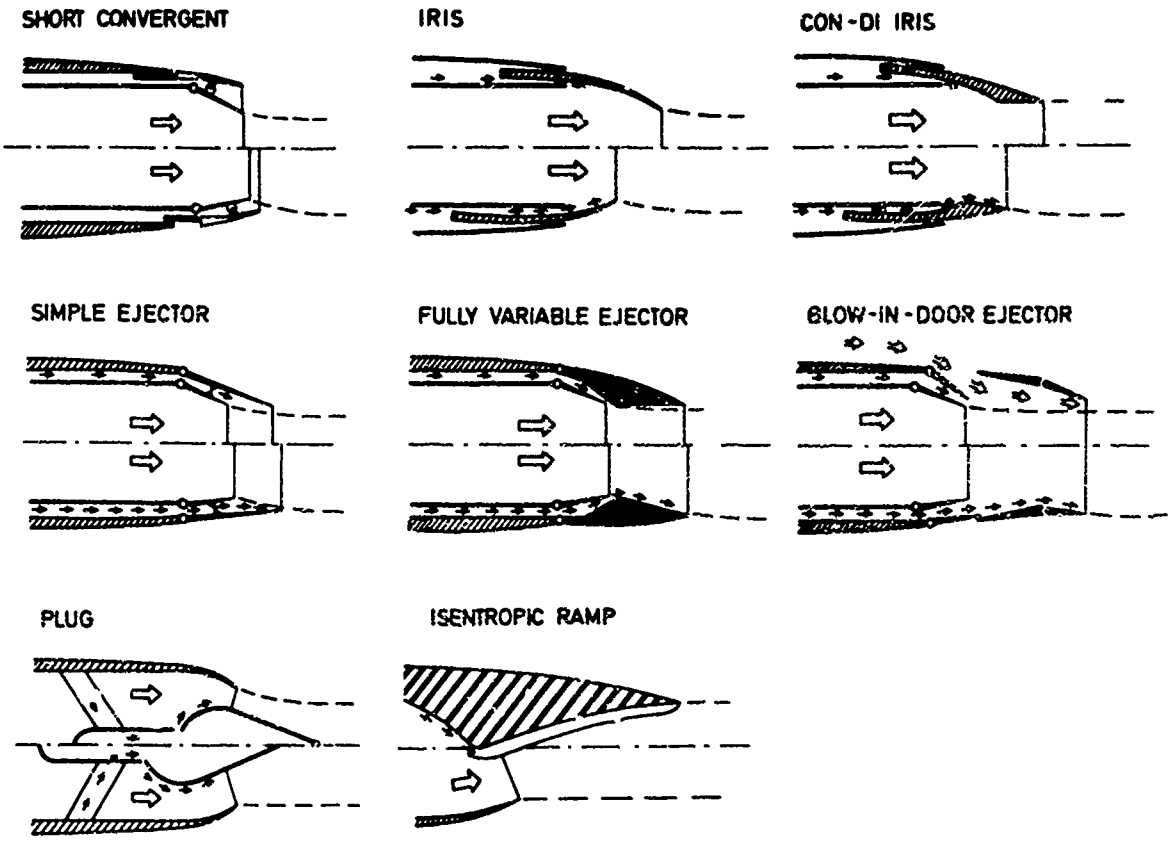

Fig. 12 Typical nozzle concepts for afterburning engines

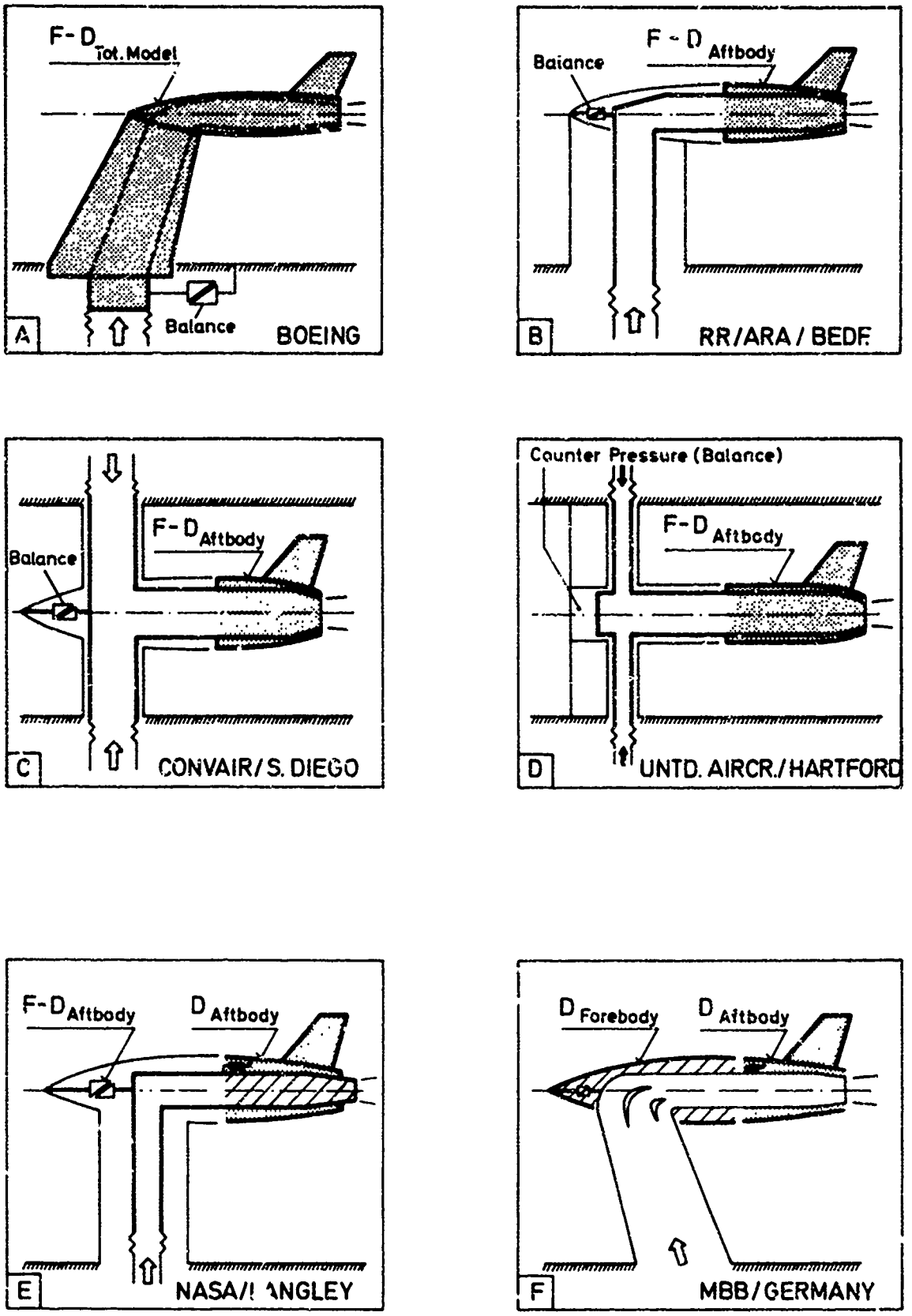

Fig. 13 Afterbody drag test rigs

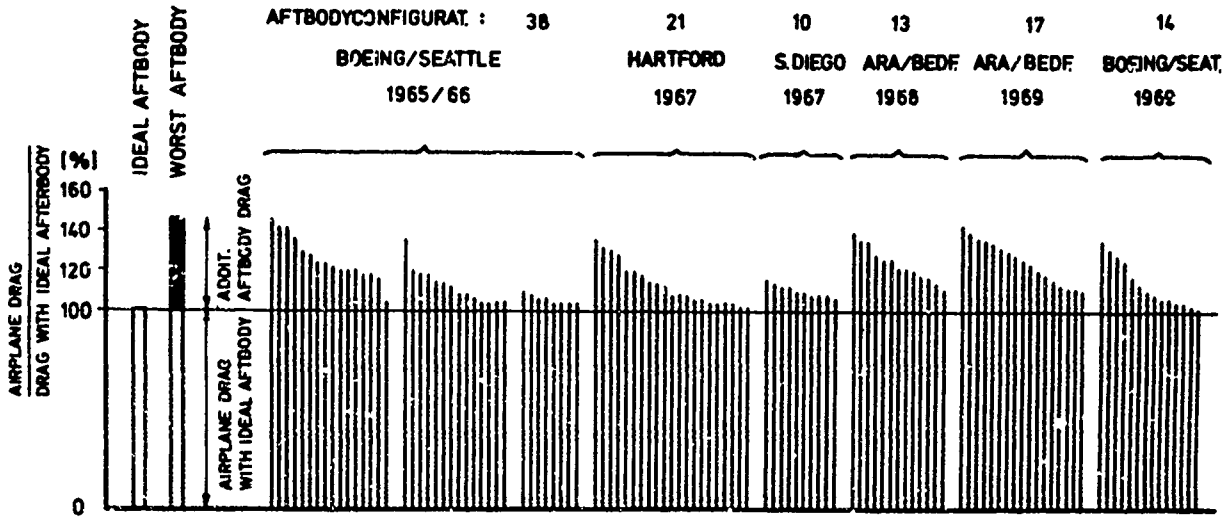

Fig. 14 Magnitude of afterbody drag

NOZZLE TYPE	BOATTAIL ANGLE	BASE AREA	NOZZLE SPACING	INTER-FAIRING LENGTH	EXCRES-CENCES
1. SHORT CONVERGENT 2 IRIS 3 EJECTOR 4. BIDE 5 PLUG 6 DOUBLE-D 7. RAMP	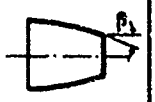	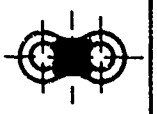	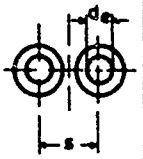	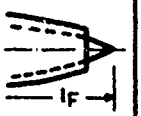	
	β = 10° 12° 15° 20°	LARGE MEDIUM SMALL ZERO	EXTRA WIDE WIDE MEDIUM NARROW EXTRA NARR.	EXTRA LONG LONG SHORT WITHOUT	SMALL LARGE WITH BASE

Fig. 15 Investigated geometric parameters

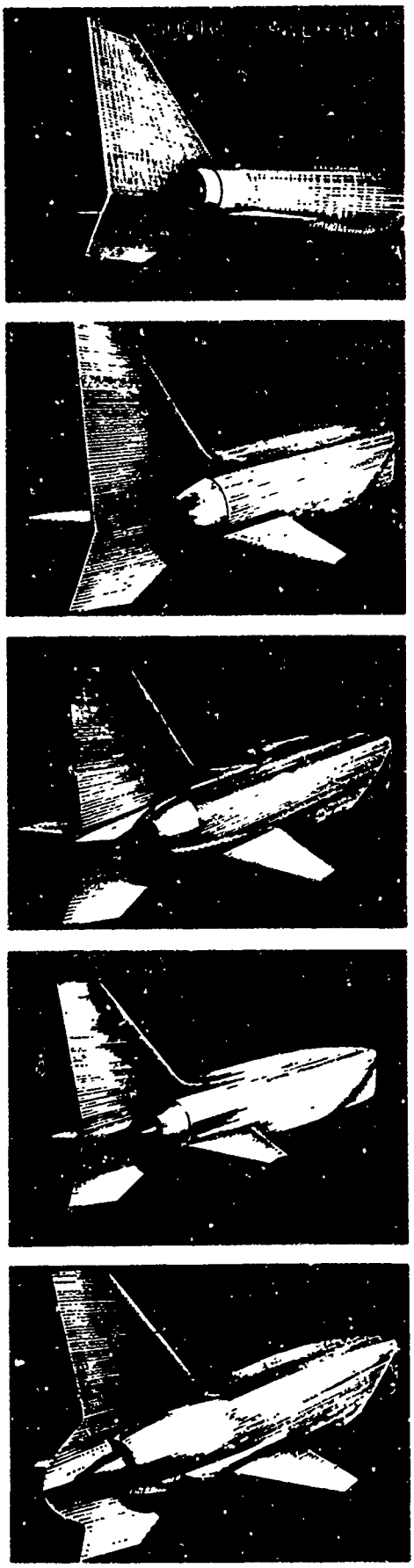

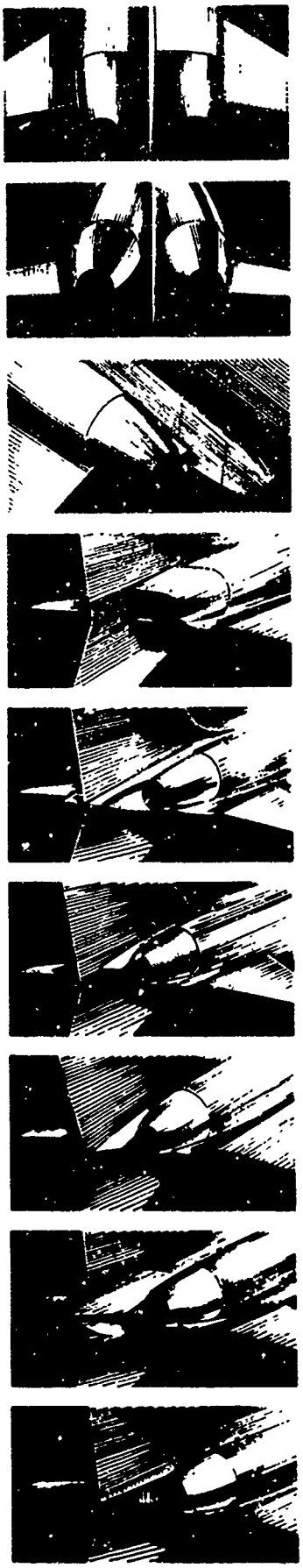

LARGE BASE

INDENTATION

VERTICAL FAIRING

SMALL BASE

FAIRED BASE

LONG FAIRING

EXTA LONG FAIRING

AREA RULE FAIRING

CUT - OUT FAIRING

NOZZLE TYPES **FAIRING TYPES**

Reproduced from best available copy.

Fig. 16 Wind tunnel models

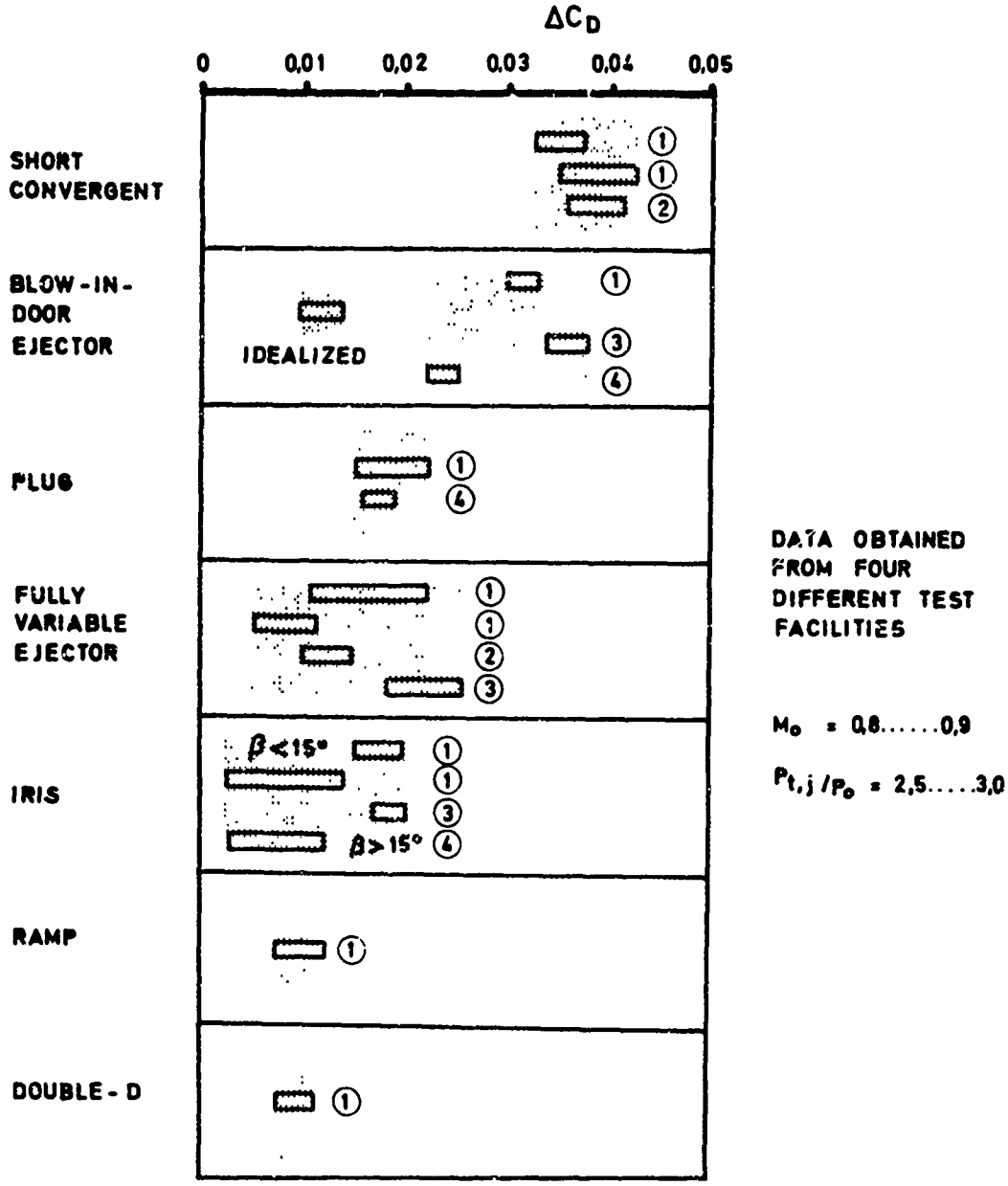

Fig. 17 Drag of various nozzle concepts obtained from different test rigs

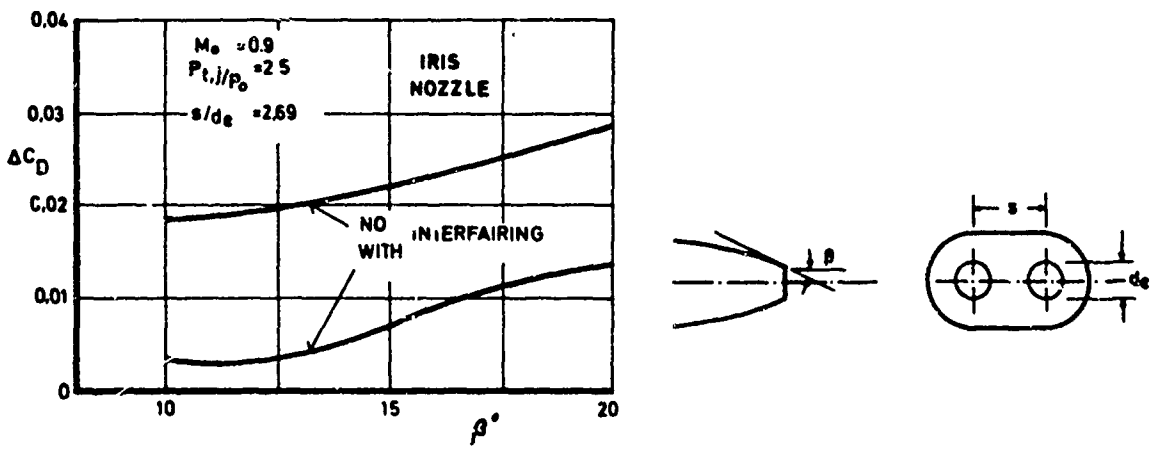

Fig. 18 Effect of boattail angle and interfairing

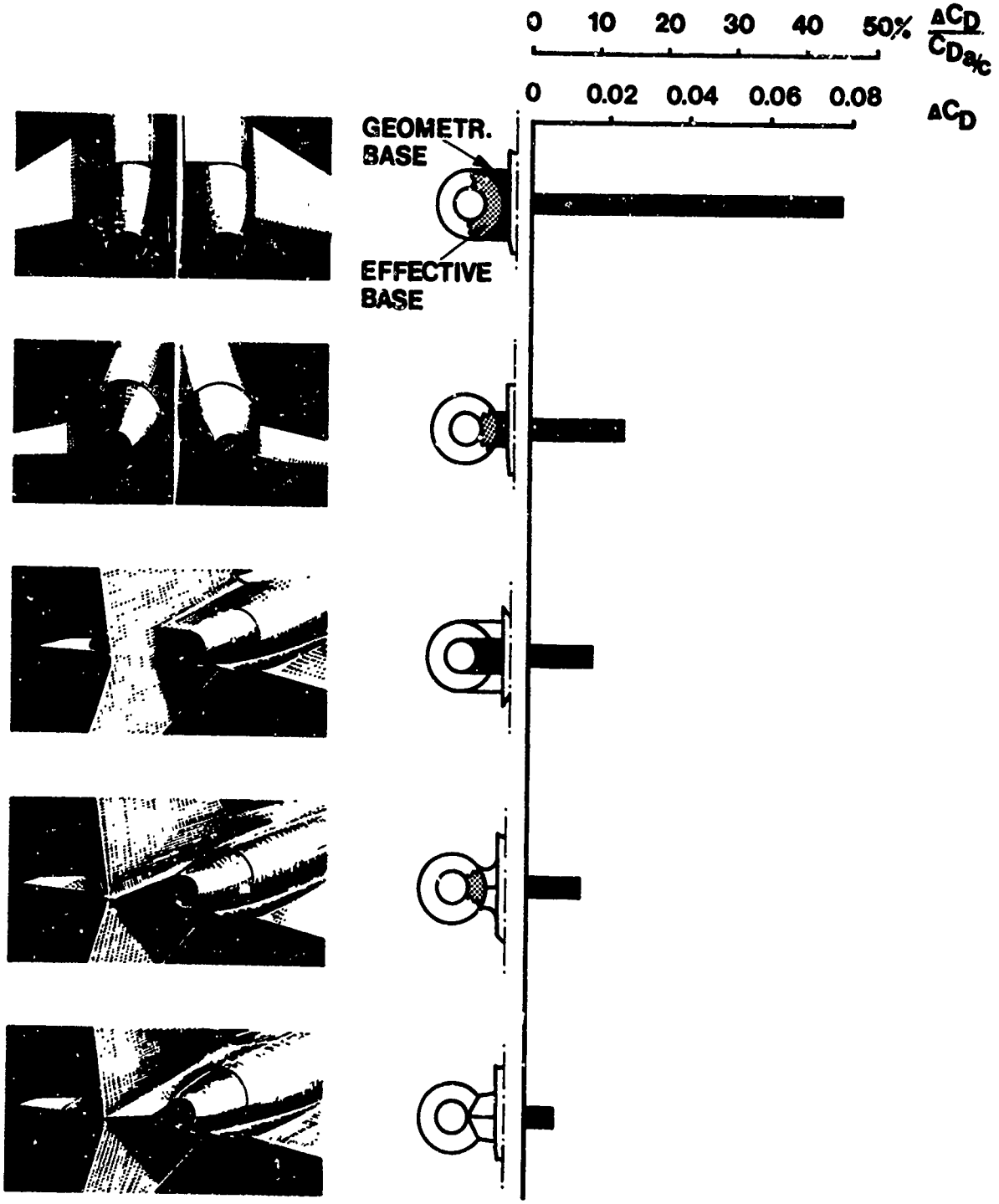

$M_0 \approx 0.9$ $P_{t,j}/P_0 = 2.5$ $s/d_e = 2.69$ $\beta = 15°$

Fig. 19 Influence of base area between nozzles on drag

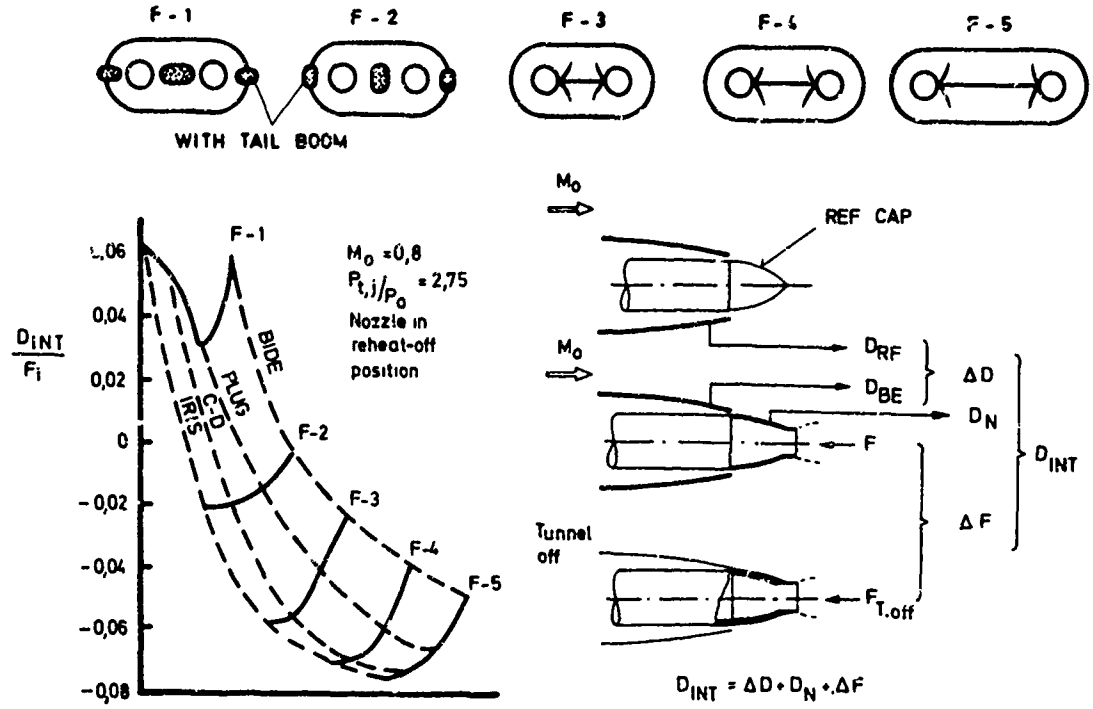

Fig. 20 Variation of interference drag with nozzle type and fuselage shape

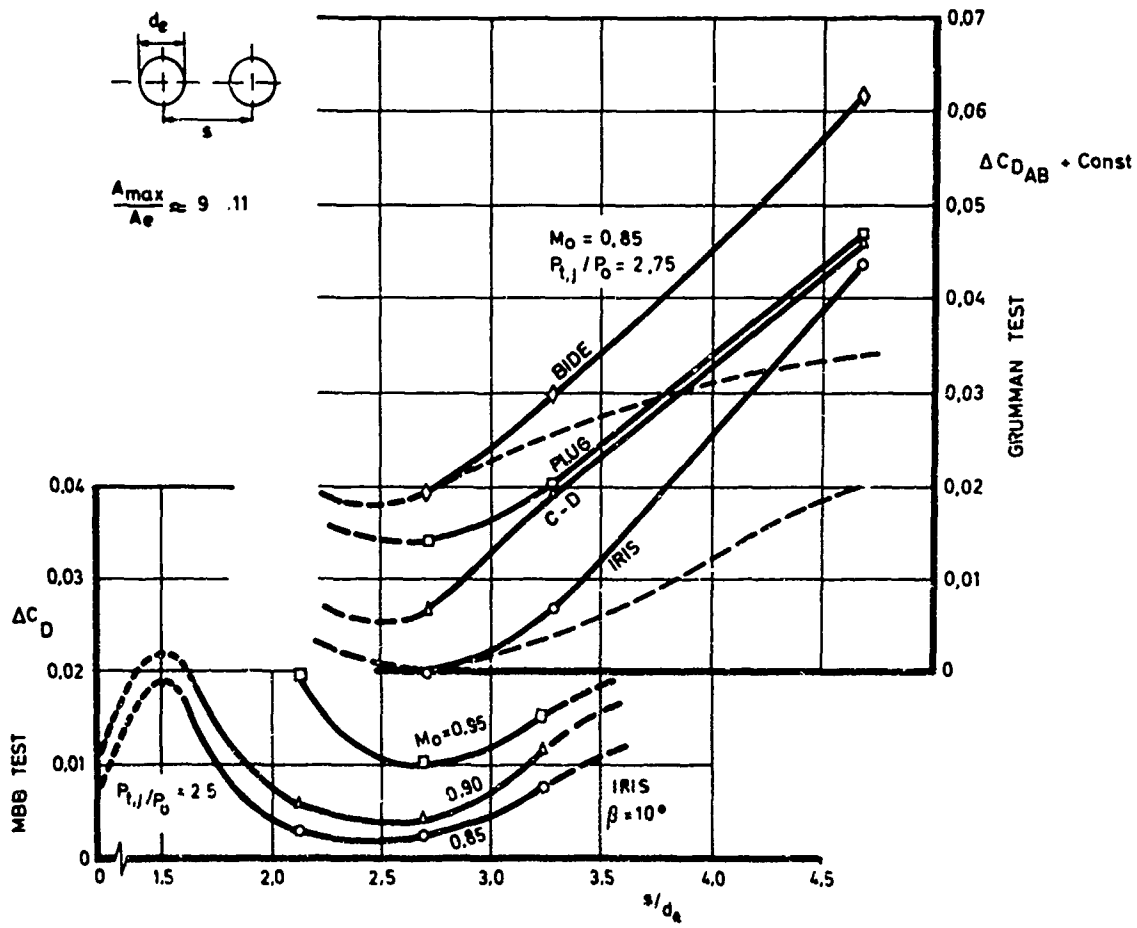

Fig. 21 Optimization of engine spacing from two different investigations

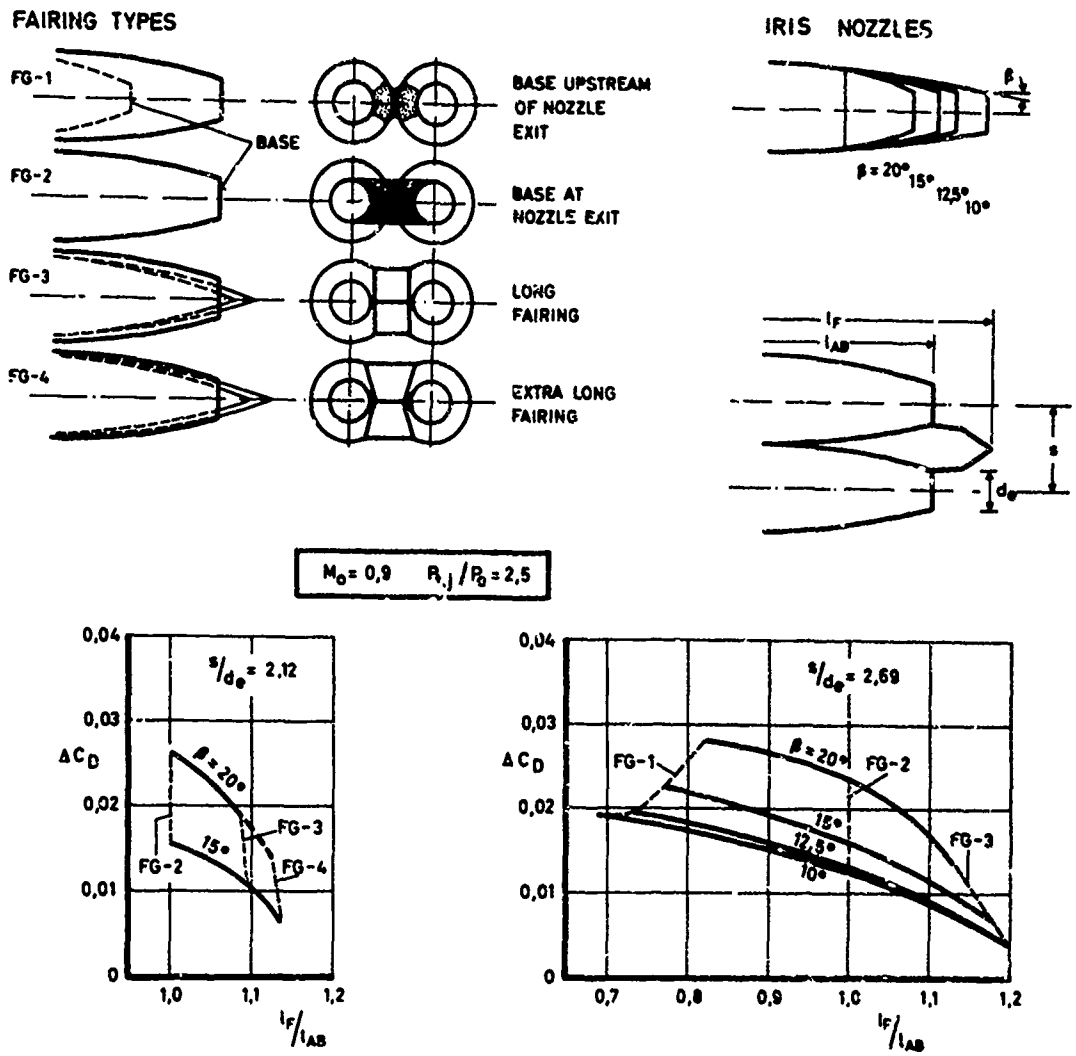

Fig. 22 Effect of interfairing length on drag for two engine spacings

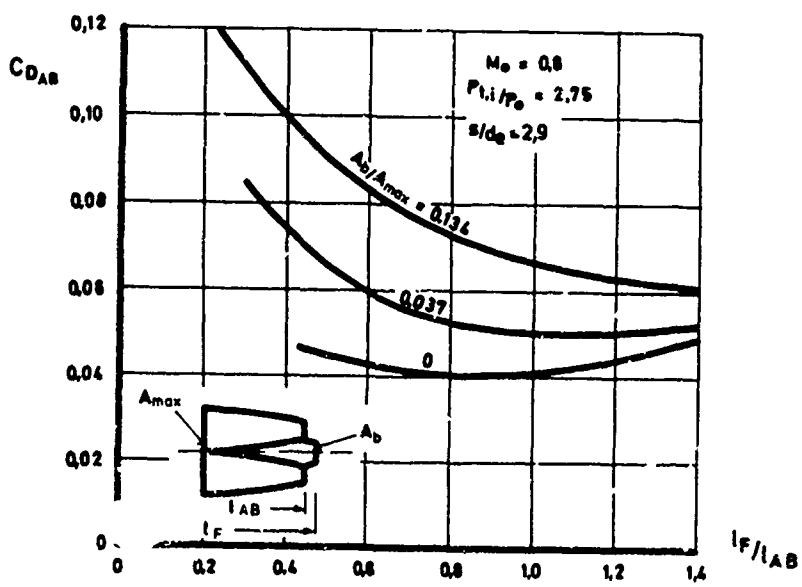

Fig. 23 Effect of interfairing length on drag for constant base areas

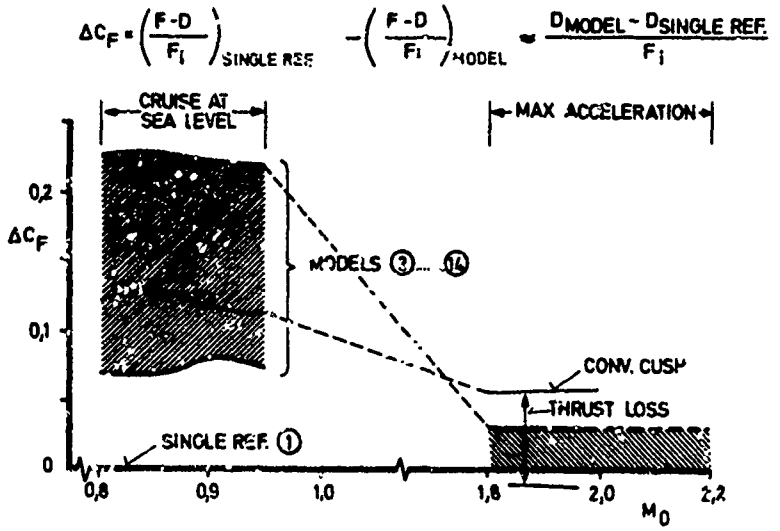

Fig. 24 Magnitude of thrust-minus-drag coefficient at subsonic and supersonic flight

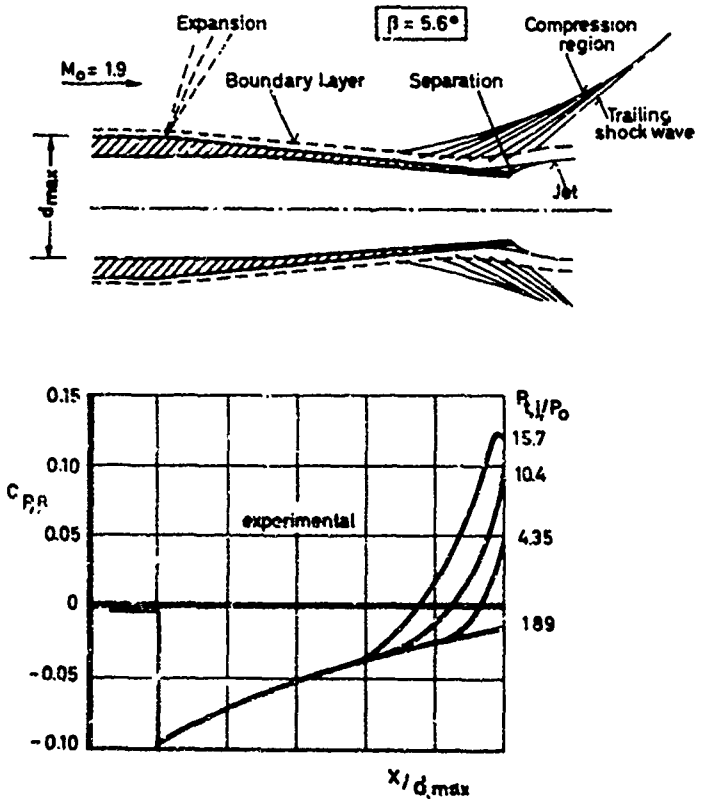

Fig. 25 Jet interference effect on boattail pressures in supersonic flow

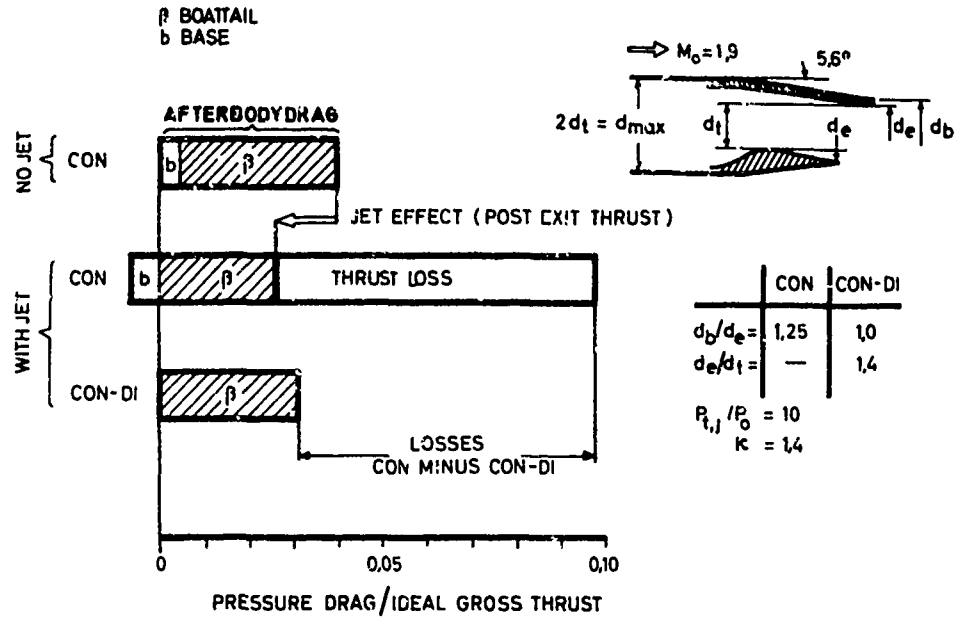

Fig. 26 Performance of matched con-di versus con nozzle at $M_0 = 1,9$

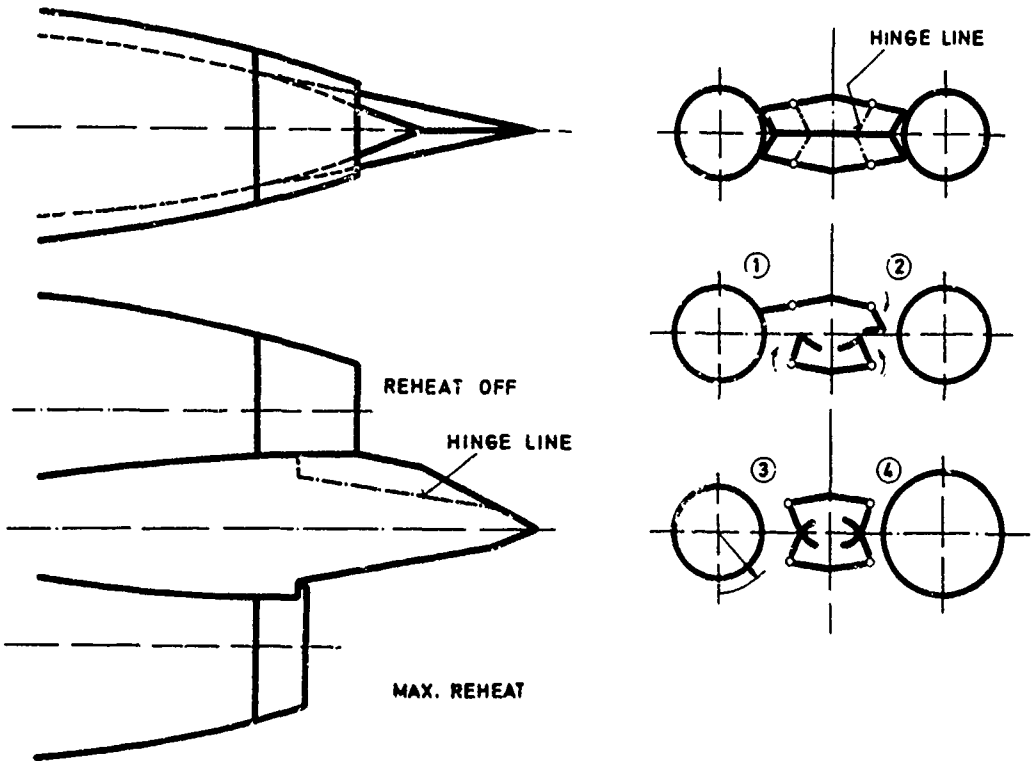

Fig. 27 Variable geometry interfairing

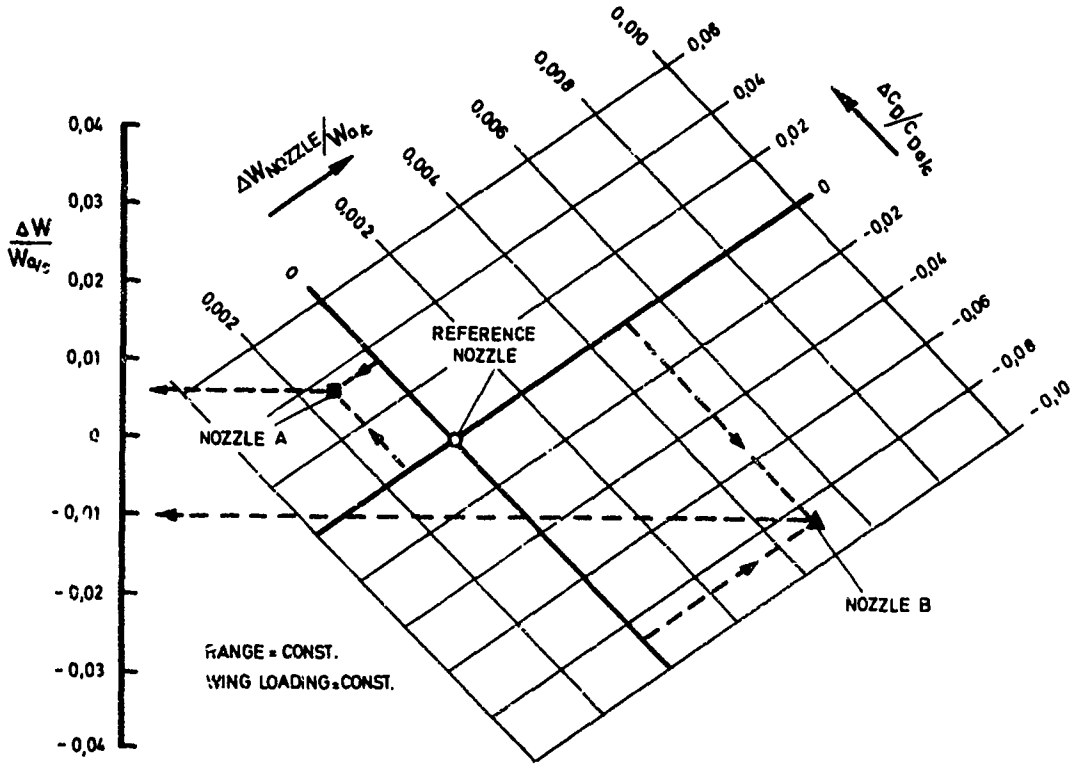

Fig. 28 Drag/weight nozzle trade study

EXPERIMENTAL DETERMINATION OF NOZZLE CHARACTERISTICS AND NOZZLE AIRFRAME INTERFERENCE

by
D. Jaarsma
National Aerospace Laboratory NLR
Sloterweg 145-Amsterdam (17)
The Netherlands

SUMMARY

First an outline is given under which circumstances certain jet flow and nozzle parameters should be simulated in the wind tunnel for both installed thrust and drag determination. The circumstances relate to the flight regimes, nozzle types and engine installation configurations (integrated or podded). Next the technical requirements for the wind tunnel and the model are given and the difficulties in fulfilling these requirements are discussed. The techniques and schemes as used by the various groups in the AGARD countries is reviewed and a discussion is made how these techniques meet the requirements. Some special attention is given to miniature turbo engine simulators.

CONTENTS

1. Introduction. 5-3
2. Accuracy. 5-3
3. Jet Simulation Requirements. 5-3
3.1. Model Configuration. 5-4
3.2. External flow Field. 5-4
3.3. Jet Flow. 5-6
- Internal thrust coefficient. 5-6
- External Nozzle Drag, Base Drag, Boattail Drag. 5-6
4. Wind Tunnel Testing Schemes for Thrust minus Drag Assessment. 5-7
5. Jet Simulation Techniques for Thrust minus Drag Assessment. 5-10
5.1. General Requirements. 5-10
5.2. Techniques, Advantages and Limitations. 5-10
5.2.1. Techniques with Faired Inlets. 5-10
- Cold Cases 5-10
- Hot Gases 5-11
5.2.2. Techniques with Complete Engine Simulation. 5-13
A. Systems with Internal Addition of Energy. 5-13
Miniature Turbine Driven Engine Simulators. 5-13
Ejectors. 5-16
B. Systems with External Addition of Energy. 5-17
6. Determination of Jet-Airframe Interference (Except Thrust-Drag). 5-17
6.1. Subsonic transport. 5-17
6.1.1. Wing Mounted Fan Engines. 5-17
6.1.2. Rear Fuselage Mounted Engines. 5-19
6.2. Integrated Airframe-Engine-Systems. 5-19
7. Non-stationary Effects of Jet Flow. 5-19
8. Corrections of Wind Tunnel Data. 5-20
9. Final Remarks 5-21
10. References. 5-21

47 figures.

LIST OF SYMBOLS

a	speed of sound
A (S)	area
c_p	specific heat at constant pressure
c_v	specific heat at constant volume
C_A	area coefficient
C_d	discharge coefficients
C_D	drag coefficient
C_L	lift coefficient
C_M	pitching moment coefficient
C_p	pressure coefficient
C_T	thrust coefficient
C_v	velocity coefficient
D	drag or diameter
d	diameter
F	measured, actual thrust
F_N	net thrust
h	throat radius
L	length
$\dot{m}$	mass flow
M	Mach number
n	jet mixing ratio (mass)
p	pressure
r	radius
R	gas constant
Re	Reynolds number
S_i^o	entropy of species i
T	temperature
v	velocity
x	axial coordinate
x_i	mole fraction of species i
X_{id}	ideal, isentropic thrust
y	radial coordinate
α	angle of incidence
β	angle of yaw or boattail angle
γ	ratio of specific heats, isentropic exponent
δ	boundary layer thickness
ρ	density
θ	tangential coordinate
μ	viscosity

SUBSCRIPTS

AB	afterbody	s	secondary
b	base	st	static
β	boattail	t	total, reservour conditions
ex	exhaust	∞	undisturbed infinity
g	gross	*	at throat
i	entering fluid		
inst	installed		
int	interference		
J	jet		
L	local		
m	model		
n	nozzle		
p	primary		
ref	reference		

1. INTRODUCTION

Once the airframe manufacturer has chosen an engine for his aircraft design he is in fact free to choose the nozzle system best suitable for the required mission. He can make a choice between ejector nozzles, variable flap ejector nozzles, blow-in-door ejector nozzles, iris nozzles, plug nozzles, short convergent nozzles or two dimensional variable throat nozzles. In this lecture no emphasis will be given to the relative performance and short comings of various nozzle designs and installations under certain conditions. These aspects will be treated in the lecture by Mr. Aulehla. Here the attention will be focused on the methods used to predict the nozzle performance from wind tunnel measurements and the methods used to determine jet interference effects at transonic and supersonic speeds. This review will closely follow the information that has been gathered from a recent AGARD ad-hoc study and is reported in reference 1. Summaries of this study are given in references 2 - 4.

As indicated in figure 1 the complete or aeroforce model tests are completed by a special afterbody and jet interference tests in the wind tunnel as is done with special inlet models. If optimum nozzle-afterbody matching is not achieved a considerable penalty on aircraft performance may result, as has been the case in many instances in the past. The actual afterbody drag, may be as large as 20 °/o to 40 °/o of the complete aircraft drag (Ref. 5). Therefore most attention of afterbody-nozzle tests particularly at transonic speeds concerns the nozzle gross thrust minus the nozzle and afterbody drag. The flight conditions to which the aircraft can be subjected to and which should be tested transonically are (a) cruise, (b) transonic acceleration, (c) transonic deceleration, and (d) high-g manoeuvre. These conditions yield various values to the nozzle area ratio, temperature ratio and pressure ratio. Figure 2 gives typical exhaust conditions at transonic speeds; other engines give different envelopes.

At supersonic speeds the drag penalties are usually less, but at supersonic cruise conditions the overall aircraft drag is very critical for flight economic reasons hence yielding a strong requirement for accurate drag assessment.

As indicated before a large variety of nozzle systems exists now-a-days, each having its particular features. Figure 3 gives a survey of various designs, since in this lecture reference will be made many times to a particular nozzle system. The fixed convergent nozzle is used with airplanes for subsonic flight, only without thrust augmentation by afterburning, such as with civil transports. Early jet fighter aircraft placed heavy emphasis on ejector nozzles. Turbojets needed a flow of secondary cooling air which could be obtained from the ejector action of the primary jet. This is still true for turbojet engines for supersonic transports. A later development was the introduction of extra tertiary air intakes at the nozzle location. These blow-in-door ejector nozzle gave performance gains at transonic flight. The introduction of the fan and bypass engines made the nozzle design easier with respect to cooling since sufficient cooling air from the fan at the same pressure ratio as the turbine flow, came available which can be ducted to the nozzle, making the other nozzle designs possible. However for optimum use, the fan engines ask for larger nozzle area variations with afterburning. Hence, in the past literature most attention was paid to the ejector nozzle installation requiring secondary flows, whereas in the recent literature more experiments are described concerning the other nozzle systems, particularly the iris and plug nozzles. Further information on nozzles can be found in references 5 - 8 for example.

In this lecture the jet parameters will be briefly described and it will be indicated as far as possible when these parameters should be simulated in the wind tunnel. Further the various testing schemes and techniques as used will be described both for the thrust-drag assessment and other jet interference problems.

In reference 1 an extensive bibliography on jet interference testing is given. That bibliography follows a convenient nozzle parameter code and may therefor be of assistance in establishing wind tunnel programs for the various speed regimes.

2. ACCURACY

The required accuracy of determination of the thrust should be compatible with the accuracy of measurement of the drag (i.e. the net thrust) of the basic airframe. Hence, the accuracy required for the gross thrust measurement depends on the ratio of the net to gross thrust, which in general will be a function of the engine bypass ratio. The following set of values can be regarded as typical as obtainable from wind tunnel tests.

	Subsonic transport	Fighters	Supersonic transport
Cruise C_D	0,023	0,030	0,018
Overall accuracy of cruise drag *	± 0,0001	± 0,0003	± 0,0005
°/o " " " " "	± 0,45	± 1,0	± 0,3
Average $\frac{\text{gross thrust}}{\text{net thrust}}$	3	2,5	2,5
Required °/o gross thrust accuracy	± 0,15	± 0,4	± 0,12

This survey shows that overall accuracy of better than ± 1/2 °/o of the cruise or critical transonic gross thrust value is desired. Achievable accuracy is difficult to assess because overall accuracy includes the combination of many instruments such as force balances, pressure transducers, thermocouples and mass flow meters, in addition to wind tunnel speed and model attitude indicators. Each model test apparatus presents individual problems in sizing, restricted internal space, pressure tares, metric break seal restraint, thermal expansion, clearances and other items which make any general statement on achievable accuracy impossible.

3. JET SIMULATION REQUIREMENTS

Before initiating nozzle and afterbody tests with or without jet simulation in the wind tunnel, questions must be answered first concerning the variables involved related the nozzle conditions. Tabel 1 gives a review of these variables and their possible values or features. After the latter have been established the next step is to define which jet and nozzle parameters should be simulated in the

* Drag values of components can be obtained more accurate.

wind tunnel experiments. Usually a compromise is found between what is desirable and what is feasible in practice. From this part on the wind tunnel model can be designed based on local possibilities, on past experience and on costs.

3.1. MODEL CONFIGURATION

The degree of necessary external flow simulation and the aircraft configuration involved strongly determine the model configuration and model support system.

Also the degree of expected mutual interference has an influence on the model configuration to be chosen. (does the external flow affect the nozzle coefficients and/or does the jet influence the external flow?). Usually the answer for choosing the model configuration involves three possibilities. The first possibility is to simulate the external flow field as good as possible by testing the afterbody and nozzle together with the complete aircraft representation for which the inlet is usually completely faired and for which the model support system causes little interference at the exhaust. The second possibility is to simulate only the afterbody geometry and determine from the relative differences the nozzle-afterbody performance. The latter test procedure is usually applied to determine nozzle-afterbody performances regardless of aircraft fore-body shape. It is performed in an early stage of aircraft development in order to obtain an early estimate of the nozzle-afterbody performance. The complete model nozzle test is usually accomplished for final checks. The third possibility is to test only the nozzle in an axisymmetric afterbody without tail planes and other (inter) fairings. This method is usually referred to an isolated nozzle test.It gives rather ideal performance. This testing is performed to establish the nozzle performance under ideal external flow conditions.

Table II gives the advantages and disadvantages of both test procedures. Figure 4 shows a typical isolated nozzle test rig for subsonic Mach numbers as it is used in the U.K. If the inlets and exhausts are far removed from the aircraft centreline, for example for podded underwing installations, it is also possible to use the halfmodel reflection plane technique. This technique is only allowed if no reflection plate boundary layer - jet interference are expected. Figure 5 is such a set-up as it is used in France for exhaust testing of the Concorde. Reference 9 gives a review of the various model support systems and the accompaning techniques.

Table 1 VARIABLES RELATED TO EXHAUSTS OF JET AIRCRAFT MODELS

	Parameter	Possible value or feature
Configuration	Number of nozzles	single, dual, multiple
	Spacing of nozzles	narrow, wide
	Mounting	podded, integrated in fuselage
	Nozzle type area ratio	Conv,Condi,Plug,BIDE,Ejector. Iris
	Geometry of afterbody	axisymmetric,non-axisymmetric,tail planes
	Direction of jet	parallel with main flow,acute angle.
External flow	Mach number	subsonic, transonic, supersonic, hypersonic
	Characteristic Reynolds number)	laminar, turbulent
	boundary layer at exhaust)	thickness
	Flow field at exhaust	basically attached, basically separated.
	Angles of incidences and yaw.	
Jet flow	Mean pressure ratio	over expanded, optimum, under expanded
	Mean temperature ratio)	dry, afterburning
	ratio of specific heats)	
	Number of nozzle streams	primary, primary+secondary, primary + secondary + tertiary
	Total pressure distortion	negligible, important
	Total temperature distortions	negligible, important
	Swirl	negligible, important
	Turbulence	negligible, important

3.2. EXTERNAL FLOW FIELD

The primary flow field parameter, the undisturbed Mach number is duplicated in all wind tunnel tests. The local flow field close to the nozzle is however generally highly three dimensional as may be seen in figure 6. This local inviscid field might be disturbed by the model support system and hence the results of the tests might be misinterpreted.

The viscous flow field is however of greatest concern for the wind tunnel experimentalist, because the exhausts always operate within the relatively thick boundary layer of the forebody or inlet. The nozzle tests in the wind tunnel are performed at reduced scale and hence at reduced Reynolds number. The degree of scaling depends on the available tunnel and testing rigs as well as on the degree of external flow field simulation. Complete external flow field simulation requires small scales, whereas large scales can be obtained with isolated afterbody tests. Boundary thickness reduction at the nozzle station towards flight conditions can be obtained in the wind tunnel by shortening the forebody, hence losing inviscid flow field simulation. The effect of the approaching boundary layer on the afterbody performance is however very large. The important non-dimensional parameters is the boundary layer thickness (δ) relative to a reference nozzle radius (r_n) (or diameter). The increase of δ/r_n, as is the case for testing a complete model at reduced Reynolds number, implies that the nozzle is immersed in a larger boundary layer field, making the viscous effects larger. An example of how this parameter affects the total afterbody and nozzle drag is shown in figure 7 for two nozzle systems (Ref. 10). It is seen that the effect of the boundary layer depends largely on the nozzle type.

Apart from the afterbody drag, the nozzle gross thrust coefficient can be also sensitive to the external flow. Figure 8 gives some nozzles which are basically sensitive to external flow and which nozzles are basically immune to the external conditions. The sensitivety is generally due to altering sonic line shapes, due to wave reflections and due to altered ejector characteristics. The internal flow field of a condi nozzle is very immune to the external conditions.

Table II ADVANTAGES AND DISADVANTAGES OF ISOLATED AND COMPLETE MODEL TESTS

ISOLATED TESTS	COMPLETE MODEL TESTS
Advantages	
- For a given size test facility, isolated nozzle tests permit larger scale models to be used with correspondingly higher Reynold's numbers.	-Complete model tests provide better external flow simulation and provide a more exact duplication of the nozzle environment that will exist on the full scale airplane (generally except for boundary layer thickness).
- Due to a possible reduced length of the forebody, the relative external boundary layer thickness at the nozzle can be properly scaled with respect to full scale.	-Complete model tests are the only means of predicting installed nozzle performance since mutual airframe-nozzle interference exists and forebody-wing influences on the afterbody-nozzle configuration are simulated.
- Higher degree of accuracy as complete model nozzle tests.	-Installation of the isolated nozzle in an airframe may produce either favourable or unfavourable effects depending on the type of nozzle and the flight speed. Results such as these are strongly dependent on the overall aircraft design.
- Larger models make the design easier and allow more instrumentation (pressures) to be included and secondary airflow systems are more easily accomodated.	-Complete model investigations of generalized research configurations with exhaust and slipstream simulation permit evaluation of effects on aircraft aerodynamics and installed nozzle performance such as exhaust nozzle axial and lateral location, effect of afterbody angle to nozzle, engine interfairing shape, and effects of empennage on nozzle performance.
- More exact detailing of the nozzle shaping is possible, i.e., roughness of variable geometry leaves and joints can be simulated and nozzle base thickness can be scaled.	-The additional effect of the exhaust plumes on control surface effectiveness and loading can be determined.
- Isolated nozzle tests are better for basic investigations, e.g., effect of jet temperature ratio, specific heat ratio, internal flow distortions.	-Plume interference on adjacent surfaces may be evaluated including both pressure and temperature increments if hot jet exhausts are employed.
- Isolated nozzle investigations are a necessary step in the development of new exhaust system concepts.	-Flow visualization studies (e.g., shadowgraph or schlieren methods) can be conducted on the complete model to aid in the analysis of results.
- Parametric studies can be conducted at less cost on external geometric variables, internal performance and initial thrust reverser and noise suppressor designs.	
- The isolated nozzle test apparatus may be used by engine manufacturers to provide the baseline for the nozzle "uninstalled performance" presented in his engine performance deck.	
- The pressure and force data obtained from isolated data can be used to substantiate or improve theoretical and empirical calculation methods.	
Disadvantages	
- A cylindrical approach section to the nozzle (near free stream flow conditions) which hardly ever occurs in practice.	-For a given size facility the complete model nozzle size will be much smaller than the isolated nozzle, making detailed scaling more difficult (lower Reynolds number etc.).
- Airframe installation effects can be very large so that a redesign of the nozzle may be required to obtain the desired installed performance.	-Complete models generally require more instrumentation, including perhaps more than one strain gauge balance, pressure instrumentation on the afterbody and other portions as well as the nozzle, requiring careful design to provide the propulsion simulation without interference of the measuring instruments of the metric section (fouling).
- Because of the wide variety of nozzle locations possible in an aircraft design, mutual nozzle-airframe interactions cannot be predicted from isolated nozzle tests.	-Space requirements in a complete model make the simulation of secondary and tertiary flows in the nozzle or base regions more difficult.
- In many large wind tunnel facilities, it is difficult to obtain the true isolated performance of the nozzle since the model requires support structure and ducting to supply the exhaust gas.	-Model size is limited by the test section available length and cross section at the most critical Mach operating condition and also by the propulsion system flow capacity.
	-Support system interference must be evaluated for the complete model in order not to invalidate all of portions of the results (Effect at all Mach numbers).

For afterbodies only, reference 11 indicates also a large external boundary layer effect. Figure 9a shows the boattail pressure drag reduction with increasing boundary layer thickness. It is stated that the thicker boundary layer appeared to effectively round the boattail corner, thus reducing drag. However, if the flow is separated an increased Reynolds number (hence reduced boundary layer thickness) reduces drag; figure 9b from reference 11. It is therefor necessary to determine the detailed flow field causing drag before conclusions can be drawn how Reynolds number (or boundary layer thickness) will affect the afterbody drag.

The importance of correct external flow field simulation is clearly illustrated in reference 12. Figure 10 is an example of this work for an variable ejector nozzle. A comparison is made between isolated nozzle tests, half-model reflection plane testing and complete model testing. From these results it is indicated that nozzle installation will increase the afterbody and external nozzle drag. The same conclusions are drawn for blow-in-door ejector nozzles and for these nozzles in supersonic external Mach numbers.

In conclusion in general a compromise must be made regarding model configuration and support considering inviscid flow field simulation (complete or partial model) and viscous flow field simulation (relative boundary layer thickness, reduced forebody, boundary layer blowing or suction). No rules can be given for optimum model design. Each aircraft configuration requires its own consideration.

3.3. JET FLOW

As has been indirectly indicated in the former section in the wind tunnel tests two items must be considered, namely the change in afterbody drag due to jet effects and the change in nozzle thrust and discharge coefficients due to installation in airframe. This section considers the influence of the jet flow parameters on the afterbody drag and nozzle characteristics.

The jet flow parameters of a turbojet or turbofan engine are shown in table I. From the fluid dynamical point of view the jets should be fully simulated.

From the practical wind tunnel point of view the jets should be simulated as simple as possible. Laws of fluid dynamics quite precisely define the scaling rules and the necessary conditions for similitude. Reference 13 gives an excellent review of the scaling rules for inviscid flows. However, the problem is to determine the consequences when some of the conditions are violated. Furthermore little is known about the similarity laws for the mixing phenomena between the jet and the main stream as it effects the flow at the exhaust.

INTERNAL THRUST COEFFICIENT

The static thrust coefficient of a particular nozzle depends primarily on the nozzle pressure ratio and on ratio of specific heats as well as on the total temperature and total pressure distortion upstream of the nozzle. In the case of a conical nozzle C_T depends also on the jet boundary contour just downstream of the nozzle edge. As is seen in figure 3, conical convergent nozzles are frequently used requiring proper simulation of mixing at the downstream boundary between the jet and the external flow in case of a simple convergent nozzle, and between the primary jet and secondary flow in case of ejector nozzles. However little is known about the actual influence of mixing downstream of a convergent (primary) nozzle on the nozzle thrust and discharge coefficients; more analytical and experimental work is needed how scaling laws should be applied. The rate of mixing depends on the ratio of the mass density flows (ρv) on both sides of the mixing boundary and on the initial upstream turbulence. In the case of ejector nozzles this means also that the secondary mass flow must be simulated. This simulation is hard to achieve for blow-in-door ejectors since the secondary mass flow depends primarily on the outer boundary layer and flow field conditions as is seen in the previous section. To a lesser extent this can also be said for plug nozzles.

In present wind tunnel nozzle test rigs the internal flow distortions and turbulence are not simulated. It is noticed in figure 11 that the total pressure distortions play an important role in the location of the sonic line and hence in the discharge coefficient and pressure distribution on the internal nozzle surface. How much the external flow field will influence the location of the sonic lines when it is already disturbed by internal flow field distortions is by now unknown. Hence, more information is needed on when (at which nozzle types and installations) these distortions can be omitted in the nozzle performance assessment in wind tunnels, when analytical or experimental corrections can be used (and how) and when these distortion should be simulated in the wind tunnel. Information is needed on the applicability of specific scaling laws.

For nozzles with internal supersonic expansion the ratio of specific heats has an influence on the characteristic lines, which means, for example, that for an ejector nozzle the initial inclination angle of the primary jet is different if γ_j is not simulated. (See for example Ref. 13 and 14). The primary jet contour can be simulated by adjusting the nozzle pressure ratio, resulting in an incorrect simulation of jet momentum. Therefore γ_j should be simulated as close as possible. If this condition can not be satisfied the nozzle for the wind tunnel model should be designed in a similar manner as the real nozzle has been designed. However, in that case off-design conditions will yield difficulties regarding interpretation of the results.

EXTERNAL NOZZLE DRAG, BASE DRAG, BOAT-TAIL DRAG

Besides the external flow field parameters, as discussed in the previous section, these drag terms are also dependent upon the jet properties. If the outer flow separates, as it often does near the nozzle exit, the separation point and pressure level in the separated region is fully determined by the viscous interaction between the jet and the ambient flow and hence on the jet boundary (shape) and mixing process (see Fig. 12). The inviscid jet shape is fully determined by the nozzle pressure ratio p_j^*/p_∞, γ_j and Mach number at the exit M_j. The jet shape (initial inclination angle) is approximately constant for convergent nozzles if $(p_j^*/p_\infty)^{1/\gamma_j}$ = constant. This relation is given in figure 13, for $M_j = 1$ which shows, that p_j^*/p_∞ must be appr. 10 % higher if a jet with $\gamma_j = 1{,}3$ is simulated with cold air ($\gamma = 1{,}4$). (If the n.p.r. is less, the corrections become relatively smaller). The base pressure or the pressure in the separated region is a function among others of the jet momentum. This quantity is determined by the nozzle pressure ratio and γ_j also. Two limiting cases can be considered; jet momentum per unit area at the exit and jet momentum per unit area along the boundary (fully expanded). The first yields $(p_j^*/p_\infty)\,\gamma_j$ = constant, the second case gives $M^2_{boundary}\cdot\gamma_j$ is constant. Both criteria are shown in figure 12 also. It is concluded from this figure that correction in p_j^*/p_∞ for correct momentum simulation is opposite from correct jet shape simulation if $\gamma_{j\,model} \neq \gamma_{j\,turbo\text{-}jet}$. Few experiments are known which verify a base pressure dependence on γ_j. However figure 14 (from Ref. 13) gives a clear indication of the influence γ_j on the base pressure of a sonic jet exhausting in a supersonic flow. The predicted base pressure at $\gamma_j = 1{,}3$ from the experimental results from $\gamma_j = 1.4$ is entirely computed on the basis of similar jet boundary inclination angles (see Ref. 14). Comparison with figure 13 shows that in this case jet contour simulation, hence adjusting the nozzle pressure ratio along the solid line of figure 13, yields the best results.

The mixing process along the jet boundary is determined by the jet properties at the boundary and by the external boundary layer characteristics at the nozzle exit. The jet properties depend on the nozzle used, particularly on the cooling system and the secondary air flow, if present (Fig. 12). If smooth uniform jet flows are assumed, the mixing parameter is $(\rho v)_j / (\rho v)_\infty$ (Refs. 15, 16, 17). This

mixing process alters the effective jet boundary shape so that the inviscid flow is affected, particularly at transonic speeds. At a given nozzle pressure ratio the mixing parameter is primarily dependent on $R_j T_{tj}/R_\infty T_{t\infty}$ (see also section 6.1.1). The entrainment effect of a cold jet on the drag of a smooth afterbody at $M_\infty = .85$ is of the order of 20 °/o of the jet plume shape effect (Ref. 18) for a convergent nozzle. Hence changes in jet entrainment, due to distortions, turbulence, jet temperature will show a strong influence on the afterbody drag.

In case of a separated flow the pressure level in the dead-air region is determined to a large extend by the condition of the external and internal mixing layers just upstream of the point of reattachment. If the external flow is transonic and the engine is of the by-pass type what means that the nozzle pressure ratio is low, the viscous layer surrounding the jet is also very dependent on the turbulence level and distortions of the jet flow just upstream of the nozzle, since these properties do not damp sufficiently during the expansion. If the outer flow is supersonic the pressure in a separated region, which is also strongly determined by the flow properties near the reattachment point, determines where the boat-tail terminal shock wave is located. A short review of this separation phenomenon is given in reference 19 for example.

However, no experiments and/or analysis are available in the open literature which consider the influence of the jet distortion and turbulence properties on the exhaust flow field, and hence on the external drag. On the contrary some experiments and analysis are known which show a strong dependance of bleeding small amounts of air in the separated base region on the base pressure. This bleed disturbes the effective stagnation point in the flow reattachment region and hence the streamline total pressure that just can overcome the pressure rise in order to flow downstream. Figure 15 shows this effect (Ref. 20). If can be concluded from this figure that leakage through the nozzle leaves will strongly affect the effective thrust minus drag of the exhaust system. Usually these conditions are not simulated in the wind tunnel in order to determine the sensitivity of the nozzle performance due to leakage, which varies between the production nozzles and which is generally unknown.

Some experiments are available on the influence of the jet temperature on base pressure using hot air (so $\gamma_j = 1.4$) at transonic speeds. Figure 16 is deduced from reference 21 yielding base pressure (C_{p_b}) base drag (C_{D_b}) and boattail drag (C_{D_β}) for a typical afterbody shape at $M_\infty = 0{,}9$ versus the total jet pressure P_{t_j}. It is clearly seen that the afterbody drag ($C_{D_\beta} + C_{D_b}$) is some 20 °/o decreased if a hot jet is used for jet simulation instead of a cold jet. A similar conclusion is reached in reference 22, where it is found that the base drag at a temperature ratio of 2,8 is 25 °/o less than it is with an unheated jet at $M_\infty = 0{,}9$ utilizing a propane-air combustion system with a convergent nozzle at a pressure ratio of 2. At supersonic external speeds the influence of the jet temperature seems to be substantially less; typically the base drag differs less than 5 °/o.

It should be noted that turbulent jet mixing is little influenced by Reynolds number effects since the characteristic mixing length is in first approximation proportional to the characteristic jet dimensions.

Summarizing the following can be concluded regarding the degree of jet simulation in transonic wind tunnels.

a) For <u>nozzle thrust coefficient</u> assessment (internal and static) the geometry, nozzle pressure ratio and ratio of specific heats should be simulated as first parameters. This is also true for the secondary mass flow in case of ejector nozzles or nozzles with substantial cooling air. The secondary parameters are the total temperature, and internal flow distortions, also swirl, upstream of the nozzle if the nozzle contraction is large ($A_{Eng}/A^* \geq 1{,}8$). For small nozzle contraction ratios these parameters become also primary.

b) For almost <u>inviscid jets</u> where mixing has a secondary importance, that is at subsonic and at supersonic speeds, the wave structure and stream line shapes, that is the initial inclination angle and wave reflection coefficients (both determining the plume shape) should be simulated regarding the influence on the external flow field. These parameters are determined by p_{t_j}/p_∞, γ_j, M_j as well as by the free stream condition. The jet temperature and upstream distortions yield corrections on the jet boundary due to mixing.

c) In cases where <u>jet mixing</u> plays an important role on the external flow field, that is at transonic speeds and if the flow separates at all speed regimes, nozzle geometry and ratio of specific heats, the nozzle temperature ratio, secondary flows (if present), external boundary layer thickness, jet distortion and turbulence should be simulated also. Scale effects due to turbulent mixing can be ignored.

4. WIND TUNNEL TESTING SCHEMES FOR THRUST MINUS DRAG ASSESSMENT

The wind tunnel testing scheme for nozzle-afterbody performance assessment that one chooses to employ for a particular aircraft design depends primarily on the available test rigs and systems in the wind tunnel and on the stage of aerodynamic testing. In recent years the main transonic wind tunnel facilities have been equiped to perform powered nozzle testing. Usually each laboratory designed its own particular system that is flexible enough to test a variety of nozzle-afterbody combinations. These test rig designs were based on jet and nozzle parameters which were thought to be of first importance, as discussed in the previous section, on the other technical requirements, as will be discussed in the next section, and on the apparatus achievable in the wind tunnel within practical limits.

The next discussion concerns primarily the engine-airframe integrated systems (e.g. fighters). Similar techniques can be used for podded subsonic installations, but in those cases the jet influence on the wing or aftfuselage is of equal importance.

The nozzle-afterbody performance must be determined from wind tunnel measurements starting from aeroforce model drag data and the engine gross static thrust. The actual installed afterbody performance can be expressed as the difference between the installed gross engine thrust (F_{inst}) minus the installed afterbody drag ($D_{AB_{inst}}$). This quantity $(F-D_{AB})_{inst}$ should be as large as possible for

maximum performance. It depends on the external parameters, such as Mach number (M_∞) and angle of attack (α) as well as on internal parameters such as engine r.p.m., degree of afterburning and exhaust area ratio. The engine parameters can be expressed in terms of the nozzle pressure ratio, temperature ratio, ratio of specific heats, geometry, etc. The engine static test bench gross thrust can in many instances be considered as the reference thrust F_{ref}, F_{st}. The reference afterbody drag ($D_{AB\ ref}$) can be determined by a model similar to the aeroforce model but with the afterbody only being metric. The afterbody drag is the drag on those parts of the afterbody which can be affected by the presence of the exhausting jet(s), such as inter-and outerfairings, tailplanes, fuselage boattail and base (if present). The split line between the forebody and afterbody is generally somewhat halfway between the inlets and exhausts. Usually the drag on the external nozzle parts (D_n) is not included in the afterbody drag but is added to the nozzle losses. The external flow can also effect the internal nozzle thrust resulting in a thrust loss (ΔF_{inst}), also called the internal nozzle drag due to the external flow (see 3.3). The interference drag is now generally defined as the difference between the net reference performance and the net installed performance of the nozzle and afterbody combination (Ref. 10 for example), that is

$$D_{int} = (F - D_{AB})_{ref} - (F - D_{AB})_{inst}$$

or $$D_{int} = \Delta F_{int} + D_n + \Delta D_{AB} ,$$

since $$\Delta F_{int} + D_n = F_{ref} - F_{inst}$$

and $$\Delta D_{AB} = D_{AB_{inst}} - D_{AB_{ref}} .$$

Sometimes $F_{ref} - D_{int} = F_{ref} - (\Delta F_{int} + D_n + \Delta D_{AB})$ is called the equivalent thrust.

Overall installed performance (thrust minus drag) is:

$$(F-D)_{inst} = F_{ref} - D_{ref} - D_{int}.$$

This quantity should have a maximum value.

In an ideal testing scheme ΔF_{int}, D_n and ΔD_{AB} should be determined independently, sothat the optimization ($\min.D_{int}$) can be performed efficiently.

Figure 17 illustrates the usual bookkeeping procedure for integrated nozzle-airframe systems where at the aeroforce model is supported by a sting located at the nozzles. Before the actual powered afterbody tests are performed, an intermediate step is done at which the model is split into a forebody and an afterbody, the latter only being metric. The forebody is grounded and may be supported by a separate sting under the fuselage or at the wing tips. Also a half model support may be used if the exhausts are sufficiently free from the tunnel walls. For these tests the inlet is closed. In other schemes with complete engine simulation the inlet flow may be completely or partially duplicated.

In figure 17 the afterbody tests are performed with the complete exhaust model. However, these tests can also be performed with an isolated afterbody model, if the powered test of the geometric similar afterbody is preceeded by a reference afterbody test. For this test the afterbody must have the same shape as the aeroforce model and must use a non-metric dummy sting at the location of the aeroforce model sting. This test yields the new reference afterbody drag $D_{AB_{ref}}$ for the actual powered afterbody/nozzle tests. The advantage and disadvantages of isolated tests have been described in the previous chapter.

The powered afterbody tests may use various schemes as is indicated in figure 18. The first scheme (A) is the simpliest one and requires only one balance. The main disadvantages of this scheme are that optimization of the afterbody-nozzle combination is hard to achieve and that the afterbody drag is overshadowed by the large installed gross thrust which is an order of magnitude larger. The accuracy must be appropriate to the net thrust level while measuring gross thrust. This difficulty is overcome by the scheme in D where the entering jet momentum is subtracted from the total measured force of A, making possible the use of a more sensitive balance. However, in this case the effective flow area (A_i) can be assessed only with difficulty and also a sealing problem exists at this high pressure location. The schemes of figure 18-B and -C are identical in practice and measure separately the installed gross thrust force and installed afterbody drag in series or in tandem respectively. The afterbody drag balance can be made more sensitive.

An alternate method to obtain the afterbody drag of simple models (e.g. axisymmetric) is to pressure tap the afterbody, which might also include a base. These pressures are integrated to obtain $D_{AB_{inst.p.}}$. Adding the calculated skin friction to this quantity yields $D_{AB_{inst}}$. This procedure is not recommended for the external drag of complicated afterbody shapes since in these cases large pressure gradients might exist yielding inaccurate date. However, some measurements of local pressure plotting and flow visualisation on afterbodies is useful in order to detect areas of drag increase and to make possible comparison with theoretical analysis.

In figure 18 only the primary mass flow is indicated. If necessary secondary flow can also be introduced in a similar manner leading to less difficulties as the primary flow since the secondary mass flow is only a few percent of the total mass flow.

The mass flow can be controlled and metered outside the tunnel test section with a high degree of accuracy. Figure 19 gives the sonic orifice method generally used and most accurate for gaseous jet fluids. The discharge coefficients for sonic line curvature, boundary layer displacement effect and virial effect which are used, are also given in figure 19. The former two discharge coefficients are well covered in the literature (see for example references 19, 23, 24), but not the discharge coefficient for the virial effect. This effect is usually neglected, but should be taken into account if the sonic orifice is operating at high pressures as it generally is the case (Refs. 24,25). If the jet fluid or one of its components is a liquid an easy and accurate technique to control and meter the flow rate is the use of a cavitating venturi, which can be accurately calibrated. The flow rate of a cavitating venturi is proportional to the square root of the product of upstream pressure times the liquid density as long as the venturi back pressure is less than the maximum venturi recovery pressure.

The nozzle gross isentropic thrust (X_{id}) can be computed based on the measured mass flow rate and the nozzle one dimensional ideal expansion from p_{t_j} to the ambient static pressure p_∞. In fact any of the theoretical isentropic thrust computations based on measured mass flow may be used as described in reference 1, chapter 3 of Part II. In the real engine isentropic thrust computations the thermal real gas effects ($p - Z\rho RT$) are usually neglected, which can be justified, but the caloric real gas effects (C_v and $C_p \neq$ constant) are taken into account. However the model tests are sometimes performed at high pressure level in order to increase the model Reynolds number. In these cases the virial effect can not be ignored, particularly if a cold jet simulating fluid is used (see fig. 20 from Ref. 26).

The gross thrust coefficient may be defined as

$$C_T = \frac{F}{X_{id}}$$

where F is the measured installed or static thrust and X_{id} the isentropic thrust for which the analytical procedure should be indicated. If secondary flow is supplied, the isentropic gross thrust is the sum of both isentropic thrusts, ($X_{idj} + X_{ids}$):

$$C_{Ts} = \frac{F}{X_{idj} + X_{ids}}$$

where X_{idj} and X_{ids} are calculated from the primary nozzle pressure ratio plus $\dot{m}_j\sqrt{T_{tj}}$ and the secondary nozzle pressure ratio plus $\dot{m}_s\sqrt{T_{ts}}$ respectively. F is again the measured total thrust.

In practice it is convenient to work with primary flows only in the bookkeeping procedure even though secondary flows are present. This can be done by subtracting from the measured thrust with primary and secondary flows the ram drag of the secondary flow $\dot{m}_s V_\infty$ and base the thrust coefficient on the isentropic gross thrust of the primary flow only:

$$C_{Tx} = \frac{F - \dot{m}_s V_\infty}{X_{idj}} .$$

The computed net thrust of the engine is then equal to

$$F_N = C_{Tx}\, X_{idj} - \dot{m}_j V_\infty$$

taking only into account the primary engine flows.

This procedure is also useful for direct comparison of the actual engine thrust with single nozzles on the static test bench.

Values of the model static thrust, which can be considered as the model reference thrust ($F_{st.model}$, $F_{ref.model}$) can be directly obtained from tunnel-off, jet-on measurements for the different nozzle operating conditions for purpose of determining the absolute installation effects:

$$F_{ref.model} = F_{st.model} = \frac{C_{Tref.model}}{C_{Tref.engine}} \frac{X_{id.model}}{X_{id.engine}} F_{st.engine}$$

$$(F_{st.eng} = X_g)$$

where $C_{Tref} = \frac{F_{st}}{X_{id}}$ which should be the same for the model nozzle and the engine nozzle (attention must be exercised that X_{id} is computed in the same manner) or the difference must be traced by analytical procedures (Refs. 19,20). The condition of obtaining identical thrust coefficients for the actual engine nozzle and for the model is very difficult to achieve (see Ref. 28 for example). If $\gamma_{jengine} = \gamma_{jmodel}$ and $(P_{tj/p_\infty})_{model} = (P_{tj/p_\infty})_{engine}$ for both primary and secondary flows than

$$\frac{X_{id.model}}{X_{id.engine}} = (\text{scale})^2 \frac{P_{tj.model}}{P_{tj.engine}} .$$

If γ_j cannot be simulated in the wind tunnel than a small correction is required. The correction depends on whether the jet plume shape is correctly simulated, but not the jet momentum, or the jet momentum is simulated yielding a non-matched plume shape (Ref. 27).

The difference between (jet-on, tunnel-off) and (jet-on, tunnel-on) thrust measurements yields:

$$(F_{ref} - F_{inst})_{model} = (\Delta F_{inst} + D_n)_{model} ,$$

i.e. the absolute nozzle installation drag, if the afterbody is measured separately. Since at some Mach numbers and simulated engine setting (r.p.m., A_{ex}), the ideal thrust and dynamic pressure are both proportional to the pressure level (for example, static pressure p_∞), the internal and external thrust losses (ΔF_{int} and D_n) can be correlated with the ideal thrust. Therefore $F_{inst}/X_{id} - C_{Tinst}$ is a meaningful quantity.

If the purpose of the afterbody tests is to compare the performance of different nozzle designs in the aircraft flow field, or even in an isolated test flow field, the simulation requirements for the jet properties are less pronounced. This method depends upon the difference between two tests on different nozzle configurations at the same free stream Mach number, nozzle expansion ratio and secondary air flow ratio. Then the comparison of installed gross thrust can be written as

$$\Delta F_{inst} = (C'_{T_{inst}} - C''_{T_{inst}})X_{id},$$

the primes referring to the two different configurations.

For $C_{T_{inst}}$ also $C_{T_{xinst}}$ can be written.

If the reference model utilizes a flow through inlet and exhaust, or a flow through nacelle, the reference afterbody drag or reference aft nacelle drag with natural flow must be determined including the natural flow jet effects on the afterbody and the natural flow thrust. This natural flow thrust minus drag term, as a function of Mach number and angle of incidence must be subtracted from the aeroforce model drag. This can be accomplished by measuring the forebody drag separately, as might be done in the inlet tests, or by measuring those values directly with a blowing reference afterbody and nozzle fed from the outside (inlet closed) for which the mass flow (cold air) is equal to the natural flow as might be done with one of the schemes of figure 18. The actual afterbody or nacelle aft configuration replaces in the next step the aeroforce configurations, at which the actual thrust and drag term are determined utilizing the proper jet simulation technique and one of the schemes of figure 18.

In case of a fan engine with a podded installation the drag acting on the turbine cowl is sometimes called the scrubbing drag. This drag term can be compared with the external nozzle drag of an integrated system. In case of under-wing engine mounting the change in drag of the wing due to jet effects should be included in the bookkeeping procedure of thrust minus drag, same as the trim drag as resulting from lift distribution changes on the wing due to the jets.

In many publications the term base drag is found. This term is generally used if the drag on the base is determined by pressure plotting, as is done with aeroforce model or inlet model drag corrections. Since the base, if present, can either be considered as part of the afterbody or part of the nozzle, the base drag will be contained in the afterbody drag or nozzle drag terms if these terms are determined by force balance measurements.

5. JET SIMULATION TECHNIQUES FOR THRUST MINUS DRAG ASSESSMENT

5.1. GENERAL REQUIREMENTS

Apart from the jet parameter simulation requirements, as described in chapter 3, other general requirements exists with respect to model construction and wind tunnel operation. These requirements are as follows:

a) The feed pipes of the jet simulating fluid should be as thin as possible in order to avoid large aerodynamic interference of the supply duct and/or support system. This requirement calls for a dense fluid in the supply duct.

b) If a thrust balance is used the system to bypass the balance without interference on the balance, should be as small as possible and/or operate at low pressures. This also calls for a dense fluid supply along the balance and/or low pressures.

c) In order to keep the possible influence of the momentum of the entering fluid on the thrust balance reading as small as possible, this momentum should be normal to the thrust axis and should be a small fraction of the momentum of the exhaust jet. This calls for a dense fluid again.

d) Within the balances, no temperature gradients should be generated due to heat flow from hot jet simulators, nor should the model deform by thermal stresses.

e) The operation of the simulator should be easily controllable, adjustable and accurately repeatable.

f) The model and simulator design should be simple and cheap.

g) The operation costs should be low.

h) The operation should be safe, therefore the number of systems should be kept small.

i) The jet flow should not contaminate the tunnel air of closed circuit tunnels, nor should explosive gas mixtures be accumulated in the tunnel.

5.2. TECHNIQUES, ADVANTAGES AND LIMITATIONS

5.2.1. TECHNIQUES WITH FAIRED INLET

The techniques for nozzle tests in wind tunnels, with closed inlets which have been utilized or suggested can be sub-divided in the following order according to the fluids used:

- Cold gases

Air or nitrogen are commonly used because of low costs, easy handling properties and reasonable gas properties for non-augmented engines (except for temperature). Cold gases give clean and continuous operation, and even with secondary flow simulation the plenum chamber of the simulator can be easily designed. However, the jet plume or jet momentum can not exactly be simulated. Nor can the mixing process of ejector nozzles and along the jet boundary be simulated. Several exhaust nozzles may be required to obtain the desired entire range of pressure ratios at high jet pressure ratios. Scaling the real nozzle for complete expansion will result in over-expanded scaled nozzle operation. Table III shows the non-matched nozzle properties (Ref. 4).

Table III. COMPARISON OF NOZZLE FLOWS FOR DIFFERENT RATIOS OF SPECIFIC HEATS

Ratio of Specific Heats	Nozzle Pressure Ratio, NPR	Area Ratio, A_{ex}/A^*, $p_{ex} = p_\infty$	Mach number Max
1.3	5.0	1.41	1.74
1.4	5.0	1.34	1.71
1.4	5.5	1.41	1.77

In order to keep the feed lines small the gas is supplied at high pressures, consequently large pressure drops in the ducts can be tolerated. The balance bypass system is generally quite voluminous and must be designed properly for detailed balancing if this system must be located inside the model. If the balance bypass system can be located outside the test section this problem can be avoided for example by utilizing long flexible hoses or pipes having a spring constant many orders of magnitude less than the spring constant of the balance. The gas must be supplied at right angles to the thrust axis. Right angle feed systems are mainly used for isolated model tests.

Figure 21 (NASA-Lewis) shows an isolated nozzle system (Ref. 29) for which the necessary flexure in the axial direction is obtained by a number of feed pipes in the support strut, using the measuring arrangement of figure 18A, incorporating secondary air. In many models the stiffness perpendicular to the thrust axis is a hard requirement to meet. Therefore often extra support bearings or flexures are incorporated as seen in this figure.

In figure 22 (NASA-Langley) a tandem arrangement is sketched (Fig. 18C) for a twin nozzle isolated afterbody model arrangement where the balance bypass is within the model (Ref. 30). However in this case no secondary air is provided.

A very popular arrangement for isolated nozzle (or afterbody) support at transonic and supersonic speeds is the shaft method for which the nozzle is at the end of the shaft extending from the tunnel plenum chamber into the test section. The advantage is the complete omission of side supports; the limitation is the large boundary layer build up along the shaft in front of the nozzle and the impossibility of incidence variation. The influence of the shaft boundary layer can however be reduced by blowing or suction just upstream of the sensitive portion of the afterbody. Figure 23 show such installations with three jet fluxes available, as they are used in various wind tunnels in France, ONERA (see Ref. 26 for example).

The sealing is obtained by balancing rubber bellows. Also details on data reduction and layout are given.

The nozzle test shown in figure 4 is also of this type as used at Rolls Royce. The rig is used primarily for the purpose of gathering comparitive information useful to select a configuration rather than obtaining absolute datums. The tests are carried out:

a) without external flow to measure nozzle internal performance.

b) with external flow to measure installed thrust minus drag.

The latter tests are made with all the significant items which might contribute to the jet interference effects - boattail, base area, tail surfaces, in the case of an afterbody - a wing and pylon in the case of a wing pod.

Figure 24 represents another afterbody shaft mounted study rig in a transonic test section which is small with respect to the scale of the model (ONERA Ref. 31). The aim of this rig is to study the afterbody performance of a podded fan engine installation by pressure plotting rather than by weighing, and to compare the results for the fan cowl with the pressure coefficients obtained from the inlet tests. In order to obtain a representative flow around the model and provide a simulated reference upstream flow, the cylindrical shaft support has been smoothly faired to the external boattail shape. However, as is shown in the lower half of this figure the common portion in the pressure coefficient is present only at the lower Mach numbers, which is probably due to the fact that the flow field induced by the lip of the inlet is not reproduced in the afterbody test. Therefore the data should not be interpreted as an absolute value of the afterbody drag as determined from pressure integration and estimated skin friction drag. Consequently improvements of this test procedure must be made, for instance by a better representation of the shape of the streamline at the leading edge and by boundary layer control (as is done in Ref. 47).

Figure 25a gives a layout of a side supported twin nozzle afterbody rig which can be installed in the transonic as well as in the supersonic wind tunnel of the Aircraft Research Association U.K. Ref. 32. The rig, which carries models of 1/10 to 1/20 scale and uses air stored at 11 atmospheres, can be used to investigate nozzle-afterbody performance over a nozzle expansion range representative of turbojet and bypass engines. The scheme used is that of figure 18A, incorporating secondary flow and tail planes at the metric afterbody. The forebody is non-metric and the strut is located at a typical wing location. The forebody is of reduced length just as figure 22 making representative boundary layer thickness simulation possible at the metric line location as is indicated in the figure 25b.This requires,however, a careful design of theforebody contour. Detailed drawings of this test facility are given in figure 25c. The instrumentation layout is shown in figure 25d along with the line diagram for data reduction in figure 25e. The data reduction scheme results in various thrust coefficients (underlined) which depend each on the definition for the isentropic thrust and the associated deduced actual model thrust. Special attention has been directed to the mass flow and discharge coefficient determination. The mass flow is measured at a special discharge chamber in the supply line as indicated in figure 25d where the total pressure (p_m) and the bell mouth depression Δp_m are measured and used to define an accurate value for $\dot{m}\sqrt{T}$. The discharge coefficient relates to the bell mouth Reynolds number and has been accurately determined against a known standard nozzle. The values of $\dot{m}\sqrt{T}$ for use in the nozzle requires correction for any total temperature change between the measuring bell mouth and nozzle plane. This can be an important item in relation to the required accuracy as 1 °/o temperature variation between the two stations gives 1/2 °/o variation in C_d. The secondary flow is measured separately in each duct by orifice plates. As is stated before, the significance of absolute discharge coefficients and thrust coefficients is subject to doubt since the rig values must be based on a defined nozzle pressure head. Also the flow distribution approaching the nozzle is likely to be very different.

If the engines are located in separate nacelles under the wings or at the aft-fuselage the semi-model test technique may be used sothat the air can be supplied through the wings and pylons to the nozzle. In this case the inlets will be faired if direct blowing is provided. Using engine simulators, such as small turbine-driven compressors. the inlet flow is also simulated partially. This technique will be discussed later. Figure 5 gives a layout of a semi-model of a supersonic transport with a half-width of 0,5 m in a 1.7 x 1.7 m^2 tunnel.

Cold gases other than compressed air or nitrogen for jet simulation in wind tunnels are proposed, since mixing air with multi-atomatic gases,such as carbon dioxide or freon, the ratio of specific heats can be adjusted (Ref. 33). By mixing a third light weight component such as He and/or H_2, the jet density can be simulated also. However, these techniques have not been used extensively due to costs, tunnel contamination and the possible accumulation of explosive or otherwise dangerous mixtures.

- Hot gases

In practice the simulation of the exhaust jets by hot gases is performed using the decomposition of hydrogen peroxide, or by burning a liquid or gaseous fuel with air. The latter method can be used in conjunction with simple cold air simulation but is of course much more complicated since an additional ignition, fuel flow and control system must be provided. In order to keep the cooling provisions and thermal flux requirements to a minimum, the heat must be generated just upstream of the nozzle,

preferrably at the actual engine location. This will mean that the loading of the burner must be rather high, resulting in incomplete combustion and hence in unpredictable simulator performance. For this reason gaseous fuels, particularly H_2, are favourable, but are more dangerous with respect to leaks, then liquid fuels and will result in rather thick fuel lines. The fuels used are generally hydrogen, methane, propane, ethylene and liquid hydrocarbons, such as kerosine. The oxidizer is usually air or oxygen, with air being more favourable due to less costs and the required moderate temperatures. Usually the problem is not to meet the highest jet temperature requirements but rather the lower jet temperature. For lower temperatures the combustor must be designed such that burning takes place in the primary zone after which cooling air is added.

The main advantage of hot gases is the correct jet simulation properties, both $R_j T_j / R_\infty T_\infty$ and γ_j. Some advantage is obtained due to the reduced required mass flow and hence, reduced supply ducts. For closed circuit wind tunnels good intermittent jet operation is required, or else an exhaust gas collector must be provided for continuous operation.

Figure 26a depicts an axisymmetric hot isolated nozzle test rig of the shaft type in a transonic/supersonic wind tunnel (RAE Ref. 22). Also non-axisymmetric nozzle and afterbodies may be attached to the shaft which extends from the tunnel plenum chamber. The shaft is 10 cm in diameter and contains a propane burner and a downstream mixer for uniform temperature distribution at the nozzle entrance. The nozzle is fed by dry compressed air heated to 600° C maximum by propane burning. The range of obtainable jet temperature and ratio of specific heats is given in figure 26b. The combustion efficiency varies between 70 °/o and 90 °/o, the highest at the highest obtainable fuel-air ratio. The temperature distortion is less than 10 °/o. This rig has been developed and refined continuously over a period of years and, apart from Reynolds number effects, simulates flight conditions very closely. The approach boundary layer on to the afterbody is, however, too thick; no boundary layer control is provided. This means for example that the efficiency of blow-in-door-ejectors can not be determined reliably by this means.

For data reduction a thrust-minus-drag balance is provided together with pressure plotting along the afterbody and base. The primary pre-determined parameters (M_∞, P_{tj}/P_∞, $T_{tj}/T_{t\infty}$) then yields data on jet thrust, boattail drag, skin friction drag, pressure drag and base drag of which the latter two terms can be obtained by pressure integration. The jet thrust and skin friction drag can be then determined after appropriate assumptions (for example estimation of skin friction drag, or assumed independence of external flow on jet thrust in choked nozzle operation).

The other way frequently used to generate hot exhaust gases is by decomposition of hydrogen peroxide in a catalyst pack producing hot steam/oxygen mixtures for which the temperature and composition depends on the peroxide concentration. It has the advantage that the ratio of specific heats and temperature of the decomposition products follow closely the values for turbojet engines as may be seen in figure 27. Peroxide decomposition yields therefore good plume shape and jet momentum simulation as well as simulation of the mixing process (Ref. 34). The silver screen catalyst pack can generally be designed small enough to be located in the model and does not require more space than a scaled engine should. Therefore this method is very suitable for jet simulation at complete aircraft-models with faired inlets. Due to the feed of cold peroxide the thermal effects have little influence on upstream components (i.e. balances). Compared to the use of cold air the following numerical values show the use of hydrogen peroxide is very attractive from a model testing requirements point of view

Density ratio $\rho_{H_2O_2}/\rho_{air} = 14$ (assumed 90 °/o H_2O_2 and compressed air at 80 atm.)

Supply mass ratio $\dot{m}_{H_2O_2}/\dot{m}_{air} = 0.46$.

Supply line diameter ratio $D_{H_2O_2}/D_{air} = 0.43$.

Supply line ultimate diameter ratio $D_{H_2O_2}/D_{air} = 0.26$.

Supply line stiffness ratio $D^3_{H_2O_2}/D^3_{air} = 0.08$.

Supply momentum ratio $(\dot{m}v_i)_{H_2O_2}/(\dot{m}v_i)_{air} = 0.08$.

Momentum ratio supply/exhaust H_2O_2 : $\dot{m}v_i/\dot{m}v_j = 0.023$.

air : $\dot{m}v_i/\dot{m}v_j = 0.28$.

This makes the use in complete afterbody model tests particularly suitable when incorporating thrust and drag balances in the model. The operation can easily be intermittent by opening and closing the supply valve. Mass flow control is easily and accurately achieved by a cavitating venturi, which also prevents chugging.

Since the feed lines are small, space is also available for secondary air flow supply as may be seen in figure 28 for an isolated nozzle test (Ref. 35), using a two-balance system. Another balance system is shown in figure 29 where the thrust balance and supply line to the simulator catalyst pack are integrated (N.L.R., The Netherlands). The afterbody drag balance is concentric with the thrust balance, yielding a testing scheme similar to figure 18 B. The balances of the system, so called ring balances, are very stiff with respect to side forces and axial forces, sothat small split lines between components of the model can be obtained. In spite of small displacement due to axial forces the output of this ring balance is relative large. Proved accuracy of this balance, electronic equipment included, is 0.5 °/o full scale. Temperature effects on the balance accuracy, caused by the hot simulator, are eliminated by cooling the contact surface between balance and simulator with water. During firing of the simulator, the balance and the front plate of the simulator are intensively cooled by the liquid hydrogen peroxide, which has an entrance temperature equal to the stagnation temperature of the tunnel air.

Though this technique has several advantages from the wind tunnel testing point of view it also has drawbacks, of which the main drawback is the cleaning and passivation procedure of components in direct contact with the hydrogen peroxide in order to operate the facility savely. This requires a skilled

operation team and a well-designed system. Fortunately dilution with only small amounts of water rapidly reduces the occurrance of fire and explosion hazards. The liquid and fumes are non-toxic. In closed circuit tunnels the humidity increases due to the large amount of steam in the jet and the tunnel air will rise in temperature. Therefore intermittent operation is required; blowing times between 4 sec. and 40 sec. are generally used. Several intermittent runs can be made before tunnel air exchange or tunnel drying is necessary due to increased humidity. Also short firing time is required due to limited catalyst pack life (one to five hours, depending on pack loading and peroxide concentration), which means in practice that the catalyst pack must be replaced a few times in a wind tunnel program. Another draw back may be the costs of H_2O_2, which is about $1,00/kg. Consequently this system will only be used in high quality wind tunnels and in wind tunnel programs for advanced aircraft design.

5.2.2. TECHNIQUES WITH COMPLETE ENGINE SIMULATION

In the previous section the exhausts are treated separately from the inlet flow, following the usual procedure as performed in the wind tunnel testing program. However, the mutual possible interference between the inlets and exhausts has been mentioned occasionally, and doubt has been expressed if separate testing is allowed.

If a wind tunnel testing scheme is set-up at which both the inlets and exhausts are simulated simultaneously, provision should be provided to energy to the inlet air flow in the form of total pressure rise and preferably also in the form of a temperature rise (temperature rise only would yield ramjet conditions). This addition of energy can be either outside the wind tunnel test section or inside the model. Depending on the inlet mass flow and required pressure rise, it can generally be stated that the required power for pumping is very large (typically between 10 and 100 h.p.) which means that the location of the pumping system inside the model would be a considerable task, though not completely impossible. Dr. Fuhs computes the power requirement for a typical example (Ref. 4) and concludes on this item: "This is like stuffing two VW engines in a three-inch pipe". Two techniques are now available, ejectors and miniature gas turbine driven engine simulators, both based on gaseous driving fluids (air or nitrogen) which is expelled through the nozzle also or which is again partially extracted from the turbine flow (Fig. 30). To obtain correct pressure ratio having a reasonable number of stages in the compressor, the speed must typically be of the order of 60.000 to 80.000 r.p.m. Use of electric power will yield too voluminous motors.

The system for which the pump system is located outside the tunnel test section can only be used if the air passages of the inlet flow can be made large enough to provide for the complete inlet mass flow particularly at transonic speeds where ρv is maximum. This means that this system cannot be used with podded engine installations since the pylon cross-sectional area is much less than the inlet area.

A. SYSTEMS WITH INTERNAL ADDITION OF ENERGY

The accompaning sketch depicts schematically the system with internal addition of energy where the primary driving fluid is expelled through the exhaust also, either mixed with the secondary flow or separated from the secondary flow in case of a fan engine simulator. If the tests are performed for thrust-drag determination or for engine-airframe interference determination, in both cases the secondary air flow must be measured (assuming the primary mass flow is measured adequately outside the test section) for correct inlet spillage and jet properties assessment. This means that careful calibration of the secondary mass flow (inlet mass flow) must be provided since the precise measurement of this quantity under wind tunnel model conditions is generally not possible. As an intermediate step in the thrust minus drag assessment sometimes also the nacelle with engine simulator is measured under isolated conditions (e.g. free from the wing) at which the interference drag can then be defined as the difference in the isolated (nacelle free) wing or airplane drag plus the net nacelle force and the complete (with powered nacelles) aircraft drag.

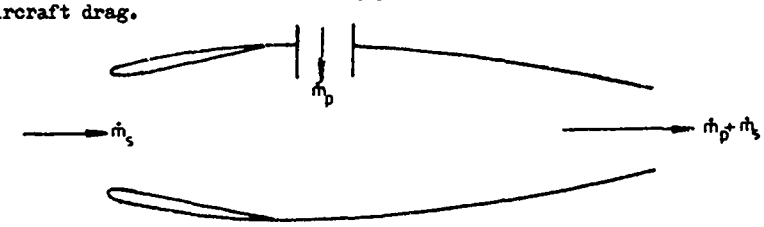

MINIATURE TURBINE DRIVEN ENGINE SIMULATORS

For a high bypass engine installed on a wing or rear fuselage in subsonic flow the performance engineer generally needs to know (a) the effect of the inlet and exhaust flow on the airframe aerodynamics, and (b) the effects of the wing flow field on the gross thrust of the nozzles and mass flow. Pressure ratios of the order of 1.7 are required to be simulated within the nacelle and this is not easily simulated by ejectors. Therefore miniature turbine driven engine simulators have recently been developed for wind tunnel use. These engine simulator units operate with a primary drive turbine using air (or N_2) at 25 atmospheres. This turbine drives a secondary duct fan (max. r.p.m. 80.000) which gives a geometrically representative secondary air flow at the correct pressure ratio. The model is usually correctly scaled and only the unrepresentative features are F, T and actual mass flow ratio. The inlet flow is less than the flight requirement but only about 15 - 25 % (for a 7 to 1 bypass ratio fan) less and is within an acceptable limit above the spill drag margin. The primary gas generator flow is unrepresentative but is probably of little importance when surrounded by the secondary flow. Figure 31 shows such a unit installed in a nacelle under the wing (Ref. 36,37).

In figure 30 a fraction of the turbine mass flow is mixed with the compressor flow, yielding flexibility in the controlling of jet plume parameters of multistage turbojet simulators. This feature is not common currently, however new simulators incorporate this feature. See for performance details of such simulators reference 38.

The degree of simulation can be described as follows:

a) Fan pressure ratio is representative of full scale.

b) Fan (secondary) nozzle can be sized correctly; thus with (a) fan nozzle exit conditions are correct in flow conditions and geometry. Distortion screens, detail struts and fairings can be incorporated within the nozzle in order to duplicate, as far as possible the exhaust flow characteristics of the full scale engine. In retrospect, it is evident that the failure to duplicate the nozzle radial total pressure profile, contributed to a discrepancy noted between model scale and full scale evaluations of the fan nozzle coefficients. At take-off power, for instance, the total pressure distortion $(P_{t_{max}} - P_{t_{min}})/(P_{t_{av}} - P_{st})$ can typically be some 30 % for large bypass ratio engines (Ref. 39).

c) The whole of the inlet flow feeds the fan nozzle, thus the inlet is wrongly matched and therefore the performance and/or the geometry must be compromised, usually by cowl modifications, in order to keep the spill margin equal.

d) Primary nozzle is geometrically near correct, the pressure ratio is close to correct but very cold. This might have consequences regarding the effects due to mixing. Bypass ratio is 2:1 instead of 5:1. As the primary jet is shielded by the fan jet these effects should probably be unimportant as far as jet interference is concerned.

Usually the following testing is performed:

a) Isolated engine on a balance without external flow with bellmouth for secondary mass flow calibration and some checks on (b).

b) Isolated nacelle on balance with external flow for thrust calibration, and

c) Nacelle(s) in position on metric model with balance measuring net forces on model, usually semi-span (Fig. 32 from Ref. 40).

The tests (a) or (a) and (b) can be replaced by "test bed" type calibration.

With respect to isolated tests it should be noted that the nacelle should be axisymmetric since a contoured nacelle in a uniform flow field would give unrealistic nacelle drag, that would not exist in the air plane flow field. This would result in apparent favourable interference effects. The installation criteria should be that the contoured nacelle operating in the airplane flow field should have essentially the same drag as an axisymmetric nacelle operating in the uniform field of the wind tunnel. Any drag increment due to improper contouring appears as interference drag and should be considered as an installation effect (Ref. 41). In test b and c the momentum of the incoming driving fluid, (air or N_2) must be perpendicular to the drag direction if the model plus simulator is metric. In test (b) care must be taken where to locate the metric line along the support strut. If the metric line is too close to the nacelle-pylon combination the measured force is unrealistic since part of the mutual interference (equal but opposite) is not measured. The distances of the metric line must be such that the pressure disturbances produced by the nacelle on the non-metric (grounded) part of the support should be small relative to the balance accuracy. In reference 41 it is considered that a distance of the metric line 1,25 nacelle diameters from the engine centerline is sufficient in this respect.

In both tests (b) and (c) it is necessary the trip the boundary layer at a fixed point in order to make the data comparable since the tests (b) and (c) will generally be performed in different wind tunnels usually having different noise intensities in the test section.

The test (c) should be done relative to the flow through nacelle, hence the compressor should be run first at such a speed that the total pressure ratio accross the fan is equal to the flow-through nacelle. This gives the reference values as obtained similarly with the aeroforce model. The overall bookkeeping procedure is than usually such that the installation drag ΔD_{inst} is defined as:

$$\Delta D_{inst} = [(T-D)_{model,\ full\ blowing\ (\alpha,\beta,n)} - (T-D)_{model,\ ref.blowing\ (\alpha,\beta)}] -$$

$$- [(T-D)_{isolated,full\ blowing(n)} - (T-D)_{isolated,ref.blowing}] = f(\alpha,\beta,n,M_\infty) .$$

The terms in the first brackets are obtained from test (c) and the terms in the last brackets from test (b). Comparison with test (a) gives break down in the various thrust and drag terms.

A typical method in use with these currently available simulators will be described next. This method for fan simulators is perhaps the most advanced and logical which has been attempted with these simulated engines, in that the thrust of the individual nozzles is related to the conditions in that nozzle in the correct environment. Certain assumptions are made of necessity, and the value of any absolute answers is dependent upon prediction methods for external drag.

Since the author does not have experience with those simulators, the method that will be described is due to the contribution of the U.K. on the AGARD questionaire as quoted in the introduction (Ref. 1).

The following methods can be used to calculate thrust.

A. In this case an attempt is made to calculate the net standard installed thrust of the engines when installed on the "complete" model. Addition of this term to the balance measured overall drag gives an aircraft external drag. As the net standard definition of thrust is used any post exit thrust is in the external drag term.

The static test (a) yields a mass flow calibration of the fan face instrumentation (typically 28 pitots, 12 statics). A flow coefficient C_d, is calculated such that

$$\dot{m}_{1_a} = C_{d_1} \times \dot{m}_{1_m} \qquad \text{(see sketch)}$$

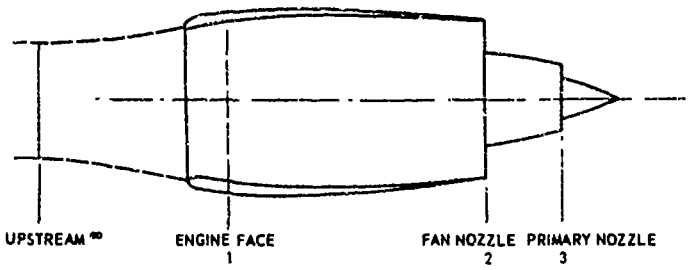

$\dot{m}$ MASS FLOW
V VELOCITY
C_A AREA COEFFICIENT
C_V VELOCITY COEFFICIENT
X_g GROSS THRUST
p_t TOTAL PRESSURE
p STATIC PRESSURE
T_t TOTAL TEMPERATURE
} FROM AREA WEIGHTED MEANS
C_{d_1} INLET MASS FLOW COEFFICIENT ((p_{t_1}/p_1) ONLY)

SUBSCRIPTS

NOTATIONS AS ABOVE
a 'ACTUAL'
m MEASURED AT PARTICULAR STATION

where $\dot{m}_{1_a}$ is obtained from a calibrated bellmouth and $\dot{m}_{1_m}$ from area weighted mean total and static pressures and freestream total temperature at the fan.

When the nacelle is tested in isolation (test b) with external flow pressure measurements can be made at the inlet, nozzle exits and on cowl external surfaces. The actual gross standard thrust for each nozzle is defined as

$$X_g = \dot{m}_m v_m C_A C_v^2 + (p_{ex} - p_\infty)A,$$

$\dot{m}_m$, v_m are determined from area weighted pressures (total and static) and total temperatures at the nozzle exit. C_A and C_v are area and velocity coefficients respectively. Obviously accurate mass flows must be used for the thrust calculations but it is also important that the same mass flow is used for the ram drag calculation as for the fan gross thrust. The inlet instrumentation is the best available (being more uniform than the nozzle) and so

$$\dot{m}_{1_a} = \dot{m}_{2_a} = C_{d_1} \times \dot{m}_{1_m} \quad \text{is taken } (c_{d_1} \text{ being taken for the relevant value of } p_{t_1}/p_1) .$$

An accurate determination of the primary mass flow can be made external to the model by a standard flow meter. In order to force the correct mass flow into the gross thrust equation above the flow coefficient can be written as

$$C_A \times C_v = \frac{\dot{m}_a}{\dot{m}_m}$$

in other words

$$X_g = \dot{m}_a v_m C_v + (p_{ex} - p \quad)A.$$

In order to determine these nozzle coefficients separately the primary nozzle C_A is taken from separate nozzle tests. Thus from the pressure, temperature and mass flow measurements the primary gross thrust X_{g3} can be calculated. The measured balance drag D_{BAL} with the isolated nacelle model is given by

$$D_{BAL} = D_{EXT} + D_{RAM} - X_{g_2} - X_{g_3}$$

where the external D_{EXT} contains all terms such as axial pressure integrals, forebody spillage drag, skin friction drag and scrubbing drag. The RAM drag can be calculated from freestream conditions and $\dot{m}_{1_a}$.

Thus the secondary gross thrust X_{g_2} is determined if all the terms in D_{EXT} are estimable or calculable. See for this procedure reference 42 for example.

In the equations

$$C_{A_2} \times C_{v_2} = \frac{\dot{m}_{1_a}}{\dot{m}_{2_m}}$$

$$X_{g_2} = \dot{m}_{2_m} \times v_{2_m} \times C_A \times C_v^2 + (p_{ex_2} - p_\infty)\, A_2$$

C_A and C_v are the only two unknons. Only one of these coefficients can be used to calculate thrust in the aircraft configuration (test c) and C_A is chosen as it is conjectured that this is likely to vary the least. It is used as a function of fan pressure ratio and Mach number.

Then the net standard thrust can be calculated when the engines are used in the installed condition and this value added to the overall measured balance drag to give model external drag. This external drag value will contain all the interference terms associated with both inlet and exhaust flows. It will also include the airframe on nacelle effects as well as the converse.

B. A similar series of tests can be conducted as in A, but interpreted differently. The static calibration (test a) is used to give a mass flow calibration but because no inlet instrumentation is available the fan nozzle instrumentation is used for the main fan mass flow measurement. The calibration is thus done in a test cell with the correct exit pressure. The calibration of the instrumentation is taken as a function not only of pressure ratio but also of corrected r.p.m., the latter because of swirl effects.

The thrust calibration with external flow (test b) is reduced as a thrust coefficient C_T defined as

$$C_T = \frac{-(D_{BAL} - D_{RAM})}{X_{g_2} + X_{g_3}}$$ 2 and 3 referring to fan and gas generator flows respectively,

where the gross thrusts are calculated using corrected mass flows and are of the fully expanded type (isentropic thrust).

This thrust coefficient is used (as a function of power and M_∞) to correct full-model balance measurements (test c). As the thrust coefficient contains the isolated nacelle external drag the model data obtained only shows differences in relation to an isolated nacelle X_g - D definition. Any adaptation to full scale results must make allowance for the change in nacelle external drag between model and full scale.

C. An alternative method would be to use an altitude test cell type technique and measuring thrust with a balance (test a). The thrust in the installed condition could then be calculated in exactly the same way as the engine manufacturer guarantees thrust. In this way the effects of the engine are determined in a "legal" sense as long as the model engine behaves similarly from test bed to installed condition. This is basically similar to A, but does not allow for changes of thrust of the model engine in the airframe environment. There is evidence that this assumption is incorrect.

In all these methods it is necessary to measure "somewhere" the full scale engine performance in the airframe environment. Evidence on the model scale shows the fan nozzle flow distribution to be considerably influenced by the wing flow since in many instances the flight envelope of the airplane results in engine operation at jet pressure ratios less than critical for both the primary (turbine) and fan nozzles. Under these conditions the external pressures in the area local to the particular nozzle can alter the flow characteristics upstream of the nozzle. This can also occur for above critical nozzle operations for conical convergent nozzles due to sonic line locations as influenced by the external pressure field. These external pressures can be significantly different when the engine is installed close to the wing. When this happens the engine can be affected in two ways:

a) The local pressure, if different from ambient at each nozzle exit plane, can cause the engine cycle to shift, and

b) The local back pressure can be affected.

Though this technique is very promising with the main features:

a) Yielding high degree of simulation, except for some increased inlet spillage and non-representative primary (turbine) jet temperature, and

b) Similar installation procedures can be followed in the wind tunnel as the actual engine in the actual airplane, it has the main draw-backs that (a) is expensive to operate, (b) it needs extensive control instrumentation for each engine, (c) it has little flexibility, each actual engine would require a different miniature turbine simulator, (d) the bearings have only limited life, (e) the repeatability is limited, (f) two equally manufactured simulators show different characteristics (as large as 5 °/o in net thrust, (reference 41) and (g) the separation of various drag and thrust terms is very difficult and sometimes speculative, mainly due to the inaccurate assessment of the nozzle coefficients.

In general it can be stated that, using small turbine driven simulators, one gains in the degree of engine simulation with respect of techniques utilizing direct nozzle blowing and direct inlet suction, but is adverse in obtainable accuracy of data assessment of each component. However, the use of these simulators is rather new, and could and will be much improved by further work.

EJECTORS

Ejectors do not contain rotating parts and are therefore much easier to manufacture and more flexible (not scale dependent) than turbine driven simulators. However, the secondary inlet mass flow is much less and the pressure ratio obtainable at the nozzle is usually limited. Furthermore large unrepresentative total pressure distortions due to the primary jets are hard to prevent. Since the ejector is a pure flow device its performance depends largely on the upstream and downstream conditions. The characteristics are usually quite different from the real engine. For these reasons the ejector is little used for thrust engine simulation; however, it is becoming popular for lift engine simulation in VTOL-aircraft, mainly due to the required low total pressure ratios in these cases. Figure 33 shows a typical

ejector unit for this purpose (Ref. 38), whereas in reference 43 a static calibration procedure is given of such a unit. Since the ejector scheme is simple and cheap to operate it seems worthwhile to do more work in order to improve its characteristics.

Due to the large flow distortions in the exhaust jet caused by the primary jets, thrust measurements with ejectors are very unrepresentative and hence usually not performed. The system is however sometimes used for assessment of jet interference effects other than thrust minus drag. For example figure 34 shows an ejector system (U.K.) for inlet and exhaust flow simulation on a fighter type model. The model is mounted on a special 6-component balance. The high pressure blowing air is ducted below the balance to a plenum box from which it feeds into a peripheral ejector in each side duct. This ejector induces intake flow through the model boosting its total pressure and mass. This air is bifurcated to the two blowing nozzles on each side with appropriate internal control to give reasonable distribution. The final jet distribution is controlled by a splitter box. Special seals must be developed for use between the metric air inlet and non-metric ejector box.

The shown ejector consists of an annular primary jet with an inner secondary inlet flow area. At the chosen design condition when operating in quiescent air conditions for each duct the primary flow was 1.65 lbs/secs, with a nozzle pressure of 4 atmospheres. The secondary or inlet flow was 0.85 lbs/secs. For the front engine the nozzle distribution was relatively poor due to the short length. The rear nozzle distribution was good. The representation of total pressure ratio for the two nozzles was good and the inlet area ratio was 0.8 ejectors off, 0.65 ejectors on.

B. SYSTEMS WITH EXTERNAL ADDITION OF ENERGY

As mentioned before the system for complete engine simulation with addition of energy outside the test section can only be used if the air passages to the outside can be made large enough for the inlet mass flow without deteriorating the external flow. In practice this scheme can only be used with integrated engine-airframe systems, using the half model technique of a twin engine aircraft. Figure 35 depicts such a set up. However, the main problem is the deteriorating effect of the reflection plate boundary layer, which probably can be kept under control for the inlet studies, but will have a disruptive effect on the phenomena looked for at the exhaust. From the point of view of engine interference testing this scheme is very attractive, and if ways could be found to omit the reflection plate boundary layer effects (shock wave-boundary layer interaction, separation, displacement, model boundary layer-plate boundary layer interactions) this method would certainly be used in the future. No examples are known which use this technique with good success. In fact these techniques would be similar to the method of simulating only the exhaust from the exhaust testing point of view. The procedure at the inlet is similar as treated with inlets only, except that space downstream of the inlets is very limited.

Of course it is possible to use a combination of external and internal addition of energy, such that the inlet mass flow is scaled same as the temperature corrected exhaust flow, without the necessary use of the semi-model technique. Though this combination of techniques might show good promise, the complexity in manufacture, control and metering rises considerably. One example is known where this method is used for interference studies of low subsonic speeds other than thrust minus drag.

6. DETERMINATION OF JET-AIRFRAME INTERFERENCE (EXCEPT THRUST-DRAG)

In many aircraft configurations the propulsive jets may influence the flow on nearby or far surfaces causing phenomena such as change in pressure distribution, shock-wave-boundary layer interaction, flow separation, surface heating and unsteady loads. These interferences depend on the engine power setting. If these phenomena are expected to occur, wind tunnel tests with full nozzle blowing should be performed for assessing the increments (in lift, moment, drag) due to the jet interference. Figure 36 gives a general impression how moment and lift increments due to jet effects can be determined. Normally the testing schemes are similar or even identical to the schemes for interference and installation drag determination. During these tests the complete external flow should be simulated, hence isolated tests are not performed. This means that complete models or semi-models are used. Semi-models can be utilized if it is certain that the reflection plate boundary layer does not deteriorate the phenomena to be examined.

Since no thrust terms are involved, the jet simulator can be non-metric (grounded) and the surfaces at which the disturbances are studied metric to a balance. Also the phenomenon can detected by pressure tapping (stationary and non-stationary if necessary) and by heat transfer measurements (base heating of launching vehicles) in which cases the complete model can be grounded. If the jet cannot be simulated, due to the small scale for example the jets may be simulated by solid body simulators representing the computed jet boundary contour, preferrably corrected for jet entrainment. However, there is a strong interference between the pressure field near the jet and the jet contour, making reliable solid body shaping for the jet very doubtful in many circumstances (Refs.44,45,46,18,11).

Since the jet interference phenomena and the testing techniques in the wind tunnel depend primarily on the aircraft configuration, the discussion in the following sections will take place according to the configuration catagory. In these sections the problems will be formulated, and the applied techniques will be discussed.

6.1. SUBSONIC TRANSPORT

6.1.1. WING MOUNTED FAN ENGINE

For these configurations the jet efflux considerably affects the local wing circulation and shock development due to the large mass flow and close position under the wing. Also the wing pressure field has a remarked influence on the flow in which the effluxes operate, affecting the shape of the sonic line and hence, altering the engine mass flow and net thrust. Therefore more attention must be paid now-a-days to these installations, than the formerly similarly installed turbojets required.

The jet simulation parameters generally are the same as discussed in section . The main parameters are the jet plume shape, jet cell structure and wave reflections, which can be expressed in terms of nozzle pressure ratio and ratio of specific heats of the jet, assuming convergent nozzles only. However, for these installations the far jet field is also important. Since the engine mass flow is relatively large the contraction or diversion of the effective jet stream as felt by the external flow due to the mixing effect (jet environment) may have a marked influence on the pressure distribution on the wing and fuselage, especially at transonic speeds. Simple analysis neglecting the kinetic energy of the flow with respect to the sensible enthalpy as a first approximation, shows that the jet mixing has a marked influence on the effective stream tube area, as may be seen in figure 37. In this figure n is the ratio of the free stream mass flow, that has been mixed with the jet flow, to this jet mass flow. It must be recognized, however,

that at a given nozzle pressure ratio the nozzle mass flow $(Av\rho)_j$ decreases as the square root of the $(RT)_j$ value at increasing jet temperature. This dependence on $(RT)_j$ mainly reduces the effect of jet temperature on the effective jet stream tube if the jet spreading were to be the same. Furthermore, it is well known that the temperature spreads faster due to turbulent mixing than the velocity (Ref. 16), which means that n should be larger than concluded from equal spreading characteristics. In general it can be stated that n depends on the detailed mixing of the jet with the external flow. Figure 37 can also be used for the effective jet stream tube near the core region of the jet. In that case the areas must be defined as indicated in the accompaning sketch, and n has an approximate constant value of the order unity, along the core region. Hence if $A_x/A_j < 1$ the jet acts as a suction region due to mixing. If $A_x/A_j > 1$ the external flow is deflected outward and the mixing acts as a source distribution along the jet boundary. In the latter case external gas heating is larger than external gas suction. The limit which the effective stream tube of the jet will obtain at long distances behind the exhaust ($n \rightarrow \infty$) is indicated in figure 37 also.

Figure 38 gives results of a more detailed analysis by prof. Ferri of the influence of the jet properties on the effective engine stream tube due to mixing. In this case the engine inlet mass flow is kept constant. The stream tubes have been calculated by assuming constant external pressure and turbulent or laminar mixing. Cases 1-1a, 2-3 represent tests where an engine simulator is used (section 5.2.2.). Case I represents a turbojet and turbulent flow; Case 1a, the same case, but with a region of laminar mixing. Case 2 represents a bypass engine, and Case 3, an engine simulator where the mass flow of the nozzle is increased to satisfy the condition of equal exhaust area and Mach number, but with different temperature. Then the increase in mass balances the difference in temperature. The data of the engines are given in the figure. Case 4 is a through flow nacelle when the engine simulator is not used. Then the geometry of the engine cannot be simulated and the exhaust is much larger than required for simulation.

It can be concluded that the mixing along the fan jet boundary will influence the effective channel between the lower surface of the wing and the jet boundary and will therefore strongly influence the transonic field in this region. This will have influence on the Mach reflections in the fan jet, as it is a little under expanded in the convergent fan nozzle.

From preliminary studies (Ref. 47), utilizing a shaft mounted fan engine nozzle (similar to Fig. 24), but with boundary layer suction, blowing under a two dimensional wing, it is shown that the jet mainly influences the wing lower side pressure distribution. The differences in pressure distribution with respect to the isolated wing is, however, very large at both sides. From these tests it can be concluded that the reference aeroforce models tests should include the podded through flow nacelles under the wing, either geometrically scaled such that the inlet mass flow is too small, or without increased exhaust such that the inlet mass flow is scaled. The main difficulty is how to represent the actual jet flow in the wind tunnel and not to disturb the effects of the inlet mass flow. Various approaches are in use, of which the most representative one is that utilizing the small turbine driven jet simulators as discussed in section 5.2.2.

If this facility is not available it is possible to utilize direct blowing of the jets and do something with the inlet flow such that the external flow around the fan cowl is best represented. In general with fan engines the simulation of fan jet is much more important than the simulation of the primary jet. This has led to the technique of reference 44 and shown in figure 39 (A.R.A., U.K.). The bullet shaped body in the inlet simulates the approach stream line on the fan inlet lip. From the results as determined by pressure plotting it appeared that with respect to the reference flow through the nacelle the pressure distributions on the wing, pylon and fan and turbine cowl hardly changed by inserting the bullet and by blowing the fan jet as reference. This means that decreasing the inlet stream tube considerably did not disturbe the flow field in the wing and exhaust regions substantially. By full blowing of the fan jet the pressure distribution on the lower side of the wing was affected markedly, as were the pressures . the turbine cowl. Or the fan cowl only the pressure distribution at the aft end was affected by blowing. (Also the inlet lip suction changed somewhat, but this must be due to static pressure changes at the free flow turbine exhaust resulting in increased spillage).

The method of direct blowing of the fan and turbine jets with complete inlet fairing has the main advantage that both jets can be represented as accurately as possible, for example using for the fan jet cold or slightly heated air and for the hot turbine jet hydrogen peroxide. Figure 40 depicts such a simulator as used at N.L.R., The Netherlands, where, however, the purpose was to determine jet effects (also heating) on the tail planes of a small airliner with engine installation at the upper side of the wing (VFW-Fokker 614)

In general for podded fan engines particularly for wing installed engines, three components can be distinguished, namely Inlet (I), Exhausts (E) and Wing plus pylon (W) for the mutual interference problem. The question for engine simulation in the wind tunnel can then generally be written as

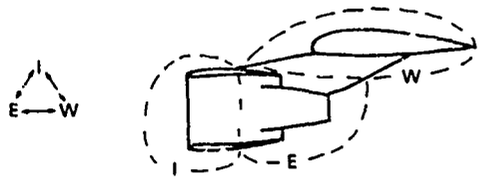

$$[(I + E) \rightarrow W] \stackrel{?}{=} [I \rightarrow W] + [E \rightarrow W]$$

where $[A \rightarrow B]$ means the effect of component A on B with respect to the reference conditions. Although not proven this question can be answered positive with good accuracy if one interference term on the R.H.S. is small with respect to the other one. From the tests as depicted in reference 44 and from unpublished data at N.L.R. it can be concluded that the exhaust interference on the wing pressure distribution is many times larger than interference from completely or partially fairing the inlet. This means that addition of the interference effects is probably allowed, making wind tunnel programmes much more easier if no miniature turbine driven simulators are available. For the installed thrust-minus-drag evaluation the similar question

$$[(W + I) \rightarrow E] \stackrel{?}{=} [W \rightarrow E] + [I \rightarrow E]$$

must be answered. Also in this case separation can be allowed since from some examples it is indicated that $[I \rightarrow E]$ is very weak provided the inlet fairing shape has been carefully determined.

With all these techniques semi-model measurements are more easily accomplished than complete, sting mounted model tests, and better accuracy is achieved due to the higher Reynolds number. The reflection plate boundary layer probably does not intefer significantly. Usually both pressure plotting and balance measurements are used.

In order to determine the jet effects on the tail plane of a large subsonic transport at low subsonic speeds and large angles of attack a rather unique complete simulator has been developed in Germany (Ref. 48). See figure 41. The engine simulators are separately mounted under a complete aircraft model and both the inlet flows and corrected exhaust flows are simulated. The bypass jet is produced by an electric motor driven fan. The motor is located inside the nacelle driving the fan with a speed up to 30,000 r.p.m. For the turbine jet compressed air is used. In order to simulate the correct inlet mass flow an adequate quantity of air is sucked through a slot at the inlet tip. However, for high subsonic speeds the fan pressure ratio obtainable would not be sufficient and the heavy engine mounting struts could not be allowed.

REAR FUSELAGE MOUNTED ENGINES

The aerodynamics of the afterbody of a fuselage containing the tail planes will be influenced by the jet efflux, either by direct impingement or by the constraint of the external flow. The influence of the engine on the wing pressure distribution is mainly caused by the inlet flow. The main phenomena caused by the exhaust jets can be a change in aircraft drag, change in angle of attack of the tail planes (hence causing change in pitching moment), surface heating (in case of direct impingement of the jets on for example brake flaps) and nonstationary aerodynamics (acoustic fatigue).

The basic measuring and jet simulation techniques as discussed in A, also apply in this case, but balance measurements seem to be more difficult. Half model techniques are not recommended, because the fuselage flow field is unrepresentative in the region of the jet interference with the rear fuselage due to the reflection plate boundary layer. Complete models require the use of wing stings and rear fuselage balances or pressure plotting. The air or jet fluid required for the jet simulators must be fed through the wings, fuselage and strut supports of the simulators to the nacelles, generally at high pressures. If balances have to be bypassed by the jet fluid the system must be located in the fuselage. However, in most circumstances the simulators will be non-metric and the rear fuselage, tail planes, and/or tail brakes will be metric as far as the jet influence is expected.

Figure 42 yields a cross-sectional view of a gasoline-air burner as used in a subsonic wind tunnel of N.L.R., simulating a low bypass jet engine installed at the fuselage aftend. The aim of the tests performed with this simulator was to determine the forces (stationary and non-stationary) and heating of aft fuselage brake flaps under descent conditions. The jet flow could be well represented.

6.2 INTEGRATED AIRFRAME-ENGINE SYSTEMS

The main jet effects on the airframe aerodynamic occurs if the jet nozzle(s) are located upstream of the fuselage aftend and/or tail planes. If the nozzles form the fuselage aftend, the jet may cause effects on the fin and tail planes, for example separation due to pluming. The treatment of these latter cases is similar to that as discussed in the complete section 5. The jet simulation parameters are similar and the technique which must be followed to determine the lift and pitching moment increments are similar to those to determine the afterbody drag. In most cases the jet nozzle and engine simulator will be non-metric and the afterbody metric on a multi-component balance. Increment determination from pressure plotting is not very attractive due to the large pressure gradients at the fuselage aftend.

If the nozzles are upstream of the fuselage aftend the jets can have important effects on the afterbody and tail plane pressure distributions, and tail plane hinge moments and may cause acoustic fatigue in the rear aircraft structure. These effects may be particularly important when the jets are not aligned with the body axis. The jet parameters are similar as discussed beforen, jet plume shape and jet mixing are probably the main jet characteristics to be simulated. For non-stationary phenomena and surface heating, hot jet tests are required.

Figure 43 depicts a direct cold air blowing system for exhaust jet flow simulation on a fighter type model as used in the U.K. The model is mounted on a standard 6-component balance. Air which passes up the centre of the sting bypasses the balance through a parallel duct into a plenum chamber ahead of the balance. From this plenum chamber 4 ducts are fed rearwards into the exit nozzles of the model. The whole of the blowing system is earthed and flexible seals are fitted between the model jet pipes and jet shrouds, and also between the model rear fuselage and sting. The latter seals being necessary to eliminate cross flows within the model. Seal constraint interference is measured by calibration with the model installed on the balance. Pressure constraints are obtained by section pressuring of the model. The direct air flow quantities were about 5 lbs/sec. at maximum pressure ratio. A faired inlet was used for these tests, with the effects of inlet spillage and a fully faired inlet being measured in a separate test. A major problem in these tests is the definition of the allocation of seal area between metric and non-metric model parts; small areas in this region can have significant effects on measured axial force.

In reference 49 some results are presented of a similar model at transonic speeds.

Figure 44 shows another very useful way to simulate the initial part of the propulsive jet by cold air as it was used in the U.K. The jet flow is brought up to the model in long thin pipes from behind the model of a strike-fighter aircraft. A six component balance measures all the forces on the model in the presence of the jet flow except, of course, the jet thrust and the nozzle base force. Pressures are measured in the balance cavity and in the cavity formed by the blanked-off intake duct. This blanked-off duct is ventilated to the annular "clearance" area between the earthed nozzles and the aircraft afterbody. This test was extended by measurements representing correct or partial inlet spillage with natural blowing exhausts either increased in area or geometrically scaled respectively. The object of this experiment was to obtain the effects of both intake spillage and jet pressure ratio on all the forces (6 components) measured on the same model. Variation of inlet flow and of jet pressure ratio were made separately. Care was taken to try to isolate the effect of variation of each of these and to minimize spurious effects caused by mis-representation of the other variable occurring at the same time.

7. NON-STATIONARY EFFECTS OF JET FLOW

The former sections all concerned steady flow phenomena .However fluctuating pressures often occur in the exhaust environment.

In reference 50 large unsteady pressures are observed on the base of a cylindrical model due to the presence of a central jet (Fig. 45). Though the steady component is already effected by the jet temperature, the average unsteady part must be strongly depended on jet velocity and therefore on temperature.

This is concluded by the authors of reference 50 and hot jet simulation in wind tunnels is recommended for similar cases. For many nozzle systems, particularly the ejector type nozzles, interaction occurs between the internal flow, external flow, and the elastic nozzle resulting in destructive instabilities.

Fixes have been obtained by trial and error, using common sense, and must be accomplished by aerodynamic means without deterioration of the nozzle performance (Ref. 51). Little fundamental knowledge exists on this phenomenon. The problem is very complex since mutual interaction exists between the generated sound pressure field., mixing, vortex formation, separation (internal and external), geometry (sound reflection) and structural dynamic characteristics. There are several ways in which time dependent flow manifest itself.

a) Mach disc oscillations in under-expanded jets due to the interaction of the generated sound field and the vortex shedding at the nozzle lips at subsonic and transonic speeds (often referred to as jet screech).

b) Shock wave oscillations in the external flow as the result of a large plume from an under-expanded nozzle at supersonic speed.

c) Unsteady separation zones close to the nozzle in the external flow; buffet like phenomenon that is amplified by the jet-mainstream interaction. In this case the flow reattachment point between the jet and ambient is also oscillating in location.

d) Also the internal flow might separate if the nozzle is overexpanded.

e) For blow-in-door ejectors the flow into the doors might be time varying, either in phase or out of phase.

f) The nozzle leaves can show flutter like oscillations, particularly for free floating diverging leaves of ejector nozzles.

g) The secondary flow might pulsate due to non-stationary flow in the inlet duct.

Little wind tunnel data are available on unsteady nozzle flow effects. Usually this phenomenon is observed at the free flight trials of the aircraft and is then cured with the real hardware.

8. CORRECTIONS FOR WIND TUNNEL DATA

The balance readings of the metric parts of wind tunnel models must be corrected for non-representative pressures acting on non-representative surfaces. For example in order to determine the forces acting on the external surface of the afterbody, the pressure forces at the inner side must be subtracted. Therefore in order to keep the internal pressure constant a sealing must be applied along the metric line and as close to outer surface as possible. Three methods are in use: the very narrow knife-edge gap (Ref. 32) the teflon seal strip (Ref. 52,53) and the self rolling seal. The sealing system used depends primarily on the local experience, the stiffness of the balance and the relative elasticity of the metric compoents. A difficulty for correcting the measured forces is the determination of the effective area on which the internal pressure is acting, hence where in the effective sealing line located. If possible the determination of this effective sealing area should be done by calibration.

The results determined with the test techniques and corrected for non-representative pressure and friction forces are normally published as they stand, either in the form of thrust and drag coefficients (based on maximum cross-sectional area) or as efficiencies (referred to the thrust of an isentropic nozzle with the same primary mass flow). Only those corrections, which have been established firmly in other wind tunnel investigations should be applied. When such corrections are made, a second set of data should also be compiled without the correction sothat a true representation of the particular correction may be evaluated by the "experienced" user. In any case the correction procedure should be clearly indicated.

If possible the experimental results should be compared with theoretical predictions. For the <u>internal</u> nozzle thrust predictions the methods as described in references 19 and 27 for example may be used if the ratio of specific heats are not matched in the wind tunnel test. If the nozzle in the wind tunnel model is designed for the γ_j of the simulating fluid in a similar manner as the actual nozzle is designed for the rear engine jet flow, the measured thrust coefficient as determined from the wind tunnel tests is directly applicable, except for a small correction for the discharge coefficient due to internal boundary layer effect. Consideration should however be paid to the fact that the ratio of specific heats increases during expansion and the rate of increase depends on the gas composition and temperature. Figure 46 gives the increase in γ_j versus expansion ratio for actual turbine engine jets, the decomposition products of H_2O_2 and of cold air. Also the computation of the ratio of specific heats at high temperatures is not unique. The coefficient of isentropic expansion $\gamma = \left(\frac{\delta \ln p}{\delta \ln \rho}\right)_s$ (where p and ρ are normalized values of the total pressure and density of the gas mixture respectively, either frozen or in equilibrium) and the ratio of specific heats $\gamma = c_p/c_v$ may be used as well as the computation from

$$\gamma = \frac{1}{1 - \dfrac{1}{\dfrac{d \sum_{i=1}^{n} x_i \, S_i^o/R}{d \ln T}}}$$

(where S_i^o = entropy of species i, x_i = mole fraction of species i of the gas mixture and R is the universal gas constant). The last equation is derived from the speed of sound definition. he latter method of equating γ_j is used in figure 46. Computer programs for real gas properties are readily available.

For correction of the external afterbody drag two cases can be distinguished; namely, separated and non-separated external flows. If the flow remains attached until the nozzle edge in the wind tunnel test, it is not very likely that the flow will separate in flight, due to the relative thinner boundary layer at full scale. In those cases and for axisymmetric and clean afterbodies the correction on the pressure contribution due the boundary layer displacement thickness can be computed with modern transonic flow field analysis for the full scale and model case and compared with the experimental wind

tunnel data, likewise the skin friction drag can be calculated. Such a technique is described in reference 54 and 55 for transonic speeds and is successful. In these computations the plume is introduced as a solid body for which corrections for mixing along the jet boundary can be applied.

The corrections give large confidence if the experimental results from the wind tunnel can be correlated or predicted by theoretical analysis. The analysis is the easiest if the afterbody can be considered as a slender body sothat small perturbation techniques can be used for the inviscid flow. The corrections on the wind tunnel data than concern changes in skin friction due to the increase in Reynolds number for the actual aircraft and changes due to reduced relative displacement thickness and entrainment. The performance goals of afterbodies should be the drag of slender axisymmetric bodies. Figure 47 as given in reference 49 shows how the computed afterbody drag compares with the results from wind tunnel tests. If this correlation can be achieved, proper determination of corrections for scale effect should be possible.

In the case flow separation does occur in the wind tunnel at the afterbody no rules are available for proper correction methods, since the extent of the separated region can not be correlated with the scale and boundary layer characteristics (see Ref. 11). For separated flows isolated tests with limited forebody length yielding simulated relative boundary layer thicknesses probably will yield the best uncorrected results. If applicable the test data should be compared with the empirical afterbody drag estimation as given in reference 56 for supersonic speeds. If this estimation is close a hot jet correction factor (change of γ_j) may be computed for which the reliability should be checked.

In general it can be stated that only little is known of Reynolds number, boundary layer and mixing effect on the afterbody drag and nozzle thrust, except for some schematic configurations and that more work is needed in this area. In reference 57 a selection is made of the best suitable methods for predicting the thrust and drag of isolated axisymmetric nozzle installations at subsonic, transonic and supersonic speeds, covering external flow problems, internal flow problems, exhaust plumes and base pressures.

9. FINAL REMARKS

From the review as given in this lecture it can be concluded that there exists no unique method which can be used to predict exhaust-airframe phenomena (and hence afterbody and nozzle performances) from wind tunnel tests. The chosen wind tunnel set-up is strongly influenced by the required accuracy, phenomena looked for, existing wind tunnel facilities and local experience. Particularly at high bypass ratio engines and transonic speeds the existing testing techniques should be improved and more information is necessary on primary jet flow parameters to be simulated in the wind tunnel. This lecture did not consider engine integration tests of V/S.T.O.L airplane models in the wind tunnel. In the future when these aircraft come in a more development stage the wind tunnel test requirements will probably be even more severe as they are now at the higher speed regimes, since other phenomena (such as reingestion will be involved, and the data are related more to safety rather than to economics and performance.

Since much information in this lecture has been taken from the AGARD Ad-Hoc study as mentioned in the introduction, the author expresses his gratitude to those groups which supplied information that has been used.

10. REFERENCES

1. A. Ferri, F. Jaarsma, R. Monti — "Engine-Airplane Interference and Wall Corrections in Transonic Wind Tunnel Tests". AGARD-AR-36-71, Aug. 1971.
2. A. Ferri — "Review of the Conclusions of the AGARD Ad-Hoc Committee on Engine-Airplane Interference and Wall Corrections in Transonic Wind Tunnel Tests". AGARD-CP-91-71, 1971. Inlets and Nozzles for Aerospace Engines.
3. F. Jaarsma — "Inlets-Airplane Testing in Transonic Wind Tunnels". AGARD-CP-91-71, Inlets and Nozzles for Aerospace Engines.
4. A.E. Fuhs — "Nozzle and Exhaust Testing in Transonic Flight Regime". AGARD-CP-91-71. Inlets and Nozzles for Aerospace Engines.
5. W.K. Greathouse — "Blending Propulsion with Airframe". Space/Aeronautics, November 1968.
6. J.J. Horgan and D.B. Waring — "Supersonic Nozzles". AGARD CP-34, 1968.
7. P. Carrière, M. Sirieix, J.H. Hardy — "Problèmes d'Adaption de Tuyères". AGARD CP-34, 1968.
8. P. Carrière — "Exhaust Nozzles". AGARDograph 120 Supersonic Turbo-Jet Propulsion systems and Components", 1967.
9. J.L. Grunnet — "Designing Jet Aircraft Wind-Tunnel Test Programs with Propulsion System Simulation". Journal of Aircraft Vol. 8 No. 6, June 1971.
10. D. Migdal and W.K. Greathouse — "Optimizing Exhaust-Nozzle/Airframe Thrust Minus Drag". SAE Paper 680294, May 1968.
11. D.N. Bowditch — "Inlet-Engine-Nozzle Wind Tunnel Test Techniques". AGARD CP-91-71 paper 7, 1971. Inlets and Nozzles for Aerospace Engines.
12. D.L. Motyoka and P.J. Skowronek Jr. — "Performance Installation Effects for Nozzles Installed on a Twin-Jet Fighter Airplane Model". SAE Paper 680296, May 1968.
13. M. Pindsola — "Jet-Simulation in Ground Test Facilities". AGARDograph No. 79, 1963.

14. E.S. Love, C.E. Grigsby, L.P.Lee and W.J. Woodling — "Experimental and Theoretical Studies of Axisymmetric Free Jets". NASA TR R-6, 1959.

15. V. Zakkay, E. Krause and S.D.L. Loo — "Turbulent Transport Properties for Axisymmetric Heterogeneous Mixing". AIAA Journal, Vol. 2, no. 11, November 1964.

16. W. Szablewski — "Turbulente Ausbreitung runden Heissluft Strahles in Bewegter Luft". Ingenieur archiv. XXVI, 1958.

17. W. Szablewski — "Turbulente Vermischung ebener Heissluft Strahlen für den Unterschall Bereich". Ingenieur Archiv XXV, Ersten Heft, 1957.

18. D. Bergman — "An Aerodynamic Drag Study of Jet Engine Nozzles". AGARD CP-91-71, 1971. Inlets and Nozzles for Aerospace Engines.

or
D. Bergman — "Effects of Engine Exhaust Flow on Boattail Drag". Journal of Aircraft, Vol. 8, no. 6, June 1971.

19. P. Carrière — "Exhaust Nozzles". AGARDOGRAPH 120.

20. P. Carrière, M. Sirieix and J.H. Hardy — "Problèmes d'Adaption de Tuyères" AGARD CP-34, 1968.

21. H. McDonald and P.F. Hughes — "A Correlation of High Subsonic Afterbody Drag in the Presence of a Propulsive Jet or Support Sting". Journal of Aircraft, Vol. 2, no. 3, May-June 1965.

22. J. Reid — "The Effect of Jet Temperature on Base Pressure". RAE TR 68176, July 1968.

23. J.E. Green — "A Design of Sonic nozzle for the Precise Measurement of Mass Flow". Zeitschrift für Flugwissenschaften, 19 (1971), Heft 3, or RAE TR 70201.

24. B. Masure, J.L. Solignac et P. Lavel — "Mass Flow Rate Measurement by Means of a Sonic Throat". ONERA, T.P. no. 956.

25. R.C. Johnson — "Real-gas Effects in Critical-Flow-Through Nozzles and Tabulated Thermodynamic Properties" NASA TN D-2565.

26. B. Masure — "Problèmes de Mesure sur Maquette de la Pousée d'un Arrière-Corps d'Avion Supersonique". Tuyères de Référence, AGARD CP-91-71, 1971, Inlets and Nozzles for Aerospace Engines.

27. J.M. Hardy — "Influence de Quelques Paramètres Caracteristiques sur les performances des Ejecteurs". AGARD CP 91-71, 1971, Inlets and Nozzles for Aerospace Engines.

28. J.C. Ascough — "Measurement Full-scale of Propelling Nozzle Performance in an Altitude Test Facility. AGARD CP-91-71. Inlets and Nozzles for Aerospace Engines 1971.

29. D.E. Harrington — "Jet Effects on Boattail Pressure Drag of Isolated Ejector Nozzles at Mach Number from 0.60 to 1.47". NASA TMX-1785, May 1969.

30. D. Migdal, E.H. Miller and U.C. Schnell — "An Experimental Evaluation of Exhaust Nozzle/Airframe Interference". AIAA Paper 69-430, AIAA 5th Propulsion Joint Specialist Conference, 1969.

31. J. Leynart and G. Meauze — "Quelques Problèmes Transoniques du Fuseau Moteur d'un Avion du Type "Airbus". AGARD CP-35, "Transonic Aerodynamics".

32. E.C. Carter — "The Use of Test Rig Measurements of thrust-Drag to Provide Correction Terms for Jet Interference". ARA memo 84, 1968.

33. K.E. Tempelmeyer — "An Analytical Study of Hot Jet Simulation with a Cold Gas Mixture". AEDC-TN-58-54, 1958.

34. J.F. Runckel and J.M. Swihart — "A Hydrogen-Peroxyde Hot-Jet Simulation for Wind Tunnel Tests of Turbojet-Exit Models". NASA Memo 1-10-59L, 1959.

35. H.T. Norton, M.D. Cassetti, C.E. Mercer — "Transonic Off-Design Performance of a Fixed Divergent Ejector Designed for a Mach Number of 2.0". NASA TM X-165.

36. J.C. Patterson Jr. — "A Wind Tunnel Investigation of Jet-Wake Effect of a High Bypass Engine on Wing-Nacelle Interference Drag of a Subsonic Transport". NASA TN D-4693, Aug. 1968.

37. J.C. Patterson Jr. and S.G. Flechner — "Jet-Wake Effects of a High-Bypass Engine on Wing-Nacelle Interference Drag of a Subsonic Transport Airplane". NASA TN D-6067, Nov. 1970.

38. "Equipment Catalogue" Techn.Development Inc., Dayton, Ohio.

39. D.T. Poland and J.C. Schwanebeck — "Turbo-Fan Thrust Determination for the C.5a". AIAA 70-611, June 1970.

40. S.E. Aldridge and J.L. Nye — "Experimental results of High-Bypass Ratio Turbo-fan and Wing Aerodynamic Interference". AGARD CP-71, Sept. 1970.

41. H.R. Welge and J.R. Ongarato — "Powered Engine Simulator Procedures and Experience for the DC-10 Wing Engine at High Subsonic Speeds". Journal of Aircraft, Vol. 8, no. 7, July 1971.

42. W. Tabakoff and H. Sowers — "Drag Analysis of Powered Nacelle for Jet Engine Model Tests". Zeitschrift für Flugwissenschaften, April 1969.

43. R.J. Margason and G.L. Gentry — "Static Calibration of an Ejector Unit for Simulation of Jet Engines in Small-Scale Wind Tunnel Models". NASA TN D-3867, 1967.

44. G. Pauley — "Interim Note on Tests with a Wing-Mounted Fan Nacelle with the Fan Jet Simulated by Cold Air Blowing and Alternatively by a Gas Generator Shroud". Aeronautical Research Council, C.P. no. 1111, 1970.

45. E. Bonner — "Expanding Role of Potential Theory in Supersonic Aircraft Design". Journal of Aircraft, Vol. 8, No. 5, May 1971.

46. L.E. Putnam and F.J. Capone — "Experimental Determination of Equivalent Solid Bodies to Represent Jets Exhausting into a Mach 2.20 External Stream". NASA TN D-5553, Dec. 1969.

47. D.J. Raney, A.G. Kurn and J.A. Bagley — "Wind Tunnel Investigations of Jet Interference for Under-wing Installation of High Bypass Ratio Engines". RAE TR 68049, 1968.

48. W. Geissler und R. Wulf — "Jet Simulation and Jet Interference Effects on Tail Planes". AGARD C.P. 71, Aerodynamic Interference, 1971.

49. J.F. Runckel — "Aerodynamic Interference between Exhaust System and Air-frame". AGARD CP-71-71. "Aerodynamic Interference, 71.

50. J.E. Rossiter and A.G. Kurn — "Wind Tunnel Measurements of the Effect of a Jet on the Time Average and Unsteady Pressures on the Base of a Bluff After-body". RAE Rep. 65187, 1965.

51. J.J. Horgan and D.B. Waring — "Supersonic Nozzles". AGARD C.P. 34, 1968.

52. B.L. Berrier and F.H. Wood Jr. — "Effect of Jet Velocity and Axial Location of Nozzle Exit on the Performance of a Twin-Jet Afterbody Model at Mach number up to 2.2". NASA, Sept. 1969.

53. D. Chamberlain — "Measurement of Drag from Interaction of Jet Exhaust and Air-frame". Journal of Aircraft, Vol. 6, no. 2. March-April 1969.

54. R.S. Armstrong and S.R. Miller — "Subsonic Aerodynamic Performance of Nozzle Installations in Supersonic Airplanes". Journal of Aircraft, Vol. 5, No. 3, 1968.

55. E. Grund, W. Presz Jr. and M. Konarski — "Predicting Airframe/Exhaust Nozzle Interactions at Transonic Mach Numbers". AIAA Paper 71-720, AIAA/SAE 7th Propulsion Joint Specialist Conference, June 1971.

56. J.A.P. Stoddard — "Jet Effects on Boattail Pressure Drag at Supersonic Speeds". AGARD C.P.-91-71, 1971. "Inlets and Nozzles for Aerospace Engines".

57. E.R. Glasgow, J.S. Divita, P.C. Everling and J.A. Laughrey — "Analytical and Experimental Evaluation of Performance Prediction Methods Applicable to Exhaust Nozzles". AIAA Paper 71-719, AIAA/SAE 7th Propulsion Joint Specialist Conference, June 1971.

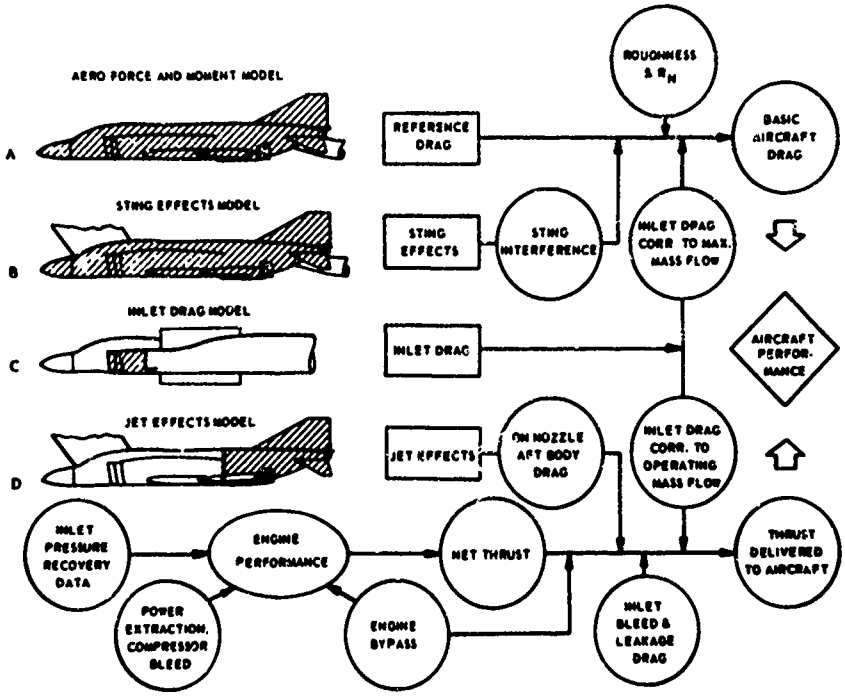

Fig. 1 Thrust and drag accounting system.

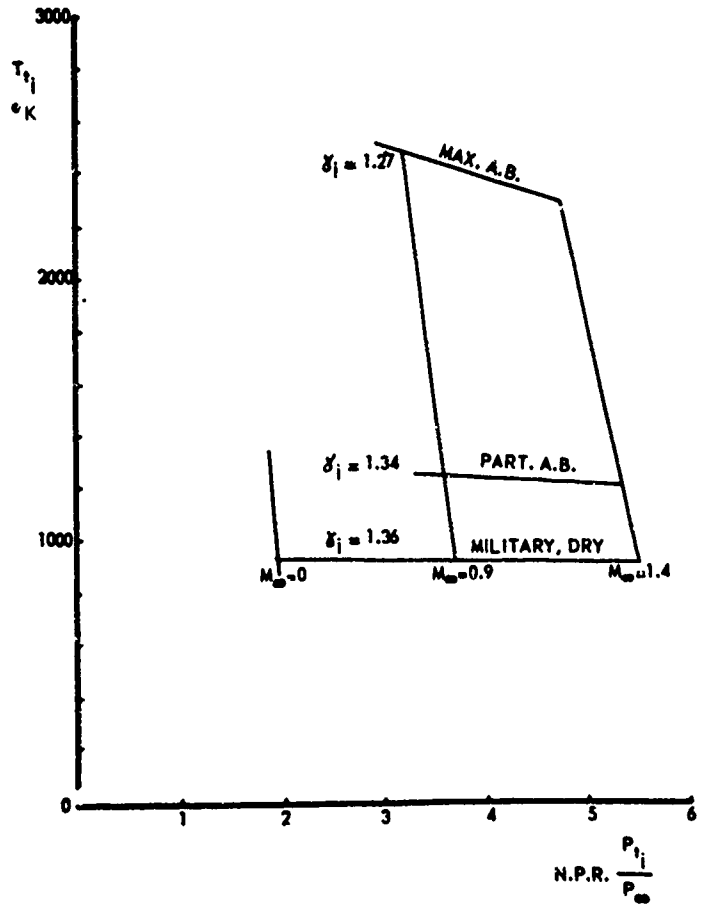

Fig. 2 Typical transonic exhaust conditions (γ_j at stagnation conditions).

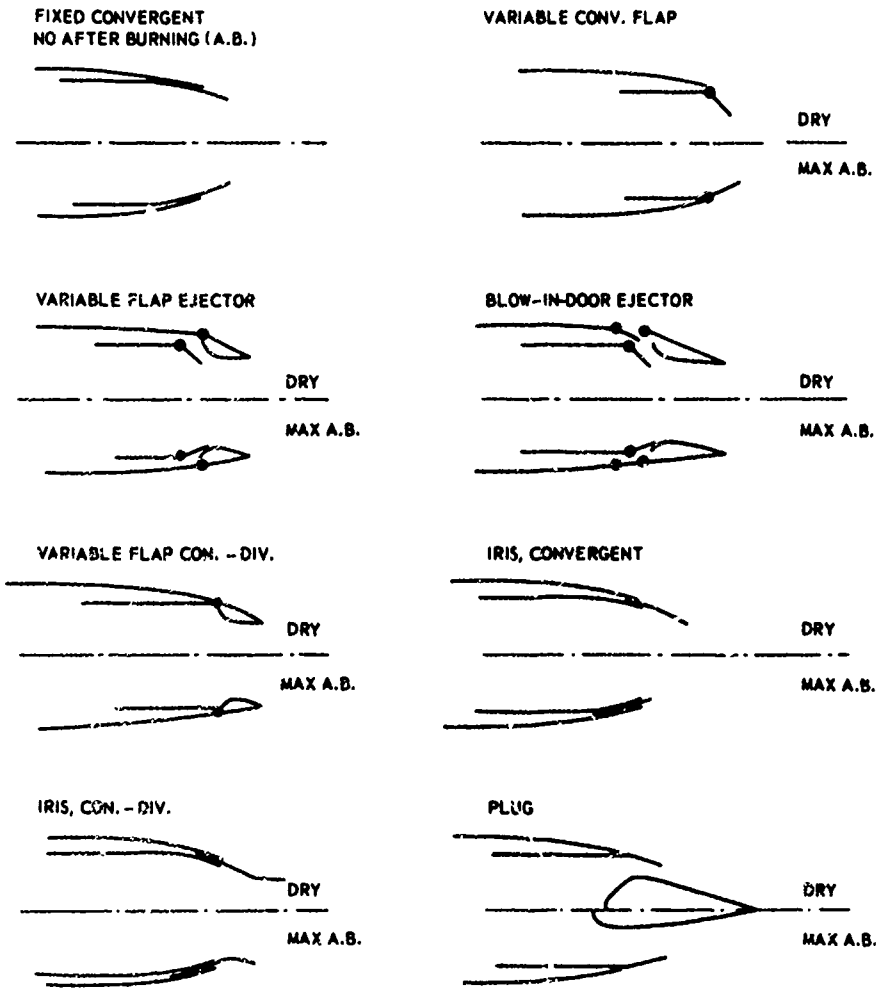

Fig. 3 Various nozzle designs, schematic.

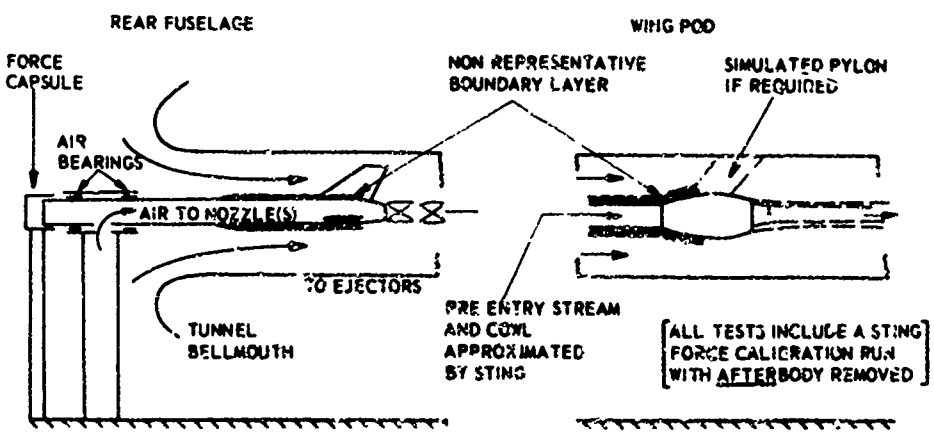

Fig. 4 Isolated nozzle test rig.

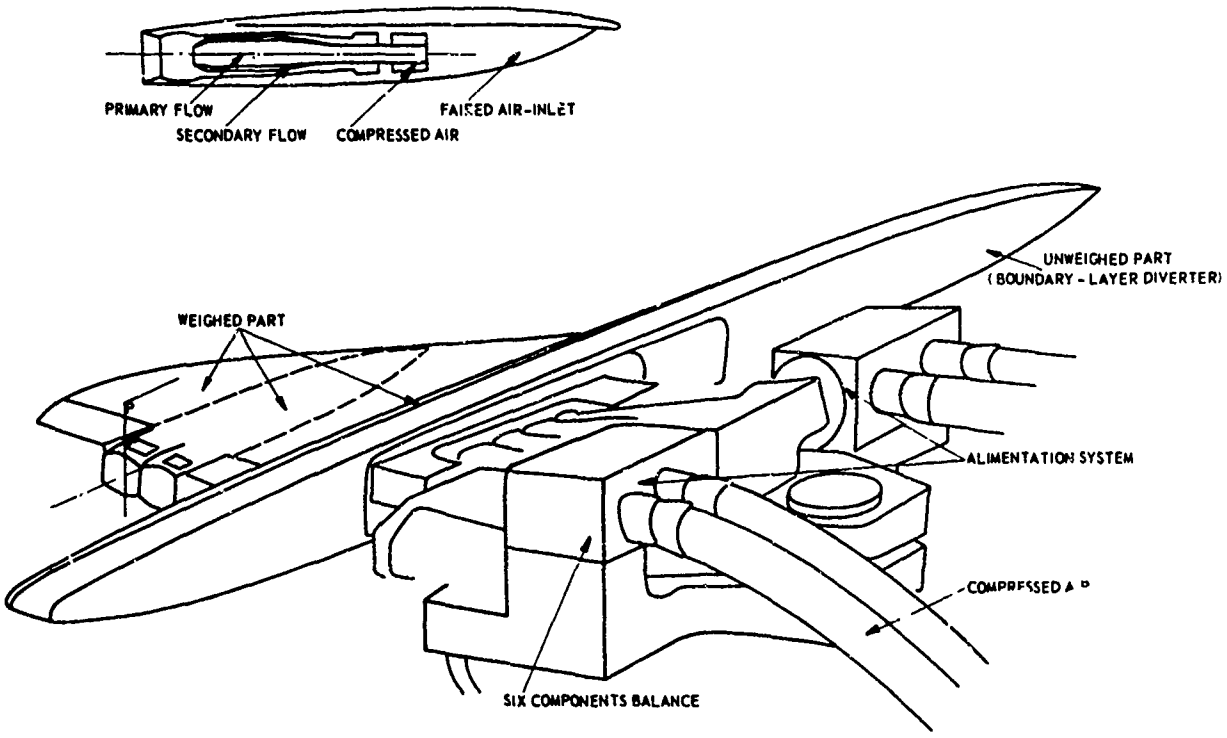

Fig. 5 Thrust-drag test semi-model of S.S.T. with integrated nacelle (scale 1/25).

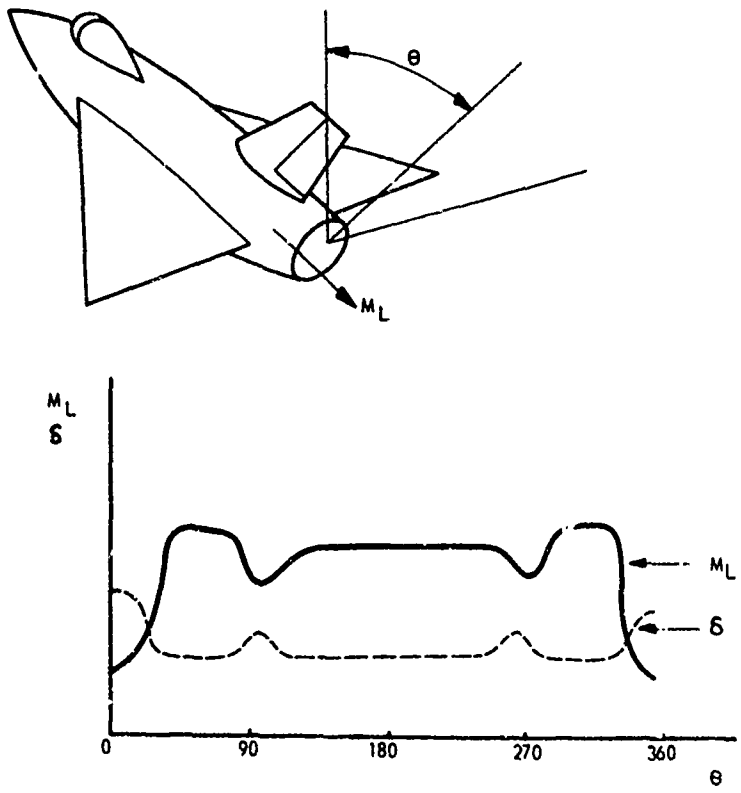

Fig. 6 Three-dimensional flow environment for nozzle.

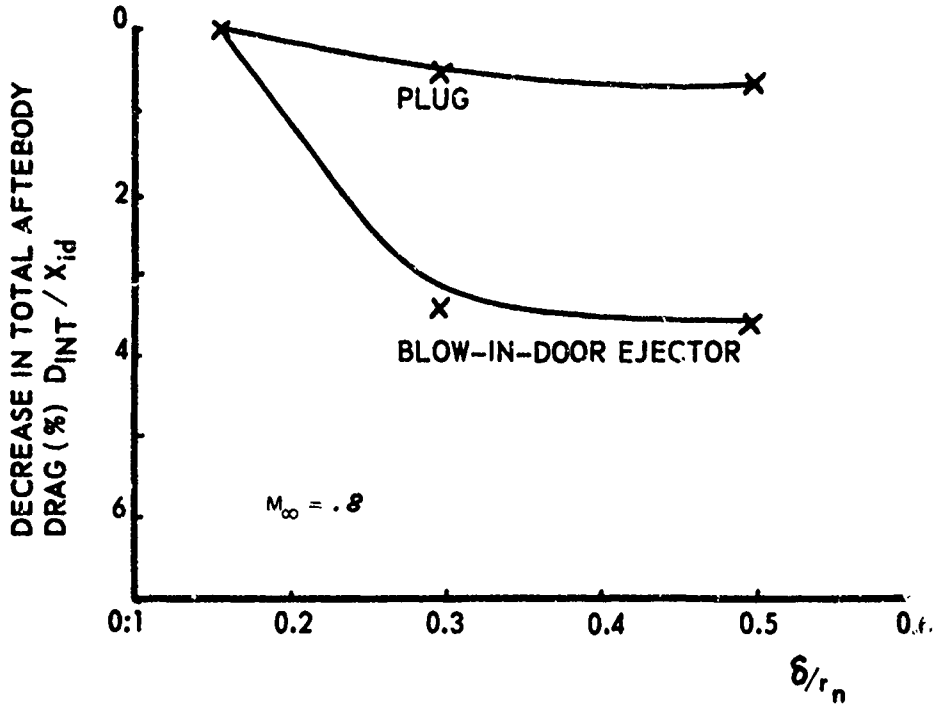

Fig. 7 Effect of relative boundary layer thickness on total interference drag (M = .8).

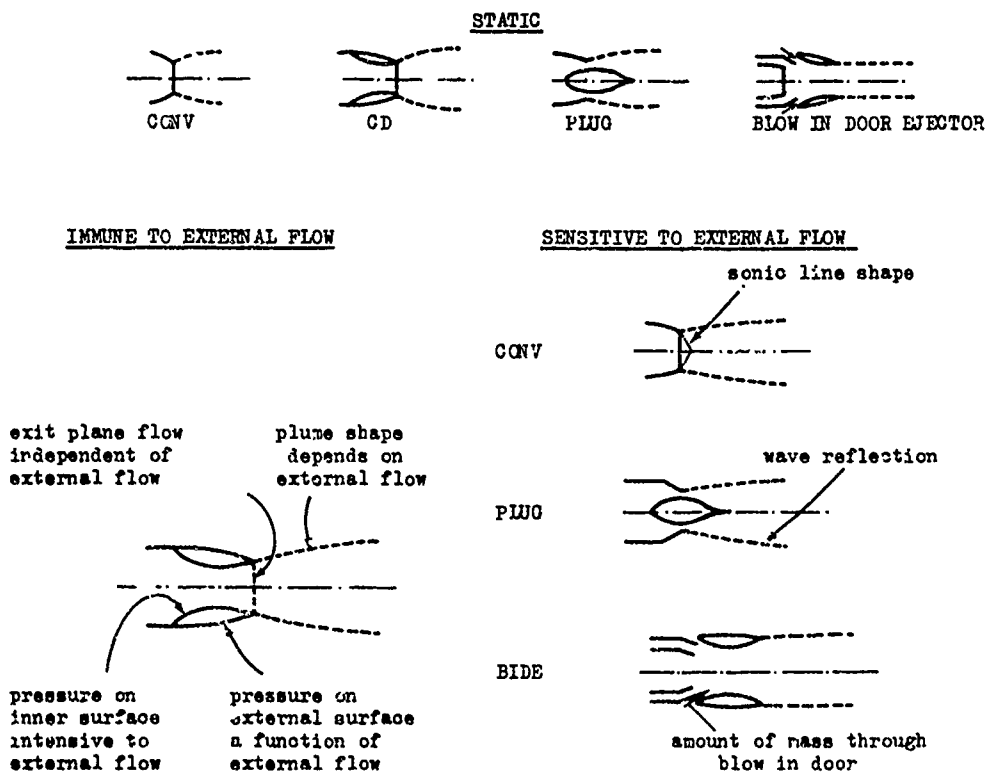

Fig. 8 Nozzles immune and sensitive to external flow.

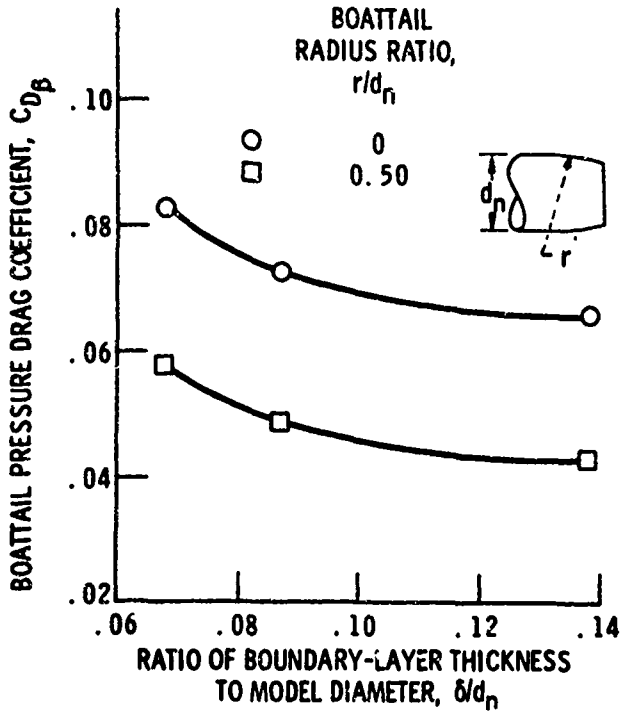

Fig. 9a Effect of relative boundary layer thickness on boattail pressure drag. $\beta = 15^{\circ}$, $M_{\infty} = .90$.

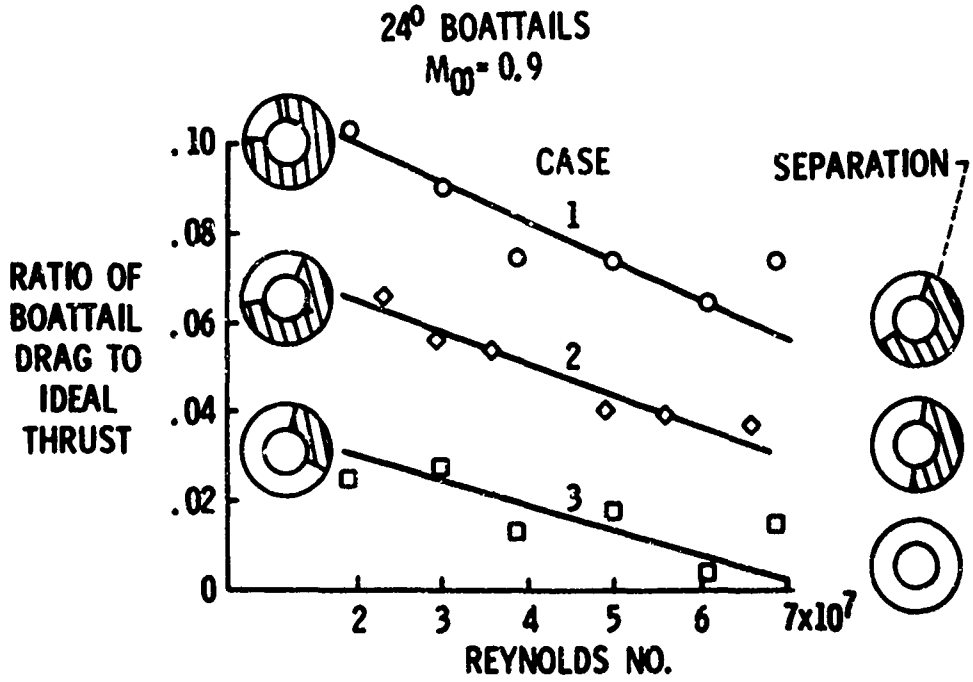

Case 1 $r/d_n = 0.72$

Case 2 $r/d_n = 0.72$ with shorter forebody

Case 3 circular arc

Fig. 9b Reynolds number effect on boattail drag.

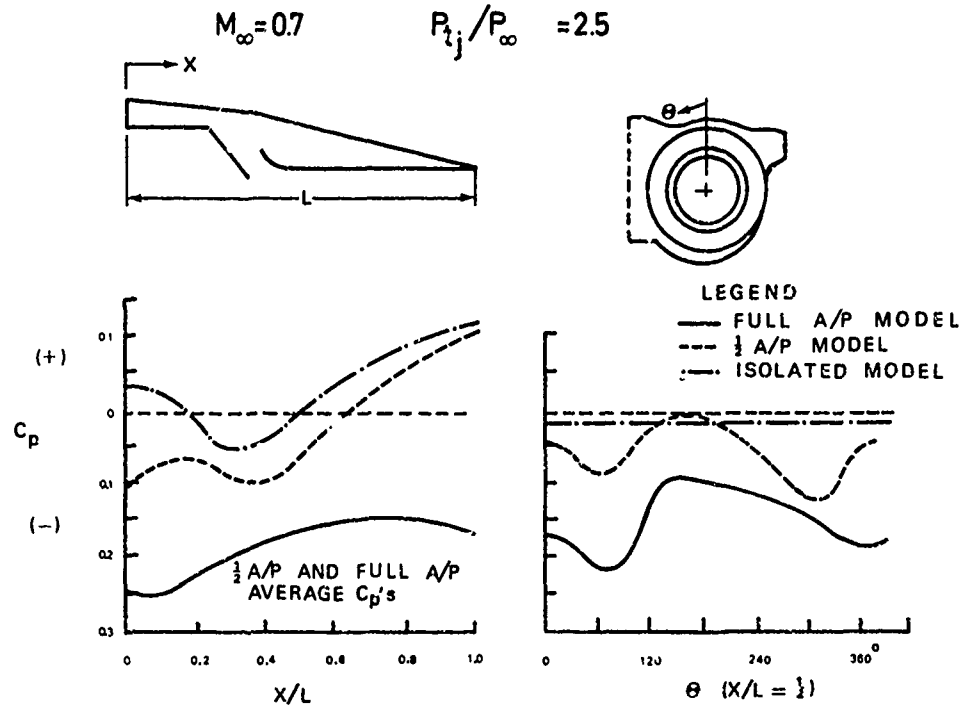

Fig. 10 External pressure on variable flap ejector nozzle for three model configurations.

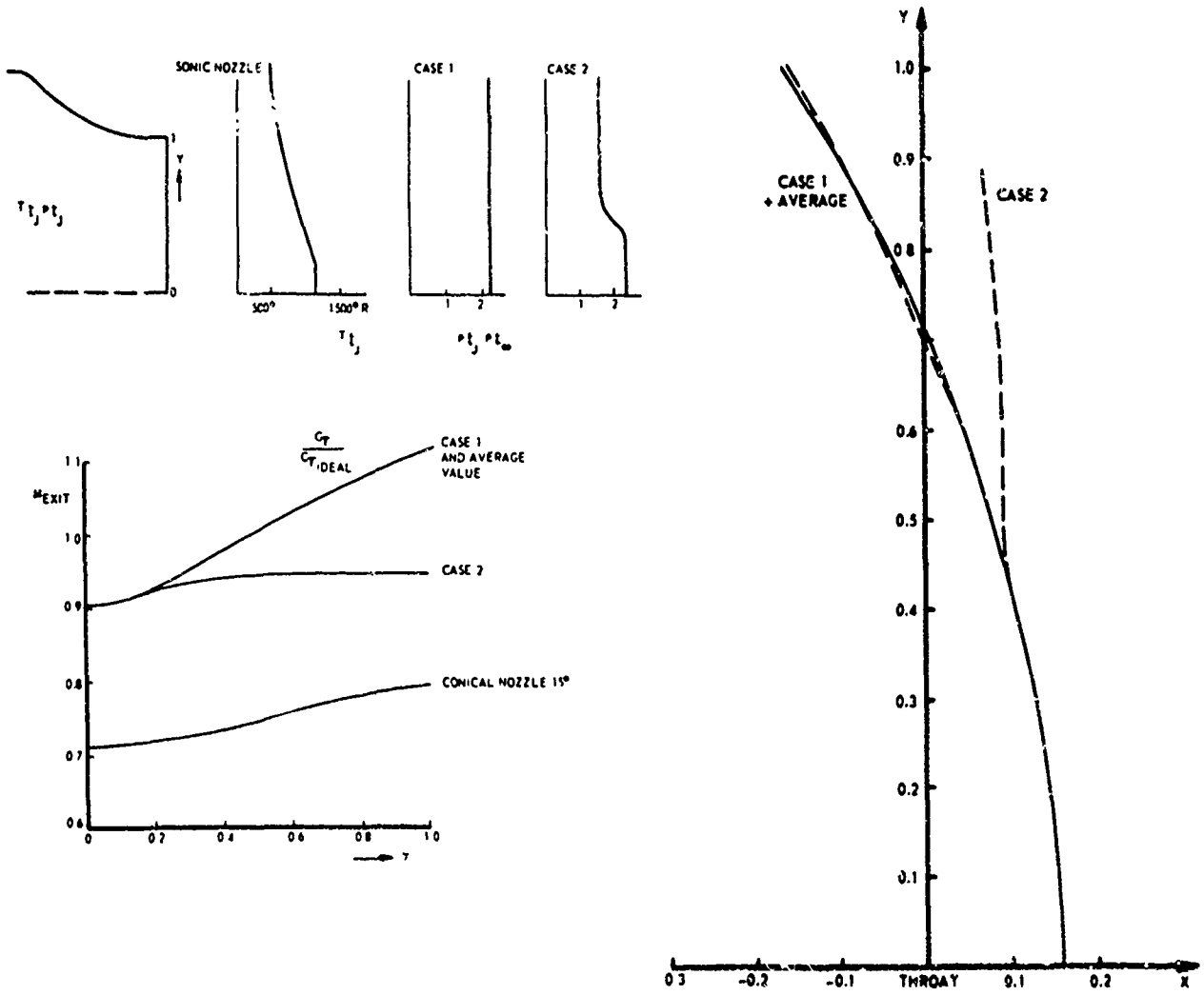

Fig. 11 Mach number distribution and sonic line shapes at the exit of a convergent nozzle for non-uniform stagnation conditions.

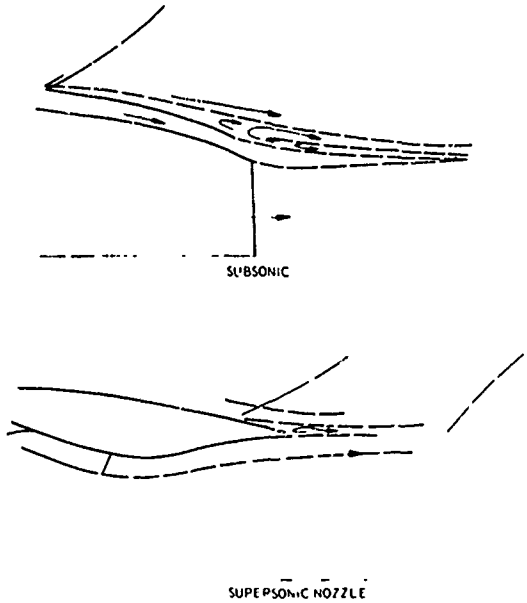

Fig. 12 Points of separation determined by mixing.

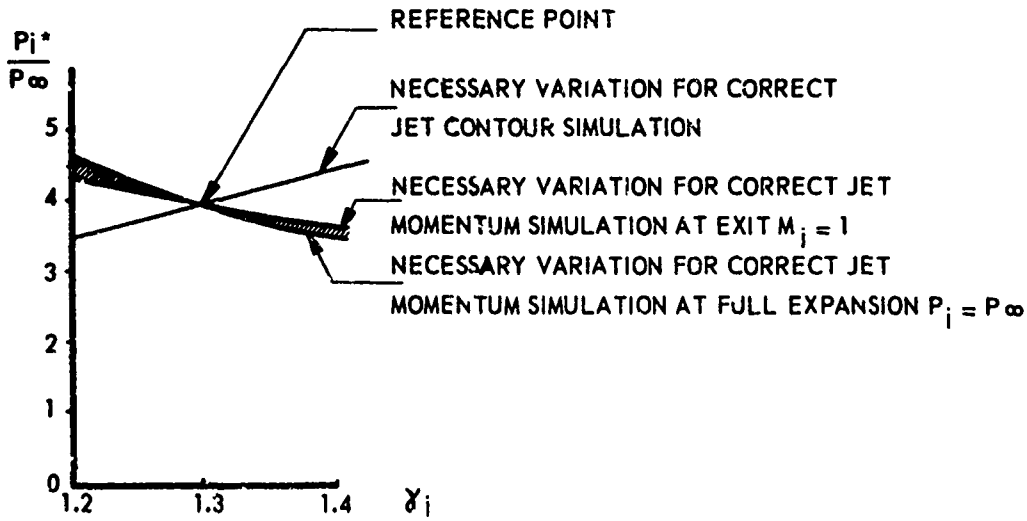

Fig. 13 Example of necessary n.p.r. variation if $\gamma_{jmodel} \neq \gamma_{jengine}$ for jet contour or jet momentum simulation.

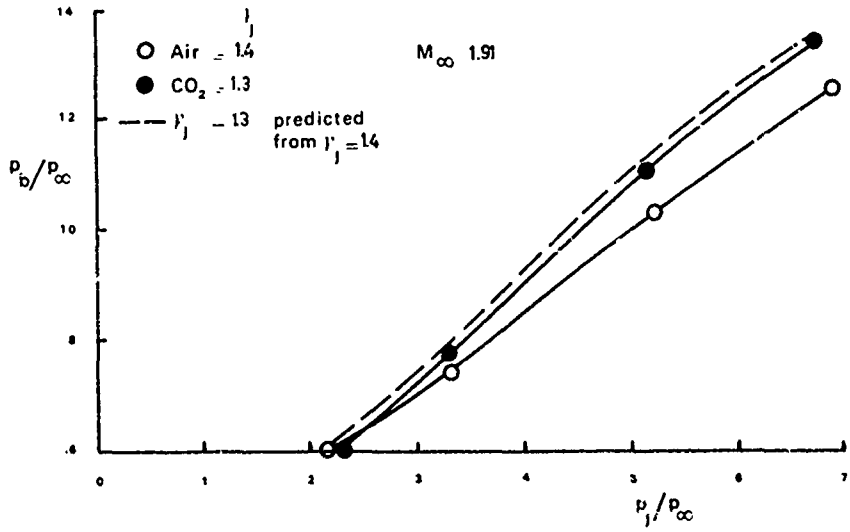

Fig. 14 Effect of a sonic jet on the base pressure at supersonic speed.

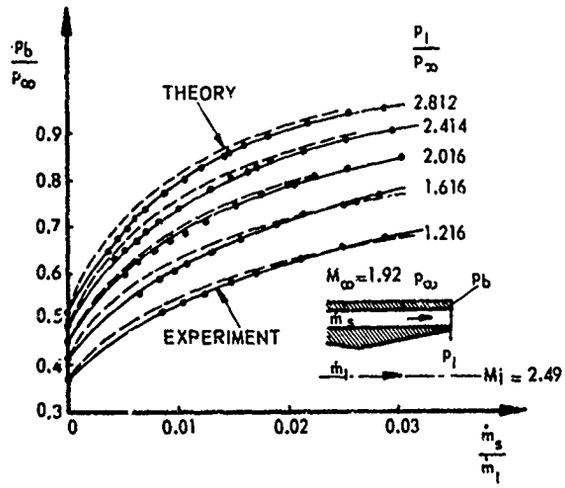

Fig. 15 Effect of mass injection at the base on the base pressure at supersonic speed.

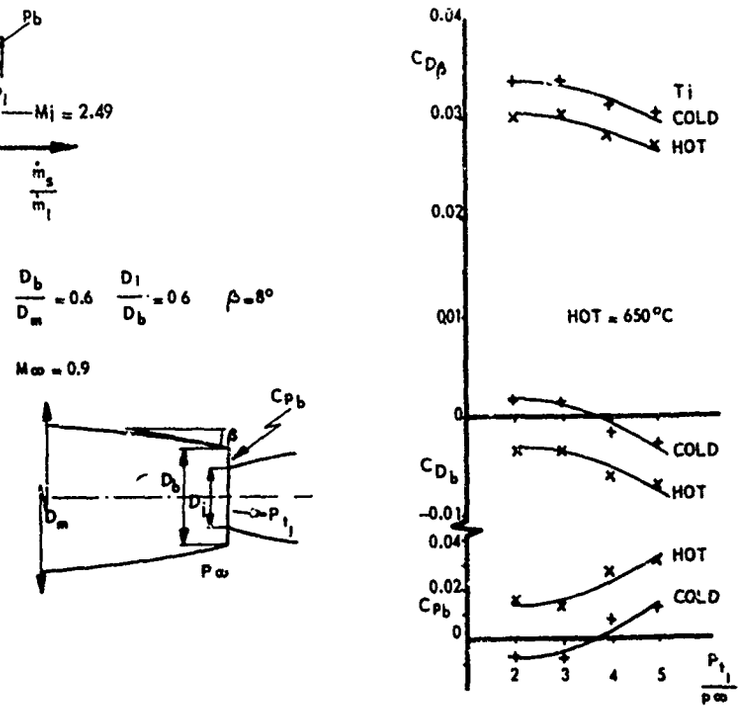

Fig. 16 Effect of jet temperature on base pressure at transonic speed. →

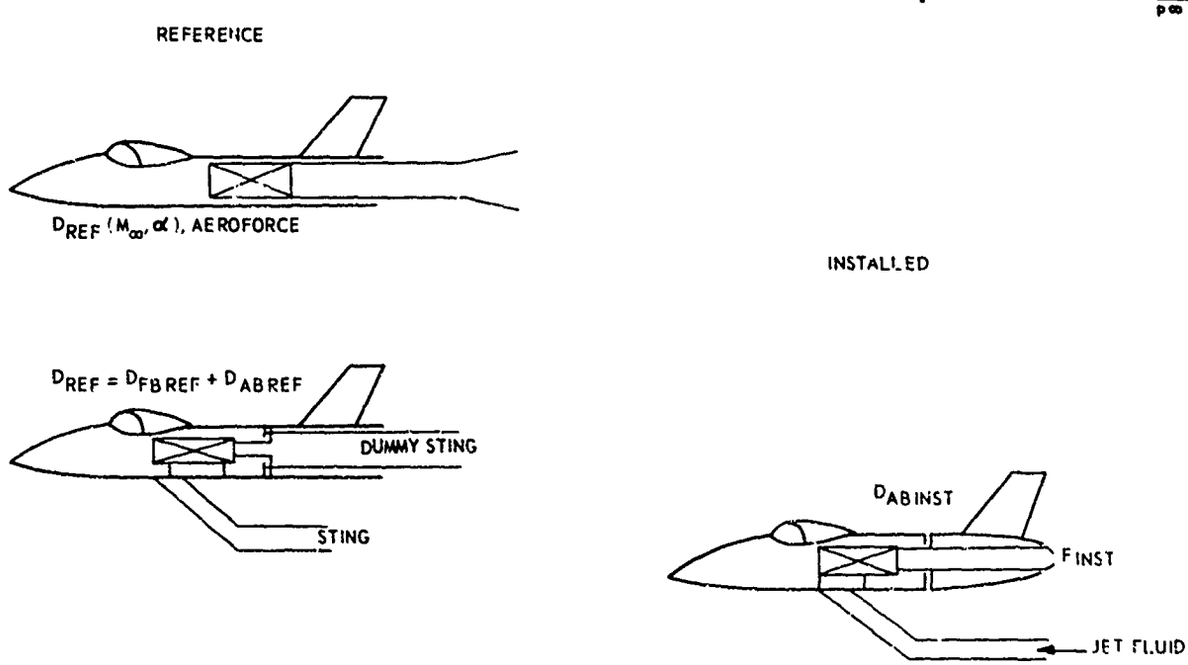

Fig. 17 Bookkeeping procedure for integrated nozzle-airframe systems.

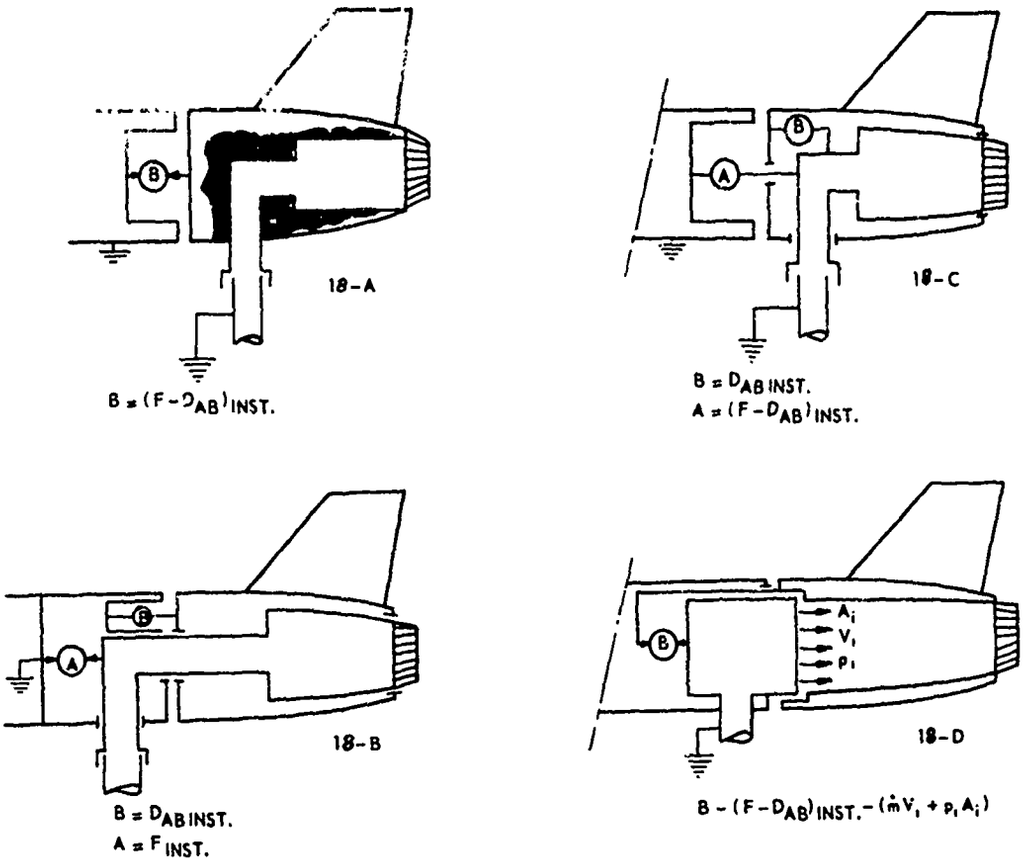

Fig. 18 Wind tunnel testing schemes for installed afterbody/nozzle performance determination.

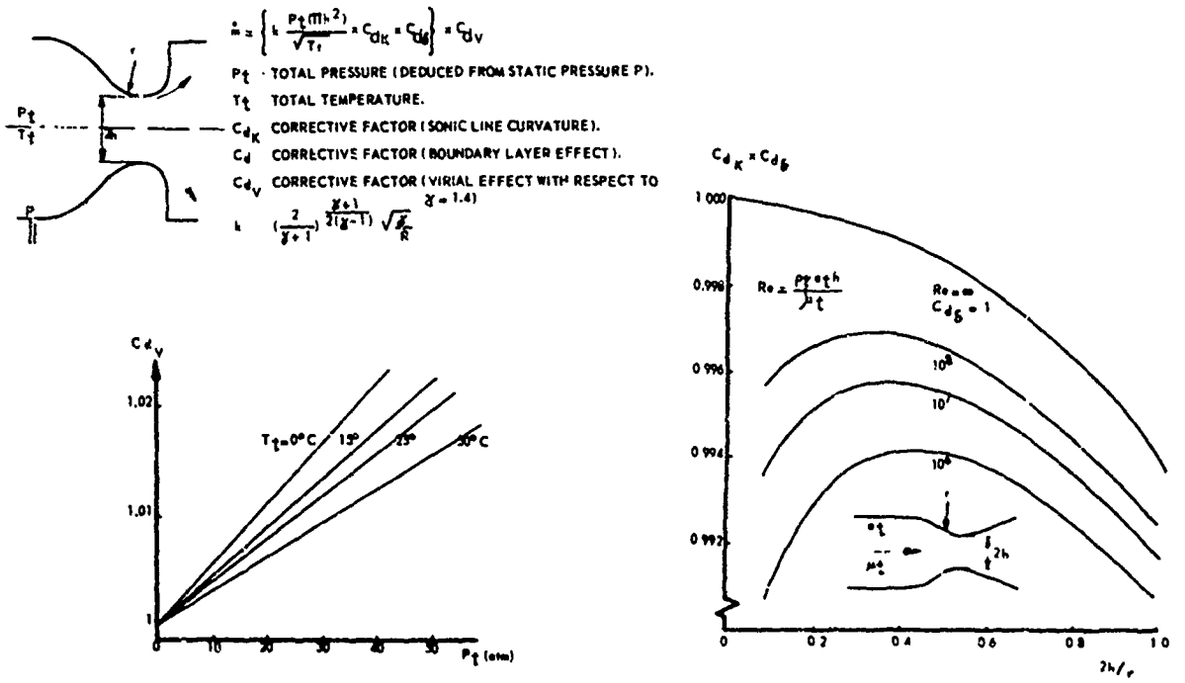

Fig. 19 Mass flow measurement by the sonic throat method.

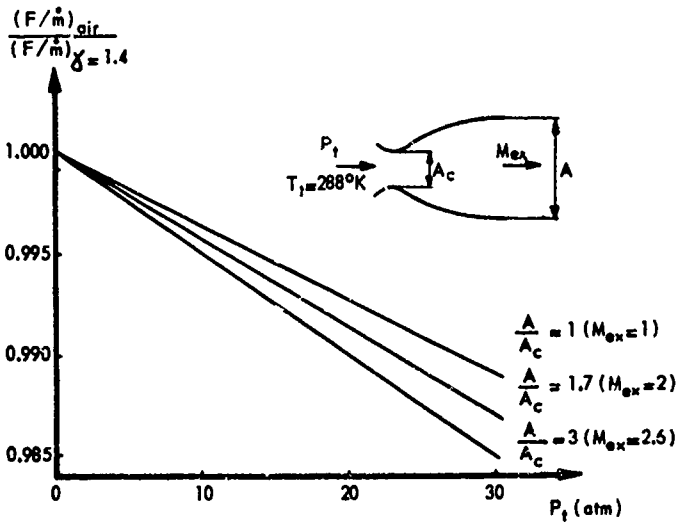

Fig. 20 Virial effect on nozzle thrust for cold air.

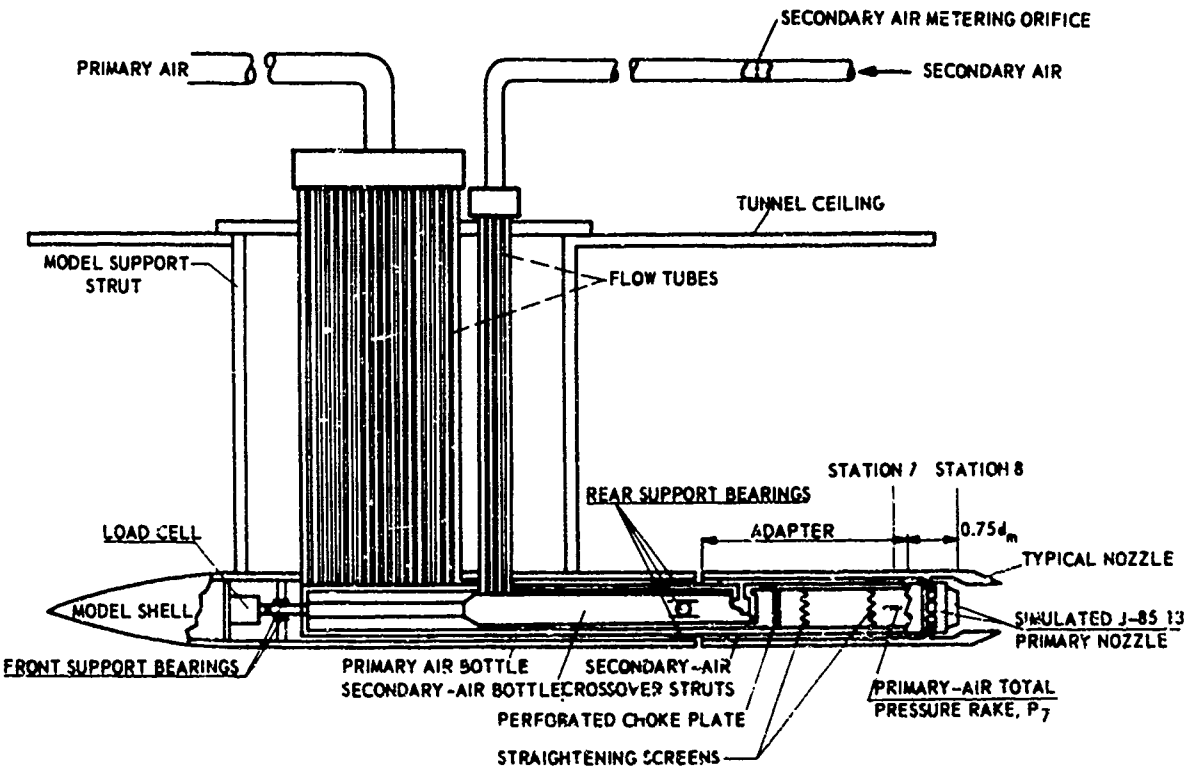

Fig. 21 Internal geometry and thrust measuring system using cold air in isolated model.

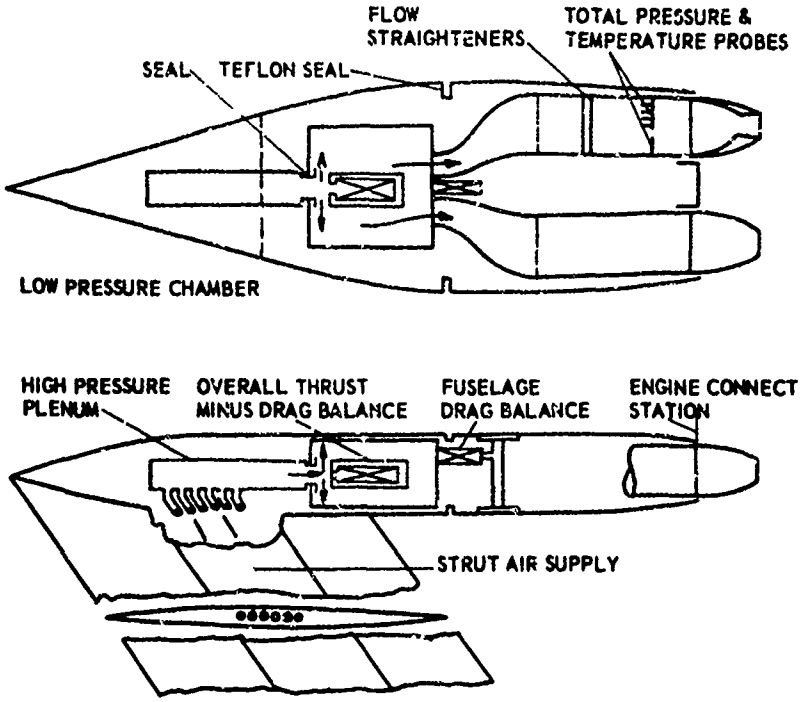

Fig. 22 Tandem, twin jet isolated afterbody test rig.

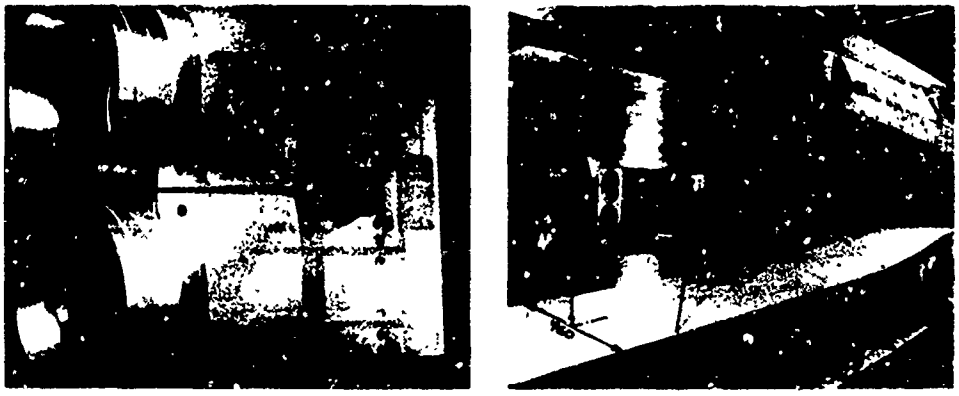

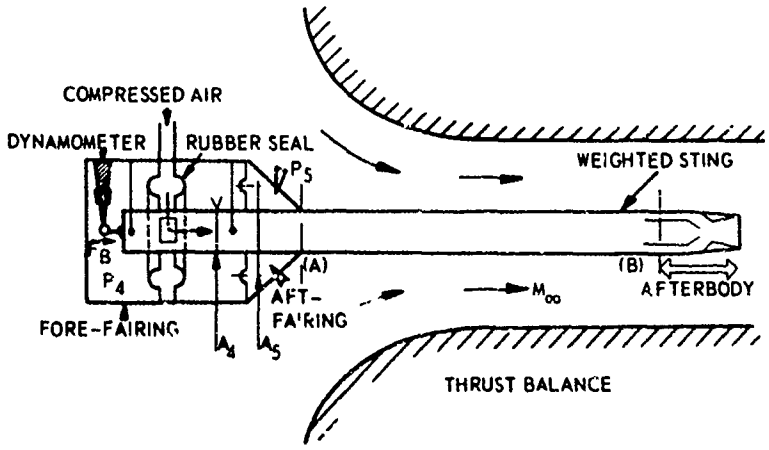

$F_B + A_4P_4 - (A_5 - A_4)P_5$ + MEMBRANES CORRECTIONS = FRICTION DRAG FROM (A) TO (B)

MEASURED THRUST (P_4 : BALANCE INTERNAL PRESSURE, A_4 . EFFECTIVE AREA) (P_5 : AFT-FAIRING PRESSURE, $A_5 - A_4$: EFFECTIVE AREA) + AFTERBODY THRUST-MINUS DRAG

Fig. 23 Shaft mounted afterbody model arrangements in transonic and supersonic wind tunnels for thrust-drag measurements.

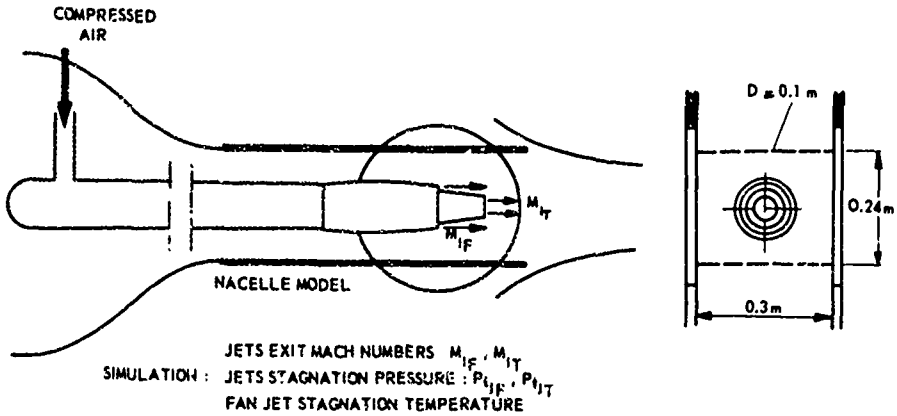

Reproduced from best available copy.

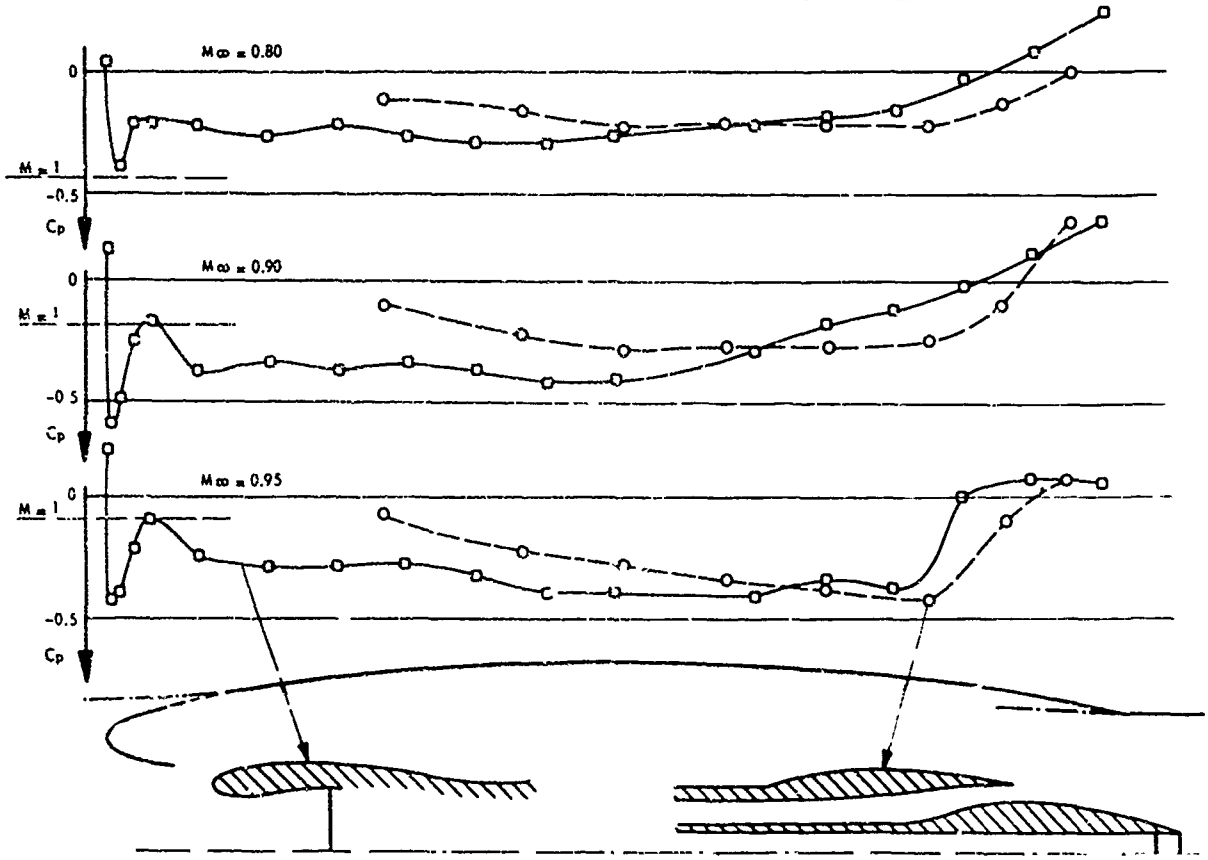

Fig. 24 Fan engine afterbody test rig in transonic wind tunnel and some test results (including inlet).

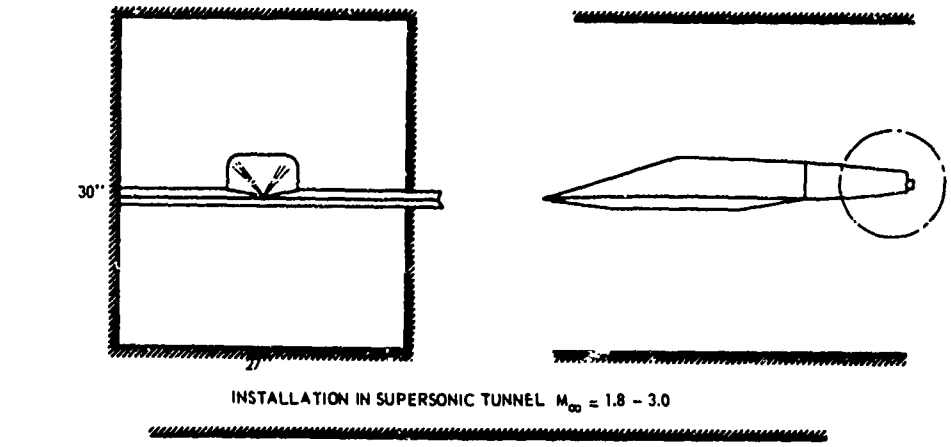

Fig. 25a Installation of a side supported twin nozzle afterbody test rig in both supersonic and transonic wind tunnel.

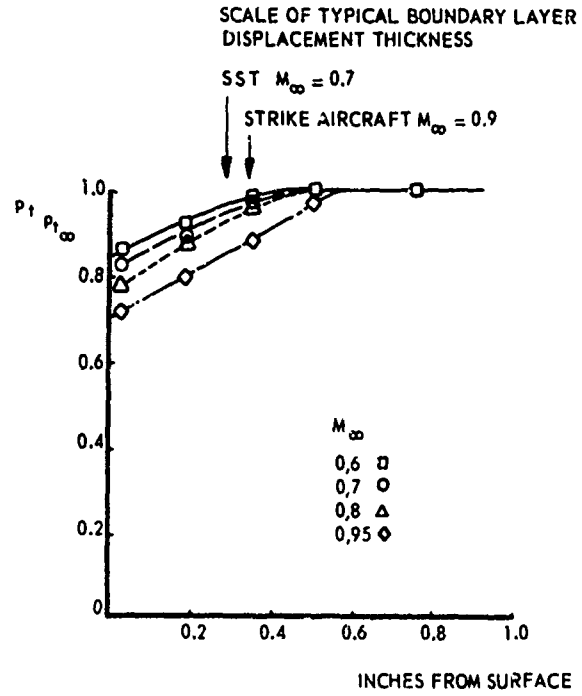

Fig. 25b Comparison between full scale boundary layer displacement thickness and model boundary layer at metric line → (fig. 25a).

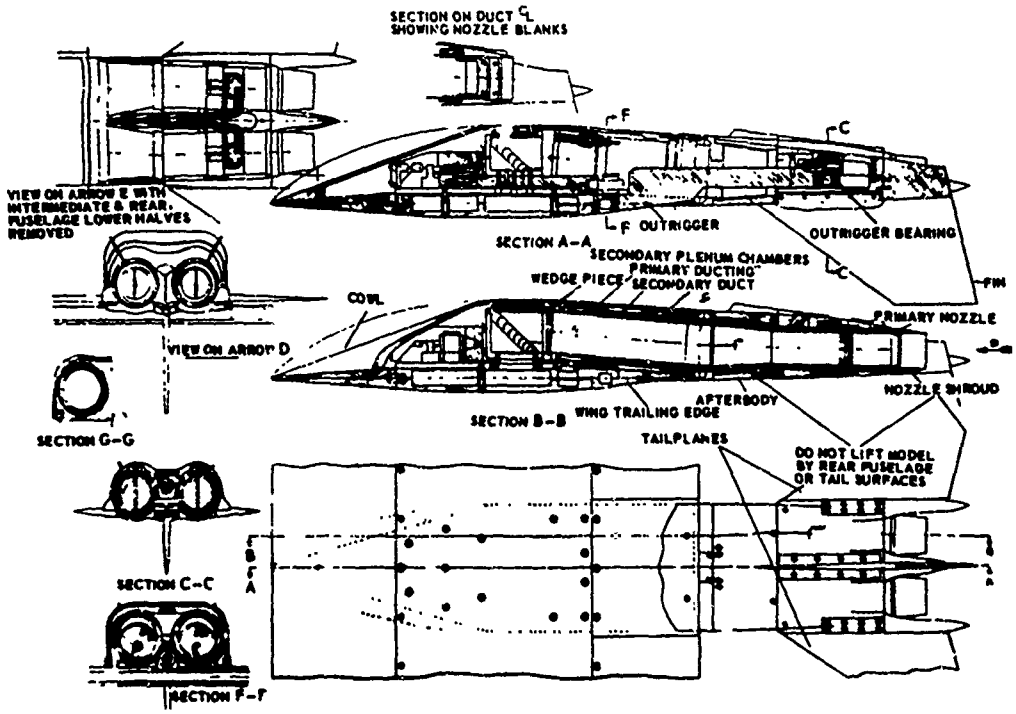

Fig. 25c Typical model assembled into rig of figure 25a.

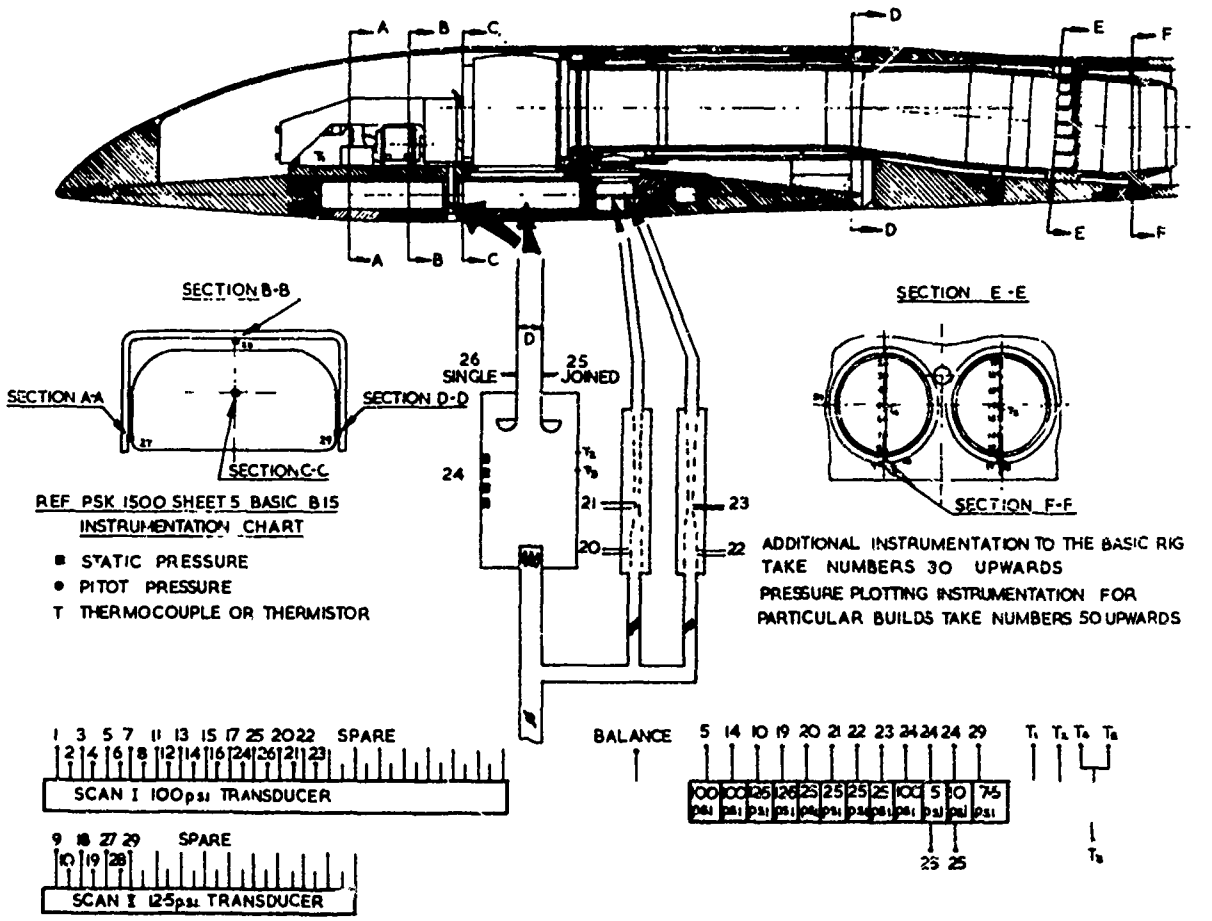

Fig. 25d Instrumentation layout (Fig. 25a)

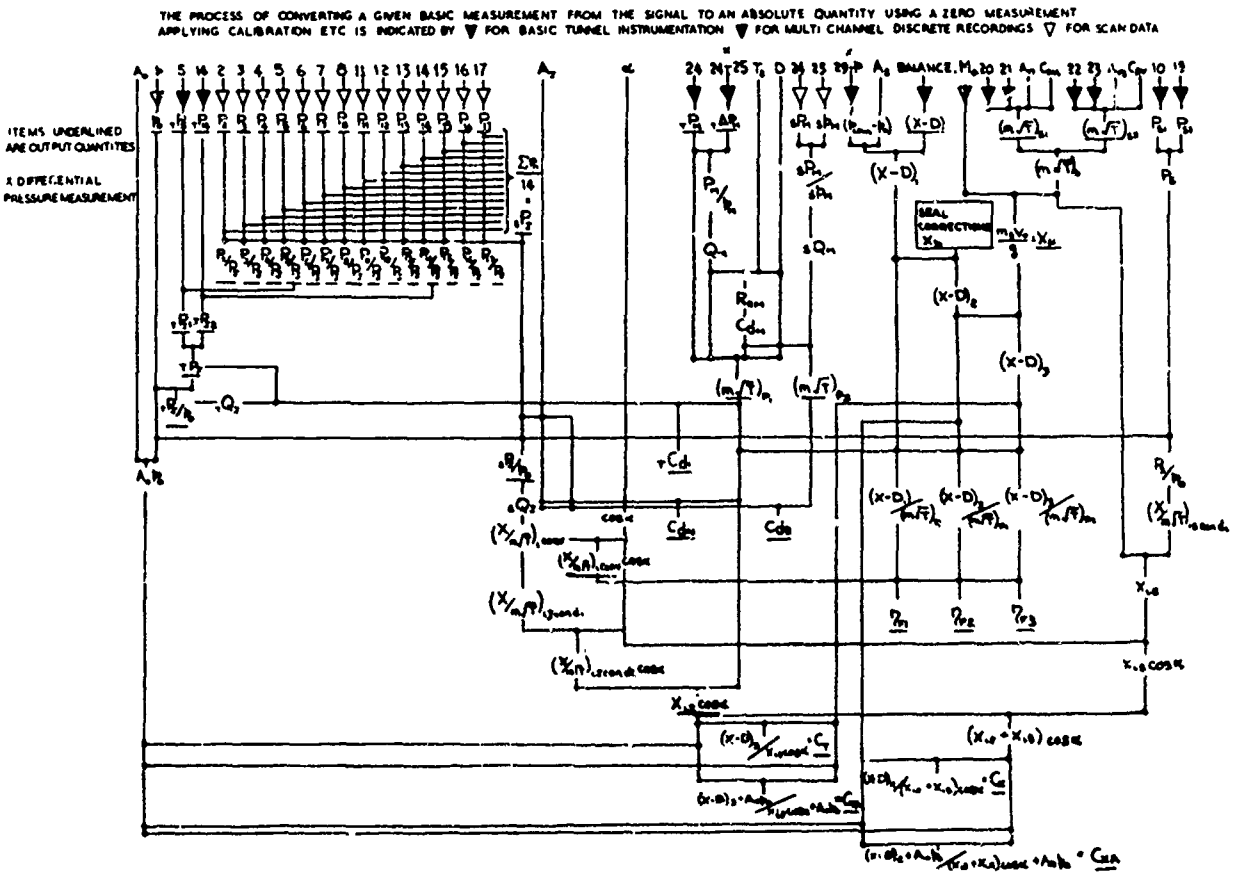

Fig. 25e Data reduction scheme (Fig. 25a).

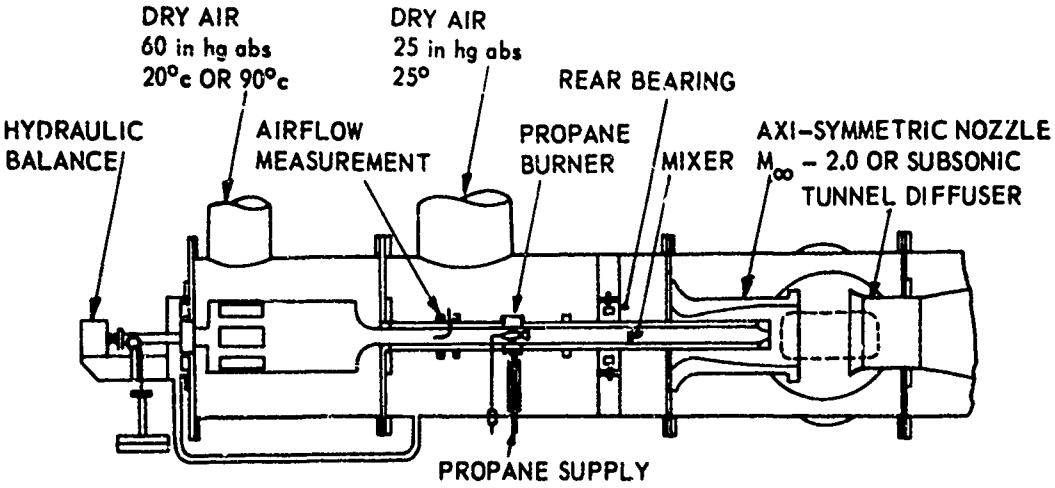

Fig. 26a Hot and cold jet interference tunnel, subsonic and transonic.

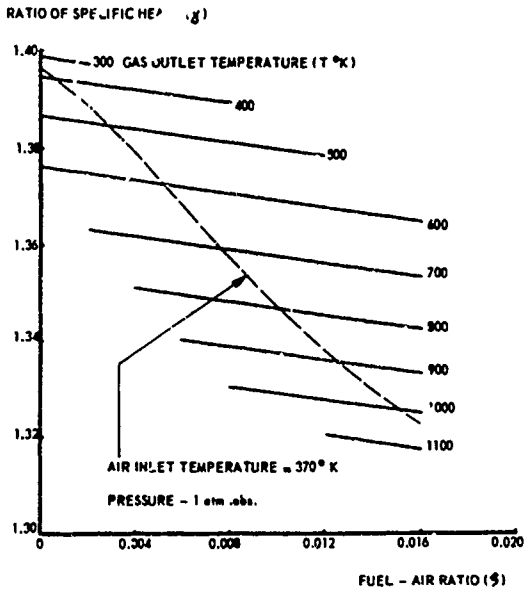

Fig. 26b Variation of ratio of specific heats with temperature and fuel-air ratio for the combustion products of propane air.

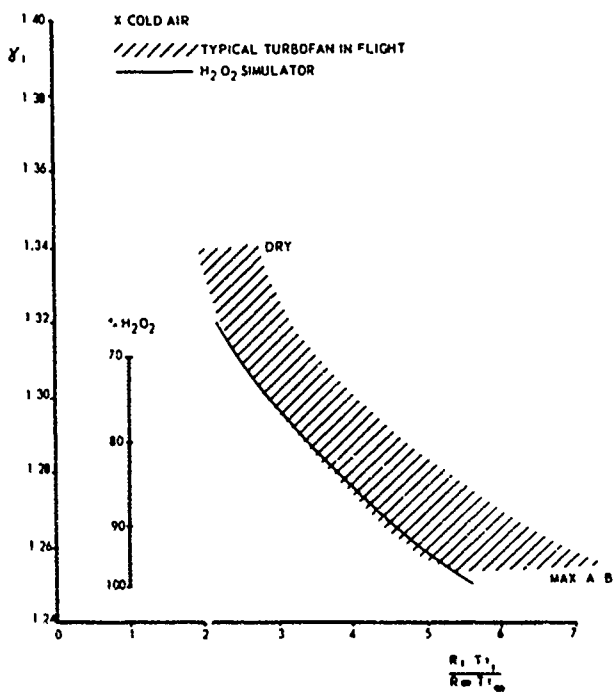

Fig. 27 Ratio of specific heat versus temperature for turbojets in flight and for decomposed H_2O_2 in wind tunnels.

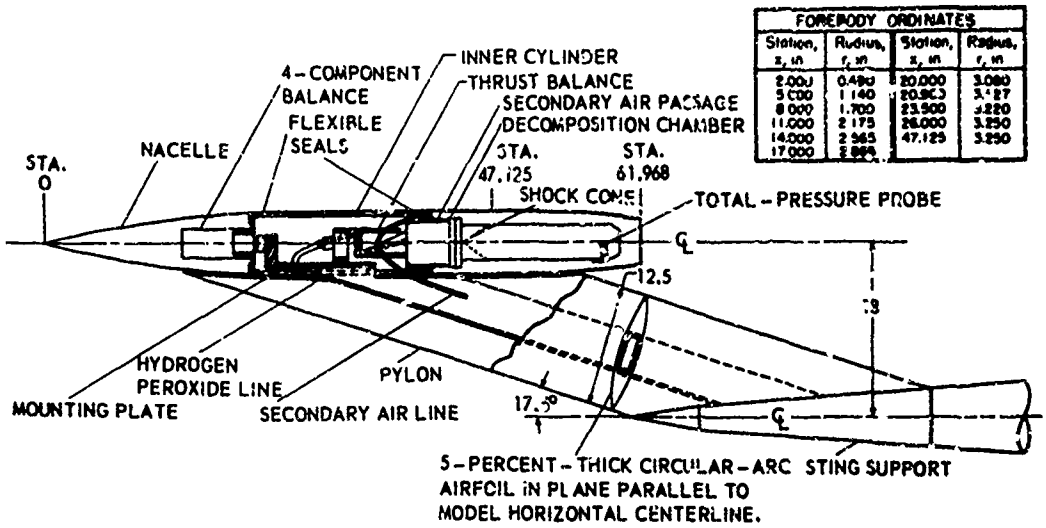

FOREBODY ORDINATES

Station, x, in	Radius, r, in	Station, x, in	Radius, r, in
2.000	0.490	20.000	3.080
5.000	1.140	20.903	3.127
8.000	1.700	23.500	3.220
11.000	2.175	26.000	3.250
14.000	2.565	47.125	3.250
17.000	2.895		

Fig. 28 Sketch of pylon-supported nacelle model using H_2O_2 and secondary flow (all dimensions in inches).

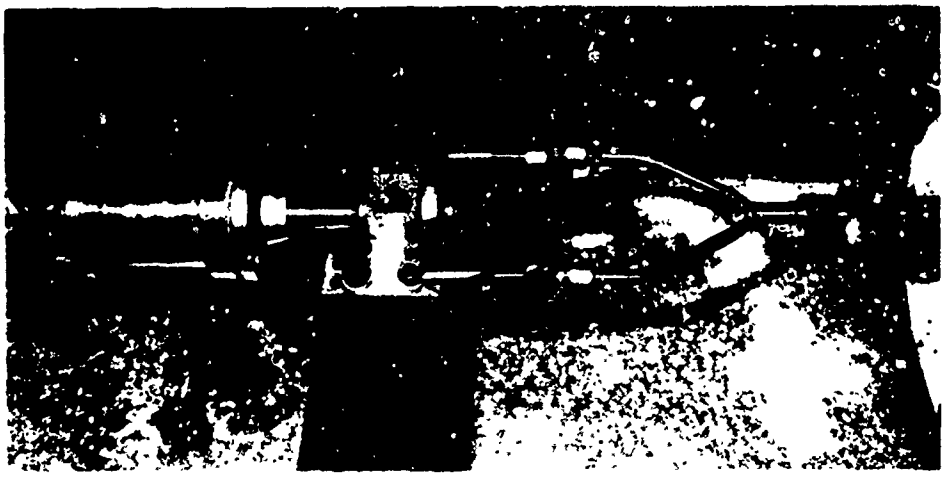

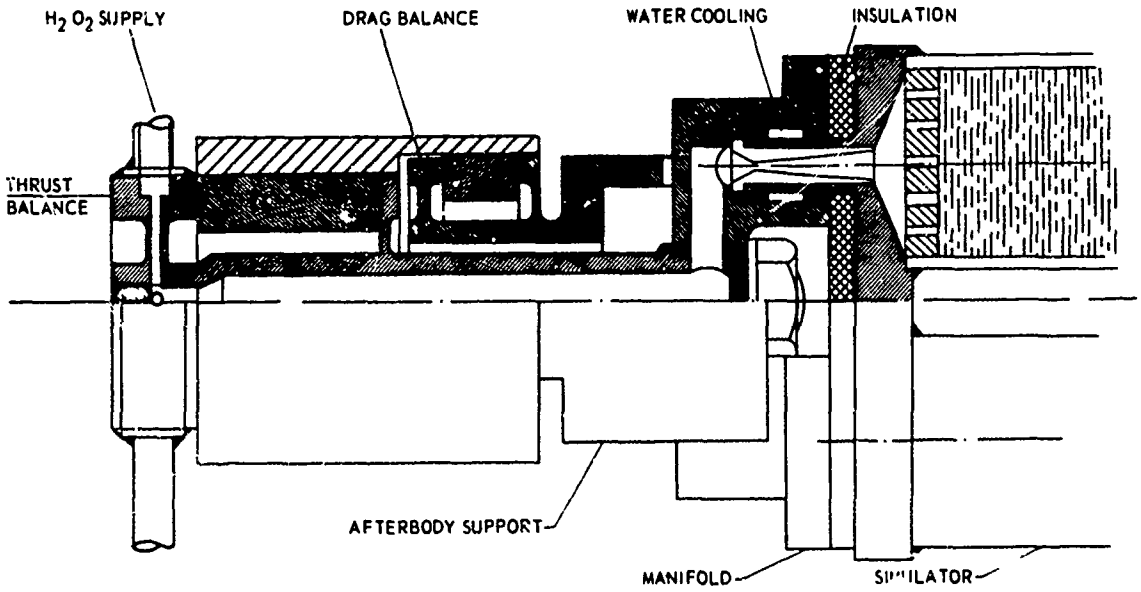

Fig. 29 Dual balance system for thrust and afterbody drag measurement using H_2O_2; thrust balance with operating H_2O_2 engine on test bench, 73 % H_2O_2.

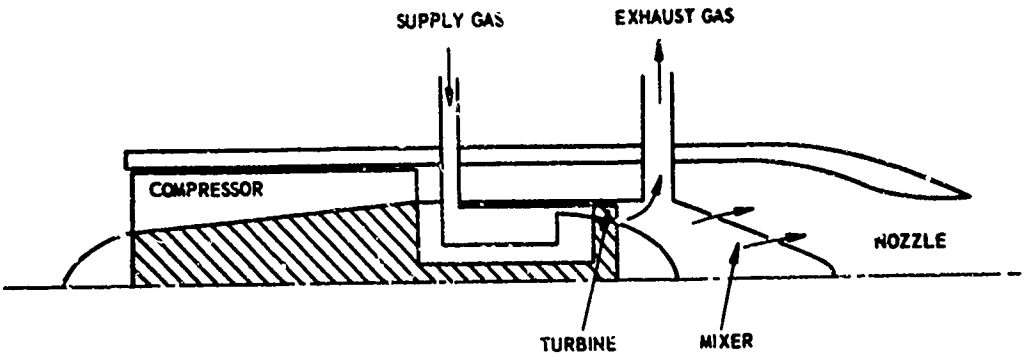

Fig. 30 Schematic miniature turbine driven turbojet simulator.

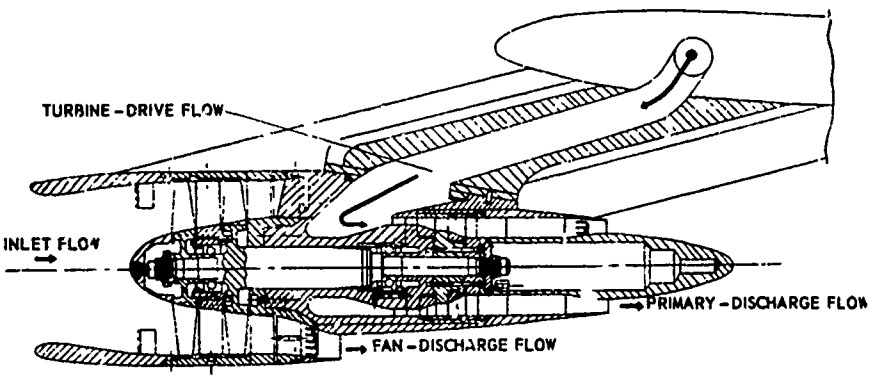

Fig. 31 Cross-sectional view of a miniature turbo-driven fan simulator.

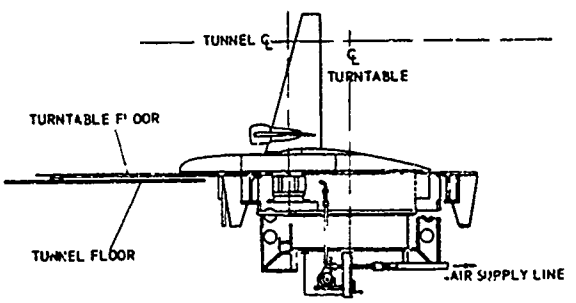

Fig. 32 Semi-span model tunnel installation with powered nacelle.

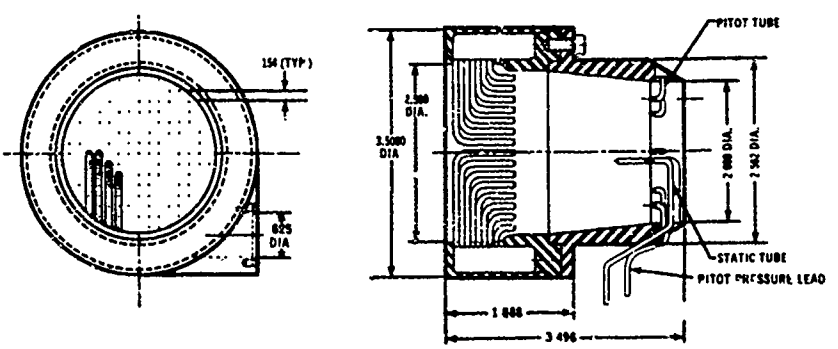

Fig. 33 Ejector unit for lift engine simulation in wind tunnels.

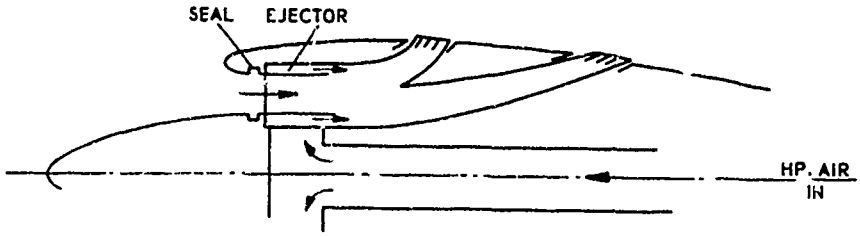

Fig. 34 Ejector system for inlet and exhaust flow.

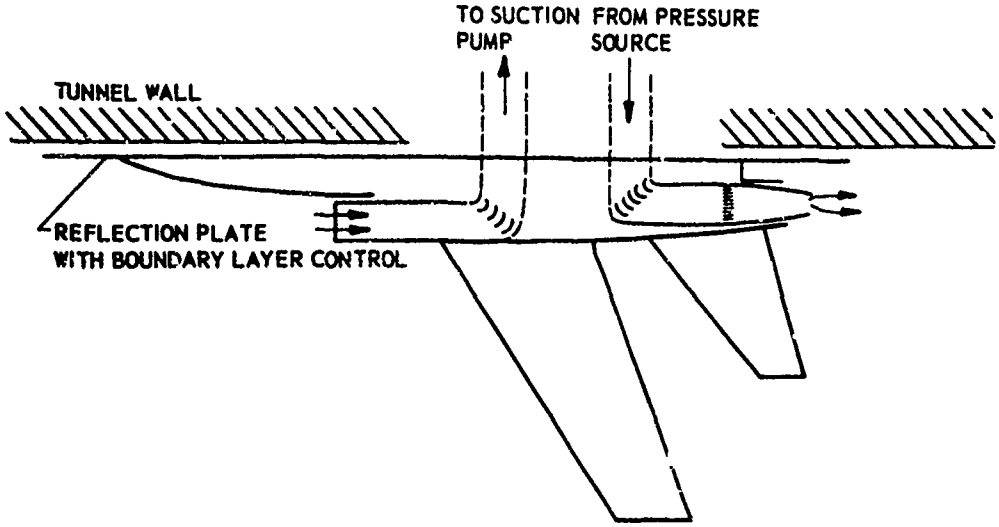

Fig. 35 Half model with direct inlet suction and nozzle blowing.

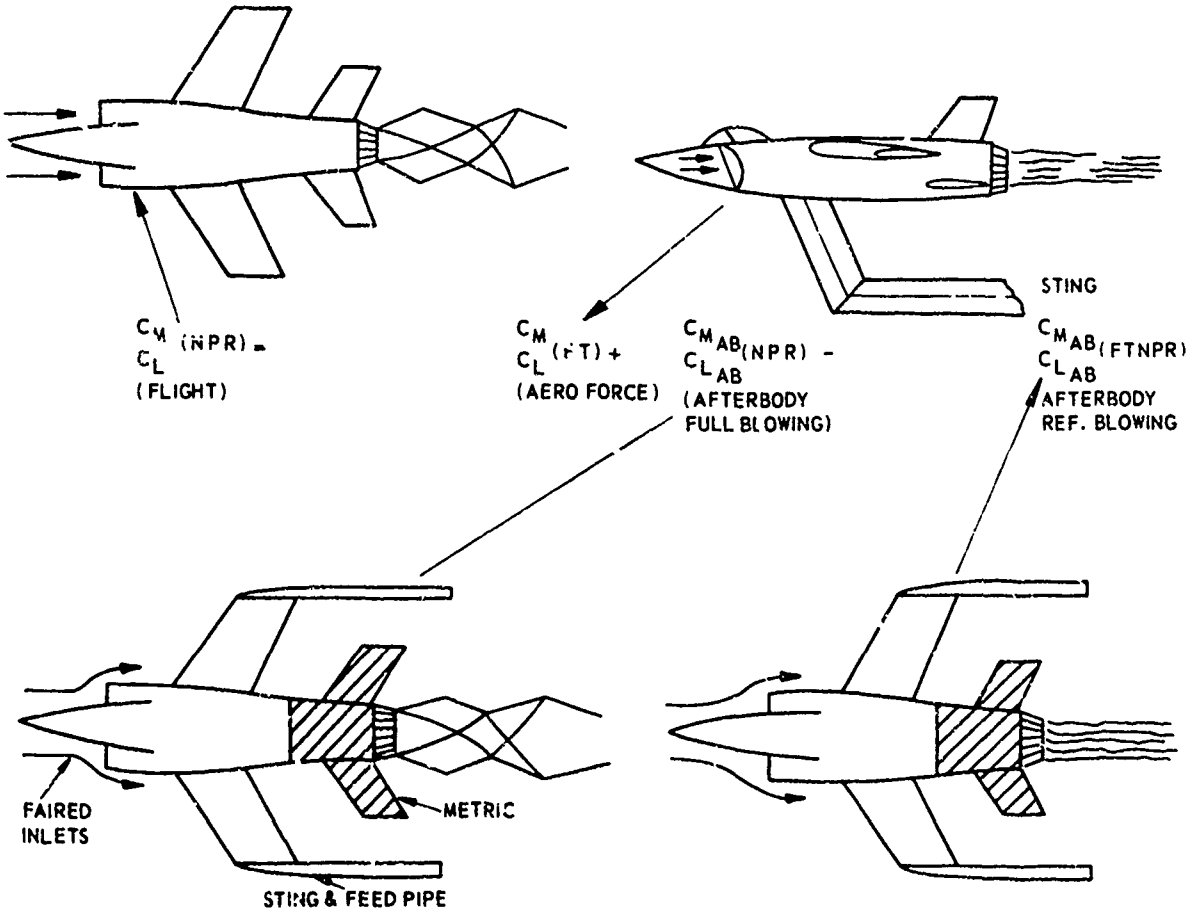

Fig. 36 Moment and lift increment determination due to jet effects.

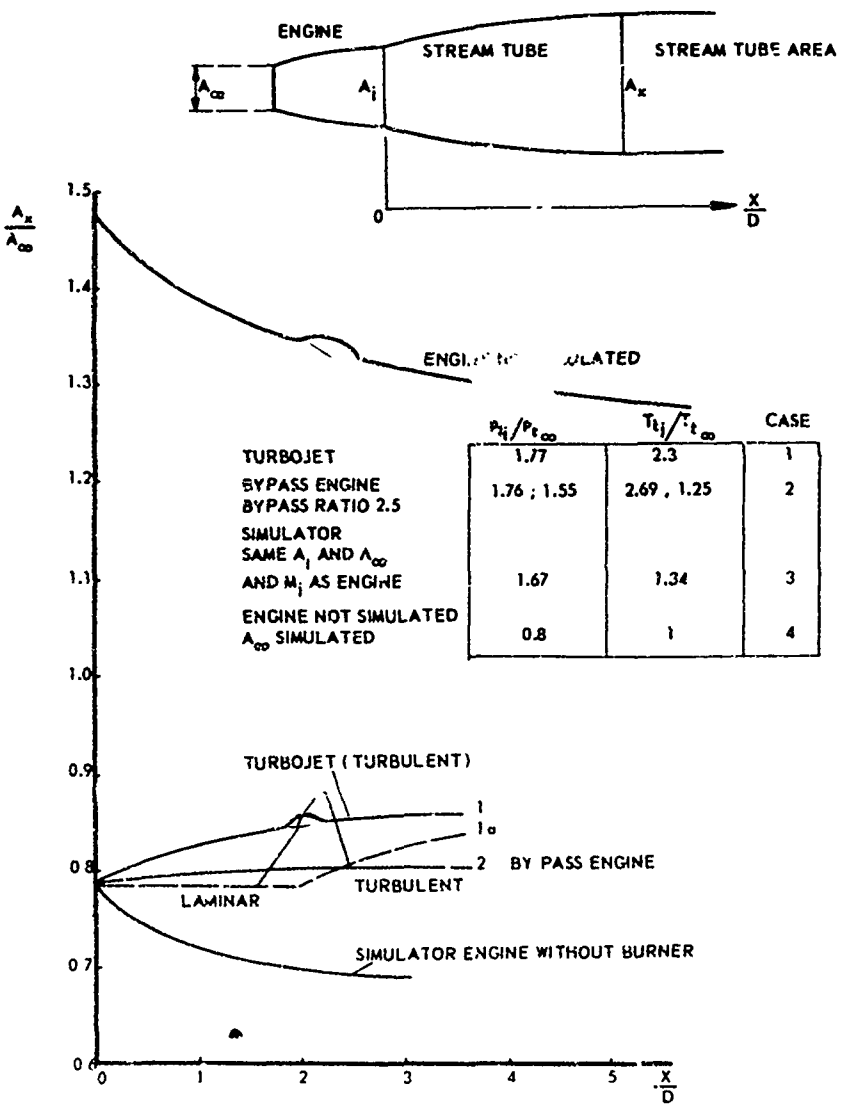

	P_{t_i}/P_{t_∞}	T_{t_i}/T_{t_∞}	CASE
TURBOJET	1.77	2.3	1
BYPASS ENGINE BYPASS RATIO 2.5	1.76 ; 1.55	2.69 , 1.25	2
SIMULATOR SAME A_i AND A_∞ AND M_i AS ENGINE	1.67	1.34	3
ENGINE NOT SIMULATED A_∞ SIMULATED	0.8	1	4

Fig. 38 Variation of jet engine effective stream tube due mixing.

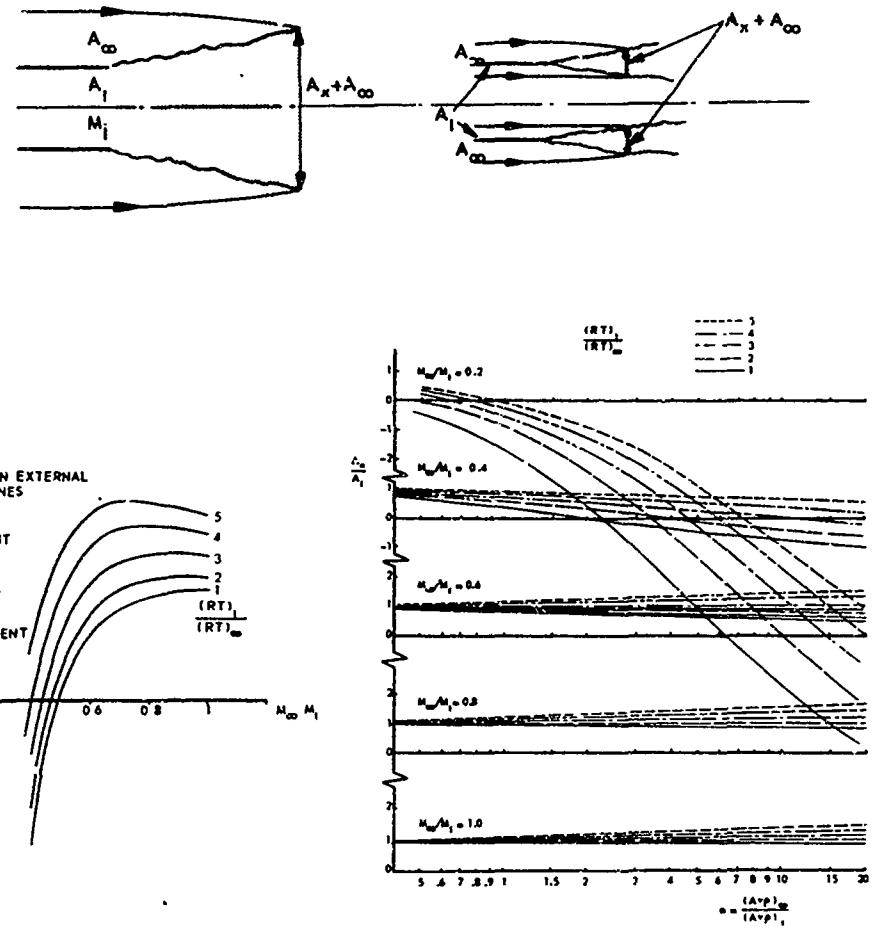

Fig. 37 Effect of mixing ratio n on the effective jet stream tube at various jet temperatures and Mach numbers (const. pressure).

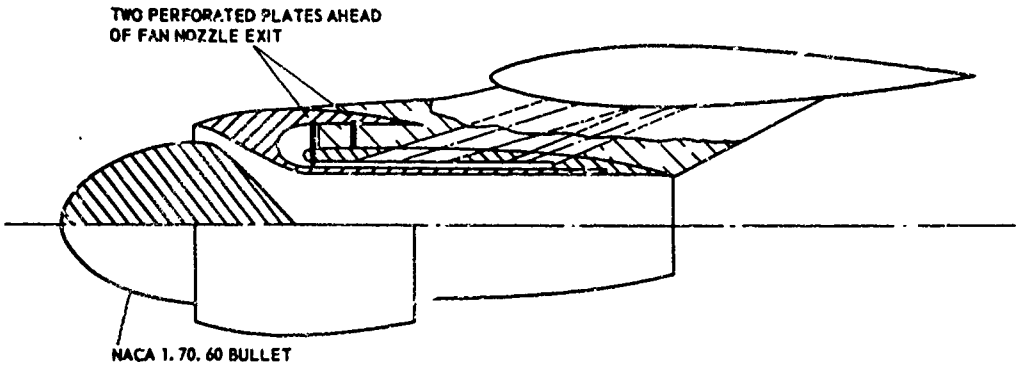

Fig. 39 Blown fan cowl model installation with partial inlet mass flow simulation.

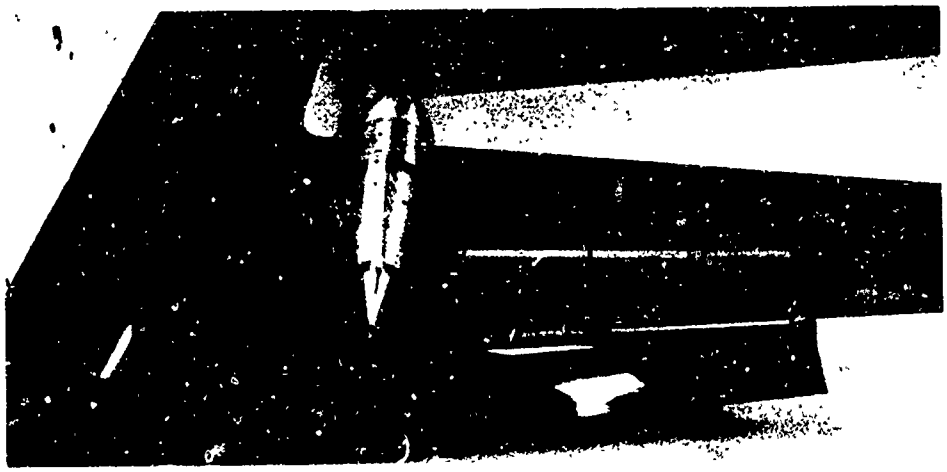

Fig. 40 Cold fan jet and hot turbine simulator with faired inlet for determination of jet effects on flaps and tailplanes.

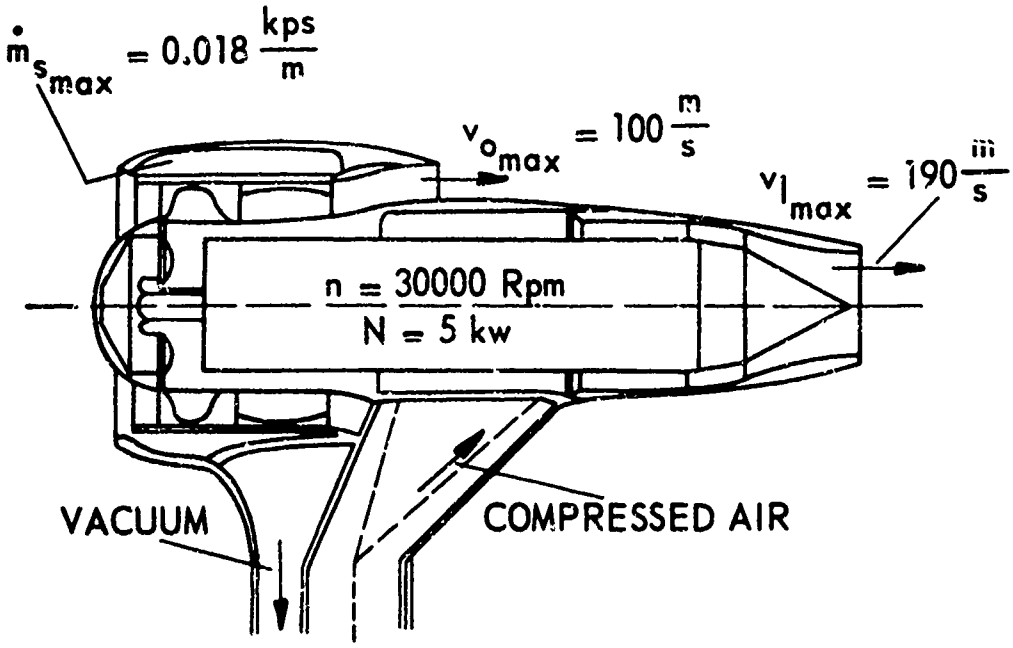

Fig. 41 Complete strut supported fan engine simulator for subsonic use.

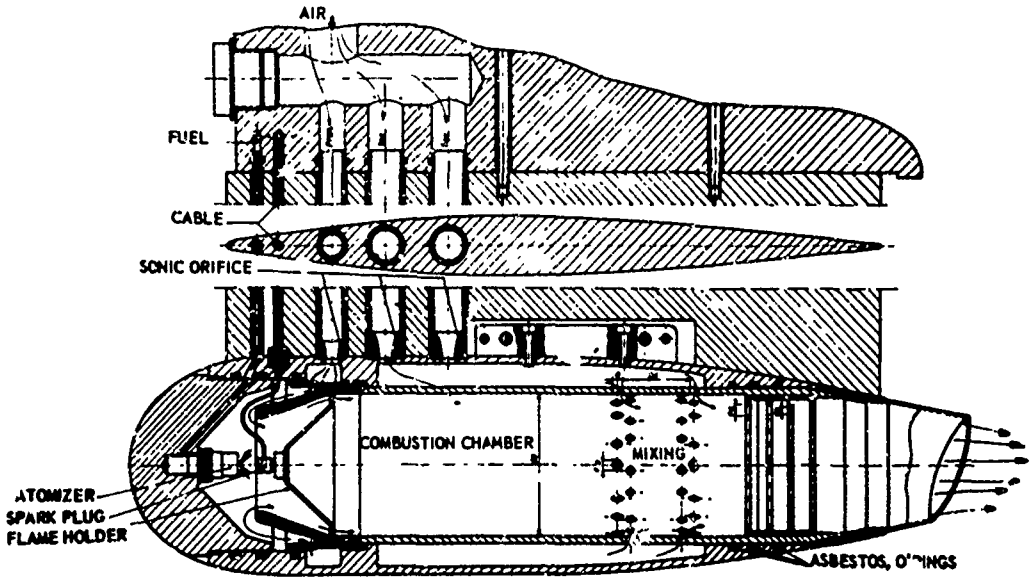

Fig. 42 Low bypass engine simulator with gasoline burner; inlet faired.

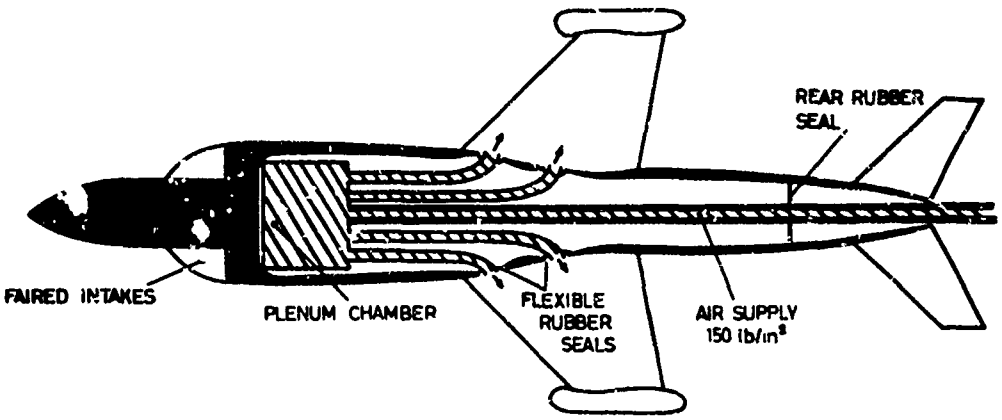

Fig. 43 Direct cold blow four jet exhaust system with faired inlets.

Fig. 44 Arrangement for ducting high pressure air to jet exit nozzles for tests with faired inlets.

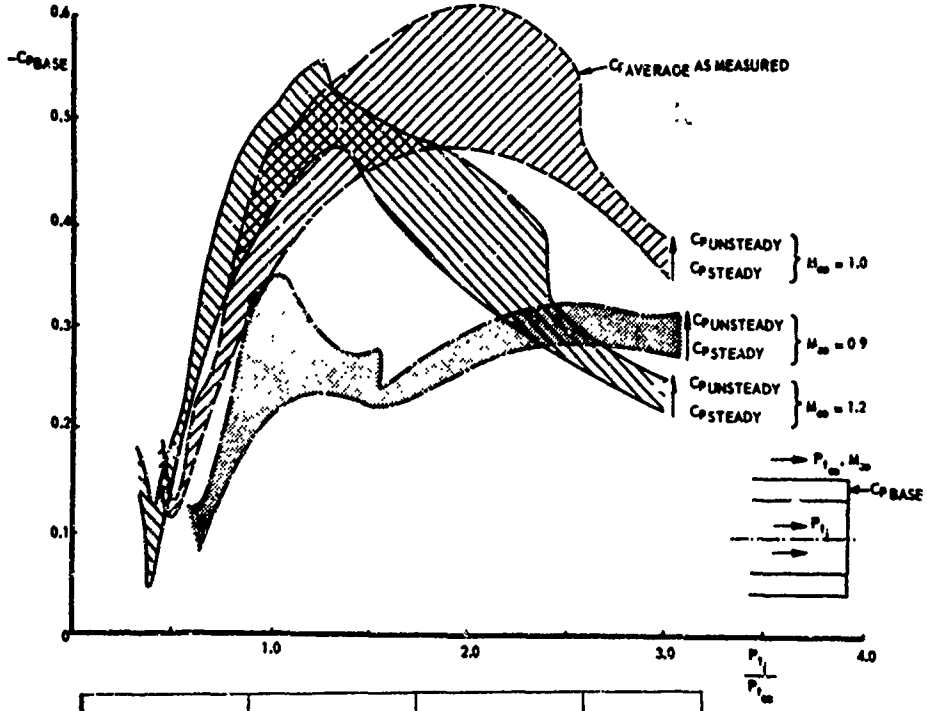

Fig. 45 Time average and unsteady pressures on the base of a bluff afterbody with jet simulation.

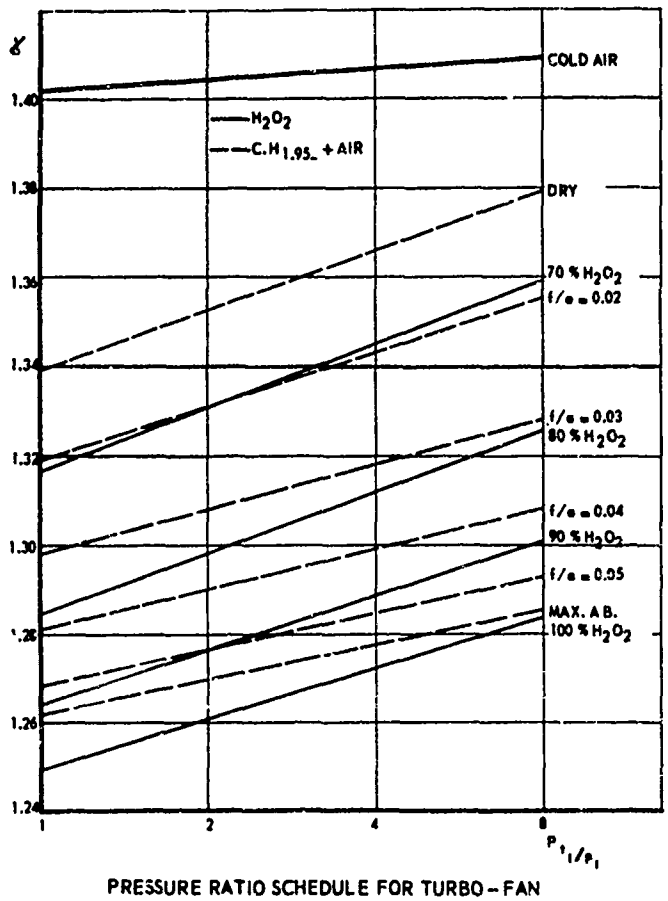

Fig. 46 Ratio of specific heats as a function of expansion ratio (f/a = fuel/air ratio).

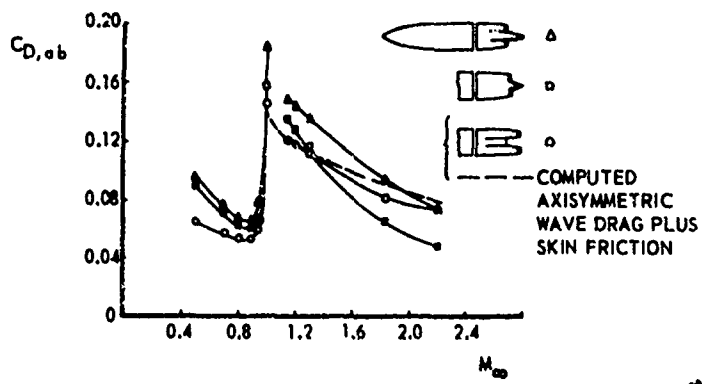

Fig. 47 Effect of jet-exit location on afterbody drag and compared with computed data.

DYNAMIC CHARACTERISTICS OF ENGINE INLETS

Dr. Demetrius Zonars
Chief Scientist
Air Force Flight Dynamics Laboratory
Air Force Systems Command
Wright-Patterson Air Force Base, Ohio 45433

SUMMARY

This paper discusses the phenomenon of inlet random pressure fluctuations and its effects on reducing the stall margin of turbojet engines. A review is accomplished of the TF-30/F-111 compatibility study over the past several years. The TF-30/F-111 portion of the paper assesses the practicality of utilizing steady state and instantaneous distortion factors to determine inlet-engine compatibility. In addition, recent advances in inlet research configurations with associated steady state and dynamic distortions are presented. Finally, a complete random data acquisition, editing, and processing method is developed for accomplishing data analysis as an inlet diagnostic tool.

I. INTRODUCTION

Historically, the engine inlet has played a secondary role in the design and development of aircraft. However, recent flight vehicle operational experience has shown the need for proper integration of the airframe and propulsion systems to achieve trouble free and effective flight performance. Specifically, engine compressor stalls have been associated with complex, distorted inlet flow fields. Development emphasis of the inlet system cannot be overlooked since this component is of primary importance in the thrust producing mechanism for transonic and supersonic flight. The details of inlet systems involve major geometrical variations which must function efficiently in a complex, changing flow environment dependent upon Mach number and aircraft orientation. These circumstances have emphasized the need for greater understanding of the airframe induced flow fields and how these fields interact with inlet systems.

In the past, the inlet and the engine have been developed on a component basis. Emphasis was placed on the inlet system to generate the proper pressure recovery with an acceptable steady-state distortion. The experience factor of current day aircraft clearly indicates that the flight vehicle performance, including stability and control must be treated on an integrated basis with due consideration for the large variations of inlet airflows. Experience has also taught us that a substantial similarity exists between the characteristics of the captured flow and the resultant flow to the compressor face. Since the inlet operates in an external flow environment which is strongly dependent upon the shape of the airframe, it behooves engineers to examine such influences as sensitivities of inlets to local flow angularities and nonuniformities of the oncoming flow.

II. F-111 FLIGHT EXPERIENCES

Advanced tactical aircraft are required to perform a number of missions which demand a high degree of airframe propulsion integration including low flow distortion over a much larger range of operating conditions (Mach number, altitude, angle of attack, engine mass flow) than previous supersonic tactical aircraft systems. Requirements for maneuvering flight in a low drag configuration necessarily implies high angle of attack flight attitudes from subsonic to supersonic speeds in excess of Mach number 2.0.

It has been, therefore, quite natural to utilize an inlet design for the F-111A which takes advantage of the flight vehicle fuselage and wing to reduce the effects of angle of attack and angle of yaw during maneuvering flight. The F-111A inlet shown in Figure 1 is an external compression 88 degree segment of an axisymmetric inlet which is integrated with the airframe fuselage-wing root intersection. Locating the inlet in the wing-fuselage flow field also provides precompression for the inlet flow in supersonic flight which means that the inlet capture area is reduced from that required at free stream conditions. Further, a significant vehicle weight savings is realized by integrating the supporting structure of the inlet and relatively short duct with the vehicle structure.

The spike system of the inlet translates fore and aft and the second cone angle varies with flight Mach number and angle of attack to vary the inlet throat area. Each of the inlets is matched to a Pratt and Whitney TF-30-P-3 afterburning turbofan engine. The modulated afterburner improves the tactical ability of the F-111A by providing a variable thrust output in afterburner mode upon demand by the throttle. Therefore, in addition to being closely integrated with the airframe, the F-111A inlet system is closely integrated with the engine to accommodate variations in airflow demand during engine transient operation.

During prototype flight tests of the F-111A, it became apparent that the desired flight envelope was restricted. Maneuverability of the aircraft at high subsonic speeds and supersonic speeds was being limited by a rapid buildup of steady and dynamic inlet flow distortion resulting in engine compressor stall. This incompatibility of the inlet and engine in the F-111A aircraft was the impetus for a comprehensive evaluation of flight test and wind tunnel data to identify the causes of the compressor stalls and define modifications to the inlet system to reduce the incidence of compressor stalls in both steady state and maneuvering flight.

In order to identify problem areas and suggest modifications to improve the inlet system and its compatibility with the engine, the inlet of a prototype airplane was equipped with diagnostic total and static pressure instrumentation in the inlet and engine. In addition, the engine compressor face was equipped with 40 total pressure probes in centroids of equal areas to map the total pressure pattern entering the fan and low pressure compressor of the engine. There were eight rakes with five probes per rake.

FIGURE 1. AFT VIEW OF TYPICAL F-111A INLET

Initially, a theoretical study was undertaken to determine the anticipated steady state distortion at the compressor face during supersonic flight. The purpose of this study was to compare such information with similar 1/6 scale wind tunnel and actual flight test data and thus provide insight as to trouble areas resulting from specific theoretical-experimental differences. The conditions of Mach number 2.2 and angle of attack of 5.5 degrees with an initial inlet cone angle of 12.5 degrees and second cone angle of 24 degrees was chosen. The theoretical approach first consisted of estimating the Mach number aft of the conical wave system resulting from the fuselage-wing glove intersection. This yielded a Mach number of 2.08 wherein the flow field was assumed to be uniform to the inlet. An exact Taylor-Maccoll solution was developed for the initial cone angle with subsequent use of the method of characteristics to generate the flow field about the second cone. A normal shock was then assumed at the entrance to the cowl lip. The resulting isobars for this 88 degree inlet segment were then uniformly expanded into a circumferential profile at the compressor face. A plane of symmetry was assumed half way between the 88 degree sector of the inlet system. The total pressures resulting from such calculations were plotted and compared with those of the 1/6 scale wind tunnel and flight case. Figure 2 shows such a comparison. The wind tunnel and flight data showed a remarkably similar profile, however the comparison with theory is understandably different due to the absence of viscous effects. More importantly, the main difference stems from a clearly identifiably low energy area on the inboard, lower portion of the compressor face which is quite different than that predicted by the inviscid theory. It was therefore clear that an investigation should be undertaken to survey the oncom' and duct flow relating to this portion of the entire airflow. Values of steady state distortion are also presented as derived from the expression K_{DA} as follows:

$$K_{DA} = \frac{\sum_{i=1}^{5} \left[\frac{P_{t_{av}} - P_{t_{min}}}{P_{t_{av}}} \right] \bar{\theta}_i C_i}{\sum_{i=1}^{5} C_i} \times 100 \qquad (1)$$

where

C = ratio of compressor inlet radius to ring radius

i = number of ring

$\bar{\theta}$ = largest continuous arc of the ring over which the total pressure is below the ring average pressure

$P_{t_{av}}$ = ring average pressure

$P_{t_{min}}$ = ring minimum total pressure

Here again, the low theoretical K_{DA} value is due to the absence of the low, inboard impact pressures and the inviscid assumptions.

In the analysis of the flight test data taken with this instrumentation, several approaches were employed. First, compressor face total pressure maps were compared, which showed the changes in flow distortion as a compressor stall condition was approached. Although this analysis indicated a low total pressure region on the inboard side, the results were inconclusive and so time variations of data from other sets of instrumentation further upstream in the duct were examined for many stall sequences in order to identify problem areas in the inlet flow field as they developed. From the time sequence plots, selected data for a particular time cut were used to define duct static pressure distributions or boundary layer total pressure profiles. The static pressure distributions were used to locate shock wave positions, indicate boundary layer bleed effectiveness, estimate stream velocities, and indicate regions of separated flow. Total pressure profiles were used to define regions of low energy flow ahead of and in the inlet, and to indicate regions of separated flow. In a parallel study coordinated with this quasi-steady data evaluation, the dynamic pressure fluctuations indicated by traces from the flight telemetry and magnetic tape output of the individual probes were being carefully analyzed. Under certain flight conditions, the traces indicated extreme "turbulence" at the compressor face. This was known to cause a loss in engine stability in other engines as reported by Gabriel, Wallner and Lubick[1] and was felt to be a contributory factor in the stall problems of the F-111A. Although a complete correlation between quasi-steady flow distortion and dynamic pressure fluctuations was not undertaken, it was realized that there was a cause and effect relationship between these two types of distortion and the approach was to address the cause of unsteady and non-uniform flow in the inlet and attempt to eliminate it. A corresponding reduction of the severity of the dynamic-pressure fluctuations (dynamic distortion) would be expected, but it was important to know the relationships between steady and dynamic flow to the limits of the instrumentation signal available.

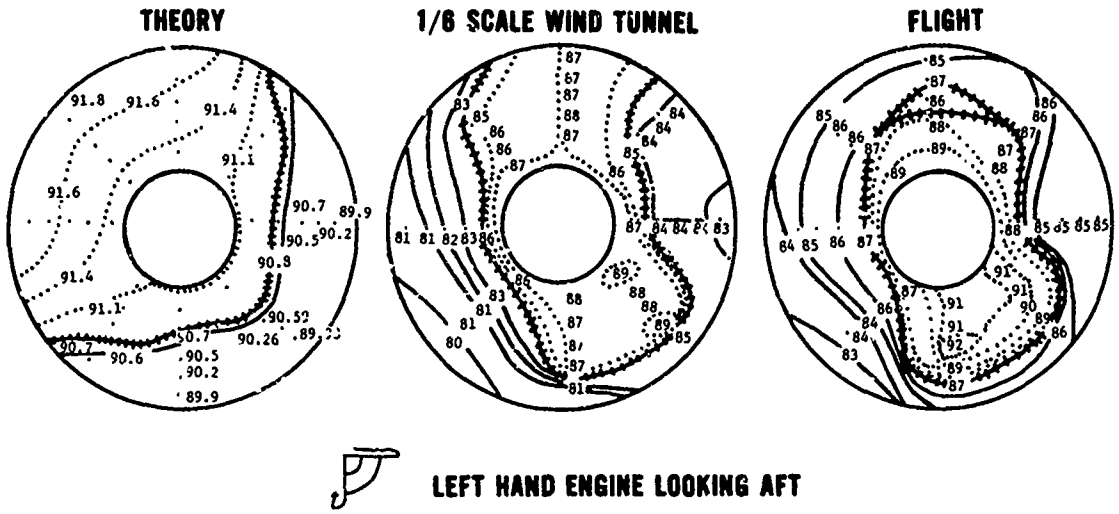

PARAMETER	THEORY	WIND TUNNEL	FLIGHT
AIR FLOW, LBS / SEC.	168	168	162
AVE. RECOVERY PRESSURE RATIO	90.8	85	87
DISTORTION FACTOR, K_{DA}	100	383	4[illegible]

FIGURE 2. COMPARISON OF F-111A COMPRESSOR FACE TOTAL PRESSURES FOR MACH NUMBER 2.2 AND AN ANGLE OF ATTACK OF 5.5 DEGREES

III. F-111 INLET PRESSURE FLUCTUATION EFFECTS

The effects of transient disturbances, or more specifically, the fluctuating nature of the measured total pressures at the compressor face were considered to have a strong influence in the stall properties of the engine. This influence and corresponding effect were considered to be above the acceptable steady-state distortion which could be accommodated by the engine. The flight regime in which this phenomenon commenced was found to be at low supersonic speeds, with increasing disturbance intensity as a function of increasing Mach number. These disturbances exhibited a wide range of amplitude-frequency content showing both slow and rapid transients. The slow transients could possibly be compensated for by inlet and engine controls. For such low frequency disturbances, engine performance is basically similar to steady-state operation since normally, the outlet pressures will follow the inlet flow variations in magnitude and phase such that the over-all compressor pressure ratio will remain the same. However, the majority of actual transient disturbances and total pressure fluctuations were found to be significantly faster than any of the aforementioned control capabilities. Under these circumstances, specific outlet pressures lag the inlet pressure variations in both amplitude and phase. Consequently, the pressure ratio across the compressor can differ considerably from the steady-state value on the operating line, and conditions can be reached wherein compressor stall margin reduction and even stall will be experienced. Data from reference 1 has shown this to be the case for a simply induced sinusoidal pressure variation input to a compressor.

It is important to note here that the original compressor face total pressure instrumentation on the prototype test aircraft was never intended for the accurate measurement and analysis of transient

disturbances. Hence, an effort to correlate transient disturbances with the lower frequency average values of the measured total pressures to the compressor face required special data reduction methods. Total pressure readout from flight magnetic tapes at conditions appropriate to engine stall were first identified and then processed through narrow band pass filters by the Field Measurements Group of the Air Force Flight Dynamics Laboratory. Figure 3 shows two typical frequency spectrums obtained from the filtering process of the flight test data wherein 85.55 inch long pressure carrying lines were provided between the pressure probes and the transducers. At first glance, the higher amplitude data would appear to occur at the lower frequencies; however, the utilization of 85.55 inch lines (tubulation) for steady-state pressure measurements suggested the possibilities of transient signal attenuation to the transducer due to classical acoustic type dissipation. In order to correct for this tubulation effect, an experimental program was undertaken by the Aero-Acoustics Branch of the Air Force Flight Dynamics Laboratory to apply corrections to the measured pressure variations for conditions just prior to engine stall. Theoretical predictions were provided by Air Force Aero Propulsion Laboratory personnel. Figure 4 shows the nature of the amplitude corrections as a function of frequency when examined for an average pressure of 14.7 psi and varying temperature. The experimental data taken at room temperature showed excellent agreement with theory.

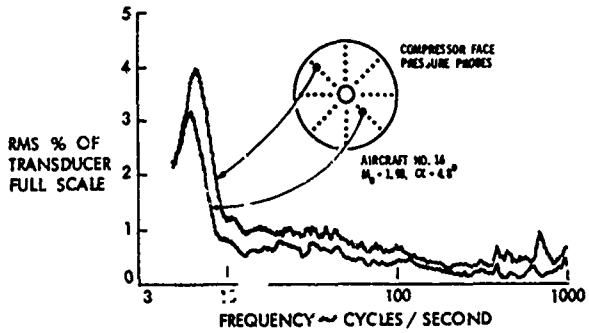

FIGURE 3. TYPICAL F-111A COMPRESSOR FACE PRESSURE AMPLITUDE-FREQUENCY SPECTRUM

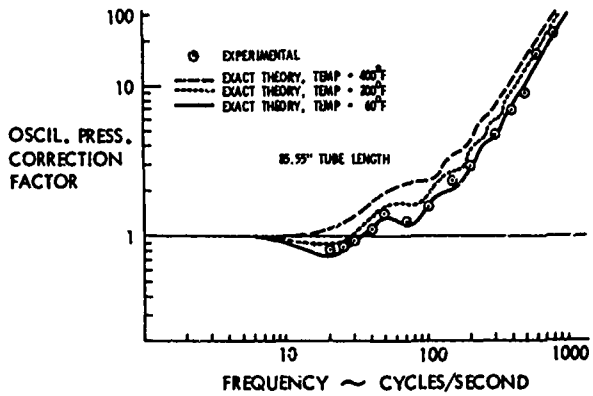

FIGURE 4. F-111A OSCILLATORY PRESSURE TUBULATION CHARACTERISTICS

Many supersonic flight conditions associated with engine stall were examined with specific emphasis on the high frequency aspects of the transient disturbances. Multiplexing of the instrumentation, as is normally accomplished on test aircraft for measuring steady-state parameters, was found to have a strong influence on the high frequency transient data. In an effort to isolate these effects, several flights were performed involving a minimum of multiplexing with a 15 inch line replacing one of the 85.55 inch lines for reduced tubulation effects. A comparison of pressure transients in a 85.55 inch line with multiplexing versus a 15 inch length tubing with minimal multiplexing is shown in Figure 5. Above approximately 250 cps it can be seen that the high frequency transients recorded with the 85.55 inch line were due to multiplexing, and not present except for some disturbances in the 525-660 cps range. It was, therefore, decided to utilize 0 - 250 cps frequency range for data analysis when transient data was subject to multiplexing, and 0 - 1000 cps for the data with minimal multiplexing.

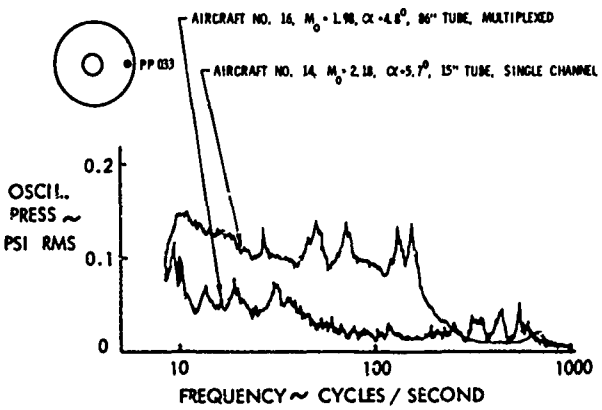

FIGURE 5. COMPARISON OF F-111A TUBULATION

A specific comparison of steady-state compressor face recovery pressures with corresponding transient disturbance values obtained from flight is shown in Figure 6. The oscillatory or transient pressure data is based on 0 to 250 cps as discussed above. Figure 6 shows, generally, that the high, steady-state recovery pressures corresponded to areas of reduced transient or oscillatory pressures, whereas low recovery pressures related to regions of higher transient values. The region in the lower left-hand corner of the oscillatory pressure map was of particular interest. This area of highest transient disturbance values corresponded directly to the lower left-hand portion of the inlet which was most susceptible to boundary layer ingestion. In addition, the steady state analysis from flight demonstrated the upward spreading of low total pressures from the bottom of the sharp cowl lip with increasing angle of attack. The data of Figure 6 would indicate that, in addition to being of a very low recovery nature, this portion of the flow possessed a high degree of flow unsteadiness sufficient to cause engine stall.

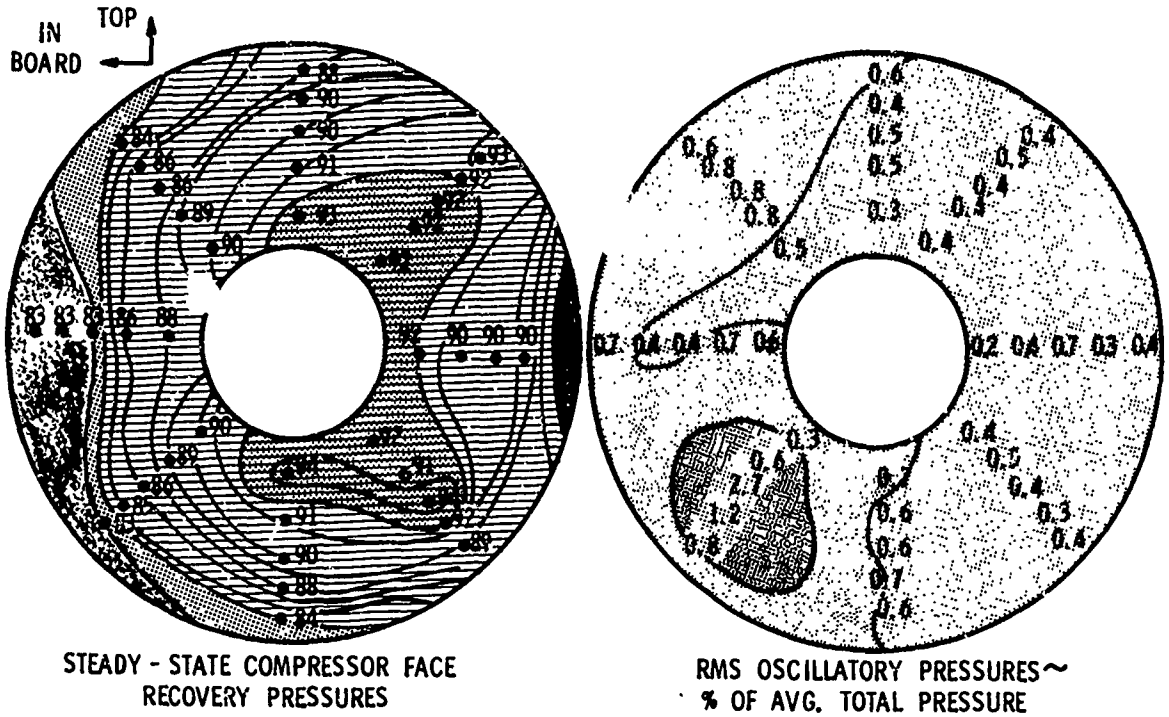

AIRCRAFT 16; $M_0 = 1.98$, $\alpha = 4.8^0$, 0.2 SECONDS BEFORE ENGINE STALL

FIGURE 6. F-111A COMPRESSOR FACE STEADY-STATE AND OSCILLATORY PRESSURES

The transient disturbance analysis for all 40 compressor face pressure measurements for a particular stall condition would have required a prohibited expenditure of manhours and it was, therefore, decided to use an available single pitot tube of 15 inch tubulation to examine the fluctuating nature of the duct flow. Figure 7 shows the effect of angle of attack on the dynamic characteristics of this probe at a constant $M_0 = 0.77$. Although many discrete frequencies were identified from the spectrum analyzer output, specific frequencies of 130, 230, and 525 cps appeared to persist with relatively high amplitude for this test condition, which was at a military power engine setting. The amplitudes of these particular frequencies appeared to be fairly constant up to moderate angle of attack with a tendency to converge and further increase in amplitude at higher angles of attack until engine compressor stall was experienced. Also shown on Figure 7 are the effects of first zone afterburner operation for cruise angle of attack. The amplitude associated with 130 cps was found to change a small amount, however, there was a substantial amplitude increase in the 230 and 525 cps frequencies.

The condition of aircraft acceleration for cruise angle of attack at maximum afterburner power was examined with results as presented in Figure 8. Here again, the influence of afterburner operation is shown in the amplitudes of the 240 and 525 cps frequencies for transonic flight conditions. However, amplitudes at these frequencies decreased with increasing Mach number and corresponding decreases in corrected air flow up to approximately Mach number 2. Beyond Mach number 2, there was a dramatic increase in all three amplitudes up to Mach number 2.2 where engine stall was experienced.

From the quasi-steady and transient disturbance data studied during 1967, it was clear that the engine compressor stall characteristics were strongly influenced by inlet pressure pulsations at high frequencies and this effect must be considered in conjunction with the "steady state" distortion.

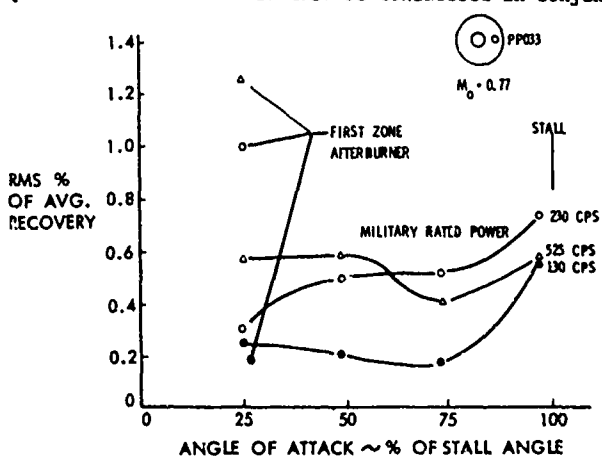

FIGURE 7. F-111A COMPRESSOR FACE PRESSURE FLUCTUATIONS VS. ANGLE OF ATTACK

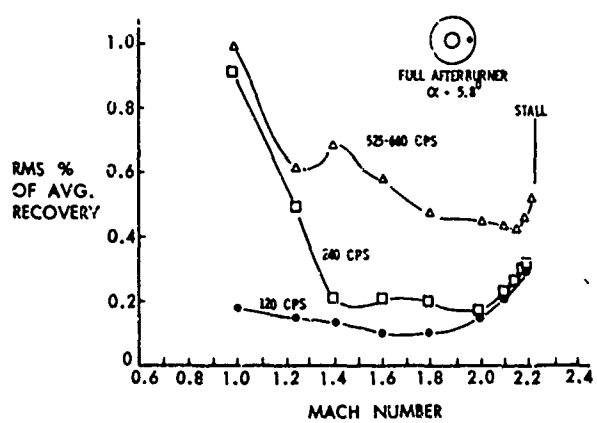

FIGURE 8. F-111A COMPRESSOR FACE PRESSURE FLUCTUATIONS VS. MACH NUMBER

IV. DETAILED STUDIES OF F-111A INLET AND ENGINE AIR FLOW FLUCTUATION EFFECTS

Subsequent to the initial study of the F-111A inlet-engine incompatibility effort discussed in Section III, a limited number of investigations [2-6] have been carried out in order to shed light on this important problem area. A typical example of one of the more significant and recent programs was reported by Plourde and Brimelow[7]. In this effort a fan and low pressure compressor of the Pratt and Whitney Aircraft TF-30 turbofan engine was selected as the test article to study the effects of "turbulence" on engine stall margin. Figure 9 shows a schematic of the TF-30 3-stage fan and 6-stage low pressure compressor system. The forward section of the compressor was connected to a "turbulence" generator duct utilizing a convergent-divergent device. Figure 10 shows a cutaway of this "turbulence" generator which included a movable plug center-body followed by a constant area duct. The purpose of this plug was to develop a sonic throat followed by supersonic flow and a normal shock system. The interaction of the shockwave with the duct boundary layer generated the fluctuating or "turbulent flow" conditions. The "turbulence" generator included a section just ahead of the compressor wherein a variety of stream obstructions such as 1/2 inch rods or 3 inch pipes could be placed in front of the compressor face to further increase or change the "turbulence" spectrum. Figure 11 shows the 3 inch rod system.

High frequency response pressure transducers were used to measure both static and total pressures at the compressor face. A typical inlet rake and total pressure probe utilizing Kistler transducers and low frequency response sensing tubes is shown in Figure 12. These total pressure rakes were positioned around the compressor inlet at 0°, 45°, 135°, 225°, 292.5°, and 315° when facing upstream.

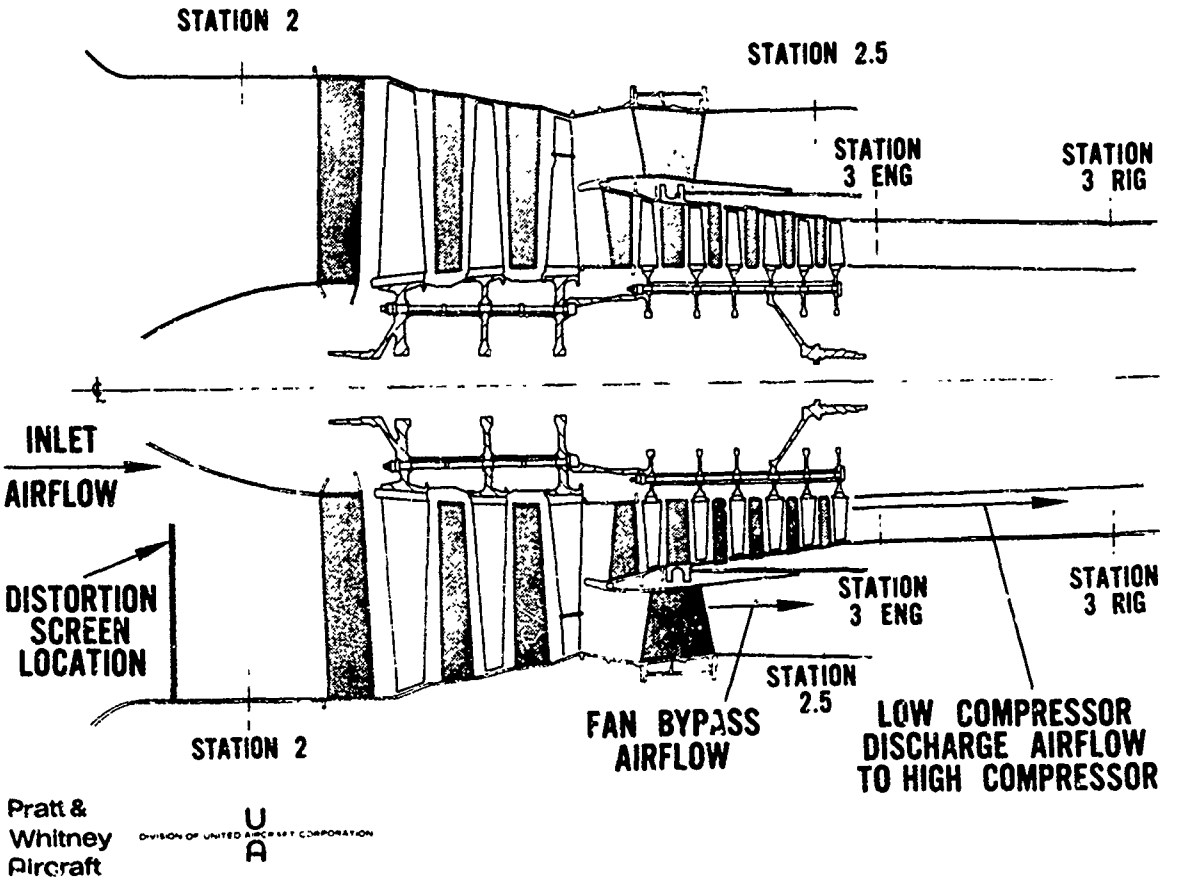

FIGURE 9. TF-30 FAN AND LOW PRESSURE COMPRESSOR SYSTEM

The power spectral densities resulting from the turbulence generators along with the spectra produced by the 1/2 inch and 3 inch rods is shown in Figure 13. The installation of the 1/2 inch grill system generated a fairly flat spectrum over the entire compressor face. The spectrum established from the 3 inch rods contained discrete frequencies as a result of shed vortices which were not yet dissipated to small scale "turbulence."

The effects of unsteady flow on compressor performance is now assessed. Gabriel, Wallner, and Lubick[1] first showed that a sinusoidal varying plane flow displayed detrimental effects on the compressor stall characteristics. In addition, their analog simulation of a turbo-jet axial flow compressor utilizing volumetric dynamics and steady-state total pressure air flow relationships was sufficient to establish the unsteady flow characteristics through an engine. A comparison of the analytical procedure with experiment showed excellent agreement. Now, the effects of "turbulence" can be described by an instantaneous spatial pressure distortion which is a function of pressure variation in amplitude and geometric location of the peak to peak pressure regions over the compressor face. The effects of this "turbulence" on the compressor performance, is shown in Figure 14. Base line characteristics for the compressor performance were determined from bellmouth tests and are so indicated. The unmodified "turbulence" generator characteristics (in other words, without the 1/2 inch and 3 inch pipe or other grill installations) showed a reduction in primary airflow, and more importantly a reduction in the stall line. Figure 14 also shows the effects of 1/4 inch and 3 inch pipe installations. As expected, further decreases in primary flow

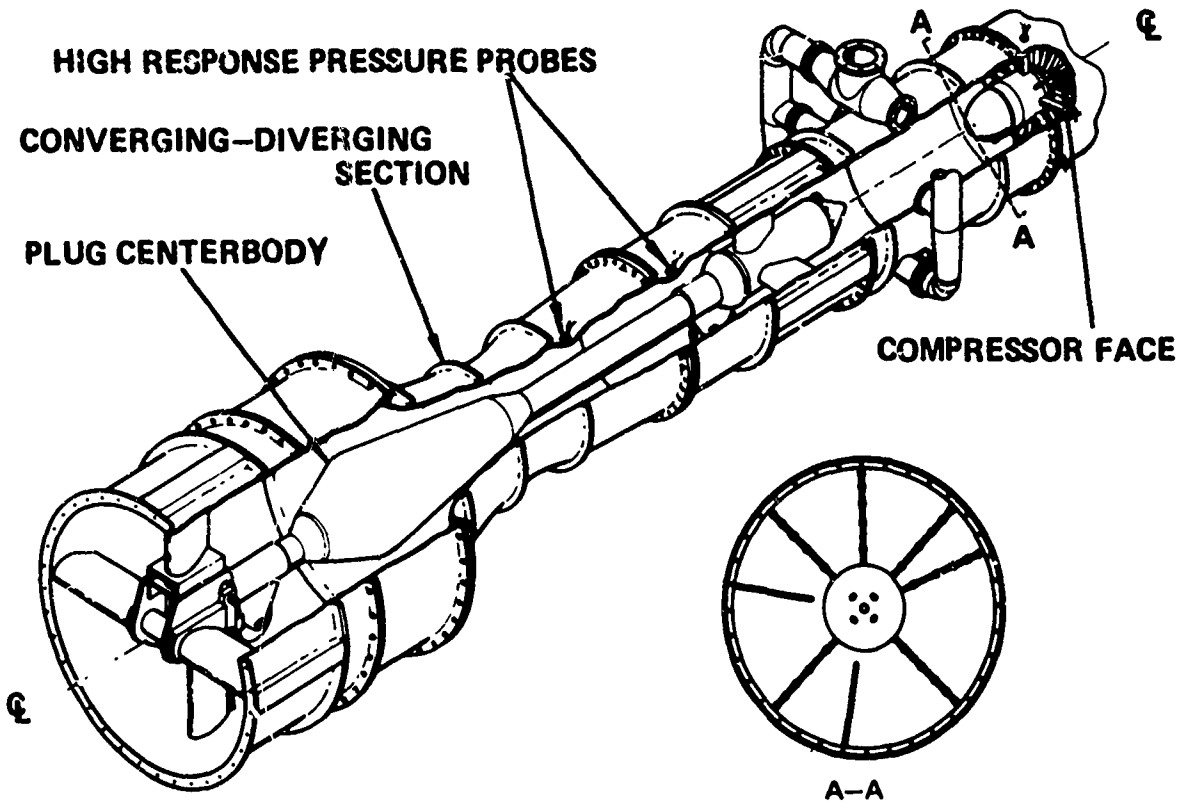

FIGURE 10. "TURBULENCE" GENERATOR

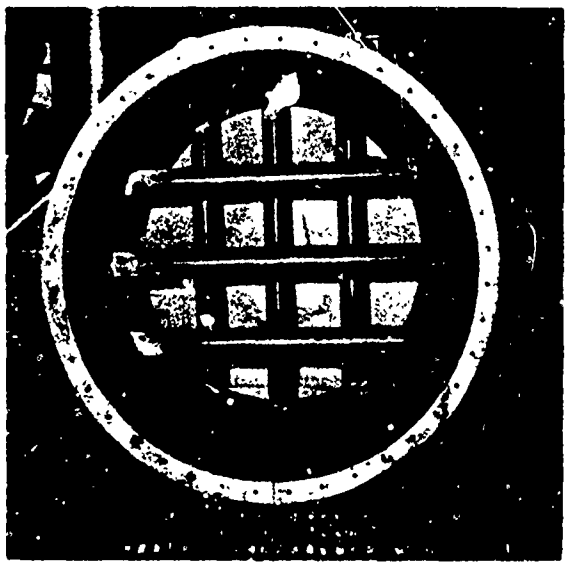

FIGURE 11. TWO ROW GRILL OF THREE-INCH DIAMETER PIPE

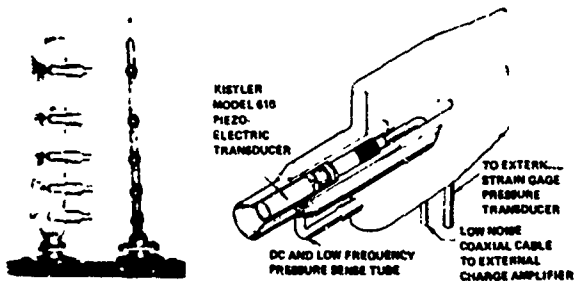

FIGURE 12. HIGH RESPONSE INLET RAKE AND TYPICAL TOTAL PRESSURE PROBE

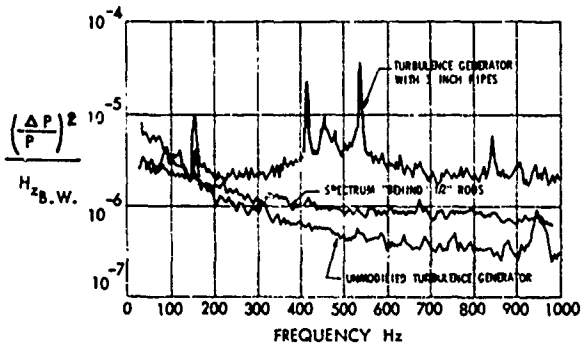

FIGURE 13. POWER SPECTRAL DENSITY COMPARISON

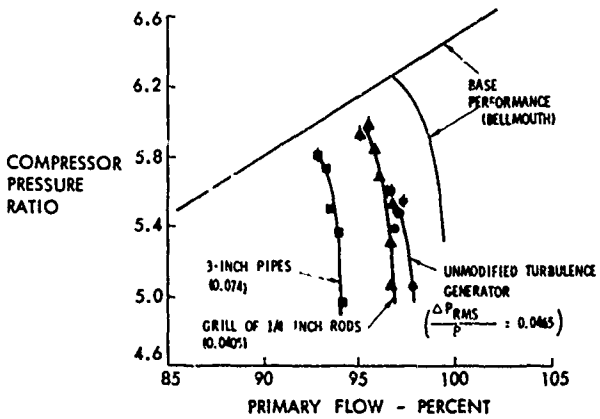

FIGURE 14. FAN LOW PRESSURE COMPRESSOR PERFORMANCE

were experienced along with some reduction in the operating stall line. Figure 15 shows the loss of compressor surge line as a function of "turbulence" level intensity. Here it is clearly shown that compressor stall is related to instantaneous spatial distortion.

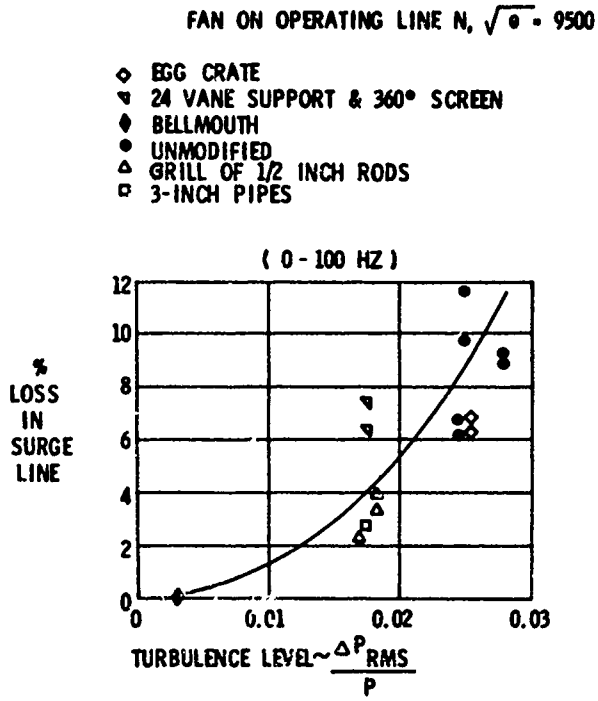

FIGURE 15. SURGE LINE REDUCTION VS "TURBULENCE" LEVEL

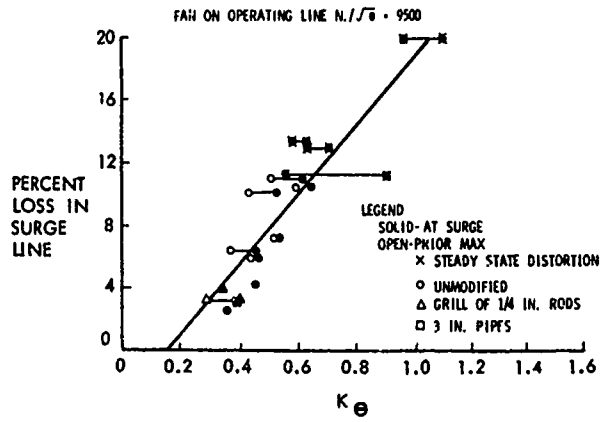

FIGURE 16. SURGE LINE LOSS VS INSTANTANEOUS SPATIAL DISTORTION

Today, there are a number of different theories advanced by numerous investigators to predict compressor stall. One effective method of describing the phenomenon is an instantaneous spatial distortion pattern. That is, although the time dependence of the fluctuations at a point is important, this effect may be approximated by the instantaneous spatial variation. With this assumption, the description of "turbulence" reduces to a weighted spatial integration producing an instantaneous distortion parameter which can be used to correlate the effects of "turbulence." The instantaneous distortion parameter K_θ[7] is expressed as follows:

$$K_\theta = \frac{\sum_{i=1}^{i} \left[\left(\frac{A_n}{n^2}\right)_{max}\right]_i \frac{P_{t_{av}}}{Q_{av}} \frac{1}{D_i}}{\sum_{i=1}^{i} \frac{1}{D_i}} \qquad (2)$$

where

i = number of pressure instrumented ring

D = diameter of the pressure instrumented ring

Q_{av} = average inlet velocity head at compressor face

$A_n = \sqrt{a_n^2 + b_n^2}$

θ = circumferencial angle

$$a_n = \frac{1}{\pi} \int_{-\pi}^{\pi} \frac{P_t(\theta)}{P_{t_{av}}} \cos n\theta d\theta$$

$$b_n = \frac{1}{\pi} \int_{-\pi}^{\pi} \frac{P_t(\theta)}{P_{t_{av}}} \sin n\theta d\theta$$

with

$$\frac{P_t}{P_{t_{av}}} = 1 + \sum_{n=1}^{\infty} a_1 \cos\theta + a_2 \cos 2\theta + \ldots a_n \cos n\theta + b_1 \sin\theta + b_2 \sin 2\theta + \ldots b_n \sin n\theta$$

and

P_t = impact pressure

$P_{t_{av}}$ = average impact pressure

Correlation of the computed instantaneous circumferential distortion parameter with experiment is shown in Figure 16. This figure shows reasonably good agreement between computation and the various configurations employed to develop "turbulence".

Recently, Burcham and Hughes[8] have modified and utilized the Pratt and Whitney K_{DA} distortion factor for predicting surge. The engine compressor face was sub-divided into 5 equal areas through concentric circles or rings. Probes were placed on rings which were maintained at a constant radii from the compressor centerline. The modified K_{DA} distortion parameter was defined as follows:

$$K_{DM} = \frac{\frac{1}{2}\sum_{i=1}^{5}\left[\frac{P_{t_{max}} - P_{t_{min}}}{P_{t_{av}}}\right]_i \bar{\theta}_i C_i}{\sum_{i=1}^{5} C_i} \times 100 \qquad (3)$$

where

C = ratio of compressor inlet radius to ring radius

i = number of ring

$\bar{\theta}$ = largest continuous arc of the ring over which the total pressure is below the ring average pressure

$P_{t_{max}}$ = ring maximum total pressure

$P_{t_{av}}$ = ring average pressure

$P_{t_{min}}$ = ring minimum total pressure

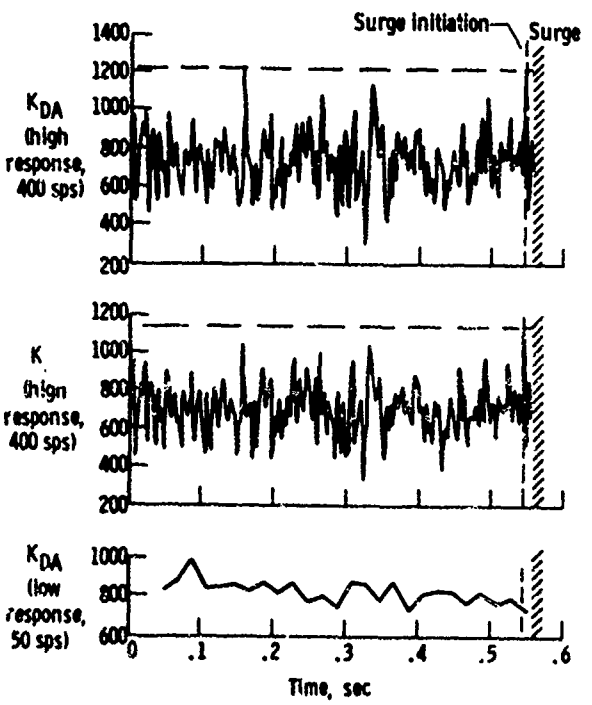

FIGURE 17. COMPARISON OF HIGH AND LOW RESPONSE K_{DA} WITH HIGH RESPONSE K_{DM}. F-111A FLIGHT CONDITIONS; MACH NUMBER = 1.6, ALTITUDE = 45,000 FEET AND OFF-DESIGN SPIKE POSITION

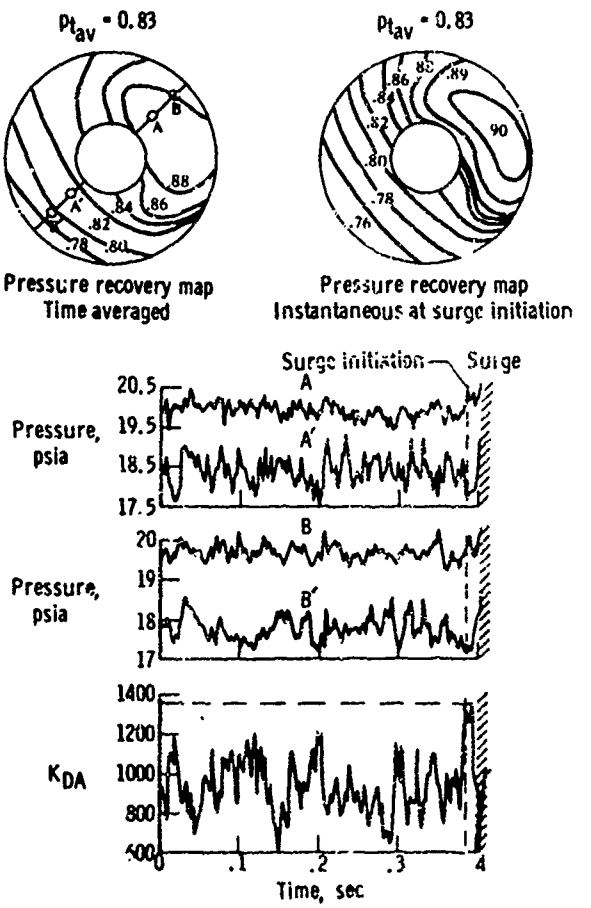

FIGURE 18. COMPARISON OF AVERAGE RECOVERY AND INSTANTANEOUS RECOVERY MAPS WITH K_{DA}. F-111A FLIGHT CONDITIONS: MACH NUMBER = 2.17, ALTITUDE = 44,000 FEET

In this specific effort a flight test F-111A aircraft was utilized to determine the dynamic nature of inlet pressure fluctuations related to engine operational stability. Derived steady state flow distortion patterns as developed from low response pressure instrumentation were compared with both the K_{DA} and K_{DM} distortion parameters calculated from high response instrumentation. A typical comparison is shown in Figure 17 for the flight case of Mach number 1.6 at an altitude of 45,000 feet with off-design inlet spike position. Here it is clearly seen that the low response data technique functioning at a sampling rate of 50 cuts per second did not yield information indicative of the compressor stall. On the other hand, utilizing the higher response data technique and calculating either the K_{DA} or K_{DM} distortion parameter at 400 samples per second did yield a substantial peak approximately 15 milliseconds prior to surge. Figure 18 shows a time history of the probe data and distortion factor for Mach number 2.17 and an altitude of 44,000 feet. Probes A and B show increases in pressure as the stall condition is approached whereas probes A^1 and B^1 are decreasing and hence result in a maximum distortion value. It is interesting to note that the instantaneous pressure recovery map shows a larger high pressure area along with a more intense low pressure area.

Figure 19 shows the surge characteristics for transonic flight at Mach number 0.9 and 30,000 feet altitude. This particular stall occurred as a result of the off-design conditions of the inlet cone and is generally recognized as a "drift" type of surge. This is demonstrated by the fact that peak values of the distortion factor occurred several times during the time period examined.

The modified distortion parameter as developed by Burcham and Hughes[8] was found to be approximately 80 percent effective in identifying surge when dynamic conditions prevailed within approximately 90 percent of the maximum steady state distortion value. Needless to say, additional information[9,10] and more exacting methods must be developed to predict engine instability due to dynamic inlet conditions.

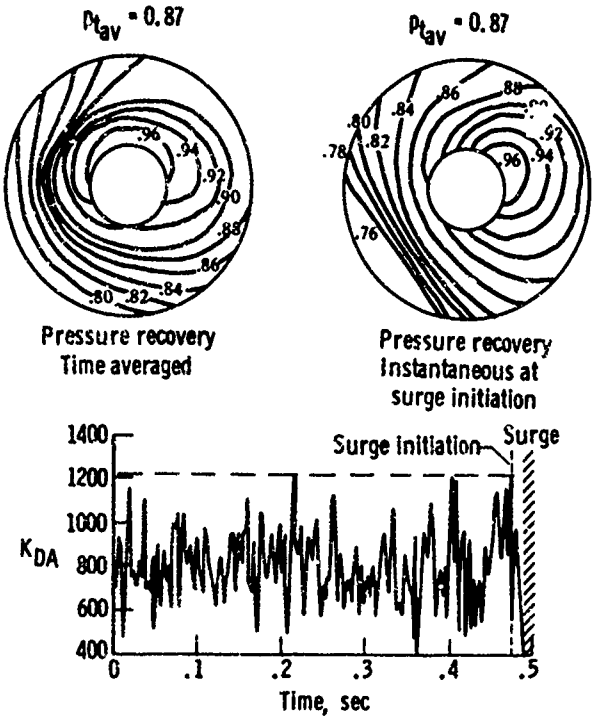

FIGURE 19. COMPARISON OF AVERAGE RECOVERY AND INSTANTANEOUS RECOVERY MAPS WITH K_{DA}. F-111A FLIGHT CONDITIONS; MACH NUMBER = 0.9, ALTITUDE = 30,000 FEET AND OFF-DESIGN SPIKE POSITION

V. ADVANCED CONFIGURATION STUDIES

Airframe-propulsion compatibility has become a critical problem area for both commercial and military high performance aircraft. Classically the solution to overcoming the problem of compressor stall has been through reduction of the pressure distortion generated by the inlet and increased distortion tolerance of the engine. Intensive efforts are presently underway in ground and flight test facilities to understand the effects of coupled steady-state and dynamic inlet distortion. Also, considerable research is being directed toward the cause and effect relationship of non-uniform flow fields entering the inlet system of turbo-jet engines. Many of these flow field examinations show local angles of attack and yaw which far exceed aircraft attitude values. Inlet designers are presently faced with a very difficult task to match inlet geometry with the large variations in flow conditions developed about many reasonable airframe geometries. Flow field studies will continue on many airframe configurations to determine optimum inlet positioning.

FIGURE 20a. TYPICAL 1/3 SCALE TAILOR-MATE WIND TUNNEL MODEL

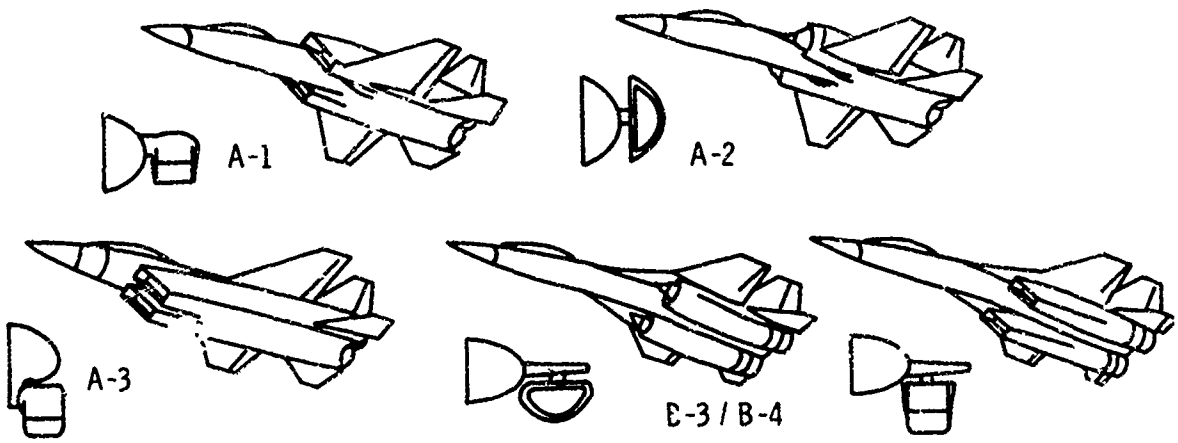

FIGURE 20b. REPRESENTATIVE CONFIGURATIONS FOR FOREBODY FLOW FIELD TESTS

More recently the Air Force Flight Dynamics Laboratory has undertaken a number of programs to investigate flows about fuselage and wing-fuselage combinations throughout the subsonic, transonic and supersonic speed regimes. The objectives of these programs are to develop a clear understanding of inlet-airframe interactions and, more importantly, to attain an experimental data bank and corresponding analytical approach for assessing the dynamic phenomena associated with engines and inlets. The Laboratory has initiated project Tailor-Mate in order to examine the effects of configuration variations on flow field dynamics and related effects to the engine system. Figures 20a and 20b show a typical 1/3 scale wind tunnel model along with various aircraft configurations studied. Configurations A-1 and A-2 are examples of side mounted type inlets whereas A-3 is an example of a fuselage shielded inlet, and wing shielded inlets are shown by configurations B-3 and B-4. One quarter scale fuselage models were constructed for wind tunnel testing purposes with appropriate fuselage static pressure distributions, boundary layer measurements and more importantly, the dynamic nature of the flow fields at the proposed inlet stations. In addition to the flow field measurements made in the area of the entrance to the inlet, two side mounted and two shielded external compression inlets were tailored for the flow fields defined by the forebody as shown in Figure 21. The detailed instrumentation for such a duct system is shown in Figure 22. Instrumentation was utilized to document the inlet performance and included static pressure rakes near the cowl lip, in the diffuser and at the simulated compressor face. It is important to note that the compressor face instrumentation contained high response type transducers to identify the fluctua-

tion nature of the inlet flow. Figure 23 shows the results of wind tunnel tests for the four configurations mentioned. These tests were performed at Mach number 2.2 with varying angle of attack. Figure 23 shows both wing shielded inlet systems experienced lower distortion as indicated by the simple distortion index along with low "turbulence" as a function of angle of attack. As might be expected the side mounted type of inlets experienced higher distortion with correspondingly higher indices of "turbulence."

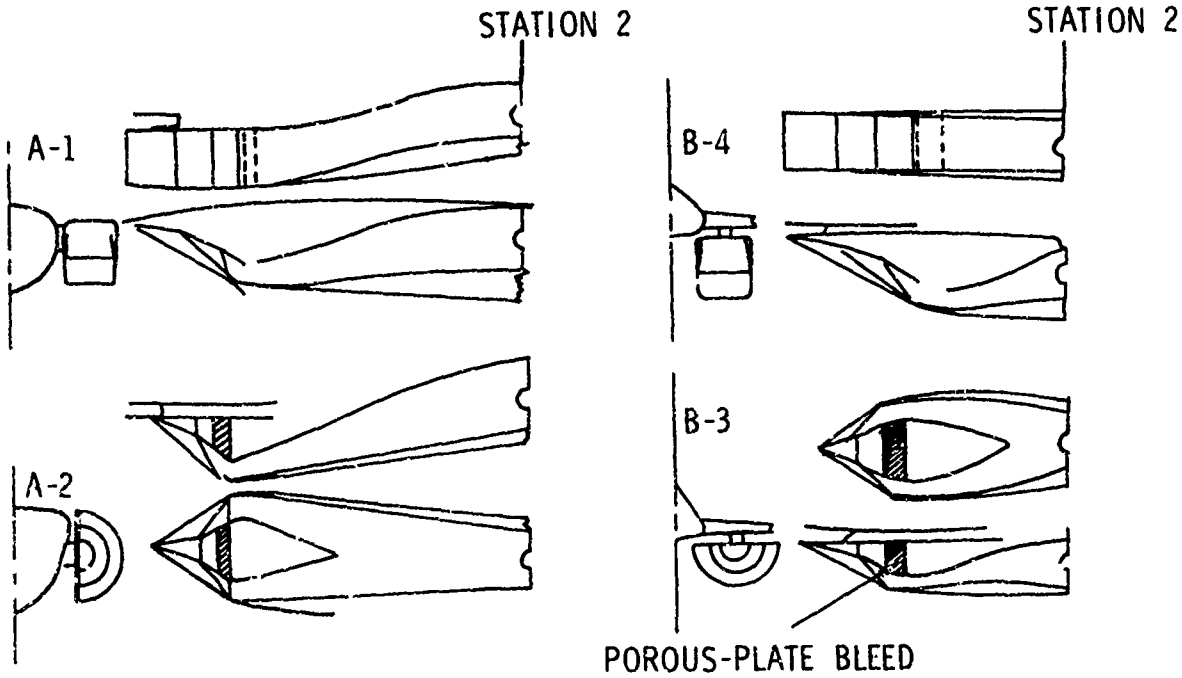

FIGURE 21. NOMENCLATURE AND COMPARISON OF FOUR (4) INLET DESIGNS

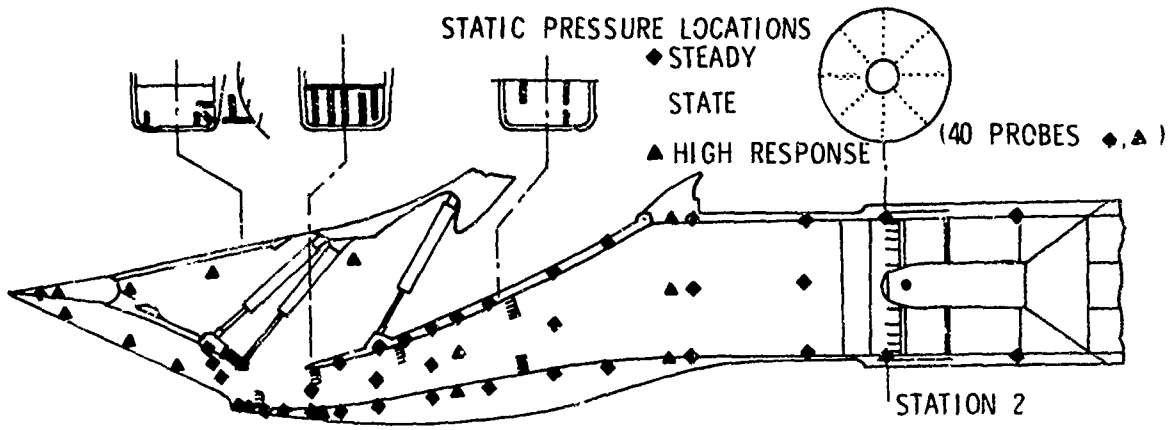

FIGURE 22. TYPICAL INLET INSTRUMENTATION

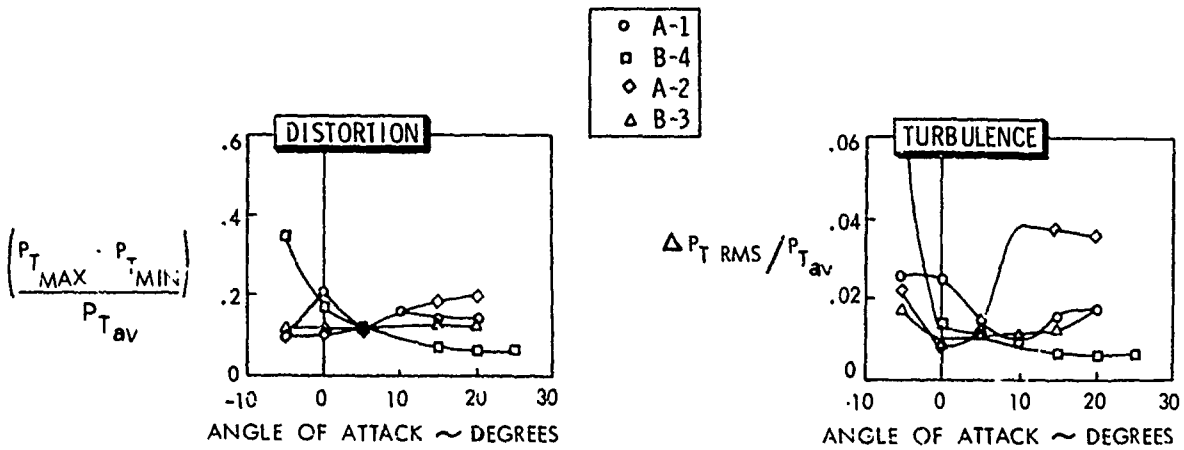

FIGURE 23. COMPARISON OF STEADY-STATE AND DYNAMIC DISTORTION FOR VARIOUS CONFIGURATIONS AT MACH NUMBER 2.2

The importance of the flo[illegible] generated by the forebody of the fuselage has been pointed out by Surber and Stevart and Zonars[12] [illegible] ple of such sensitivity is shown in Figure 24 wherein the side mounted 2-dimensional inlet o[illegible] A-1 was examined in conjunction with body A-2. This figure shows the vastly different characteristic of distortion vs "turbulence." Surprisingly enough, the small change in contour of the A-2 fuselage was found to have a substantially better characteristic than A-1. This is undoubtedly due to a lower local outwash and hence a reduced tendency toward flow separation on the inboard sid[illegible] of the inlet. In the event the designer is confined to the A-1 inlet configuration and cannot readjust [illegible] body contour as shown by the A-2 characteristics, he must then look for other means by which he can suppress both the steady state and "turbulent" distortion. A longer inlet duct has a surprisingly favorable characteristic as denoted in Figure 25. There is a considerable reduction in both distortion parameters which puts the operational mode of the inlet well within the stable bounds of engine operation.

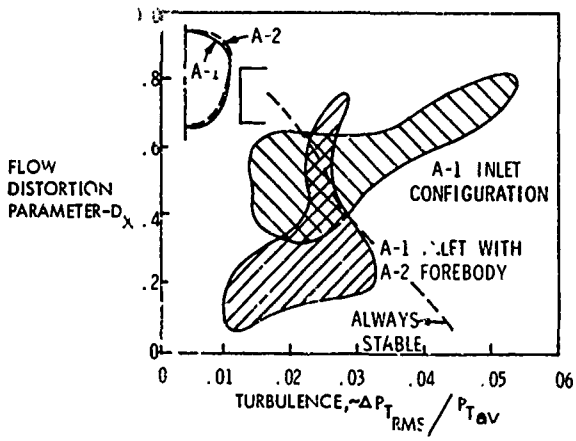

FIGURE 24. INFLUENCE OF FOREBODY CONTOUR ON ENGINE STABILITY AT MACH NUMBER 2.2

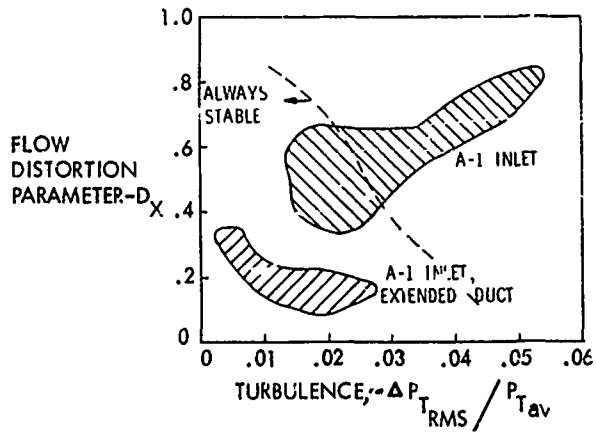

FIGURE 25. EFFECT OF LONGER DUCT ON SUPPRESSING STEADY STATE AND "TURBULENT" DISTORTION

VI. DYNAMIC DATA HANDLING TECHNIQUE

Among the problems that exist in handling dynamic data are the tremendous quantities of analog data tapes generated during inlet development programs and that past efforts to analyze dynamic data has depended heavily upon what has been seen relative to the behavior of the steady state or average component of compressor face total pressure. As a consequence, only about one percent of the data is actually examined since considerable digitization is required to review one case. More specifically, the area of interest centers on the analysis of the dynamic or fluctuating component of total pressure measured at the compressor face plane of a trisonic type inlet. The pressures are measured by means of fast response instrumentation located in rakes radiating from the hub. This data is recorded on analog tape and represents the beginning of our problem.

The solution to this problem has been to develop an analog editing system for screening and editing inlet dynamic data based on the use of engine distortion parameters. As a result, large quantities of tape can be screened and those parts of the data identified which would have adverse effects on airframe-propulsion compatibility.

A typical Air Force Flight Dynamics Laboratory inlet program consists of 5000 data points wherein one Mach number, angle of attack and yaw, and capture area ratio comprises a single data point. At least 200 feet of tape are used for each data point and as a result, it can be seen that about 10 reels of tape are required for a program of this magnitude. For a more extensive inlet development program, such as associated with advanced flight vehicles, as many as 500 tapes are required. In any event, the data of interest is contained on only about one percent of the tape which is not necessarily the same one percent of tape mentioned previously. The principle question that arises is how does one expeditiously and economically locate the data of interest?

In the development of the analog editing system, certain goals were established. First, it was desirable to utilize parameters involving all the compressor face steady-state and dynamic data which had a direct relationship to engine stability. Second, a scheme was desired that would identify high levels of dynamic flow activity on the tapes and where this event occurred. Third, a fast response capability was a requirement in order to account for model scale. For example, if a particular engine is sensitive to pressure fluctuations up to 200 cycles/second, and the inlet wind tunnel model is one-tenth scale then valid data out to 2000 cycles/second is required from the model. Model scaling characteristics have been hypothesized by Sherman and Motycka[13]. Fourth, a desirous capability was to use more than one parameter in the screening process to determine which was most meaningful and acceptable and hence avoid tape re-runs. Fifth, the system should be flexible to permit digitization of data and possess a data playback capability at the recorded speed.

Among the parameters selected for data screening was the Pratt & Whitney engine distortion parameters K_θ, K_{RAD} and K_A which have been formulated on the basis of experimental data. The expressions shown below, which in part relates to Equation 2, describe the level of distortion associated with a particular compressor face pattern.

$$K_A = K_\theta + bK_{RAD} \tag{4}$$

$$K_{RAD} = \left[\frac{1}{Q_{av}\sum_{i=1}^{i} D_i^{-x}}\right]\sum_{i=1}^{i}\left[D_i^{-x}\left(P_{t_{av}} - P_{t_{av,i}}\right)\right] \tag{5}$$

where

b = constant depending on engine design and entrance Mach number

x = weighting factor depending on distortion sensitivity

K_θ describes the influences associated with a circumferential distortion pattern while K_{RAD} describes the pattern variation associated with radial distortion. When a combined pattern exists, which is typically the case, K_θ and K_{RAD} are added together in a weighted manner to form K_A. In addition to the Pratt and Whitney parameters, a set of General Electric engine distortion parameters have been programmed. These expressions are used to identify high levels of dynamic activity in the air flow process. These data are subsequently subjected to further analysis which in turn aids in determining the necessary modifications required to alleviate the compatibility problem.

The dynamic data screening device or system was developed jointly between the Air Force Flight Dynamics Laboratory and the Aeronautical Systems Division Computer Center using a hybrid computer. This program was initiated in January 1970 by Sedlock and Marou,[14] with the acquisition of a 72 channel multiplex discriminator system, a 14 track direct playback tape transport, tape search unit peak detectors, and a 48 channel data filtering system. The complete system shown in Figure 26 became operational in July 1971. The system described above is similar to that developed by Crites and Heckart[15], Crites[16], Lynch and Slade[17] except for the added flexibility due to a hybrid computer capability.

The current status of the Air Force Flight Dynamics Laboratory system is that both General Electric and Pratt and Whitney engine distortion parameters have been programmed on the computer and up to five parameters can be tracked simultaneously with an order of priority established for each parameter. The primary requirement of the system is to identify dynamic peaks and the time of occurrence. The resolution of the tape search unit permits identification of the peak value within one millisecond. Center frequencies used in the discriminators have been selected for greatest compatibility with those being used by USAF and contractor facilities. The dynamic data can be filtered from 125 to 9000 cycles/second in six discrete increments in order to account for model scale and filtering of any unwanted high frequency information such as probe resonance. Both the engine distortion parameters and pressure data can be digitized at various sampling rates.

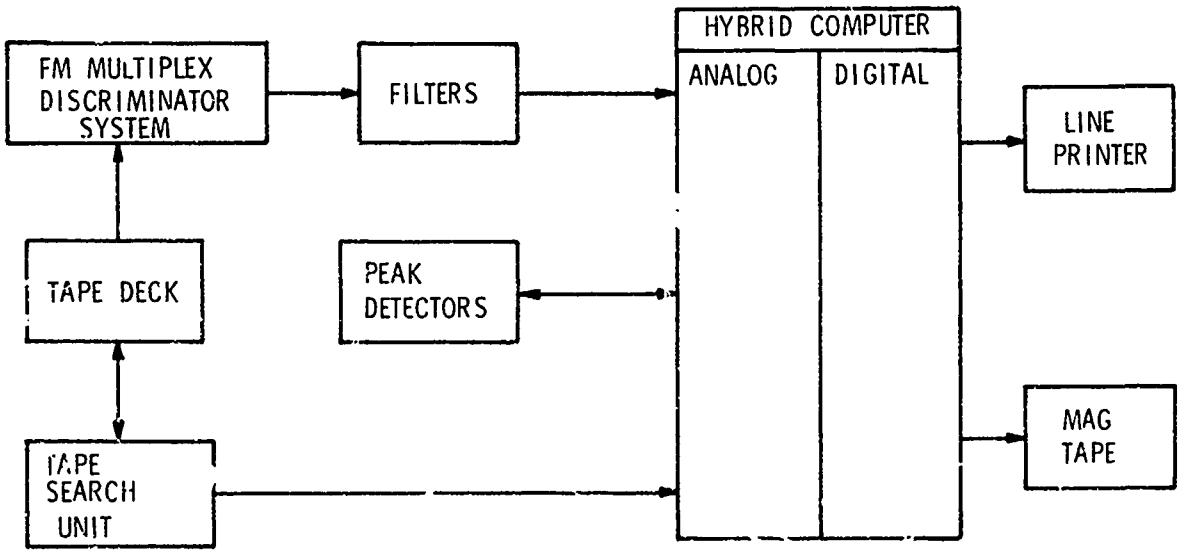

FIGURE 26. DYNAMIC DATA SCREENING AND EDITING SYSTEM

Our past and current efforts have included review of the compatibility points in the B-1 Interface Control Document and the Arnold Engineering Development Center 1/10 scale inlet test data. In addition to continued support of the B-1 program, data from the RA-5C wind tunnel-flight test correlation and Tailor-Mate programs will be reviewed.

McDonnell-Douglas personnel [16] have developed a screening system for use during the F-15 inlet development program. In examining this capability to review dynamic data based on conventional means, it was estimated that six manyears and one million dollars were required to review one percent of a 250 data point program which represented some four million pressure distributions. The development of an analog editing system reduced this task to six weeks with less than 1000 feet of tape to be examined. Our own experience has shown that one reel of tape containing 30 data points can be examined in approximately one hour. To accomplish the same task with a digital computer would require 15 hours to digitize the data and approximately 20 hours of computer time to process the information. This estimate is based on 200 samples per data point. The development described above represents a major step in handling the extremely large amount of data associated with an inlet development program.

A description of how the engine distortion parameters are implemented on the analog/digital computer to accomplish the goal of editing and screening the data will now be addressed. This can be accomplished by relating the expression for K_θ to a particular configuration of total pressure probes at the compressor face. In this particular case, consider a configuration that consists of 48 probes with six rings and eight rakes. The implementation of Equation (2) on the analog computer is quite simple. The steady state and gain adjusted fluctuating pressure are summed together to form the total component of pressure. Each pressure is multiplied by its respective sine θ and cosine θ, summed around each ring, and then squared. These two terms are added together and then the square root is taken of this summation. Finally, this value is multiplied by the value of the leading term to attain K_θ for one ring. This process is repeated for each ring and then the individual ring K_θ are summed together to form the total K_θ. While the value of this expression is being calculated, a similar process is occurring simultaneously for the other parameters.

The editing process is accomplished by considering the time history of the parameter K_θ. K_θ can be generated as a continuous function since an analog computer is a continuous type of machine. The operator has the ability to set a threshold level for each of the parameters such that only information occurring about that level will be examined. The engineer must know when a peak in K_θ has been experienced and the time of this occurrence. In addition, he is interested in the value of K_θ when it exceeds a given threshold level and when it returns to a lower value. Special peak detector networks are utilized to accomplish these objectives. These peak detectors track an increasing signal to the peak level and maintain that level until it is reset. The peak detectors are normally reset when the value of the parameter drops below the threshold level in order that successive peaks can be detected even though such peaks may be of a lower value than a preceding peak. In addition, the peak detectors can be used as a signal generator that signifies a peak has been detected. Judgement must be made as to identifying both threshold crossings and peaks or peak values alone. When a threshold crossing occurs, an interrupt signal is generated, and the information is transferred from the analog to the digital computer. No on-line manipulation of this information is permitted in order to transfer the data as quickly as possible. The current response time from signal interrupt thru information transfer is 300 microseconds. An important feature of the program is the identification of which parameters triggered the interrupt signal. Whenever the interrupt signal occurs, the peak value of the parameter is stored as well as the value of the other parameters at this particular instant. The next output from the editor is the time when the peak was detected. The time resolution is to within one millisecond.

Many electronic components make up the editing system. A 14 track tape transport is used to playback the dynamic data through the discriminator system which de-multiplexes the individual signals. Each pressure signal is filtered before it is sent to the analog computer. Coupled with the tape deck and hybrid computer is the tape search unit. The search unit allows one to find a particular time-pressure history on the tape while it also serves as the time reference frame for the hybrid computer. The peak detectors, mentioned earlier, are coupled to the analog computer. The information stored in the digital computer can be printed out on the line printer or stored on magnetic tape.

VII. CONCLUSION

The effects of "turbulence," or specifically, the fluctuating nature of the measured total pressures at the compressor face have been found to have a strong influence on the stall margin of most engines. This phenomenon normally commences at low supersonic speeds with increasing disturbance intensity as a function of increasing Mach number. This "turbulence" exhibits a wide range of amplitude-frequence content. For low frequency disturbances, engine performance is basically similar to steady state operation since the engine outlet pressures will follow the inlet flow variations in magnitude and phase, such that overall compressor pressure ratio will remain the same. However, the majority of time dependent total pressure fluctuations are found to be significantly faster than the aforementioned flow properties. Under these circumstances, outlet pressures lag the inlet pressure variations in both amplitude and phase. Consequently, the pressure ratio across the compressor can differ considerably from a steady-state value, and conditions can develop wherein compressor stall margin is completely negated. For years the use of a frequently referred to "turbulence factor", $(\Delta P_t)rms/P_{t_{av}}$, averaged over the compressor face has raised many doubts concerning its usefulness. The results of the study presented in this paper clearly indicates that instantaneous spatial distortion calculations are necessary to judge the performance characteristics of the ducted flow as caused by a number of physical phenomenon such as shock wave-boundary layer interaction and flow separation. The development of small-scale powered simulators for wind tunnel use can be very beneficial in establishing inlet-engine compatibility. Although only the affects of "turbulence" on engine stability have been addressed, future efforts should be directed toward identifying unsteady flow influences on the vitally important thrust aspects of the inlet.

REFERENCES

1. Gabriel, D. S., Wallner, L. E., and Lubick, R.J., "Some Effects of Transients in Inlet Pressures and Temperatures on a Turbojet Engine," Institute of the Aeronautical Sciences Twenty-Fifth Annual Meeting, (January 1957).

2. Martin, A. W. and Kostin, L. C., "Propulsion System Dynamic Test Results," North American Aviation, Inc., Report No NA-67-386, (April 1967).

3. Winslow, L. J., et. al., "Inlet Distortion Investigation, Upstream Engine Influence and Screen Simulation," The Boeing Company, Technical Report AFAPL-TR-68-140, (January 1969)

4. Wasserbauer, J. F. and Willoh, R. G., "Experimental and Analytical Investigation of the Dynamic Response of a Supersonic Mixed Compression Inlet," AIAA Preprint 68-651 (1968).

5. Martin, A. and Kostin, L., "Dynamic Distortion at the Exit of a Subsonic Diffuser of a Mixed Compression Inlet," North American Rockwell, Report TFD-69-588 (1969).

6. Oates, G. C., Sherman, D. A., Motycka, D. L., "Experimental Study of Inlet-Generated Pressure Fluctuations," PWA Report 3682 (1969).

7. Plourde, G. A. and Brimelow, B., "Pressure Fluctuations Cause Compressor Instability," Air Force Airframe/Propulsion Compatibility Symposium, (June 1969).

8. Burcham, F. W., Jr. and Hughes, D. L., "Analysis of In-Flight Pressure Fluctuations Leading to Engine Compressor Surge in an F-111A Airplane for Mach Number to 2.17," AIAA Preprint 70-264 (1970).

9. Calogeras, J. E., Burstadt, P. L., and Coltrin, R. E., "Instantaneous and Dynamic Analysis of Supersonic Inlet-Engine Compatibility," AIAA Preprint 71-667 (1971).

10. Jansen, W., "Compressor Sensitivity to Transient and Distorted Transient Flows," AIAA Preprint 71-670 (1971).

11. Surber, L. E. and Stava, D. J., "Supersonic Inlet Performance and Distortion During Maneuvering Flight," AGARD Propulsion and Energetics Panel Specialists' Meeting on "Inlets and Nozzles for Aerospace Engines," AGARD Conference Proceedings CP-91-71, (1971)

12. Zonars, D., "Problems on Inlets and Nozzles," 7th Congress of the International Congress of the Aeronautical Sciences, (August 1970).

13. Sherman, D. A., and Motycka, D. L., "Experimental Evaluation of a Hypothesis for Scaling Inlet Turbulence Data," AIAA Preprint 71-669 (1971).

14. Sedlock, D. and Marcus, J., private communication, (1972).

15. Crites, R. C. and Heckar., M. V., "Application of Random Data Techniques to Aircraft Inlet Diagnostics," AIAA Preprint 70-597 (1970).

16. Crites, R. C., "The Philosophy of Analog Techniques to the Analysis and High Speed Screening of Dynamic Data, "AIAA Preprint 70-595 (1970).

17. Lynch, F. R. and Slade, C. J., "Data Acquisition and Automated Editing Techniques for Engine-Inlet Tests," AIAA Preprint 70-596 (1970).

ENGINE INTEGRATION AND THRUST/DRAG DEFINITION

by

Dr. Allen E. Fuhs
Professor of Aeronautics
Naval Postgraduate School
Monterey, California, 93940
United States of America

SUMMARY

Careful attention is given to various definitions relating to thrust and drag. Since thrust minus drag is of primary interest, the background on drag determination is discussed. This is followed by testing techniques for full scale propulsion systems. Many of the testing techniques yield uninstalled engine thrust levels significantly greater than installed values. Sources of installation losses are, hence, of considerable interest. Several different methods have evolved to account for various terms in a drag/thrust determination. Bookkeeping of forces and momentum flux is described. Any aircraft development is controlled by schedules and fixed resources. Influence of these constraints on engine-airframe integration is discussed. Some special integration problems, e.g., engine bleed air, are considered.

I. INTRODUCTION

In recent times there have been examples of aircraft, both military and commercial, with inaccurate prediction of performance during development. The aircraft are committed to production without knowledge of substandard performance. The consequence is a non-competitive aircraft. Prediction of aircraft performance is based mainly on static tests of the aircraft engine and wind tunnel tests on subscale models of the aircraft. Sources of inaccuracy in the prediction are the changes of thrust from uninstalled to the installed condition and the mutual interaction between engine and airframe.

As a result of past experience with faulty predictions, there has been greater emphasis on accurate testing and consistent bookkeeping procedures. Some of these tests and procedures are described.

After defining many of the forces associated with an aircraft, the determination of aircraft drag in a wind tunnel is discussed. These tests are almost solely subscale. It is not practical to build subscale models of aircraft engines. As a result, full scale engines are tested starting with demonstrator engines. Methods and techniques for testing full scale engines and propulsion systems are presented.

A critical component in a propulsion installation is the exhaust system. External flow and aerodynamic interference add complexity to the determination of exhaust performance. Isolated and complete model tests of nozzles are discussed. A method for estimating installed gross thrust knowing uninstalled gross thrust and subscale nozzle data is presented.

Many of the factors that cause losses when an engine is installed in an aircraft are briefly examined. This is followed by a discussion of a thrust and drag bookkeeping system. Certain aspects of system management are included to emphasize the fact that any test program is constrained by resources and schedules.

II. DEFINITIONS

A series of definitions will be stated before the main discussion of engine integration. Definitions, which are quite uninteresting, should appear perhaps in a remote appendix; however, due to the fact that the definitions are essential to the understanding of the paper, they appear in this prominent location.

Some quantities, e.g., ram drag, are defined much the same throughout the propulsion community. As a result of the diversity of aircraft types and different powerplant installations, there are many specially defined drag and thrust quantities which are not universally defined. This is another motivation for providing a definitions chapter.

Notation and nomenclature differ widely with different symbols for the same concept or the same symbols for different concepts. Additive drag and pre-entry drag are identical quantities with different nomenclature. In view of the different symbols in use, a more efficient set of symbols is suggested and used herein. A capital subscript is used to denote an increment while a lower case subscript indicates the quantity itself and not an increment.

A. Drag Associated with Inlets

D_e drag of the external surfaces of inlet extending from stagnation point on inlet lip aft to an appropriate point on nacelle or fuselage. Alternate names are forebody drag, especially for nacelles and cowl drag.

D_ℓ drag on the internal surfaces of inlet extending from stagnation point to fan or compressor face. Important for flow-through nacelles in wind tunnel models. Usually lumped with engine internal net thrust when engine is installed.

D_d diverter drag due to the spacer which moves inlet outward so as to avoid ingestion of boundary layer along aircraft forebody.

D_A additive drag, which is equal to integral of gage pressure along streamtube from a point far ahead of inlet to the entrance of inlet; also equal to change in momentum in freestream to momentum at inlet entrance. Note this is an increment. D_A is a term resulting from desire to use freestream conditions to define ram drag.

D_S spillage drag equal to difference of D_A and the change in external drag. The charge in D_e due to spillage of air is often termed cowl suction.

D_B increment of drag due to boundary layer bleed somewhere along inlet compression surfaces.

D_Y increment of drag due to air which is taken on board via the inlet but which bypasses the engine and is dumped overboard.

D_r ram drag equal to product of mass flow rate entering inlet and flight velocity.

D_i inlet drag equal to sum of D_e and D_d.

D_I increment in inlet drag equal to increments D_A, D_B, D_Y, and D_S.

B. Drag Associated with Nozzles and Exhausts

D_t boattail drag is force on external surfaces of fuselage or nacelle that decrease cross sectional area from maximum area to nozzle exit area.

D_b base drag is force due to the annular region between nozzle and boattail.

D_n nozzle external drag due to forces on nozzle external surfaces extending beyond nacelle or boattail. Variable geometry nozzles usually extend beyond boattail to permit changes in nozzle exit area.

D_a afterbody drag is sum of boattail drag and drag due to fairings, rudder, and elevators.

D_E increment of exhaust system drag due to changes in D_t, D_b, D_n, and D_a.

D_{st} sting drag is force on sting which supports model in the wind tunnel.

C. Engine Thrust Definitions

F_g gross thrust is force produced by momentum flux across exit plane and by gage pressure over exit area.

F_n net thrust is gross thrust less ram drag.

F_t net internal thrust (sometimes termed internal thrust) is equal to stress tensor integral over all internal surfaces wetted by engine air streamtube. Net thrust and net internal thrust differ by additive drag.

F_u uninstalled gross thrust is gross thrust measured in engine test facilities using reference nozzle without external flow.

F_f flange thrust is force obtained by an ideal expansion of actual flow of gases at some station downstream of turbine; the flow includes distortions or profiles in P_T or T_T present in actual engine.

F_i ideal thrust is force obtained by one-dimensional isentropic expansion of gases from P_{T6} and T_{T6} to P_∞.

D_s scrubbing drag is force due to skin friction on pylon and nacelle surfaces wetted by fan discharge streamtube.

$(\ )_6$ subscript to denote the nozzle charging station.

In addition to the various drag and thrust terms, there are related coefficients defined, e.g., gross thrust coefficient. These will be discussed later.

III. AIRFRAME DRAG DETERMINATION IN WIND TUNNEL

A. Scope of Testing

There are many different kinds of aircraft ranging from supersonic transports, supersonic fighters, VTOL, to piston powered sport planes. To provide propulsion for the gamut of aircraft, there are a wide variety of propulsion systems. A major variable for aircraft gas turbines is bypass ratio. Supersonic aircraft tend to have zero or small bypass ratio (less than unity). High subsonic cruise aircraft tend to have large bypass ratio up to 8 or so. Lower Mach number cruise yields higher bypass ratio as the optimum, thus transforming the turbofan to a turboprop. Large bypass engines are mounted in nacelles, whereas turbojets may be buried within the fuselage. In this lecture we limit the discussion to buried and large bypass ratio podded engines.

There are at least three mounting locations for jet engines in nacelles on high subsonic cruise aircraft: below the wing, above the wing, and rearward on the fuselage. For low pressure ratio fans the loc[illegible] pressure distribution due to wing or fuselage can alter fan performance.

The scope and kinds of testing are determined by the point in the development cycle. Figure 1 illustrates schematically the engine/airframe integration process for an engine mounted in a

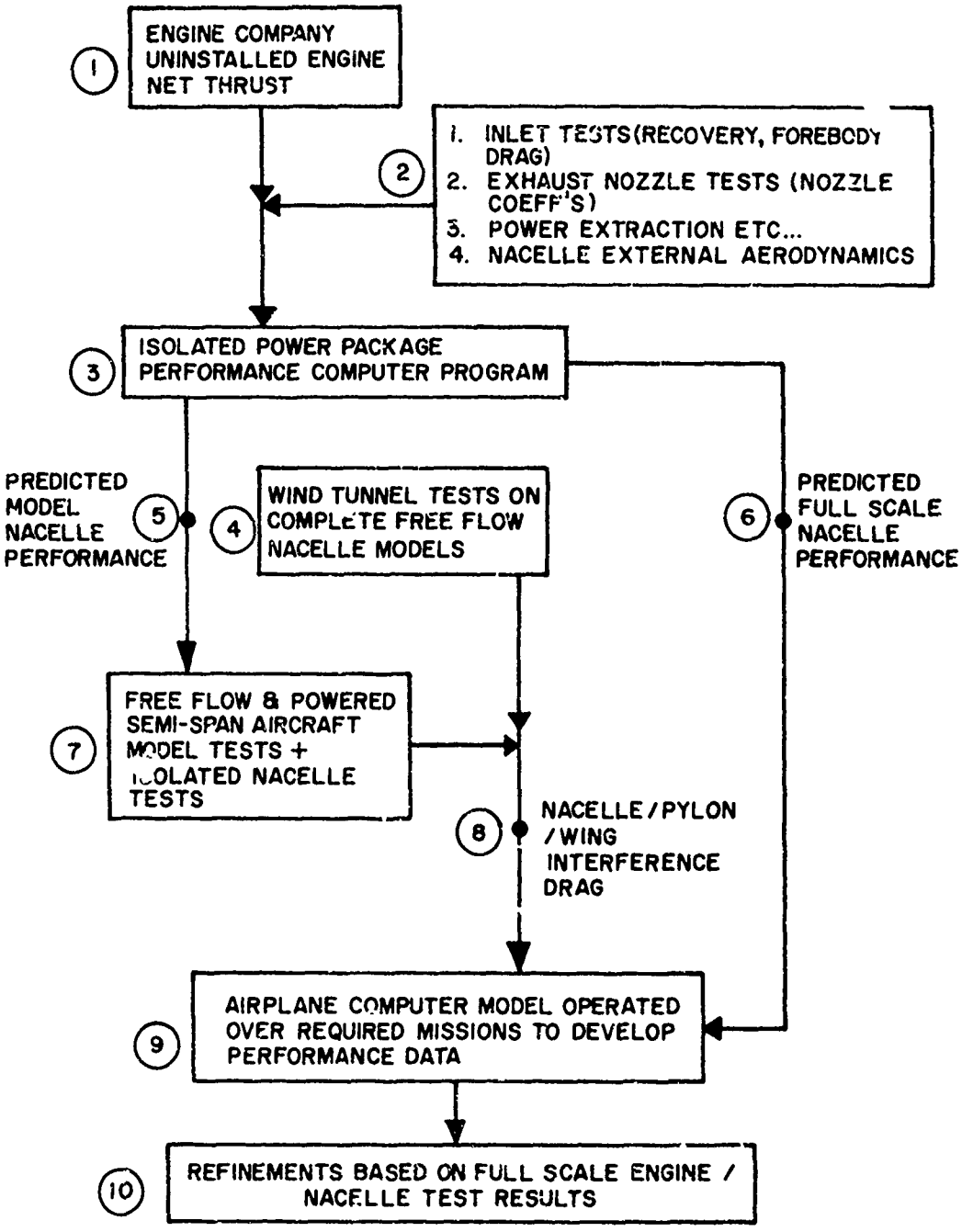

Figure 1. Engine/Airframe Integration Process.

nacelle. Figure 2 shows major elements of wing/pylon/nacelle flow field. Figures [illegible] and 2 are reproduced from the Lockheed-Georgia response to the AGARD ad hoc study on transonic testing.[1] For the procedures shown in Figure 1, the aircraft preliminary design and configuration layout is complete. The work that remains is the verification of design calculations, accumulation of wind tunnel data to predict performance, and specification of many of the details not part of initial design.

For an aircraft with the engine buried in the fuselage, a bookkeeping system is illustrated in Figure 3. Figure 3 was reproduced from Reference 1. The various models necessary to obtain drag and thrust increments are also shown. Figure 3 represents the same span of development cycle illustrated by Figure 1.

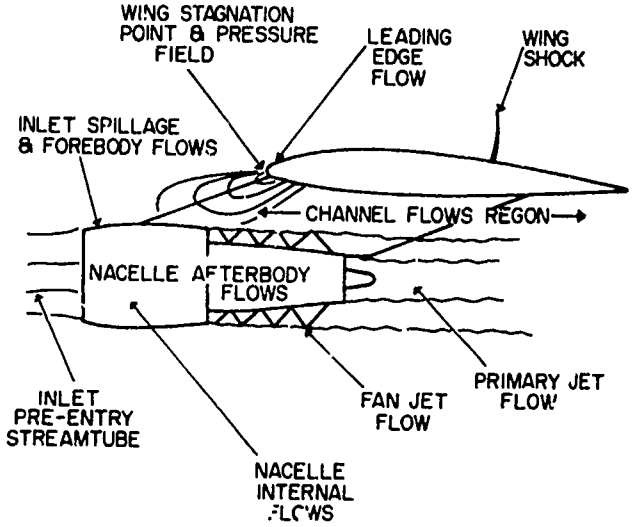

Figure 2. Major Elements of Wing/Pylon/Nacelle Flow Field.

B. Variables

In addition to the flight or operational variables, e.g., Mach number and altitude, there are many geometrical variables. For key operational points a reference configuration is chosen from among the possibilities. A change in geometry gives rise to a drag or thrust increment. Some of the geometrical variables are nozzle exit area, nozzle throat area, wheels up or down, wing sweep angle, flap position, control position, bleed door position, bypass door position, and inlet throat area. If the flight condition is defined, then many of these variables become fixed. For example, cruise of a supersonic aircraft at a supersonic Mach number, which is a key operational point, has wing sweep at maximum angle, wheels and flaps up, etc. A model is built with these geometric variables fixed at an appropriate value. For transonic cruise of a supersonic aircraft at the transonic drag rise, the geometrical variables have changed compared to supersonic cruise. Another model is needed.

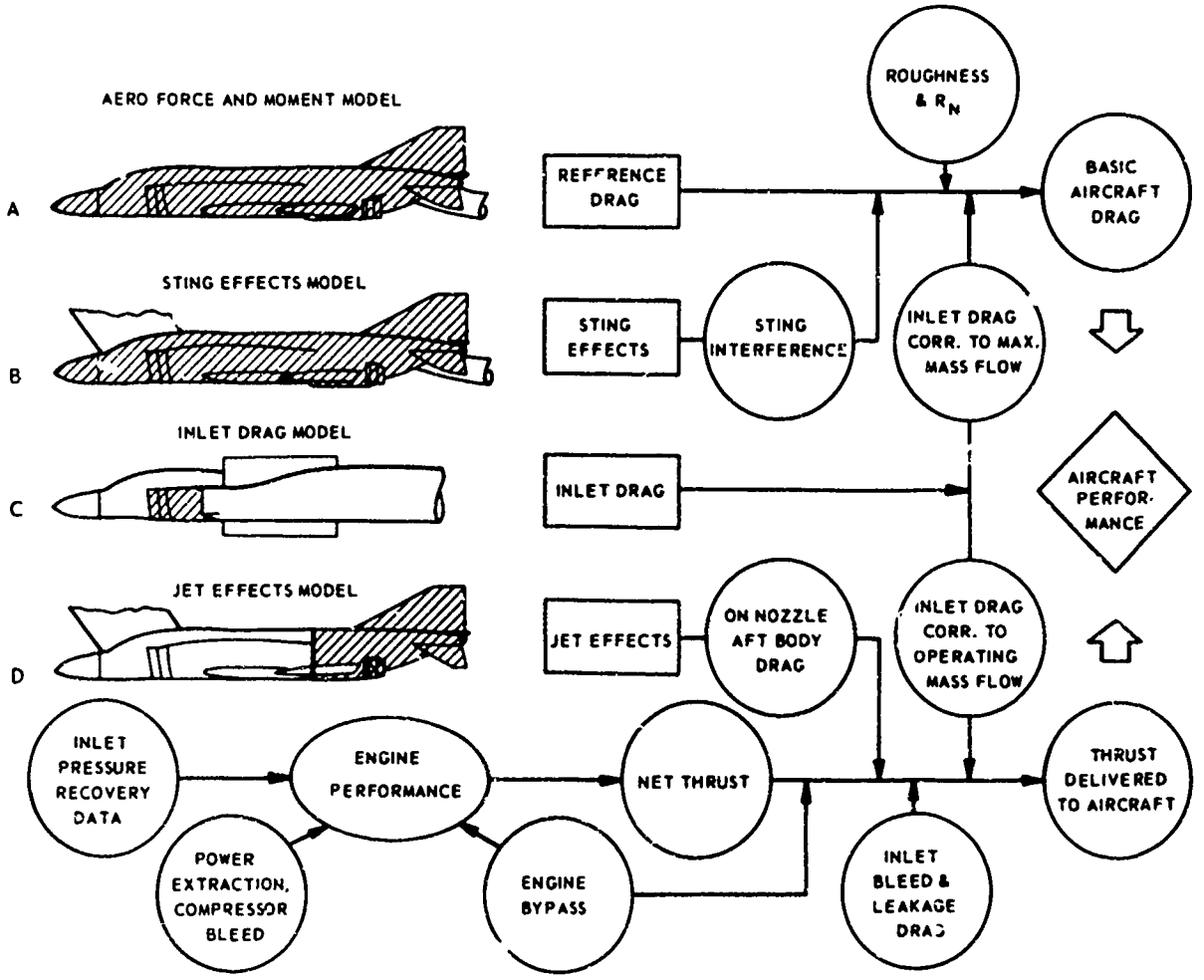

Figure 3. Thrust and Drag Accounting System.

Propulsion variables, other than geometry, that influence drag and thrust are mass flow ratio for the inlet, exhaust nozzle pressure ratio, and afterburner operation. These propulsion related variables must be duplicated in the inlet or afterbody models to obtain thrust minus drag throughout the operating envelope.

C. Subscale Testing

For each test Mach number there is a reference geometrical configuration. A model of the aircraft is made for that configuration. Usually it is too difficult to manufacture a variable geometry model so that additional models are needed for each reference geometry. The aircraft mission specifies

performance for certain key points within the operating envelope. Models will be built as appropriate for these key points.

Scale of the model is determined to a large extent by wind tunnel size. Transonic testing is the most complex within the Mach number range from subsonic through supersonic. Transonic wind tunnel blockage restrictions, expressed as ratio of model cross sectional area normal to mainstream to wind tunnel flow area in test section, yield small models. Blockage of 0.5 per cent to 1 per cent are common. Scale has an influence not only on Reynolds number but also on model construction. It is not possible to duplicate surface roughness or small details in a small model. Models less than 1/20 scale usually have so many compromises relative to geometric detail and Reynolds number that tests are not attempted. There are exc[illegible], of course, with sonic boom models being an example.

[illegible]alized models such as the inlet model or the jet effect model shown in Figure 3 can be of relatively large scale, e.g., 1/6 scale. Only part of the airframe needs to be duplicated for inlet or exhaust models.

There are special tests which are conducted subscale. Spin tests are an example. These are not discussed here.

D. Propulsion System Representation

There are three common techniques for representing the propulsion system as part of a wind tunnel model: faired over inlets, flow through nacelles, and powered simulators. With faired over inlets, there is, of course, no flow entering the model. If exhaust gases are piped into the model with faired inlet, the exhaust plume can be simulated. Without an exhaust gas supply, neither inlet nor exhaust flow is simulated.

Flow through nacelles, also called free flow nacelles, give partial simulation of inlet and exhaust flows. The nozzle pressure ratio is usually in error. Figure 4 compares the nozzle pressure ratio for an optimum, ideal turbojet with the flow through nacelle. At a Mach number of 1 the turbojet has NPR [illegible]ut two and one half times greater than flow through nacelle.

To obtain the aircraft drag using a flow through nacelle, it is necessary to subtract the drag of the internal surfaces of the nacelle. The internal drag can be obtained by flow surveys at the exit plane of the nacelle.

Figure 3 indicates separate models to obtain inlet forces and to obtain exhaust/afterbody interference. Powered simulators permit simultaneous simulation of both inlet and exhaust flows. If it is possible to obtain the desired information from a single model with a powered simulator, why are the separate inlet and exhaust models employed? Simulators for supersonic aircraft are currently being developed. Simulators for large bypass turbofans have been in use for some time. Figure 1 indicates that these simulators play an important role in the engine/airframe integration of a high bypass ratio engine. Figure 5a is a photograph of a supersonic propulsion simulator. Figure 5b is a photograph of the simulator undergoing tests; this bears a striking similarity to a real gas turbine under test!

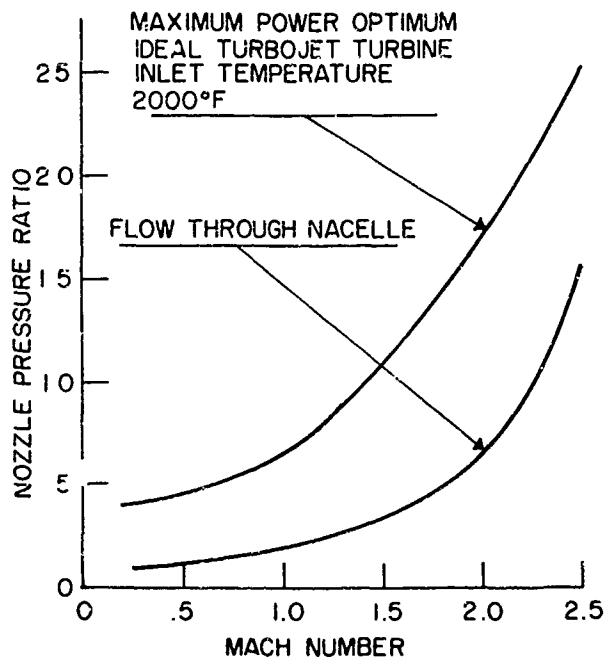

Figure 4. Nozzle Pressure Ratio VS Mach Number for an Optimum, Ideal Turbojet and a Flow Through Nacelle.

E. Summary

To summarize Section III, an aeroforce model is used to obtain airframe drag polar at specified reference conditions. Propulsion may be simulated in several ways as discussed above. A specialized inlet model, usually of larger scale than aeroforce model, is used to obtain drag increments for varying mass flow ratio, angle of attack, and angle of yaw. Another specialized exhaust model, also called jet effects model in Figure 3, is used to obtain thrust minus drag increments due to varying nozzle pressure ratio, mass flow ratio, and nozzle geometry. For podded engines a large scale, at least large scale relative to aeroforce model, powered simulator is used to determine propulsion characteristics and interference with airframe.

IV. ENGINE THRUST--FULL SCALE PROPULSION TESTING TECHNIQUES

There are four testing techniques applicable to full scale engines: sea level static, altitude, wind tunnel with inlet and partial airframe, and flight testing. Altitude testing is described as direct connect testing. In direct connect testing all the air supplied passes through the engine. In the wind tunnel tests, spillage of air can occur. This is called free jet testing. Sea level static and altitude testing give the internal or uninstalled thrust. Wind tunnel testing with inlet, exhaust, and partial airfr[illegible]e becomes a reasonable approximation for installed thrust. Flight testing provides installed thrust.

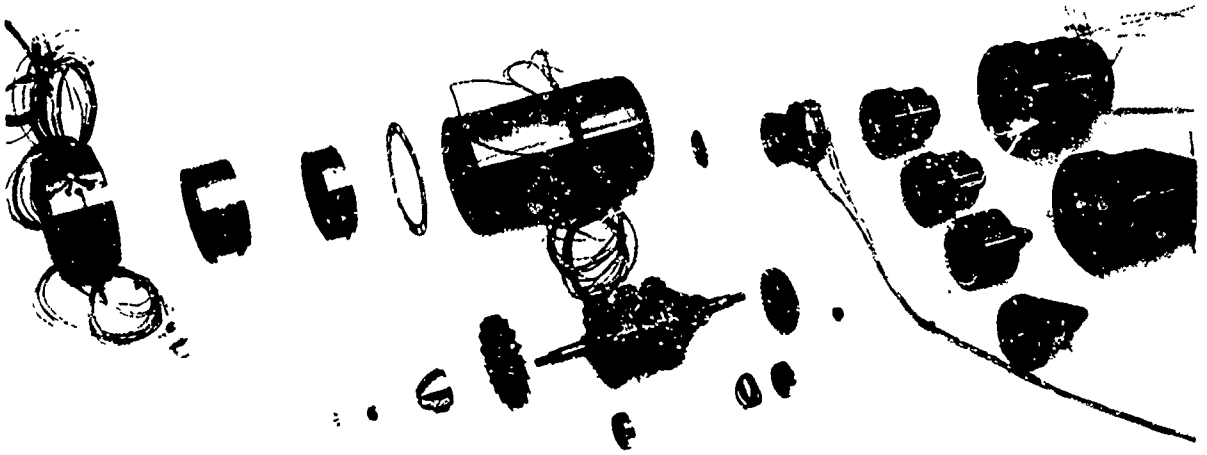

SUPERSONIC PROPULSION SIMULATOR

CONTRACT NO. F33615-69-C-1909

TD 680

TECH DEVELOPMENT, INC.

DAYTON, OHIO

Reproduced from best available copy.

a. Exploded View.

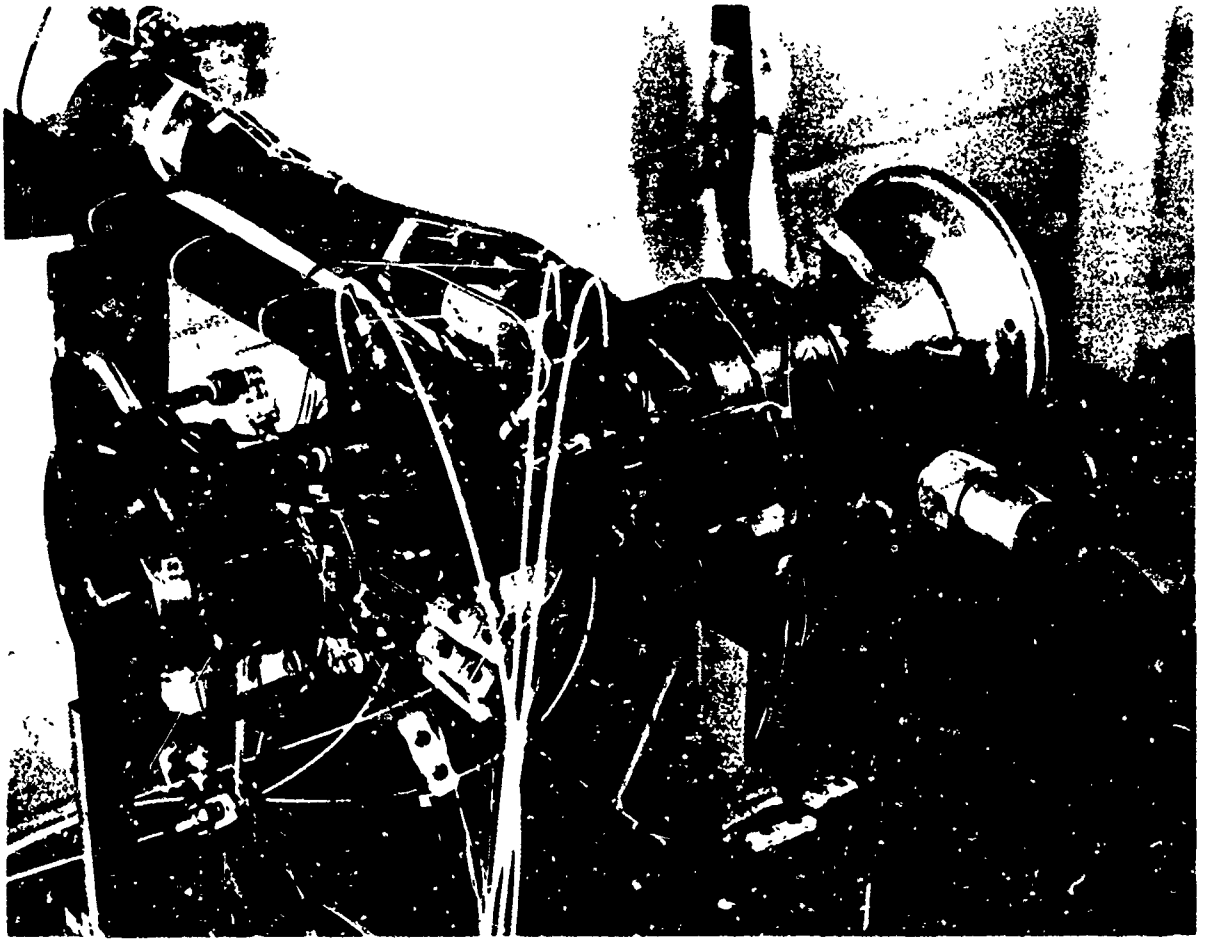

b. Simulator on Test Stand.

Figure 5. Supersonic Propulsion Simulator.
(Figure 5 was supplied to the author by Captain Steve Piller of USAF AeroPropulsion Laboratory.)

Engine companies specify that their engines will have a certain magnitude of gross thrust when tested sea level static under certain conditions. When the customer buys an engine, the specification usually indicates a definite value of gross thrust during sea level static or altitude testing. Thrust is a function of many variables including the following: (a) altitude, which determines free-stream pressure and temperature, (b) flight Mach number, (c) inlet pressure recovery, (d) distortion of flow into compressor, (e) power level angle or throttle position, (f) power extraction by bleed air or torque at accessory pad, (g) secondary airflow, and (h) exhaust nozzle position (when nozzle geometry is variable). As can be seen in Figure 6, a major problem is the conversion of uninstalled thrust to installed thrust. Conditions at Station ② the compressor face, may be only partially simulated. The nozzle differs. There is external flow over the nozzle. For static testing a simple convergent nozzle may be used, whereas a more complicated nozzle, e.g., blow in door ejector, may be used in the aircraft. Subsequent discussion should answer some of the questions posed in this paragraph.

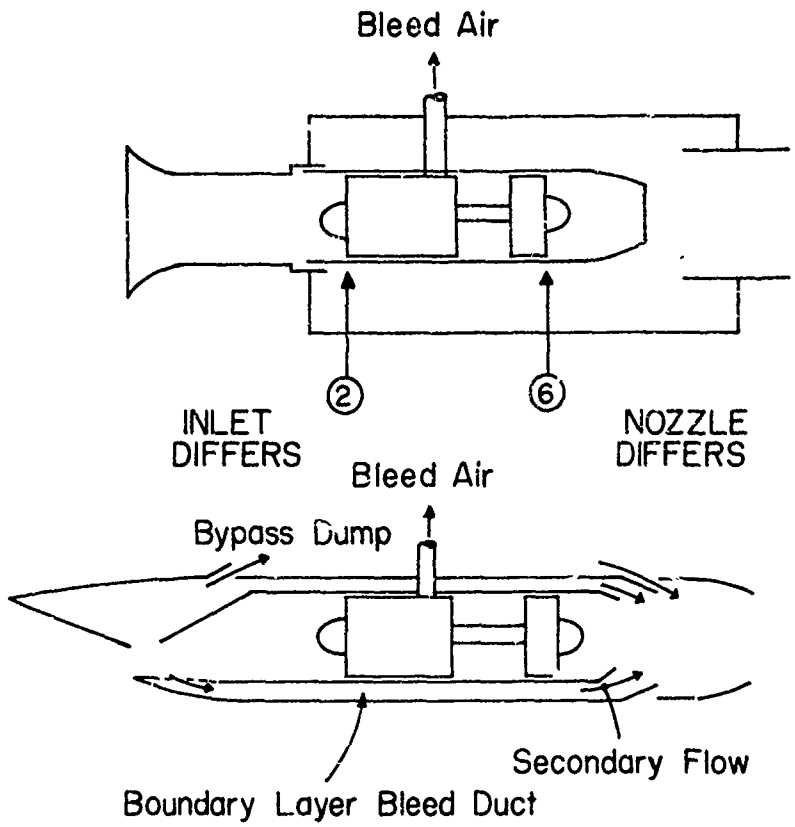

Figure 6. Aircraft Engine in Altitude Test Facility and Installed in Aircraft.

A. Sea Level Static Testing

Sea level static testing is the most economical, by a wide margin, of all the techniques. The engine is mounted on a base plate supported by flexure strips. A bell mouth is bolted to the engine face, and a reference nozzle is installed. Thrust of the engine and bell mouth is measured directly by a load cell. By calibration or pressure taps along the bell mouth inner wall, the force on the bell mouth is known. Momentum flux into the bell mouth is also determined. After suitable correction, the gross thrust of an uninstalled engine is obtained. To avoid bell mouth corrections a labyrinth seal may be used at the junction between engine and bell mouth.

Accuracies of 0.5 per cent for F_g are commonly attained. With this level of accuracy, care must be taken to have uniform pressure over the engine external surfaces. Fuel must be introduced normal to thrust axis or else a correction needs to be made for fuel momentum. Figure 7 illustrates base plate, flexure strips, etc.

Data are reported in terms of gross thrust coefficient defined as

$$C_{Fg} = \frac{F_g}{\dot{m}_e v_i} = \frac{F_g}{F_i}$$

where $\dot{m}_e$ is the mass flow at engine exit, Station ⑥ in Figure 6. Mass flow at engine exit is the sum of mass flow of air plus fuel. The velocity v_i is an ideal velocity obtained by isentropic expansion from P_{T6} and T_{T6} to P_a. The gross thrust coefficient is, in a sense, an efficiency comparing actual thrust to ideal thrust. C_{Fg} provides a link between the installed and uninstalled engine gross thrusts. From that point of view, it is valuable. Cycle analyses are one dimensional and can yield values for F_i. The thrust coefficient provides a means for estimating F_g. C_{Fg} also eliminates engine size or scale. However, C_{Fg} mixes one-dimensional concepts with three-dimensional flow. The question arises concerning how to define P_{T6} and T_{T6}. It is necessary to use an averaging procedure, e.g., area weighted or mass flow weighted averages, to arrive at a single number. An average cannot be defined which simultaneously satisfies the conservation equations; if averages are used, one of the conservation equations is being violated. Flange thrust F_f has [illegible] recognize the three-dimensional aspects of flow at the charging station. Defining a C_{Fg} with [illegible] laced by F_f would add realism but would be complicated to use.

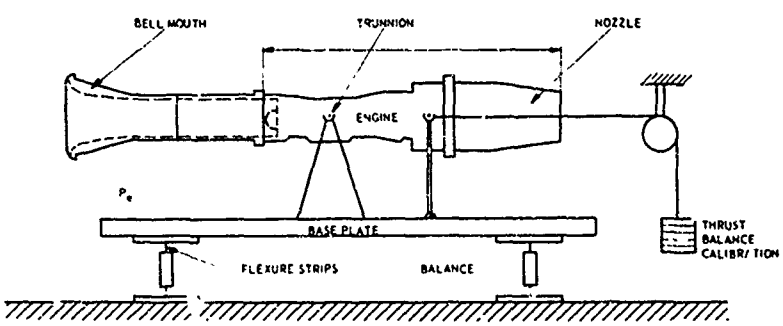

Figure 7. Engine Static Thrust Measurement at Sea Level.

To obtain C_{Fg} from a sea level static measurement of F_g, it is necessary to determine the mass flow rate of air at engine inlet $\dot{m}_a$. Compressor maps yield corrected weight flow rate as a function of engine speed $N/\sqrt{\theta}$ and compressor pressure ratio. Separate means of measuring $\dot{m}_a$ are calibrated bell mouth, venturis or orifices. Calibration of engine air flow in terms of $N/\sqrt{\theta}$ and pressure ratio provides useful data for flight testing. Pressure rakes and temperature rakes are used to determine P_{T6} and T_{T6}. Since specific fuel consumption and ideal thrust require knowledge of the mass flow of fuel $\dot{m}_f$, the specific gravity of the fuel must be measured at the engine. Most flow meters yield volume flow rate.

The station where P_{T6} and T_{T6} are measured is frequently called the nozzle charging station. The charging station must be accessible for instrumentation in both full scale and model nozzles.

The thrust coefficient C_{Fg} includes losses due to flow divergence, skin friction on internal nozzle surfaces, leakage, non uniform profiles, and swirl. These are some of the flow phenomena and loss mechanisms which make C_{Fg} less than unity.

B. Altitude Testing

Conditioned air is supplied at the compressor face. The stagnation pressure and stagnation temperature are determined by calculations knowing flight altitude and Mach number. A suitable inlet pressure recovery is assumed. Compressors and heaters (or refrigerators) are necessary to supply correct T_T and P_T at engine face. The engine external surfaces are maintained at ambient pressure suitable for altitude being simulated. Exhausters are required to maintain a low pressure. Figure 8 shows a schematic of the altitude test facility at the Naval Air Propulsion Test Center.[2] From the scale of

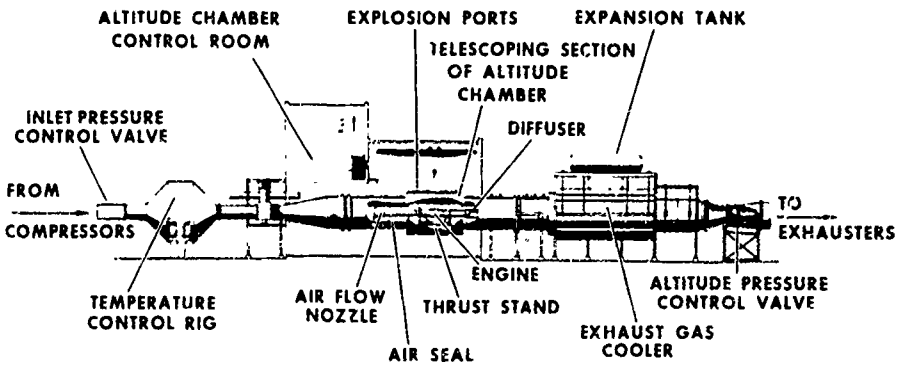

Figure 8. Schematic of Altitude Test Facility at Naval Air Propulsion Test Center. (Reproduced from Reference 2.)

the engine one can judge the scale of the facility. To aid the exhausters the high velocity jet from the engine is used as an ejector enhancing the facility capability in terms of altitude and mass flow rate of air. Altitude testing is expensive. For large engines with high $\dot{m}_a$, the costs may be a few thousand dollars for each hour of test time.

Altitude testing yields an uninstalled thrust value. As in the case of sea level static testing, thrust is measured using apparatus similar to that shown in Figure 7. An alternate method to determine F_g is to make exhaust surveys as illustrated in Figure 9. Within current testing philosophy this is generally regarded as a secondary method. The pressure and temperature rakes are upstream of the sonic line to avoid measurements in a supersonic stream. By careful attention to experimental details, it is possible to obtain agreement within 1 per cent between F_g from load cell and F_g from survey.

C. Wind Tunnel Testing with Partial Airframe

For fighter size aircraft it is possible to test a full scale engine along with its inlet and exhaust in a wind tunnel. Those parts of the fuselage, usually the forebody, and wing which influence the inlet flow are duplicated. Figure 10, which is reproduced from Reference 3, is a sketch of such a test.

For large aircraft it is not possible to test the complete propulsion full scale. Although this section is on full scale testing, we show the photograph of B-70 propulsion in the 16-foot wind tunnel to illustrate the concept. The scale is .577. Figure 11 is from Reference 4.

Part of the motivation for conducting tests as illustrated in Figures 10, 11, and 12 is to determine inlet engine compatibility, inlet controls, nozzle controls, influence of angle of attack, etc. Another reason for the tests is to obtain installed thrust.

D. Flight Testing

Flight testing of a propulsion system occurs late in the development cycle. To fly, the engine must be flight rated, and this rating is issued only after a long series of tests. If anything is wrong, it is late, and the changes to correct a propulsion system become expensive.

There are several cases of flight testing full scale propulsion systems: a new engine mounted on an old aircraft, a new engine in the new aircraft, and an old engine on an old aircraft as part of a comprehensive ground and flight test program.

A new engine under development can be flown on an old aircraft to check operation in a flight environment. There are phenomena, e.g., gyroscopic forces, that cannot be examined on the ground. Engine performance can be verified. The drag polar of the old aircraft is well documented so that engine thrust can be estimated from aircraft performance. Engine thrust may be determined by inverse procedure of sea level static test. C_{Fg} is assumed known. $N/\sqrt{\theta}$ and compressor pressure ratio are measured; from these data $\dot{m}_a$ is determined. Stagnation pressure and stagnation temperature are measured at the nozzle charging station so that v_i can be calculated. It then follows

$$F_g = C_{Fg} \dot{m}_a v_i$$

Of course, the new engine in a new aircraft is always flight tested. As stated before, this is very late in the development, and correction of any deficiencies is expensive.

NASA has been conducting flight tests of a J-85 on a F106 aircraft. This is an example of an old engine on an old aircraft. These tests were part of a comprehensive wind tunnel and flight test program. Several different nozzle configurations were flown. The program, besides supporting SST development, provides badly needed data for checking wind tunnel results with flight tests.

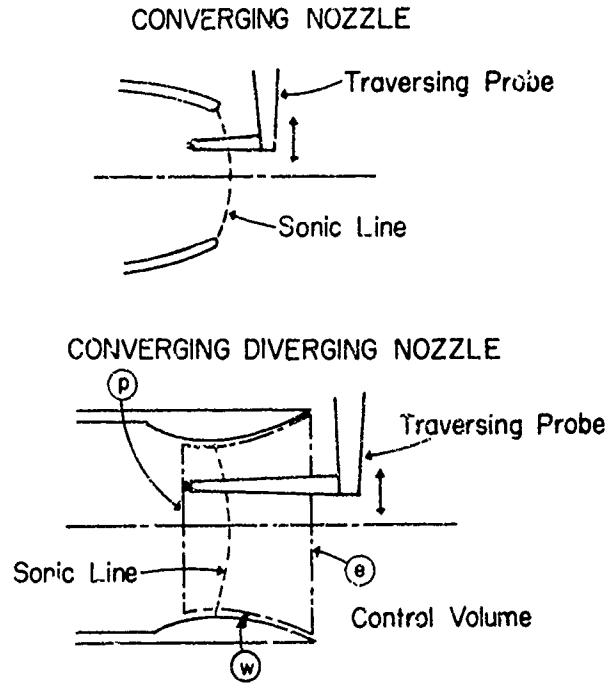

Figure 9. Exhaust Survey for Converging and Diverging Nozzles.

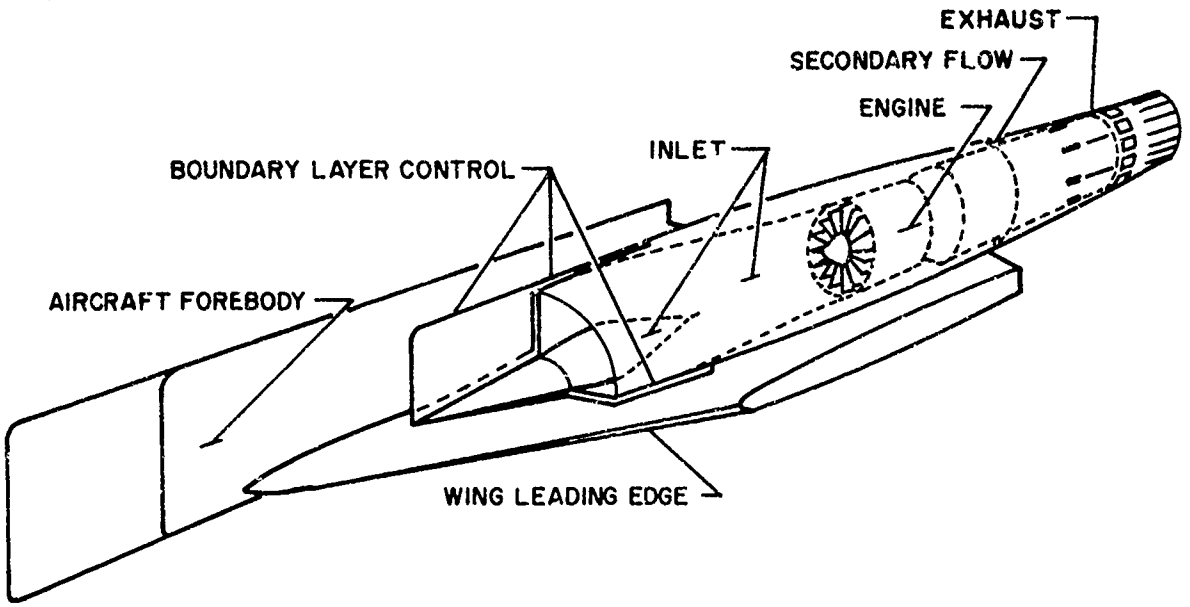

Figure 10. Full Scale Propulsion Integration Test. (Reproduced from Reference 3.)

E. Difference Between Uninstalled Thrust and Installed Thrust

In sea level static and altitude testing, the uninstalled thrust is measured. For fan engines mounted on pylons, the uninstalled thrust includes scrubbing drag. To arrive at the installed thrust, it is necessary to add or subtract increments due to the following: (a) inlet additive or spillage drag, (b) momentum losses due to flow extracted from the engine inlet for boundary layer bleed, bypass, or secondary cooling air, (c) thrust recovery from air extracted from the engine (See Figure 6.) for customer use, (d) scrubbing drag on adjacent airframe not previously included, (e) nacelle friction or pressure losses due to airframe/engine interference, (f) changes in pylon pressure distribution due to aerodynamic interference, (g) alteration of C_{Fg} due to external flow, and (h) change in boattail or base drag due to exhaust flow.

V. EXHAUSTS[5]

A. Introduction

Once a given jet engine has been selected, the nozzle selection remains open. As shown in Figure 12, there is a wide variety of nozzle designs from which to choose. The aim of this section is to

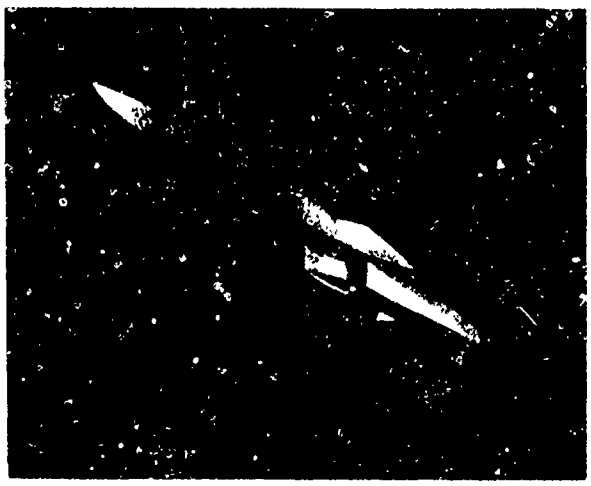

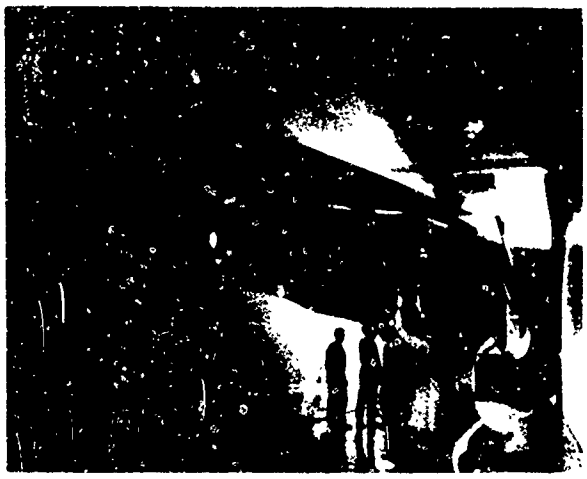

B-70 Wind Tunnel Models

Figure 11. Photographs of B-70. (Reproduced from Reference 4.)

indicate how a prediction of installed thrust can be made based on wind tunnel data and engine test cell data. The techniques for estimating nozzle performance and jet interference will be discussed.

To make an obvious statement, a supersonic aircraft will fly subsonically, transonically, and supersonically in any supersonic mission. Aircraft performance must be verified in each flight regime. Comments concerning transonic flight will be made; similar statements can be made for the other operating conditions.

The transonic flight regime is a region where afterbody and nozzle drag is high. There are at least four operating conditions that must be thoroughly investigated: (1) transonic cruise, (2) transonic acceleration, (3) transonic deceleration, and (4) high-g maneuvers. These four operating conditions have different nozzle pressure ratio, exhaust stagnation temperature, nozzle area ratio, heat capacity ratio, and aircraft angle of attack. Figure 13 shows the typical range for some of these variables.

Afterbody models are used to complete the necessary drag data. These models are in addition to the aeroforce model, which is a reproduction of the complete aircraft. Afterbody drag and nozzle drag may be 20 to 40 per cent of complete aircraft drag at transonic flight. A variety of bookkeeping procedures has been developed to define, identify, measure, diagnose, and correct forces of various components.

The trend in nozzle design has been to iris and plug nozzles. Development of fan engines has made cooling air available. Turbojets needed a flow of cooling air which could be obtained from ejector action of the primary jet. Early jet fighter aircraft placed heavy emphasis on ejector nozzles. For some supersonic aircraft, blow-in door ejector nozzles provide performance gains in transonic flight. Variable geometry nozzles are essential for multiple Mach number design points.

There is a wide number of variables related to nozzles and exhausts. Table I lists these variables. A particular nozzle problem can be stated or specified by taking one adjective for each variable from the right-hand column. When this is done, there are 62,208 different combinations, implying that number of nozzle configurations!

An important aspect of nozzle and exhaust testing is the fidelity of jet simulation. Jet simulation will be discussed.

Test planning involves many considerations including the type of nozzle and type of installation. Extent of simulation, as mentioned previously, must be decided. Compromises are required by constraints of local facilities and program goals; decisions concerning compromises are based on past experience.

B. Accuracy

Accuracy of determination of thrust should be, of course, compatible with the accuracy of measurement of drag. Since the aircraft senses net thrust and the procedures yield gross thrust, it is necessary to have a more precise measurement of gross thrust. The ratio F_g/F_{net} is 2 to 3 for transonic flight. Assessment of accuracy is complicated by the many instruments employed in the measurement sequence, the many models used for obtaining drag increments and seperate portions of overall drag, and the complex test apparatus. Desired accuracy in the transonic region is 0.5 per cent for F_g.

Figure 14, which is reproduced from Reference 6, shows the range sensitivities for various installation parameters. A 3 per cent decrease in propulsion package weight causes an increase in range of about 40 n.m. A 3 per cent increase in C_{F_g} yields a range increase of 300 n.m. Nozzle performance, for a SST, is a most sensitive parameter.

C. Isolated Nozzle Versus Complete Model Tests

Isolated nozzle tests are a very close approximation to a two-dimensional flow problem. The geometry is usually axisymmetric without fins, elevators, or other features. An afterbody or complete model test duplicates the geometry of the aircraft. This is a three-dimensional problem. Isolated nozzle tests, which are valuable for comparing different nozzle designs, are usually conducted early in

the development phase. In later phases of the aircraft development, absolute values for nozzle performance parameters are needed. For these purposes complete model tests are usually conducted. Advantages and disadvantages for isolated and complete model tests are summarized in Tables II and III. Figure 15 illustrates two test arrangements for a wind tunnel.

Figure 16 shows schematically a complete model test using tandem balances. Nozzle gross thrust is obtained by adding readings of balances (A) and (B). Information is obtained about the sum of afterbody plus base drag. Tandem balances offer many advantages. Both balances (A) and (B) in Figure 16 can be sized to match the force. The main disadvantage is the complexity of the model.

D. Installed Gross Thrust from Uninstalled Gross Thrust

From the tests depicted by Figure 6 or 7, a gross thrust coefficient is obtained, and the gross thrust can be calculated by

$$F_g = C_{Fg} F_i$$

From the tests schematically shown in Figure 16, another gross thrust coefficient is obtained

$$F'_g = C'_{Fg} F'_i$$

A prime is used to denote the complete model tests. Taking the ratio of the above two equations, one obtains

$$\frac{F'_g/\dot{m}'_e}{F_g/\dot{m}_e} = \frac{C'_{Fg}}{C_{Fg}}$$

The ideal velocity v_i has cancelled out since each nozzle has been run with the <u>same</u> P_T and T_T at the nozzle charging station. Specific thrust, i.e., thrust per unit mass flow rate, is equal to the ratio of gross thrust coefficients. The engine of Figure 7, when installed in an airframe of the geometry of Figure 16, should give a specific thrust $F'_g/\dot{m}'_e$.

This discussion illustrates the usefulness of C_{Fg} and demonstrates how test cell results can be combined with complete model data to predict performance. The accuracy of the prediction depends on how well v_i matches v'_i. Profiles of P_T or T_T, swirl, nozzle leakage, and similar flow properties can cause inaccuracies.

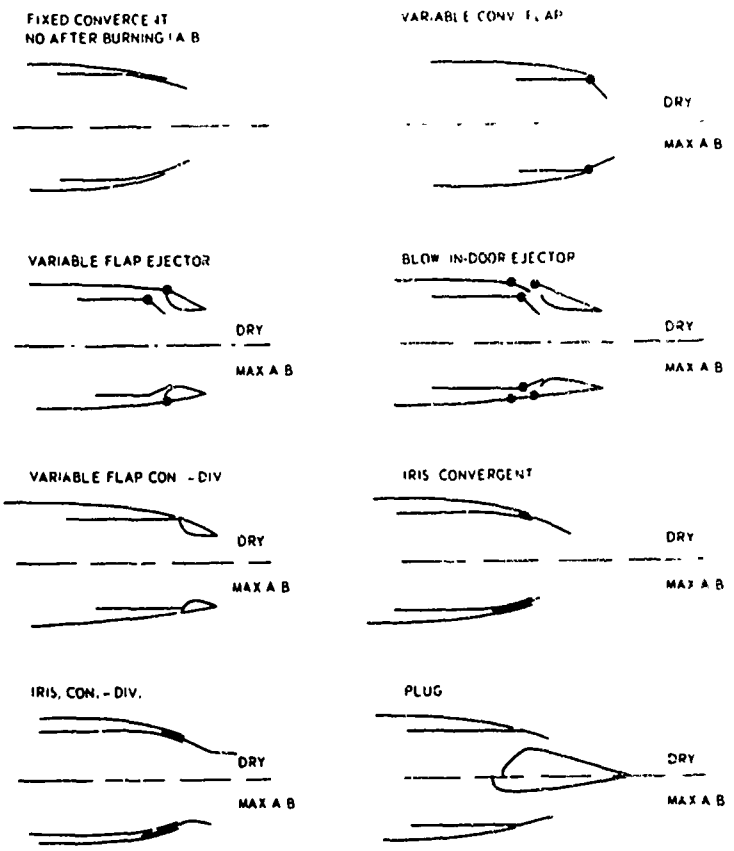

Figure 12. Schematic of Various Nozzle Designs.

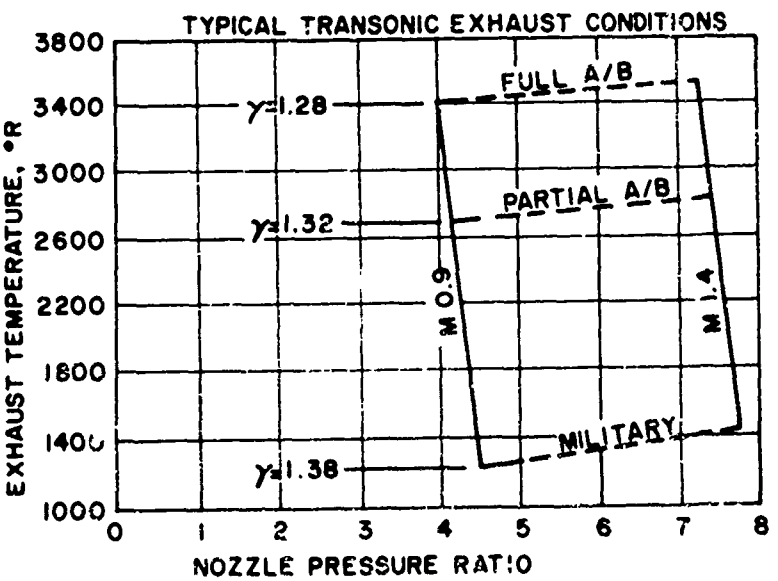

Figure 13. Map of Exhaust Variables for a Fighter Aircraft.

E. Summary Remarks on Exhausts

In this part of the "Exhausts" Section various items will be listed and briefly discussed.

1. Models tested in the wind tunnel do not represent accurate scaled models of the actual airplane. Development programs are paced by schedules and constrained by resources. In a development program wind tunnel data are of importance only to the extent that the data help to produce a good performing airplane. The wind tunnel data are relegated to the file cabinet as soon as the aircraft is certified. Most aircraft programs do not include resources to reexamine the quality of wind tunnel

TABLE I. VARIABLES RELATED TO EXHAUSTS

Variable	Possible Values or Feature
Mainstream Mach Number	Subsonic - Transonic - Supersonic - Hypersonic
Jet Mach Number	Subsonic - Transonic - Supersonic - Hypersonic
Nozzle Pressure Ratio	Overexpanded - Optimum - Underexpanded
Direction of Jet	Parallel - Acute Angle - Normal
Number of Exit Ports	Single - Dual - Multiple
Spacing of Multiple Jets	Narrow - One Jet Diameter - Wide
Number of Nozzle Streams	Primary - Primary and Secondary - Primary, Secondary, and Tertiary
Geometry of Afterbody	Axisymmetric - Nonaxisymmetric
Shape of Afterbody	Blunt Base - Smooth Contour
Boundary Layer, Internal	Laminar - Turbulent
Boundary Layer, External	Laminar - Turbulent
Ratio δ^* to Jet Diameter	(Smooth Variation of This Parameter)
Sensitivity to External Flow	None - Influenced

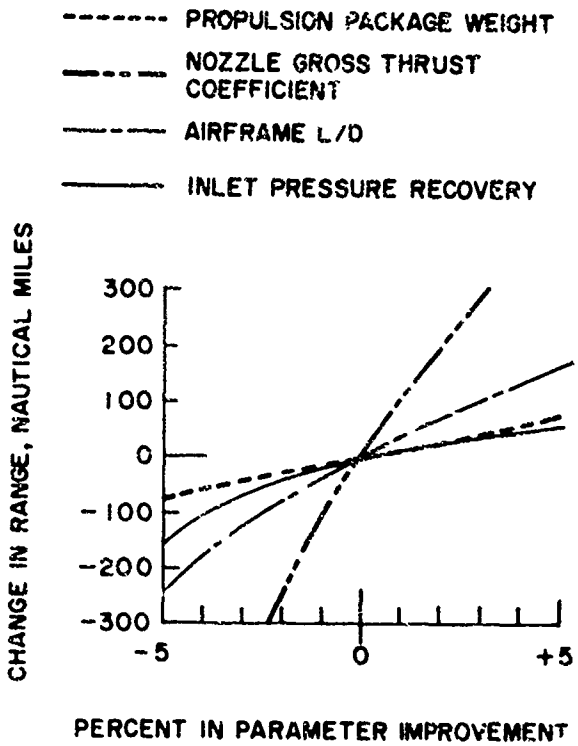

Figure 14. Performance Sensitivity of Propulsion-System Installation for a Typical Supersonic Transport. M = 2.7; Range, 3500 Nautical Miles. (Reproduced from Reference 6.)

data in the light of flight test results. Since the model may not match the airplane, some key points may need checking in the wind tunnel with a new, accurate model.

2. Similarity rules of fluid mechanics are violated in nearly every wind tunnel test. Rarely is Reynolds number correctly duplicated. The problem with interpretation of wind tunnel exhaust data is to know the consequence of inexact similitude and scaling. With the advances in computational fluid mechanics coupled with analytical approaches, new insight may be gained.

3. Unsteady aerodynamics certainly occurs in the external flow field in the transonic regime. Time dependent exhaust flow may be an overlooked feature when evaluating exhaust system performance--or when evaluating the lack of performance.

4. Thrust coefficients are based on an ideal nozzle. Thrust coefficients are a one-dimensional concept trying to quantitatively define performance of a three-dimensional flow device. Thrust coefficients and ideal thrust neatly tie cycle analysis to exhaust system hardware and its performance. The tie becomes confusing and has sources of error in the number to assign to ideal thrust when there are profiles of P_T or T_T.

5. Bookkeeping procedures based on increments have several advantages such as conceptual simplicity; however, to fully exercise the complete bookkeeping procedure, numerous additions and subtractions of data obtained from many different models of widely varying scales must be accomplished. Bookkeeping procedures which do not clearly define the division of responsibility between the engine and airframe companies do not gain acceptance. Being practical and astute, this is a recognized requirement on bookkeeping procedure; however, the aircraft responds to thrust minus drag. Is the split of responsibility a factor which hinders optimization of thrust minus drag?

6. Present methods of defining thrust permit verification of full scale engine quality by testing outside the aircraft. This is certainly desirable.

7. Inlet spillage may have an influence on exhaust performance. Remember the accuracy goals are 0.5 per cent. Limited work has been done to define inlet interference on exhausts for engines buried in the fuselage. More extensive work has been done on pylon mounted turbofan engines. Paired inlets may distort installed nozzle performance.

8. A Mach number of unity is difficult to achieve in a wind tunnel. Wind tunnel tests near M = 1 are difficult to conduct without tunnel interference.

TABLE II. ISOLATED NOZZLE TESTS

Advantages	Disadvantages
Larger Scale, Hence Larger Re	Flow Is 2-D Instead of 3-D
Larger Scale, Easier to Instrument	Installation Effects May Require Nozzle Redesign
Larger Scale, Exact Detailing Possible	Do not Form Basis for Predicting Interference in 3-D Models
Necessary for Checking New Nozzle Concepts and Basic Studies	Support Structure Eliminates Possibility for True Isolated Tests
Baseline for Uninstalled Performance	Not Adequate for Interference Between Multiple Nozzles
Substantiate Calculations; Easier Geometry for Which to Make Predictions	
Relatively Economical	

TABLE III. COMPLETE MODEL TESTS

Advantages	Disadvantages
Better External Flow Simulation	Small Size Nozzle or Else Very Large Tunnel Needed
Only Means Available to Predict Installed Nozzle Performance	Complex Shape Requires More Extensive Instrumentation
Verifies Aircraft Design	Simulation of Secondary or Tertiary Flow Difficult
Influence on Aircraft Aerodynamics Can Be Measured	Support System Interference Needs Careful Checking
Influence of Exhaust Plume on Control Surface Effectiveness Can Be Determined	Models Are Complex and Costly
Pylon Design Verified	Low Re for Nozzle Due to Size
Flow Visualization Possible	Changes in Geometry Are Difficult to Make
Multiple Nozzle Designs Verified	Hot Jets Difficult to Incorporate
	Profile into Nozzle May Be Poor
	Difficult to Measure Mass Flow Accurately

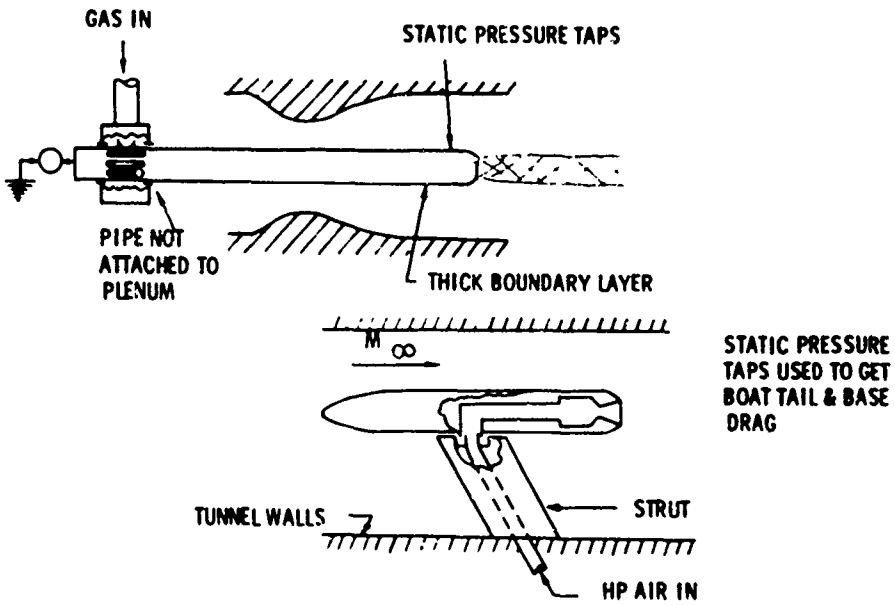

Figure 15. Isolated Nozzle Tests in a Wind Tunnel

9. Pressure ratios are small in the streamtube passing through the fan. The potential for mutual interference between a wing and a turbofan is great.

10. Sources of error in exhaust testing include struts to hold model, roughness in the model flow channel, omission of small detail due to model scale, and incorrect profiles at nozzle entrance.

VI. INSTALLATION LOSSES

An uninstalled engine, as shown in Figure 6 or 7, has a level of performance. This level of performance is not achieved in an aircraft. Various aircraft demands erode the performance. Various

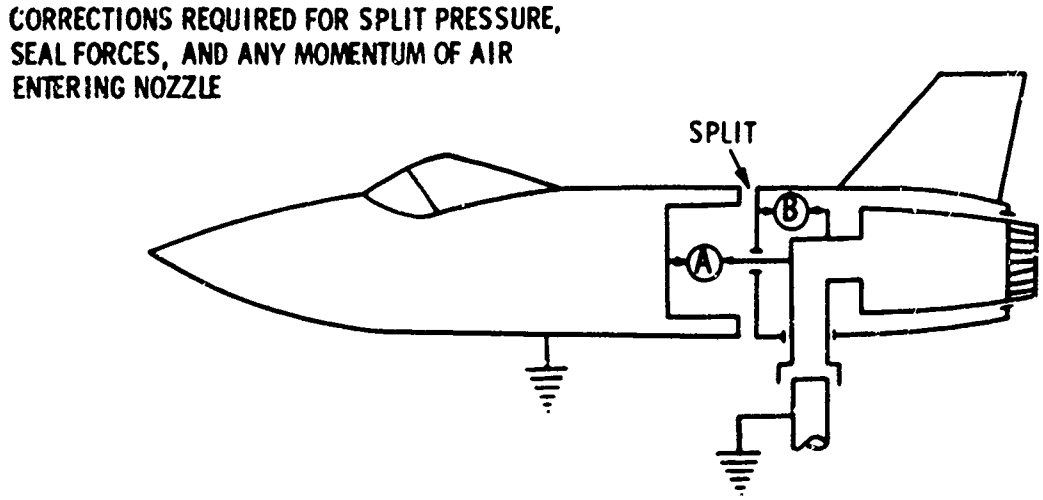

Figure 16. Tandem Balances. Balance (A) reads $F_g - D_a - D_b$. Balance (B) reads $D_a + D_b$.

installation factors alter performance.

A. Losses Due to Inlet

A price is paid for the air taken on board the aircraft; it is the ram drag. At the engine face the stagnation pressure is less than that attained by an isentropic compression. This is a loss which degrades performance. The impact of pressure recovery on SST range is shown in Figure 14.

The inlet provides distorted flow to the fan and compressor. Distorted flow may cause the compressor to stall and the engine to surge. Adequate stall margin must be incorporated to avoid stall. The margin degrades performance of the engine compared to what it could have been. For the same pressure ratio additional stages of compression may be needed.

The inlet is sized for maximum air flow requirement. For operating conditions off the maximum design point, air must be spilled or taken on board and dumped. Spillage of air causes a drag, or alternatively, a loss of thrust.

B. Losses Due to Engine Accessories

Engine accessories include fuel pumps, fuel controls, and lubrication pumps. To drive the accessories power is taken from the engine. Accessories tend to increase engine frontal area increasing nacelle drag or airframe drag which effectively decreases thrust minus drag.

C. Losses Due to Power Bleed

Power may be removed from the engine in the form of compressed air. The compressed air may provide air conditioning for electronic equipment and crew, drive pneumatic actuators, provide boundary layer control, and force the flow of cooling air.

Power may be removed from the engine in the form of torque on a shaft. Modern aircraft have large electrical power needs for radar, galley heaters, etc. Hydraulic pumps for the aircraft control system are driven by the engine.

D. Installation Structure

It is necessary to transfer engine thrust to the airframe. Structure is needed for this task and adds weight. Figure 14 shows impact of propulsion package weight on SST performance.

E. Environmental Factors

Closely related to the inlet distortion discussed in A is clear air turbulence which can be a source of distorted flow at the compressor. Ingestion of foreign gases, e.g., steam during a catapult launch, can cause stall. Stall margin must be built into the compressor.

Gas turbines have limits on turbine inlet temperature. On hot days it is necessary to decrease fuel flow to avoid over temperature in the turbine. When operated in similarity conditions, thrust of a gas turbine falls off linearly with ambient pressure. Decreasing pressure, e.g., at altitude, decreases performance.

F. Acceleration and Safety Margins

For an engine to accelerate, turbine torque must exceed compressor torque requirements. Adding fuel to accelerate tends to drive the transient operating line toward stall. The operating point must be sufficiently far from surge line so that transients do not cause surge. This necessitates more stall margin.

G. Nozzle Performance

External flow and aerodynamic interference can cause loss of gross thrust coefficient. Figure 17 shows drag, thrust, and thrust coefficient as a function of Mach number for a supersonic aircraft. In the transonic region, C_{F_g} has a pronounced dip, which gives a corresponding dip in thrust.

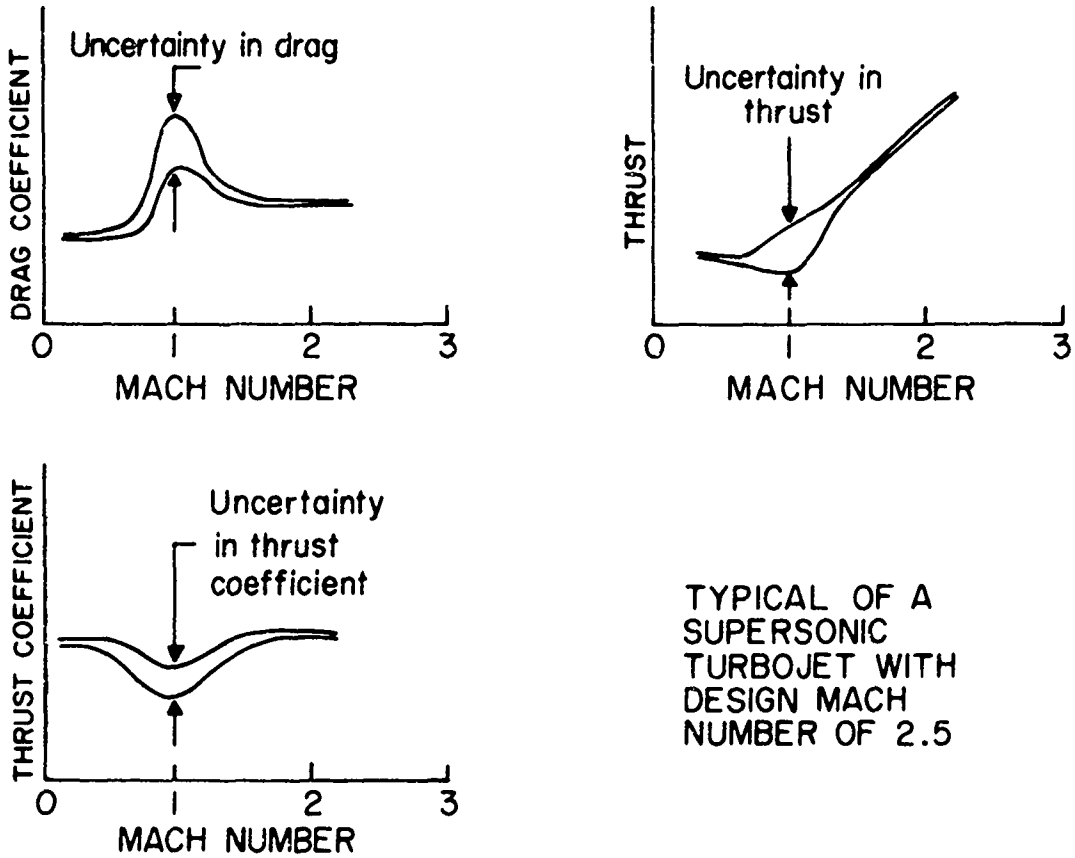

Figure 17. Thrust and Drag as a Function of Mach Number.

Installation losses are due to inlet and exhaust inefficiencies, safety margins of one nature or another, and power bleed.

VII. THRUST AND DRAG ACCOUNTING SYSTEMS

There are numerous schemes for obtaining drag, thrust, and thrust minus drag. One such method will be discussed here to illustrate the scope of a complete test and to show how afterbody and inlet tests fit into the procedures.

Aircraft performance is defined in part by thrust minus drag. The engine company sells thrust, and the airframe manufacturer minimizes drag. Since there are items in the force bookkeeping procedure which must be assigned to drag or to thrust, careful definitions are required.

Bookkeeping of forces usually involves increments to drag or thrust for operation at some point other than the reference condition. At a given M_∞, three variables are usually specified as standard or reference values. These are nozzle pressure ratio P, nozzle area ratio, and angle of attack; subscript r denotes reference values. Deviation from these reference conditions gives rise to force increments. One philosophy for assignment of the force increments is to alter thrust if the increment results from a throttle change. If the increment is due to a change in angle of attack, it is assigned to drag.

The drag of inlets depends on mass flow ratio m into the air induction system. The drag of exhaust systems depends on nozzle pressure ratio P for a given flight condition. Variable geometry of inlets or nozzle adds complexity and alters drag. Changes in m, P, and area ratios are mainly due to throttle changes and hence are assigned to thrust.

The aeroforce model is mounted on a sting and force F_1 determined; see Figure 18. For this test there are reference values of m_R and P_R which may not be the same as, or even close to, the values chosen as the standard flight configuration and denoted by subscript r. At m_r and P_r, drag increments due to the inlet or nozzle flow are set equal to zero.

Figure 18 shows schematically how drag is obtained from the aeroforce model, the inlet model, and the exhaust model. Variation of force due to variation of m or P is readily obtained from the test data. The change in the force on the inlet represented by $F_3 - F_4$ would be charged to thrust since it is

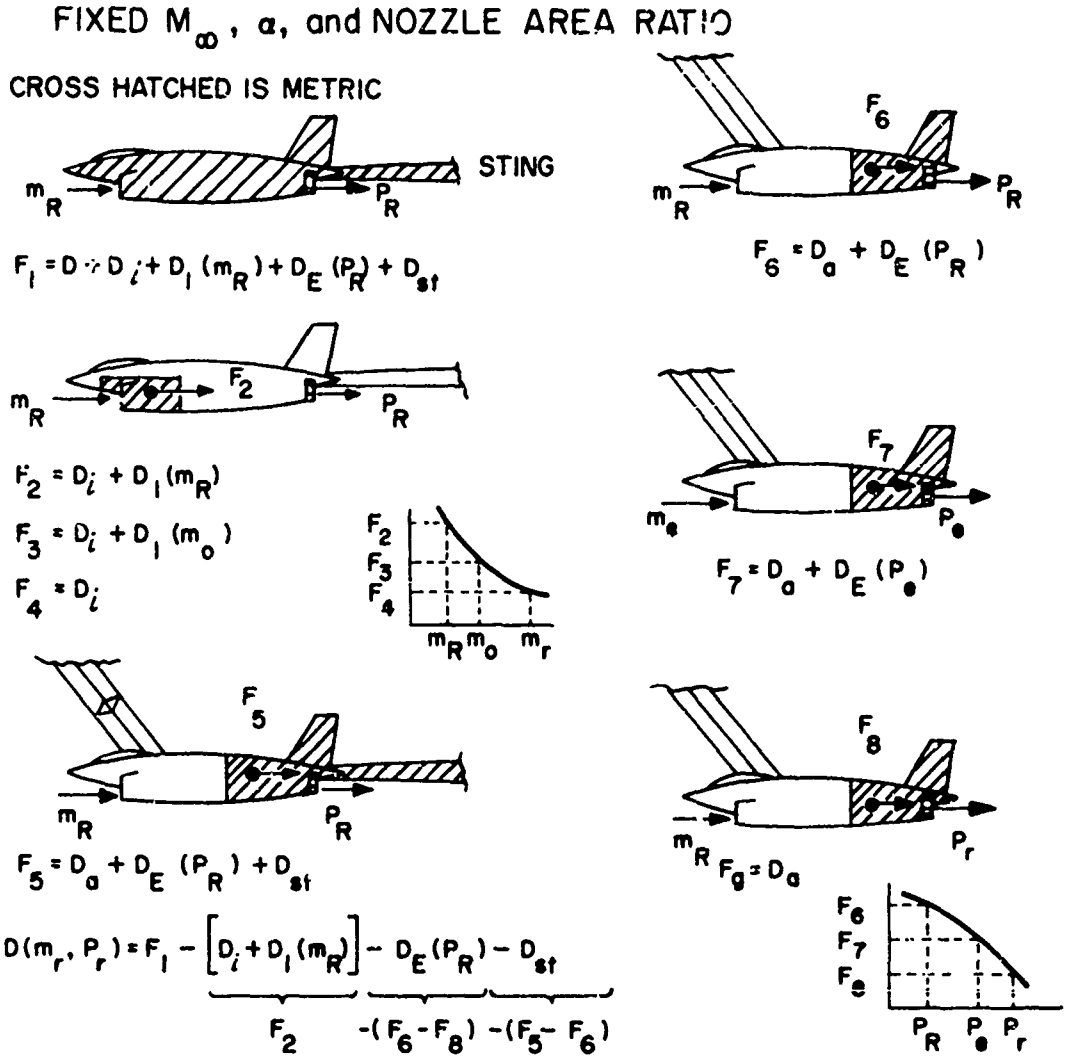

Figure 18. Bookkeeping for Drag.

a result of throttle (mass flow) changes. The change of force represented by $F_7 - F_8$ would also be charged to thrust since nozzle pressure ratio is a function of throttle setting.

Propulsion system installed gross thrust is obtained from

$$\begin{pmatrix}\text{installed}\\ \text{gross}\\ \text{thrust}\end{pmatrix} = \begin{pmatrix}\text{test cell}\\ \text{gross}\\ \text{thrust}\end{pmatrix} + \begin{pmatrix}\text{increment}\\ \text{due to}\\ \text{inlet}\end{pmatrix} + \begin{pmatrix}\text{increment}\\ \text{due to}\\ \text{exhaust}\end{pmatrix} + \begin{pmatrix}\text{increment}\\ \text{due to}\\ \text{engine}\end{pmatrix} + \begin{pmatrix}\text{increment}\\ \text{due to}\\ \text{secondary}\\ \text{flow}\end{pmatrix}$$

The test cell F_g was discussed previously. The increment terms need to be defined and discussed.

The increment due to the inlet includes the following: (1) spillage drag, (2) bleed drag, and (3) bypass drag. Spillage drag consists of additive drag and the change in force on the inlet cowl. Usually data are reported in terms of C_{Dspill} or C_{Dadd} plus C_{Dcowl}. To control shock-wave-boundary-layer interaction, it is necessary to partially remove the boundary layer at critical portions of the inlet. The bleed air is dumped overboard. For some flight conditions it is better to take excess air on board and then dump it overboard. Inlet stability or the trade off between spillage and bypass drag may make it desirable to swallow air in excess of engine needs.

Several factors determine the size of the drag increment due to the exhaust: (1) correction for external flow, (2) base drag, (3) boattail drag, and (4) exhaust interference. Installed gross thrust is at some flight Mach number. The test cell gross thrust is at static conditions. A correction must be made for the external flow influence on internal flow. For the CD nozzle illustrated in Figure 19, this correction may be very small. For the CONV. PLUG, or BIDE nozzles of Figure 19, this may be a relatively large correction. The correction is obtained from the subtraction of static nozzle thrust from the thrust of the same nozzle installed in an afterbody model. The nozzle is metric within the afterbody model. An example of the correction for external flow is shown in Figure 20 for a plug nozzle. Also the boattail and base drag corrections are shown. Figure 20 was reproduced from Reference 7.

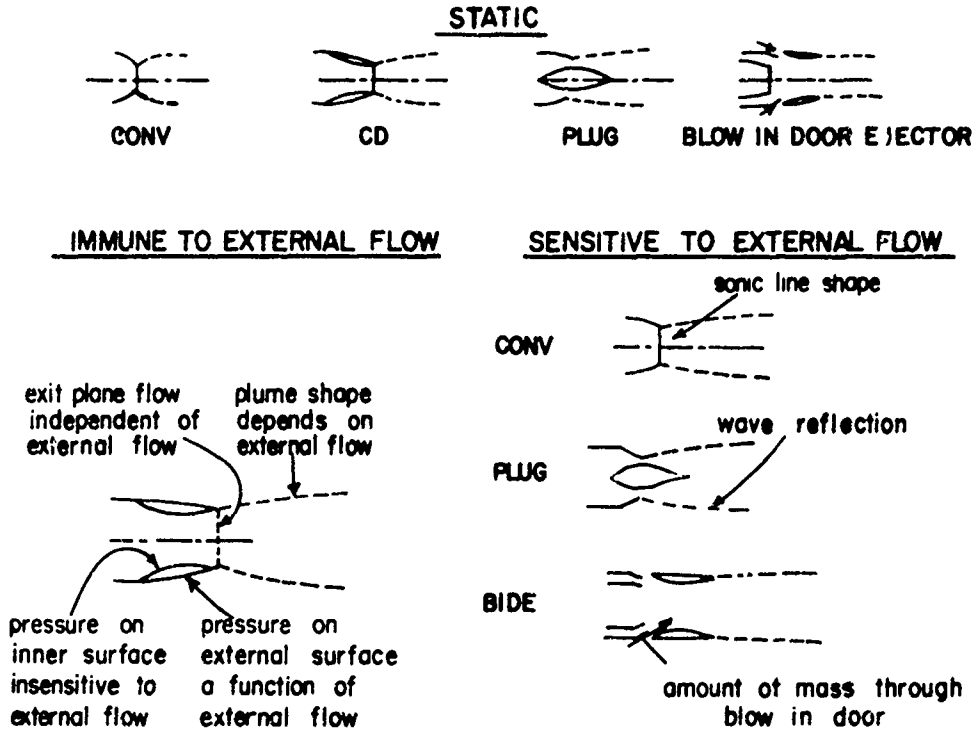

Figure 19. Static and Dynamic Nozzle Tests

Before proceeding with additional discussion of base drag, boattail drag, etc., it is worthwhile to reread Section II and examine Figure 16. Notice the split between the forebody and afterbody of the aircraft model; this indicates that the afterbody is metric. Afterbody drag includes tail, fairings, and boattail. The boattail is the surface which reduces the area from the forebody-afterbody split to the area at the nozzle exit. For variable geometry nozzles, there are usually external nozzle surfaces exposed to the external flow giving rise to external nozzle drag, D_n. The drag D_n may be included with boattail drag. Base flow is a downstream flow region where the streamlines do not follow the body contour. Such an annular area is illustrated in Figure 16. The internal nozzle drag is not important for these discussions having been accounted for by C_{F_g}.

When the base flow region is an annulus surrounding the nozzle exit, as shown in Figure 16, the correction for base drag can be lumped into boattail drag. When there are multiple exhaust nozzles, there may be base flow regions not at the nozzle exit plane. If this is the case, the base drag can be included with the exhaust interference term.

Changes in nozzle pressure ratio, use of afterburner for thrust augmentation, and other propulsion system operating points cause changes in the exhaust plume geometry. As a result, the external flow is modified. Changes in the external flow may alter the pressure distribution on the elevator, rudder, wing, or fuselage. The drag increment termed exhaust interference accounts for this aspect of the exhaust.

Continuing with the various terms on the right-hand side of the installed gross thrust equation, consider now the increment due to the engine. As a result of m different from m_r, inlet pressure recovery and level of distortion at the compressor face may change. These changes can influence engine operation. Based on data obtained from test programs in sea level static test cells or altitude facilities, corrections can be made.

Power may be extracted from the engine either by bleeding air off the compressor or by driveshafts for alternators, pumps, etc. Bleed air from the compressor to provide boundary layer control on the wing, air conditioning for the crew, or to actuate pneumatic devices causes a loss of thrust. This thrust loss is accounted for in the term "increment due to engine."

The final term in the installed gross thrust equation is the increment due to secondary flow. (Secondary flow can be defined as air taken on board from freestream conditions and returned to the ambient atmosphere without forming part of the engine working fluid.) When the secondary flow, e.g., cooling air, forms part of the nozzle flow, there is a thrust increment which changes with the engine operating conditions. The secondary air may be dumped overboard through its own nozzle or exit door. Pressures on the aircraft may be changed. The ram drag associated with secondary air is the mass flow rate of secondary air times vehicle velocity.

The installed F_g equation indicates the corrections which must be made to convert test cell gross thrust to installed gross thrust. The number of corrections becomes quite large as the preceding

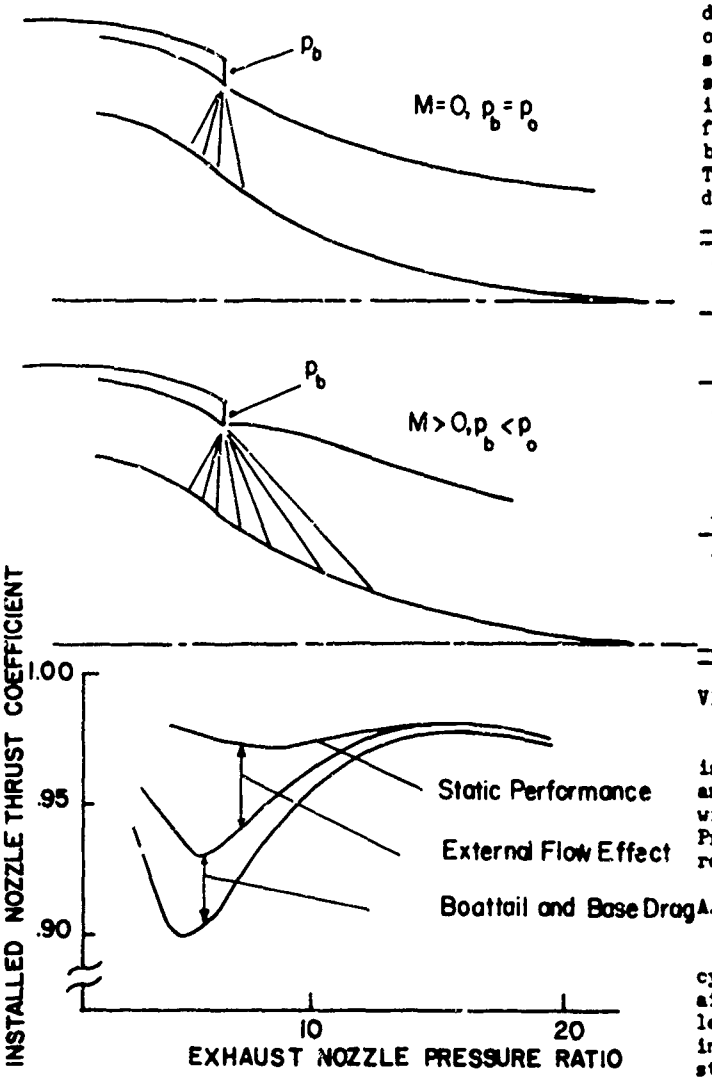

Figure 20. Static and Installed Thrust Coefficient for a Plug Nozzle. (Reproduced from Reference 7.)

discussion has indicated. Each correction or increment has its own accuracy and is a source of error. The bookkeeping schemes should strive for the minimum number of increments required to adequately describe forces on an aircraft. The increments may be based on a variety of model sizes. Typical model sizes providing data are indicated in Table IV.

TABLE IV. TRANSONIC TESTING MODEL SIZES* (TYPICAL FIGHTER AIRCRAFT)

Model	Percentage of Full Scale
Aeroforce Model	5
Inlet Model	8-10
Isolated Nozzle Test	25
Afterbody Model	8-10

*Models less than 1/20 scale have so many compromises relative to geometric detail and Reynolds number that tests are not attempted.

VIII. ASPECTS OF SYSTEMS MANAGEMENT

The motivation for this section is to support the argument that the kinds and goals of testing depend on the phase within the aircraft development cycle. Procedures and scope of tests are limited by resources and schedules.

A. Aircraft Development Cycle

A major aircraft development cycle spans several years; likewise, a major aircraft gas turbine development is a lengthy process. Figure 21, which is based in part on Reference 8, outlines some milestones along the cycle. Figure 21a deals with the airframe. Once vehicle requirements have been defined, various vehicle configurations are explored. Questions such as high wing versus low wing, engines mounted on wing versus engines on fuselage, etc., are examined. A most likely configuration is picked. Small scale (1/12) models of the inlet are being tested. As testing progresses, larger scale inlets (1/6) are built. Based on 1/12 scale data, decisions are made about axisymmetric versus ramp, external versus mixed compression, etc. Using 1/6 scale inlets, questions concerning boundary layer bleed, diverter height, interaction with forebody, etc., are answered.

Early in the development cycle rather crude simulation of the propulsion system is possible. The aeroforce models become larger scale and incorporate better propulsion representation. As the freeze point in design is approached, powered simulators may be employed.

For engine development the first steps are to define cycle parameters, i.e., pressure ratio, turbine inlet temperature, bypass ratio, etc. Based on the required cycle parameters, a demonstrator engine is designed using technology and hardware from previous exploratory and advanced development programs. If the cycle calls for a high turbine inlet temperature, the demonstrator engine should operate at that temperature. If the fan performance pushes the state of the art in tip speed, then the demonstrator engine should run at that tip speed. The demonstrator engine can be boilerplate, i.e., it can have heavy components. It need not be dimensionally correct. It should demonstrate successful operation of all new technology to be incorporated into the final design.

Figure 21c continues the engine development cycle to production. PFRT is preliminary flight rating test. It answers the question of whether or not the engine is safe to fly. Once PFRT has been passed, flight testing can proceed. MQT is military qualification test. This certifies the engine meets all specifications in regard to performance, endurance, weight, etc., and is ready to enter production. As mentioned previously, flight testing is late in the program, although it is before MQT.

B. Types of Tests and Scheduling

Figure 21 gives testing highlights. Some of the tests related to airframe/engine are grouped in the lower part of the figure. Also Figures 1 and 3 are correlated with Figure 21. At the start of the program there are many choices. For example, see Figure 12 for all of the nozzle choices. Early testing is conducted to screen possible candidates and to give relative performance. As the design

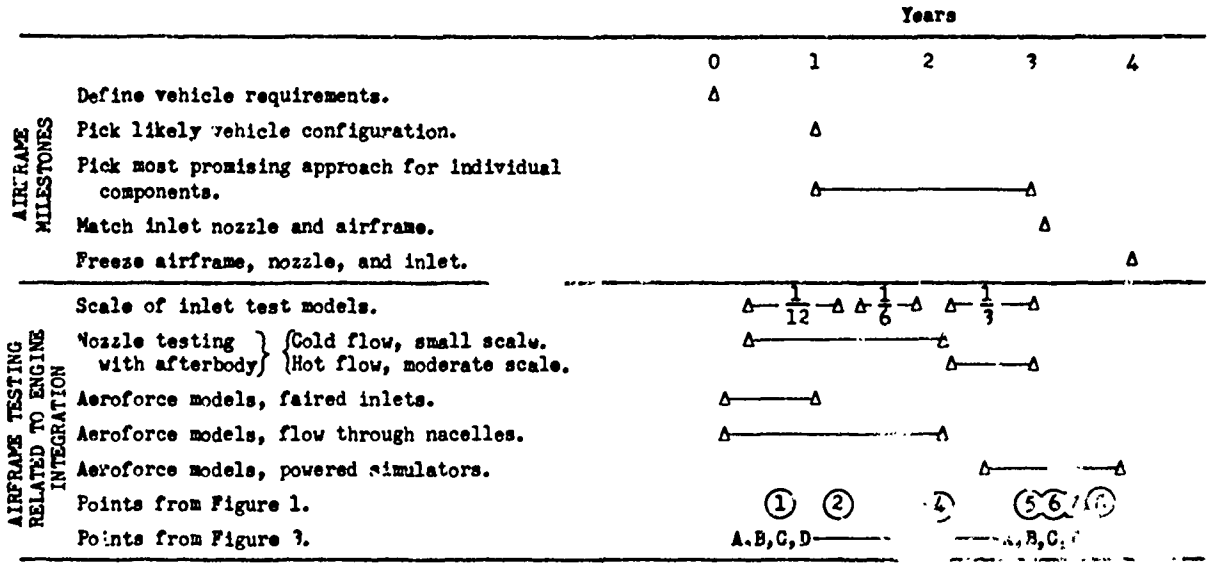

a. Airframe.

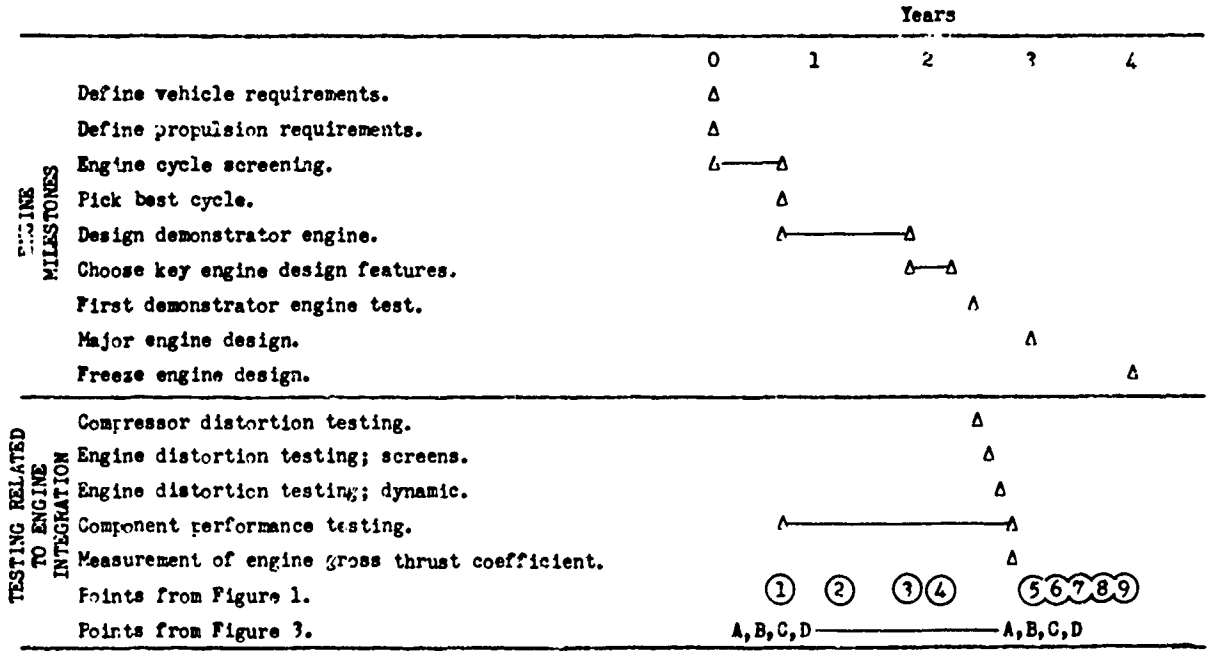

b. Early Engine Events.

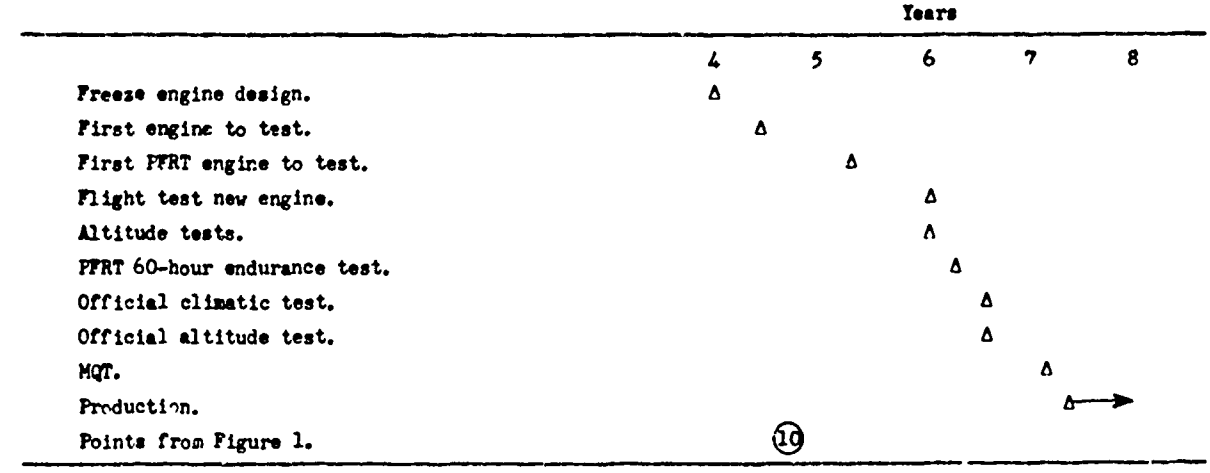

c. Later Engine Events.

Figure 21. Aircraft Development Cycle.

freeze point approaches, emphasis is on absolute thrust and drag levels. Tests become more exhaustive and more precise.

Since there are two major groups, the engine and the airframe manufacturers, working on pieces of the aircraft, there is interchange of data. Engine tests must be scheduled to provide necessary information to the airframe contractor when needed and vice versa.

C. Assessing Progress and Prognosis for Success

About 2 1/2 years into the program, the engine manufacturer has run his first demonstrator engine. Shortly thereafter, as indicated in Figure 21b, engine sensitivity to distorted inlet flow is being tested.

At the same time into the program, the airframe manufacturer has gathered some data from his 1/3 scale inlet. For example, he knows the value of distortion index for $M = 0.95$, $\alpha = 20^\circ$, and $\beta = 5^\circ$. If the engine and airframe manufacturer use the same distortion index, it is possible to evaluate likelihood of engine surge. If a distortion index of 500 causes surge and if distortion indices of 1000 are measured, then some urgent issues need to be solved before design freeze. If the numbers are interchanged, then one may want to make the inlet less fancy--e.g., cut down of bleed air--or else decrease stall margin.

About 3 years into the program, the engine contractor has a value for C_{F_g} based on the demonstrator engine. At the same time, the airframe manufacturer has a fairly precise drag coefficient using an aeroforce model with powered simulators and hot flow afterbody tests. Combining the data available at this point, the performance can be estimated. Based on the outcome of this estimation, the time before design freeze may be hectic or tranquil.

Obviously program management is not quite as simple as the preceding paragraphs might imply. Information is needed at the correct time to make decisions. Need for information must be anticipated.

D. Validity of Test Data

While the design is on paper, there is room for judgment and opinion. Once tests have been conducted, the level of performance is no longer in doubt, assuming careful attention to experimental detail. Possible uncertainty in test results can result from correction factors. Such correction factors may be wind tunnel wall corrections, correction for pressure or temperature difference from reference values, labyrinth seal corrections, etc. Decisions are based on test results.

E. Consistent Definitions

One consistent definition was already denoted; that was distortion index. Both engine and airframe manufacturers need to use the same definition for distortion index, including frequency cut off for time dependent data, number of transducers, curve fitting, etc. Methods for calculating ideal gross thrust need to be standard. There are numerous other interface quantities that need to be defined.

In addition to consistent definitions, identical format for data acquisition and compatible computer programs for data reduction can facilitate information exchange between the two major contractors.

IX. SUMMARY AND CONCLUDING REMARKS

Failure of some aircraft designs to meet performance goals in recent times has focussed attention on procedures and techniques to determine thrust minus drag. Extensive wind tunnel test programs are necessary. Two types of wind tunnel tests may be conducted: subscale testing of aeroforce models along with specialized inlet and exhaust models and full scale testing of propulsion system with partial airframe. The former tests are always conducted, whereas the latter depend on program and aircraft.

Full scale static testing of the engine is conducted at both sea level and simulated altitude yielding F_u and C_{F_g}. It is necessary to convert these values to installed F_g. The method employed is by means of C_{F_g} obtained from exhaust tests. At the conclusion of Section V, there are several summary remarks concerning aircraft exhausts which will not be repeated. These remarks discuss the validity of C_{F_g} approach.

In the early days of wind tunnel testing of propeller driven aircraft, variable frequency electrical motors were developed to provide simulation. More elaborate simulators have been developed for large bypass turbofans and have been utilized in several major test programs. Turbine driven simulators for turbojets are under development making possible one aeroforce model which simulates simultaneously inlet and exhaust flows. Due to the expense of powered simulators, specialized inlet and exhaust models will not be discarded.

Airframe and engine development occur in a parallel fashion. There are numerous critical interfaces between airframe and engine. The major factors of interface at inlet are pressure recovery, mass flow requirements, and distortion levels. For the exhaust system, the interface involves nozzle pressure ratio, nozzle area schedule, exhaust temperature, and secondary flows. There is a significant interface with aircraft power needs. Power is extracted from engine by compressed air bleed or by shaft torque. A timely flow of information between the airframe and engine contractors concerning the interfaces is necessary, and one function of the program manager is to facilitate this flow.

An exceptional aircraft requires a superior engine with superior integration into a superior airframe. A poor engine in a good airframe yields an inferior aircraft. A good engine in a poor

airframe yields a poor aircraft. A good engine improperly installed in a good airframe yields an inferior aircraft.

X. REFERENCES

(1) A. Ferri, F. Jaarsma, and R. Monti, Editors, "Engine-Airplane Interference and Wall Corrections in Transonic Wind Tunnel Tests," AGARD Advisory Report No. 36-71, August 1971.

(2) C. J. Pirello, R. D. Hardin, M. V. Heckart, and K. R. Brown, "An Inventory of Aeronautical Ground Research Facilities. Volume II--Air Breathing Engine Test Facilities," NASA CR-1875, November 1971.

(3) J. Franklin Montgomery, "Engine Altitude Test Procedure," USAF AeroPropulsion Laboratory Technical Memorandum APTP-TM-69-20, May 1969.

(4) M. Pindzola and J. B. Delano, "Wind Tunnel Testing of Propulsion Systems," AIAA Paper 65-477.

(5) A. E. Fuhs, "Nozzle and Exhaust Testing in Transonic Flight Regime," Paper No. 3, Conference Proceedings No. 91, Inlets and Nozzles for Aerospace Engines, AGARD NATO, 1972.

(6) M. R. Nichols, "Aerodynamics of Airframe-Engine Integration on Supersonic Aircraft," NASA TN D-3390, August 1966.

(7) G. R. Rabone, "Low-Angle Plug Nozzle Performance Characteristics," AIAA Paper 66-664.

(8) T. F. Stirgwolt, "TF34 Seminar," Naval Postgraduate School Seminar, 13 October 1971.